



**NAM**

# **Geophysical measurements of shear wave velocity at KNMI accelerograph stations in the Groningen gas field area**

---

**Deltares: Marco de Kleine, Rik Noorlandt, Ger de Lange, Marios Karaoulis, Pauline Kruiver**

Datum June 2016

Editors Jan van Elk & Dirk Doornhof



## General Introduction

The accelerations experienced at surface as a result of the earthquakes induced by the production of gas from the Groningen field are locally dependent on the shallow geological and soil conditions. This is called the site response effect. To be able to take this effect into account NAM has asked Deltares to build a detailed model of the shallow subsurface below Groningen.

A study was done in 2014 and 2015 by Deltares to describe the quaternary geology of the Groningen area. This work was described in the report: "Geological schematisation of the shallow subsurface of Groningen for site response to earthquakes for the Groningen gas field", which was issued in June 2015. As an introduction to the quaternary geology of the Groningen area, Erik Meijles of the Rijksuniversiteit Groningen has written a report titled: "De ondergrond van Groningen: een geologische geschiedenis". Both reports can be downloaded from:

[www.namplatform.nl/feiten-en-cijfers/onderzoeksrapporten](http://www.namplatform.nl/feiten-en-cijfers/onderzoeksrapporten)

In preparing the model of the shallow subsurface below Groningen, Deltares made use of the beta-version of the GEOTOP database of TNO Geologische Dienst Nederland (TNO-NITG) supplemented by more recent data. Additional data collected over the years in support of foundation design and other activities was sourced from Fugro and Wiertsema. These are mainly CPT (Cone Penetration Test) measurements. Additionally, data from the shallow geophone wells was used.

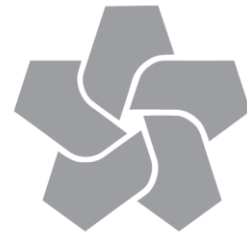
Following the completion of this study, Deltares performed site response measurements near geophone and accelerometer stations of the KNMI geophone network. These measurements combined with the model for the shallow geology form the basis for an enhancement of the Ground Motion Prediction methodology, which includes site response based on the local soil conditions.

Several methods to measure the shear wave velocity at these sites were used and the results have been compared in the report. Both passive methods, making use of the every-day noise vibrations at the measurement site, and active methods, based on vibrations made with a hammer, have been used.

Next step is to expand the shear wave velocity measurements and cover more geological settings and also focus additionally on sites where the shallow sub-surface has been disturbed by human activities. An example are the dwelling mounds, locally called Wierden. The preparatory work for site investigation of the wierden has been carried out by the Rijksuniversiteit Groningen and is reported in "Terp composition in respect to earthquake risk in Groningen" by Dr. ir. E. W. Meijles, Dr. G. Aalbersberg and Prof. dr. H. A. Groenendijk. This report is also available on:

[www.namplatform.nl/feiten-en-cijfers/onderzoeksrapporten](http://www.namplatform.nl/feiten-en-cijfers/onderzoeksrapporten)



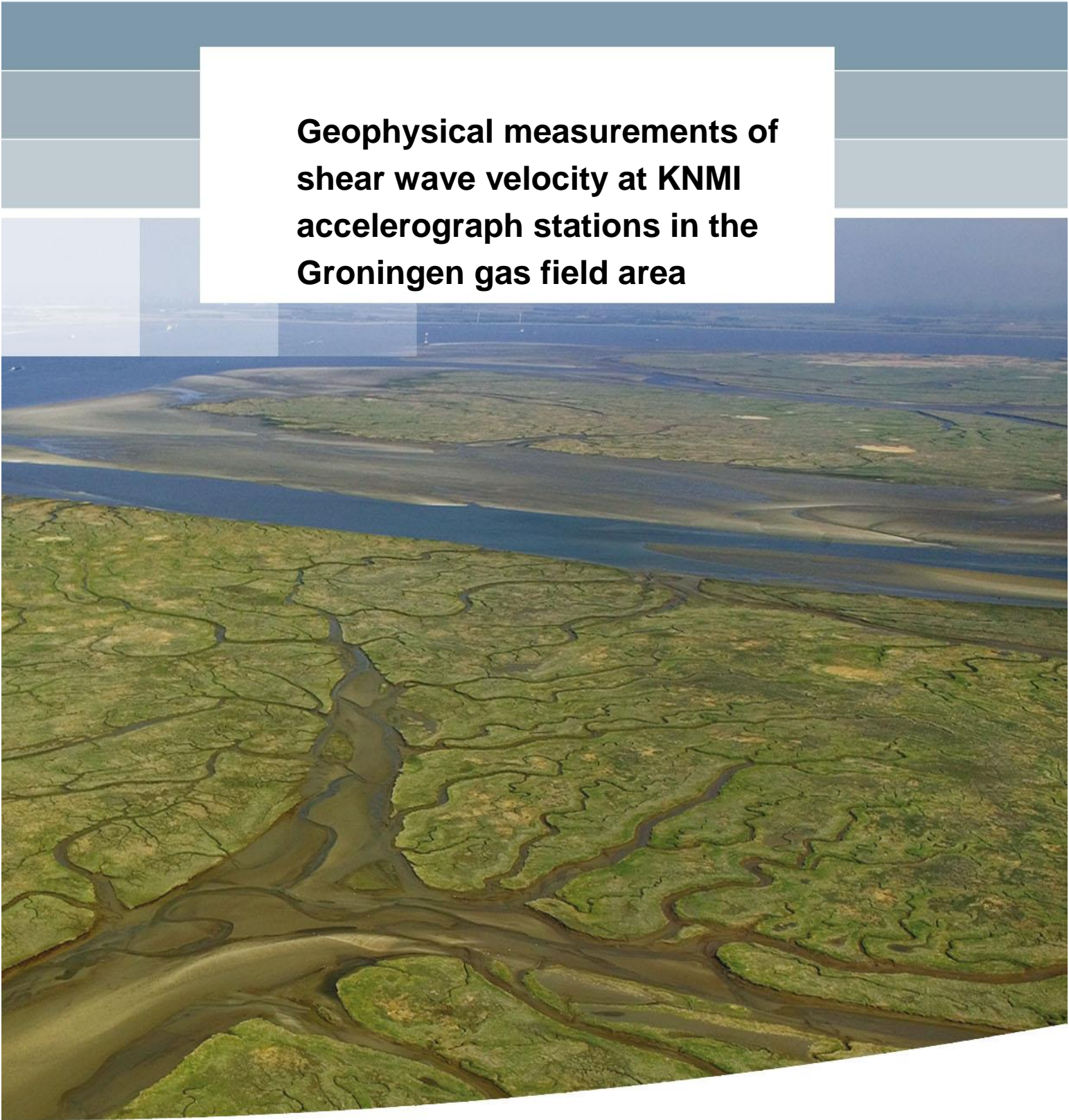


**NAM**

<b>Title</b>	<b>Geophysical measurements of shear wave velocity at KNMI accelerograph stations in the Groningen gas field area</b>		<b>Date</b>	June 2016
			<b>Initiator</b>	NAM
<b>Author(s)</b>	Deltares: Marco de Kleine, Rik Noorlandt, Ger de Lange, Marios Karaoulis, Pauline Kruiver	<b>Editors</b>	Jan van Elk Dirk Doornhof	
<b>Organisation</b>	Deltares	<b>Organisation</b>	NAM	
<b>Place in the Study and Data Acquisition Plan</b>	<p><u>Study Theme: Ground Motion Prediction</u></p> <p><u>Comment:</u> The accelerations experienced at surface as a result of the earthquakes induced by the production of gas from the Groningen field are locally dependent on the shallow geological and soil conditions. This is called the site response effect. NAM has asked Deltares to build a detailed model of the shallow subsurface below Groningen. This was followed in 2015 by measurements of the site response at the sites of KNMI accelerometer and geophone stations. This report describes the results of these measurements.</p>			
<b>Directly linked research</b>	<ol style="list-style-type: none"> <li>1. Introductory text: “De ondergrond van Groningen: een geologische geschiedenis” by Erik Meijles of the Rijksuniversiteit Groningen</li> <li>2. Model of Shallow Geology: “Geological schematisation of the shallow subsurface of Groningen. For site response to earthquakes for the Groningen gas field” by Pauline Kruiver, Ger de Lange, Ane Wiersma, Piet Meijers, Mandy Korff, Jan Peeters, Jan Stafleu, Ronald Harting, Roula Dambrink, Freek Busschers and Jan Gunnink of Deltares and TNO Geologische Dienst Nederland (TNO-NITG).</li> <li>3. Investigations into Wierden: “Terp composition in respect to earthquake risk in Groningen.” by Dr. ir. E. W. Meijles, Dr. G. Aalbersberg and Prof. dr. H. A. Groenendijk</li> <li>4. Follow-up Site-Response measurements near the new geophone / accelerometer stations of the extended monitoring network.</li> </ol>			
<b>Used data</b>	<p>GEOTOP Beta-version and CPT data sourced through Fugro and Wiertsema. New data acquisition described in this report.</p>			
<b>Associated organisation</b>	Deltares, Department of geography of the natural environment of the Rijksuniversiteit Groningen and TNO Geologische Dienst Nederland (TNO-NITG).			
<b>Assurance</b>	Internal			



**Geophysical measurements of  
shear wave velocity at KNMI  
accelerograph stations in the  
Groningen gas field area**





**Geophysical measurements of  
shear wave velocity at KNMI  
accelerograph stations in the  
Groningen gas field area**

Marco de Kleine  
Rik Noorlandt  
Ger de Lange  
Marios Karaoulis  
Pauline Kruiver

1210624-000



**Title**

Geophysical measurements of shear wave velocity at KNMI accelerograph stations in the Groningen gas field area

Client	Project	Reference	Pages
Nederlandse Aardolie Maatschappij B.V.	1210624-000	1210624-000-BGS-0007	329

**Keywords**

Shear wave velocity, spatial scales, active and passive MASW, SCPT, cross-hole measurements, P-S suspension logging.

**Summary**

As part of the development of Ground Motion Prediction Equations (GMPE) for the Groningen field, a fieldwork campaign has been conducted to determine the shear-wave velocity ( $V_S$ ) in situ at 18 recording stations of the KNMI monitoring network. The measured  $V_S$  profiles serve as input for the calibration of the GMPE using records of earthquake motions registered by the network.

The campaign of in situ measurements was performed in two phases: in the first phase, a wide range of techniques was applied at three pilot stations in order to test and optimise the different approaches and select those most suitable for general application across the networks. The multiple measurement approach was also designed to provide insight into the inherent uncertainty in the resulting  $V_S$  profiles and, to some extent, the degree of lateral heterogeneity at each site. The techniques used included Seismic Cone Penetration Tests (SCPT, with varying offsets), active Multichannel Analysis of Surface Waves (MASW, with multiple sources), passive MASW, cross-hole tomography measurements and P-S suspension logging. Classic CPT and borehole logging provided information on the composition and stratigraphy of the subsurface. The full range of measurement techniques has been applied at three pilot stations. SCPT and MASW proved to be suitable techniques to determine  $V_S$  during phase 1, due to the swiftness of performance and no boreholes need to be drilled. These techniques were applied at the 15 remaining stations as well, because fast progress was critical at this stage of the project. The cross-hole tomography was not selected for the remaining stations, mainly for logistic reasons and the need for progress in the second phase of the survey. This technique results in useful and detailed  $V_P$  and  $V_S$  sections, clearly showing the subsurface heterogeneity, but it needs several boreholes. The P-S suspension logging was not used in the second phase, because it did not perform as expected. This was probably due to the combination of the borehole construction, grouting and the local geological setting.

The results from the various techniques to determine  $V_S$  compare well, considering their difference in spatial resolution and sampling volumes. The discussion on sampling volumes of different techniques and the representativeness of the  $V_S$  profile, however, is still pending. For pragmatic reasons, the final  $V_S$  profile at a recording station was chosen as the SCPT  $V_S$  profile that was measured closest to the station. However, in some cases, the  $V_S$  results from first 1 to 4 metres of the SCPT were unreliable. In these cases, the  $V_S$  values from the active MASW results were assigned to the final profile. The maximum depth of the final  $V_S$  profiles is 30 m, unless the SCPT did not reach this end depth. Therefore, the maximum depth of the final  $V_S$  profiles varies between 21.5 and 30 m.

For one station (coded "BOWW"), no choice could be made between the two SCPTs for a representative  $V_S$  profile. The two SCPTs at that location show very different  $V_S$  profiles, local geological setting/stratigraphy and have the same distance to the station. Therefore, both  $V_S$  profiles were provided to the GMPE team.

**Title**

Geophysical measurements of shear wave velocity at KNMI accelerograph stations in the Groningen gas field area

Client	Project	Reference	Pages
Nederlandse Aardolie Maatschappij B.V.	1210624-000	1210624-000-BGS-0007	329

The measured  $V_S$  profiles were converted to  $V_{S30}$  values (the time averaged  $V_S$  for the first 30 m below the surface) and compared to the modelled  $V_{S30}$  map of GMPE V3 (Bommer et al., 2016, Kruiver et al., 2016b), which represent regional  $V_{S30}$  values for geologically similar zones. The measured  $V_{S30}$  values lie within two standard deviations of the modelled  $V_{S30}$  for all stations. The measurements, however, provide more accurate data on a local scale. This stresses the importance of acquiring *local*  $V_S$  profiles for the purpose of determining local ground motions, e.g. for the calibration of the GMPE.

**References**

NAM PO Number 4512273020, contract UI46802

Version	Date	Author	Initials	Review	Initials	Approval	Initials
2	June 2016	Marco de Kleine		Rogier Westerhoff		Bob Hoogendoorn	
		Rik Noorlandt					
		Ger de Lange					
		Marios Karaoulis					
		Pauline Kruiver					

**Versioning**

Version	Date	State	Remark
1	December 18 <sup>th</sup> , 2015	Draft	Prepared for the expert session held at Deltares on January 5 <sup>th</sup> , 2016
2	June 27, 2016	Final	

**State**

final

## Contents

<b>1</b>	<b>Introduction</b>	<b>1</b>
<b>2</b>	<b>Fieldwork and survey methods</b>	<b>3</b>
2.1	Selection of field techniques	3
2.2	Operational aspects	5
2.3	Cone penetration testing	6
2.4	Multichannel Analysis of Surface Waves (active)	11
2.5	Passive MASW	14
2.6	Cross-hole Tomography	15
2.7	P-S suspension logging	18
2.8	Borehole logging	19
<b>3</b>	<b>Processing and analysis</b>	<b>21</b>
3.1	Seismic Cone penetration testing (SCPT)	21
3.2	Offset SCPT (OSCPT)	23
3.3	Multichannel Analysis of Surface Waves	24
3.4	Passive Seismic	26
3.5	Cross-hole Tomography	26
3.6	P-S suspension logging	27
3.7	Borehole logging	27
3.8	$V_{S30}$	27
<b>4</b>	<b>Results</b>	<b>29</b>
4.1	Reading Guide	29
4.2	Appingedam- BAPP	33
4.3	Uithuizen- BUHZ	47
4.4	Westeremden- BWSE	63
4.5	Kolham- BFB2	79
4.6	Gartshuizen-BGAR	93
4.7	Harkstede-BHAR	103
4.8	Garrelsweer- BHKS	113
4.9	Kantens- BKAN	123
4.10	Loppersum- BLOP	133
4.11	Middelstum 1-BMD1	145
4.12	Middelstum 2- BMD2	157
4.13	Oosternieland- BONL	167
4.14	Oosterwijdwerd- BOWW	177
4.15	Stedum- BSTD	189
4.16	Winneveer- BWIN	199
4.17	Wirdum- BWIR	209
4.18	't Zandt- BZN1	221
4.19	Zeerijp- BZN2	231

<b>5 Final <math>V_S</math> profiles from the measurements</b>	<b>243</b>
5.1 General observations	243
5.2 Selection of final $V_S$ profile	244
5.3 Link between $V_S$ and local geological setting	249
5.4 Comparison of measured $V_{S30}$ and GMPE V3 $V_{S30}$ map	250
<b>6 Conclusions and recommendations</b>	<b>253</b>
<b>Appendices</b>	
<b>A References</b>	<b>A-1</b>
<b>B Abbreviations</b>	<b>B-1</b>
<b>C Results of borehole logging</b>	<b>C-1</b>
<b>D SCPT locations and station codes</b>	<b>D-1</b>
<b>E OSCPT profiles</b>	<b>E-1</b>
<b>F Dispersion fitting plots MASW 200m array</b>	<b>F-1</b>
<b>G Dispersion envelopes CMPcc</b>	<b>G-1</b>
<b>H Tomography reports from Geotomographie</b>	<b>H-1</b>

## 1 Introduction

The province of Groningen, the Netherlands, is experiencing induced earthquakes due to the production of gas. The largest induced earthquake to date had a local magnitude of 3.6 (moment magnitude  $M=3.4$ ) and occurred in 2012. This earthquake initiated a study program of NAM to develop a hazard and risk model to determine the potential effects of the induced earthquakes. To manage the related risks, a probabilistic seismic hazard and risk analysis has been carried out for the area (Winningsplan, technical addendum part III and IV). During the study program, the GMPEs have become more sophisticated and more specific for the Groningen situation. The latest improvement of the GMPE is taking into account actual profiles of shear-wave velocity ( $V_S$ ) at KNMI recording stations. The records of ground motions due to earthquakes are used to calibrate the Groningen specific GMPE using the measured  $V_S$  profiles. This work has been performed in a parallel track and is reported in Bommer et al. (2016). The team that performs the study program for NAM consists of experts from Deltares, Shell, NAM, TNO and several independent consultants (relevant for the  $V_S$  profiles are Julian Bommer, Adrian Rodriguez-Marek and Ben Edwards).

This report describes the results of a field campaign to determine measured  $V_S$  profiles at the locations of 18 KNMI accelerograph stations. The aim of the survey was to provide  $V_S$  profiles down to a minimum depth of 30 metres at these stations and gain detailed (numerical) insight in the lateral representativeness of these profiles. The location of the stations is shown in Figure 1.1, the codes of the stations are included in Table 1.1. Deltares has designed and executed a geophysical survey at these stations in the Groningen region.

An overview of the fieldwork and survey techniques is given chapter 2. The processing and analysis of the field data are described in chapter 3. The results are presented in chapter 4 with one section for each station. The construction of the final  $V_S$  profiles to be used in the GMPE analysis is described in chapter 5, alongside a comparison to the local geological setting. The report ends with a conclusions and recommendations chapter. Abbreviations are provided in Appendix B.

Table 1.1 Codes for the KNMI accelerograph stations

Accelerograph station code	Located in or near the town of	Accelerograph station code	Located in or near the town of
BAPP	Appingedam	BONL	Oosternieland
BFB2	Kolham	BOWW	Oosterwijdwerd
BGAR	Gartshuizen	BSTD	Stedum
BHAR	Harkstede	BUHZ	Uithuizen
BHKS	Garrelswaer	BWIN	Winneweer
BKAN	Kantens	BWIR	Wirdum
BLOP	Loppersum	BWSE	Westeremden
BMD1	Middelstum	BZN1	t Zandt
BMD2	Middelstum	BZN2	Zeerijp

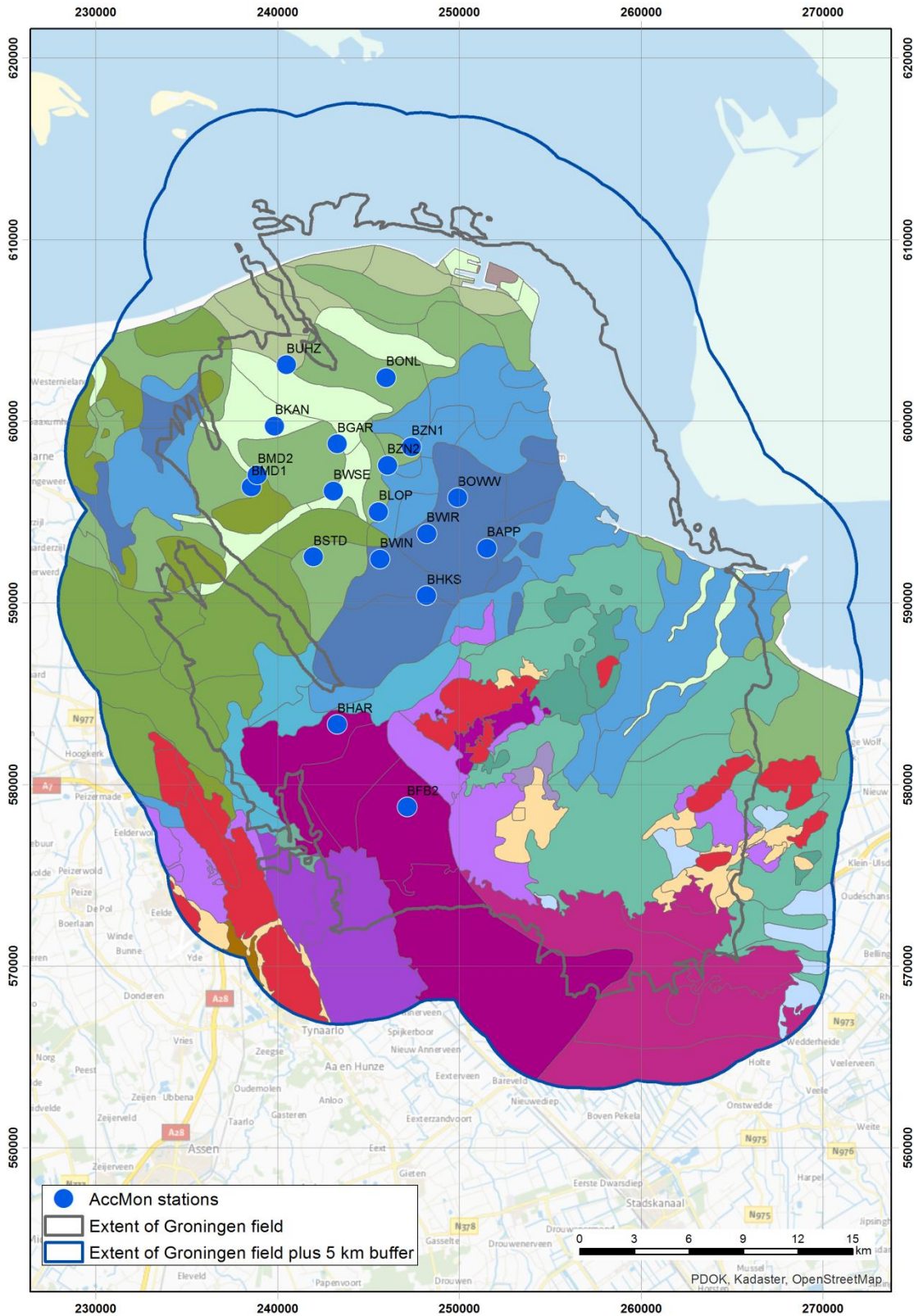


Figure 1.1 Location of accelerograph stations (blue dots) in the Groningen region plotted geological zones (Kruiver et al, 2015 and 2016).

## 2 Fieldwork and survey methods

The  $V_S$  survey has been executed in two phases. In phase one, a series of survey techniques have been tested on three pilot locations (BUHZ, BAPP and BWSE, codes in Table 1.1). The selection of field techniques is described in section 2.1. Operational aspects are included in section 2.2. The field techniques are subsequently described in sections 2.3 to 2.8.

### 2.1 Selection of field techniques

In order to obtain the best results in an efficient way, the fieldwork was set up in two phases. The first phase consisted of applying a wide range of potentially applicable techniques at a selection of the sites. In the second phase, based on the results of this pilot, a number of techniques was selected to be applied at the remaining sites.

The survey setup has been designed to capture relevant horizontal and vertical scales of variability in the subsurface. The selection of potentially applicable techniques is based on the following design criteria:

- Suitability to determination of  $V_S$ ;
- Need to use multiple methods, e.g. for cross validation;
- Need to capture and describe lateral heterogeneity;
- 1D and 2D aspects;
- Logistical aspects (operation impact on surroundings and duration of measurements);
- Vertical resolution and depth of investigation;
- Quality and resolution;
- Time schedule;
- Costs.

Based upon these criteria a team of experts selected a number of most promising techniques for the first phase. This team consisted of experts from Deltares and Shell (Steve Oates, Antonio Di Matteo) from the GMPE team lead by Julian Bommer. The following techniques were selected for the pilot sites in the first phase:

- 1 Cone Penetration test (CPT)
- 2 Seismic Cone Penetration Test (SCPT)
- 3 Offset Seismic Cone Penetration Test (OSCPT)
- 4 Multichannel Analysis of Surface Waves (MASW) with active source
- 5 Passive MASW using ambient noise as source
- 6 Cross-hole tomography, both P-wave and S-wave
- 7 P-S suspension logging
- 8 Borehole logging

A detailed description of these techniques is given in sections 2.3 to 2.8 of this chapter. However, some general considerations of these techniques are described here. Using these different techniques, information at different length and volume scales could be acquired. Because different frequencies of ground shaking are sensitive to different scales of heterogeneity in the subsurface, the methods applied should cover approximately the same range, or be transportable over the different scales. At the smallest scale, the SCPT “samples” only a small volume of soil of approximately 2 metre around the cone. At the other

end of the range, the MASW methods sample an area of approximately 200 metre. The setup used for the OSCPT and cross-hole measurements have intermediate scales. An overview of these scales is shown in Figure 2.1.

The different techniques also have different depth of investigation (DOI) and intrinsic vertical resolution (Table 2.1). The DOI depends on the setup used. For the CPT based methods it depends on the properties of the soil and the maximum cone pressure that can be applied (15 ton), before damage to the instrument occurs. In this project, the maximum achievable depth varies between 20 and 30 metres. For the borehole based methods it merely depends on the depth of the borehole and cable lengths. For this project, the DOI has been fixed to 30 metres. The DOI of the active and passive MASW depends on the local geological setting, survey layout and instrumentation choices. For this project, the DOI for active and passive MASW varies between 15 and 50 metres.

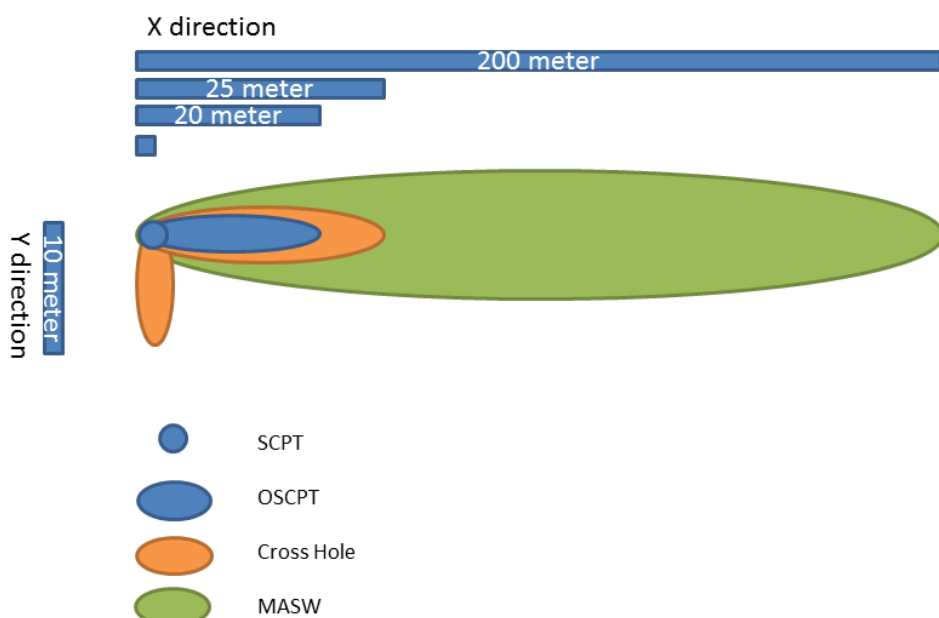


Figure 2.1 Top view (X-Y) schematic presentation of the lateral 'sampling' area of the applied techniques. For corresponding depths (Z), see DOI in Table 2.1.

The vertical resolution of the techniques is highest for the techniques in which the instruments are going into the ground (CPT, Cross-hole, P-S suspension, borehole logging) and less for techniques where instruments are only applied at the surface (MASW). Furthermore, the resolution can be controlled with the CPT and borehole methods, using a denser sampling scheme, but cannot be as well controlled with the MASW methods. The sensitivity of the MASW method to  $V_s$  is very high for the shallow most layers, but decreases rapidly with depth. For the SCPT, the resolution of the shallow layers is difficult. Therefore, MASW and SCPT methods are complementary. For this project, the SCPT typically samples layers up to 0.5 metres in thickness whereas the MASW samples layers on a varying depth scales of metres, i.e. less than 0.5 m to several metres.

After completion of the first phase, a selection of the field techniques has been made based on first results and operations aspects, such as terrain conditions and available time. In the second phase, the selected techniques were SCPT, active and passive MASW and these

have been applied to the remaining 15 locations. During the second phase, still some improvements have been made to the survey approach.

Table 2.1 Overview of the used techniques. Passive MASW DOI was expected to be complementary to the active MASW DOI.

Technique	Fieldwork phase	DOI (m)*	Lateral averaging (m)	Vertical resolution
CPT	1 & 2	20~30	~1	Highest
SCPT	1 & 2	20~30	~2	High, except shallow part
OSCPT	1 & 2	20~30	~20	High, except shallow part
MASW active	1 & 2	15~50	Up to ~200	Medium, decreasing with depth
MASW passive	1 & 2	>30**	~200	Medium, decreasing with depth
Cross-hole tomography	1	30	~25	High
PS suspension	1	30	~1	Highest
Borehole logging	1	30	~1	Highest

\* DOI = Depth of investigation as obtained in the field using current setup.

\*\* In reality shallower than expected.

## 2.2 Operational aspects

The fieldwork has been executed in two phases. During the first phase, all techniques mentioned above were to be evaluated. In the second phase, a subset of techniques was applied on the remaining locations. For the first phase, four representative test sites have been selected based on geological information, such as the classification of the high resolution geological model GeoTOP of the Geological Survey of The Netherlands – TNO (GDN-TNO). However, due to unforeseen difficulties with the obtaining permission to access these sites, three new sites had to be selected for the first phase. After the survey in phase one, the first results have been presented to all parties involved. In a joint session of NAM, Shell, Deltares and external experts it was decided only to apply the first five techniques to the remaining 15 locations.

Due to access and operational issues (e.g. space needed to execute some types of measurements) it was not always possible to execute all measurements in the direct vicinity of the accelerograph station. If that was the case, a SCPT was placed at the site of the accelerograph station and an additional SCPT was positioned on the location of the rest of the measurements. In this way, the data from both locations could be related.

The timing of the two phases of field work was: phase 1 in July 2015 and phase 2 in August and September 2015. Because of the difficulty in getting permits to access the terrain the available time for the fieldwork was very limited. Therefore, pragmatic choices had to be made in the field.

The CPT, SCPT and OSCPT (section 2.3) were executed by Wiertsema en Partners in cooperation with Deltares. For each OSCPT, approximately 2 days of fieldwork were required. During phase 2, Wiertsema en Partners mobilised 2 CPT rigs, and in total 4 seismic cone acquisition sets were deployed simultaneously. During data acquisition, staff from Deltares assisted during the performance of the soundings and performed on-site QC. The simultaneous mobilization of 4 units (2 trucks) and the special design of the OSCPT

(especially considering the holiday season) required optimal flexibility of the team. A certain degree of inefficiency could therefore not be avoided.

The active MASW and the passive data (section 2.4 and 2.5) were acquired by a Deltares field crew. In general, 1 day per location was required to perform the geophysical survey program.

The cross-hole tomography (section 2.6) was executed in cooperation with a subcontractor from Germany, Geotomographie. The required boreholes were provided by Wiertsema and Partners. The measurements took 2 to 3 days per locations. Because of the limited time frame and the delays in the project the German crew had to mobilise 3 times. The cross-hole tomography technique was only applied at the pilot locations. This technique was not selected for the remainder of the stations, because of the logistics of the boreholes required for these measurements (i.e. inconvenience caused by drilling rigs, time needed for drilling, relatively large distance to accelerograph station).

The P-S suspension logging (section 2.7) was executed by Robertson Geologging from the UK. With this technique, two locations were logged over a period of 2 days.

The borehole logging measurements (section 2.8) were executed by Deltares. The 3 sites from phase 1 were logged in 1 day.

## 2.3 Cone penetration testing

### 2.3.1 Introduction

Cone Penetration Testing (CPT) is a method to determine the properties of unconsolidated soils. This method was developed in The Netherlands and is frequently applied for geotechnical evaluation of the subsurface, to determine the geo-engineering properties of soils and to delineate soil stratigraphy. The cone penetration test consists of pushing a cone penetrometer using a series of push rods into the soil at a constant rate of penetration (Figure 2.2). During penetration, measurements of cone resistance and sleeve friction are recorded. The cone size, penetration rate and instruments are standardised. The test results can be used for interpretation of stratification, classification of soil type and evaluation of engineering soil parameters (ISO 22476-1:2012(E)).

The DOI for CPTs is equal to the maximum achievable depth of penetration and depends on the soil properties and the maximum pressure that can be applied by the CPT truck. Typically, a maximum pressure of approximately 15 ton can be applied by the CPT truck, which is sufficient to reach depths of well over 30 metres in unconsolidated sediments. However, when stiff Peelo Clay ("Potklei") is present, the DOI is limited. Based on the sensors and setup used, the measurements performed in Groningen can be divided in three groups; regular CPTs (CPT, section 2.3.2), seismic CPTs (SCPT, section 2.3.3) and offset seismic CPTs (OSCPT, section 2.3.4).

### 2.3.2 Regular CPT (CPT)

The regular CPTs were carried out with a cone equipped with sensors to record the cone resistance, local friction, inclination and the pore water pressure continuously with depth. At each location, a regular CPT was performed to delineate the soil stratigraphy based on the standard CPT profile. Based on this stratigraphy, the optimal depth interval for sampling  $V_S$  with the SCPT was determined.

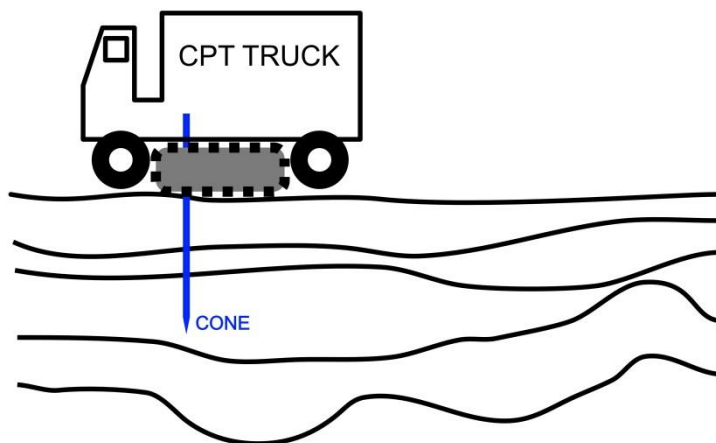


Figure 2.2 Sketch of the CPT setup (not to scale).

### 2.3.3 Seismic CPT (SCPT)

In the seismic CPT setup, the cone is equipped with a vibration sensor that is used to record seismic waves traveling from the surface to the cone at depth. The seismic velocity in the subsurface can be determined with this method. Figure 2.3 shows an overview sketch of the SCPT setup. In order to acquire high quality SCPT data, the following precautions were made once the sensors reach the intended depth: penetration was halted, the hydraulics were decoupled and the engine was turned off. Next, the shear waves were generated by striking a 10 kg sledgehammer on opposite sides of 2.5 m hardwood beams, placed on the surface. To further enhance the data quality the hammer blows at each side of the beam were repeated three times and the resulting records were stacked (averaged).

The shear wave velocity profile is determined from the travel times of the shear waves from source to receiver and the geometries of the setup.

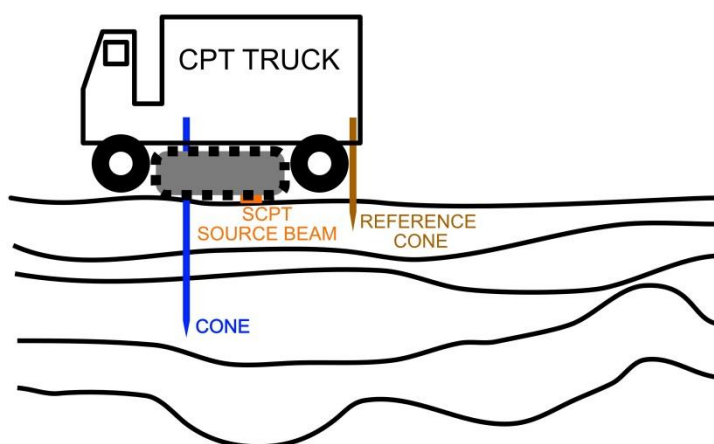


Figure 2.3 Sketch of the SCPT setup (not to scale)

For the SCPT setup the source beam was placed underneath the tracks of the CPT truck and typically at an offset of 1.1 m from the seismic cone. Placing the beam underneath the truck ensured that the beam is well coupled to the ground.

To prevent overestimation and underestimation of the seismic velocity, the measuring intervals used in the SCPTs were carefully chosen based on the preceding CPT. In contrast to a fixed regular sampling setup, this method ensures that the velocities of different layers are not mixed together. Thus, the velocities of peat layers and high density sand layers could be determined more reliably. The velocity boundaries are more accurate and velocity extremes (both low and high) within the velocity profile are better preserved using the optimised sampling interval. This is specifically important in case peat (low-velocity) layers are present. A regular sampling method would overestimate its shear wave velocity, because the thickness of peat layers in Groningen is generally less than 2 m.

A second seismic cone was installed at a fixed depth of 0.5 metre to monitor the quality of signals generated by the hammer blows. The variation of the source signal, due to bad impacts of the hammer and gradual compaction of the soil below the source beam, could be recorded with this sensor and later taken into account in the processing stage.

Both the seismic cones (at depth and at the surface) were manufactured by Geomil. These cones are equipped with a triple axis accelerometer sensor unit. The signals were recorded on a notebook computer using a system made by BCE Engineers. All shear wave signal traces were recorded using a fixed system amplification factor, to enable analysis of trace amplitude degradation with depth. Triggering of the recorder systems was achieved by an electric contact between the hammer head and a striking plate at the ends of the beam. Triggering accuracy was checked by examining the timing consistency of the shear wave arrivals registered by the stationary sensors. A spot check of the triggering accuracy on two locations (Zeerijp, BZN2 and Stedum, BSTD) revealed that the accuracy typically is within 0.1-0.2 ms. The triggering error was corrected for using the stationary sensor of the reference cone.

The recording and processing of the signal traces were performed by Wiertsema and Partners with commercially available dedicated software packages from BCE Consultants.

1210624-000-BGS-0007, Version 2, 27 June 2016, final



Figure 2.4 The SCPT truck with the hammer source on the side, the beam is locked under the tracks guaranteeing sufficient coupling between soil and seismic source.

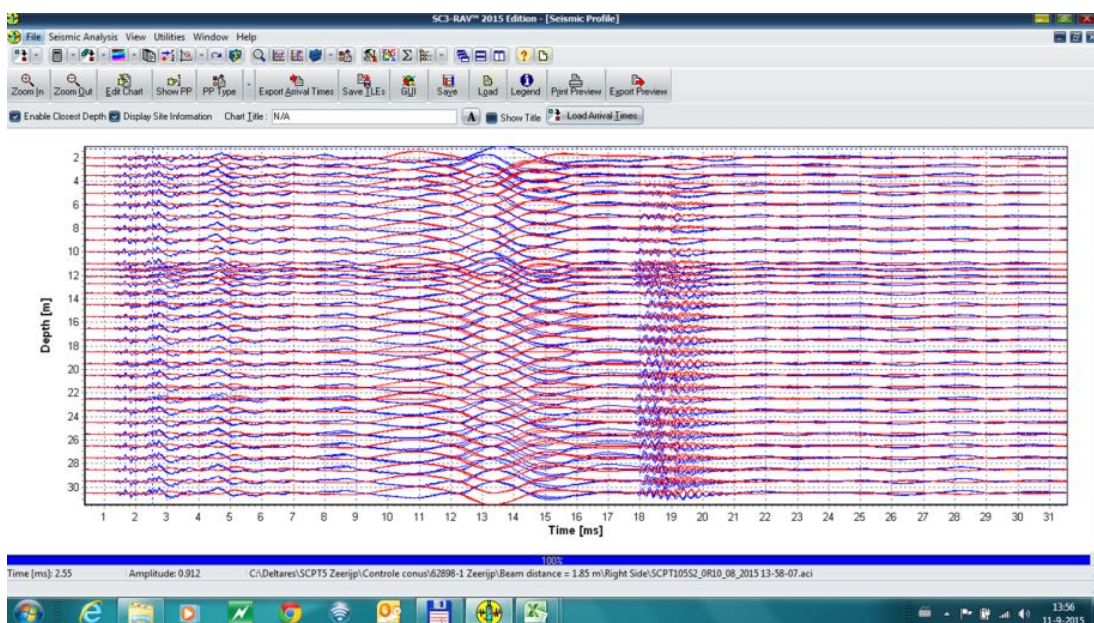


Figure 2.5 Example of raw SCPT data, red and blue represent the impact from left and right.

### 2.3.4 Offset SCPT (OSCPT)

In order to gain more insight in short-spaced lateral variations in  $V_s$ , the SCPT method was expanded by using multiple offsets of the source. These soundings are referred to as offset seismic cone penetration test (OSCPT). Figure 2.6 shows an overview sketch of the OSCPT setup.

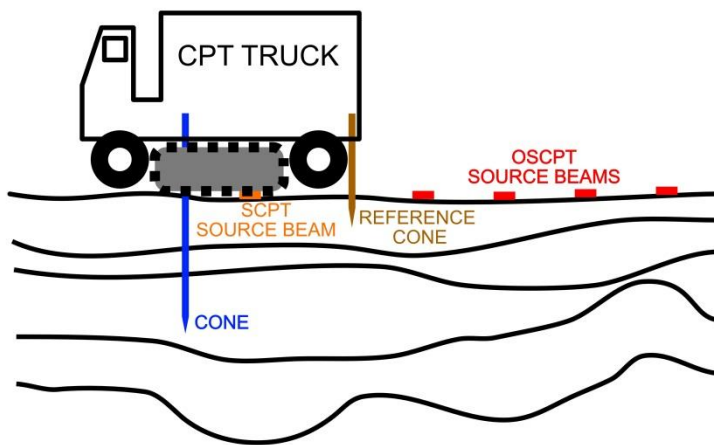


Figure 2.6 Sketch of OSCPT setup (not to scale)

In our OSCPT setup, we used four beams at offsets of 5, 10, 15 and 20 m in addition to the standard SCPT beam at 1.1 m offset (Figure 2.6 and Figure 2.7). These offset beams were ballasted with sand bags. An excavator was available to one of the field crews and was used to improve the coupling of the 20 m offset beam. The other field crew increased the number of hammer blows from three to four each side of the 20 m offset beam to improve the data quality.



Figure 2.7 The field setup for the OSCP acquisition. A standard CPT truck with 4 additional S-wave sources (beams) with on left and right hammers. The beams have been weight down for improved coupling. Later on in the project the coupling of largest offset has been improved by adding even more weight.

## 2.4 Multichannel Analysis of Surface Waves (active)

### 2.4.1 Introduction

Multichannel Analysis of Surface Waves (MASW) is a method to obtain dispersion maps, i.e. information on the frequency dependent velocity of surface waves, from seismic records. Surface waves travel along the interface between air and soil and contain the major part of the induced seismic energy of a surface source. Their behaviour depends on the mechanical properties – density and stiffness – of the upper tens of metres below ground level. By analysing the dispersion maps, the shear wave velocity distribution of the subsurface can be obtained. MASW can be performed on data recorded with an active source, but can also be applied on passive data were only ambient noise is recorded. Both methods were applied in this project. During phase one, two seismic sources were evaluated. An explosive impulse source, called ‘Sissy’, and an accelerated weight drop source, here referred to as ‘impactor’ (Figure 2.8). During evaluation of phase 1, it was decided that the impactor was more suitable for the MASW survey. The impactor provided lower frequency data and has operational advantages.



Figure 2.8 Impactor source behind towing vehicle as used in the field

The maximum depth of  $V_S$  information that can be acquired is determined by the frequency generated by the source; the local geological setting and the fieldwork setup; and measurement instrumentation. MASW is an indirect method, because advanced processing is needed to infer shear wave velocities (inversion, section 3.3.1). However, the advantage of the method is that acquisition of field data is fast. With MASW, both the vertical and the lateral distribution of  $V_S$  can be determined. From this, subsurface heterogeneity and the representativeness of single SCPT (point measurement) can be estimated.

The MASW setup used has been evaluated in the field in the first phase and adapted in the second phase of the survey. Table 2.2 gives an overview of setups for MASW used in both phases.

Table 2.2 Overview of MASW setups in different phases of the project.

	Phase 1	Phase 2
Number of planted geophones	96 x 4.5 Hz 12 x 1 Hz	120 x 4.5 Hz 12 x 1 Hz
Use of streamers	Tried, found not feasible in most cases	No
Source	<ul style="list-style-type: none"> <li>• Impactor</li> <li>• Sissy at BAPP and BUHZ as well, found not to be beneficial for the MASW survey.</li> </ul>	Impactor only
Passive recordings	BAPP: 120x 16s at 1ms sampling BUHZ: 70x 32s at 2ms sampling BWSE: 70x 32s at 2ms sampling	~80 x 32s at 2ms sampling

## 2.4.2 Phase 1

At the three pilot sites, the active MASW survey was executed using two different methods. For the first method, a 72 channel land streamer equipped with 10 Hz vertical geophones spaced 1 metre apart was deployed (Figure 2.9). This streamer has been repositioned 3 times per locations with a lateral shift of 72 metres. Shots (i.e., weight striking on a steel plate) were positioned at 11 locations at each position of the streamer. With this a setup a virtual streamer line of 216 geophones could be made for each shot position. At least 3 shots per location were made for stacking purposes to improve signal to noise ratio. At some locations, a pre shot was given to compact the - often muddy - soil before recording started. This was done to avoid abrupt changes in the source signal.

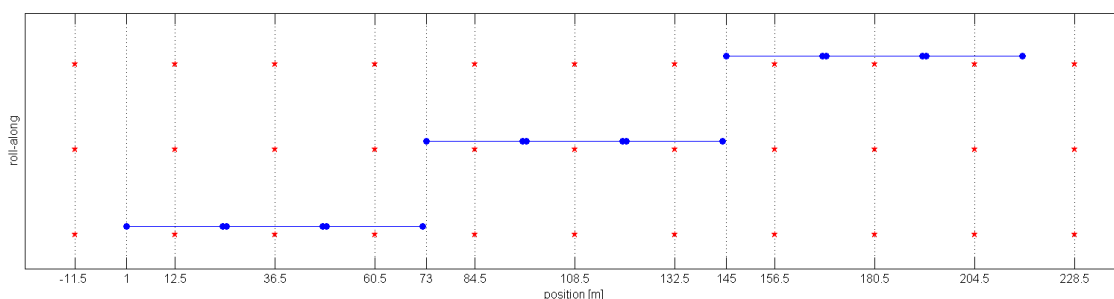


Figure 2.9 MASW land streamer setup for phase 1. In blue, the position of the land streamer and in red the shot locations. For presentation purpose, the positions are shown with a lateral offset, but in the field these were positioned along a single survey line.

The second method consisted of a fixed array using planted 4.5 Hz vertical geophones, combined with a group of twelve 1Hz vertical geophones (Figure 2.10). The spacing between the 4.5 Hz geophones was 3 metres, the 1Hz geophones were placed at 4 metre spacing. In total, 108 geophones have been used in a “T” shaped array, with a “long” and a “short” line.

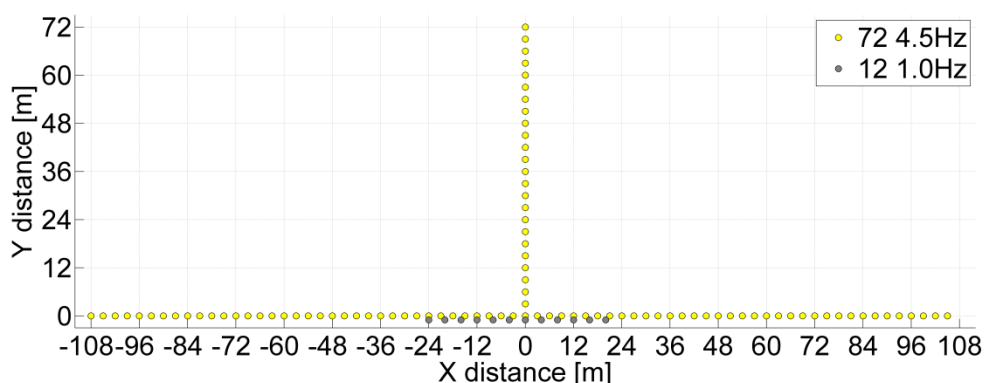


Figure 2.10 Design of the planted geophone array for MASW during phase 1. The “long” line is in the X direction and measures ~ 200 m. The “short” line is perpendicular to the long line and measures ~ 70 m. The “1 Hz” line spans a distance of ~45 m.

The same shot positions as with the land streamer array were used, but also shots at both sides of the perpendicular array were added. At BAPP and BUHZ not only the impactor source was used, but also the Sissy impulse source. This was done to verify if the frequency content and amplitude range of the impactor could be complemented by the Sissy source. Although it was found that the Sissy source produced slightly wider frequency spectrum

(more high frequencies), the difference was not significant enough for the extra effort of operating two sources. Therefore it was decided only to continue with the impactor.

### 2.4.3 Phase 2

During phase 2, the land streamer measurements were abandoned (Table 2.2). In general, the land streamer setup works well on sealed surfaces and grass land. However, due to the windy conditions and the general roughness of the terrain the contact between the land streamer and the surface was not optimal. This resulted in a worse signal-to-noise ratio than the planted array. Generally, deploying and using a streamer array is less cumbersome than a planted array. However, the operational advantage of the streamer over a planted array was limited in this case, because the planted array needed to be deployed anyway for the passive measurements.

For phase 2, some adjustments were made to the planted array (Figure 2.11). The spacing between the geophones on the main survey line was reduced to 2 metre. The perpendicular (“T”) array had a geophone spacing of 4 metres, as did the 1 Hz geophones. The latter were positioned in the middle of the array. In total, 18 shot locations have been used. Shots were positioned at either end of the receiver lines. The data acquired from these different shots allow for comparison of dispersion maps and subsequent selection of the best quality data. The shots in between the receivers along the “long” line were performed for the CMPcc analysis.

Stacking at each shot location was at least 4 times, and when the soil was soft a pre shot was given to improve ground coupling of the impactor.

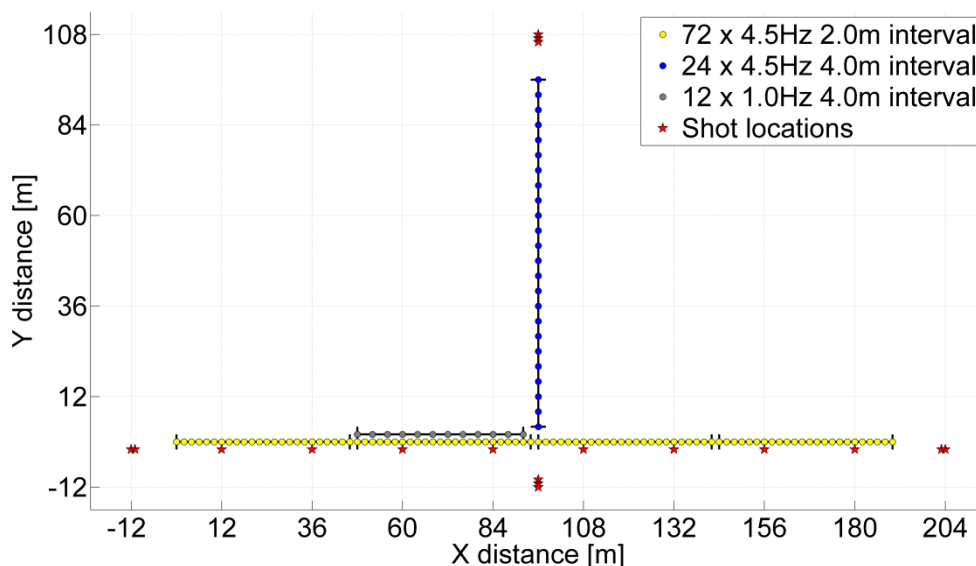


Figure 2.11 Design of the planted geophone array for MASW during phase 2. The “long” line is in the X direction and measures ~ 190 m. The “short” line is perpendicular to the long line and measures ~ 90 m. The “1 Hz” line spans a distance of ~45 m.

## 2.5 Passive MASW

For the passive measurements, the ‘planted geophone’ arrays were used. The main aim of performing the passive recording was to extend the DOI of the active MASW soundings (Table 2.1). However, the DOI depends on local soil and noise conditions. With passive seismics, the seismic waves are not generated by an active source, but ‘natural’ noise acts as

the seismic source. This noise can either be continuous, i.e. waves breaking on the shoreline or movement of trees by wind, or more event-driven, i.e. passing of cars and trucks. Passive MASW data is generally acquired by many seismic records over a long time period (e.g. 1 hour) and stacking the data. Commonly, passive MASW data set contain lower frequencies (i.e. larger wavelength) than the active MASW dataset. Because of the lower frequency data, a larger DOI can be achieved.

When acquiring passive seismic data, the exact origin and position of the seismic source energy is unknown. However, the direction of the source signal is important in order to determine the true velocities of the seismic waves and the true dispersion. A wave traveling parallel to the main survey line (as done with the active MASW) will yield correct values, but a source location perpendicular could theoretically yield almost infinite seismic velocities since all waves appear to arrive at the same time. Therefore, knowing the main source location of the source signal is important for determining true velocities. A complicating factor is that source locations ('events') can be everywhere and also vary over time. The potential effects of events can be limited by recording over a long period. A "T"-shaped array has been used in order to enable determining the direction of the seismic source (Figure 2.10 and Figure 2.11).

Twelve 1Hz geophones have been included in the array to determine whether the 4.5 Hz geophones have sufficient resolution at the low end of the frequency range (Figure 2.12).

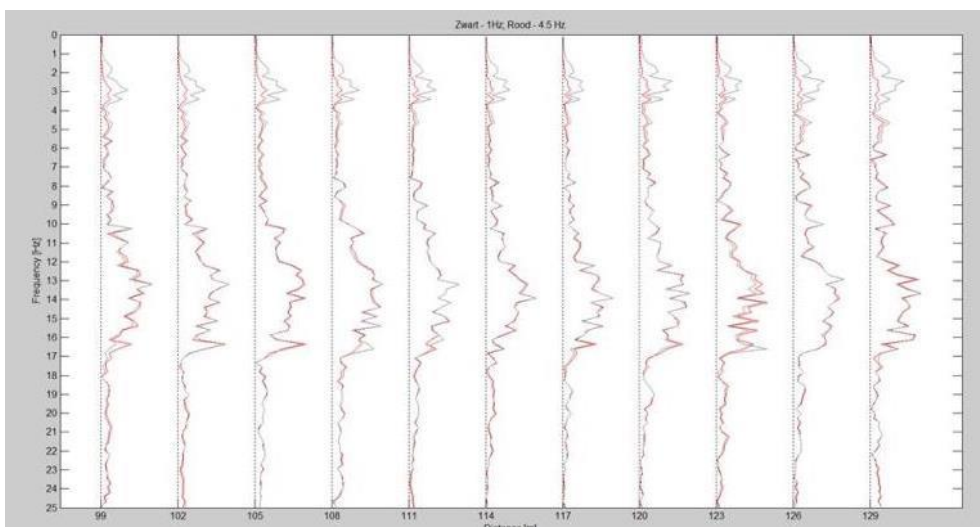


Figure 2.12 Comparison of 1Hz geophones (black) with 4.5 Hz geophones (red), in the range from 0 to 25 Hz. Especially below 4 Hz the differences become significant.

## 2.6 Cross-hole Tomography

P- and S-Wave tomographic measurements were executed on the three locations of phase 1 (BUHZ, BAPP and BWSE). Seismic tomography is a geophysical method used to delineate structures between boreholes and map spatial changes in soil properties. Seismic waves are generated by an impulsive source in one borehole. The propagation of the seismic waves is influenced by the varying soil properties between the boreholes leading to slow or fast wave arrivals at the receivers in the second borehole. The boreholes were positioned in an "L" shape, with the source in the corner of the L (Figure 2.13). There is a short distance between two boreholes in the "short leg" and a longer distance between the two boreholes in the "long leg". This geometry is chosen to generate tomographic images at 2 different scales. The

spacing between boreholes was ~10 metres in the short leg of the L, whereas the spacing was ~25-26 m in the long leg of the L and at an angle of ~90°.

The boreholes were drilled using the sonic drilling technique (provided by Bolten Drilling). The boreholes were finished using a blind liner. The annulus between liner and formation was grouted.

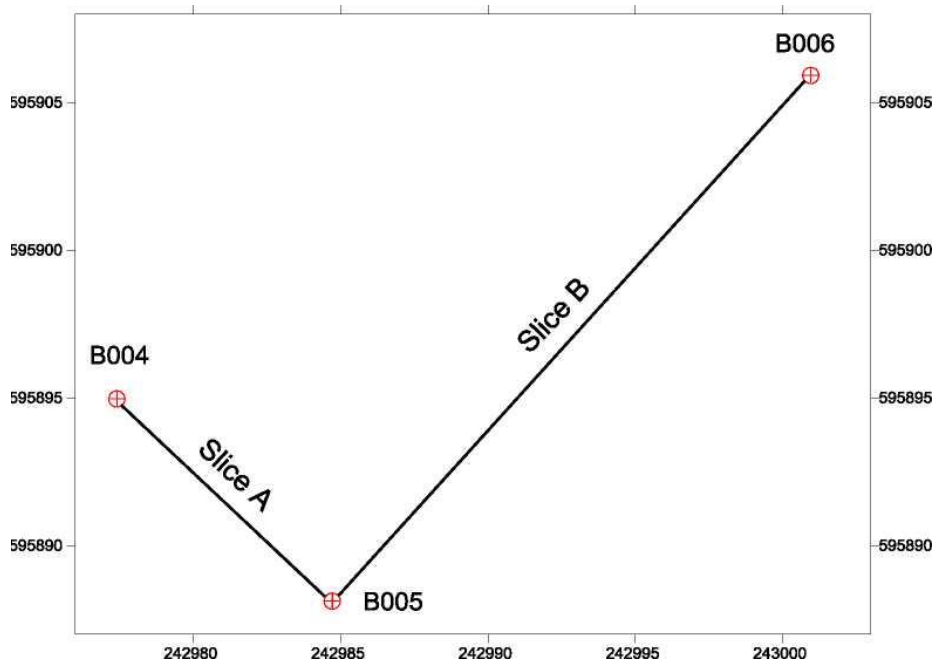


Figure 2.13 Top view of layout of boreholes used for the tomographic survey, slice A and B represent the position of the resulting tomographic panels.

## 2.6.1 P-Wave tomography

Hydrophones were connected in a vertical multichannel string with 24 or more sensors to receive the seismic signals in the second borehole. Once sufficient signal data quality was achieved, the seismic source was moved to the next position in the first borehole and shots were repeated. As a result, ray paths from one borehole to the other build up a very dense and detailed ray coverage.

Because of the good transmission properties of the soil, it was decided to use the same source for both the P- and S-wave tomographic measurements (Figure 2.14). Therefore, the SH-wave source type BIS-SH source (Figure 2.15) was used for both P- and S-wave measurements, as the BIS-SH generates both horizontally polarised shear waves (SH) and compressional waves (P) with a high repeatability. The borehole source is coupled to the borehole wall by a pneumatic clamping system (inflatable bladder). The orientation of the source is controlled from the surface by a torsional stiff hose.

The seismic blow direction was aligned towards the receiver borehole in order to generate P-waves with the highest amplitude. For the P-wave tomography measurements, one record was recorded for each depth interval. A hydrophone array type BHC2 with 24 channels at 1 m spacing was used to receive the signals (Western Atlas 2512). A specialised 24 channel compact seismograph was used for data acquisition.

The equipment used to measure the P-wave arrival times consists of an electric surge generator, a remote control unit and a down-hole probe. Triggering of the seismic acquisition system is performed by the remote control unit. The remote control unit converts the reference signal of the surge generator into a trigger signal.

More detailed field-acquisition descriptions are provided in Appendix H.



Figure 2.14 P-wave tomography equipment with 5 kV HV unit (upper left), downhole probe BIS-SH (upper middle), remote control unit (upper right) and hydrophone (lower middle)

## 2.6.2 S-wave tomography

S-wave tomography is a direct way to measure shear wave velocity. It can be used to infer soil stiffness if the soil density is known. Another advantage of the S-wave tomography is that shear wave velocities are not influenced by the groundwater table.

The generation of the S-wave requires a source which is able to generate SH or SV waves in opposite directions. In order to generate S-waves the SH-wave source type BIS-SH was used (Figure 2.15). The borehole source BIS-SH generates horizontally polarised shear waves (SH) and compressional waves (P). The seismic signals are highly repeatable. This source works in dry or water filled boreholes. The borehole source is coupled to the borehole wall by a pneumatic clamping system (inflatable bladder). The orientation of the source is controlled from surface by a torsional stiff hose. The seismic blow direction was aligned perpendicular to the receiver borehole in order to generate SH-waves. To get the opposite blow direction the source was rotated by 180° and thus generating S-waves with opposite polarities. For each shot direction a separate seismic record was acquired and stored.

The seismic signals were received using the Multi-Station Borehole Acquisition System (MBAS) receiver unit. The MBAS is a digital three-component (X, Y, and Z direction) geophone string used to receive P- and S-waves in dry or water filled boreholes. Up to ten

individual stations with tri-axial sensors can be connected.

The MBAS stations are aligned to ensure that all horizontal sensors are oriented in the same direction. The system can be oriented from the surface by a torsional stiff hose. Each station is clamped to the borehole wall by two pneumatic cylinders. An external trigger can be plugged into the USB interface on a laptop at the surface. The operation is entirely controlled by the acquisition software. A separate seismograph is not required.

An MBAS unit with seven 3C units at 1m station interval was used. The MBAS unit was aligned with their X-sensor direction parallel to the source blow direction. Thus, these sensors should give the best seismic signal when evaluating the horizontally polarised shear wave. The MBAS was pneumatically clamped to the borehole wall. The S-wave source was moved in the other borehole in 1m intervals.

More detailed field-acquisition descriptions are provided in Appendix H.



Figure 2.15 SH-wave equipment with 5 kV HV unit (upper left), down-hole probe BIS-SH (upper middle), remote control unit (upper right) and MBAS receiver (lower middle)

## 2.7 P-S suspension logging

P-S suspension logging was performed by Robertson Geologging from the UK. The Digital P-S suspension probe is a low-frequency acoustic probe designed to measure compressional and shear-wave velocities in soils and soft-rock formations. The probe contains a powerful hammer source and two receivers, separated by acoustic damping tubes. The probe is lowered in a water filled borehole. To acquire data, the probe is stopped at the required depth and the source is fired. Firing causes a pressure doublet in the surrounding fluid. The

resultant fluid motion produces a tube wave at the borehole wall with velocity close to the shear velocity of the formation together with a compressional wave. The motions are detected by two 3D hydrophone receivers, allowing the wave velocity to be directly measured.

## 2.8 Borehole logging

### 2.8.1 Natural Gamma Ray

The Natural Gamma Ray radiation was recorded by Deltares with Century or Antares tools. These recordings can be used to determine the lithology and accurately determine the vertical transitions between layers. However, not all types of lithologies can be distinguished using the gamma ray signal alone. For example, coarse sand and peat can yield the same gamma reading. Combining the gamma recordings with other borehole parameter, it becomes possible to distinguish between layers of these different lithologies.

For the Groningen region, threshold values for lithologies are presented in Table 2.3.

Table 2.3 Natural gamma ray values (in counts per second, cps) translated to lithology.

Gamma radiation (cps)	Lithology
< 15	Medium to coarse sand, peat
15 - 40	Fine sand
> 40	Clay

### 2.8.2 Electromagnetic induction (EM)

The electromagnetic induction tool is manufactured by Century Geophysical Corporation, USA. The tool uses an electromagnetic field from that induces an electrical current in the surrounding formation. A secondary magnetic field is created by the induced current, and is measured, amplified and then transmitted to the surface as a direct current. The magnitude of the direct current is proportional to the electrical conductivity of the formations, which is a function of lithology and pore-fluid conductivity (Metzger and Izbicki, 2012).

### 2.8.3 Deviation

The deviation of the boreholes was inferred from the slant angle and azimuth measurements. The measurements are corrected for the local magnetic declination estimated value (<http://www.ngdc.noaa.gov/geomag-web/>). With these measurements, it is possible to determine the real position of each measured point in the lateral and the vertical direction.

### 2.8.4 Magnetic susceptibility

The magnetic Susceptibility tool is manufactured by Century Geophysical Corporation, USA. The tool has a length of 241 cm and a mass of 18 kg. The tool is used to measure the deviation of the borehole with X-Y Inclinerometers and an Azimuth metre.

### 2.8.5 Well logging operation

The well logging took place after the standard casing of the well was installed. The optimum operating speeds are 2 m/min for the sonic tool, 6 m/min for the electromagnetic induction and the magnetic susceptibility tool.



## 3 Processing and analysis

The data have been processed and analysed by both standard techniques (e.g. SCPT, MASW) and tailor made interpretation methods, such as tomography of offset SCPT (section 3.2) and CMPcc analysis of MASW data (section 3.3.2). The sections in this chapter describe the processing and analysis steps for each of the techniques.

### 3.1 Seismic Cone penetration testing (SCPT)

The SCPT data were analysed using BCE SC3-RAV 2015 seismic data analysis software (Version 15.0.1-june 2015) by Deltares and Wiertsema and Partners. This software allows semi-automatic interval time picking using cross correlation of the wave trains of subsequent test depths. The algorithm uses a simple ray tracing principle based on a horizontal stratigraphy model to determine the travel path length to calculate the interval shear wave velocities. The processing consists of the following steps: file gathering, first arrival picking, left and right picking and classification.

#### File gathering

For each location, data files are grouped based on the source offset and the polarization of the source (shear wave left or right blow, section 2.3.3). Header information on location and polarization was manually checked and occasionally corrected. This grouping was useful in order to keep an overview of the amount of data files.

#### First arrival picking

Data were analysed automatically by the software using cross-correlation to pick first arrivals on the SCPT records. Automatic analysis minimises human bias associated with visually selecting. However, if the data quality is poor, cross-correlation can give an unreliable outcome. In these cases, automatic interval time picking was not possible and the first arrivals were picked manually.

#### Left and right picking

On each SCPT location, shear wave data were generated on both left and right side of the truck. In theory, the travel times from both sides should be the same. Therefore, an extra quality control is to compare the travel times from the left and the right blow.

In most cases, the results compare well. However, at some locations the travel time determined using the cross-correlation method for the left blow was slightly different from the right blow. For some datasets, this could be solved by improved (re)picking of the first arrivals (manually), but still some 'left' and 'right' datasets remained that did not show comparable travel times. A probable cause for this discrepancy is the position of the offset source: possibly the beam was not placed exactly in the middle relative to the CPT cone with geophones.

The interval velocities were determined using the so-called Forward Modelling/Downhill Simplex Method (FMDSM) (Baziw, 2002). The resulting shear wave velocity profiles obtained by SCPT are presented in Chapter 4 for each location.

## Classification

The cone penetration test data are used to determine the lithology of the encountered layers using a modified nomogram as developed by Douglas and Olsen (1981). An interactive nomogram allows the adjustment of the position of lines dividing zones of equal lithology (e.g. Figure 3.1). The classification can be easily modified to fit the local “penetrometer stratigraphy”. The derived lithological columns are included in the SCPT-shear wave velocity plots (Section 4.X.3, in which X are the locations). The legend for the lithologies is given in Table 3.1.

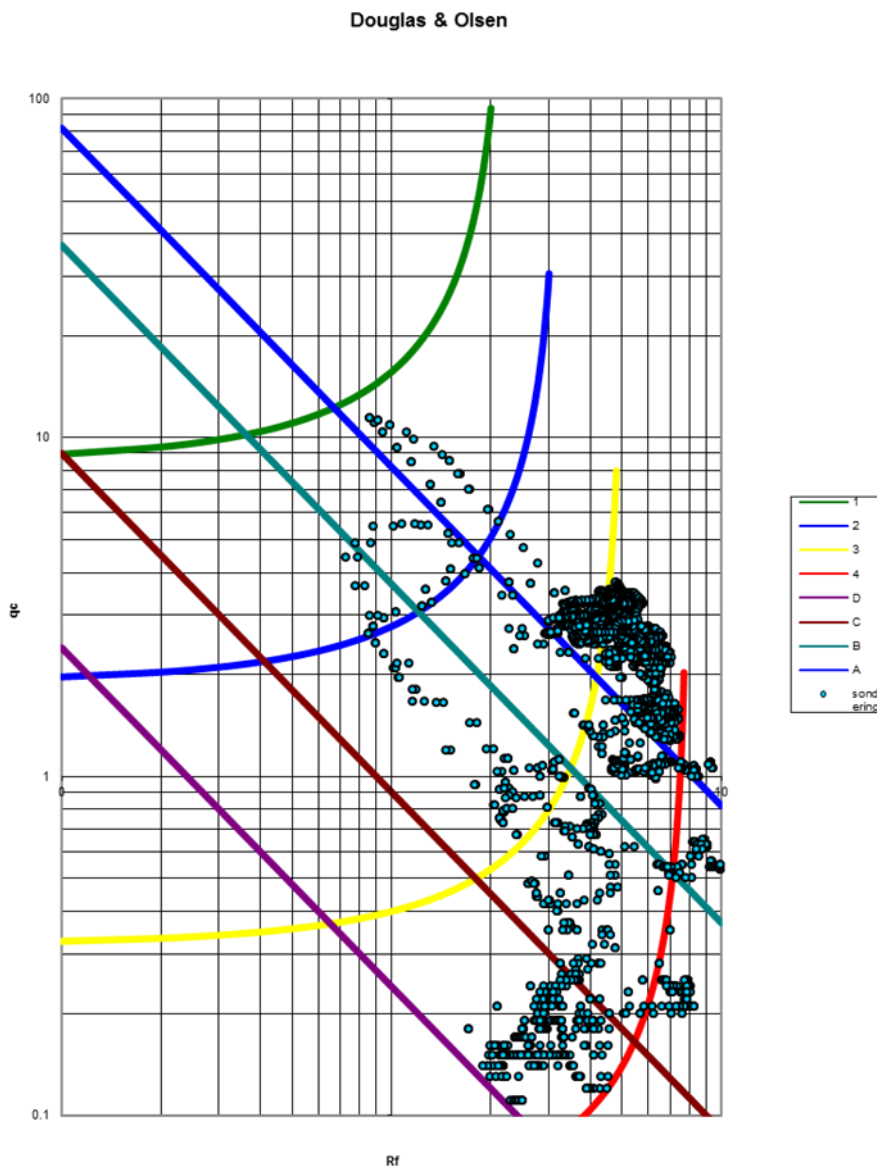
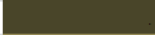


Figure 3.1 Nomogram based on Douglas & Olsen (1981), as used for the interpretation of the CPT data.

Table 3.1 Legend for lithological classification of CPT

very dense F-C Sand	
dense F Sand-moderately dense C Sand	
dense M-C Sand	
loose F Sand - moderately dense M Sand	
very stiff Clay/Silt	
sandy Clay/clayey Sand	
very stiff Clay	
stiff (organic) Clay	
soft-firm (organic) Clay	
very dense Peat	
Peat	

### 3.2 Offset SCPT (OSCPT)

Additionally to the standard SCPT acquisition, the SCPT data were acquired with different offsets of the source (section 2.3.4). In a first step, data were processed using the method described in the section 3.1. Specifically for OSCPT analysis, several processing steps were added in order to provide tomographic images of  $V_s$ . The additional steps are related to quality control and the construction of tomographic images. The steps are described this section.

#### Quality control

The consistency of all individual blows at the offset sources was checked for each location. Due to the lower signal-to-noise ratio of the offset beam records, the arrival times had to be picked manually. Differences in arrival times between left and right blows were calculated. This analysis showed that differences of up to 6 ms occurred at the field survey. The differences can be attributed to imperfect coupling between the beam and the ground. The difference was smallest for the 20 m offset, where the coupling was better due the additional excavator weight to the ballast of the sand bags.

#### Construction of tomographic images

The model subsurface was discretised using a grid of nodes, with a node distance of 0.5 m. For each of the nodes, the optimum  $V_s$  was determined by minimising the misfit between the modelled travel times and the measured travel times. The 'fast marching method' (Sethian, 1999) was used to calculate the modelled travel times of seismic waves from source to receivers. For the optimisation, the Fresnel ray-path approach (Watanabe et al., 1999) was used. The misfit is represented by the root-mean-square (RMS) of the differences between the model and the measured travel times. For each OSCPT plot, the RMS value is shown. In general, RMS values of <10% represent good quality. Profiles with RMS values > 10% should be used with care as they exhibit a higher degree of uncertainty.

An example of a tomographic image of  $V_s$  from OSCPT is given in Figure 4.7, showing  $V_s$  information in the top left corner. The right lower corner is not illuminated by the rays, because of the geometry of the sources and receiver locations. Therefore, the tomographic images of  $V_s$  are presented in the shape of a triangle.

### 3.3 Multichannel Analysis of Surface Waves

#### 3.3.1 Workflow and processing methodology

The workflow for the processing of MASW data consisted of the following steps:

- 1 Quality control and creation of the 'meta table'. This table includes the coordinates of shots and receivers and information about bad shot records and traces, or traces with a wrong reversed polarity.

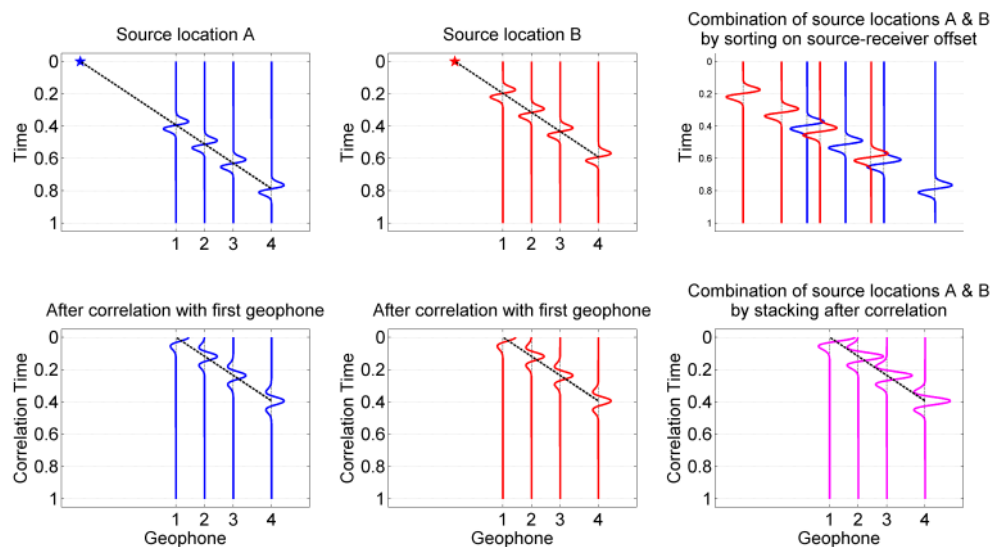


Figure 3.2 Basic procedures for combining individual shots in step 2. Top row: combining different shots to increase the number of offset in active MASW (step 2a). Bottom row: combining the same shots relative to the first geophone position for CMPcc (step 2b) and passive MASW (step 2c). In a simplistic way, the method in the top row shifts the records left-right to obtain the results, while the method in the bottom row shifts the records up-down to obtain the result.

- 2 Processing:
  - a. "Regular" MASW: For each line (long line, short line and 1 Hz line, Figure 2.11) the shots are selected that are in line with the corresponding receiver array. The shots at both ends of the lines were analysed separately. The different shot offsets were combined in a virtual record that has a denser sampling than the actual array to increase the resolution of the dispersion map (step 3). This method is visualised in the top part of Figure 3.2. For example, combining the two shots separated by 1 metre with the long array (96 traces separated by 2 metre) results in a virtual record of 192 traces separated by 1 metre. The virtual records of each line are further processed as described in step 3.
  - b. "Active Common Mid Point cross-correlation MASW" (CMPcc): For the "long" line (Figure 2.10 and Figure 2.11), cross-correlations are calculated for every pair of traces. The long line with 96 traces thus forms a correlation record of  $(96 \cdot 95) / 2 = 4560$  traces. Each of these correlation traces has an associated mid-point and offset, being the mid-point of, and the distance between, the traces forming the correlation pair. All correlation pairs with the same mid-point form a virtual record. The two sets of virtual records (one with "left-to-right" traveling waves and one with "right-to-left"

traveling waves) were combined into 72 virtual records along the array (Figure 3.3). These virtual records were further processed as described in step 3.



Figure 3.3 Schematic representation of CMPcc sampling, blue dots are geophones and red lined are groups of 24 channels used for each individual CMPcc. By virtually shifting the array (i.e. selecting a different group of geophones and source signals) a different section of the survey line is sampled.

- c. "Passive CMPcc Beam" MASW: The processing is similar to the Active CMPcc, with the exception that no active source was used. Instead, ~ 80 records of 30 seconds length were used to record ambient waves traveling by. In this case, the correlation uses the full 2D shape of the array, combining traces from the long and short cross line. In this way, the azimuth of the waves traveling by is determined. The apparent distance between the 1 Hz geophones is determined using the known azimuth. Next, the "CMPcc" stack of the 1 Hz geophones together with their apparent distances can be further processes as described in step 3.
- 3 Creation of the dispersion map. A dispersion map is an image showing the energy distribution as a function of frequency and velocity as measured in the field. The time domain records are first transformed to the frequency domain. Next, for each frequency the records are shifted in "time" by their offset divided by a set of predefined velocities. For every velocity, the different offsets are stacked and produce an amplitude density pixel. Repeating this for all velocities and frequencies, a map can be constructed showing the energy distribution as a function of frequency and velocity. Dispersion maps often show aligned energy curves. These are also known as dispersion curves. Dispersion maps were made for all virtual records described in step 2. The best dispersion maps for active MASW and active CMPcc, i.e. containing the widest frequency range and sharpest defined energy, were selected for inversion (step 4).
  - 4 Determining the best  $V_S$  layer model. The dispersion maps are inverted to find the best  $V_S$  model. An inversion algorithm searches the model space to find the  $V_S$  profile, which dispersion curve is as close as possible to the measured dispersion map. The most likely  $V_S$  model was determined with in-house software in two different ways:
    - a. Manual optimization. In this project,  $V_S$  information from the SCPT and borehole measurements was available. This information was used as a starting model for manual optimization. The emphasis was on obtaining a  $V_S$  model that fitted all modes and the particular shapes of the modes, such as curvatures at certain frequencies.
    - b. Automatic genetic algorithm. This algorithm automatically generated numerous  $V_S$  model realizations, each associated with a modelled dispersion curve. The best model from the manual optimization was used to define the search space of the automatic algorithm. The energy of the dispersion map along the modelled dispersion curve is a measure of the goodness of fit. This is used by the algorithm to combine good models to generate new models. After a number of iterations, this process

converges to a group of likely models. The best  $V_S$  model is chosen from this group based on its goodness of fit.

### 3.3.2 Interpretation of CMPcc

The CMPcc analysis for the active MASW yields 72 individual dispersion maps (Figure 3.3, section 3.3.1), spanning the centre ~ 100 m of the long line. These 72 dispersion maps can be regarded as a moving average along the array. Each of the dispersion maps was inverted to a  $V_S$  model. The 1D  $V_S$  models are plotted next to each other as a profile to visualise the CMPcc results. These profiles can be used to visualise the lateral and vertical  $V_S$  variation and yield information on the maximum and minimum velocities present within this area. In the synthesis of all data, the 72 individual CMPcc  $V_S$  profiles are averaged to one overall profile. Due to all averaging involved this final profile shows no discrete steps and changes very smoothly with depth.

## 3.4 Passive Seismic

The processing of the passive data set is to a large extent similar to the process described in paragraph 3.3.1. However, this initial processing did not yield any information in the dispersion map additional to the active MASW dispersion map. Experts from Shell and Utrecht University confirmed this after analysis of one of the data sets.

We do observe, however, that the 1 Hz geophone recordings contain lower frequency data than the 4.5 Hz geophones. The layout of the 1Hz array is not suitable to determine dispersion maps due to the limited number of geophones and the linear layout (no directionality). Additionally, the passive data can be improved by increasing the recording duration in the field.

We therefore recommend the following to improve the passive MASW acquisition for future fieldwork:

- Different layout of 1 Hz geophones (more geophones and directional sensitivity).
- Longer duration of measurement.

## 3.5 Cross-hole Tomography

### P-wave tomography

During seismic data processing, first arrival travel times of the waves related to the P-waves are picked for each source-hydrophone pair. Using an iterative numerical inversion procedure, a seismic velocity distribution between the two boreholes was calculated based on the travel times and the known source and hydrophone locations.

### S-wave tomography

Data processing requires different steps compared to P-wave tomography, as typically the number of receivers is limited and identification of the S-wave requires the overlap of the opposite shot directions. After arrival travel times of the S-waves, the iterative numerical inversion procedure determines the seismic velocity distribution between the two boreholes.

More details on the acquisition and processing of the cross-hole tomographic data set are provided in appendix H. Deltares has performed QC on this data set and for one location the data has been reprocessed to review the method. The results were very similar proving the high quality of this data set. It should be noted that when interpreting the resulting P and S-wave models that the smaller anomalies should be interpreted with care. There are

alternative solutions possible for these anomalies. Considering the data quality the representativeness of the data set is high.

### 3.6 P-S suspension logging

The P-S suspension logging data have been acquired and processed by Robertson Geologging from the UK. The data quality was average to poor, due to the combination of the borehole construction, grouting and the local geological setting. For now, this dataset has not been analysed.

### 3.7 Borehole logging

The lithology was inferred from the gamma ray data alone, based on threshold values from Table 2.3. Three lithological units are distinguished, i.e. medium coarse sand, fine sand and clay. Peat was not distinguished as a lithological unit, as the gamma radiation of peat is generally low and will often be classified as coarse sand. The classification is based on expertise from other projects in the region. The lithological interpretations are presented with the well logs and the measured electromagnetic induction in Appendix C.

### 3.8 $V_{S30}$

Generally, the parameter  $V_{S30}$  is regarded as a measure of strength of the soil. The  $V_{S30}$  is the time-averaged  $V_S$  in the first 30 m below the surface:

$$V_{S30} = \frac{30}{\sum V_S} \quad \text{Eq. 3.1}$$

where  $V_S$  the shear wave velocity of the layer with thickness  $\Delta x$ .

Additionally, the  $V_{S30}$  is used as one of the inputs in the seismic hazard and risk analysis for Groningen and therefore part of the GMPE (Bommer et al., 2016). For the Groningen  $V_{S30}$  map, the SCPT database, consisting of older SCPTs and the SCPTs measured in this project, were used to derive Groningen specific  $V_S$  distributions as a function of stratigraphy, lithology and depth. These  $V_S$  distributions were applied to the GeoTOP model of TNO-GSN and the geological zonation (Kruiver et al., 2015, 2016a) to obtain a  $V_{S30}$  map (Kruiver et al, 2016b).

In section 5.4, the measured  $V_{S30}$  are compared to the GMPE V3  $V_{S30}$  map. In those cases where the measured  $V_S$  profile did not reach the full 30 m, the profile was extended using the modelled  $V_S$  from GMPE V3 to fill the gap (Kruiver et al, 2016b).



## 4 Results

### 4.1 Reading Guide

This chapter presents the results for all 18 locations and all 6 techniques. Each location is explained in a separate sub-section (4.2 to 4.19). This sub-section (4.1) serves as a reading guide, i.e., it explains the template that is followed for description of results for each location.

#### 4.1.1 Location

This section shows a map of the location that includes:

- Location and coordinates of the accelerographs (in RD and WGS84 coordinates). In some cases, the exact coordinates of the accelerograph was not clear: the coordinate list of NAM and of KNMI had different coordinates. In those cases, all possible coordinates are shown.
- Shot points and survey lines of the MASW survey.
- Location of SCPT (one or two).
- Geological zonation from the GMPE V2 (Kruiver et al. 2015). This information was used to obtain a first insight in the local geological setting that is to be expected at the station location. In some cases, the accelerograph is situated close to the boundary of the geological zones. These boundaries, however, are no exact lines. In those cases, the local geological setting at the station is less certain, based on the geological zonation. Other sources, such as the CPTs will give more information on the actual geological setting at the station.

#### 4.1.2 Geological setting

A short geological description is provided for each location. This is based on the 1D “apple corer” section through the DGM model (GDN-TNO), a section from the Delfstoffen online model (GDN-TNO) and a selection of borehole descriptions of deep borings near the site. These are presented in two figures and one table. Dutch geological nomenclature and corresponding colours in the DGM and GeoTOP geological models is summarised in Table 4.1. The apple corer shows the modelled geology at the site on formation level. The Delfstoffen online section shows the volume percentage of the lithologies (peat, clay and sand) versus depth.

Additionally, two descriptions are given:

- (1) The character of the Holocene deposits and the transition to the Pleistocene formations.
- (2) The position of the station with respect to the presence of ‘Peelo Valleys’, which are deep incised valleys. The channel infill has and can have different stiffness than the surrounding subsurface because of the possible presence of stiff Peelo clay (“Pot Klei”).

Next, three maps are presented, which show from top to bottom the thickness of the Holocene peat, the thickness of the Peelo Formation and the top of the Pleistocene surface. The survey lines, SCPT, accelerograph station locations and geological zonation are presented on these maps as well. These maps serve to illustrate of heterogeneity can be expected (at different scales).

Table 4.1 Abbreviations and colour scheme in geological nomenclature in the Northern part of the Netherlands. Additionally, HL is short for Holocene in the DGM model.

<b>Anthropogenic deposits</b>		<b>Boxtel Formation</b>	
<b>AAOP</b>	Anthropogenic deposits	<b>BX</b>	Boxtel Formation
<b>Naaldwijk Formation</b>		<b>BXKO</b>	Boxtel Formation, Kootwijk Member
<b>NASC</b>	Naaldwijk Formation, Schoorl Member	<b>BXSI1</b>	Boxtel Formation, Singraven Member, upper unit
<b>NAZA</b>	Naaldwijk Formation, Zandvoort Member	<b>BXWI</b>	Boxtel Formation, Wierden Member
<b>NA</b>	Naaldwijk Formation, no differentiation between Wormer and Walcheren Members	<b>BXSI2</b>	Boxtel Formation, Singraven Member, lower unit
<b>NAWA</b>	Naaldwijk Formation, Walcheren Member	<b>Other units</b>	
<b>NAWO</b>	Naaldwijk Formation, Wormer Member	<b>EE</b>	Eem Formation
<b>Nieuwkoop Formation</b>		<b>DR</b>	Drente Formation
<b>NINB</b>	Nieuwkoop Formation, Nij Beets Member	<b>DRGI</b>	Drente Formation, Gieten Member
<b>NIHO</b>	Nieuwkoop Formation, Hollandveen Member	<b>DN</b>	Drachten Formation
<b>NIBA</b>	Nieuwkoop Formation, Basal Peat Bed	<b>URTY</b>	Urk Formation, Tynje Member
		<b>PE</b>	Peelo Formation
		<b>UR</b>	Urk Formation, Tynje Member
		<b>ST</b>	Sterksel Formation
		<b>AP</b>	Appelscha Formation
		<b>PZWA</b>	Peize and Waalre Formations (Peize in this area)

### 4.1.3 SCPT

This section shows the classic CPT measurement (tip resistance, sleeve friction and friction ratio) with an indicative automatically generated lithological column and the SCPT  $V_S$  profile. The SCPT  $V_S$  profile shows the results from the left blow, the right blow and the average of the two blows.

When two SCPTs are performed at one station location, the next figure presents the difference between the two SCPTs. This plot provides an indication of the degree of heterogeneity at the station location and the representativeness of the SCPTs.

At one station, BFB2, an additional array of CPTs was measured between the two SCPTs to investigate the lateral heterogeneity. The results are described in the SCPT section of BFB2 (4.5.3).

### 4.1.4 OSCPT

The OSCPT is presented as a tomographic profile (showing the upper right half of the model space, as explained in section 3.2). These graphs show the short spaced lateral variations in velocity due to heterogeneity.

### 4.1.5 MASW

This section presents three plots of active MASW results:

1.  $V_S$  profile as a result from the inversion of the dispersion data (e.g. Figure 4.8). Two results are shown in the left panel: the inverted results using the automatic genetic algorithm and the result using manual optimisation of the  $V_S$  profile (section 3.3.1). Both associated dispersion curves are shown in the frequency – velocity domain in the right panel (e.g. Figure 4.8, right panel).
2. The CMPcc results are presented in three plots (e.g. Figure 4.9). The first profile (top left panel) shows the best 72 models along the CMPcc array. This image illustrates the lateral and vertical variations. The bottom left panel shows the standard deviation of these best models. It is important to note that these two panels do not represent lateral profiles, but they indicate the variations in model outputs. The third profile (right panel) shows the  $V_S$  depth profile result of the CMPcc analysis, and plots the best fit

curve of all 72 models (black), including the standard deviation (light-red and blue), as well as the maximum and minimum value of all 72 models (red and blue).

3. Dispersion curves as calculated from the SCPT  $V_S$  sounding are shown on the dispersion energy plot (e.g. Figure 4.10). The top 3 layers of the SCPT are replaced by the minimum  $V_S$  found in this range, because of the limited reliability of SCPT results in the top layers. The alignment of the modelled dispersion curves for the different modes based on the  $V_S$  profile from the SCPT with MASW dispersion energy is an extra quality control measure.

Additionally, two appendices provide extra background information on the MASW analysis. Appendix F shows the top 1% (best fit) of the fitted models on top of the dispersion plots and the resulting models. This provides a range of average models over the entire 200 m line. Appendix G includes the total envelope of energy for the CMPcc method.

#### 4.1.6 Cross-hole tomography

The results from the cross-hole tomography at the three pilot locations are shown as panels for  $V_P$  and for  $V_S$  between the boreholes at the location. The figures are provided by Geotomographie. The boreholes are situated in an L-shape (Figure 2.13). In reality, the two panels of seismic velocity information are perpendicular, but for presentation purposes they are unfolded. The centre borehole in the corner of the L is shown in the centre of the plot.

#### 4.1.7 Borehole logging

The borehole logs for the three pilot stations (BAPP, BUHZ, BWSE) are provided in Appendix C.

#### 4.1.8 P-S suspension logging

The results from the P-S suspension logging at two of the pilot stations show depth profiles of  $V_P$ ,  $V_S$  and the ratio  $V_P/V_S$  for the three boreholes at the station.

#### 4.1.9 Synthesis

The synthesis of the  $V_S$  measurements is shown in two plots. These plots aim at cross-validating all techniques and from these, final  $V_S$  that serve as input for the GMPE V3 (Bommer et al, 2016) were constructed (Chapter 5).

The first plot shows the  $V_S$  profiles for each method in panels next to each other with uncertainty bands. From left to right the panels show:

- CMPcc result with the average profile and the standard deviation.
- MASW result showing both the automatic inversion with the range between minimum and maximum  $V_S$  and the best model for manually optimised  $V_S$  profile.
- OSCPT result shows the average  $V_S$  at 1 to 5 m distance from the CPT location based on the OSCPT tomogram. The uncertainty band indicates the minimum and maximum  $V_S$  in the first 5 metres. One or two curves are shown, depending on the amount of SCPTs performed at the location.
- SCPT results. The uncertainty band represents the results between the left and the right blow. One or two curves are shown, depending on the amount of SCPTs performed at the location.

- 1D representation of cross-hole 2D  $V_S$  result: the average  $V_S$  value was determined for each depth interval. The average, minimum and maximum  $V_S$  in the 2D section is plotted.

The second plot shows the SCPT results that form the basis for the final  $V_S$  profiles in the left panel, the MASW and CMPcc in the second plot and the CPT results and the indicative lithological column in the right panels. Intervals that are not reliable (e.g. poor data quality or insufficient resolution) are shown in red.

## 4.2 Appingedam- BAPP

### 4.2.1 Location

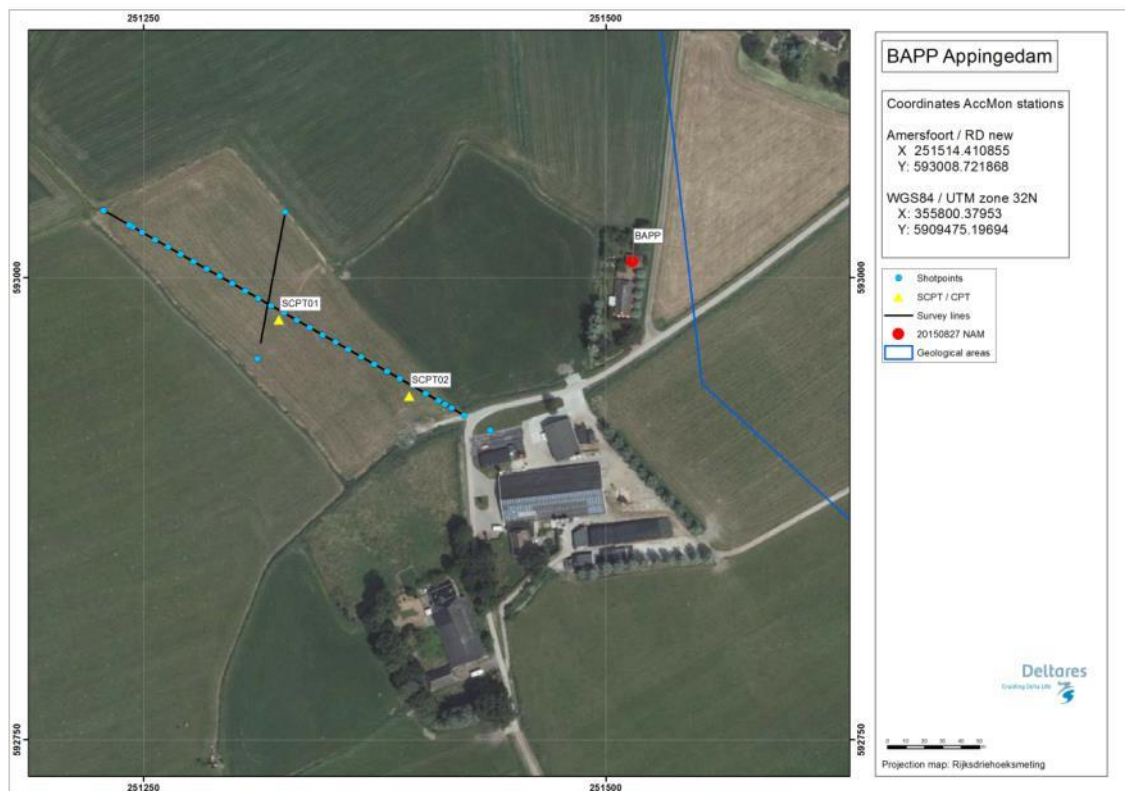


Figure 4.1 Map of location BAPP, showing the KNMI accelerograph station, SCPT location and MASW survey lines and shot locations.

### 4.2.2 Geological setting

The location is situated in a non-erosive area. The Holocene deposits consist of clay with a peat layer in between at the depth of 1 metre. The basal peat is present in this area.

Top of the Pleistocene is found at a depth of  $\pm 5$  metres with a slope to the east to 6 metres. The location is situated in the middle of a Peelo valley with a depth of 180 metres.

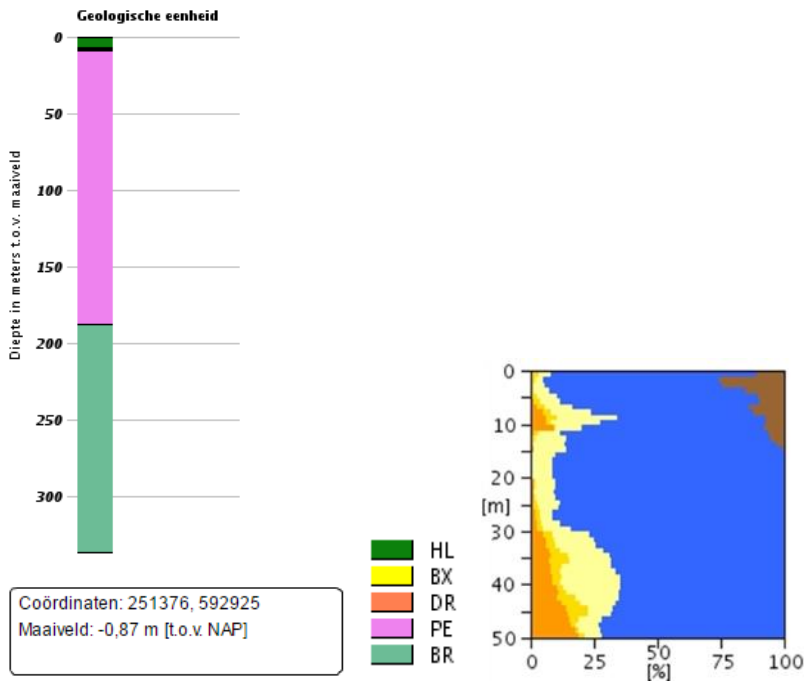


Figure 4.2 Geological information at station BAPP. Left: 1D section from the DGM model. Right: Section from the “delfstoffen online” model (GDN-TNO). Colour coding: brown = peat, blue = clay, yellow to orange = fine sand to coarse sand. The horizontal scale shows the volume percentage of each of the lithologies present at the location, the vertical scale is depth below the surface.

Table 4.2 Descriptions of representative deep boreholes near station BAPP from the DINO database ([www.dinoloket.nl](http://www.dinoloket.nl)).

<i>Drilling</i>	<i>Distance from drilling</i>	<i>top</i>	<i>bottom</i>	<i>sediment type</i>	<i>Min. grain size</i>	<i>Max. grain size</i>	<i>Formation</i>
B07F0005	1100mtr NE	0,38	-2,13	Clay			Formation of Naaldwijk
		-2,13	-3,13	Peat			Formation of Nieuwkoop
		-3,13	-5,88	Clay			Formation of Naaldwijk
		-5,88	-5,98	Peat			Formation of Nieuwkoop
		-5,98	-9,88	Sand	Fine		Formation of Bortel
		-9,88	-114,38	Clay			Formation of Peelo
		-114,38	-181,38	Sand	Fine		Formation of Peelo
B07F0116	1400mtr NE	0,00	-0,50	Clay			Formation of Naaldwijk
		-0,50	-2,00	Peat			Formation of Nieuwkoop
		-2,00	6,00	Clay			Formation of Naaldwijk
		6,00	6,20	Peat			Formation of Nieuwkoop
		6,20	9,00	Sand	Fine		Formation of Bortel
		9,00	-130,00	Clay			Formation of Peelo
B07F0149	1500mtr NE	0,00	-1,50	Clay			Formation of Naaldwijk
		-1,50	-2,00	Peat			Formation of Nieuwkoop
		-2,00	-4,70	Clay			Formation of Naaldwijk
		-4,70	-6,20	Sand	Fine		Formation of Bortel
		-6,20	-50,00	Clay			Formation of Peelo
		-50,00	-56,00	Sand	Fine		Formation of Peelo
		-56,00	-61,00	Sand	Coarse		Formation of Peelo
		-61,00	-66,00	Sand	Fine		Formation of Peelo
-66,00	-72,00	Sand	Coarse		Formation of Peize		

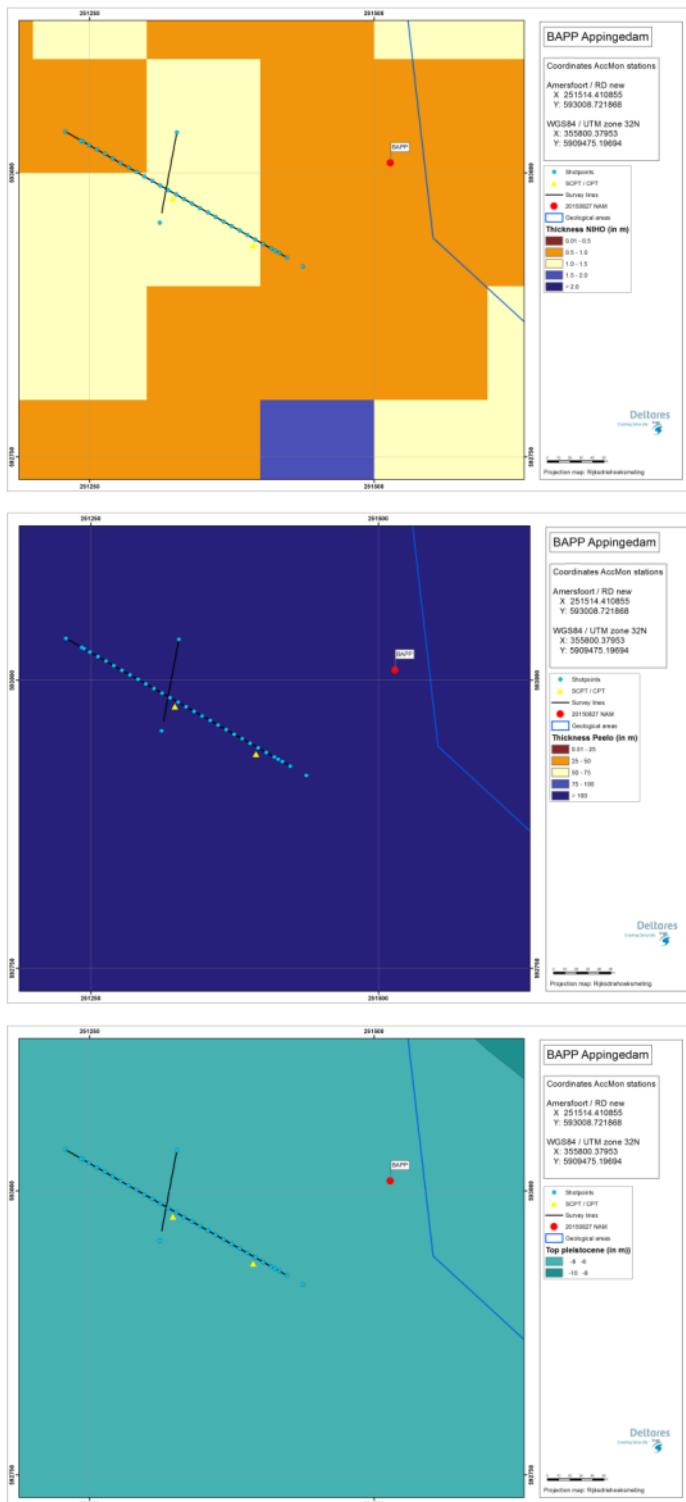


Figure 4.3 Overview map of geological setting based on beta version of GeoTOP model. Top panel: Thickness of the Holocene peat. Middle panel: Thickness of the Peelo Formation, blue colour indicates thick Peelo layer, hence in the centre of the channel; red and orange colour indicates thin Peelo layers, hence areas outside the channel; yellow indicates transition zone. Lower panel: Top of Pleistocene surface relative to Dutch Ordnance Datum NAP.

## 4.2.3 SCPT

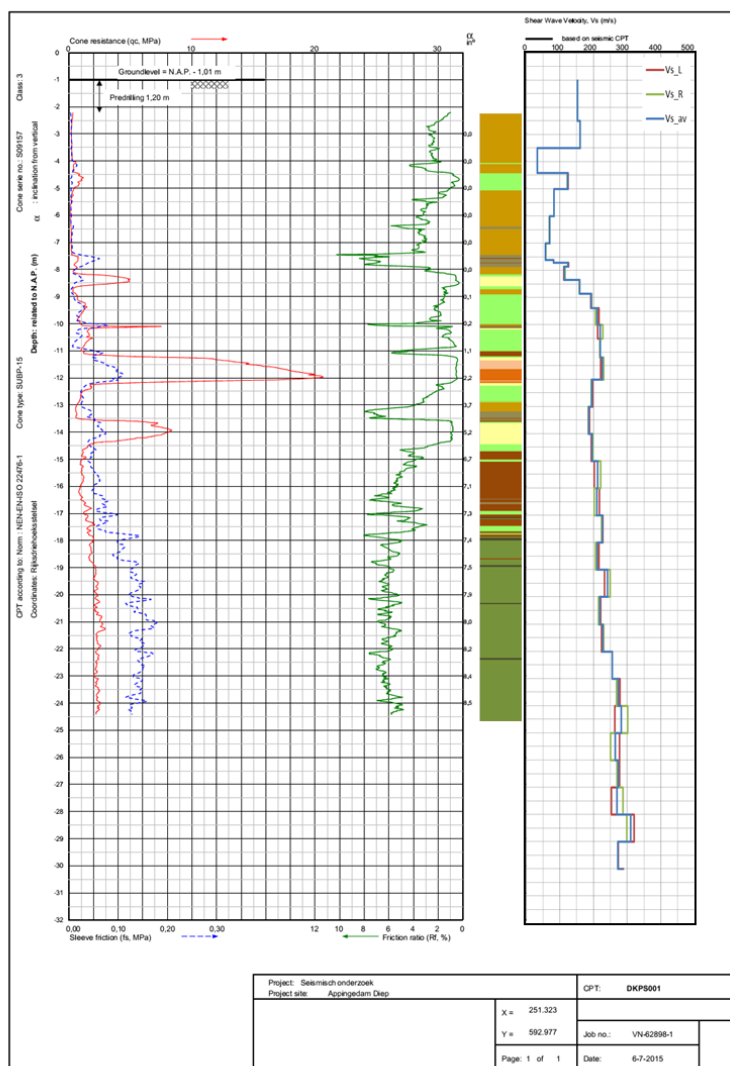


Figure 4.4 SCPT01. From left to right: CPT measurement, showing tip resistance, sleeve friction and friction ratio; automatically generated lithology (indication, for legend see Table 3.1); Vs profile (red = left blow, green = right blow, blue = average).

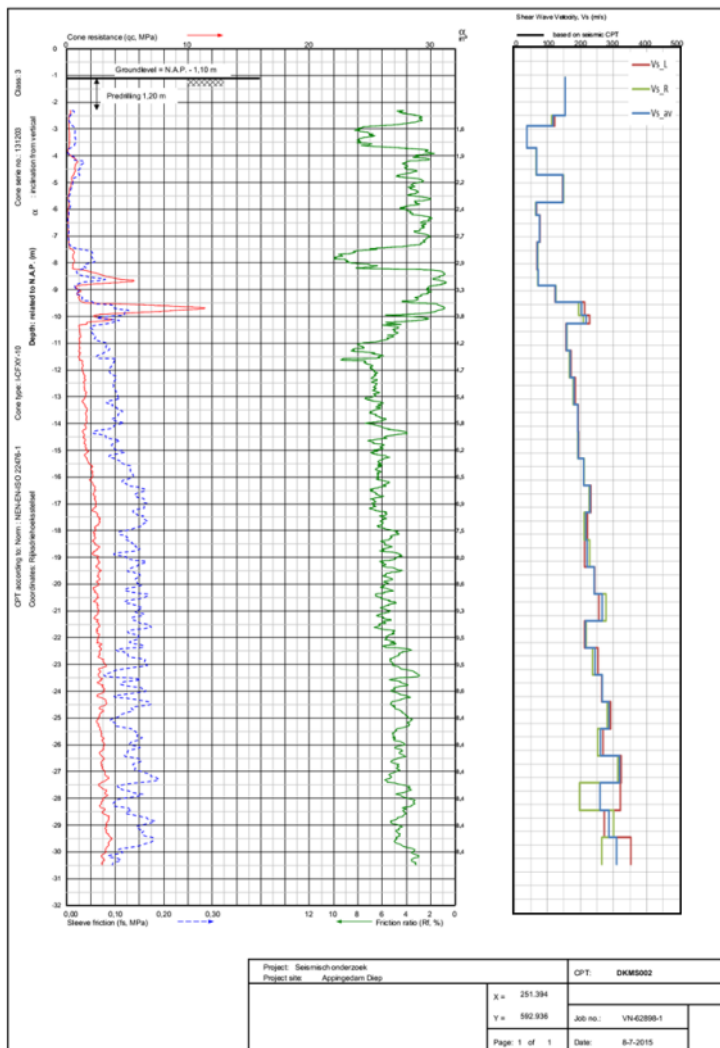


Figure 4.5 SCPT02. From left to right: CPT measurement, showing tip resistance, sleeve friction and friction ratio; automatically generated lithology (indication, for legend see Table 3.1);  $V_s$  profile (red = left blow, green = right blow, blue = average).

1210624-000-BGS-0007, Version 2, 27 June 2016, final

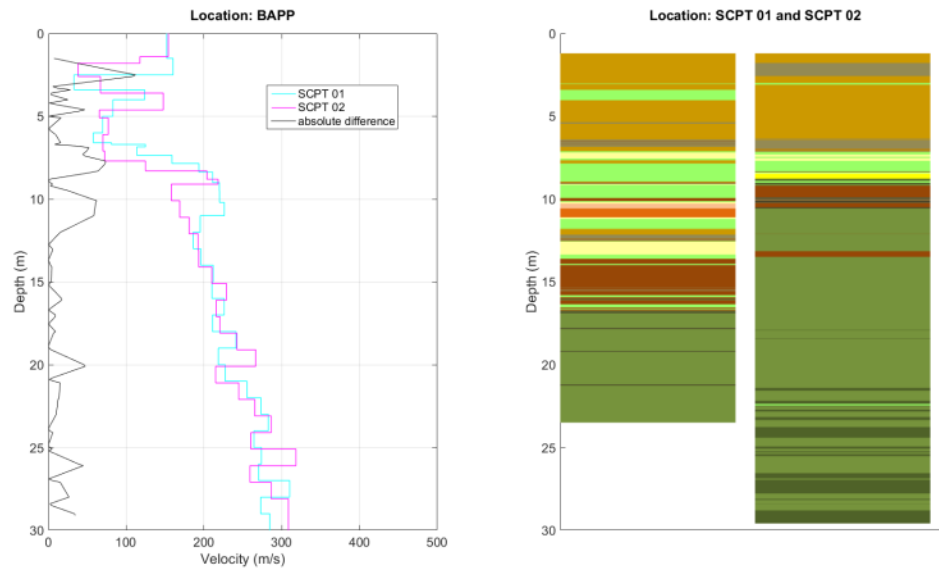


Figure 4.6 Station BAPP. Left: Difference between the two SCPTs measured at the same station location. Right: automatically generated lithology (indication).

## 4.2.4 OSCPT

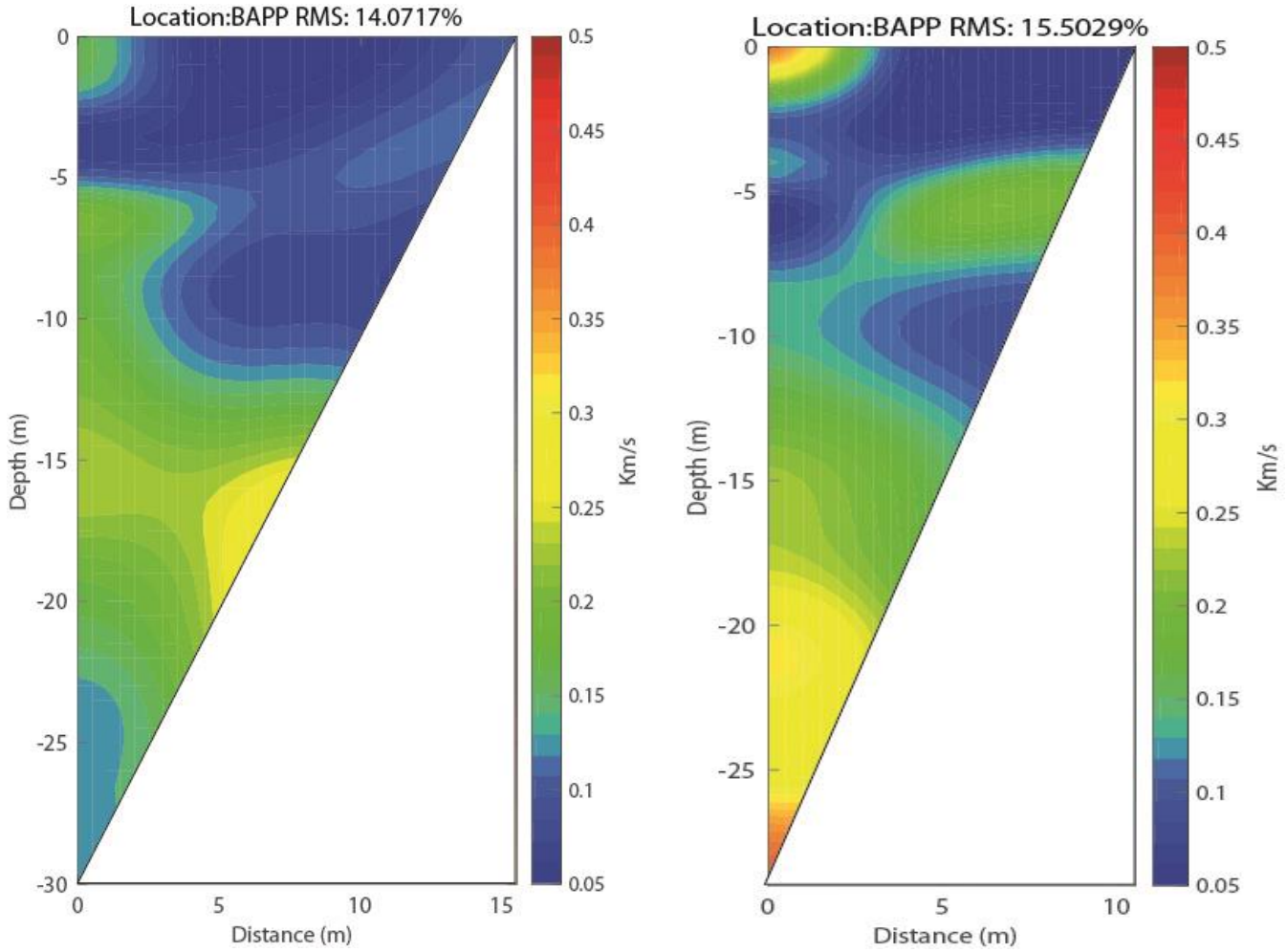


Figure 4.7 Tomographic images based on OSCPT results from two SCPTs for station BAPP (left SCPT01; right SCPT02).

## 4.2.5 MASW

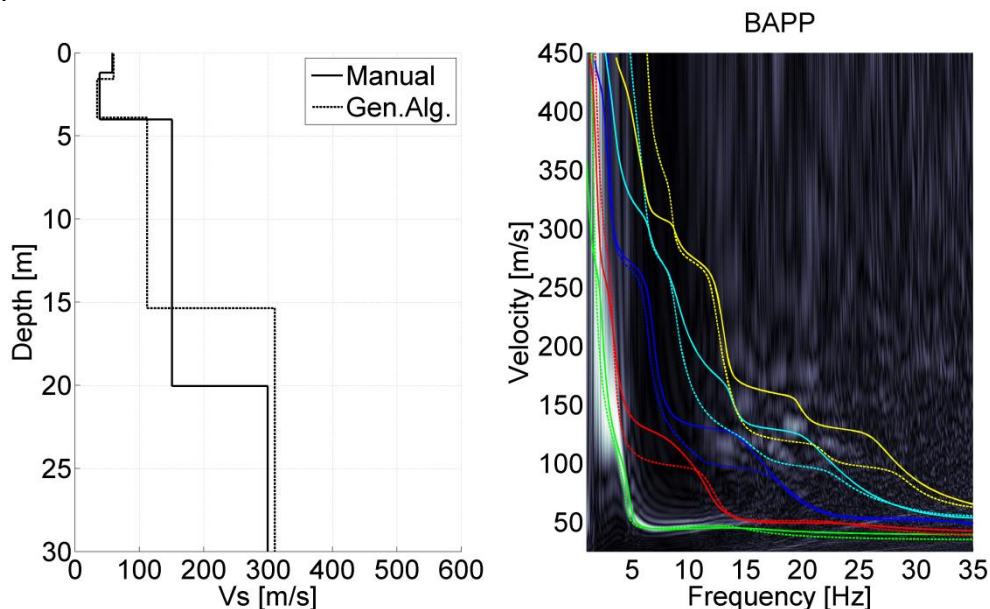


Figure 4.8 MASW result for BAPP. Left panel:  $V_s$  profiles from active MASW. Solid line from manual fitting of dispersion curves; dashed line for automatic inversion. Right panel: energy in the dispersion plot in greyscale; solid lines are the dispersion curves for different modes of the hand fitted  $V_s$  profile; dashed lines for the different modes of the automatic inversion  $V_s$  profile.

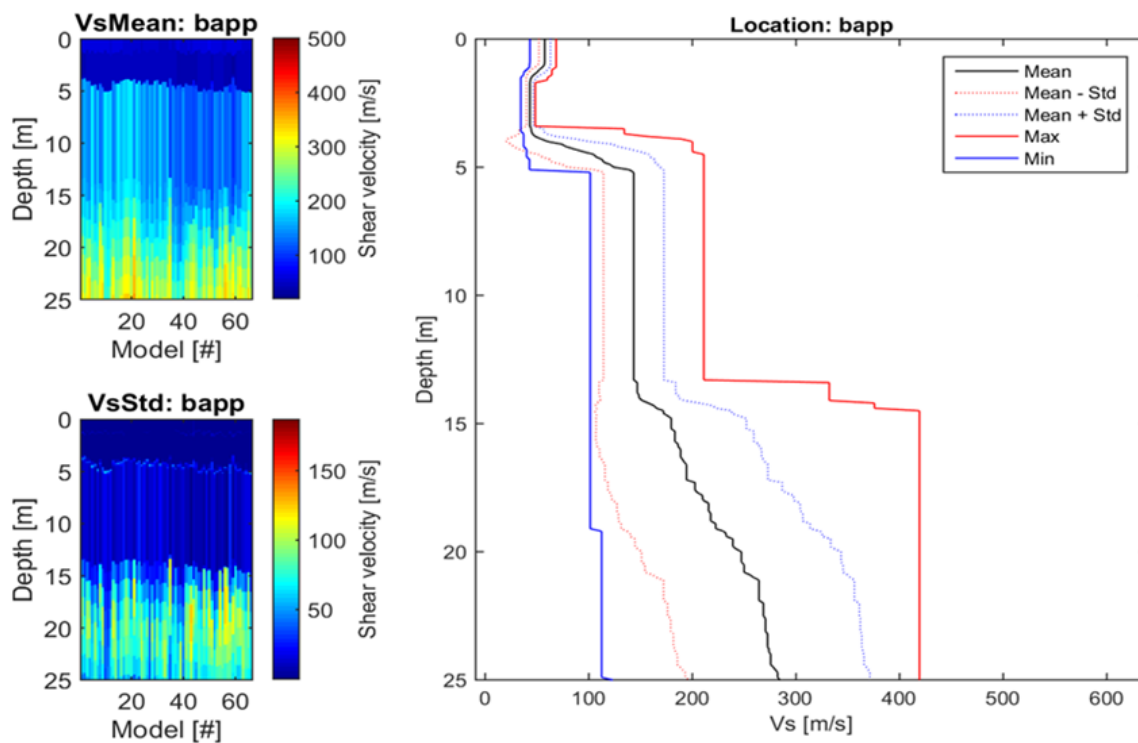


Figure 4.9 CMPcc result for BAPP. Top left: average velocity along the CMPcc array. Bottom left: statistical misfit standard variation along the CMPcc array. Right: best fit curve of all 72 models together with the maximum and minimum value observed in the whole CMPcc and the standard deviation (misfit) from all the models.

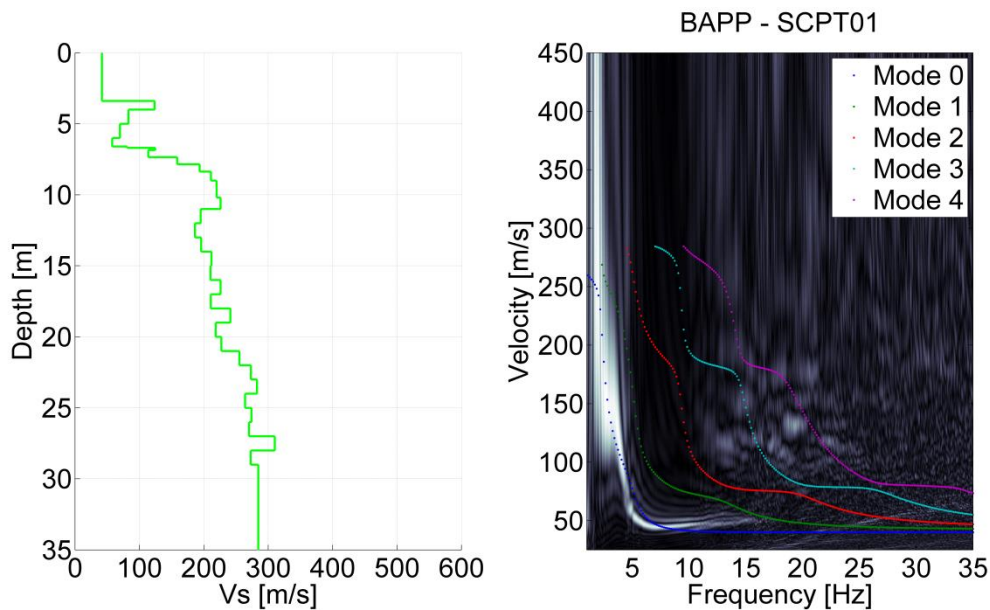


Figure 4.10 Comparison for BAPP of SCPT01 and MASW result. Left:  $V_s$  profile from SCPT. The  $V_s$  from the top 2 layers of the SCPT is generally unreliable and replaced by the minimum  $V_s$  of the first 3 layers. Right: theoretical dispersion plot of SCPT  $V_s$  profile in coloured lines on the energy of MASW dispersion plot in greyscale.

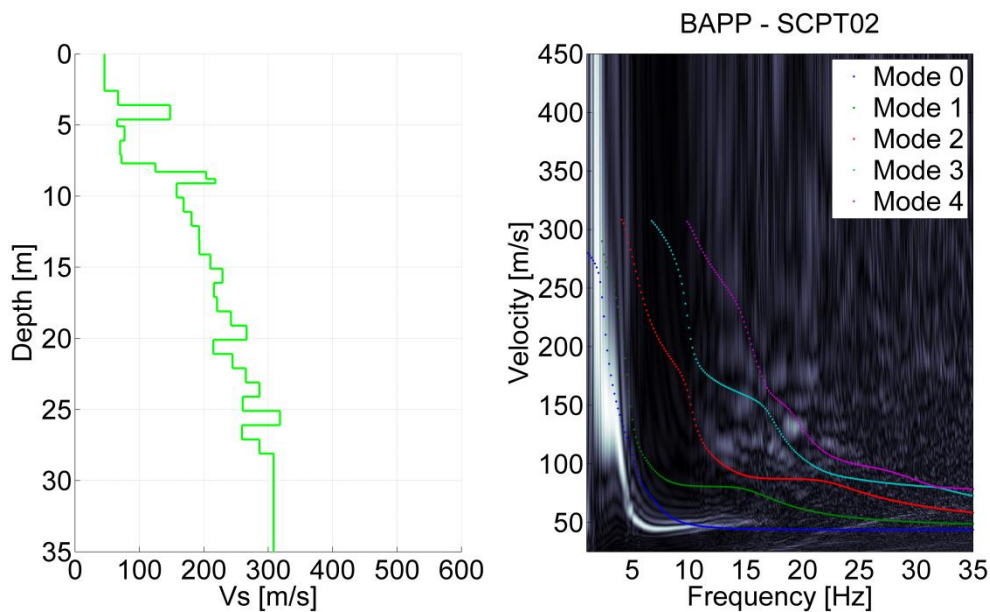


Figure 4.11 Comparison for BAPP of SCPT02 and MASW result. Left:  $V_s$  profile from SCPT. The  $V_s$  from the top 2 layers of the SCPT is generally unreliable and replaced by the minimum  $V_s$  of the first 3 layers. Right: theoretical dispersion plot of SCPT  $V_s$  profile in coloured lines on the energy of MASW dispersion plot in greyscale.

## 4.2.6 Cross-hole Tomography

The data quality of the tomography varies the upper layers are of moderate to poor because of the very soft soil condition, for this reason part of the shallow data is not presented. The patterns in the P and S wave tomograms do show both a significant transition at -10 metres. It appears that the short panel shows higher average velocities than the long panel.

The other variations in the spatial velocity distribution do not appear to align between the P and S wave tomograms.

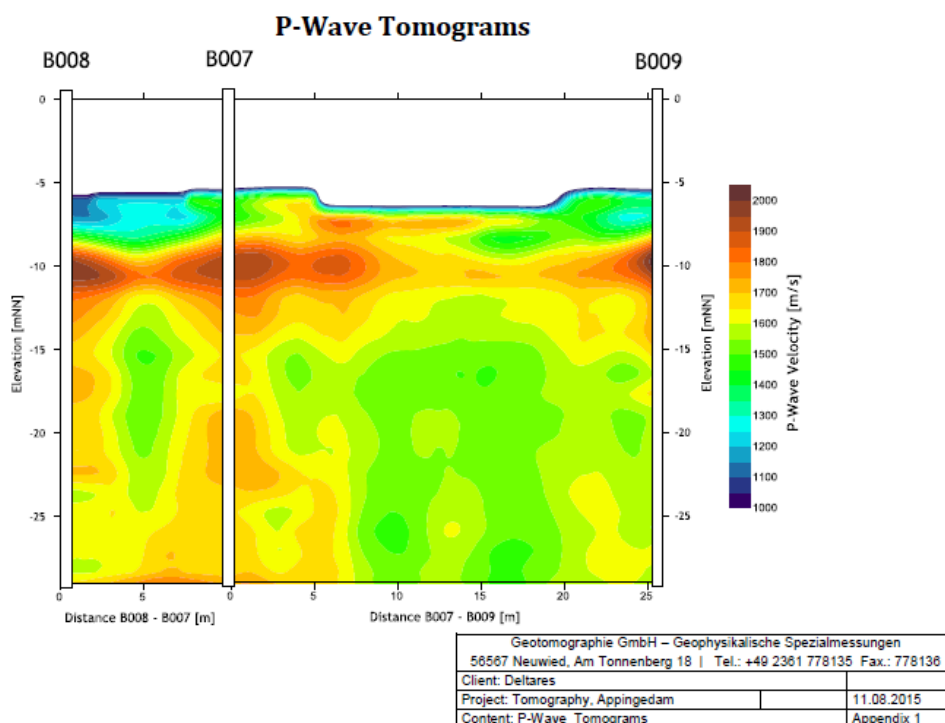


Figure 4.12  $V_p$  tomogram for station BAPP, from Geotomographie. The cross section in the figure has an L shape in the field (see Figure 2.13): the short leg (left) is perpendicular to the long leg of the borehole setup (right). B numbers indicate the borehole code. The top layer in the tomograms has been removed, because of poor data quality.

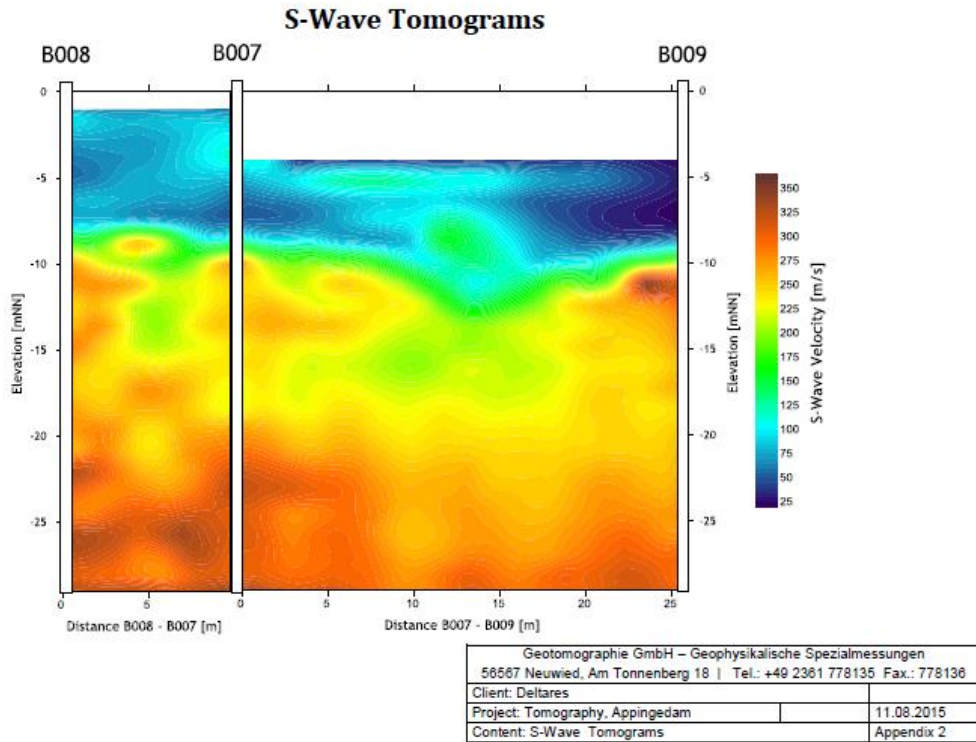


Figure 4.13  $V_s$  tomogram for station BAPP, from Geotomographie. The cross section in the figure has an L shape in the field (see Figure 2.13): the short leg (left) is perpendicular to the long leg of the borehole setup (right). B numbers indicate the borehole code. The top layer in the tomograms has been removed, because of poor data quality.

4.2.7 P-S suspension logging

Due to low quality P-S suspension logging data at BUHZ and BWSE, no P-S suspension logging has been performed at BAPP.

## 4.2.8 Synthesis

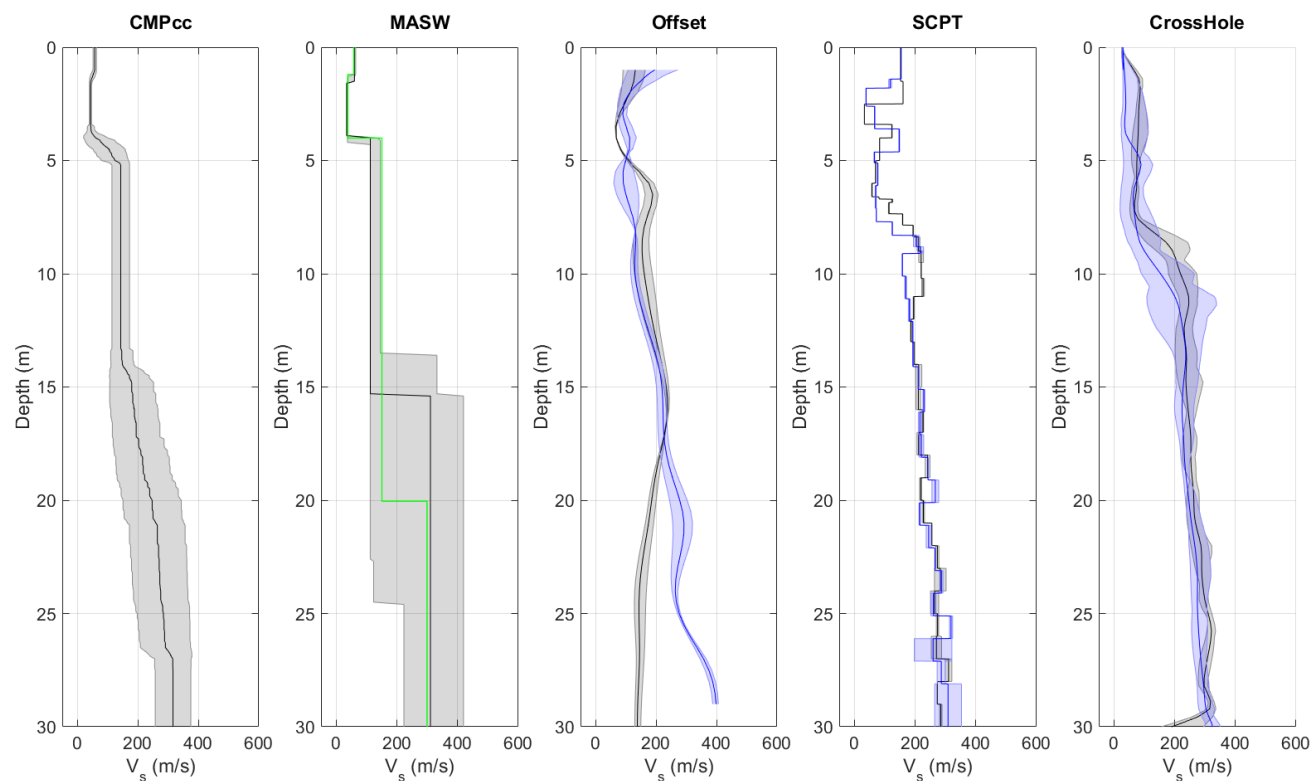


Figure 4.14  $V_s$  profiles from different measurement techniques, including uncertainty bands. From left to right: CMPcc based on active MASW array, shaded band indicates standard deviation; active MASW with manual fit in green and automatic inversion in black with grey shaded band indicating the minimum and the maximum  $V_s$ ; average profile for offset SCPTs between 1 and 5 m offset for 1 or 2 SCPTs with shaded band indicating the minimum and the maximum  $V_s$ ; SCPTs with band indicating variation between left and right blow; cross-hole average profiles for long leg in blue and short leg in grey with shaded band indicating the minimum and the maximum  $V_s$ .

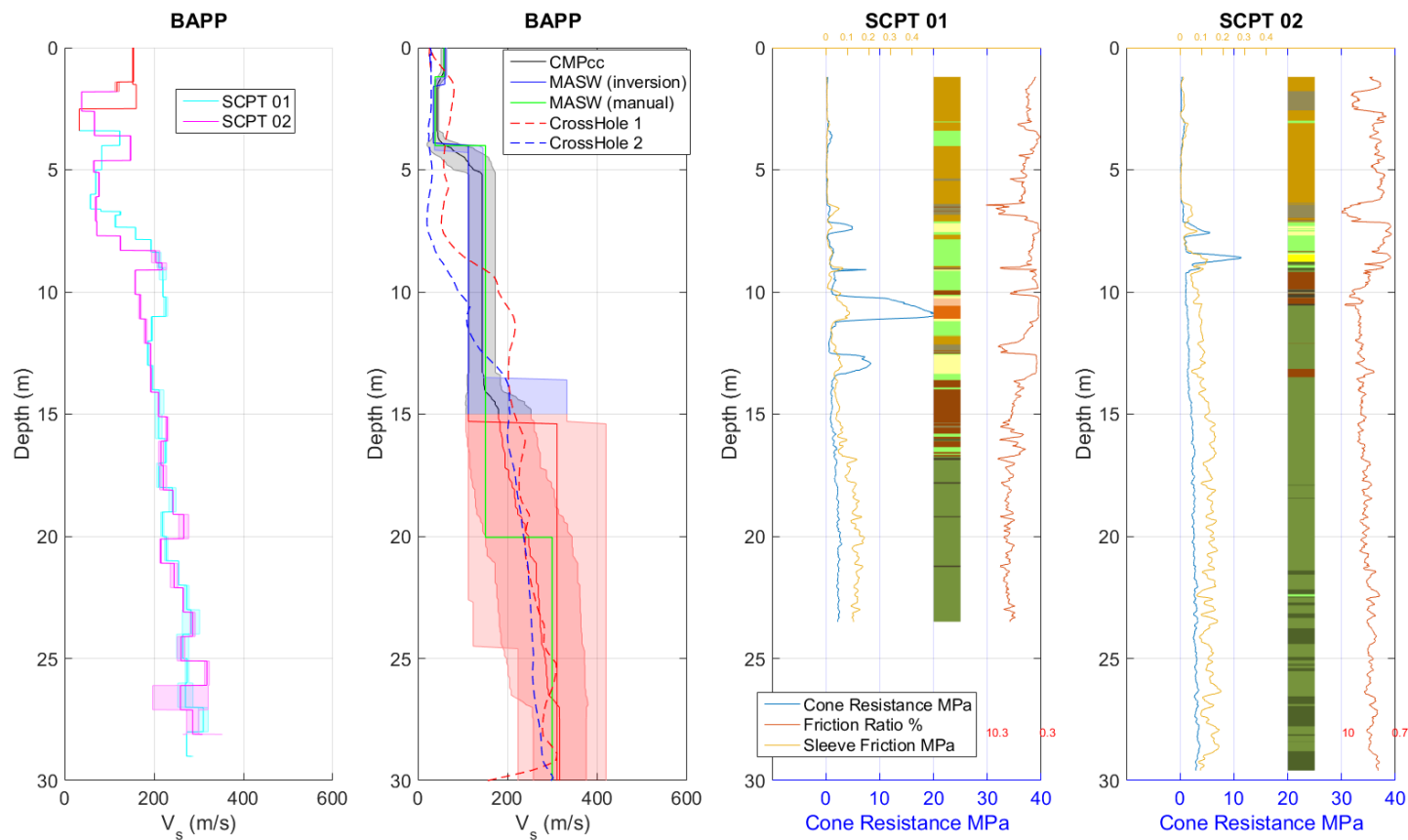


Figure 4.15 Synthesis of  $V_s$  results. Unreliable results are shown in red. From left to right: SCPT with band indicating variation between left and right blow; CMPcc, MASW and average cross-hole results with uncertainty bands; CPT with cone resistance, friction ratio, sleeve friction and automatically generated lithology (indication, for legend see Table 3.1).

### 4.3 Uithuizen- BUHZ

#### 4.3.1 Location

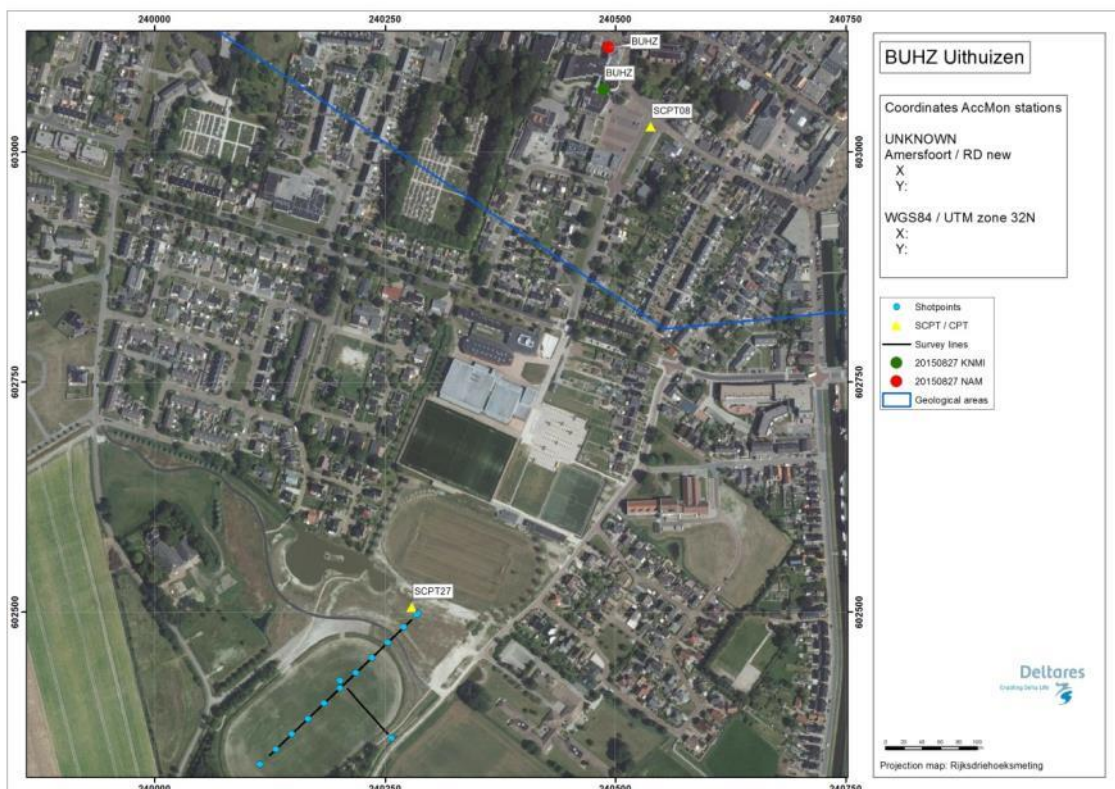


Figure 4.16 Map of location BUHZ, showing the KNMI accelerograph station (exact location ambiguous), SCPT location and MASW survey lines and shot locations.

#### 4.3.2 Geological setting

The location of the geophysical is situated in an erosional valley bordered in the east by a non-erosive area. Pleistocene is covered with erosive Holocene deposits consisting of fine sand. Thickness of the Holocene differs from 14 metres in the east of the line up to 30 metres to the west in the centre of the erosive channel.

The site is positioned outside of the Peelo valley.

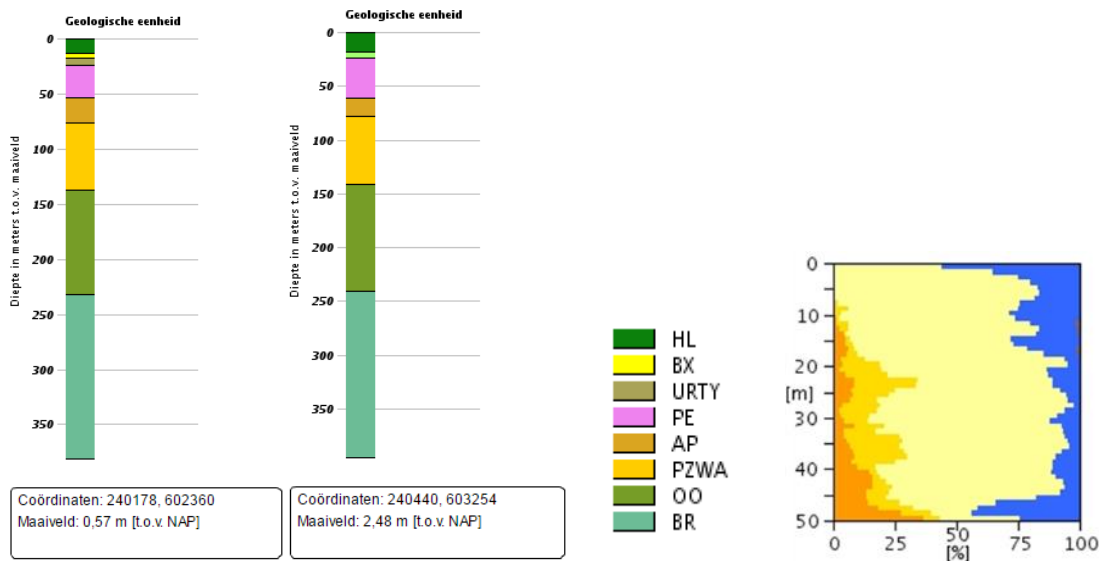


Figure 4.17 Geological information at station BUHZ. Left: 1D section from the DGM model. Right: Section from the “delfstoffen online” model (GDN-TNO). Colour coding: brown = peat, blue = clay, yellow to orange = fine sand to coarse sand. The horizontal scale shows the volume percentage of each of the lithologies present at the location, the vertical scale is depth below the surface.

The accelerograph is positioned on the non-erosive area which has a different composition of the Holocene. At that location the Holocene consists of 18 metre of fine silt-bearing sands.

Table 4.3 Descriptions of representative deep boreholes near station BUHZ from the DINO database ([www.dinoloket.nl](http://www.dinoloket.nl)).

Drilling	Distance from drilling	top	bottom	sediment type	Min. grain size	Max. grain size	Formation
B03G0002	180mtr N	2,21	-15,95	Sand	Very fine		Formation of Naaldwijk
		-15,95	-20,79	Sand	Very fine		Eem Formation
		-20,79	-22,29	Sand	Very coarse	Gravel	Eem Formation
		-22,29	-28,79	Clay			Formation of Peelo
		-28,79	-44,79	Sand	Very fine		Formation of Peelo
		-44,79	-50,29	Clay			Formation of Peelo
		-50,29	-61,29	Sand	Medium coarse		Formation of Peelo
		-61,29	-74,49	Sand	Very coarse		Formation of Appelscha

1210624-000-BGS-0007, Version 2, 27 June 2016, final

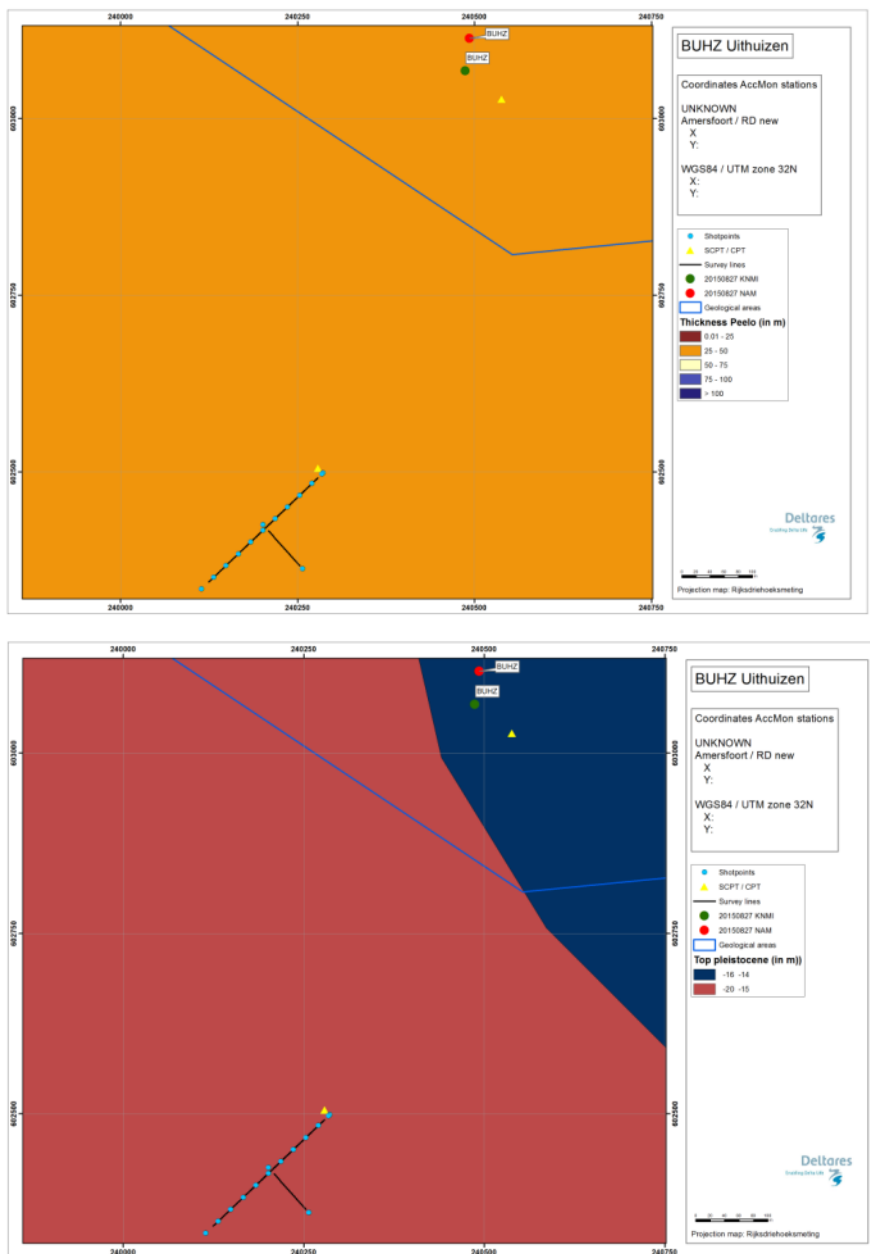


Figure 4.18 Overview map of geological setting based on beta version of GeoTOP model. Top panel: Thickness of the Peelo Formation, blue colour indicates thick Peelo layer, hence in the centre of the channel; red and orange colour indicates thin Peelo layers, hence areas outside the channel; yellow indicates transition zone. Lower panel: Top of Pleistocene surface relative to Dutch Ordinance Datum NAP.

## 4.3.3 SCPT

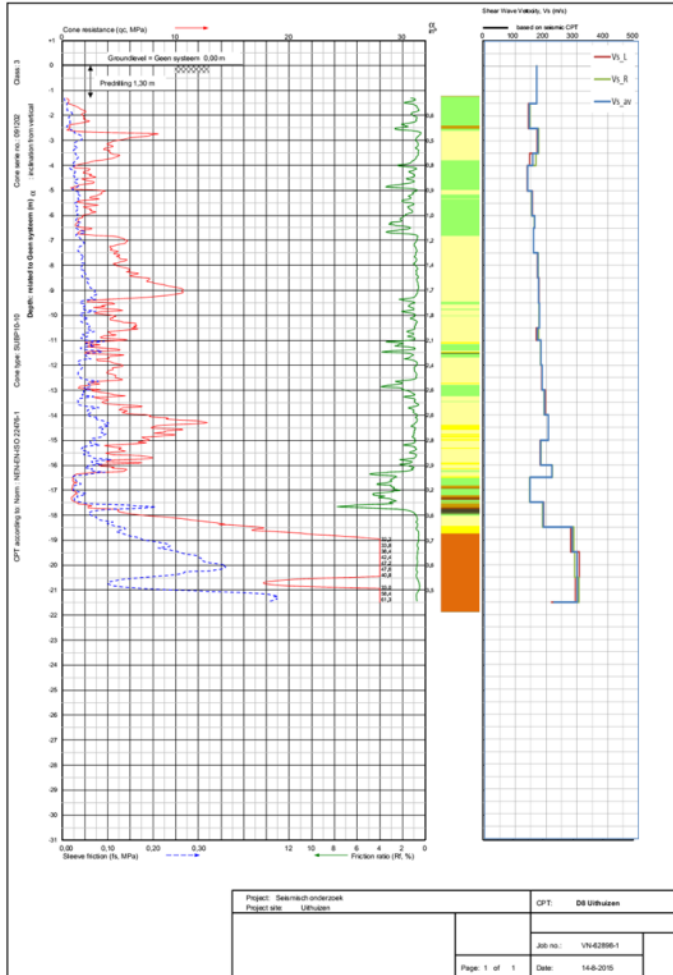


Figure 4.19 SCPT08. From left to right: CPT measurement, showing tip resistance, sleeve friction and friction ratio; automatically generated lithology (indication, for legend see Table 3.1);  $V_s$  profile (red = left blow, green = right blow, blue = average).

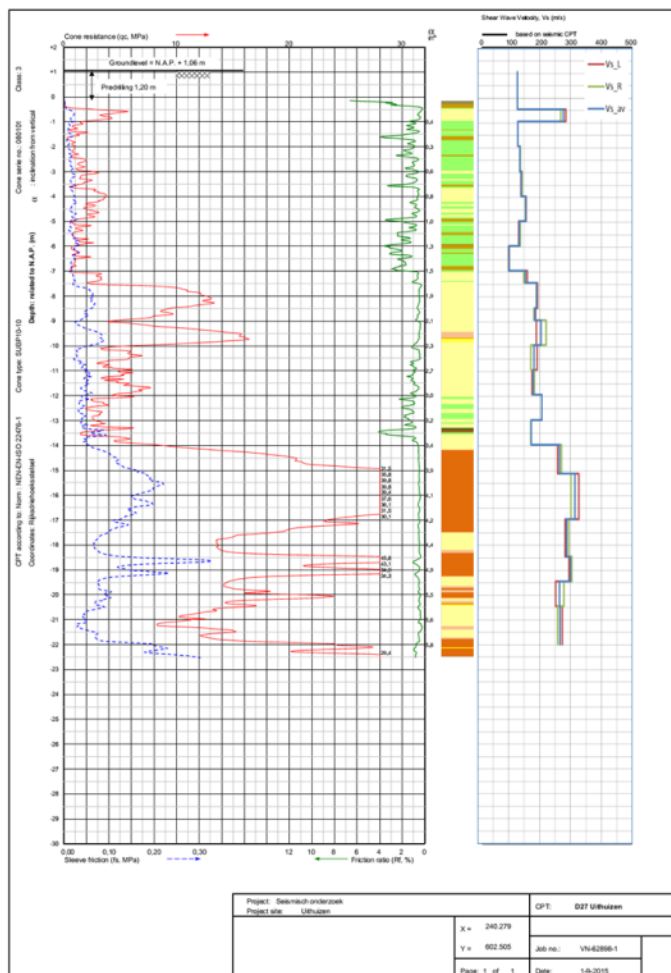


Figure 4.20 SCPT27. From left to right: CPT measurement, showing tip resistance, sleeve friction and friction ratio; automatically generated lithology (indication, for legend see Table 3.1);  $V_s$  profile (red = left blow, green = right blow, blue = average).

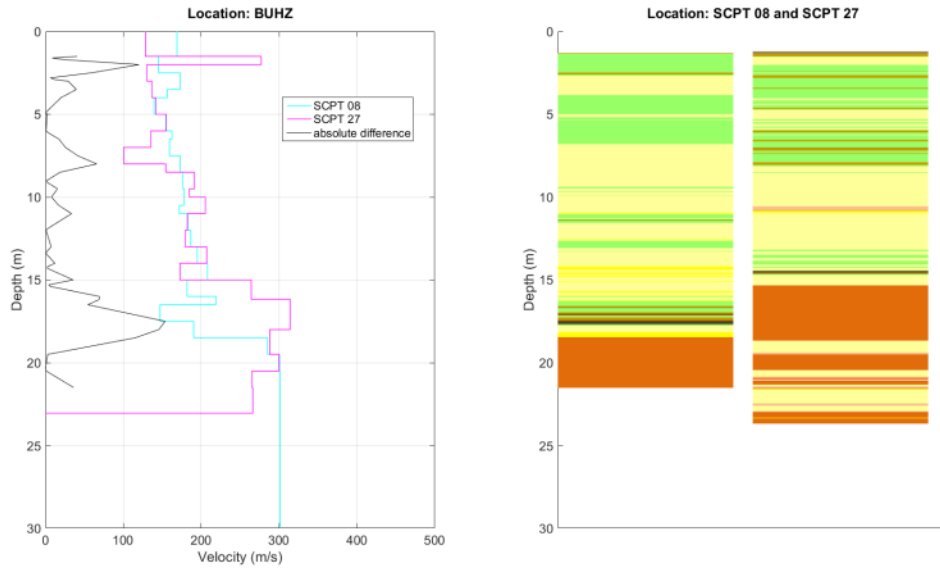


Figure 4.21 Station BUHZ. Left: Difference between the two SCPTs measured at the same station location. Right: automatically generated lithology (indication).

## 4.3.4 OSCPT

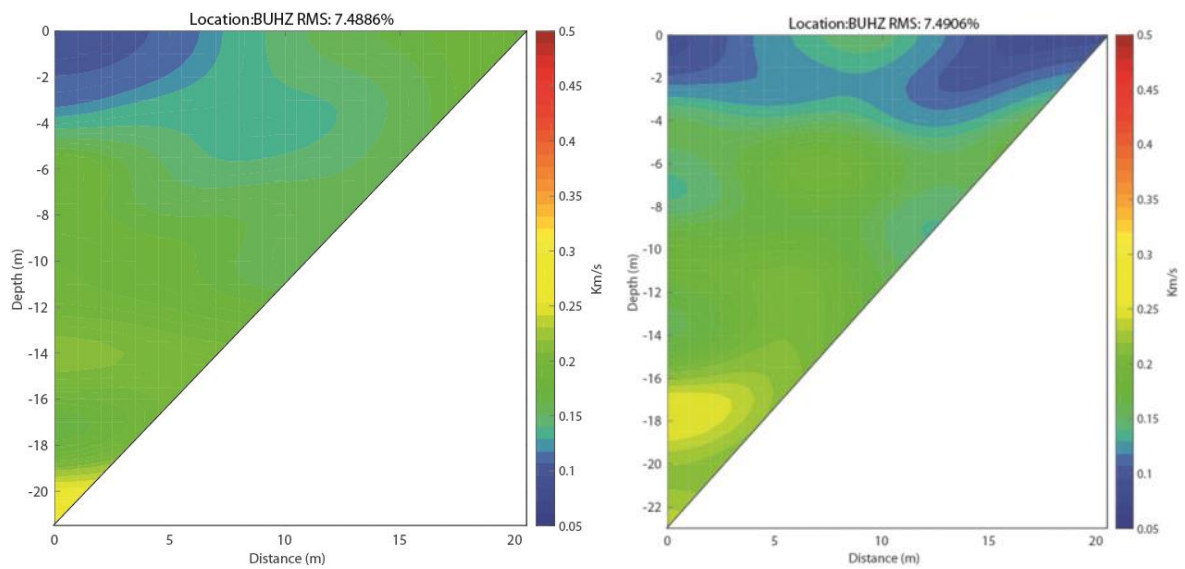


Figure 4.22 Tomographic images based on OSCPT results from two SCPTs for station BUHZ (left SCPT08; right SCPT27).

## 4.3.5 MASW

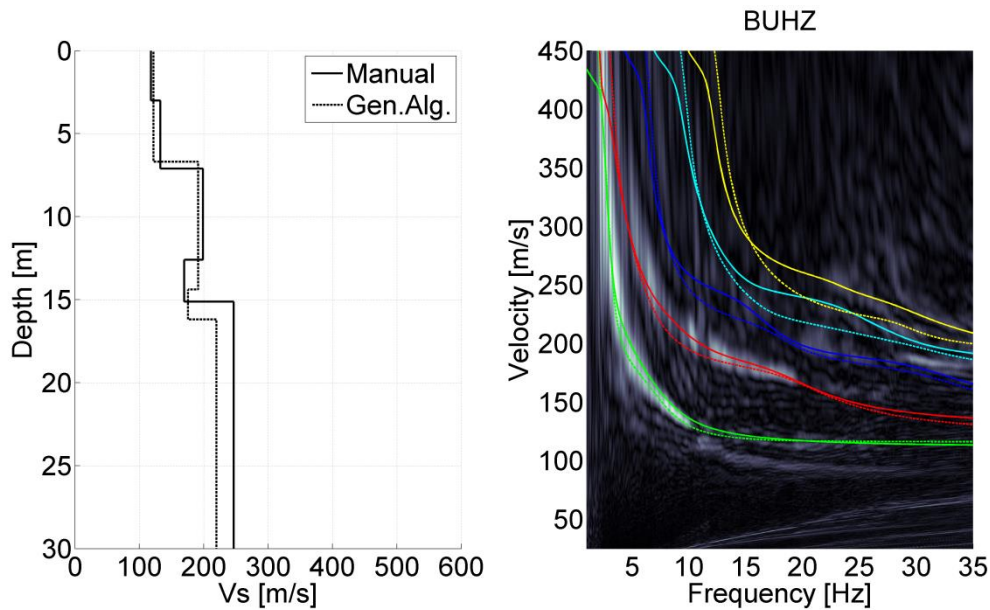


Figure 4.23 MASW result for station BUHZ. Left panel:  $V_s$  profiles from active MASW. Solid line from manual fitting of dispersion curves; dashed line for automatic inversion. Right panel: energy in the dispersion plot in greyscale; solid lines are the modelled dispersion curves for different modes of the manually fitted  $V_s$  profile; dashed lines for the different modes of the automatically inverted  $V_s$  profile.

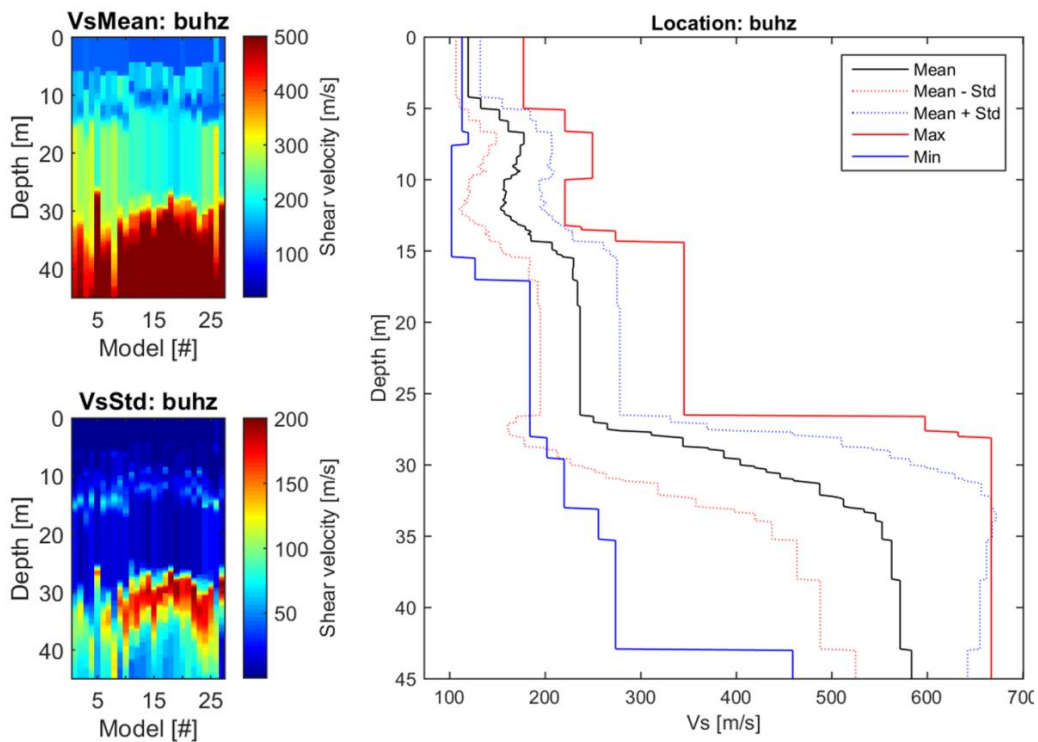


Figure 4.24 CMPcc result for BUHZ. Top left: average  $V_s$  along the CMPcc array. Bottom left: standard deviation of  $V_s$  along the CMPcc array. Right: best fit curve of the 72 models with the maximum and minimum value observed in the whole CMPcc and the standard deviation from all models.

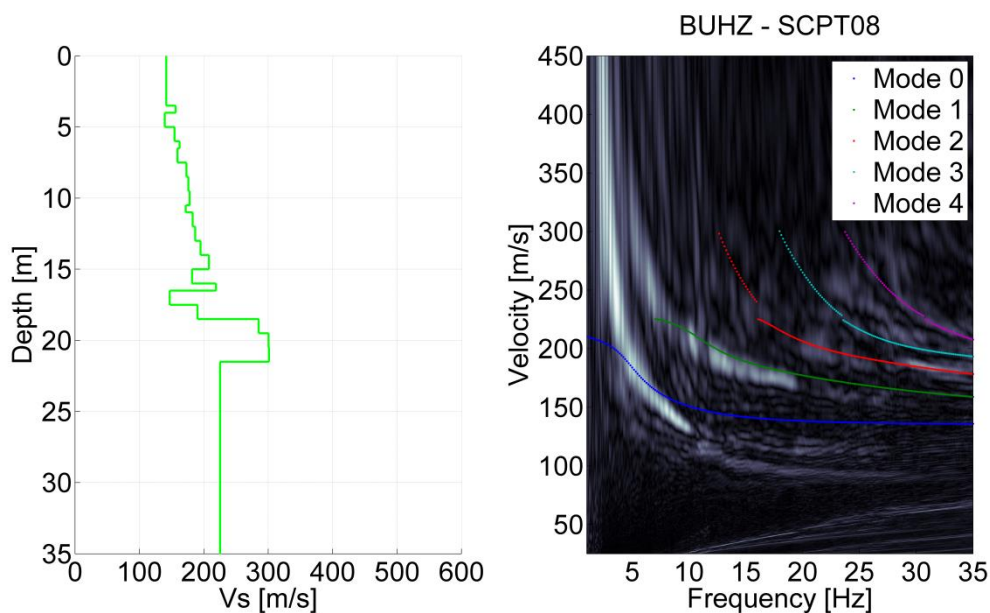


Figure 4.25 Comparison for BUHZ of SCPT08 and MASW result. Left:  $V_s$  profile from SCPT. The  $V_s$  from the top 2 layers of the SCPT is generally unreliable and replaced by the minimum  $V_s$  of the first 3 layers. Right: modelled dispersion curves of different modes based on the SCPT  $V_s$  profile in coloured lines plotted on the energy of MASW dispersion plot in greyscale.

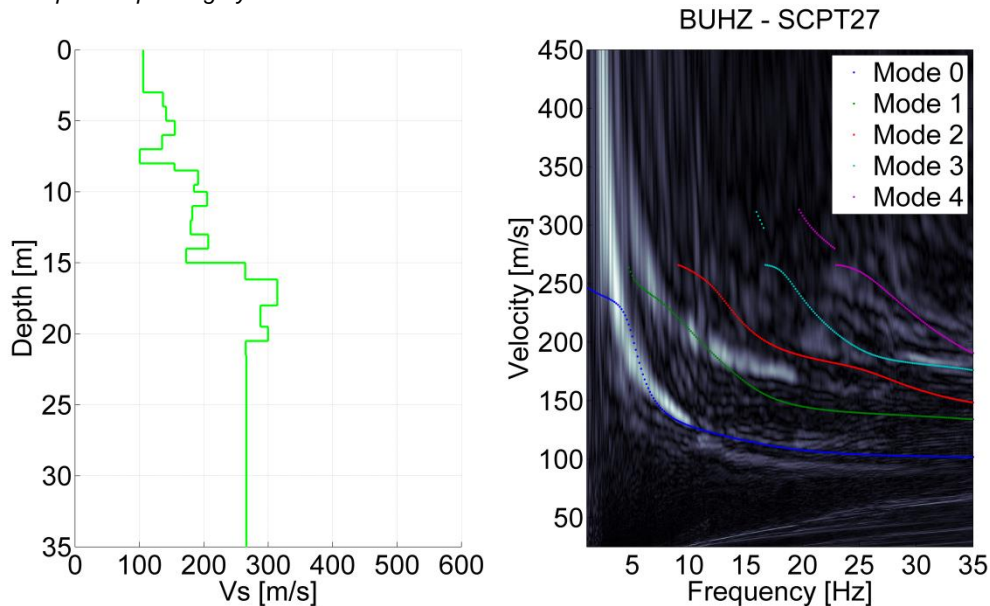


Figure 4.26 Comparison for BUHZ of SCPT27 and MASW result. Left:  $V_s$  profile from SCPT. The  $V_s$  from the top 2 layers of the SCPT is generally unreliable and replaced by the minimum  $V_s$  of the first 3 layers. Right: modelled dispersion curves of different modes based on the SCPT  $V_s$  profile in coloured lines plotted on the energy of MASW dispersion plot in greyscale.

## 4.3.6 Cross-hole Tomography

The cross-hole tomography data for station BUHZ is very good to excellent. Both tomograms show a major increase in velocity at around -5 to -6 and again around -15 metres. The first transition represents the transition from Holocene peat and clay to a sand layer. The second transition represents the top of the Pleistocene.

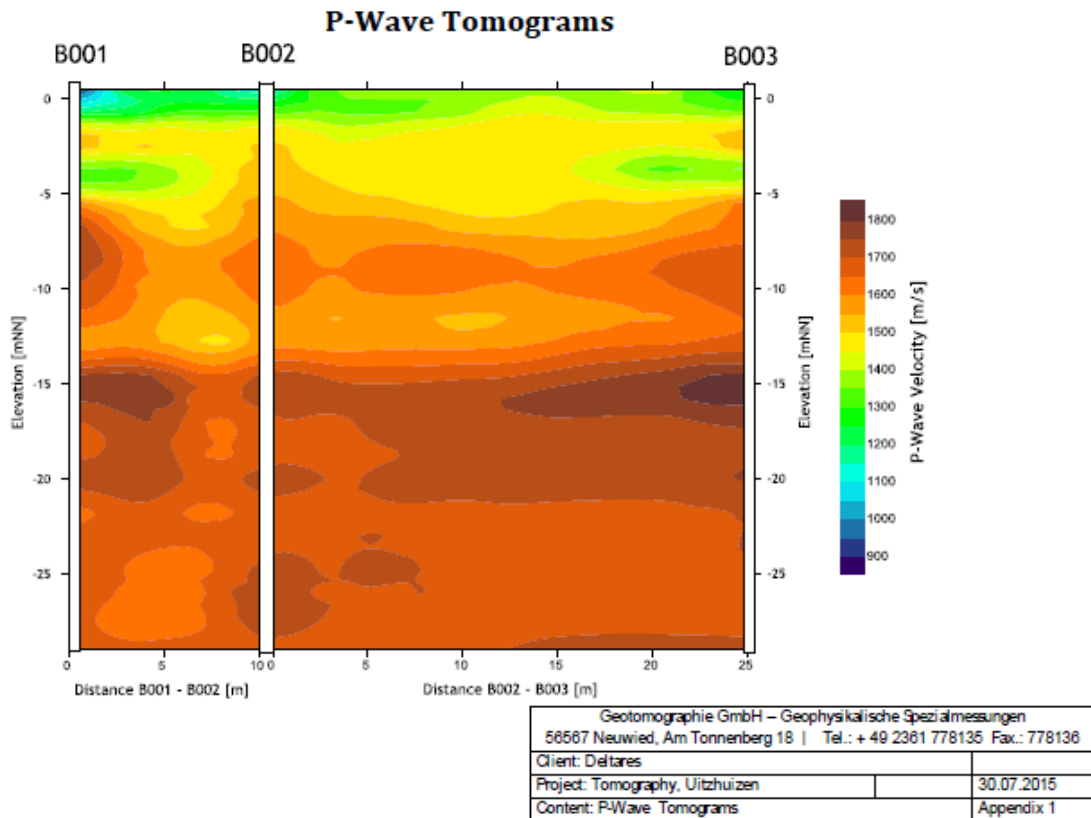


Figure 4.27  $V_P$  tomogram for station BUHZ, from Geotomographie. The cross section in the figure has an L shape in the field (see Figure 2.13): the short leg (left) is perpendicular to the long leg of the borehole setup (right). B numbers indicate the borehole code.

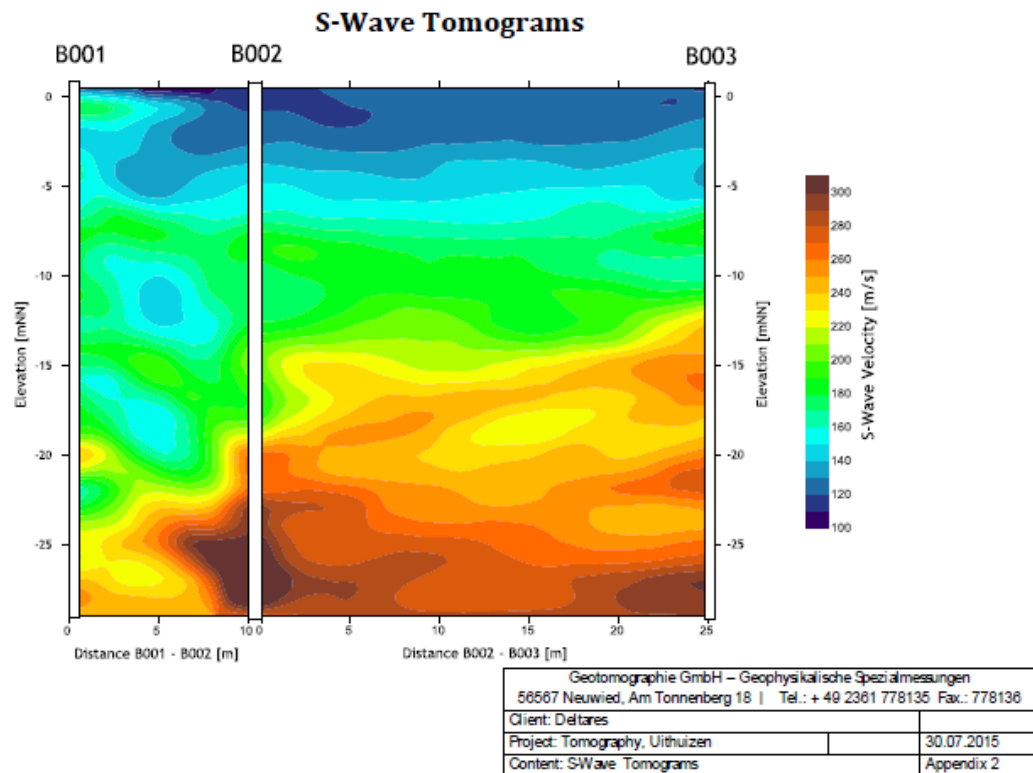


Figure 4.28  $V_S$  tomogram for station BUHZ, from Geotomographie. The cross section in the figure has an L shape in the field (see Figure 2.13): the short leg (left) is perpendicular to the long leg of the borehole setup (right). B numbers indicate the borehole code

#### 4.3.7 P-S suspension logging

The quality of the suspension logging is low, the resulting values are probably not representative. The trends in both P and S wave velocities are not comparable to that of the other techniques used in this project.



1210624-000-BGS-0007, Version 2, 27 June 2016, final

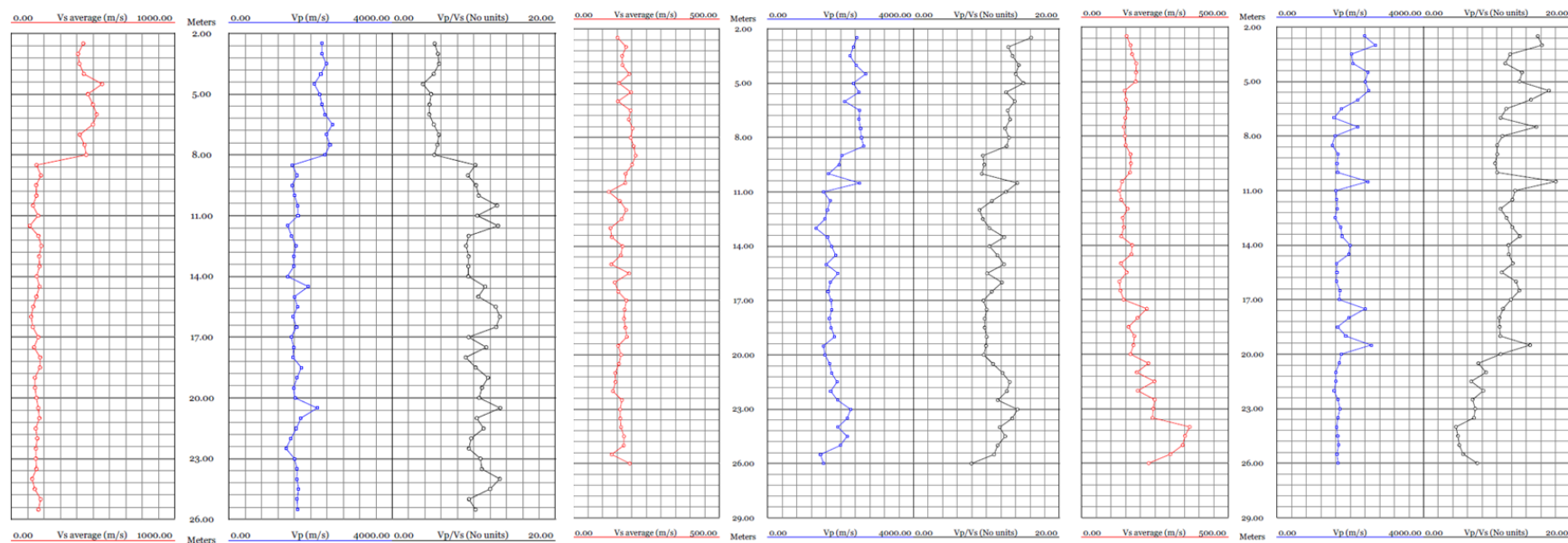


Figure 4.29 P-S suspension logging results for station BUHZ for three boreholes, from left to right:  $V_S$ ,  $V_P$  and the  $V_P/V_S$  ratio.



## 4.3.8 Synthesis

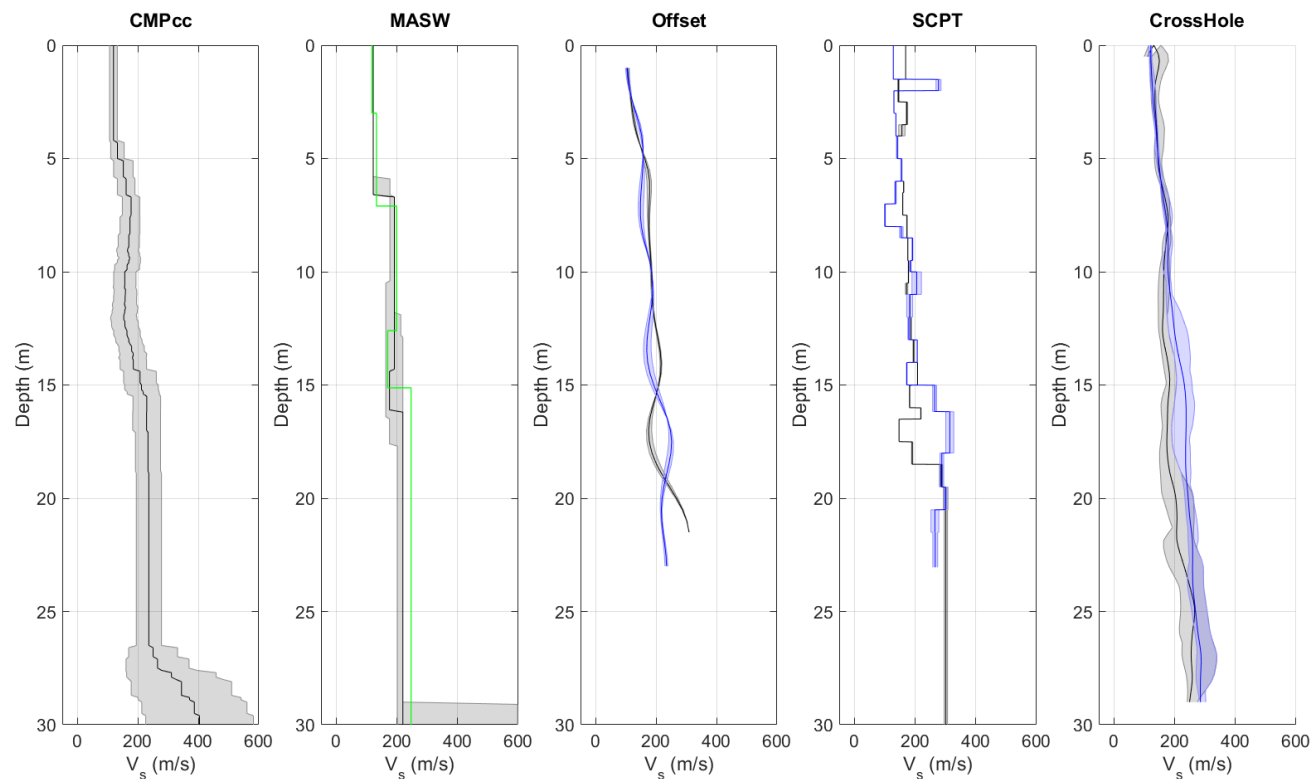


Figure 4.30  $V_s$  profiles from different measurement techniques, including uncertainty bands. From left to right: CMPcc based on active MASW array, shaded band indicates standard deviation; active MASW with manual fit in green and automatic inversion in black with grey shaded band indicating the minimum and the maximum  $V_s$ ; average profile for offset SCPTs between 1 and 5 m offset for 1 or 2 SCPTs with shaded band indicating the minimum and the maximum  $V_s$ ; SCPTs with band indicating variation between left and right blow; cross-hole average profiles for long leg in blue and short leg in grey with shaded band indicating the minimum and the maximum  $V_s$ .

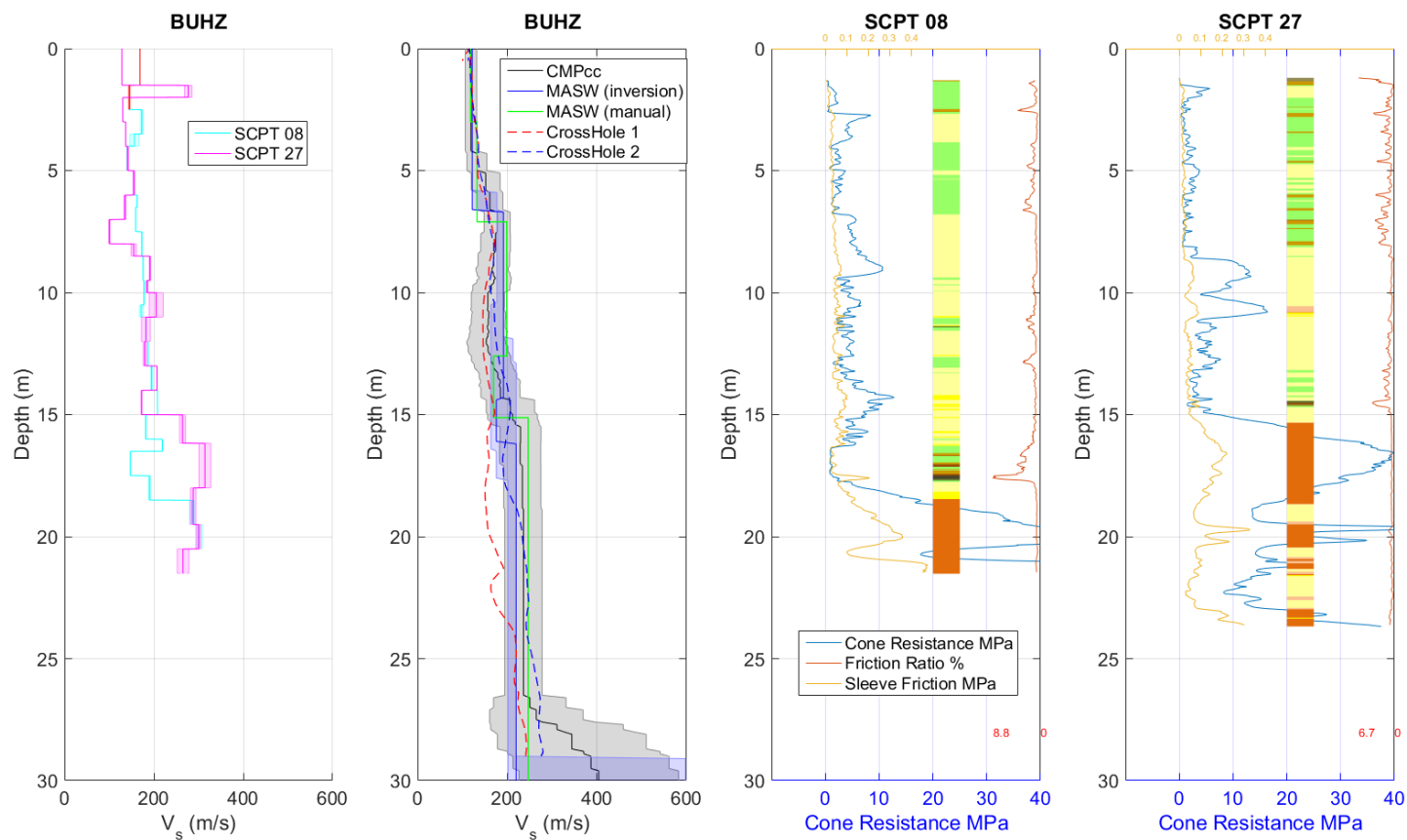


Figure 4.31 Synthesis of  $V_s$  results. Unreliable results are shown in red. From left to right: SCPT with band indicating variation between left and right blow; CMPcc, MASW and average cross-hole results with uncertainty bands; CPT with cone resistance, friction ratio, sleeve friction and automatically generated lithology (indication, for legend see Table 3.1).

## 4.4 Westeremden- BWSE

### 4.4.1 Location

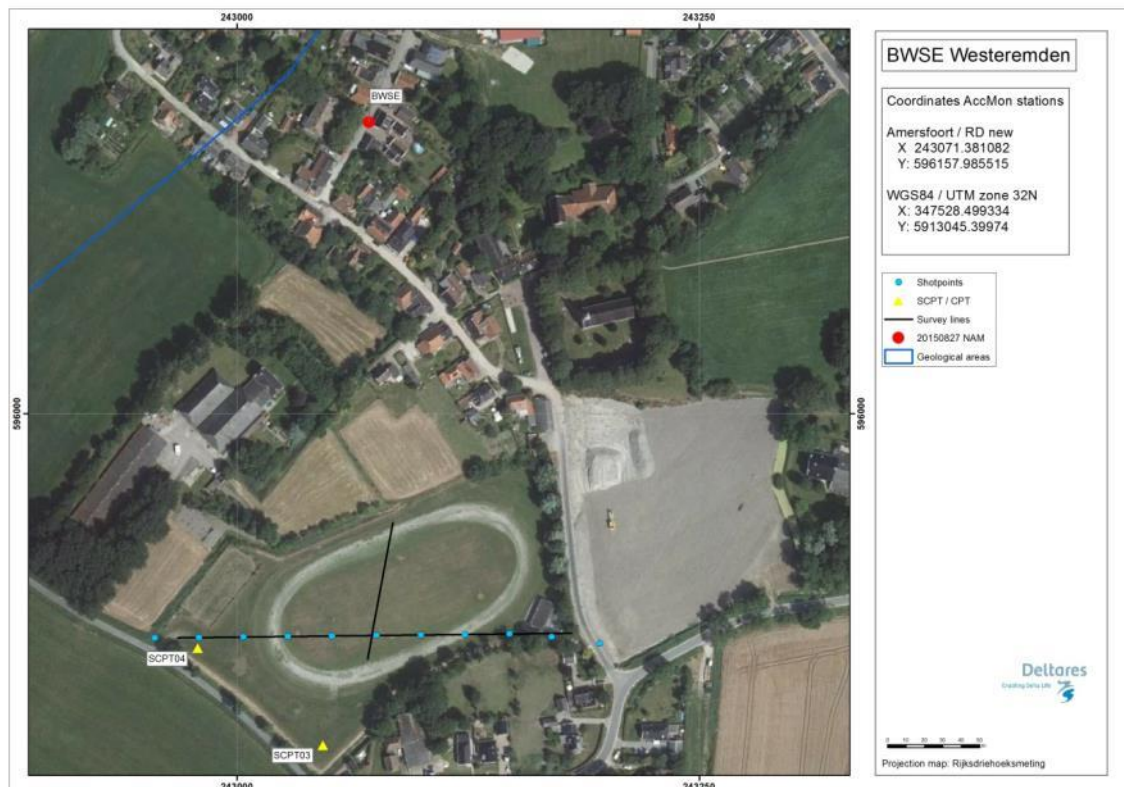


Figure 4.32 Map of location BWSE, showing the KNMI accelerograph station, SCPT location and MASW survey lines and shot locations.

### 4.4.2 Geological setting

The location is situated in a narrow Holocene erosive valley with a width of approximately 800 metres. The depth of the valley is 12 metres southwest of the location and deepening up to approximately 20 metres to the northeast.

The Holocene fill of the valley is in the southwest in majority clay and to the northeast a mix of sand and clay. In the non-erosive surrounding area, the basal peat is found on the top of the Pleistocene. The accelerograph is positioned either within or just outside this Holocene valley.

The site is positioned outside of the Peelo valley.

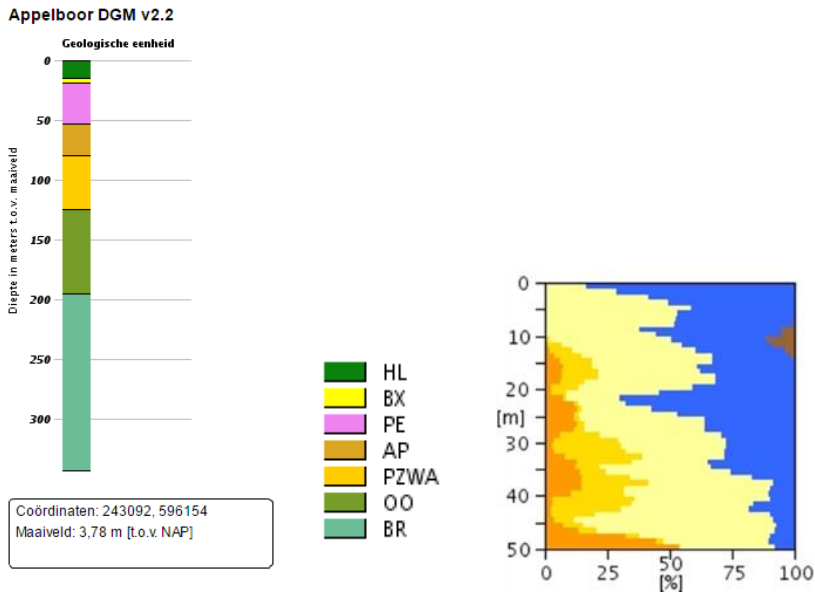


Figure 4.33 Geological information at station BWSE. Left: 1D section from the DGM model. Right: Section from the “delfstoffen online” model (GDN-TNO). Colour coding: brown = peat, blue = clay, yellow to orange = fine sand to coarse sand. The horizontal scale shows the volume percentage of each of the lithologies present at the location, the vertical scale is depth below the surface.

Table 4.4 Descriptions of representative deep boreholes near station BWSE from the DINO database ([www.dinoloket.nl](http://www.dinoloket.nl)).

Drilling	Distance from drilling	top	bottom	sediment type	Min. grain size	Max. grain size	Formation
B07E0048	2000mtr NE	1,30	-3,70	Clay			Formation of Naaldwijk
		-3,70	-15,00	Sand	Extreme fine		Formation of Naaldwijk
		-15,00	-17,20	Sand	Medium coarse	Extreme coarse	Formation of Naaldwijk/Eem
		-17,20	-26,20	Clay			Formation of Peelo
		-26,20	-59,70	Sand	Medium fine	Medium coarse	Formation of Peelo

1210624-000-BGS-0007, Version 2, 27 June 2016, final

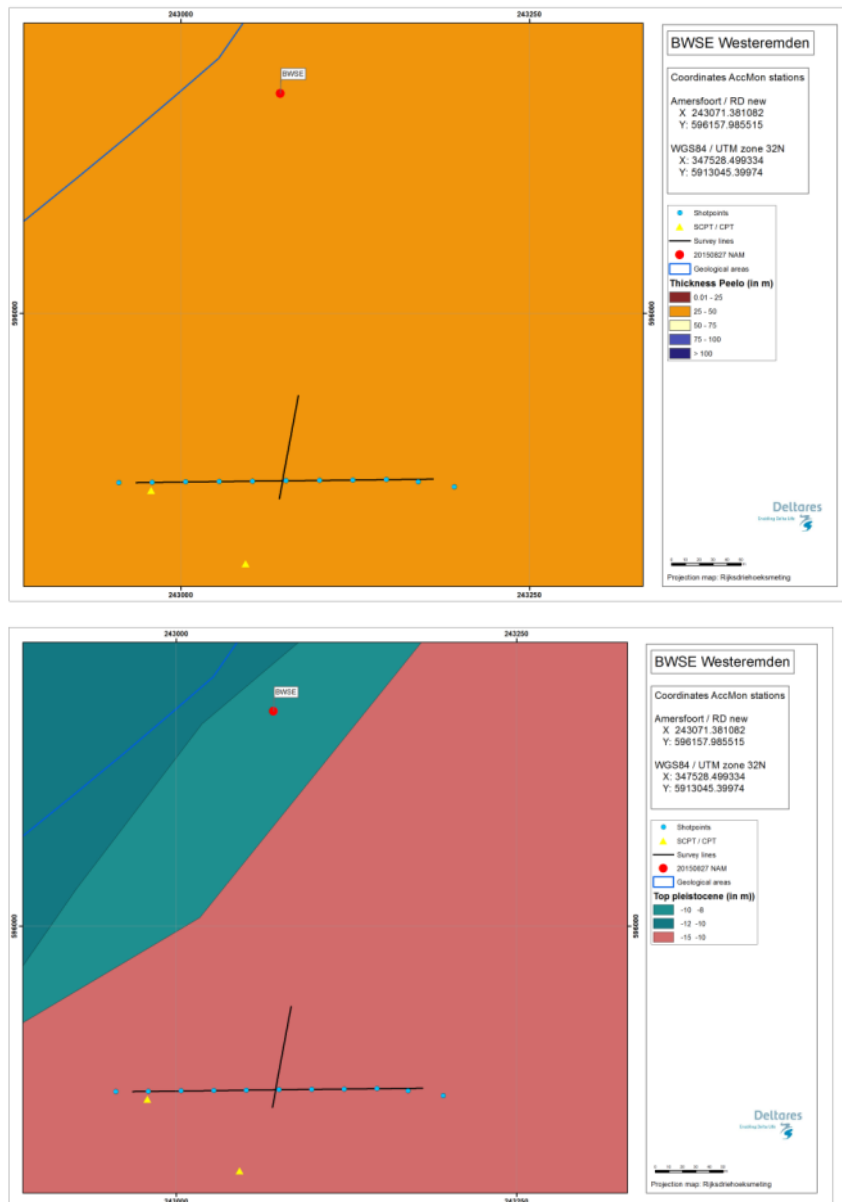


Figure 4.34 Overview map of geological setting based on beta version of GeoTOP model. Top panel: Thickness of the Peelo Formation, blue colour indicates thick Peelo layer, hence in the centre of the channel; red and orange colour indicates thin Peelo layers, hence areas outside the channel; yellow indicates transition zone. Lower panel: Top of Pleistocene surface relative to Dutch Ordnance Datum NAP.

## 4.4.3 SCPT

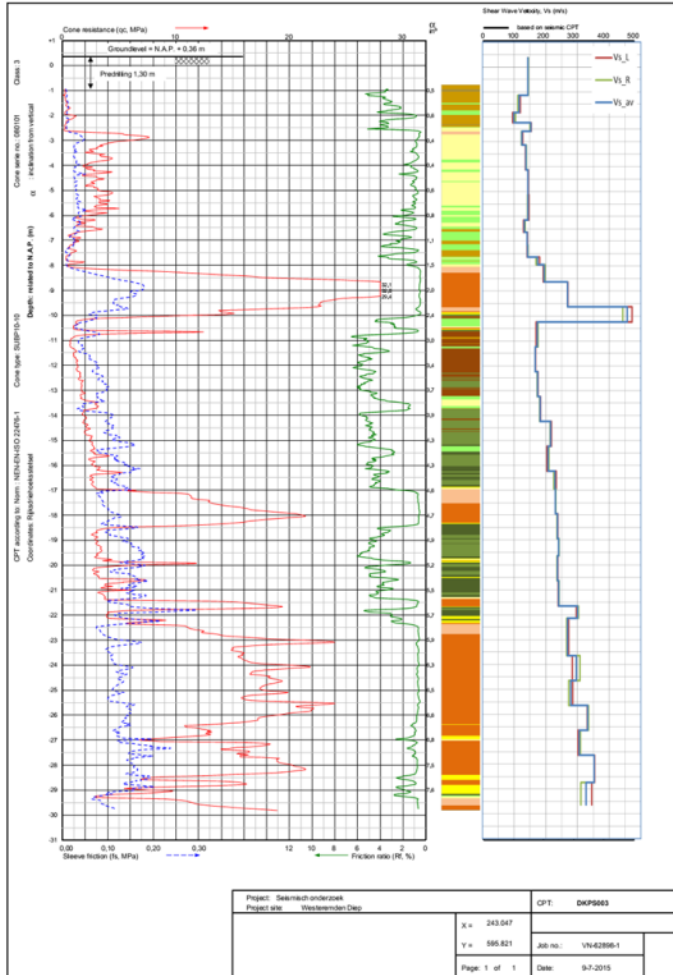


Figure 4.35 SCPT03. From left to right: CPT measurement, showing tip resistance, sleeve friction and friction ratio; automatically generated lithology (indication, for legend see Table 3.1); Vs profile (red = left blow, green = right blow, blue = average).

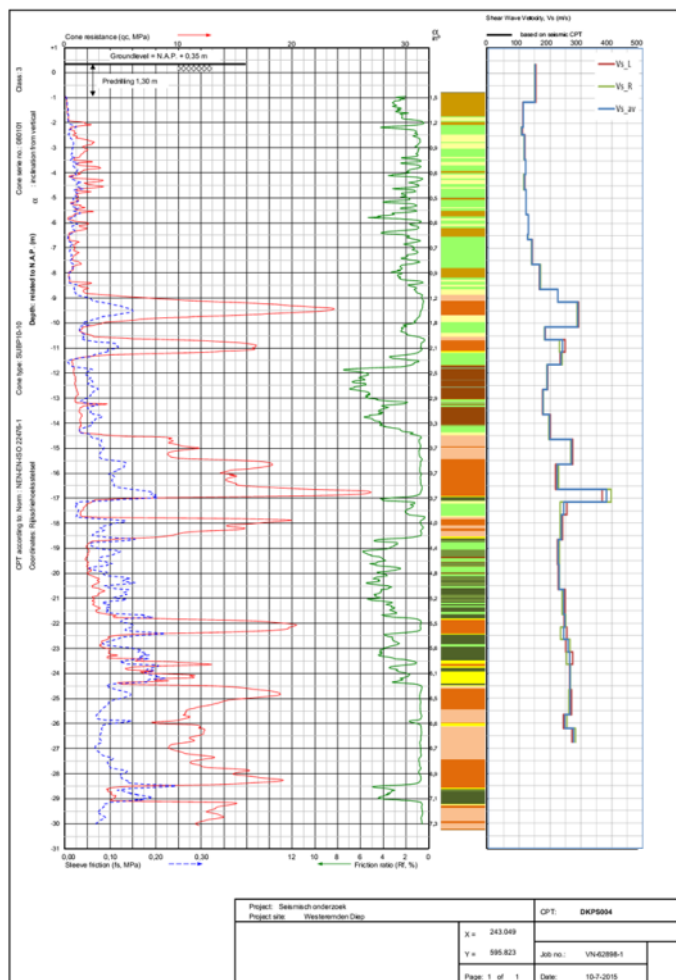


Figure 4.36 SCPT04. From left to right: CPT measurement, showing tip resistance, sleeve friction and friction ratio; automatically generated lithology (indication, for legend see Table 3.1);  $V_s$  profile (red = left blow, green = right blow, blue = average).

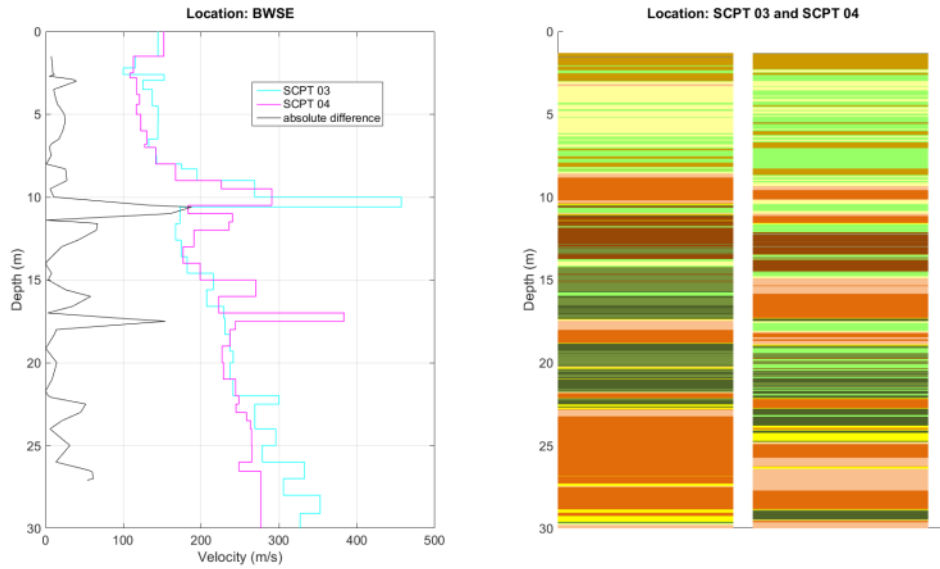


Figure 4.37 Station BWSE. Left: Difference between the two SCPTs measured at the same station location. Right: automatically generated lithology (indication).

## 4.4.4 OSCPT

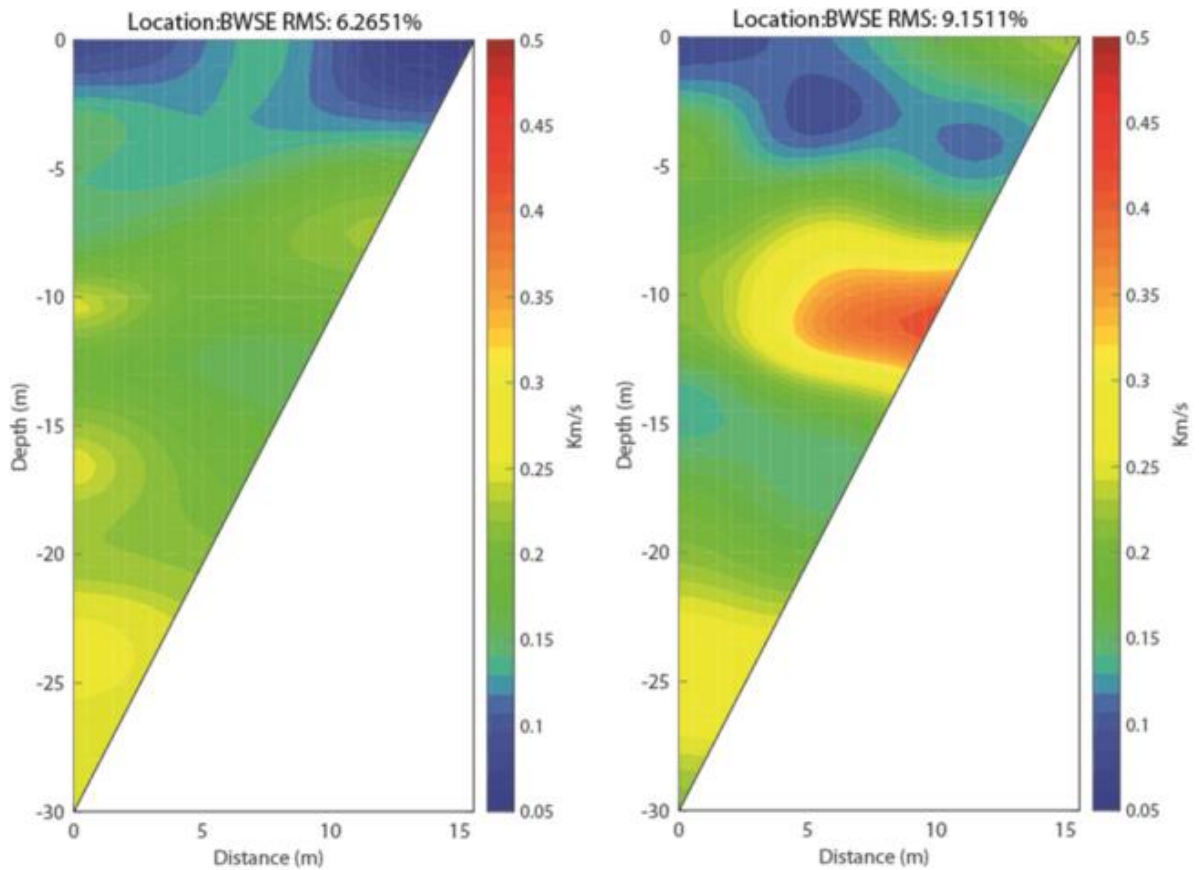


Figure 4.38 Tomographic images based on OSCPT results from two SCPTs for station BWSE (left SCPT04; right SCPT03).

## 4.4.5 MASW

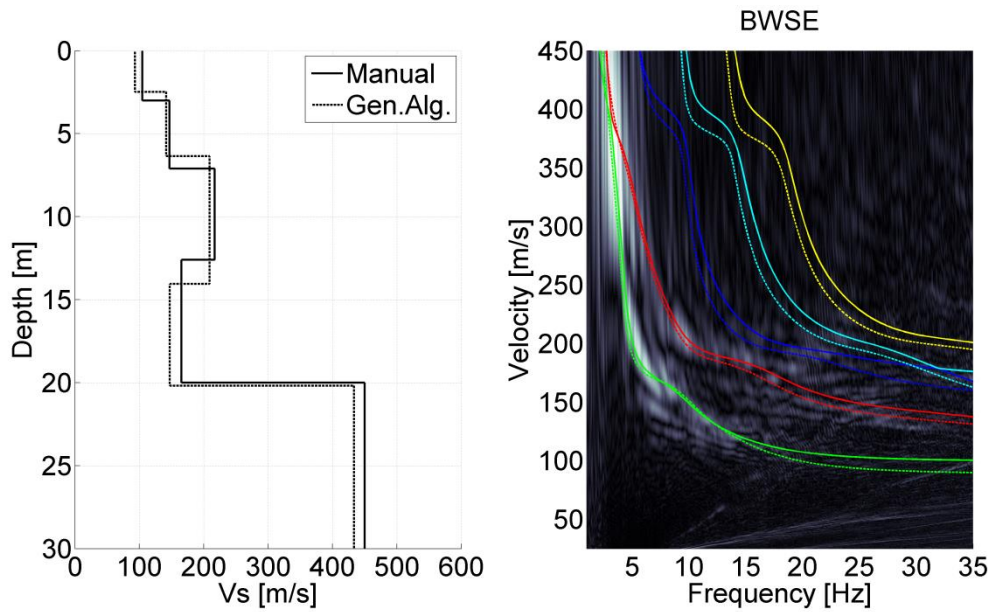


Figure 4.39 MASW result for station BWSE. Left panel:  $V_s$  profiles from active MASW. Solid line from manual fitting of dispersion curves; dashed line for automatic inversion. Right panel: energy in the dispersion plot in greyscale; solid lines are the modelled dispersion curves for different modes of the manually fitted  $V_s$  profile; dashed lines for the different modes of the automatically inverted  $V_s$  profile.

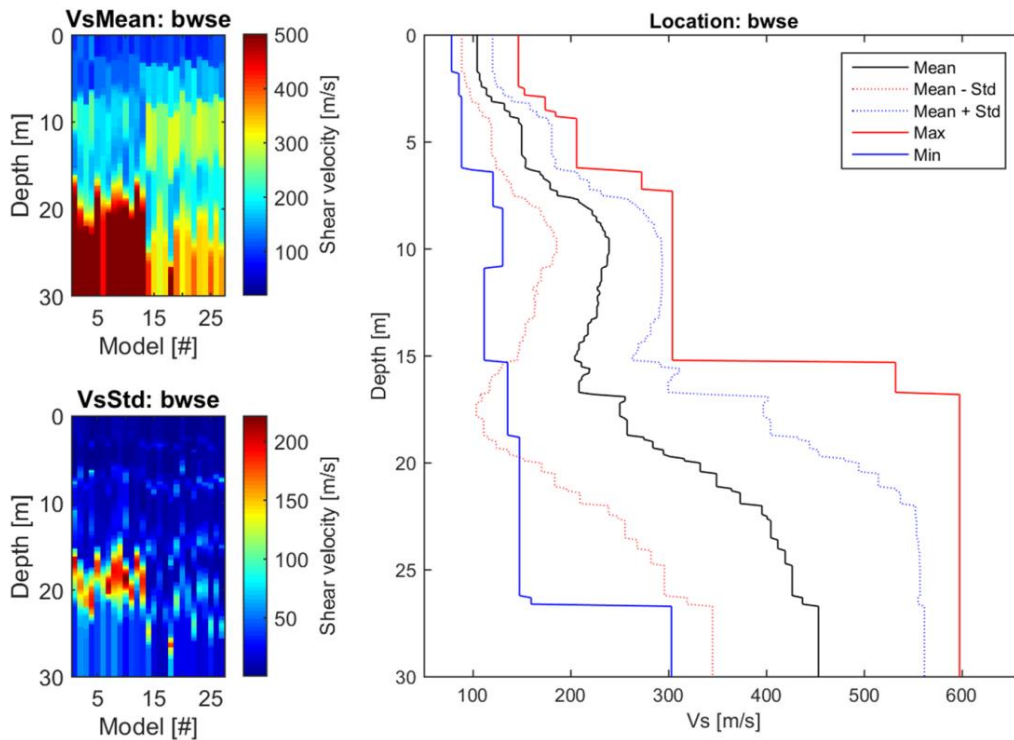


Figure 4.40 CMPcc result for BWSE. Top left: average  $V_s$  along the CMPcc array. Bottom left: standard deviation of  $V_s$  along the CMPcc array. Right: best fit curve of the 72 models with the maximum and minimum value observed in the whole CMPcc and the standard deviation from all models.

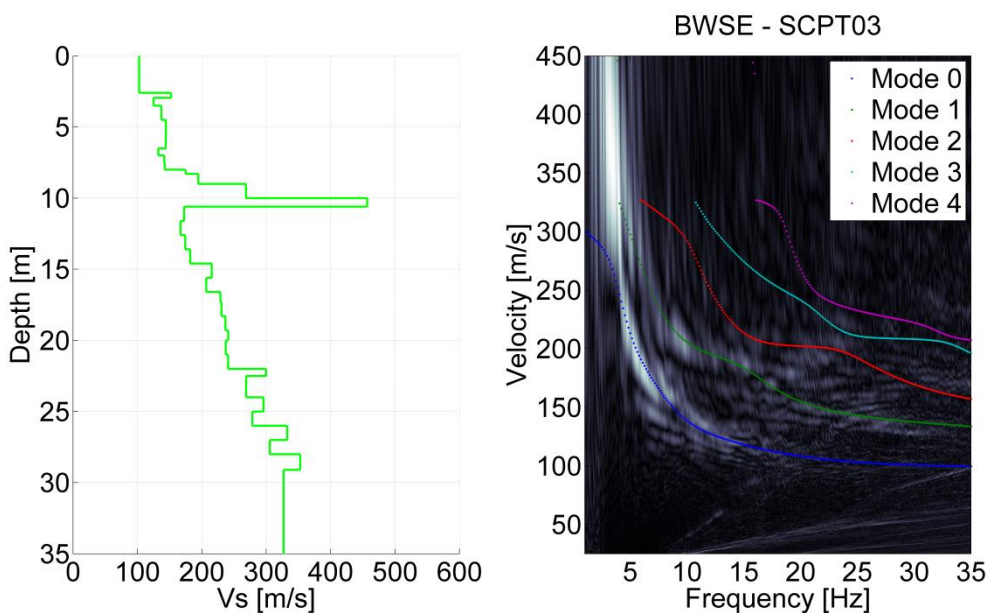


Figure 4.41 Comparison for BWSE of SCPT03 and MASW result. Left:  $V_s$  profile from SCPT. The  $V_s$  from the top 2 layers of the SCPT is generally unreliable and replaced by the minimum  $V_s$  of the first 3 layers. Right: modelled dispersion curves of different modes based on the SCPT  $V_s$  profile in coloured lines plotted on the energy of MASW dispersion plot in greyscale.

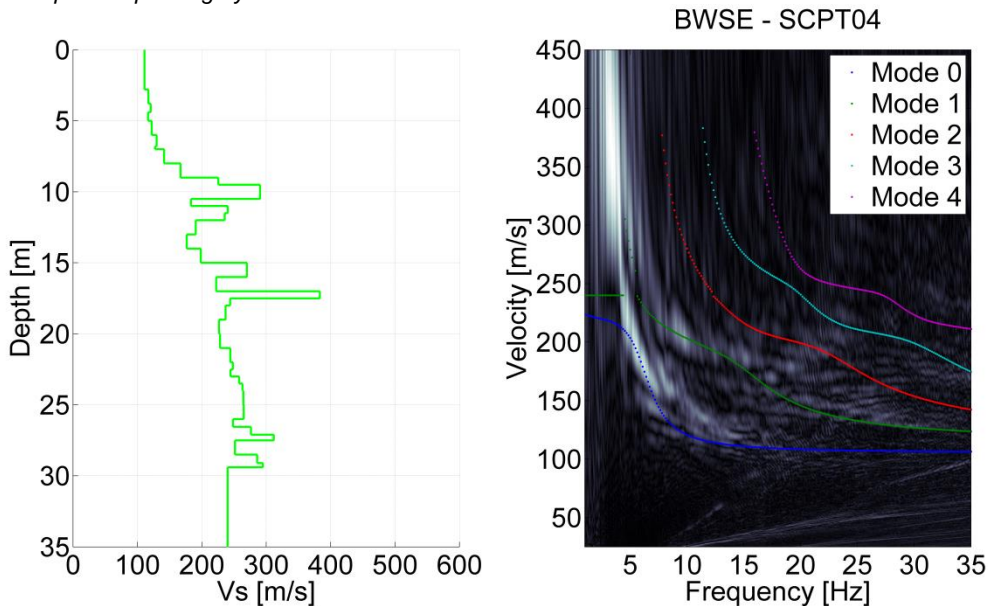


Figure 4.42 Comparison for BWSE of SCPT04 and MASW result. Left:  $V_s$  profile from SCPT. The  $V_s$  from the top 2 layers of the SCPT is generally unreliable and replaced by the minimum  $V_s$  of the first 3 layers. Right: modelled dispersion curves of different modes based on the SCPT  $V_s$  profile in coloured lines plotted on the energy of MASW dispersion plot in greyscale.

## 4.4.6 Cross-hole Tomography

The data is very good to excellent, both tomograms show a major increase in velocity at around -9 to -10 metres, this transition represents is the base of the Holocene deposits. The S-wave tomogram suggests more heterogeneity than the P-wave tomogram. The high velocity zone in the P wave tomogram around -3 to -5 metre depth coincides with a sand layer in the otherwise soft Holocene top layer. This zone is not visible in the S-wave panel.

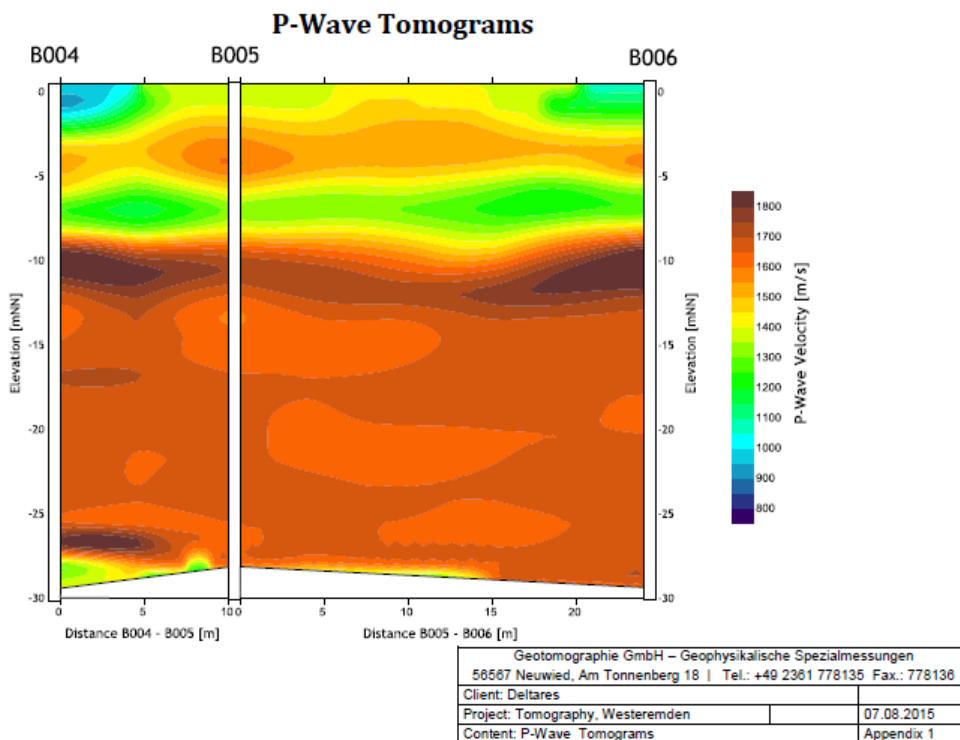


Figure 4.43  $V_P$  tomogram for station BWSE, from Geotomographie. The cross section in the figure has an L shape in the field (see Figure 2.13): the short leg (left) is perpendicular to the long leg of the borehole setup (right). B numbers indicate the borehole code.

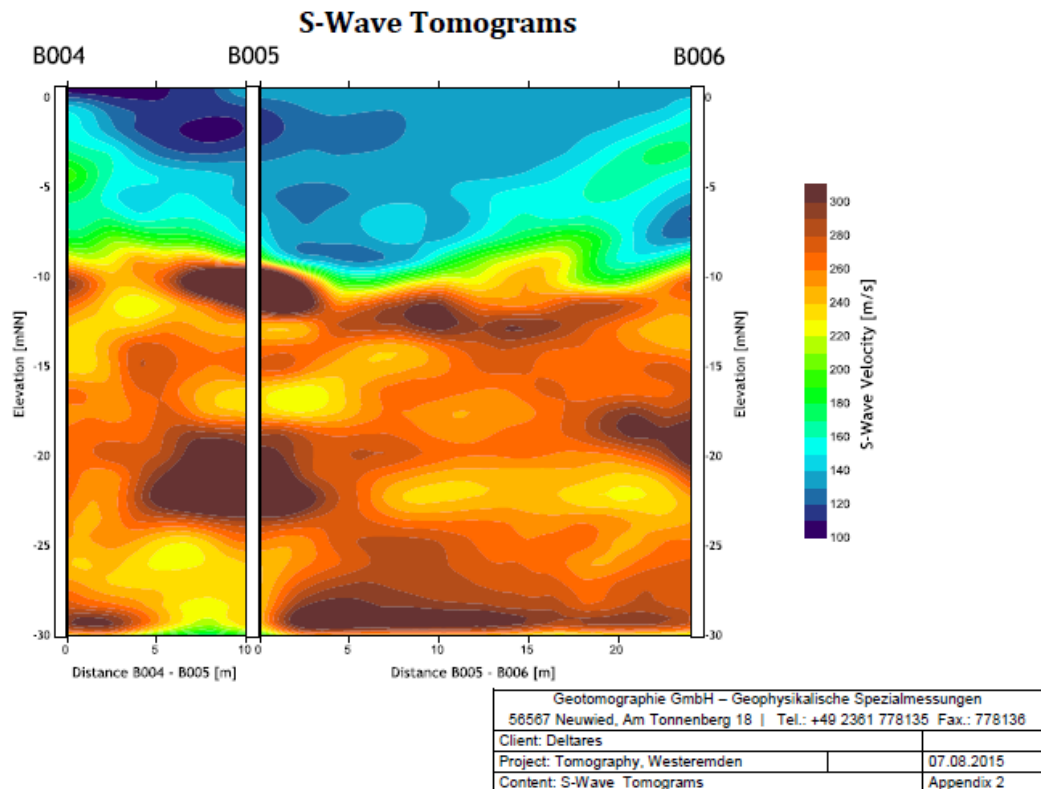


Figure 4.44  $V_S$  tomogram for station BWSE, from Geotomographie. The cross section in the figure has an L shape in the field (see Figure 2.13): the short leg (left) is perpendicular to the long leg of the borehole setup (right). B numbers indicate the borehole code

#### 4.4.7 P-S suspension logging

The quality of the suspension logging is low, the resulting values are probably not representative. The trends in both P and S wave velocities are not comparable to that of the other techniques used in this project.



1210624-000-BGS-0007, Version 2, 27 June 2016, final

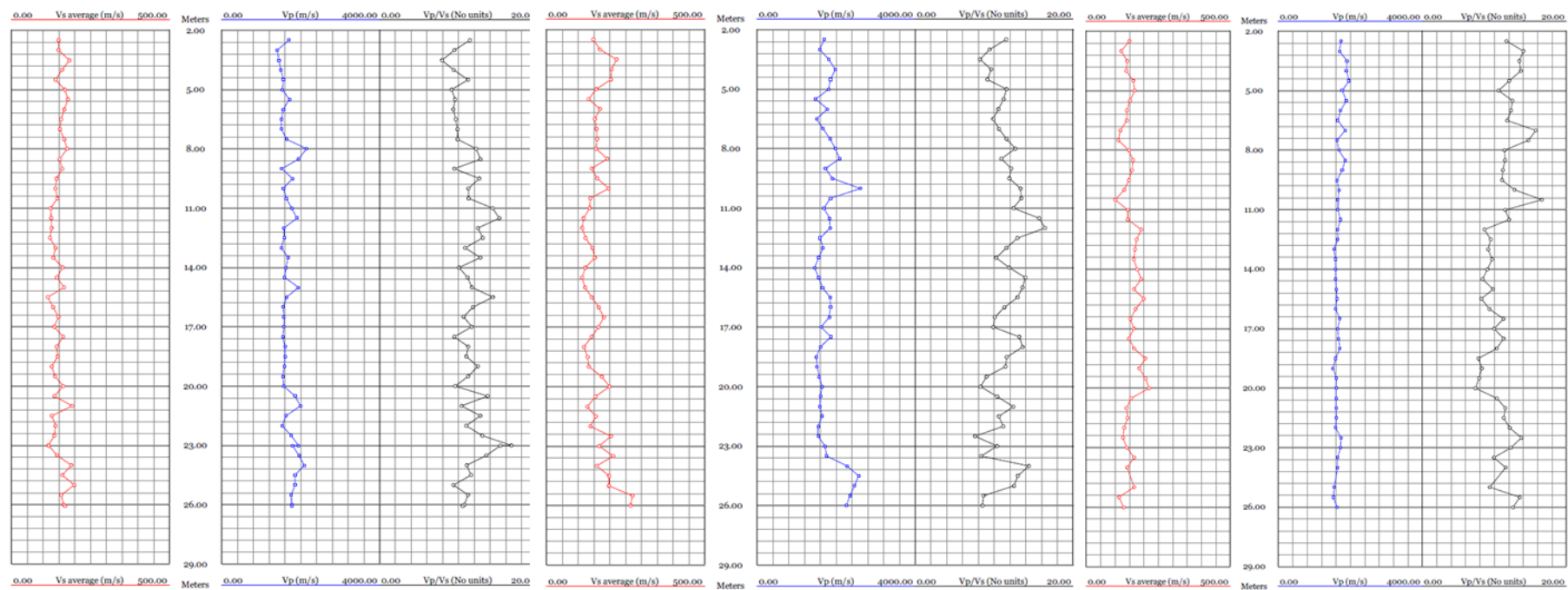


Figure 4.45 P-S suspension logging results for station BWSE for three boreholes, from left to right:  $V_S$ ,  $V_P$  and the  $V_P/V_S$  ratio.



## 4.4.8 Synthesis

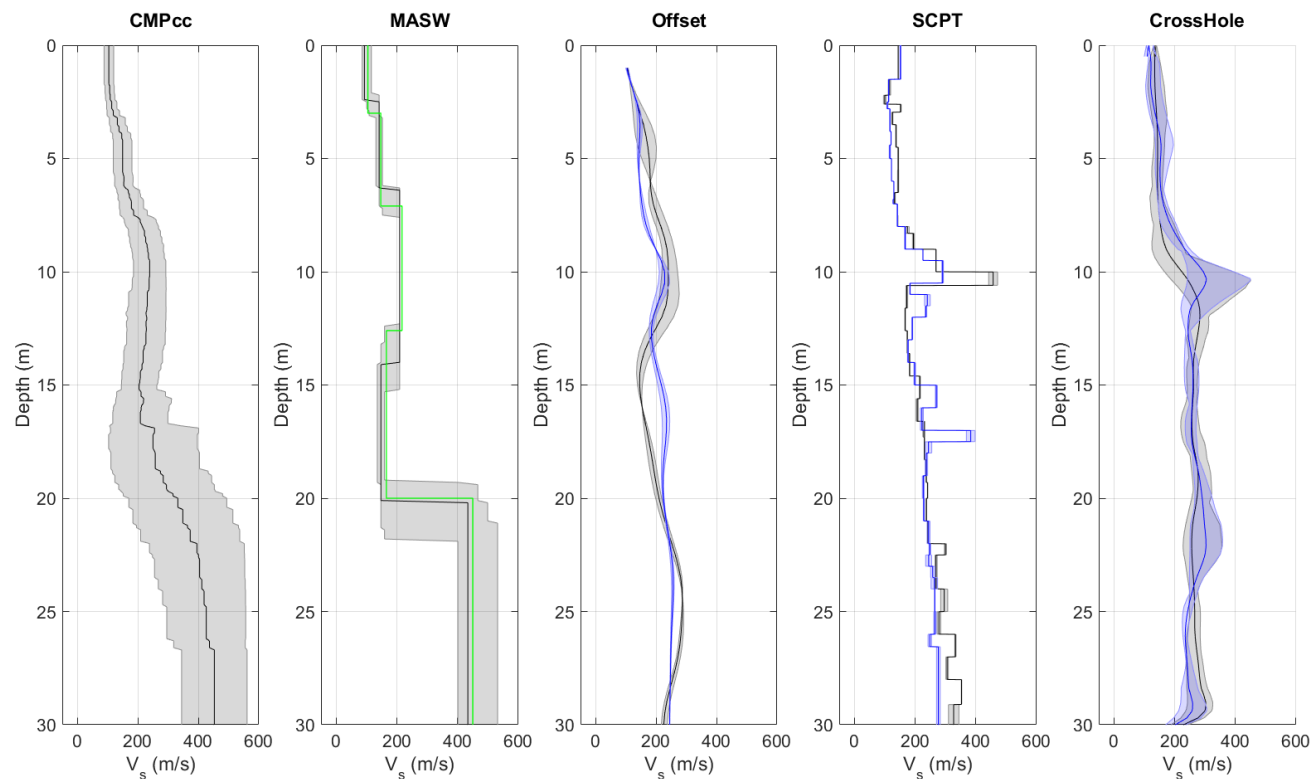


Figure 4.46  $V_s$  profiles from different measurement techniques, including uncertainty bands. From left to right: CMPcc based on active MASW array, shaded band indicates standard deviation; active MASW with manual fit in green and automatic inversion in black with grey shaded band indicating the minimum and the maximum  $V_s$ ; average profile for offset SCPTs between 1 and 5 m offset for 1 or 2 SCPTs with shaded band indicating the minimum and the maximum  $V_s$ ; SCPTs with band indicating variation between left and right blow; cross-hole average profiles for long leg in blue and short leg in grey with shaded band indicating the minimum and the maximum  $V_s$ .

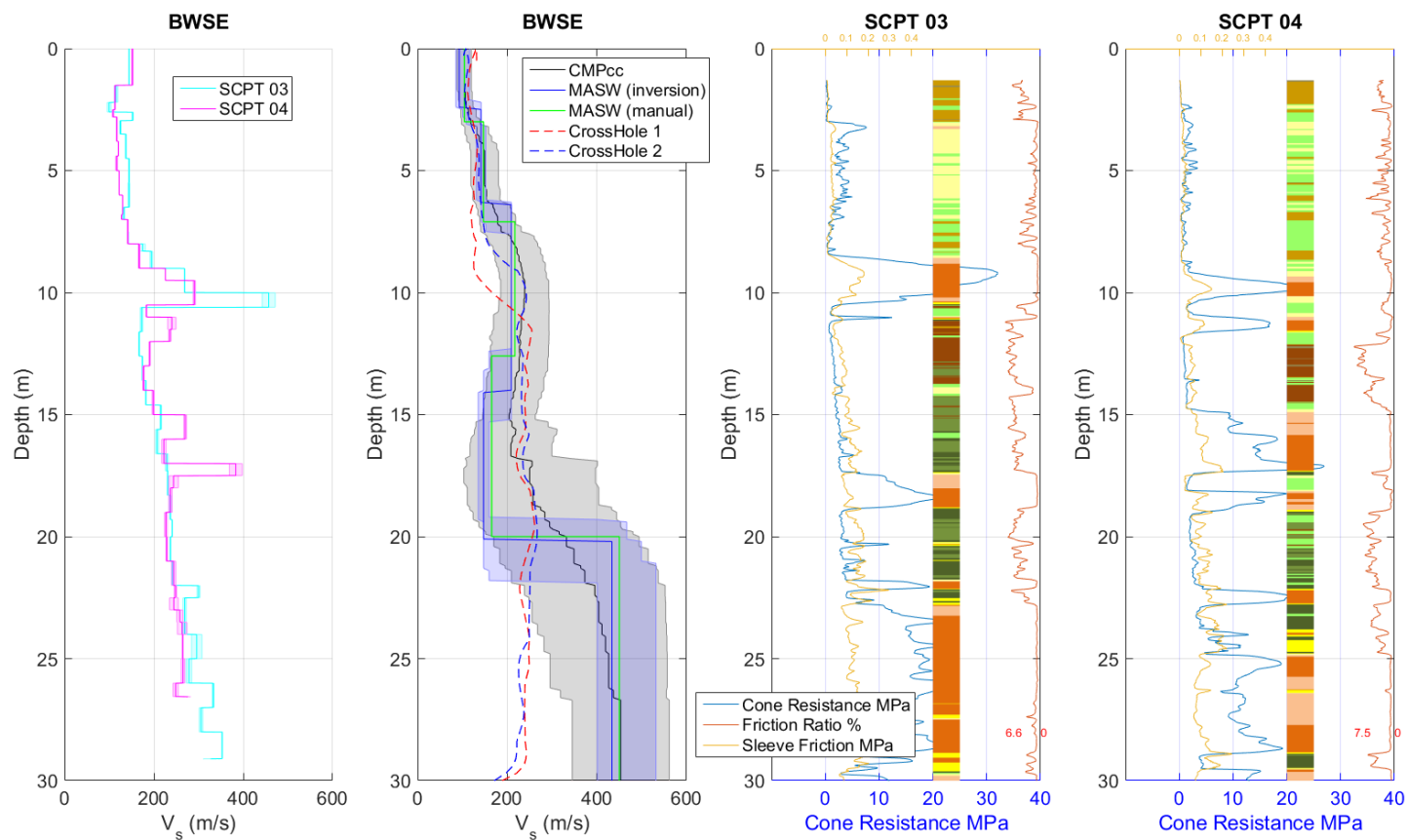


Figure 4.47 Synthesis of  $V_s$  results. Unreliable results are shown in red. From left to right: SCPT with band indicating variation between left and right blow; CMPcc, MASW and average cross-hole results with uncertainty bands; CPT with cone resistance, friction ratio, sleeve friction and automatically generated lithology (indication, for legend see Table 3.1).

## 4.5 Kolham- BFB2

### 4.5.1 Location

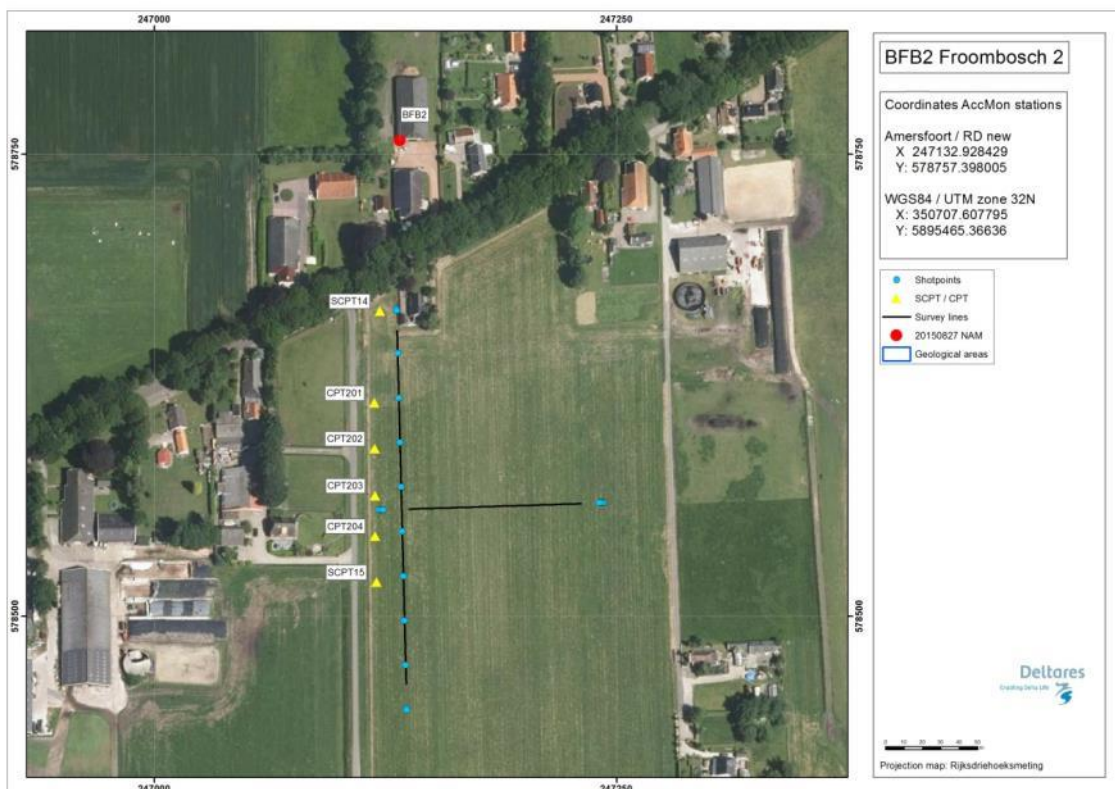


Figure 4.48 Map of location BFB2, showing the KNMI accelerograph station, SCPT location and MASW survey lines and shot locations.

### 4.5.2 Geological setting

The location is situated in an area with cover sand (Boxtel Formation) at the surface. There are no Holocene deposits present.

Locally some thin peat layers can be found at or near the surface.

The location is situated on a declining slope of a Peelo valley that reaches from 78 metres at the location up to a maximum depth of 100 metres in the centre of the valley, over a distance of 1 kilometre to the southwest.

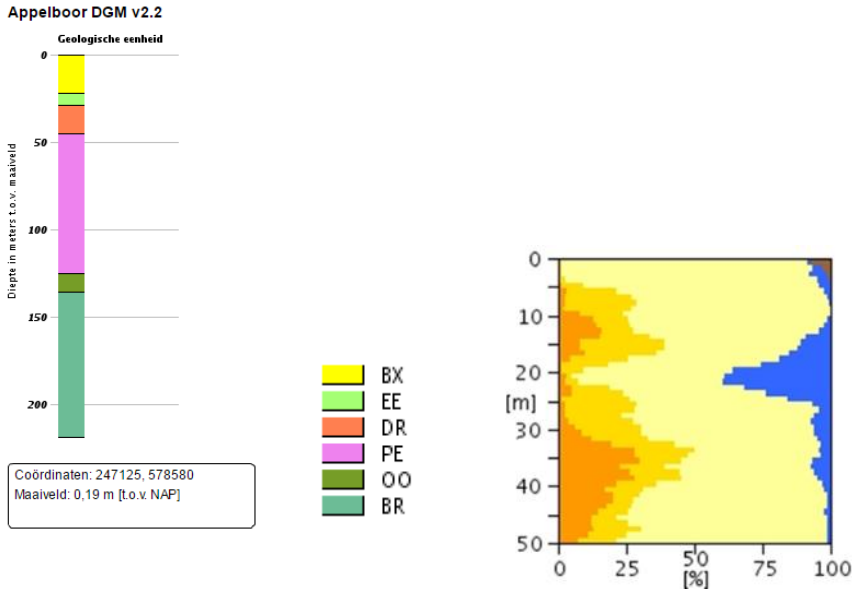


Figure 4.49 Geological information at station BFB2. Left: 1D section from the DGM model. Right: Section from the “delfstoffen online” model (GDN-TNO). Colour coding: brown = peat, blue = clay, yellow to orange = fine sand to coarse sand. The horizontal scale shows the volume percentage of each of the lithologies present at the location, the vertical scale is depth below the surface.

Table 4.5 Descriptions of representative deep boreholes near station BFB2 from the DINO database ([www.dinoloket.nl](http://www.dinoloket.nl)).

Drilling	Distance from drilling	top	bottom	sediment type	Min. grain size	Max. grain size	Formation
B07G0175	2900mtr SE	-1,50	-19,50	Sand	Very fine	Medium fine	Formation of Boxtel
		-19,50	-24,50	Clay			Eem Formation
		-24,50	-35,50	Sand	Medium fine	Medium coarse	Eem Formation
		-35,50	-38,50	Gravel	coarse		Formation of Drente
		-38,50	-39,50	Clay			Formation of Drente
		-39,50	-45,50	Sand	Very fine	Medium fine	Formation of Drente
		-45,50	-49,50	Sand	Extreme coarse	Gravel	Formation of Peelo
		-49,50	-52,50	Sand	Medium fine	Medium coarse	Formation of Peelo
		-52,50	-59,50	Sand	Very coarse	Extreme coarse	Formation of Peelo
		-59,50	-61,50	Clay			Formation of Peelo
		-61,50	-114,50	Sand	Extreme coarse	Gravel	Formation of Peelo
		-114,50	-137,50	Sand	Very coarse	Gravel	Formation of Peize
		-137,50	-140,50	Sand	fine		Formation of Peize
		-140,50	-150,50	Sand	Medium coarse	Extreme coarse	Formation of Peize
		-150,50	-206,50	Sand	Medium fine		Formation of Peize/Oosterhout
B07G0097	1900mtr SE	0,70	-20,93	Sand	Medium fine		Formation of Boxtel
		-20,93	-22,43	Clay			Eem Formation
		-22,43	-27,93	Sand	Medium fine		Formation of Boxtel
		-27,93	-33,93	Sand	Extreme coarse		Formation of Drente
		-33,93	-82,93	Sand	Medium fine	Medium coarse	Formation of Peelo/Peize
		-82,93	-88,43	Clay			Formation of Peize
		-88,43	-136,73	Sand	Very fine	Medium fine	Formation of Oosterhout
		-136,73	-143,93	Clay			Formation of Oosterhout
		-143,93	-148,43	Sand	Medium fine		Formation of Oosterhout
		-148,43	-152,93	Clay			Formation of Oosterhout
		-152,93	-160,93	Sand	Medium fine		Formation of Oosterhout
		-160,93	-175,43	Clay			Formation of Breda

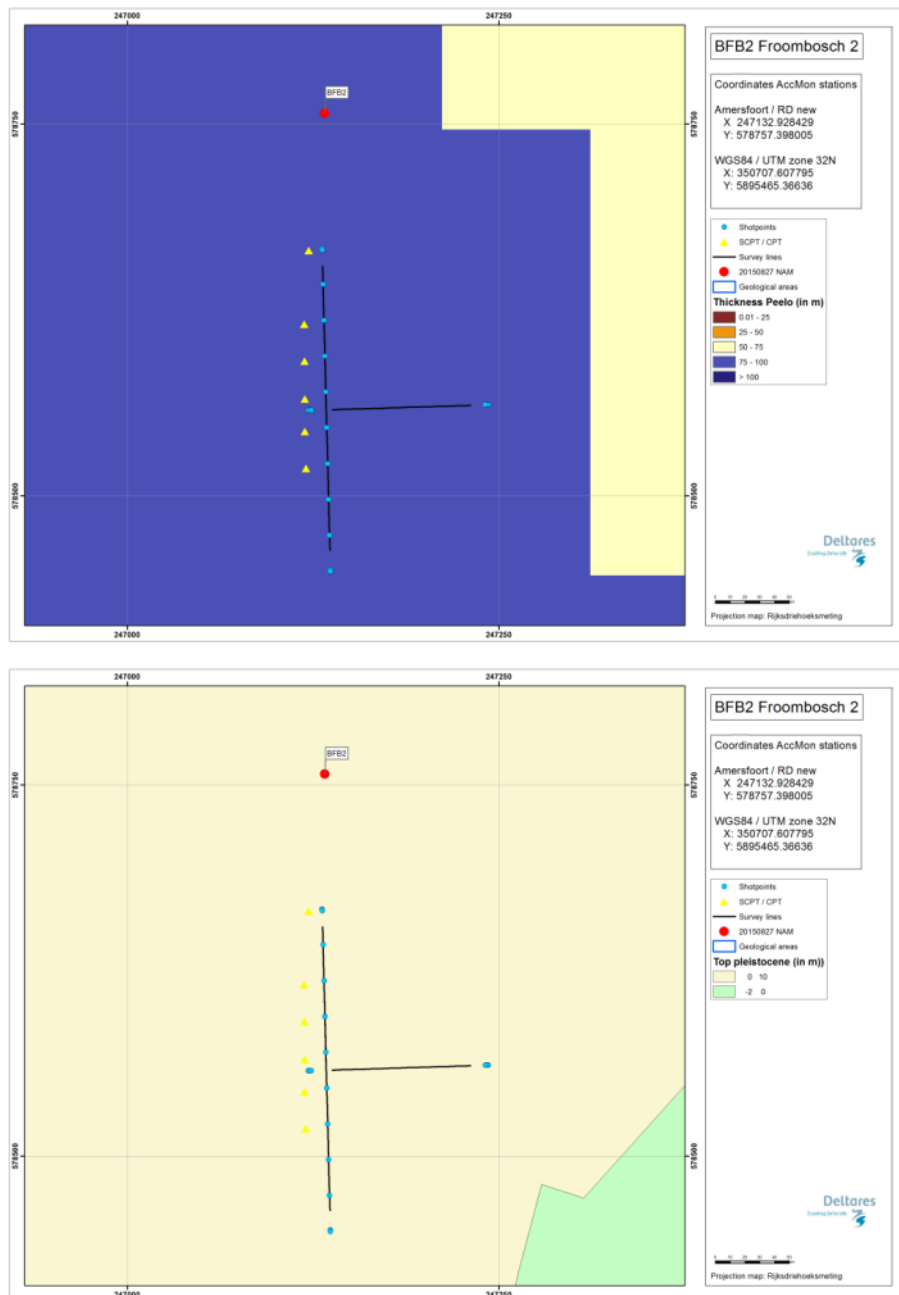


Figure 4.50 Overview map of geological setting based on beta version of GeoTOP model. Top panel: Thickness of the Peelo Formation, blue colour indicates thick Peelo layer, hence in the centre of the channel; red and orange colour indicates thin Peelo layers, hence areas outside the channel; yellow indicates transition zone. Lower panel: Top of Pleistocene surface relative to Dutch Ordnance Datum NAP.

## 4.5.3 SCPT

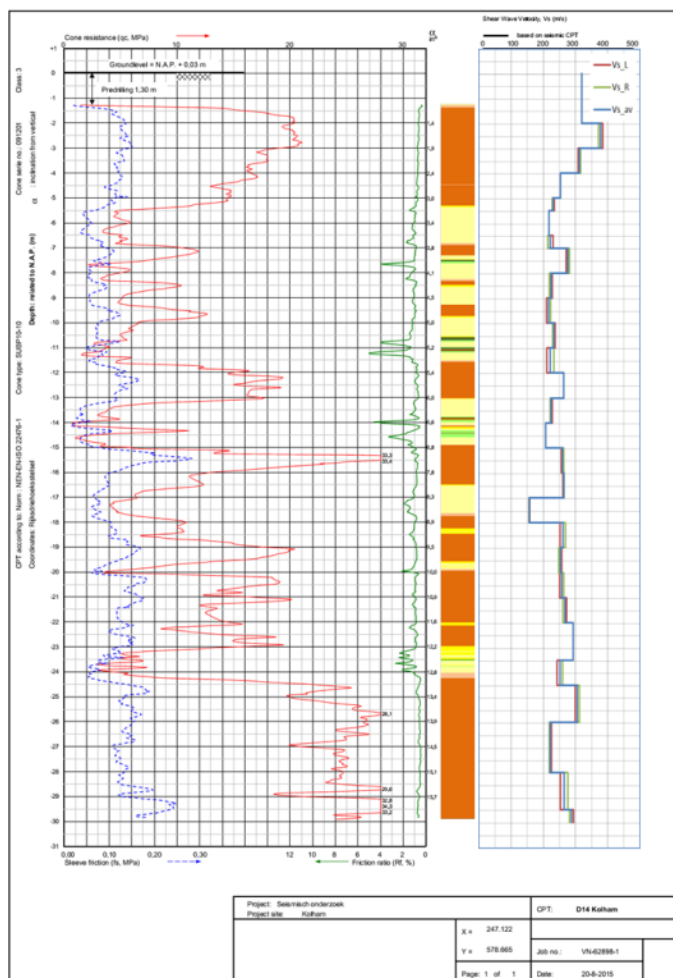


Figure 4.51 SCPT14. From left to right: CPT measurement, showing tip resistance, sleeve friction and friction ratio; automatically generated lithology (indication, for legend see Table 3.1);  $V_s$  profile (red = left blow, green = right blow, blue = average).

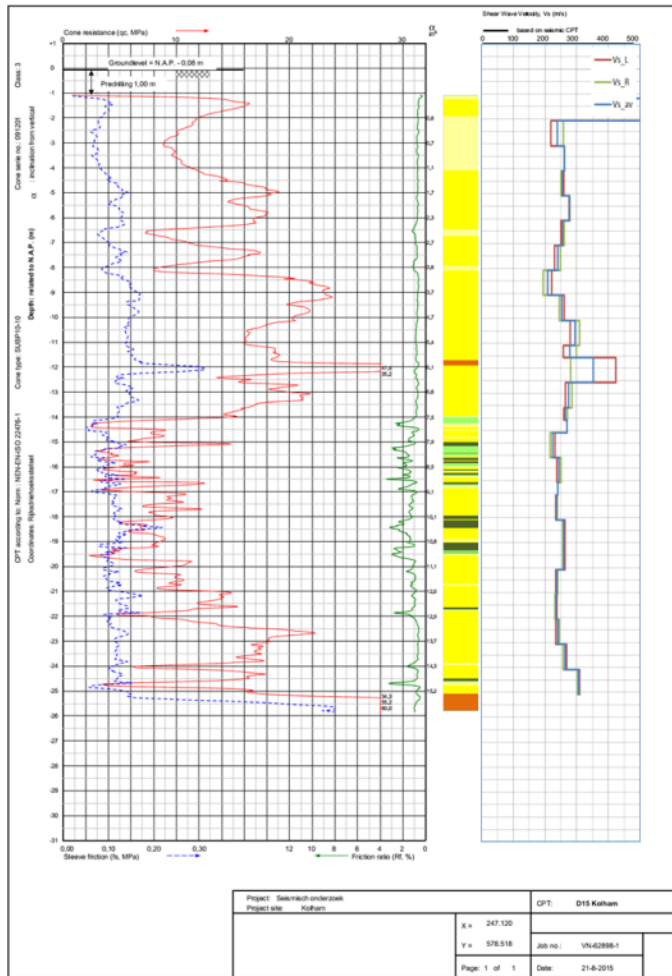


Figure 4.52 SCPT15. From left to right: CPT measurement, showing tip resistance, sleeve friction and friction ratio; automatically generated lithology (indication, for legend see Table 3.1);  $V_s$  profile (red = left blow, green = right blow, blue = average).

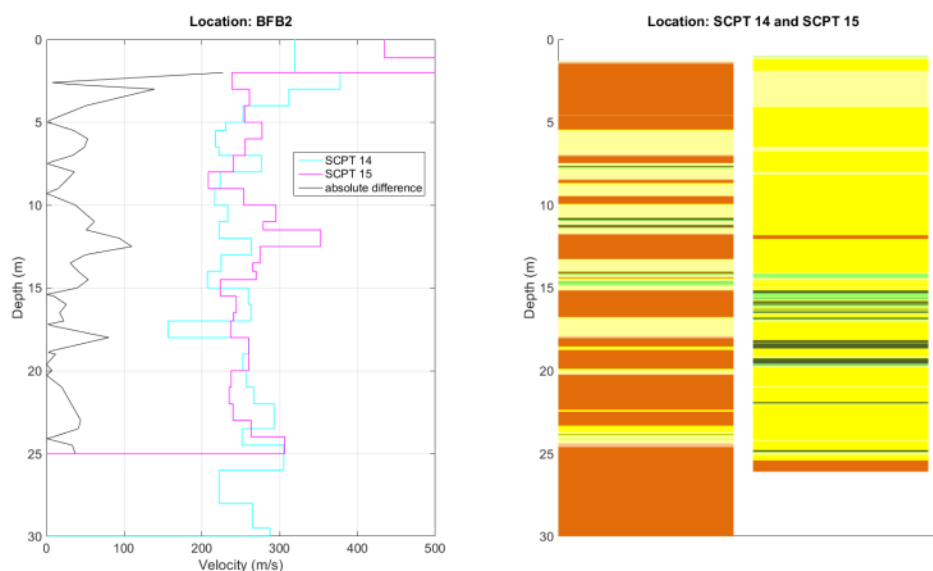


Figure 4.53 Station BFB2. Left: Difference between the two SCPTs measured at the same station location. Right: automatically generated lithology (indication).

### Subsoil variability

At each location, the different site investigation techniques cover an area of at least 100 m in diameter. In some cases, the accelerometer station is not within this area of investigation due to logistical limitations.

To illustrate soil variability, a trajectory of 6 CPT over a horizontal distance 150 is measured at station BFB2 at Kolham. Based on the GeoTOP model and formation characteristics, we expect a simple, sand dominated Pleistocene succession. The preliminary analysis of the MASW data, however, indicated that the soil within the investigated depth range showed lateral variability. Therefore, two SCPTs were performed at both ends of the MASW line and 4 infill CPTs spread along the line. The SCPTs and CPTs are presented in Figure 4.54. The location of the 6 (S)CPTs is shown in Figure 4.55.

The vertical succession at this location consists of (from the top) Boxtel aeolian sand, Boxtel fluvial sand and clay and Eem marine sand. Lateral variability is apparent in two characteristics. As expected, the cone resistance of the sands varies laterally. The difference in stratification succession of the sand and clayey layers on this lateral scale is more surprising. The clay layer in CPT201 between 7 m and 9 m depth is not present in the other CPTs and seems to be a feature. The clayey layer below 15 m is less pronounced in SCPT14. The top of the Eem Formation is characterised by a sharp contrast in cone resistance, but the level varies between 24 and 27 m depth. Additionally, SCPT14 lacks this contrast. Moreover, at this location it seems that a correlation between cone resistance and  $V_s$  is rather poor.

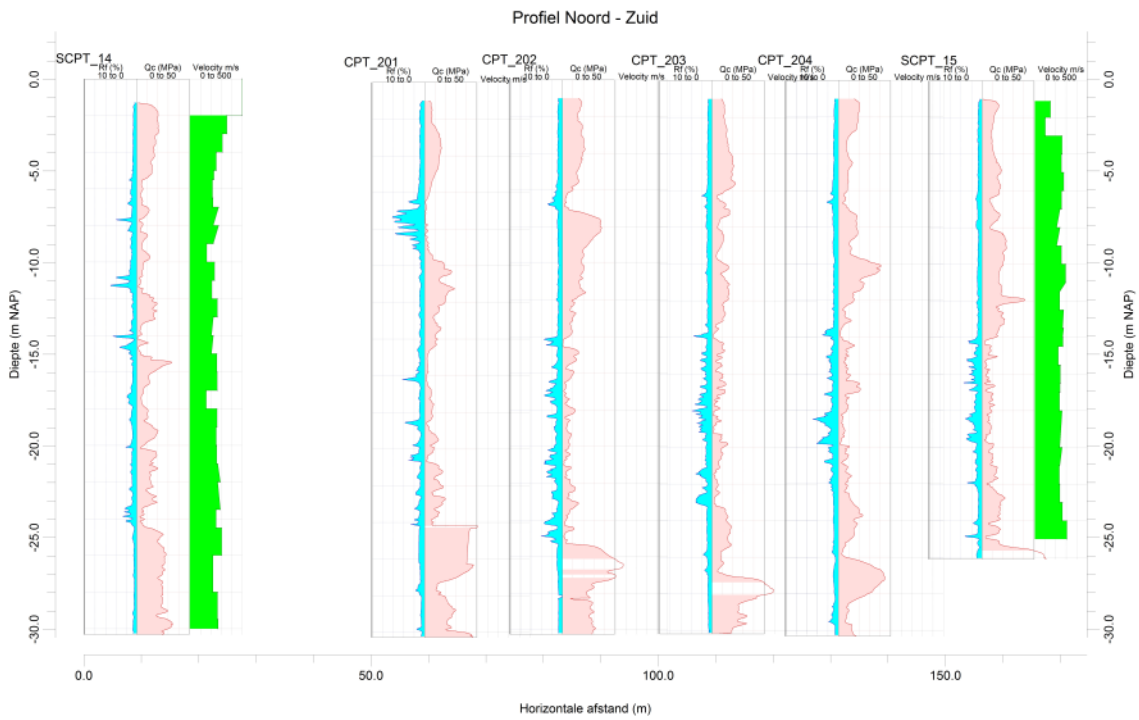


Figure 4.54 CPT profiles covering a horizontal distance of 150 m at station BFB2 to illustrate lateral subsoil variability. Holocene strata are absent at this location.



Figure 4.55 Location of (S)CPTs at station BFB2

## 4.5.4 OSCPT

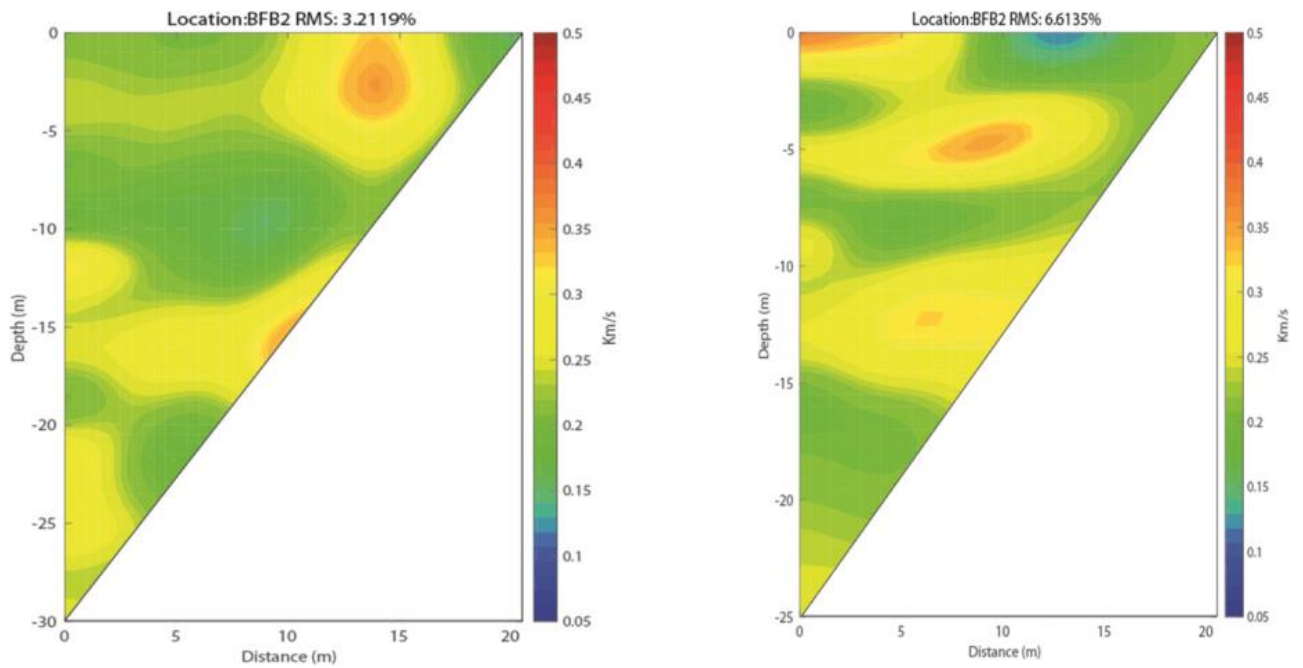


Figure 4.56 Tomographic images based on OSCPT results from two SCPTs for station BFB2 (left SCPT14; right SCPT15).

## 4.5.5 MASW

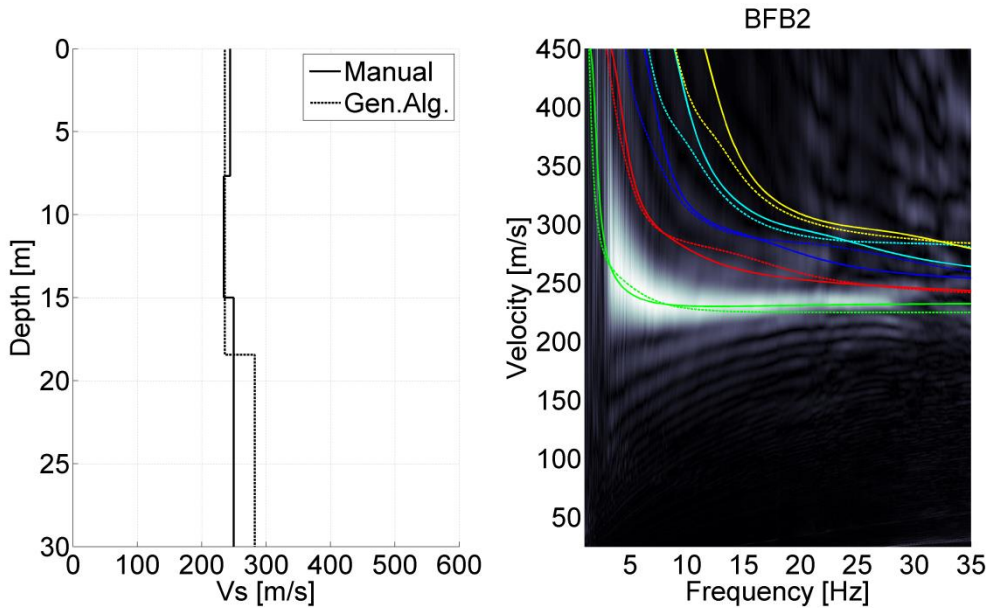


Figure 4.57 MASW result for station BFB2. Left panel:  $V_s$  profiles from active MASW. Solid line from manual fitting of dispersion curves; dashed line for automatic inversion. Right panel: energy in the dispersion plot in greyscale; solid lines are the modelled dispersion curves for different modes of the manually fitted  $V_s$  profile; dashed lines for the different modes of the automatically inverted  $V_s$  profile.

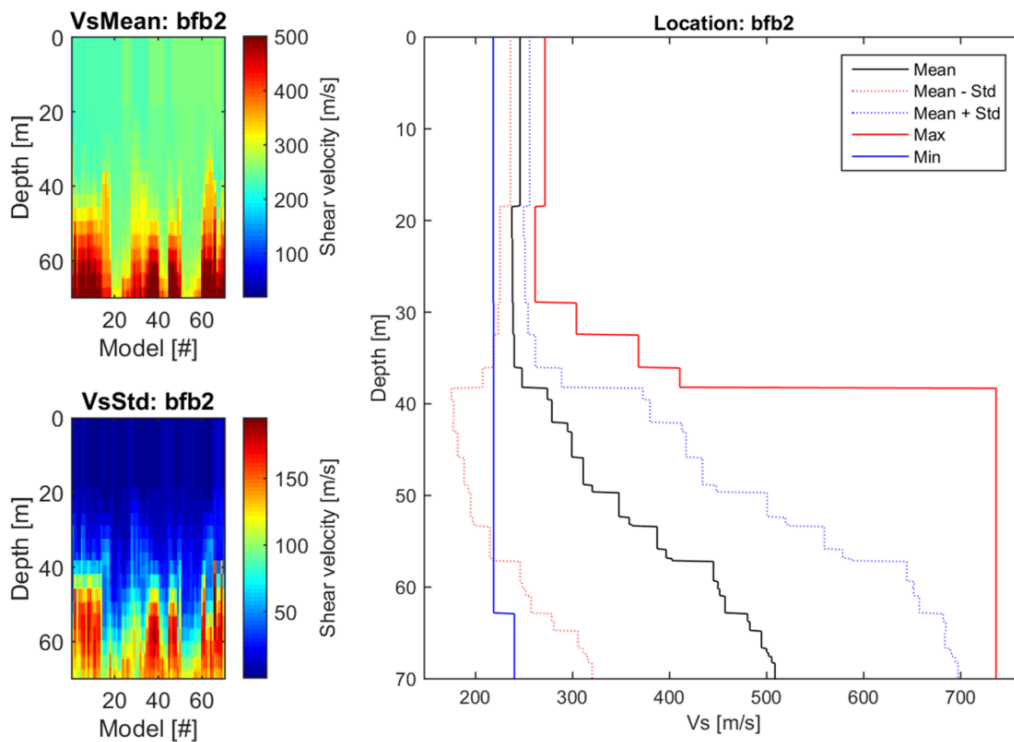


Figure 4.58 CMPcc result for BFB2. Top left: average  $V_s$  along the CMPcc array. Bottom left: standard deviation of  $V_s$  along the CMPcc array. Right: best fit curve of the 72 models with the maximum and minimum value observed in the whole CMPcc and the standard deviation from all models.

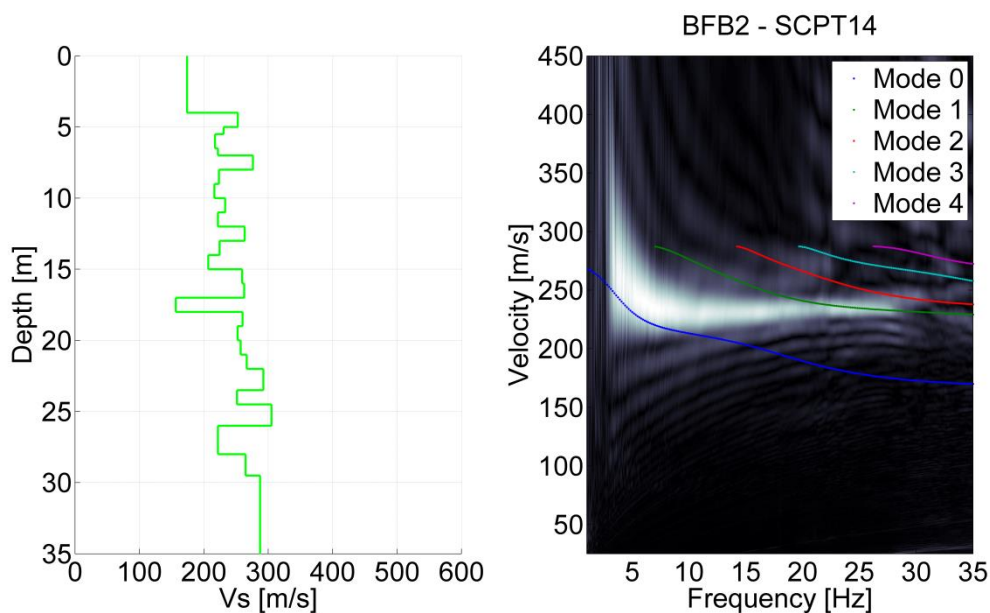


Figure 4.59 Comparison for BFB2 of SCPT14 and MASW result. Left:  $V_s$  profile from SCPT. The  $V_s$  from the top 2 layers of the SCPT is generally unreliable and replaced by the minimum  $V_s$  of the first 3 layers. Right: modelled dispersion curves of different modes based on the SCPT  $V_s$  profile in coloured lines plotted on the energy of MASW dispersion plot in greyscale.

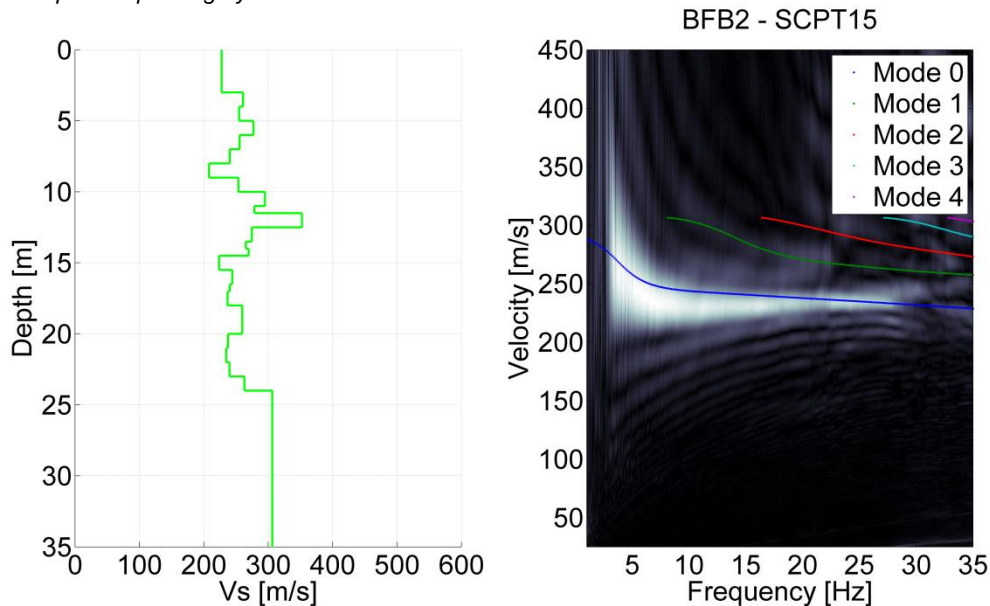


Figure 4.60 Comparison for BFB2 of SCPT15 and MASW result. Left:  $V_s$  profile from SCPT. The  $V_s$  from the top 2 layers of the SCPT is generally unreliable and replaced by the minimum  $V_s$  of the first 3 layers. Right: modelled dispersion curves of different modes based on the SCPT  $V_s$  profile in coloured lines plotted on the energy of MASW dispersion plot in greyscale.



## 4.5.6 Synthesis

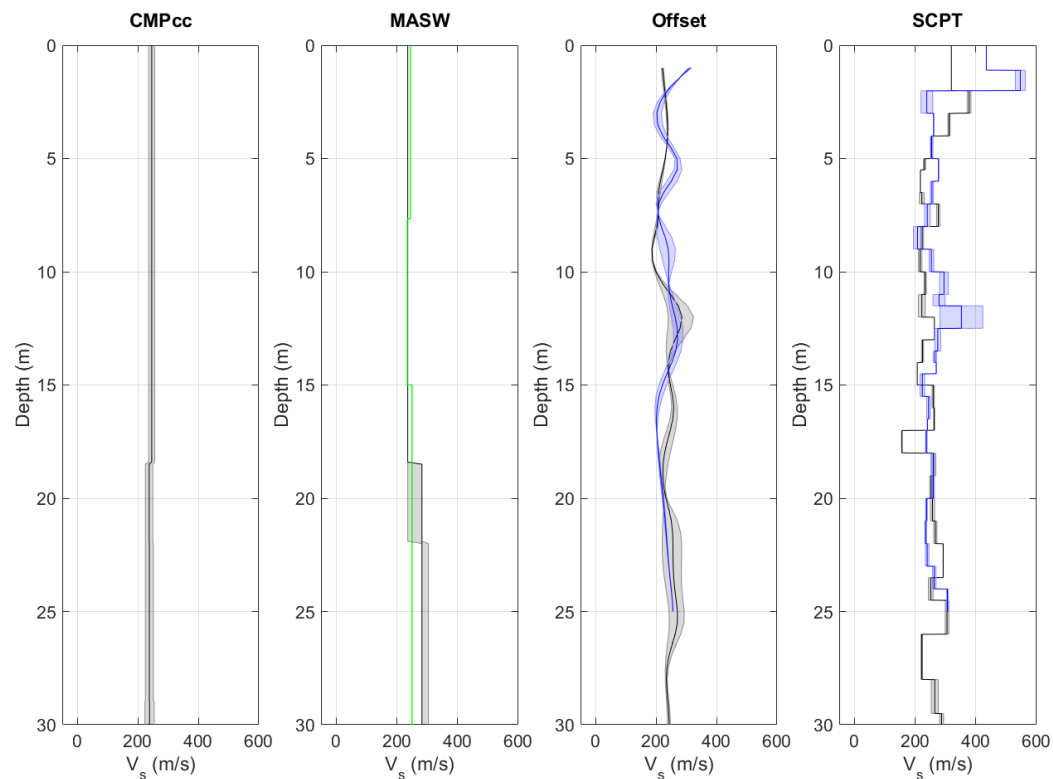


Figure 4.61  $V_s$  profiles from different measurement techniques, including uncertainty bands. From left to right: CMPcc based on active MASW array, shaded band indicates standard deviation; active MASW with manual fit in green and automatic inversion in black with grey shaded band indicating the minimum and the maximum  $V_s$ ; average profile for offset SCPTs between 1 and 5 m offset for 1 or 2 SCPTs with shaded band indicating the minimum and the maximum  $V_s$ ; SCPTs with band indicating variation between left and right blow; cross-hole average profiles for long leg in blue and short leg in grey with shaded band indicating the minimum and the maximum  $V_s$ .

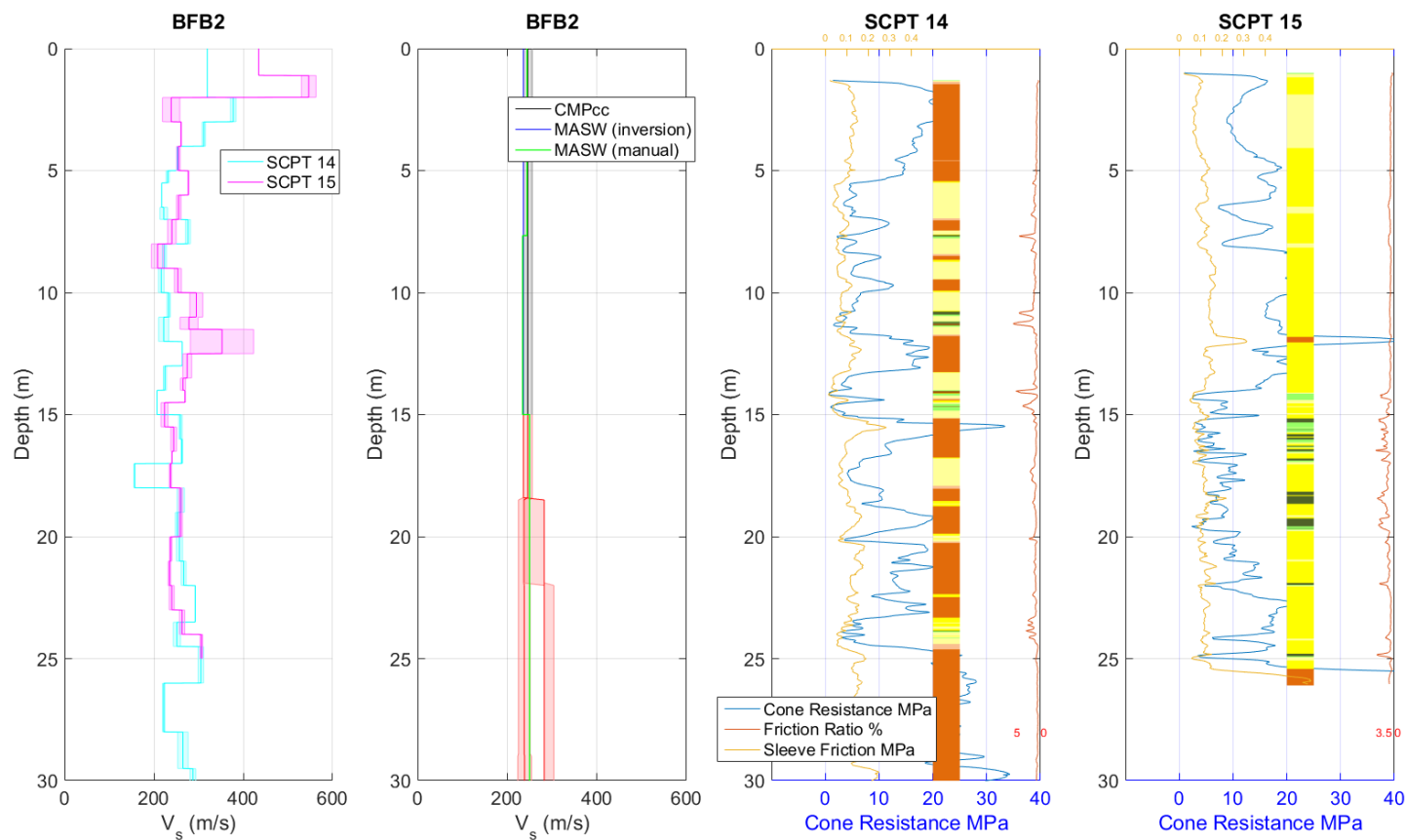


Figure 4.62 Synthesis of  $V_s$  results. Unreliable results are shown in red. From left to right: SCPT with band indicating variation between left and right blow; CMPcc, MASW and average cross-hole results with uncertainty bands; CPT with cone resistance, friction ratio, sleeve friction and automatically generated lithology (indication, for legend see Table 3.1).

## 4.6 Gartshuizen-BGAR

### 4.6.1 Location

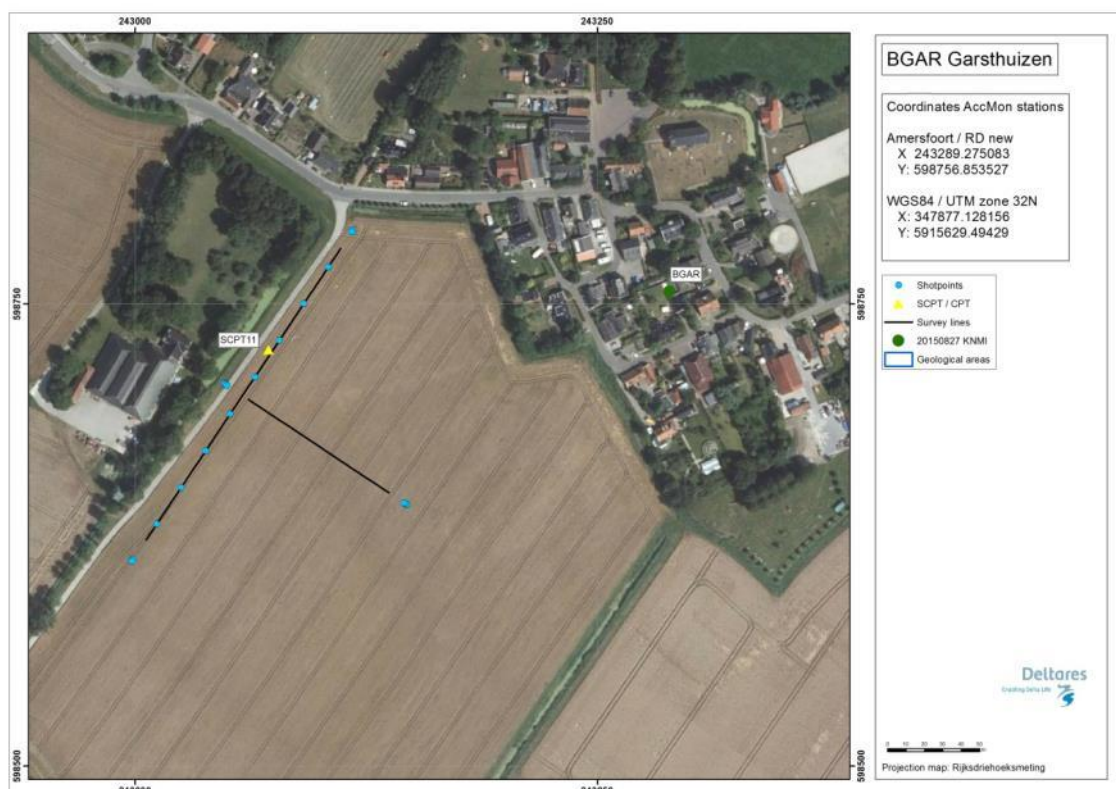


Figure 4.63 Map of location BGAR, showing the KNMI accelerograph station, SCPT location and MASW survey lines and shot locations.

### 4.6.2 Geological setting

The location is situated on the edge of a non-erosive area bordering an erosive valley in the east. The Pleistocene is covered with approximately 14 metres of Holocene deposits consisting of sands and clay. The base of the Holocene consists of Basic peat or humid clay and therefore the top of the Pleistocene is not eroded.

This location is positioned outside the Peelo valley. The erosive valley (outside project area) is covered with up to 20 metres of Holocene deposits.

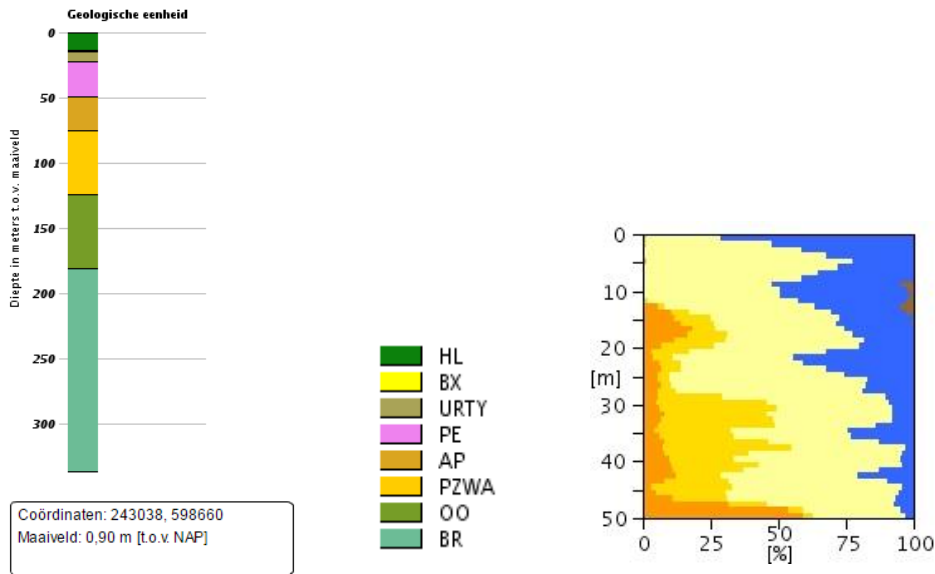


Figure 4.64 Geological information at station BGAR. Left: 1D section from the DGM model. Right: Section from the “delfstoffen online” model (GDN-TNO). Colour coding: brown = peat, blue = clay, yellow to orange = fine sand to coarse sand. The horizontal scale shows the volume percentage of each of the lithologies present at the location, the vertical scale is depth below the surface.

Table 4.6 Descriptions of representative deep boreholes near station BGAR from the DINO database ([www.dinoloket.nl](http://www.dinoloket.nl)).

Drilling	Distance from drilling	top	bottom	sediment type	Min. grain size	Max. grain size	Formation
B07E0049	1300mtr NW	0,00	-1,00	Clay			Formation of Naaldwijk
		-1,00	-4,00	Sand	Extreme fine		Formation of Naaldwijk
		-4,00	-10,70	Clay			Formation of Naaldwijk
		-10,70	-12,00	Sand	Medium fine		Formation of Boxtel
		-12,00	-20,00	Sand	Very coarse	Extreme coarse	Formation of Boxtel/Eem
		-20,00	-21,00	Clay			Formation of Peelo
		-21,00	-32,00	Sand	Medium fine	Very coarse	Formation of Peelo
		-32,00	-54,00	Sand	Very coarse	Extreme coarse	Formation of Peelo/Appelscha

1210624-000-BGS-0007, Version 2, 27 June 2016, final

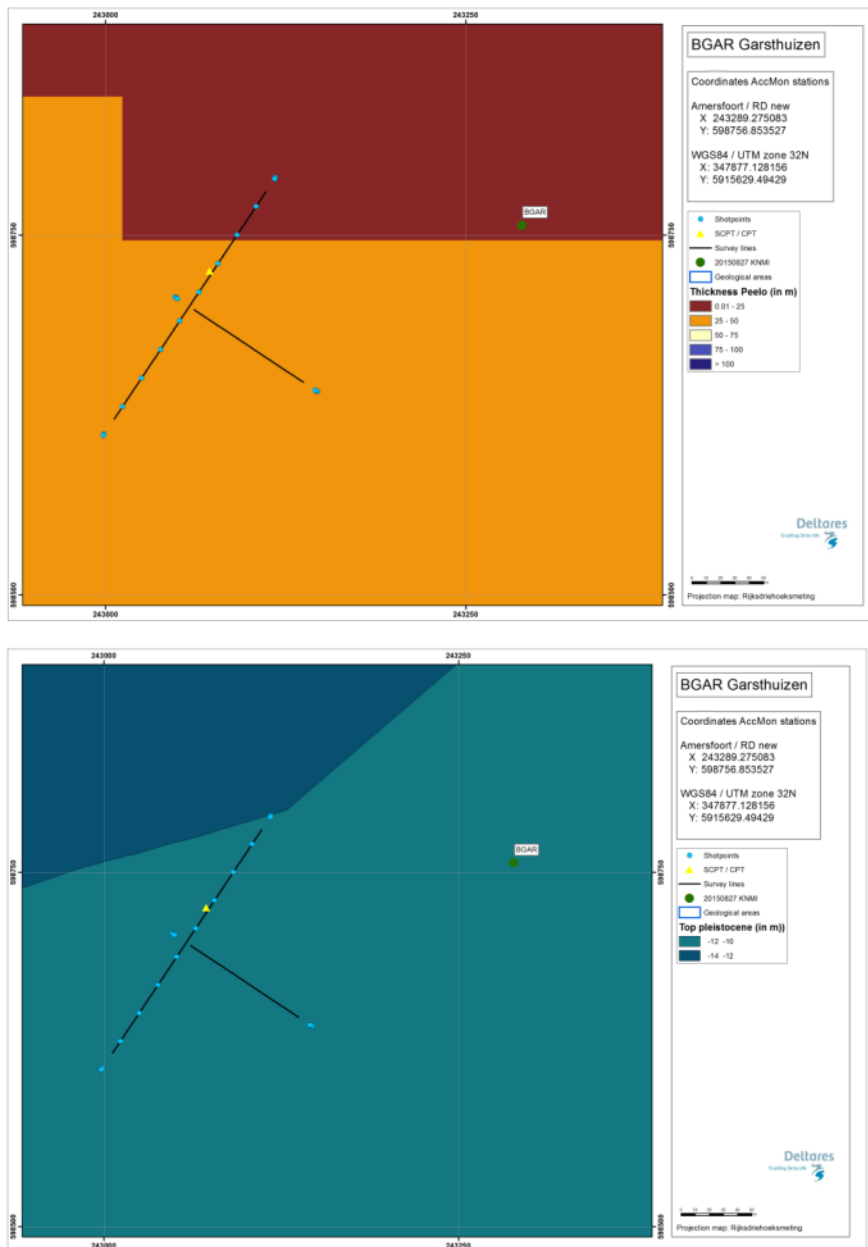


Figure 4.65 Overview map of geological setting based on beta version of GeoTOP model. Top panel: Thickness of the Peelo Formation, blue colour indicates thick Peelo layer, hence in the centre of the channel; red and orange colour indicates thin Peelo layers, hence areas outside the channel; yellow indicates transition zone. Lower panel: Top of Pleistocene surface relative to Dutch Ordnance Datum NAP.

## 4.6.3 SCPT

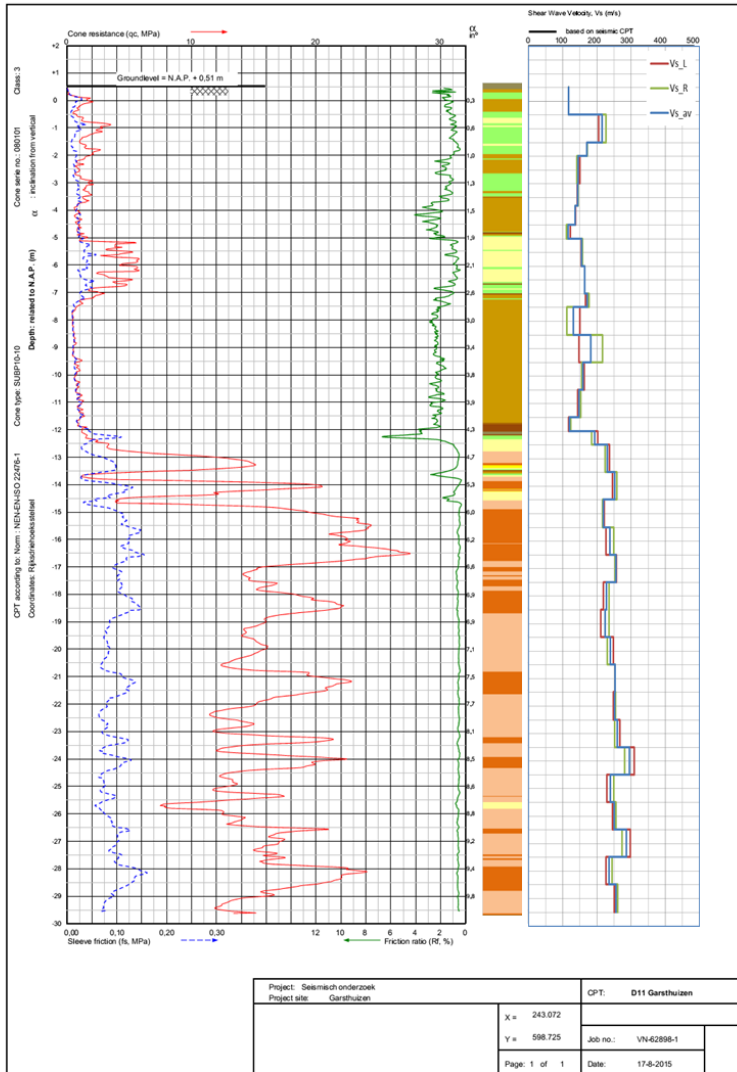


Figure 4.66 SCPT11. From left to right: CPT measurement, showing tip resistance, sleeve friction and friction ratio; automatically generated lithology (indication, for legend see Table 3.1); Vs profile (red = left blow, green = right blow, blue = average).

## 4.6.4 OSCPT

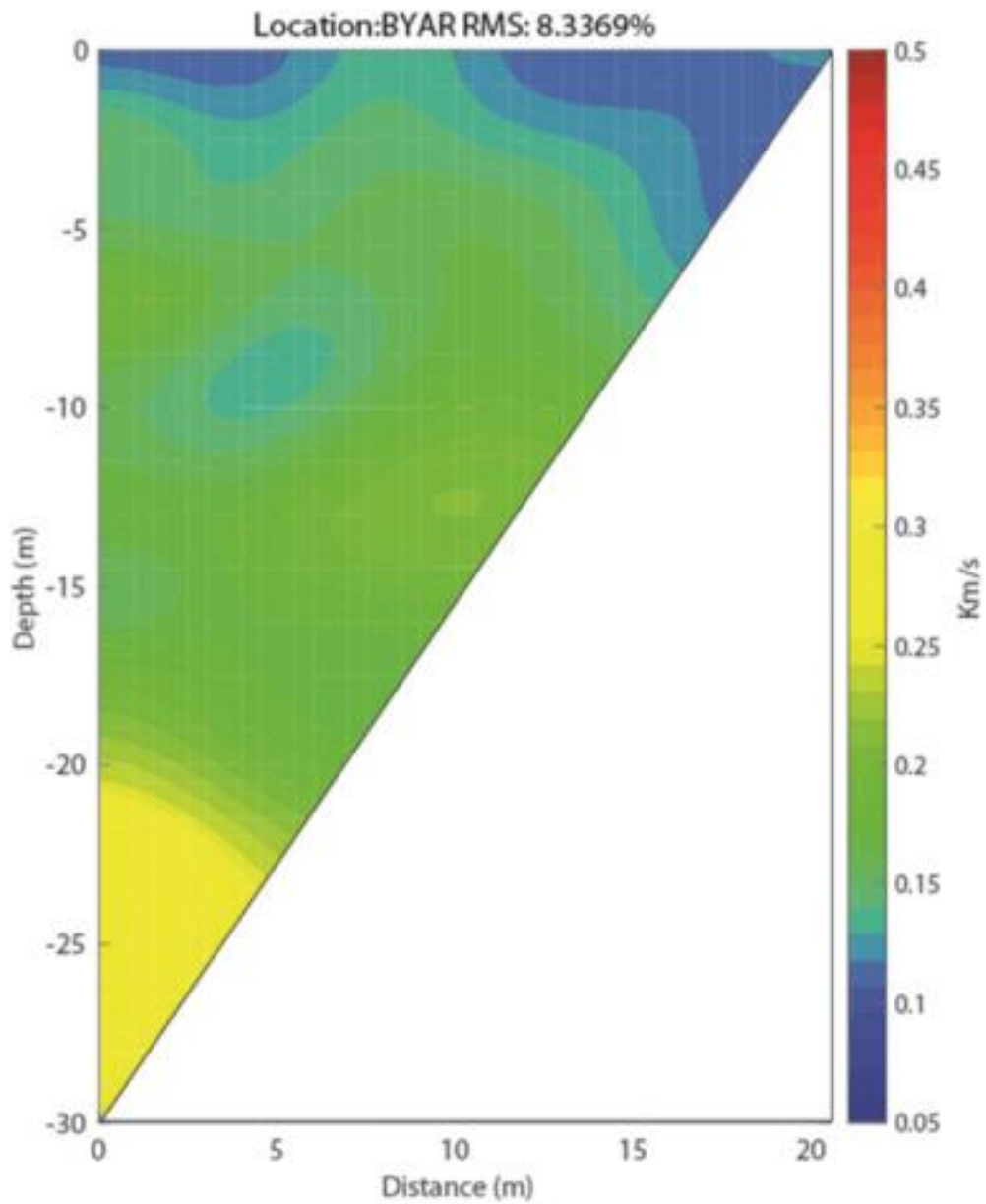


Figure 4.67 Tomographic images based on OSCPT result from SCPT for station BGAR (SCPT11).

## 4.6.5 MASW

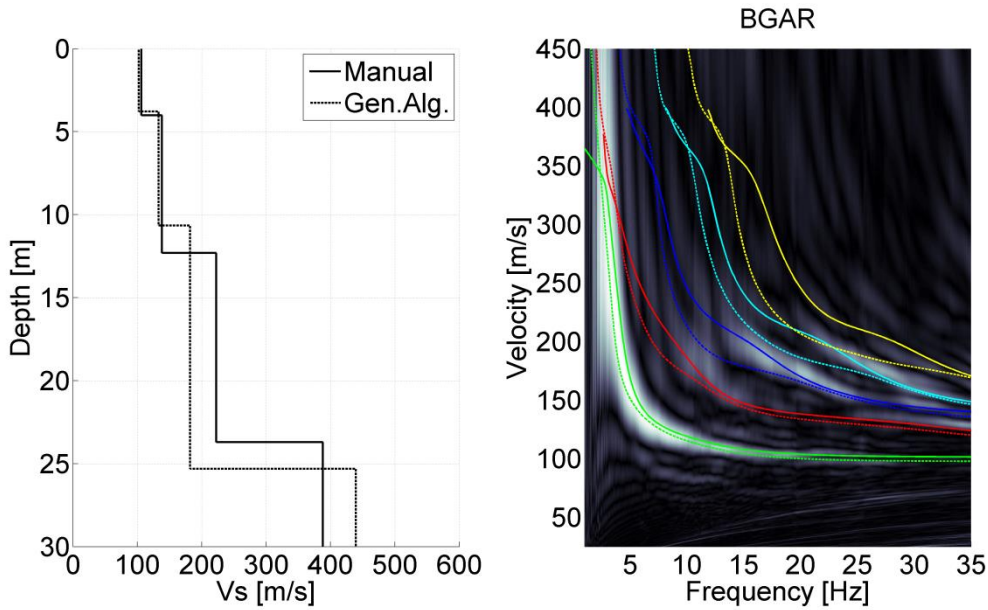


Figure 4.68 MASW result for station BGAR. Left panel:  $V_s$  profiles from active MASW. Solid line from manual fitting of dispersion curves; dashed line for automatic inversion. Right panel: energy in the dispersion plot in greyscale; solid lines are the modelled dispersion curves for different modes of the manually fitted  $V_s$  profile; dashed lines for the different modes of the automatically inverted  $V_s$  profile.

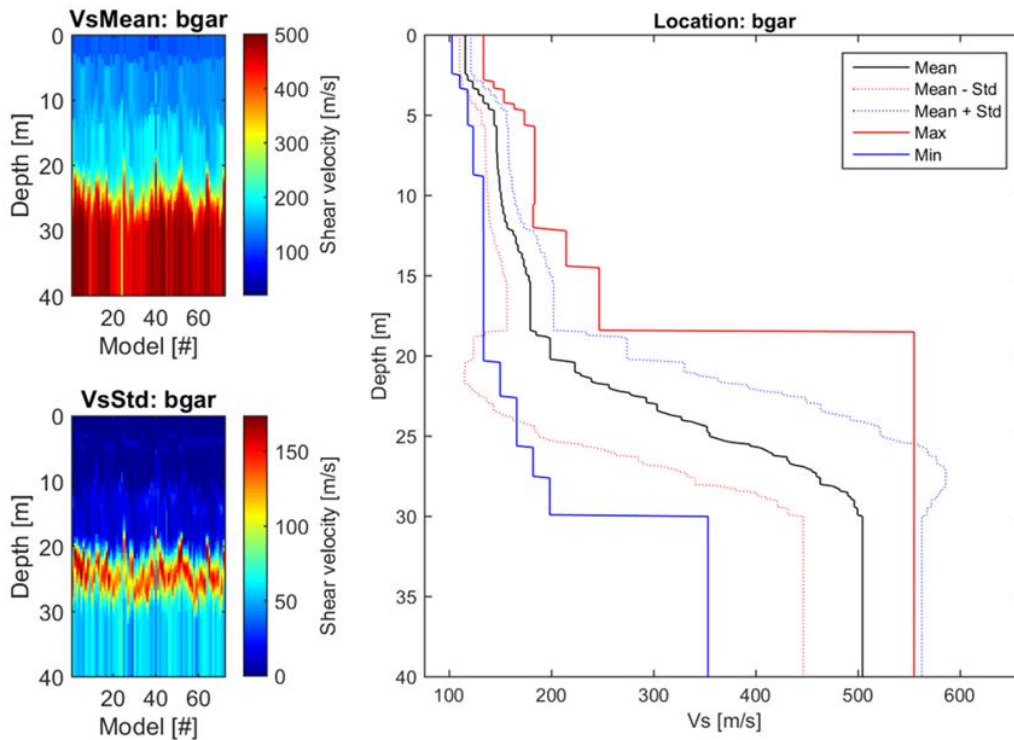


Figure 4.69 CMPcc result for BGAR. Top left: average  $V_s$  along the CMPcc array. Bottom left: standard deviation of  $V_s$  along the CMPcc array. Right: best fit curve of the 72 models with the maximum and minimum value observed in the whole CMPcc and the standard deviation from all models.

1210624-000-BGS-0007, Version 2, 27 June 2016, final

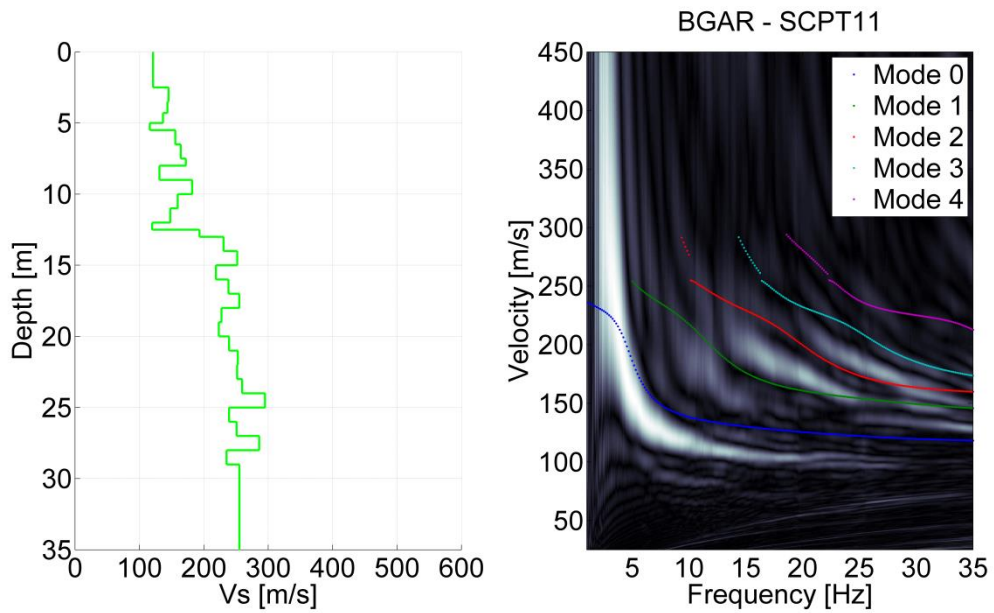


Figure 4.70 Comparison for BGAR of SCPT11 and MASW result. Left:  $V_s$  profile from SCPT. The  $V_s$  from the top 2 layers of the SCPT is generally unreliable and replaced by the minimum  $V_s$  of the first 3 layers. Right: modelled dispersion curves of different modes based on the SCPT  $V_s$  profile in coloured lines plotted on the energy of MASW dispersion plot in greyscale.



## 4.6.6 Synthesis

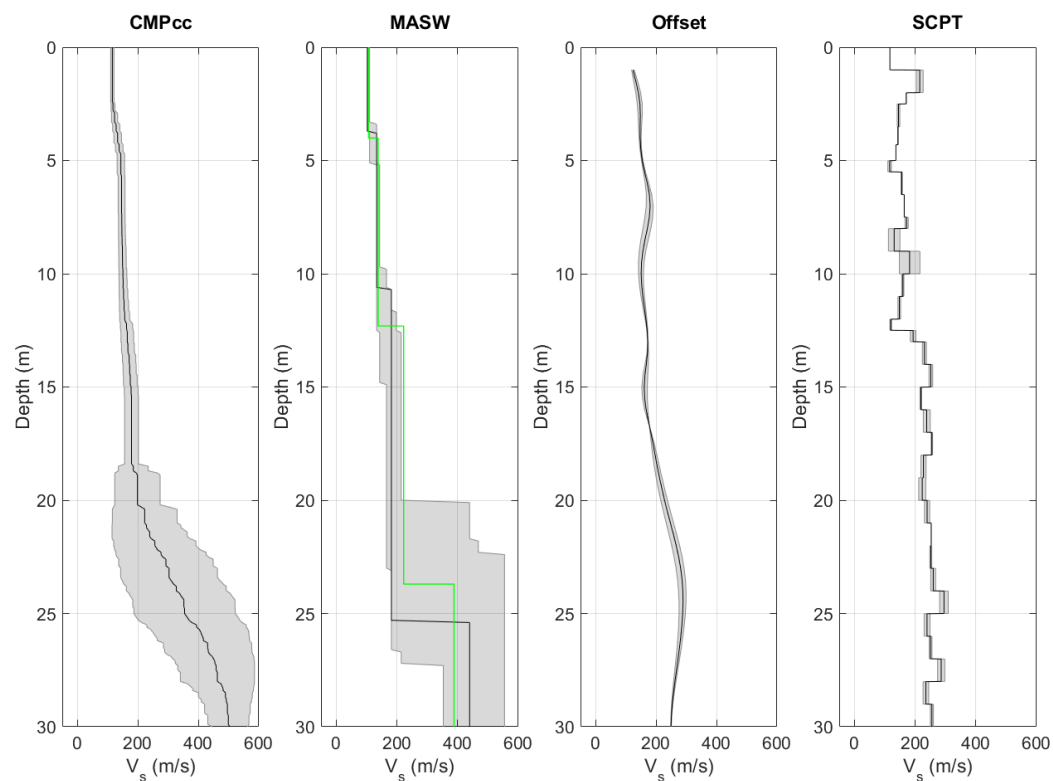


Figure 4.71  $V_s$  profiles from different measurement techniques, including uncertainty bands. From left to right: CMPcc based on active MASW array, shaded band indicates standard deviation; active MASW with manual fit in green and automatic inversion in black with grey shaded band indicating the minimum and the maximum  $V_s$ ; average profile for offset SCPTs between 1 and 5 m offset for 1 or 2 SCPTs with shaded band indicating the minimum and the maximum  $V_s$ ; SCPTs with band indicating variation between left and right blow; cross-hole average profiles for long leg in blue and short leg in grey with shaded band indicating the minimum and the maximum  $V_s$ .

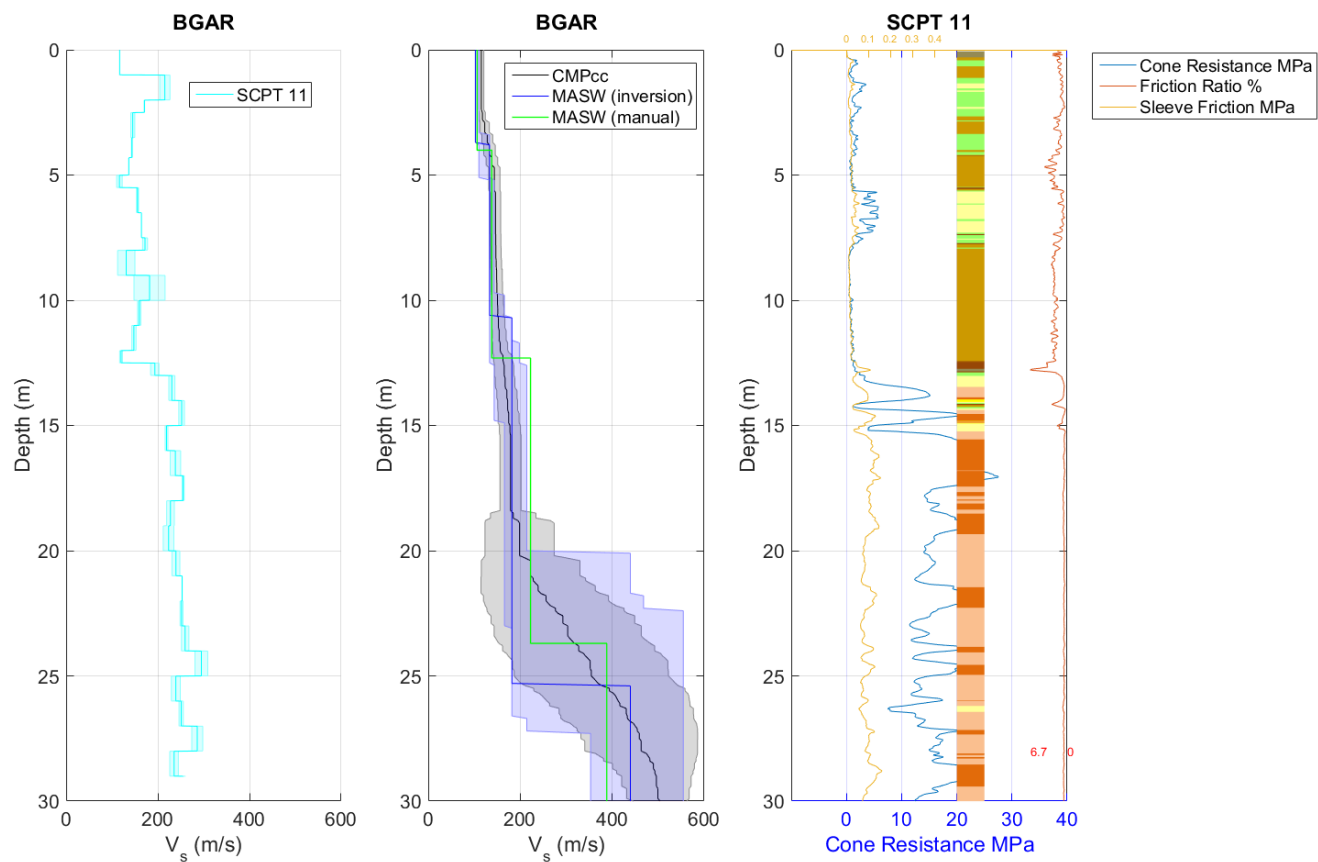


Figure 4.72 Synthesis of  $V_s$  results. Unreliable results are shown in red. From left to right: SCPT with band indicating variation between left and right blow; CMPcc, MASW and average cross-hole results with uncertainty bands; CPT with cone resistance, friction ratio, sleeve friction and automatically generated lithology (indication, for legend see Table 3.1).

## 4.7 Harkstede-BHAR

### 4.7.1 Location

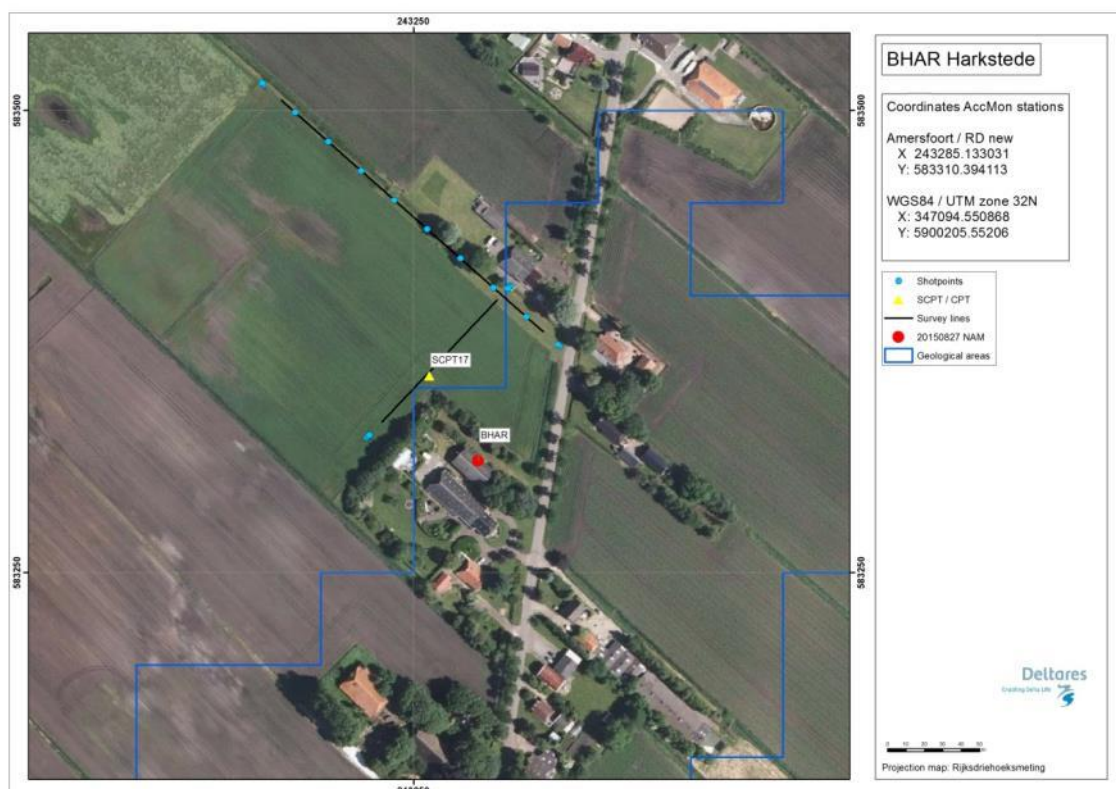


Figure 4.73 Map of location BHAR, showing the KNMI accelerograph station, SCPT location and MASW survey lines and shot locations.

### 4.7.2 Geological setting

The location is situated in a non-erosive area. The Holocene clay has not been deposited only a peat layer is found on top of the Pleistocene. The peat layer has a thickness of 40 cm. To the north the peat layers thicken up to 1 metre.

The location is situated on the end of a declining slope of a Peelo valley that reaches from 70 metres at the location up to the maximum depth of 106 metres in the centre over a distance of 1.3 kilometres to the northwest.

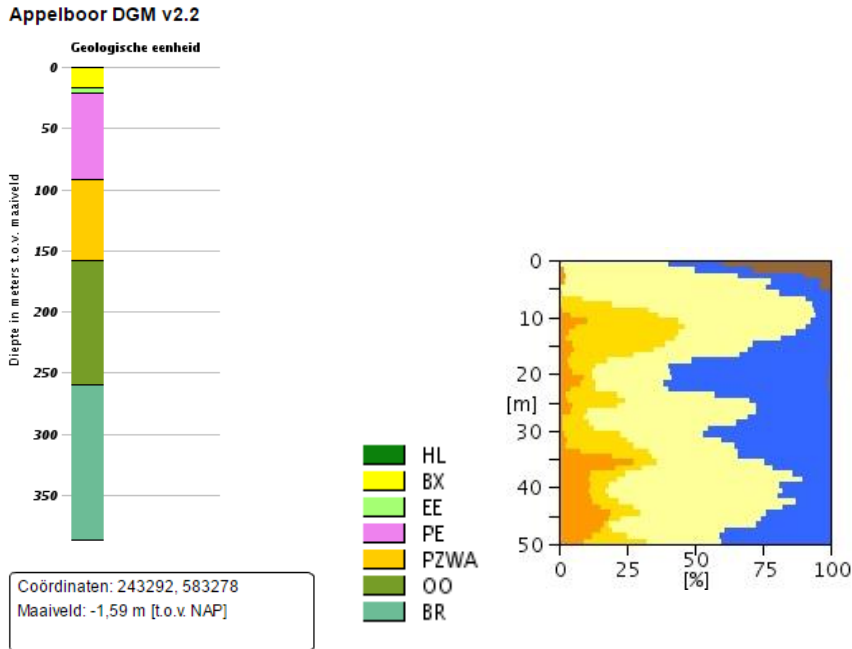


Figure 4.74 Geological information at station BHAR. Left: 1D section from the DGM model. Right: Section from the “delfstoffen online” model (GDN-TNO). Colour coding: brown = peat, blue = clay, yellow to orange = fine sand to coarse sand. The horizontal scale shows the volume percentage of each of the lithologies present at the location, the vertical scale is depth below the surface.

Table 4.7 Descriptions of representative deep boreholes near station BHAR from the DINO database ([www.dinoloket.nl](http://www.dinoloket.nl)).

<b>Drilling</b>	<b>Distance from drilling</b>	<b>top</b>	<b>bottom</b>	<b>sediment type</b>	<b>Min. grain size</b>	<b>Max. grain size</b>	<b>Formation</b>
B07G0158	1400mtr NW	-1,80	-4,60	Peat			Formation of Nieuwkoop
		-4,60	-11,80	Sand	Medium fine		Formation of Bortel
		-11,80	-19,30	Sand	Medium coarse	Extreme coarse	Formation of Bortel
		-19,30	-38,80	Clay			Formation of Peelo
		-38,80	-40,80	Sand	Extreme fine		Formation of Peelo
		-40,80	-41,80	Clay			Formation of Peelo
		-41,80	-48,80	Sand	Extreme fine		Formation of Peelo
		-48,80	-78,80	Clay			Formation of Peelo
		-78,80	-80,80	Sand	Medium fine		Formation of Peelo
		B07G0175	2900mtr SE	-1,50	-19,50	Sand	Very fine
-19,50	-24,50			Clay			Eem Formation
-24,50	-35,50			Sand	Medium fine	Medium coarse	Eem Formation
-35,50	-38,50			Gravel	coarse		Formation of Drente
-38,50	-39,50			Clay			Formation of Drente
-39,50	-45,50			Sand	Very fine	Medium fine	Formation of Drente
-45,50	-49,50			Sand	Extreme coarse	Gravel	Formation of Peelo
-49,50	-52,50			Sand	Medium fine	Medium coarse	Formation of Peelo
-52,50	-59,50			Sand	Very coarse	Extreme coarse	Formation of Peelo
-59,50	-61,50			Clay			Formation of Peelo
-61,50	-114,50			Sand	Extreme coarse	Gravel	Formation of Peelo
-114,50	-137,50			Sand	Very coarse	Gravel	Formation of Peize
-137,50	-140,50			Sand	fine		Formation of Peize
-140,50	-150,50	Sand	Medium coarse	Extreme coarse	Formation of Peize		
-150,50	-206,50	Sand	Medium fine		Formation of Peize/Oosterhout		

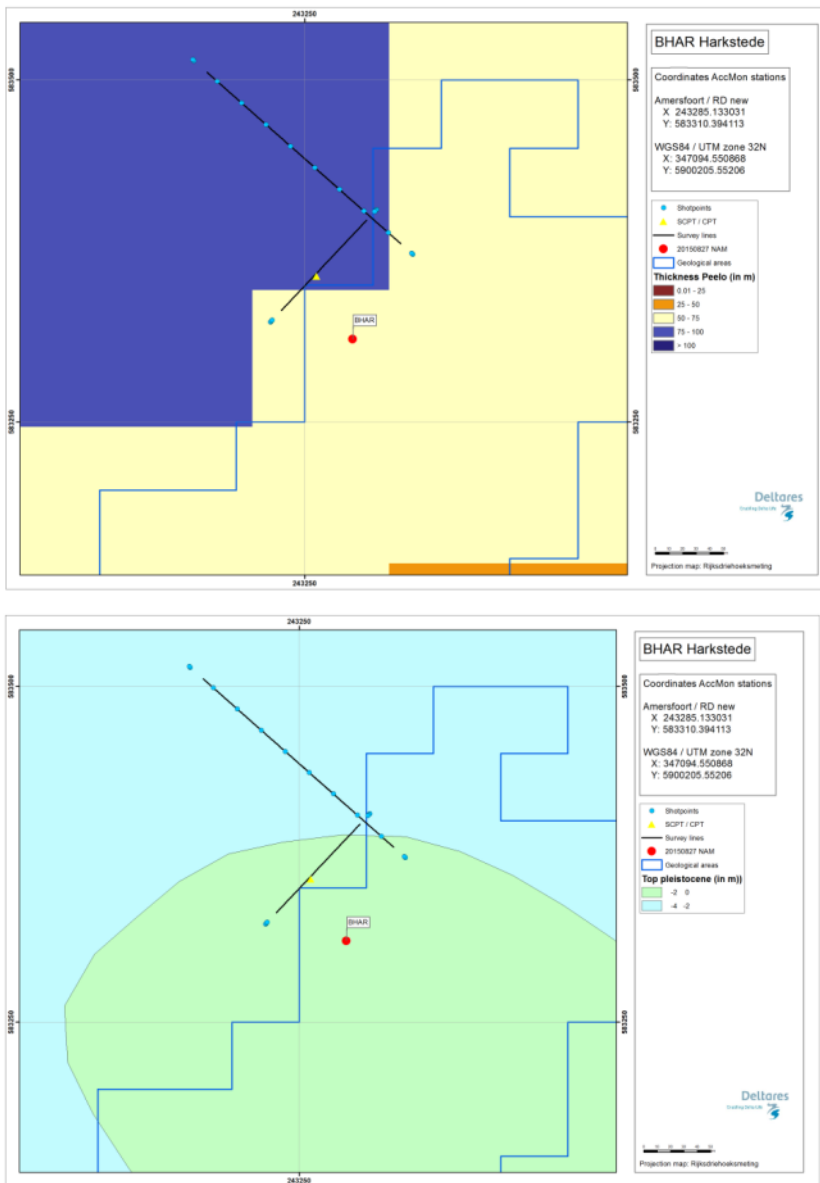


Figure 4.75 Overview map of geological setting based on beta version of GeoTOP model. Top panel: Thickness of the Peelo Formation, blue colour indicates thick Peelo layer, hence in the centre of the channel; red and orange colour indicates thin Peelo layers, hence areas outside the channel; yellow indicates transition zone. Lower panel: Top of Pleistocene surface relative to Dutch Ordnance Datum NAP.

## 4.7.3 SCPT

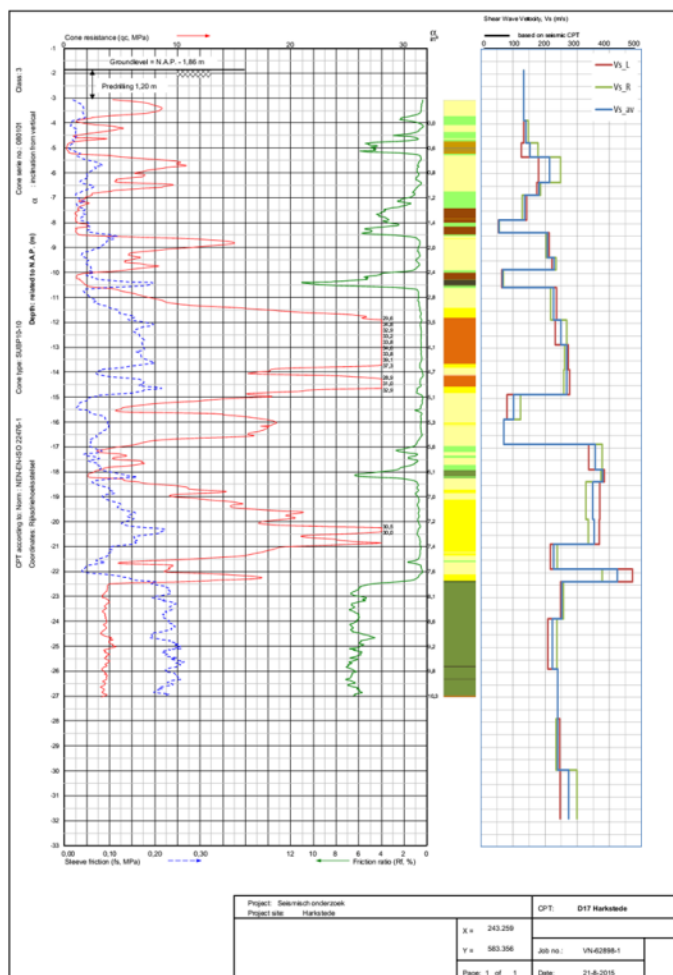


Figure 4.76 SCPT17. From left to right: CPT measurement, showing tip resistance, sleeve friction and friction ratio; automatically generated lithology (indication, for legend see Table 3.1);  $V_s$  profile (red = left blow, green = right blow, blue = average).

## 4.7.4 OSCPT

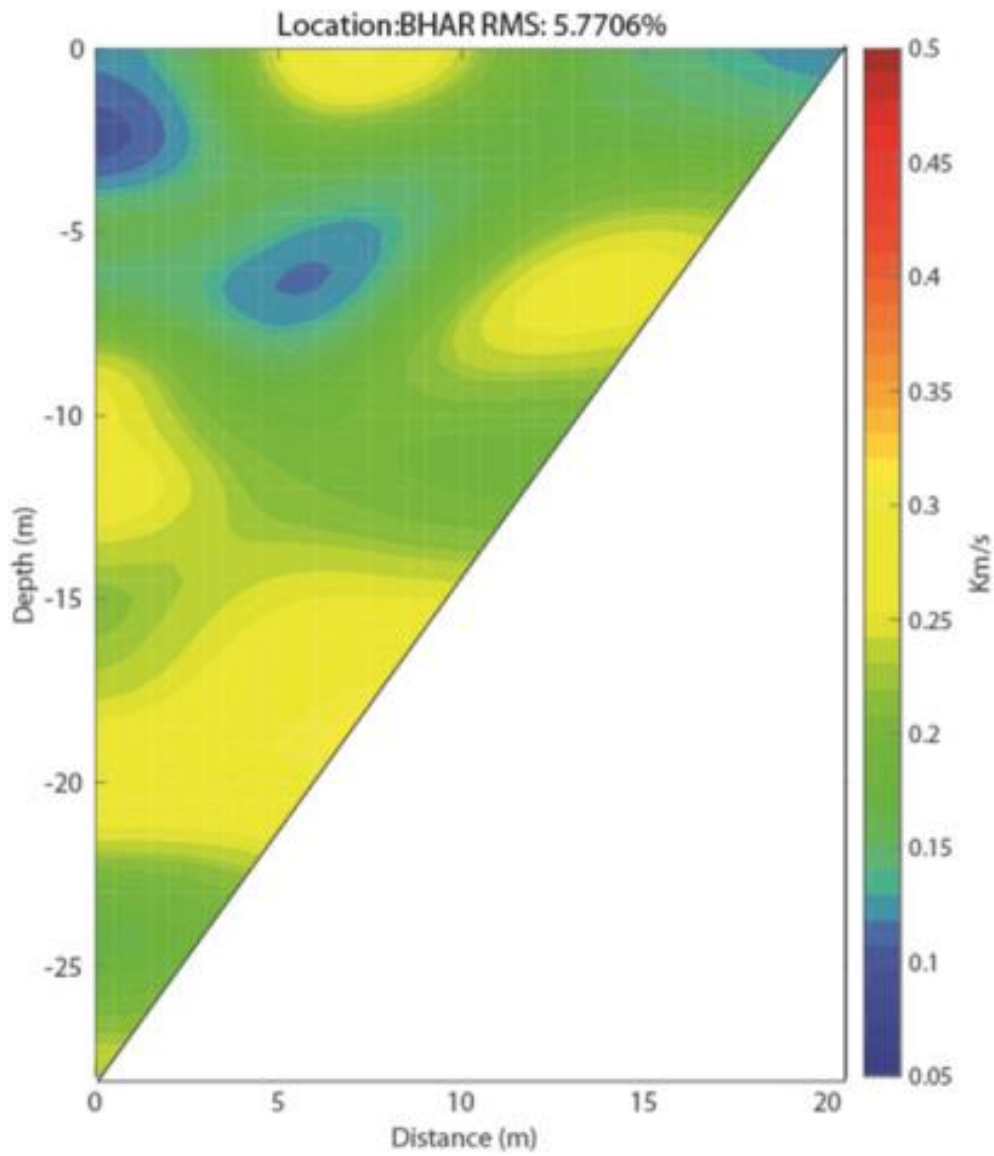


Figure 4.77 Tomographic images based on OSCPT result from SCPT for station BHAR (SCPT17).

## 4.7.5 MASW

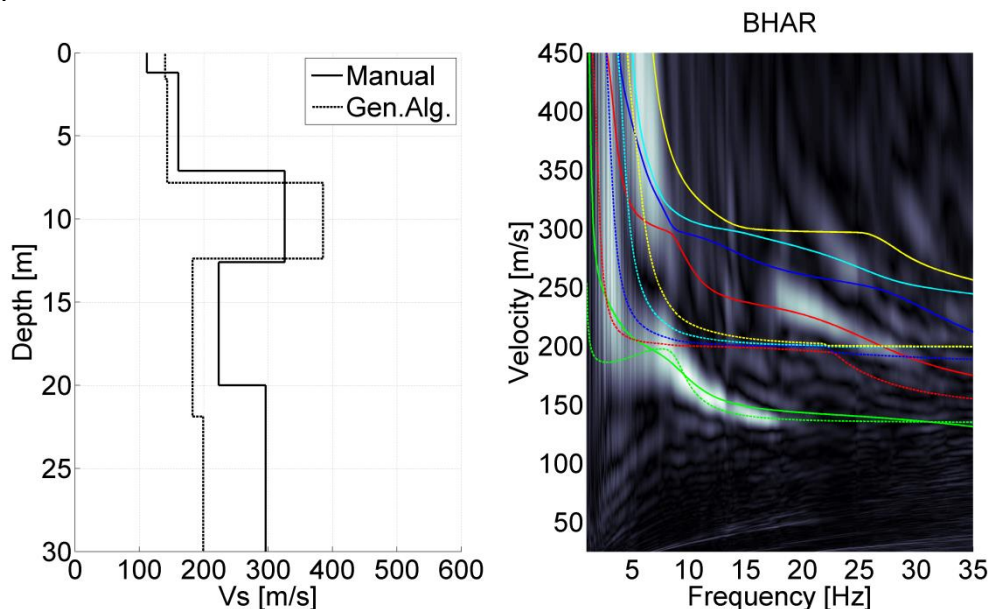


Figure 4.78 MASW result for station BHAR. Left panel:  $V_s$  profiles from active MASW. Solid line from manual fitting of dispersion curves; dashed line for automatic inversion. Right panel: energy in the dispersion plot in greyscale; solid lines are the modelled dispersion curves for different modes of the manually fitted  $V_s$  profile; dashed lines for the different modes of the automatically inverted  $V_s$  profile.

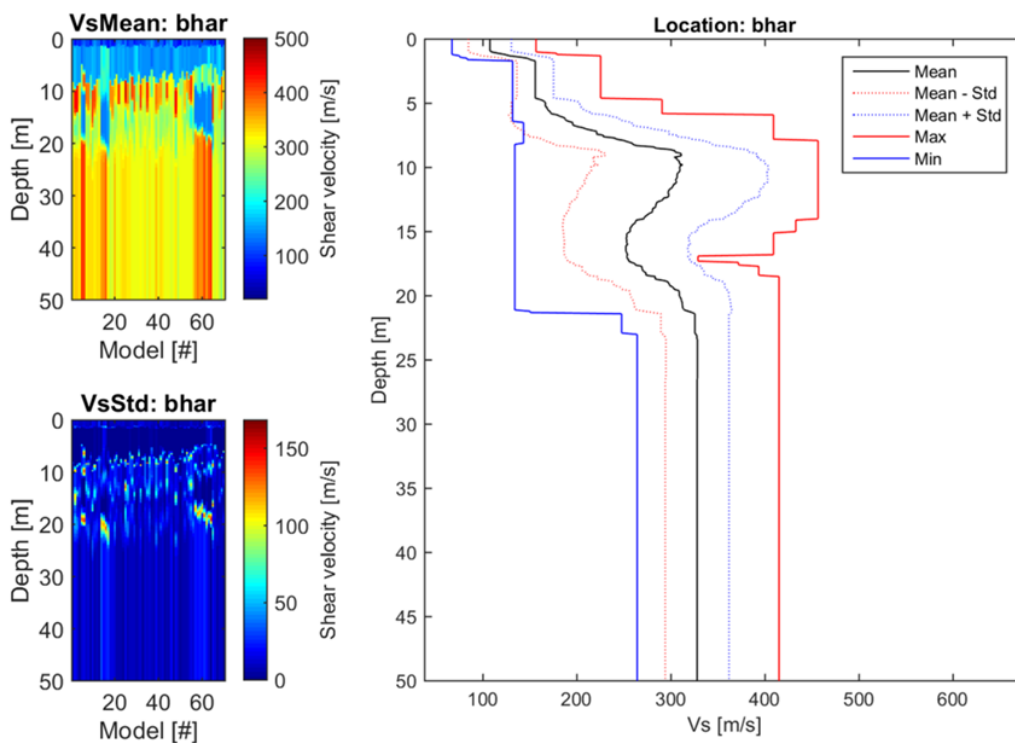


Figure 4.79 CMPcc result for BHAR. Top left: average  $V_s$  along the CMPcc array. Bottom left: standard deviation of  $V_s$  along the CMPcc array. Right: best fit curve of the 72 models with the maximum and minimum value observed in the whole CMPcc and the standard deviation from all models.

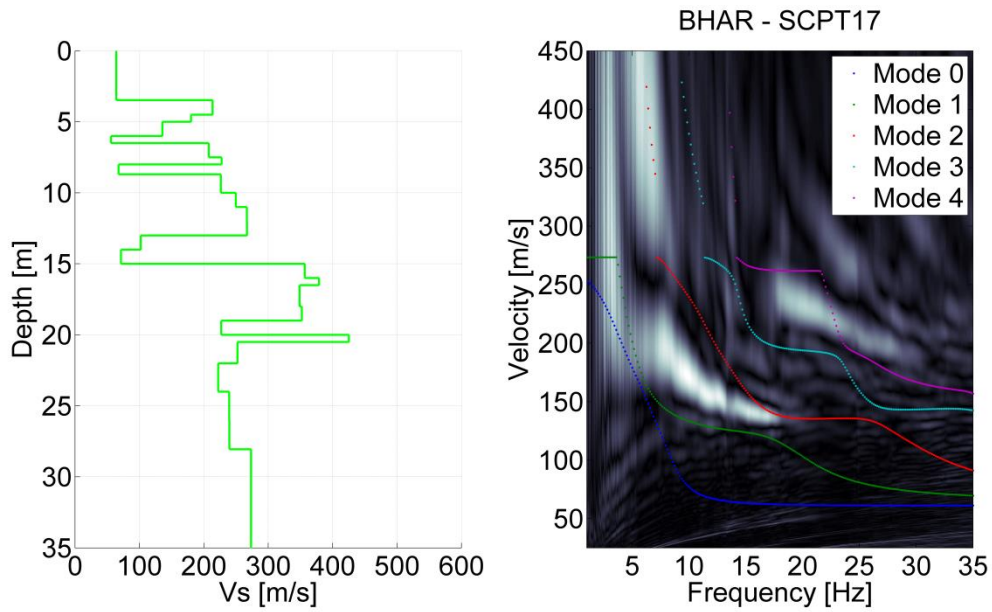


Figure 4.80 Comparison for BHAR of SCPT17 and MASW result. Left:  $V_s$  profile from SCPT. The  $V_s$  from the top 2 layers of the SCPT is generally unreliable and replaced by the minimum  $V_s$  of the first 3 layers. Right: modelled dispersion curves of different modes based on the SCPT  $V_s$  profile in coloured lines plotted on the energy of MASW dispersion plot in greyscale.

## 4.7.6 Synthesis

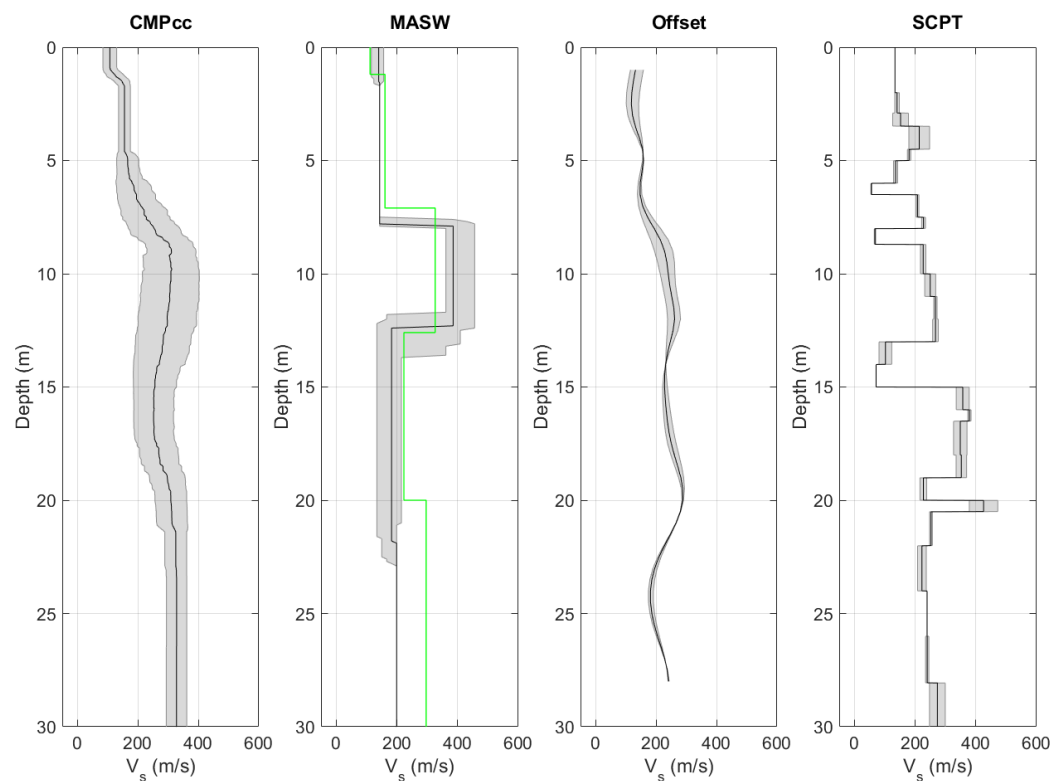


Figure 4.81  $V_s$  profiles from different measurement techniques, including uncertainty bands. From left to right: CMPcc based on active MASW array, shaded band indicates standard deviation; active MASW with manual fit in green and automatic inversion in black with grey shaded band indicating the minimum and the maximum  $V_s$ ; average profile for offset SCPTs between 1 and 5 m offset for 1 or 2 SCPTs with shaded band indicating the minimum and the maximum  $V_s$ ; SCPTs with band indicating variation between left and right blow; cross-hole average profiles for long leg in blue and short leg in grey with shaded band indicating the minimum and the maximum  $V_s$ .

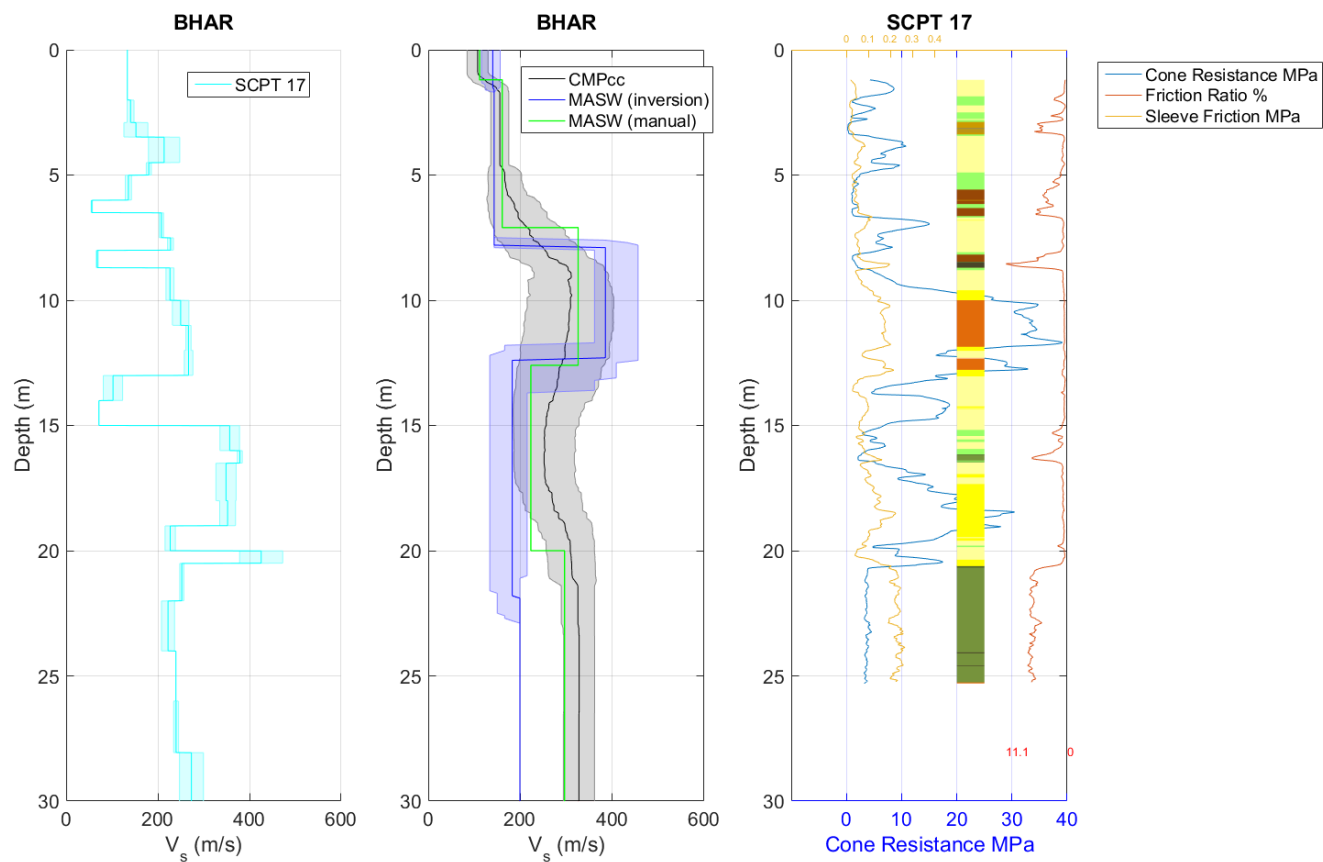


Figure 4.82 Synthesis of  $V_s$  results. Unreliable results are shown in red. From left to right: SCPT with band indicating variation between left and right blow; CMPcc, MASW and average cross-hole results with uncertainty bands; CPT with cone resistance, friction ratio, sleeve friction and automatically generated lithology (indication, for legend see Table 3.1).

## 4.8 Garrelsweer- BHKS

### 4.8.1 Location



Figure 4.83 Map of location BHKS, showing the KNMI accelerograph station, SCPT location and MASW survey lines and shot locations.

### 4.8.2 Geological setting

The location is situated in a non-erosive area. The Holocene deposit consists of clay with a peat layer in between at the depth of 0.5 metre. Basic peat is present in this area. Top of the Pleistocene is found at a depth of approximately 5 metres.

At a distance of 1 kilometre to the west of the line an erosive valley with a depth of approximately 8 metre can be found oriented towards the northeast. Here the Holocene clay layer is present on the Pleistocene that consists of boulder clay or cover sand.

The location is situated on a flat part of a Peelo valley between two deeper valleys, the base of the valley varies from 63 metres at the accelerograph station up to the maximum depth of 174 metres in the centre of the valley over a distance of 1.5 kilometre to the southwest.

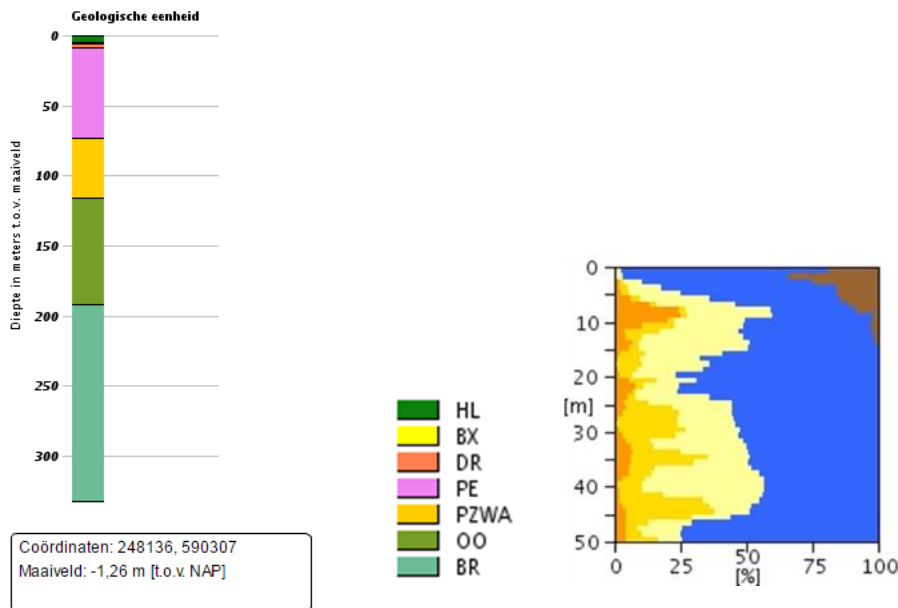
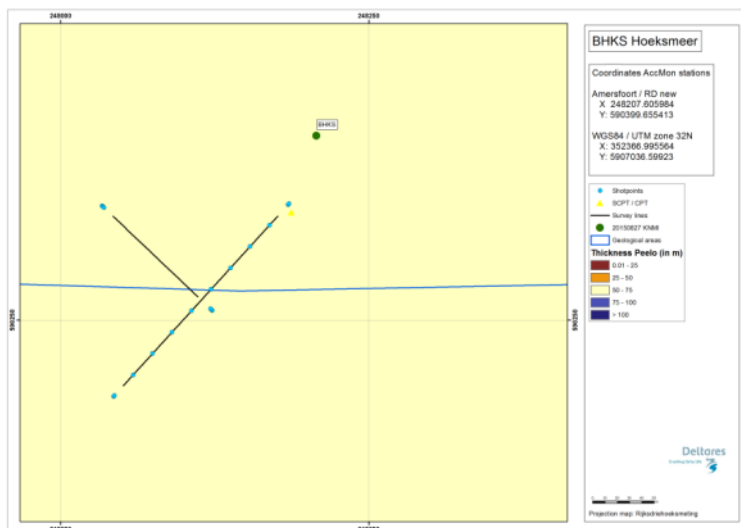
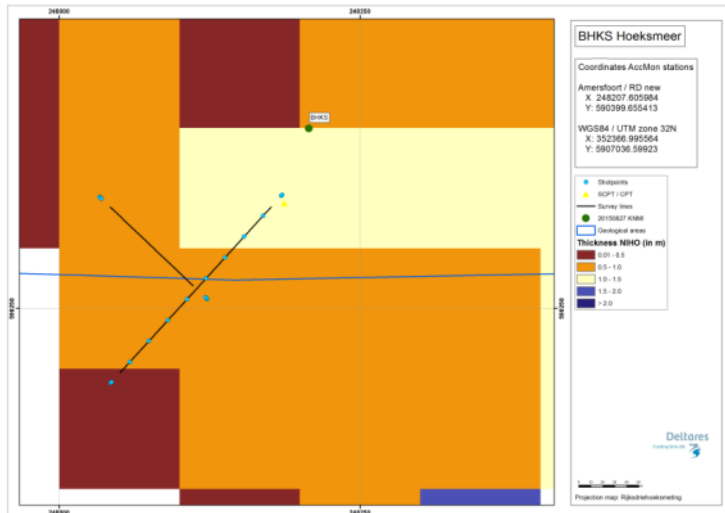


Figure 4.84 Geological information at station BHKS. Left: 1D section from the DGM model. Right: Section from the “delfstoffen online” model (GDN-TNO). Colour coding: brown = peat, blue = clay, yellow to orange = fine sand to coarse sand. The horizontal scale shows the volume percentage of each of the lithologies present at the location, the vertical scale is depth below the surface.

Table 4.8 Descriptions of representative deep boreholes near station BHKS from the DINO database ([www.dinoloket.nl](http://www.dinoloket.nl)).

Drilling	Distance from drilling	top	bottom	sediment type	Min. grain size	Max. grain size	Formation
B07F0076	4400mtr SE	1,50	-1,85	Clay			Formation of Naaldwijk
		-1,85	-3,75	Peat			Formation of Nieuwkoop
		-3,75	-16,00	Sand	Medium fine		Formation of Boxtel
		-16,00	-38,50	Clay			Formation of Peelo
		-38,50	-46,90	Sand	Medium fine		Formation of Peelo/Appelscha
		-46,90	-69,15	Sand	Medium coarse	Very coarse	Formation of Appelscha/Peize
		-69,15	-74,15	Sand	Medium fine	Medium coarse	Formation of Peize
		-74,15	-86,20	Sand	Medium coarse	Very coarse	Formation of Peize
B07E0004	3300mtr NW	-86,20	-92,00	Loam			Formation of Peize
		0,00	-7,80	Clay			Formation of Naaldwijk
		-7,80	-12,30	Sand	Fine		Formation of Boxtel
		-12,30	-77,00	Clay			Formation of Peelo
		-77,00	-99,00	Sand	Fine		Formation of Peelo
		-99,00	-118,30	Sand	Medium coarse		Formation of Peelo
-118,30	-130,00	Sand	Fine		Formation of Peelo		

1210624-000-BGS-0007, Version 2, 27 June 2016, final



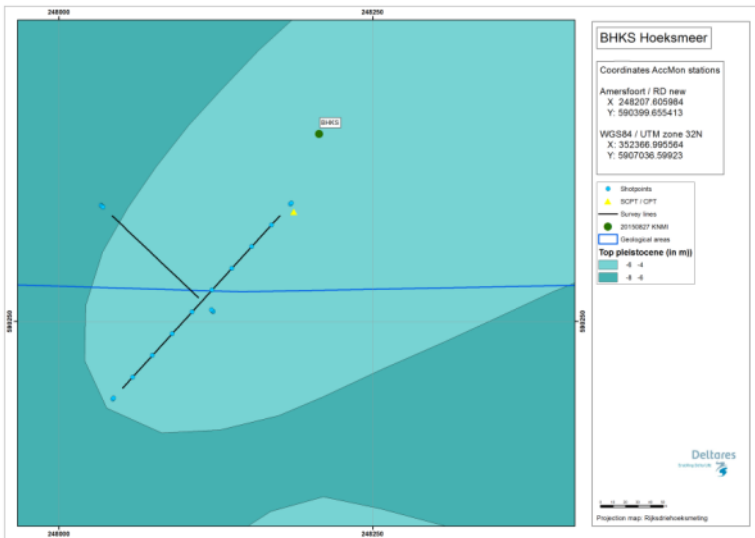


Figure 4.85 Overview map of geological setting based on beta version of GeoTOP model. Top panel: Thickness of the Holocene peat. Middle panel: Thickness of the Peelo Formation, blue colour indicates thick Peelo layer, hence in the centre of the channel; red and orange colour indicates thin Peelo layers, hence areas outside the channel; yellow indicates transition zone. Lower panel: Top of Pleistocene surface relative to Dutch Ordnance Datum NAP.

## 4.8.3 SCPT

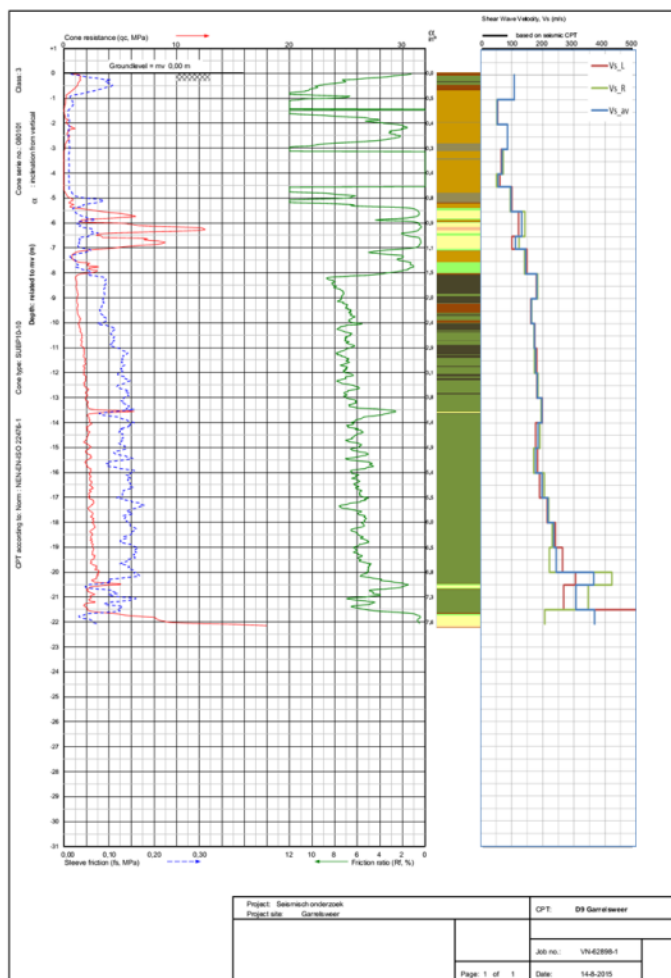


Figure 4.86 SCPT09. From left to right: CPT measurement, showing tip resistance, sleeve friction and friction ratio; automatically generated lithology (indication, for legend see Table 3.1);  $V_s$  profile (red = left blow, green = right blow, blue = average).

## 4.8.4 OSCPT

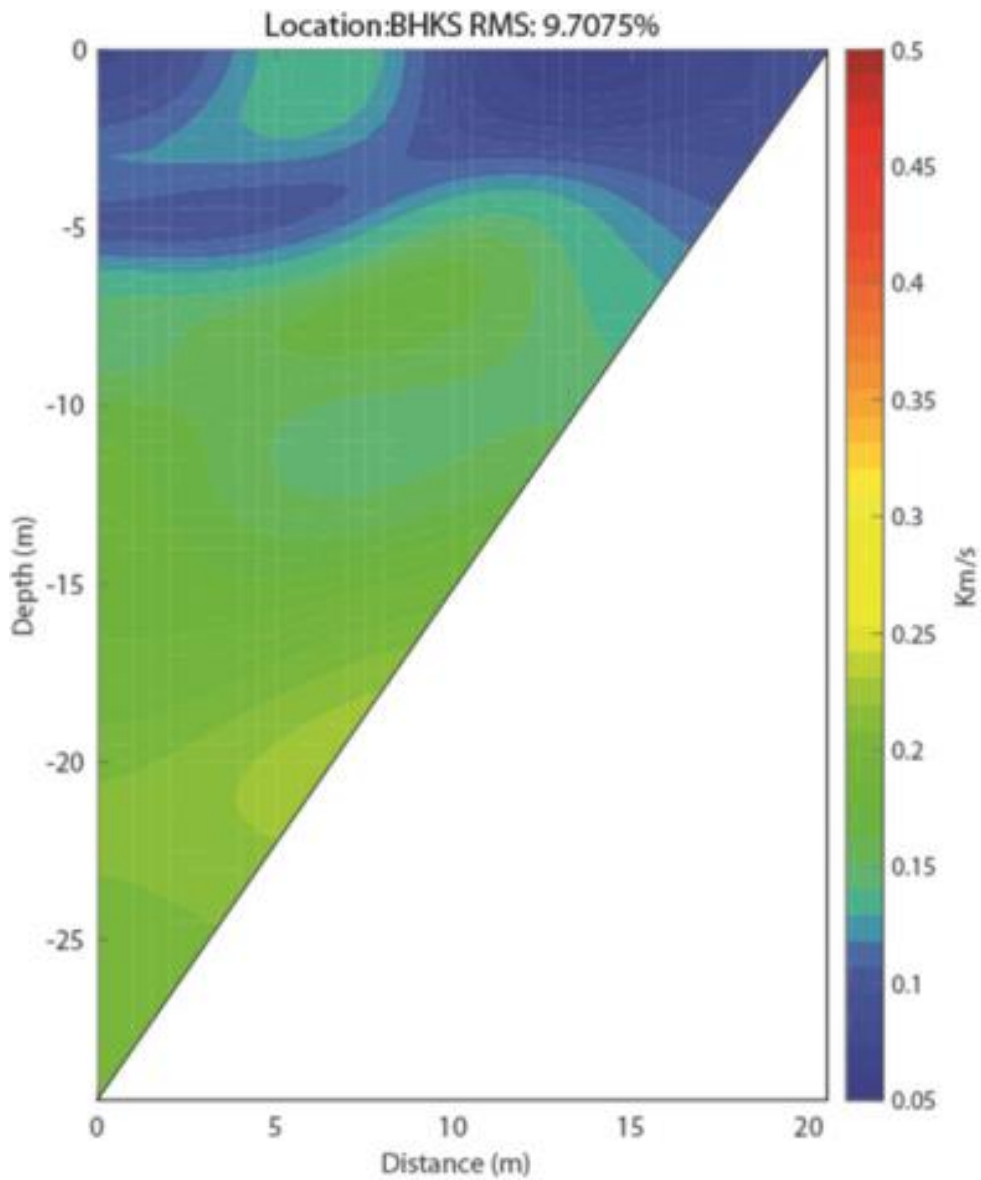


Figure 4.87 Tomographic images based on OSCPT result from SCPT for station BHKS (SCPT09).

## 4.8.5 MASW

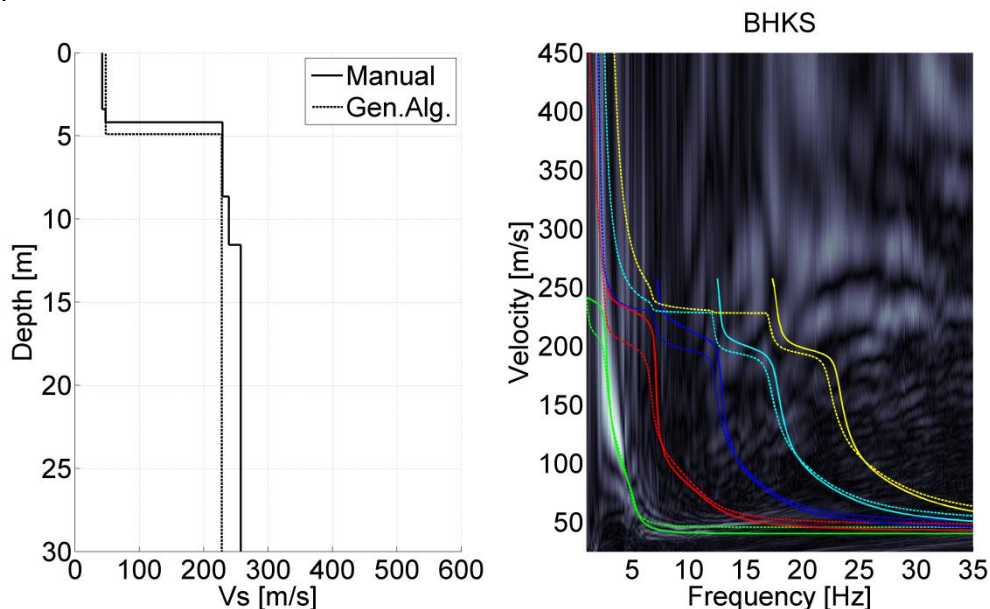


Figure 4.88 MASW result for station BHKS. Left panel:  $V_s$  profiles from active MASW. Solid line from manual fitting of dispersion curves; dashed line for automatic inversion. Right panel: energy in the dispersion plot in greyscale; solid lines are the modelled dispersion curves for different modes of the manually fitted  $V_s$  profile; dashed lines for the different modes of the automatically inverted  $V_s$  profile.

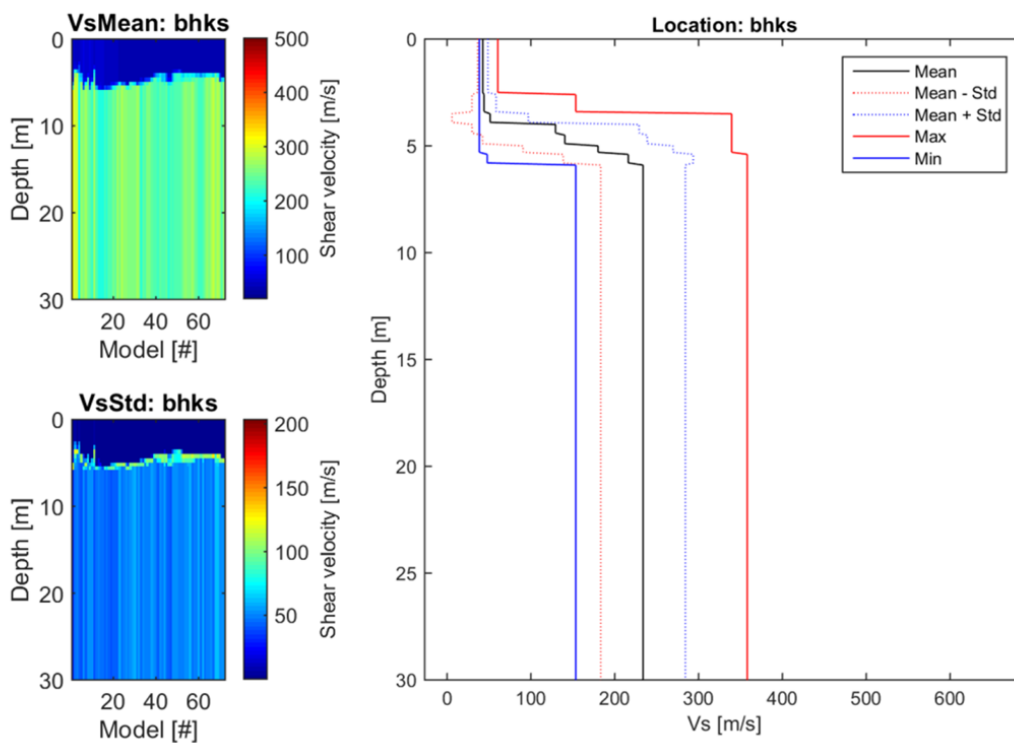


Figure 4.89 CMPcc result for BHKS. Top left: average  $V_s$  along the CMPcc array. Bottom left: standard deviation of  $V_s$  along the CMPcc array. Right: best fit curve of the 72 models with the maximum and minimum value observed in the whole CMPcc and the standard deviation from all models.

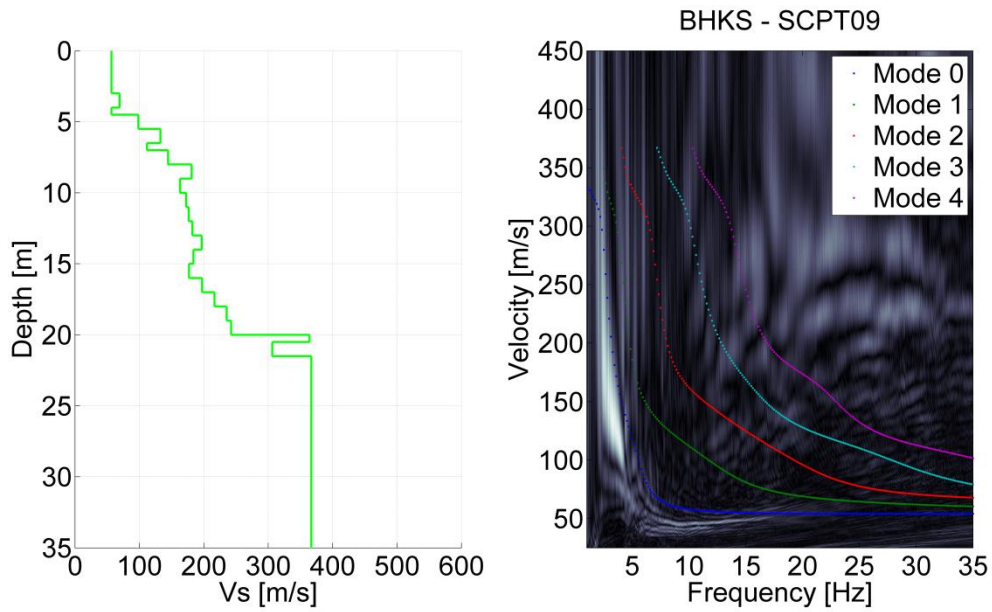


Figure 4.90 Comparison for BHKS of SCPT09 and MASW result. Left:  $V_s$  profile from SCPT. The  $V_s$  from the top 2 layers of the SCPT is generally unreliable and replaced by the minimum  $V_s$  of the first 3 layers. Right: modelled dispersion curves of different modes based on the SCPT  $V_s$  profile in coloured lines plotted on the energy of MASW dispersion plot in greyscale.

## 4.8.6 Synthesis

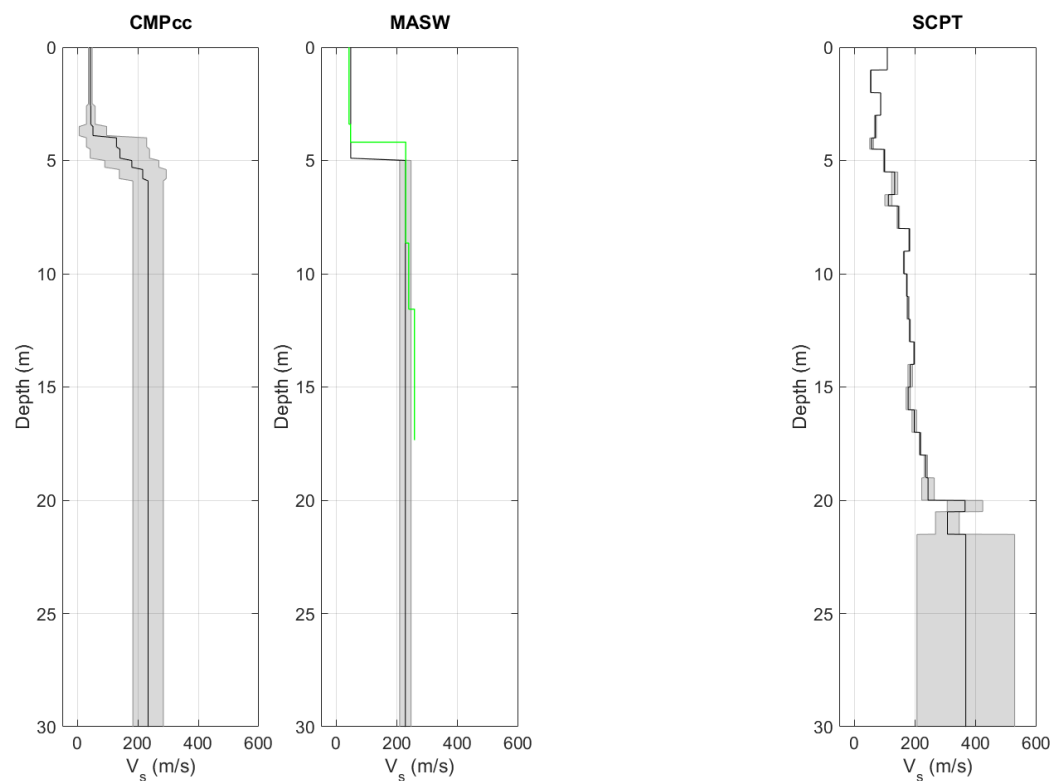


Figure 4.91  $V_s$  profiles from different measurement techniques, including uncertainty bands. From left to right: CMPcc based on active MASW array, shaded band indicates standard deviation; active MASW with manual fit in green and automatic inversion in black with grey shaded band indicating the minimum and the maximum  $V_s$ ; average profile for offset SCPTs between 1 and 5 m offset for 1 or 2 SCPTs with shaded band indicating the minimum and the maximum  $V_s$ ; SCPTs with band indicating variation between left and right blow; cross-hole average profiles for long leg in blue and short leg in grey with shaded band indicating the minimum and the maximum  $V_s$ .

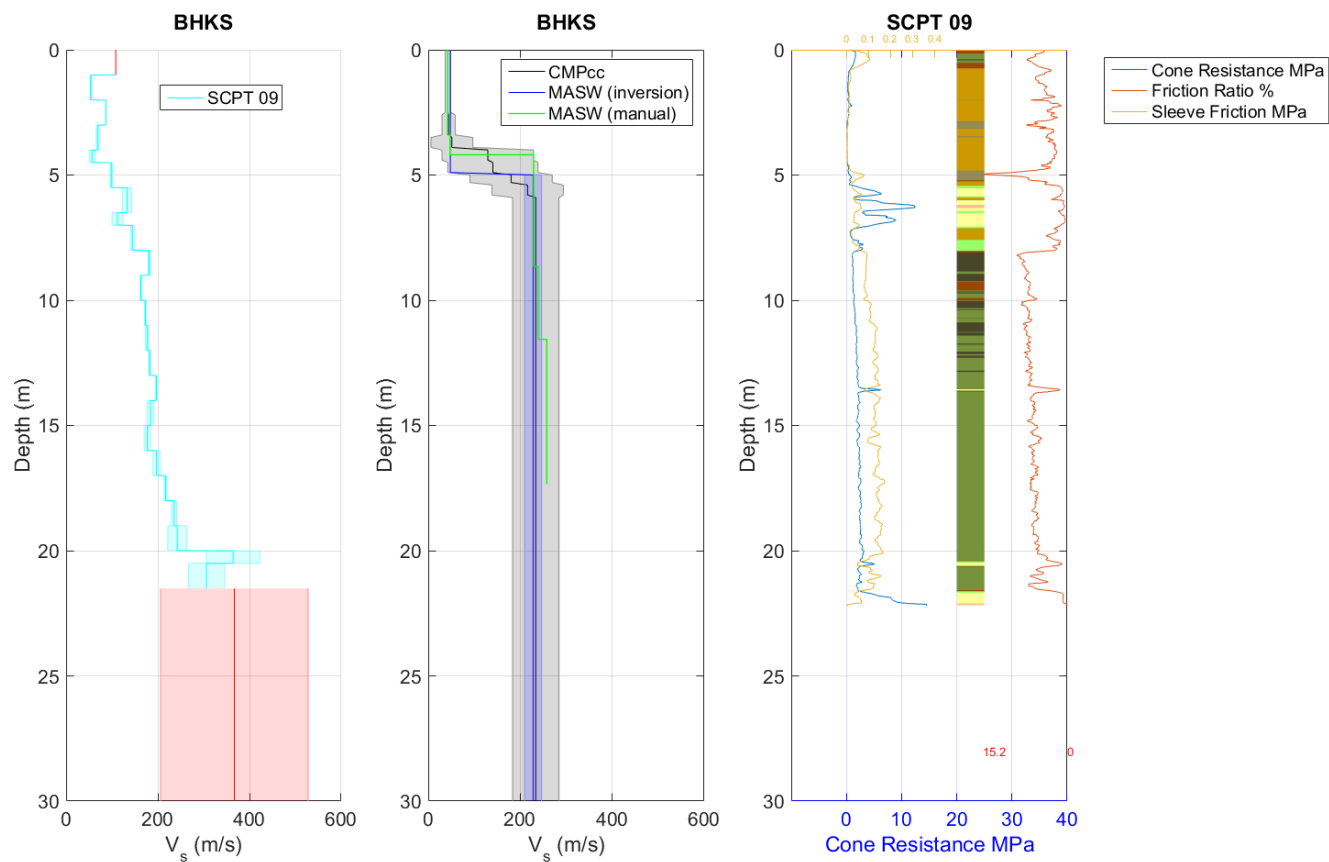


Figure 4.92 Synthesis of  $V_s$  results. Unreliable results are shown in red. From left to right: SCPT with band indicating variation between left and right blow; CMPcc, MASW and average cross-hole results with uncertainty bands; CPT with cone resistance, friction ratio, sleeve friction and automatically generated lithology (indication, for legend see Table 3.1).

## 4.9 Kantens- BKAN

### 4.9.1 Location

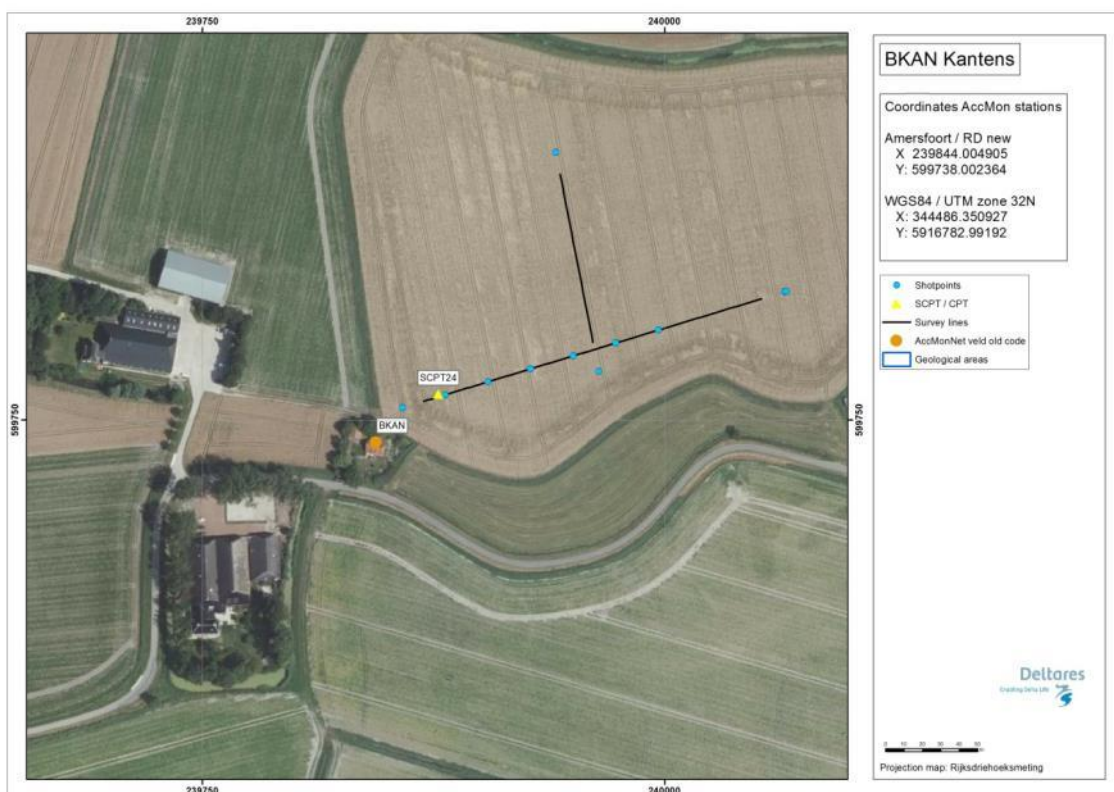


Figure 4.93 Map of location BKAN, showing the KNMI accelerograph station, SCPT location and MASW survey lines and shot locations.

### 4.9.2 Geological setting

The location is situated in an erosive area within distance of 750 metres from a non-erosive area in the southeast. The Holocene deposits consist of clay with an erosive sand base on top of a thin Pleistocene sand layer. Underneath 'Pot clay' (Peelo formation) can be found. Top of the Pleistocene at the location is found at a depth of approximately 20 metres. In the southeast the top Pleistocene depth is approximately 10 metres with a slope to the north and the northeast to 25 metres.

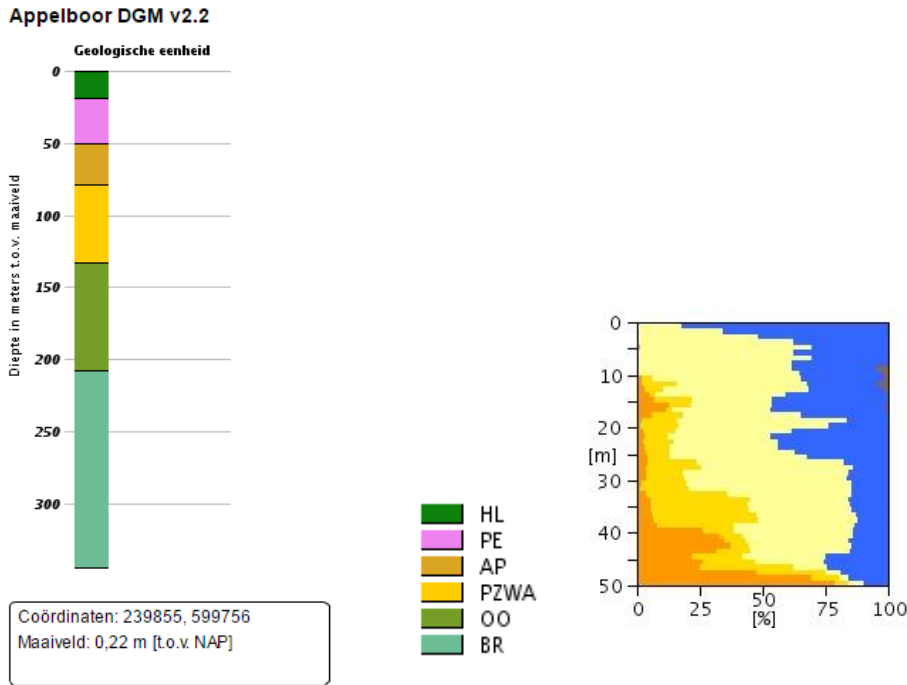


Figure 4.94 Geological information at station BKAN. Left: 1D section from the DGM model. Right: Section from the "delfstoffen online" model (GDN-TNO). Colour coding: brown = peat, blue = clay, yellow to orange = fine sand to coarse sand. The horizontal scale shows the volume percentage of each of the lithologies present at the location, the vertical scale is depth below the surface.

Table 4.9 Descriptions of representative deep boreholes near station BKAN from the DINO database ([www.dinoloket.nl](http://www.dinoloket.nl)).

Drilling	Distance from drilling	top	bottom	sediment type	Min. grain size	Max. grain size	Formation
B07E0049	2700mtr E	0,00	-1,00	Clay			Formation of Naaldwijk
		-1,00	-4,00	Sand	Extreme fine		Formation of Naaldwijk
		-4,00	-10,70	Clay			Formation of Naaldwijk
		-10,70	-12,00	Sand	Medium fine		Formation of Boxtel
		-12,00	-20,00	Sand	Very coarse	Extreme coarse	Formation of Boxtel/Eem
		-20,00	-21,00	Clay			Formation of Peelo
		-21,00	-32,00	Sand	Medium fine	Very coarse	Formation of Peelo
		-32,00	-54,00	Sand	Very coarse	Extreme coarse	Formation of Peelo/Appelscha
B07B0071	2500mtr W	0,00	-15,10	Clay			Formation of Naaldwijk
		-15,10	-16,00	Sand	Medium fine		Formation of Naaldwijk
		-16,00	-18,00	Clay			Formation of Peelo
		-18,00	-21,00	Sand	Very fine		Formation of Peelo
		-21,00	-26,00	Clay			Formation of Peelo
		-26,00	-31,50	Sand	Medium fine	Medium coarse	Formation of Peelo
		-31,50	-39,00	Sand	Medium coarse	Very coarse	Formation of Peelo
		-39,00	-58,00	Sand	Medium coarse	Extreme coarse	Formation of Peelo/Appelscha

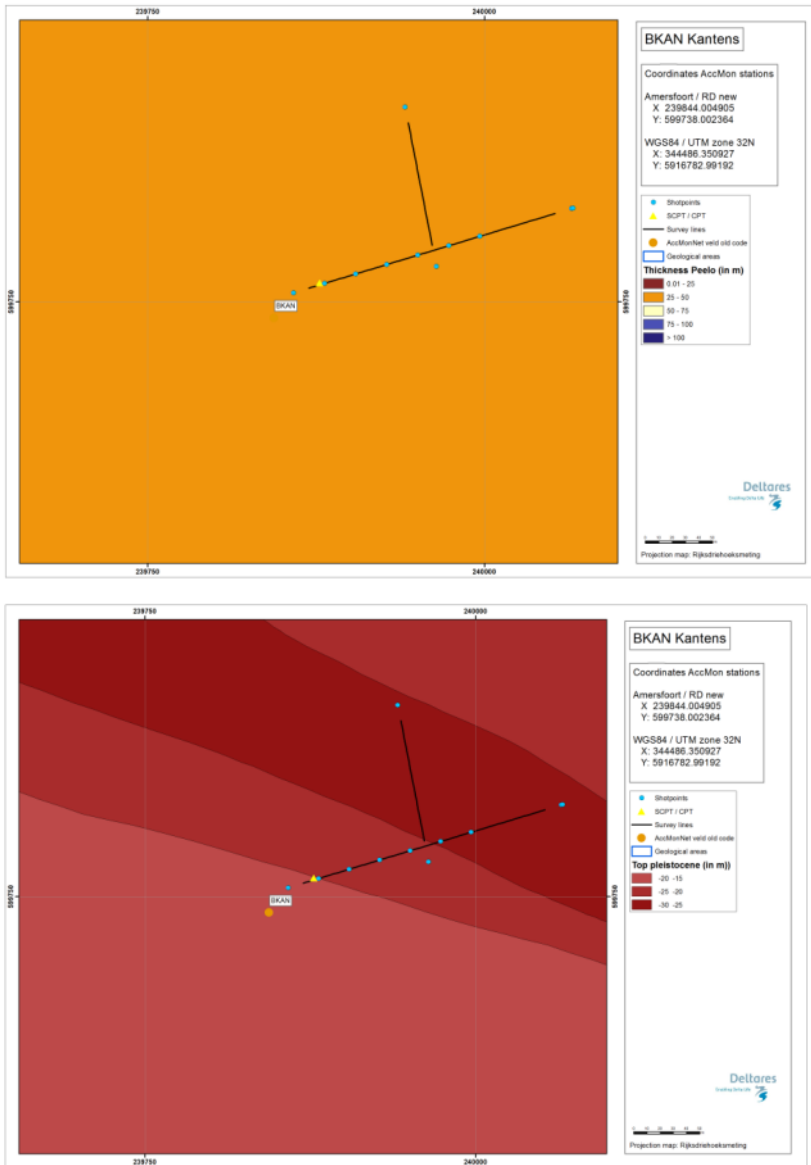


Figure 4.95 Overview map of geological setting based on beta version of GeoTOP model. Top panel: Thickness of the Peelo Formation, blue colour indicates thick Peelo layer, hence in the centre of the channel; red and orange colour indicates thin Peelo layers, hence areas outside the channel; yellow indicates transition zone. Lower panel: Top of Pleistocene surface relative to Dutch Ordnance Datum NAP.

## 4.9.3 SCPT

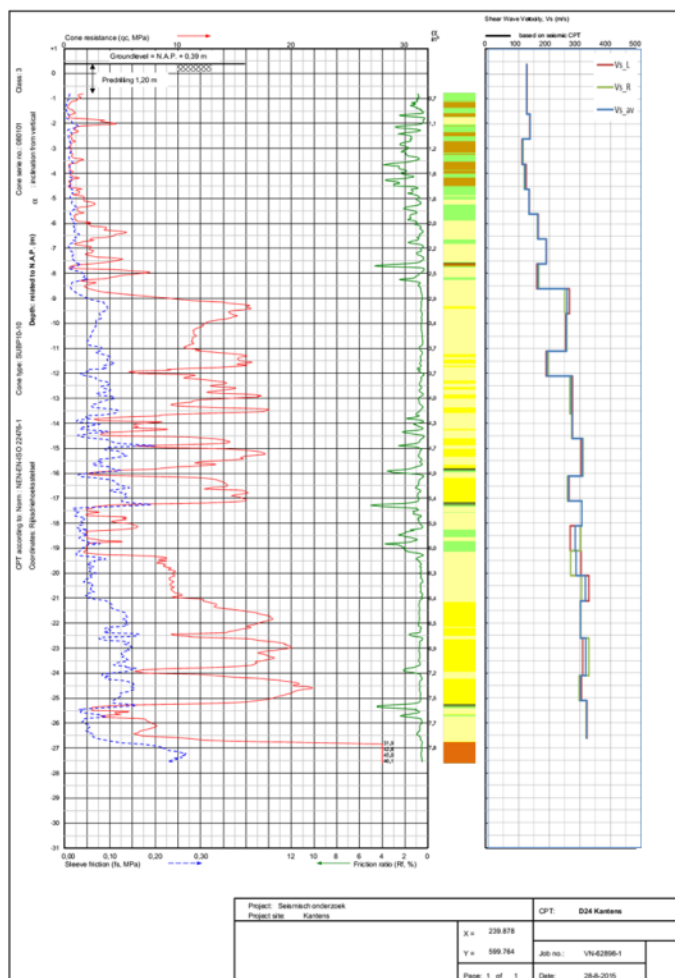


Figure 4.96 SCPT24. From left to right: CPT measurement, showing tip resistance, sleeve friction and friction ratio; automatically generated lithology (indication, for legend see Table 3.1);  $V_s$  profile (red = left blow, green = right blow, blue = average).

## 4.9.4 OSCPT

The OSCPT for this location is not available.

## 4.9.5 MASW

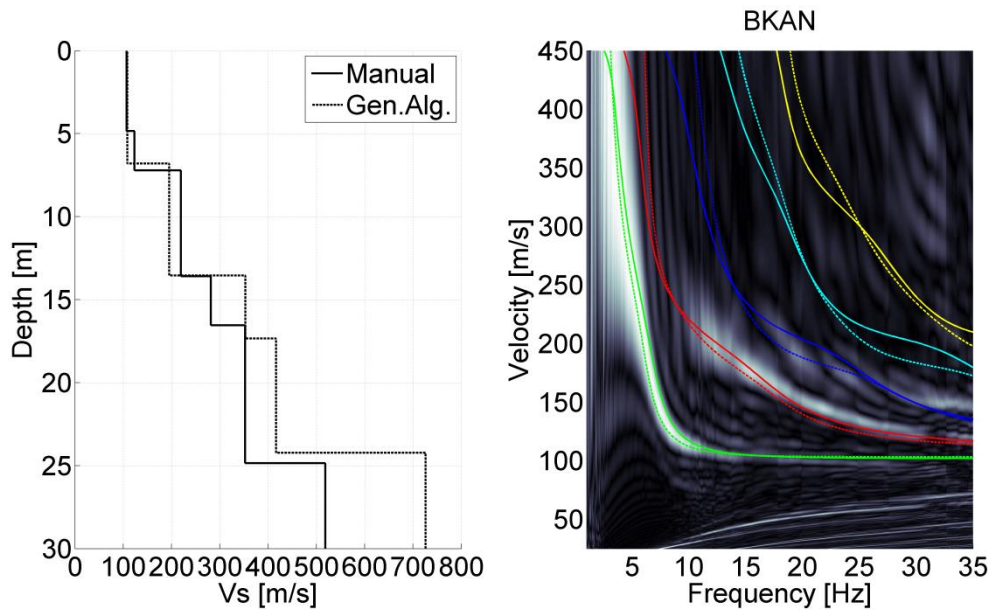


Figure 4.97 MASW result for station BKAN. Left panel:  $V_s$  profiles from active MASW. Solid line from manual fitting of dispersion curves; dashed line for automatic inversion. Right panel: energy in the dispersion plot in greyscale; solid lines are the modelled dispersion curves for different modes of the manually fitted  $V_s$  profile; dashed lines for the different modes of the automatically inverted  $V_s$  profile.

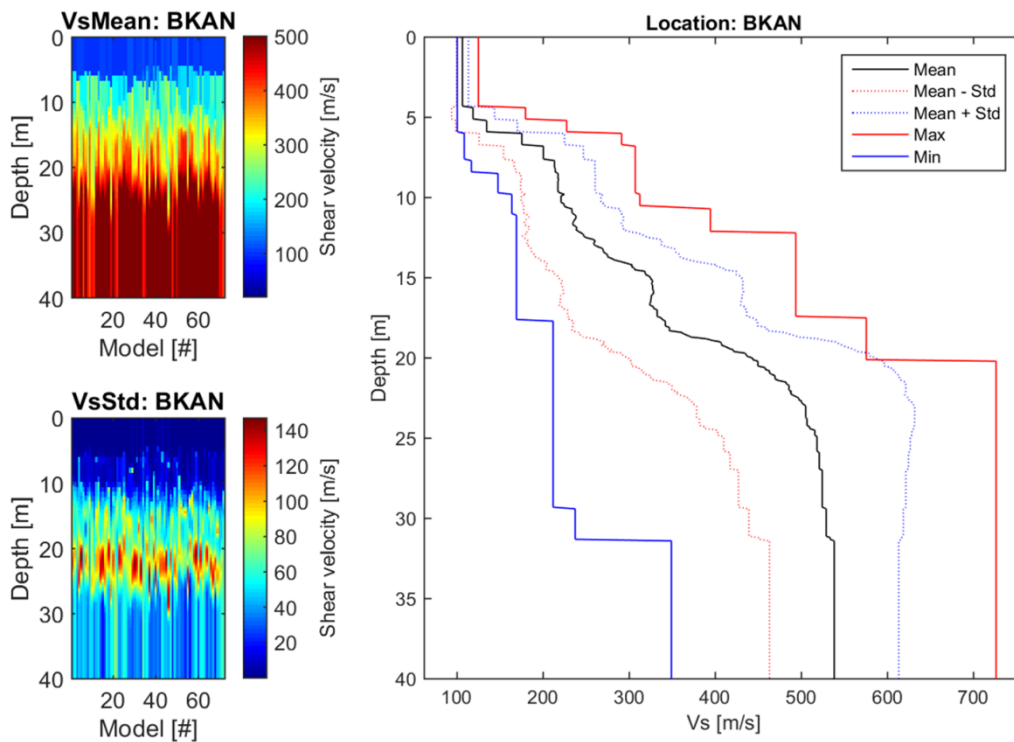


Figure 4.98 CMPcc result for BKAN. Top left: average  $V_s$  along the CMPcc array. Bottom left: standard deviation of  $V_s$  along the CMPcc array. Right: best fit curve of the 72 models with the maximum and minimum value observed in the whole CMPcc and the standard deviation from all models.

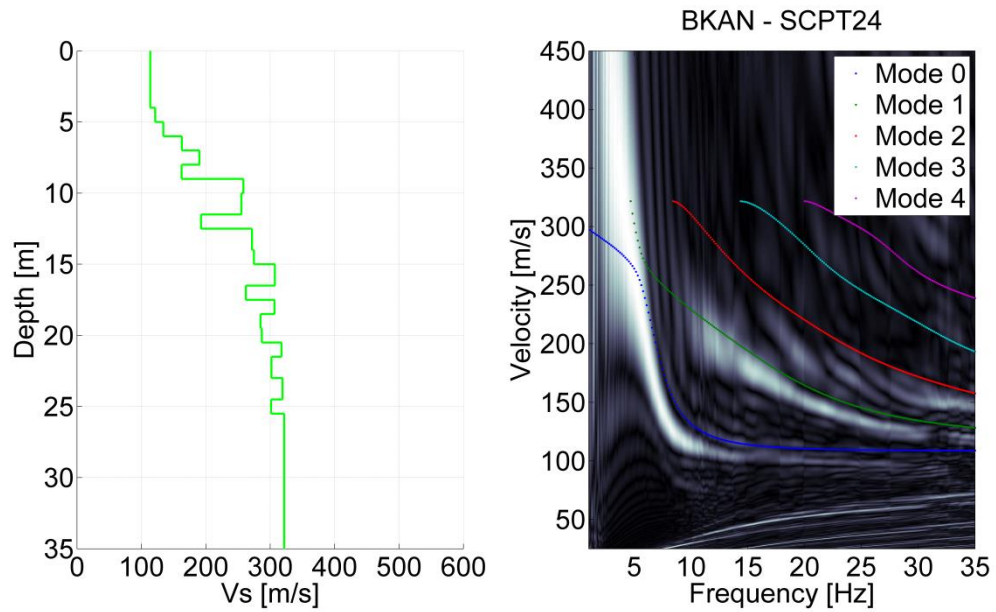


Figure 4.99 Comparison for BKAN of SCPT24 and MASW result. Left:  $V_s$  profile from SCPT. The  $V_s$  from the top 2 layers of the SCPT is generally unreliable and replaced by the minimum  $V_s$  of the first 3 layers. Right: modelled dispersion curves of different modes based on the SCPT  $V_s$  profile in coloured lines plotted on the energy of MASW dispersion plot in greyscale.



## 4.9.6 Synthesis

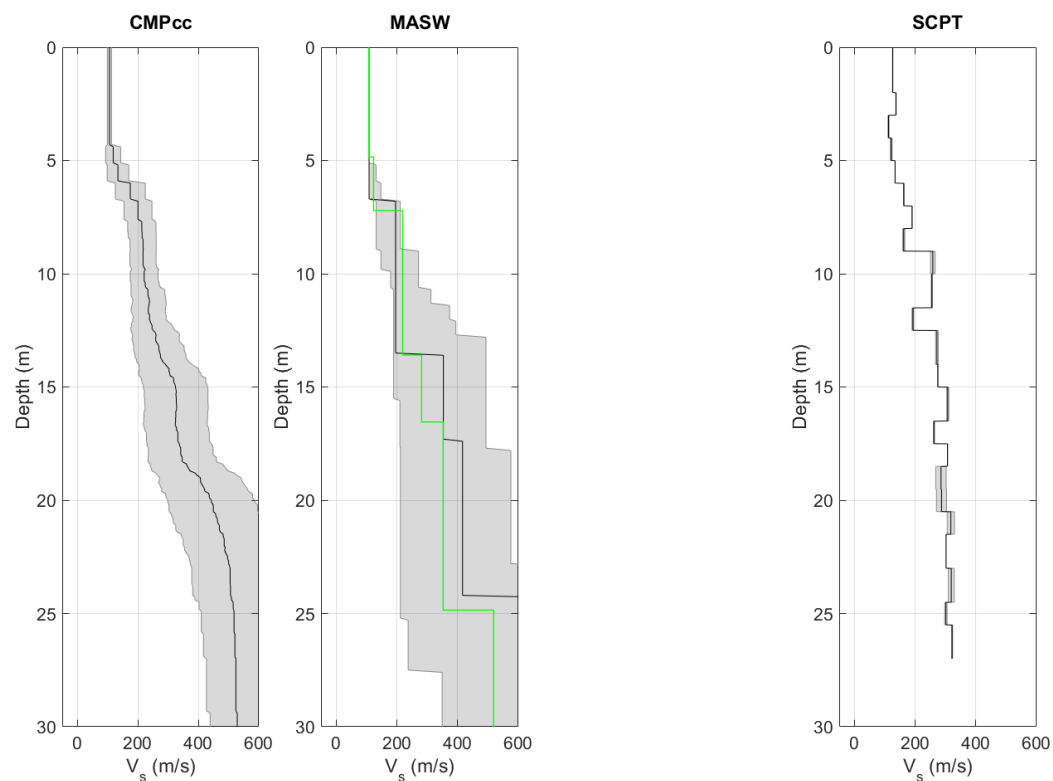


Figure 4.100  $V_s$  profiles from different measurement techniques, including uncertainty bands. From left to right: CMPcc based on active MASW array, shaded band indicates standard deviation; active MASW with manual fit in green and automatic inversion in black with grey shaded band indicating the minimum and the maximum  $V_s$ ; average profile for offset SCPTs between 1 and 5 m offset for 1 or 2 SCPTs with shaded band indicating the minimum and the maximum  $V_s$ ; SCPTs with band indicating variation between left and right blow; cross-hole average profiles for long leg in blue and short leg in grey with shaded band indicating the minimum and the maximum  $V_s$ .

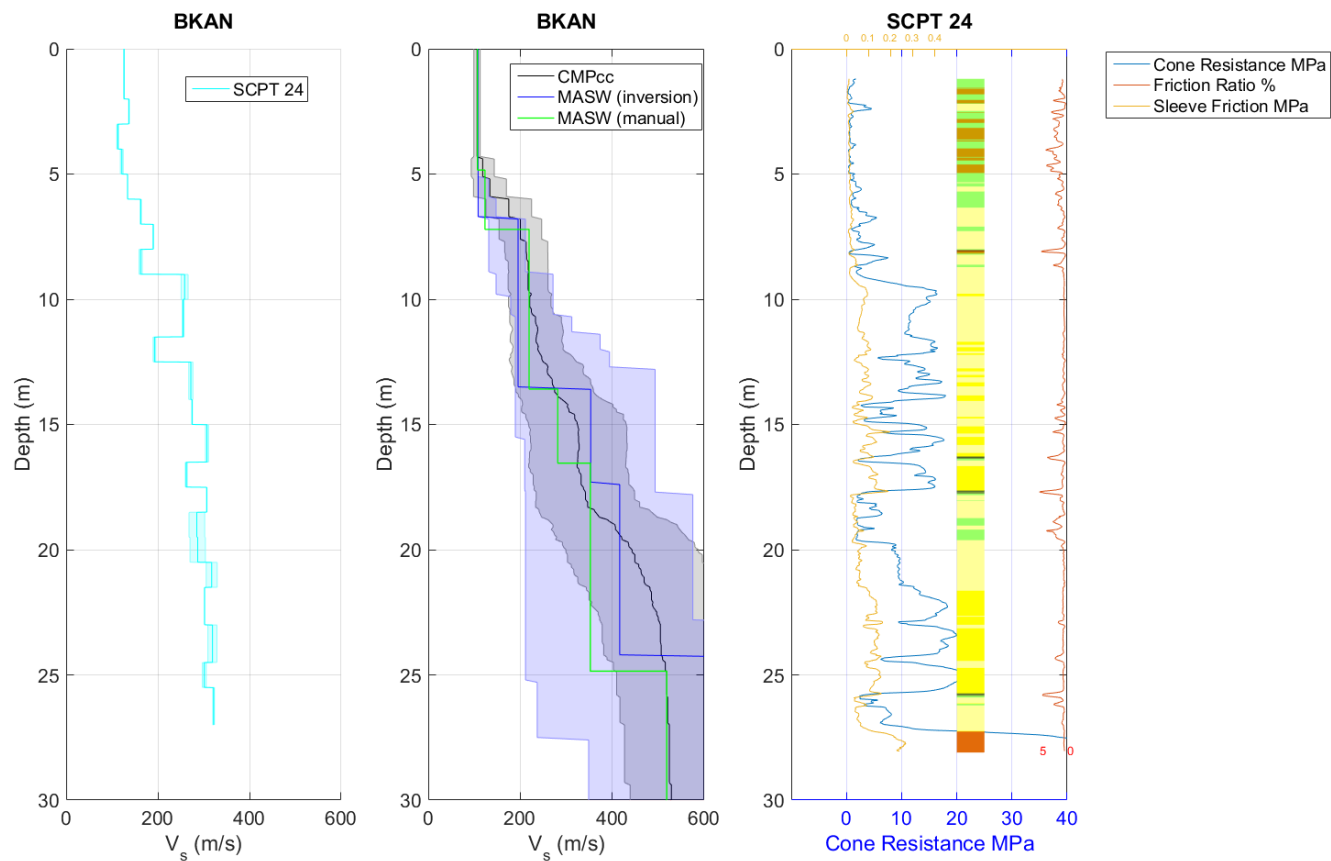


Figure 4.101 Synthesis of  $V_s$  results. Unreliable results are shown in red. From left to right: SCPT with band indicating variation between left and right blow; CMPcc, MASW and average cross-hole results with uncertainty bands; CPT with cone resistance, friction ratio, sleeve friction and automatically generated lithology (indication, for legend see Table 3.1).

## 4.10 Loppersum- BLOP

### 4.10.1 Location

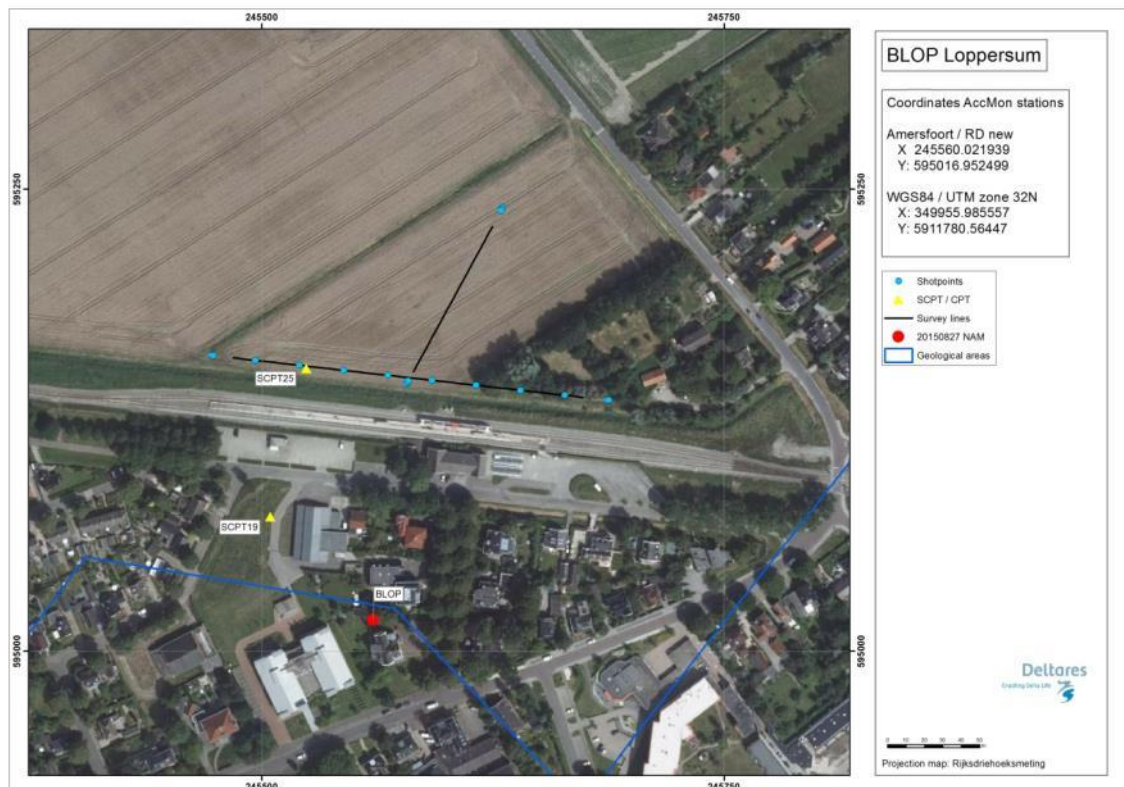


Figure 4.102 Map of location BLOP, showing the KNMI accelerograph station, SCPT location and MASW survey lines and shot locations.

### 4.10.2 Geological setting

The location is situated in an erosive area with clay on top of the Pleistocene. The top of the Pleistocene is situated at a depth of  $\pm 10$  metres. The Holocene deposits consist mainly of Clay. To the south east at a distance of 500 metres a thin layer of basic peat covers the Pleistocene. The location is situated on a declining slope of a Peelo valley that reaches from 70 metres at the location up to the maximum depth of 115 metres in the centre over a distance of 2 kilometres to the southeast.

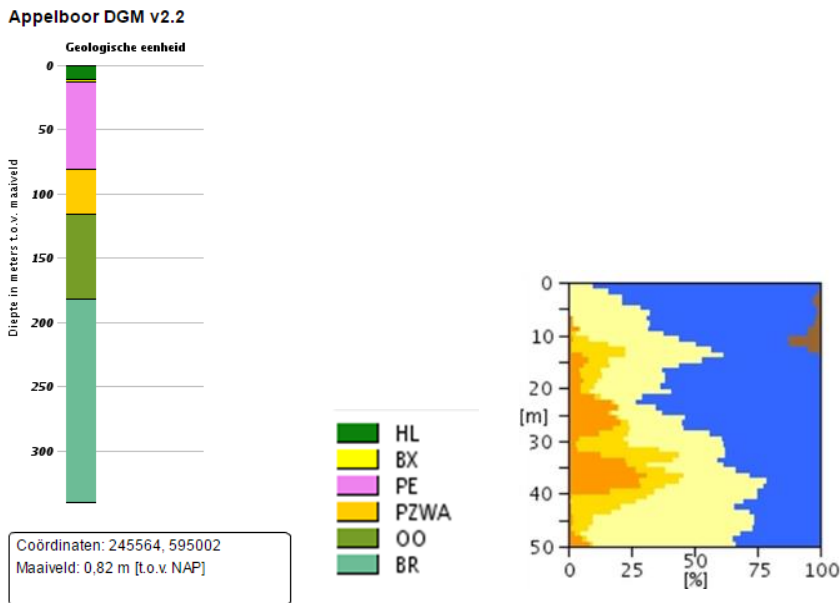


Figure 4.103 Geological information at station BLOP. Left: 1D section from the DGM model. Right: Section from the “delfstoffen online” model (GDN-TNO). Colour coding: brown = peat, blue = clay, yellow to orange = fine sand to coarse sand. The horizontal scale shows the volume percentage of each of the lithologies present at the location, the vertical scale is depth below the surface.

Table 4.10 Descriptions of representative deep boreholes near station BLOP from the DINO database (www.dinoloket.nl).

Drilling	Distance from drilling	top	bottom	sediment type	Min. grain size	Max. grain size	Formation
B07E0022	100mtr W	1,00	-3,00	Clay			Formation of Naaldwijk
		-3,00	-6,00	Sand	Fine		Formation of Naaldwijk
		-6,00	-8,00	Clay			Formation of Naaldwijk
		-8,00	-10,00	Sand	Fine		Formation of Boxtel
		-10,00	-13,50	Boulderclay			Formation of Drente
		-13,50	-59,50	Sand	Medium coarse		Formation of Peelo
		-59,50	-69,00	Sand	Coarse		Formation of Peelo/Appelscha
B07E0004	3000mtr S	0,00	-7,80	Clay			Formation of Naaldwijk
		-7,80	-12,30	Sand	Fine		Formation of Boxtel
		-12,30	-77,00	Clay			Formation of Peelo
		-77,00	-99,00	Sand	Fine		Formation of Peelo
		-99,00	-118,30	Sand	Medium coarse		Formation of Peelo
		-118,30	-130,00	Sand	Fine		Formation of Peelo

1210624-000-BGS-0007, Version 2, 27 June 2016, final

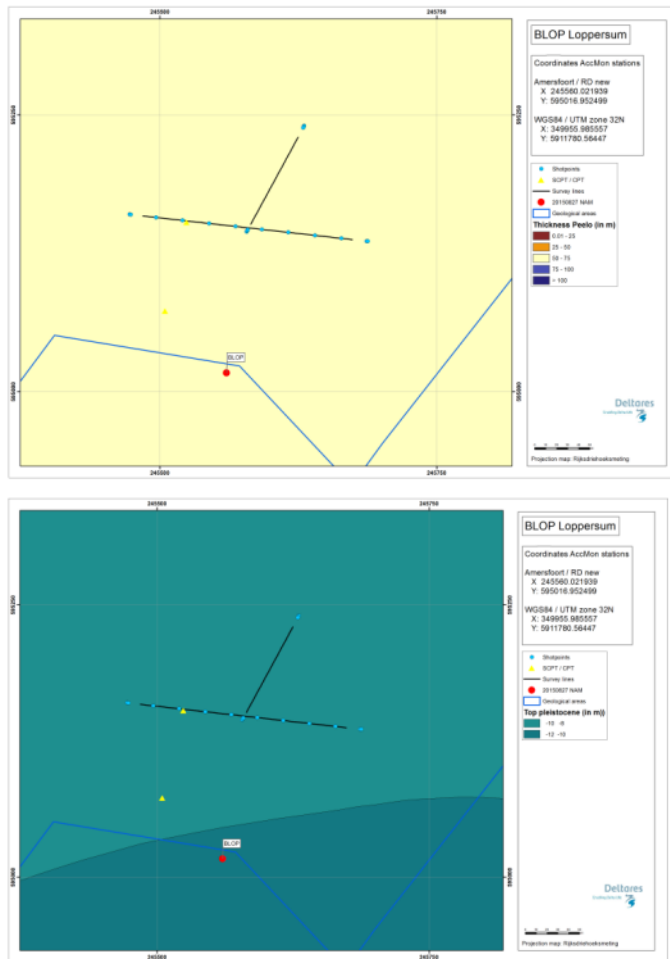


Figure 4.104 Overview map of geological setting based on beta version of GeoTOP model. Top panel: Thickness of the Peelo Formation, blue colour indicates thick Peelo layer, hence in the centre of the channel; red and orange colour indicates thin Peelo layers, hence areas outside the channel; yellow indicates transition zone. Lower panel: Top of Pleistocene surface relative to Dutch Ordnance Datum NAP.

## 4.10.3 SCPT

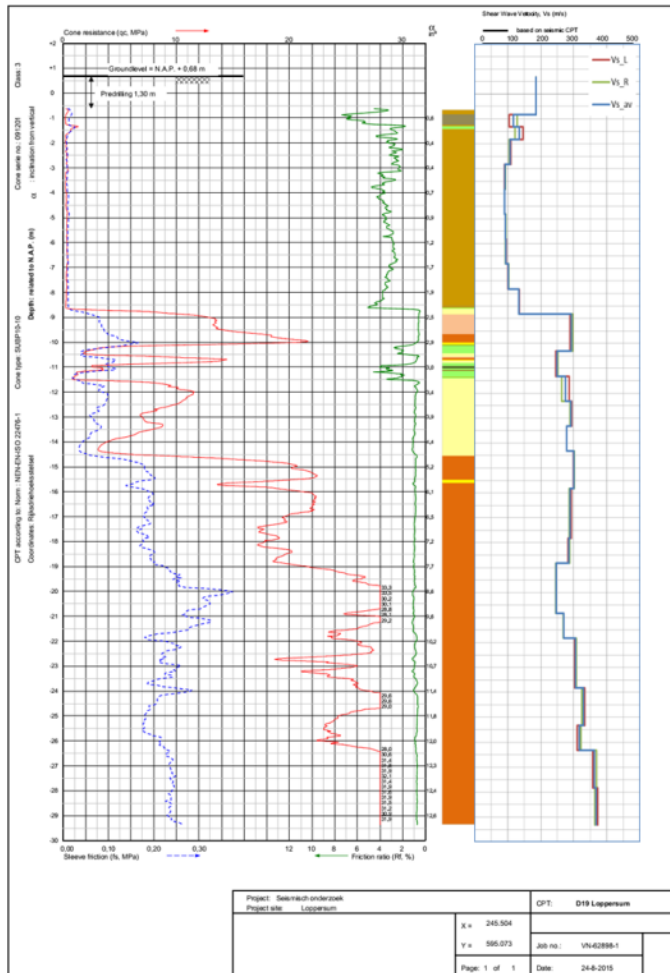


Figure 4.105 SCPT19. From left to right: CPT measurement, showing tip resistance, sleeve friction and friction ratio; automatically generated lithology (indication, for legend see Table 3.1);  $V_s$  profile (red = left blow, green = right blow, blue = average).

1210624-000-BGS-0007, Version 2, 27 June 2016, final

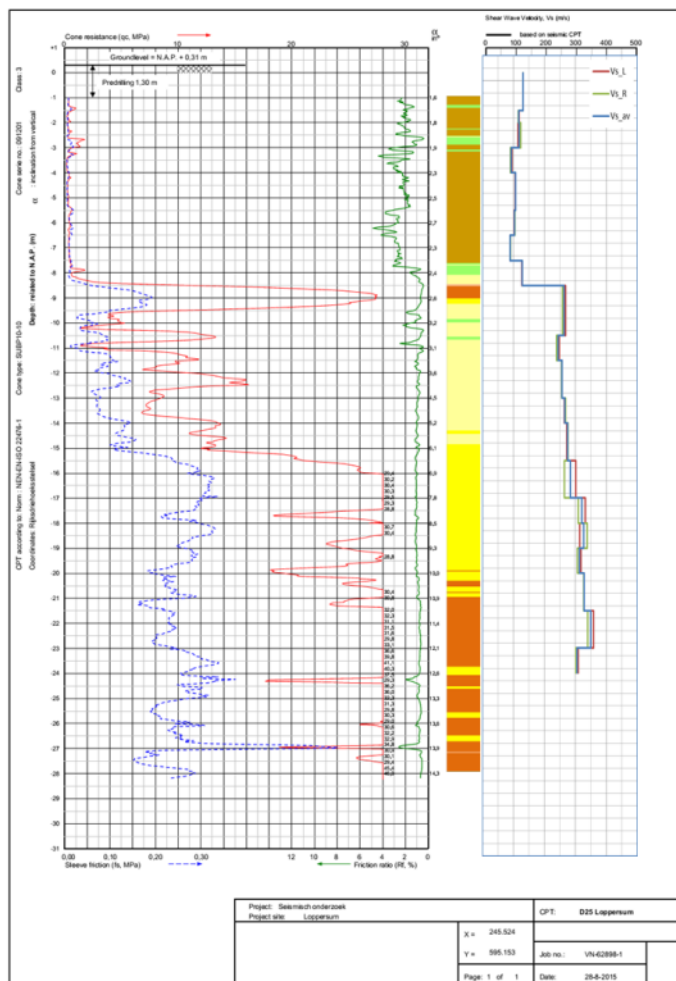


Figure 4.106 SCPT25. From left to right: CPT measurement, showing tip resistance, sleeve friction and friction ratio; automatically generated lithology (indication, for legend see Table 3.1);  $V_s$  profile (red = left blow, green = right blow, blue = average).

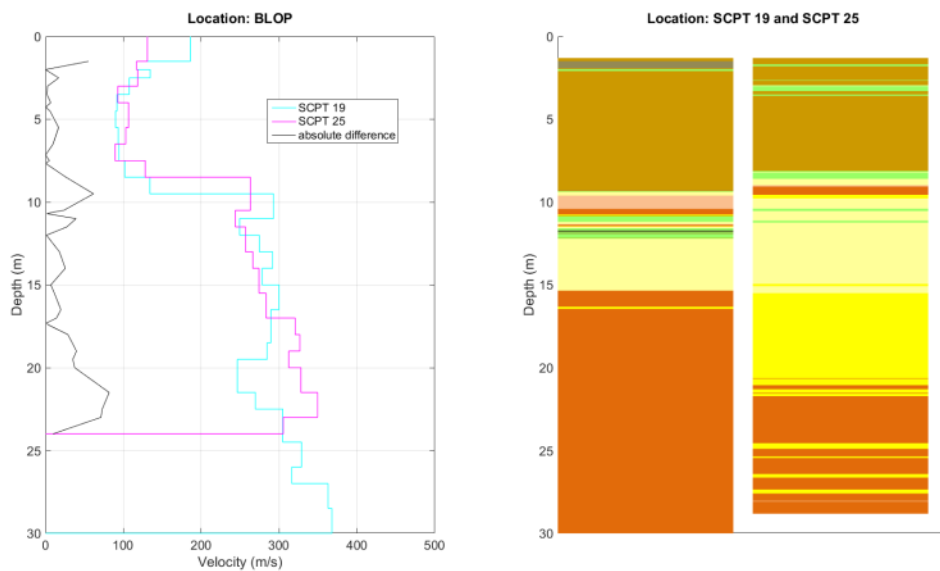


Figure 4.107 Station BLOP. Left: Difference between the two SCPTs measured at the same station location. Right: automatically generated lithology (indication).

## 4.10.4 OSCPT

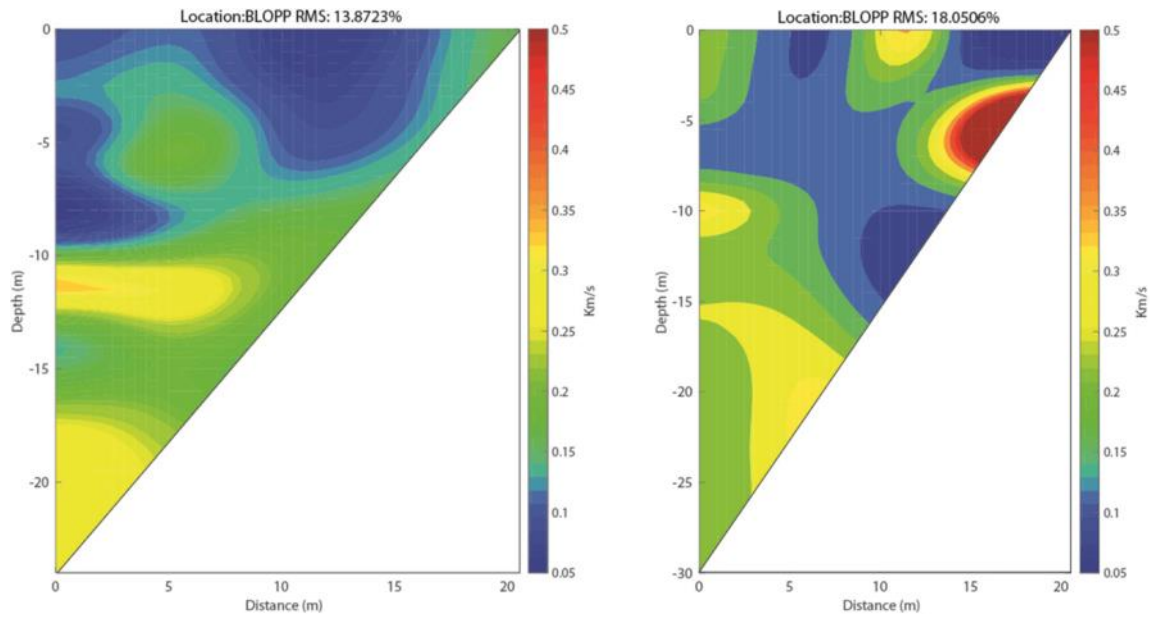


Figure 4.108 Tomographic images based on OSCPT results from two SCPTs for station BLOP (left SCPT25; right SCPT19).

## 4.10.5 MASW

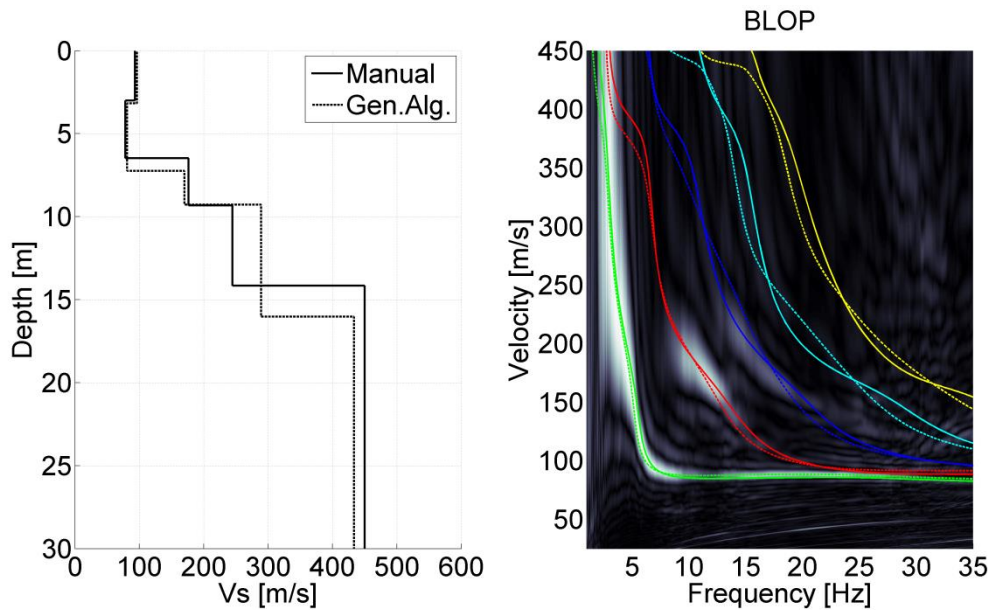


Figure 4.109 MASW result for station BLOP. Left panel:  $V_s$  profiles from active MASW. Solid line from manual fitting of dispersion curves; dashed line for automatic inversion. Right panel: energy in the dispersion plot in greyscale; solid lines are the modelled dispersion curves for different modes of the manually fitted  $V_s$  profile; dashed lines for the different modes of the automatically inverted  $V_s$  profile.

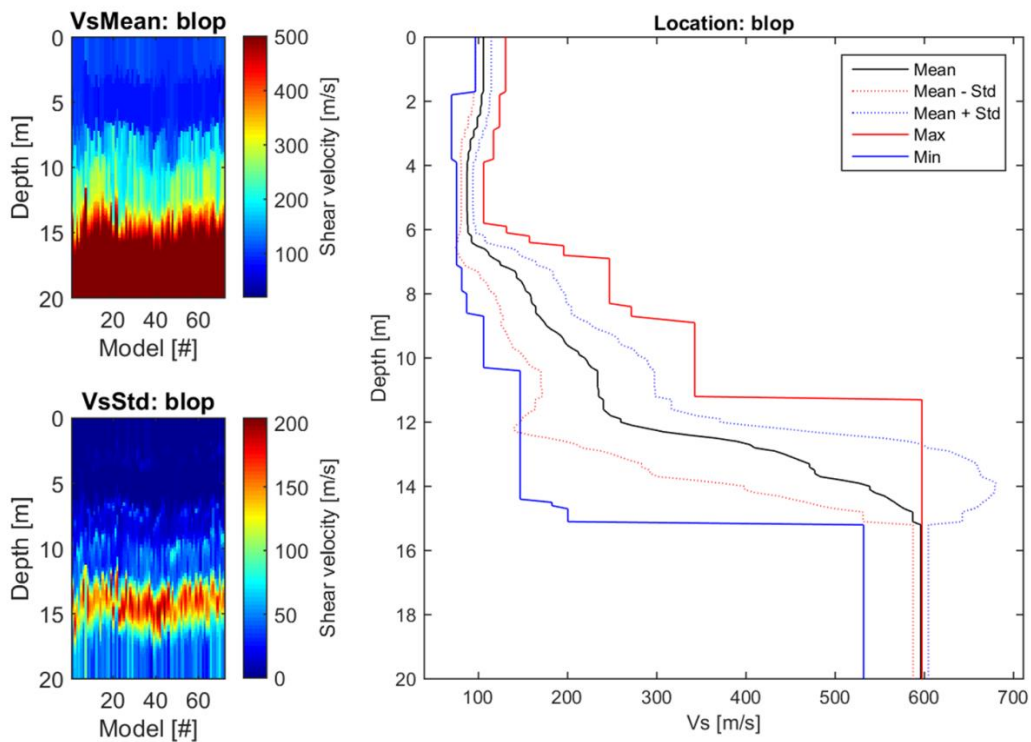


Figure 4.110 CMPcc result for BLOP. Top left: average  $V_s$  along the CMPcc array. Bottom left: standard deviation of  $V_s$  along the CMPcc array. Right: best fit curve of the 72 models with the maximum and minimum value observed in the whole CMPcc and the standard deviation from all models.

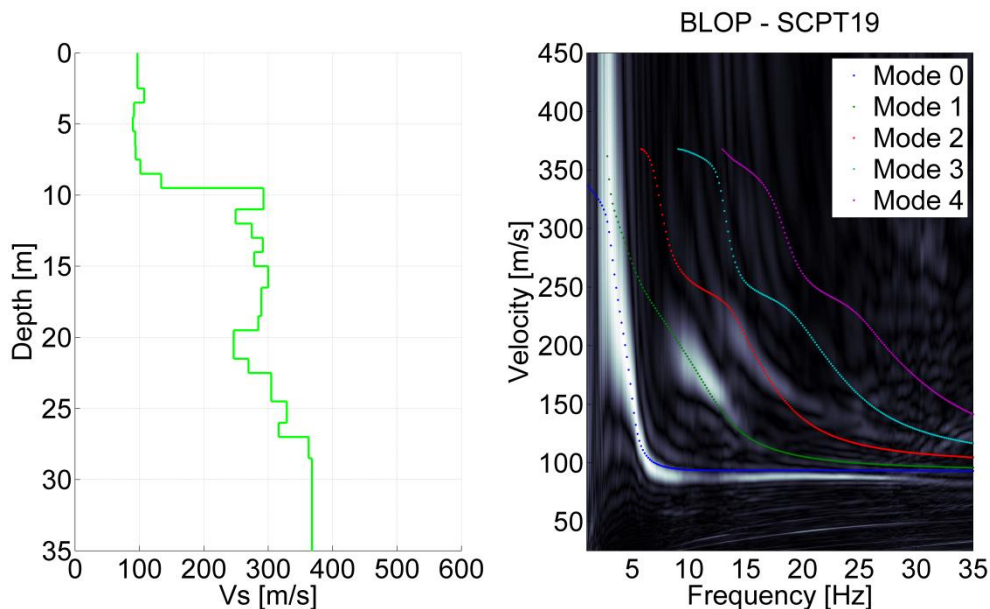


Figure 4.111 Comparison for BLOP of SCPT19 and MASW result. Left:  $V_s$  profile from SCPT. The  $V_s$  from the top 2 layers of the SCPT is generally unreliable and replaced by the minimum  $V_s$  of the first 3 layers. Right: modelled dispersion curves of different modes based on the SCPT  $V_s$  profile in coloured lines plotted on the energy of MASW dispersion plot in greyscale.

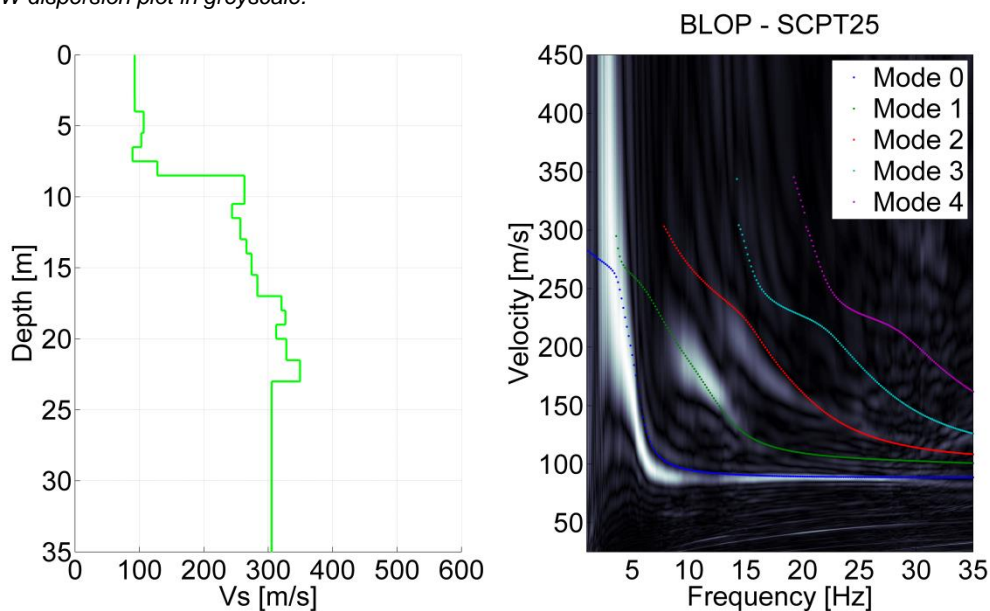


Figure 4.112 Comparison for BLOP of SCPT25 and MASW result. Left:  $V_s$  profile from SCPT. The  $V_s$  from the top 2 layers of the SCPT is generally unreliable and replaced by the minimum  $V_s$  of the first 3 layers. Right: modelled dispersion curves of different modes based on the SCPT  $V_s$  profile in coloured lines plotted on the energy of MASW dispersion plot in greyscale.



## 4.10.6 Synthesis

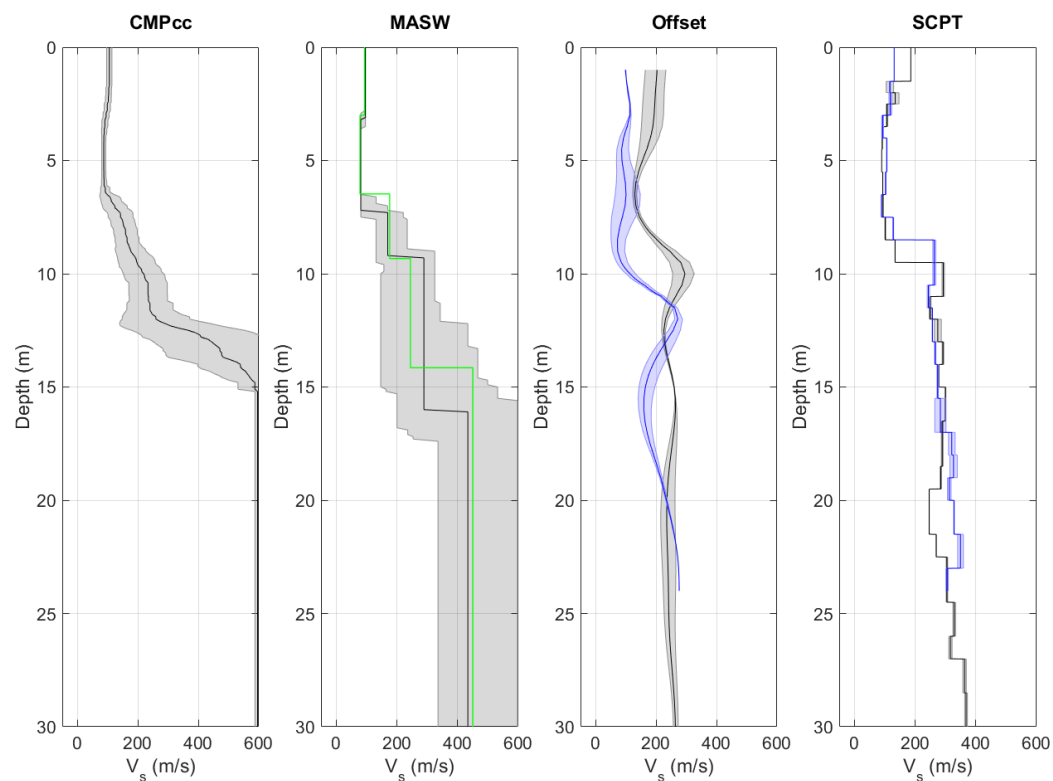


Figure 4.113  $V_s$  profiles from different measurement techniques, including uncertainty bands. From left to right: CMPcc based on active MASW array, shaded band indicates standard deviation; active MASW with manual fit in green and automatic inversion in black with grey shaded band indicating the minimum and the maximum  $V_s$ ; average profile for offset SCPTs between 1 and 5 m offset for 1 or 2 SCPTs with shaded band indicating the minimum and the maximum  $V_s$ ; SCPTs with band indicating variation between left and right blow; cross-hole average profiles for long leg in blue and short leg in grey with shaded band indicating the minimum and the maximum  $V_s$ .

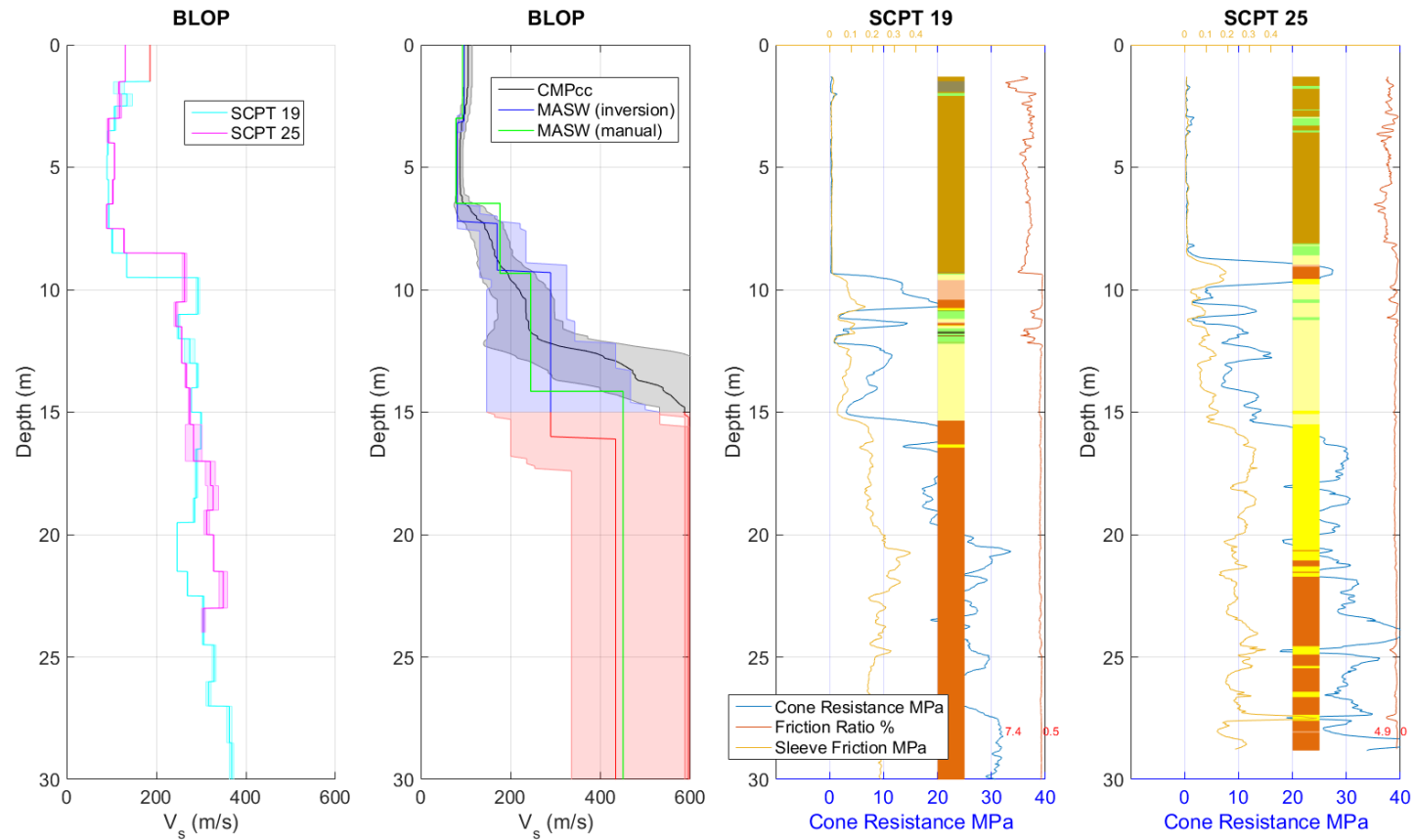


Figure 4.114 Synthesis of  $V_s$  results. Unreliable results are shown in red. From left to right: SCPT with band indicating variation between left and right blow; CMPcc, MASW and average cross-hole results with uncertainty bands; CPT with cone resistance, friction ratio, sleeve friction and automatically generated lithology (indication, for legend see Table 3.1).

## 4.11 Middelstum 1-BMD1

### 4.11.1 Location



Figure 4.115 Map of location BMD1, showing the KNMI accelerograph station, SCPT location and MASW survey lines and shot locations.

### 4.11.2 Geological setting

The location is situated in a non-erosive area bordering a small erosive valley in the north at a distance of 700 metres with a depth up to 15 metres. Pleistocene is covered by Holocene deposits with a thickness of approximately 10 metres. The deposits can be divided in a coverage layer of clay with a thickness of approximately 3 metres on a sandy layer. The basal peat and older clay were not eroded and are still present.

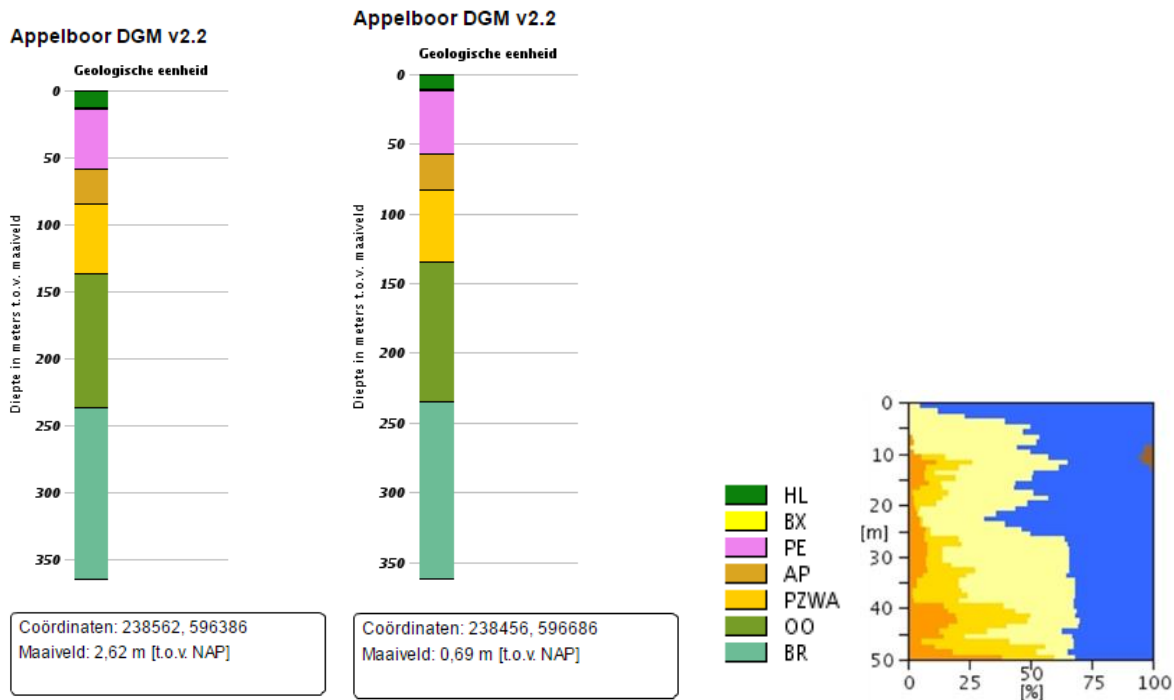
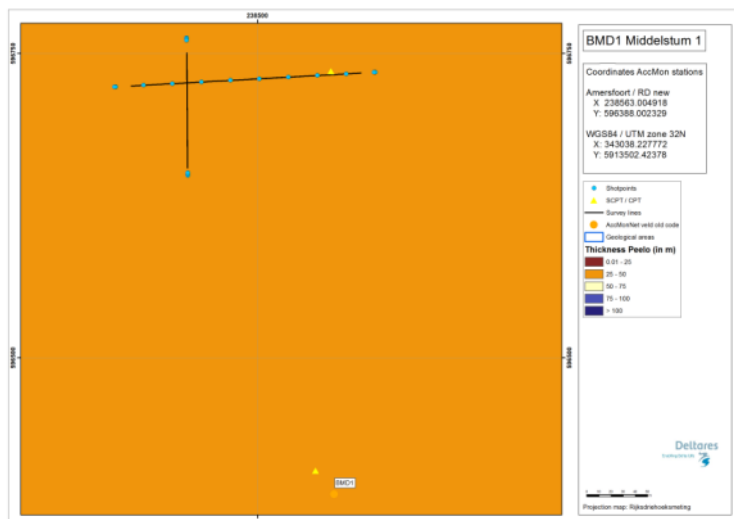
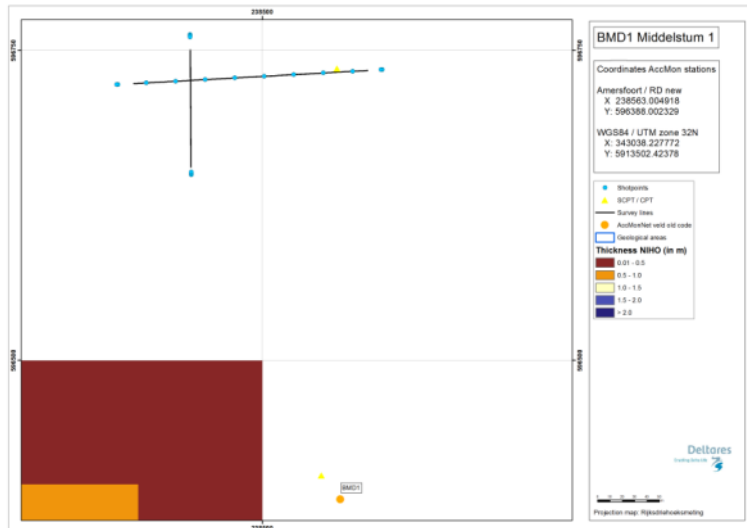


Figure 4.116 Geological information at station BMD1. Left: 1D section from the DGM model. Right: Section from the “delfstoffen online” model (GDN-TNO). Colour coding: brown = peat, blue = clay, yellow to orange = fine sand to coarse sand. The horizontal scale shows the volume percentage of each of the lithologies present at the location, the vertical scale is depth below the surface.

Table 4.11 Descriptions of representative deep boreholes near station BMD1 from the DINO database ([www.dinoloket.nl](http://www.dinoloket.nl)).

Drilling	Distance from drilling	top	bottom	sediment type	Min. grain size	Max. grain size	Formation
B07B0001	260mtr NW	1,86	-1,04	Clay			Formation of Naaldwijk
		-1,04	-9,19	Sand	Very fine		Formation of Naaldwijk
		-9,19	-9,64	Clay			Formation of Naaldwijk
		-9,64	-9,94	Peat			Formation of Nieuwkoop
		-9,94	-10,89	Sand	Fine		Formation of Boxtel
		-10,89	-54,14	Clay			Formation of Peelo
		-54,14	-68,14	Sand	Coarse		Formation of Appelscha
		-68,14	-68,34	Sand	Medium coarse		Formation of Peize

1210624-000-BGS-0007, Version 2, 27 June 2016, final



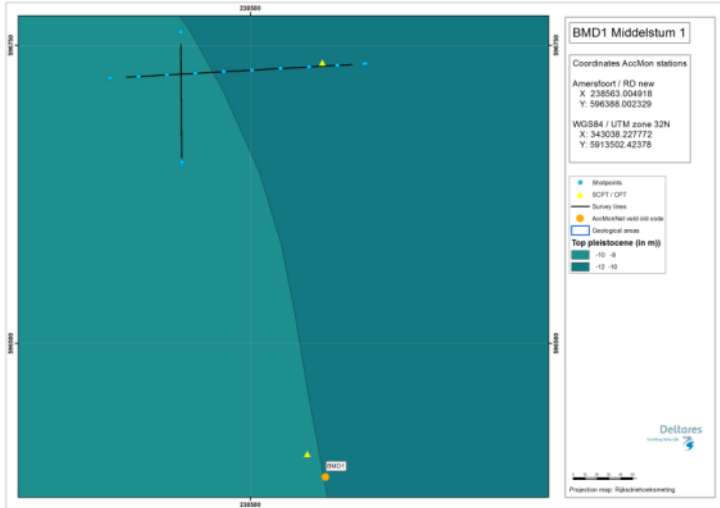


Figure 4.117 Overview map of geological setting based on beta version of GeoTOP model. Top panel: Thickness of the Holocene peat. Middle panel: Thickness of the Peelo Formation, blue colour indicates thick Peelo layer, hence in the centre of the channel; red and orange colour indicates thin Peelo layers, hence areas outside the channel; yellow indicates transition zone. Lower panel: Top of Pleistocene surface relative to Dutch Ordnance Datum NAP.

## 4.11.3 SCPT

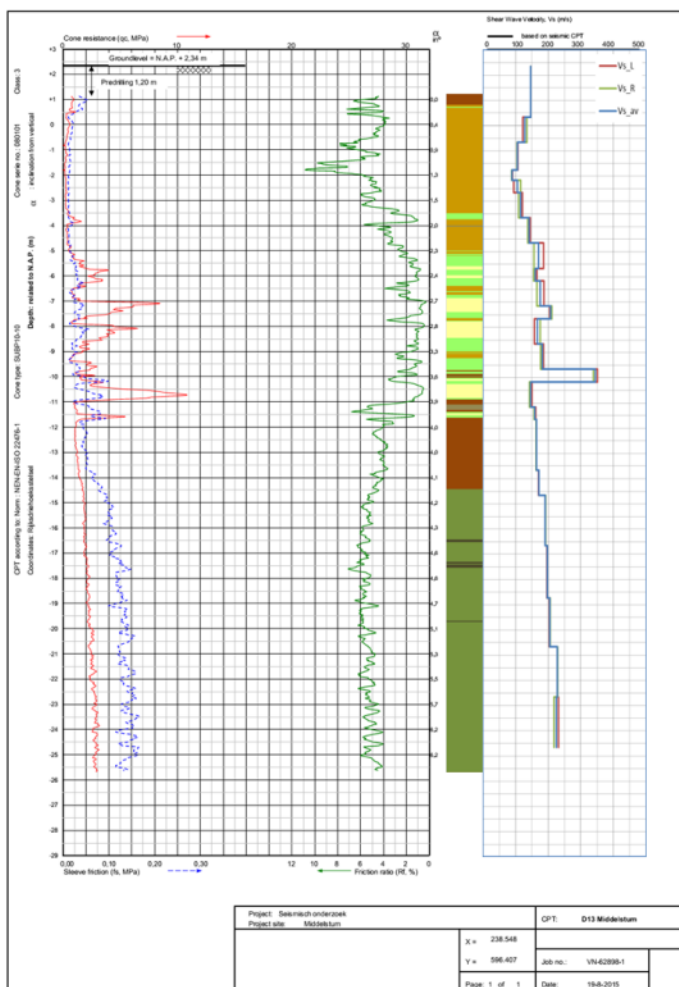


Figure 4.118 SCPT13. From left to right: CPT measurement, showing tip resistance, sleeve friction and friction ratio; automatically generated lithology (indication, for legend see Table 3.1);  $V_s$  profile (red = left blow, green = right blow, blue = average).

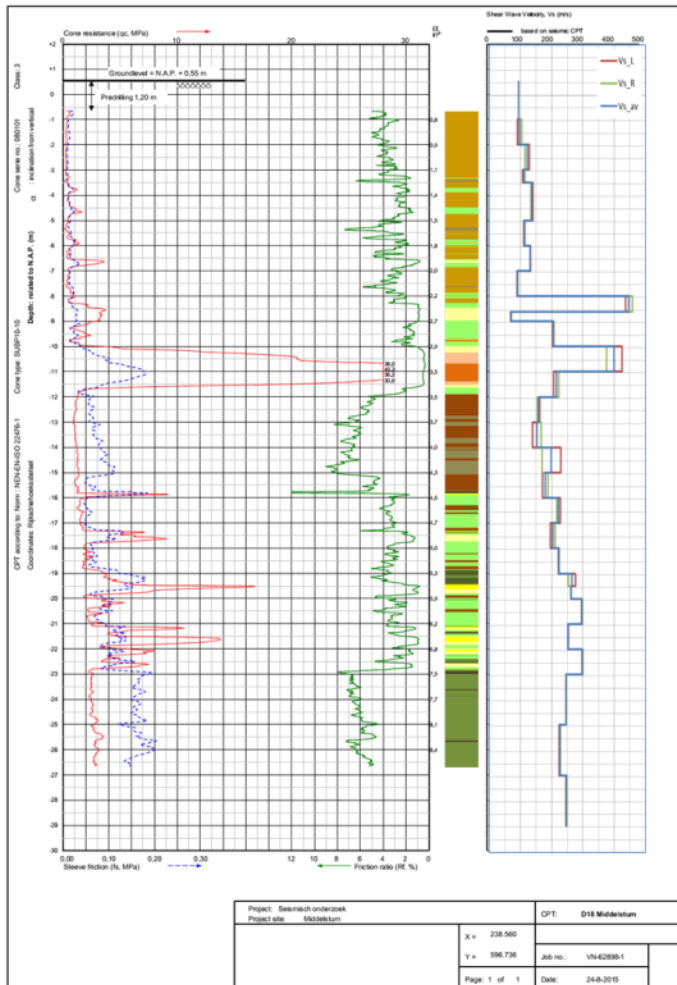


Figure 4.119 SCPT18 (in between BMD1 and BMD2). From left to right: CPT measurement, showing tip resistance, sleeve friction and friction ratio; automatically generated lithology (indication, for legend see Table 3.1);  $V_s$  profile (red = left blow, green = right blow, blue = average).

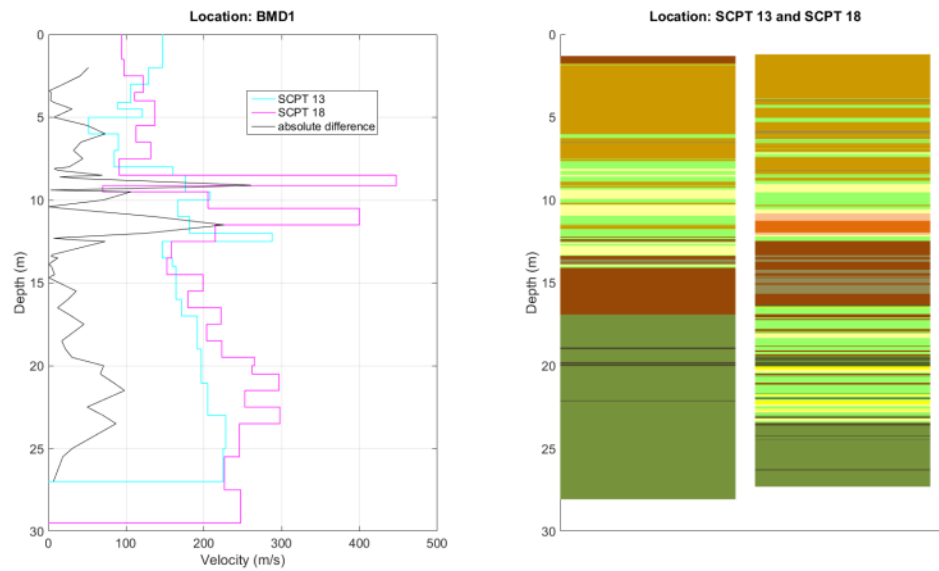


Figure 4.120 Station BMD1. Left: Difference between the two SCPTs measured at the same station location. Right: automatically generated lithology (indication).

## 4.11.4 OSCPT

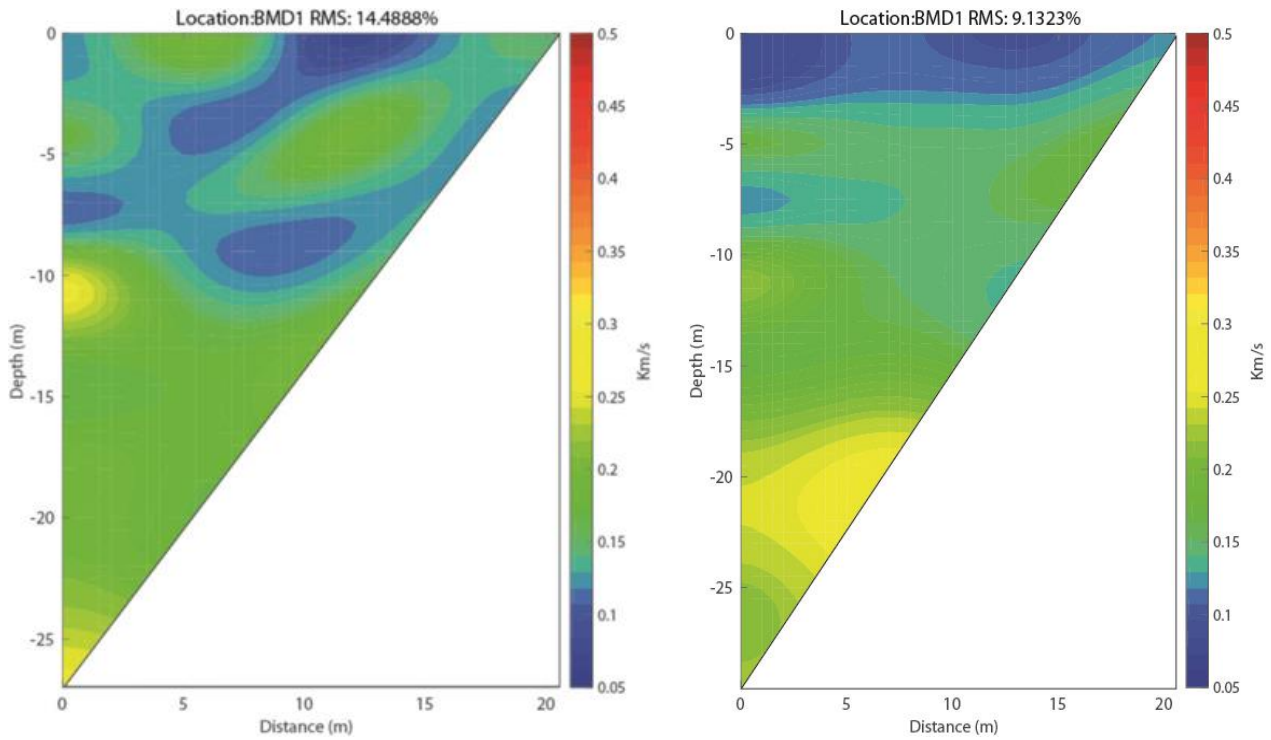


Figure 4.121 Tomographic images based on OSCPT results from two SCPTs for station BMD1 (left SCPT13; right SCPT18).

## 4.11.5 MASW

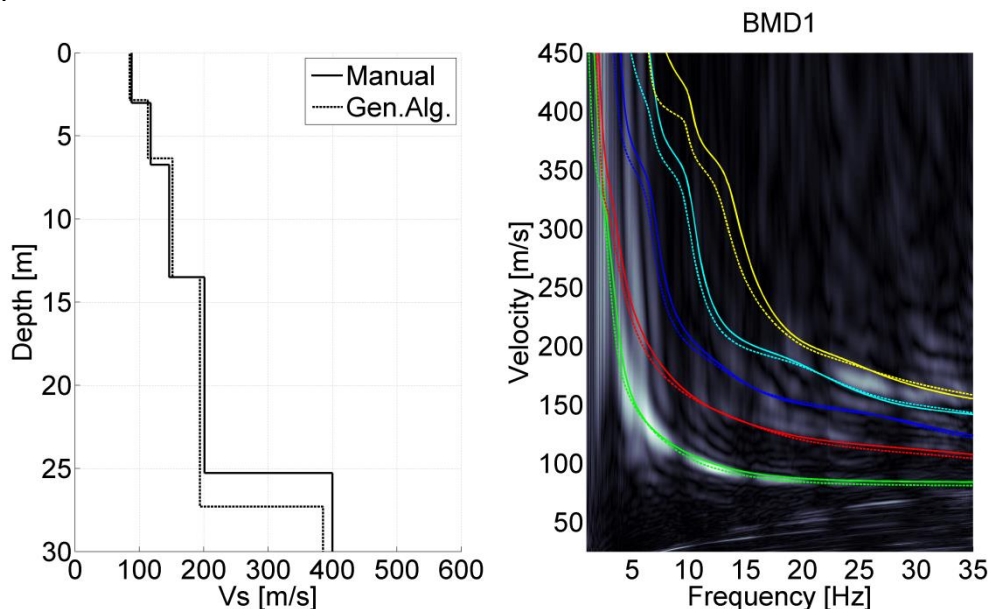


Figure 4.122 MASW result for station BMD1. Left panel:  $V_s$  profiles from active MASW. Solid line from manual fitting of dispersion curves; dashed line for automatic inversion. Right panel: energy in the dispersion plot in greyscale; solid lines are the modelled dispersion curves for different modes of the manually fitted  $V_s$  profile; dashed lines for the different modes of the automatically inverted  $V_s$  profile.

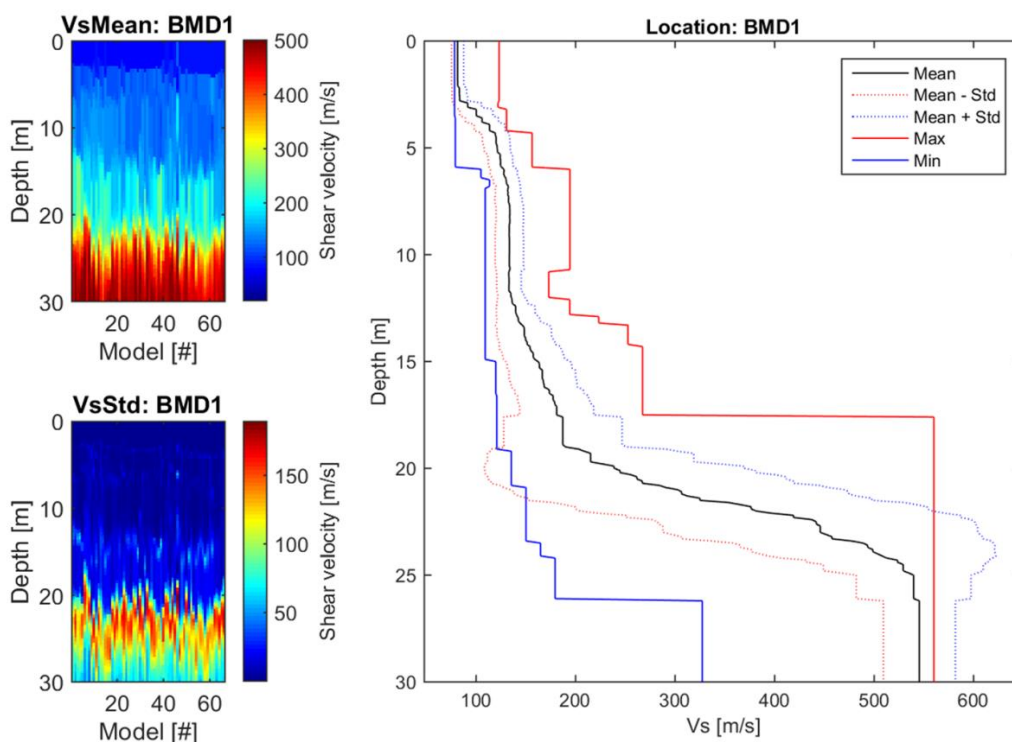


Figure 4.123 CMPcc result for BMD1. Top left: average  $V_s$  along the CMPcc array. Bottom left: standard deviation of  $V_s$  along the CMPcc array. Right: best fit curve of the 72 models with the maximum and minimum value observed in the whole CMPcc and the standard deviation from all models.

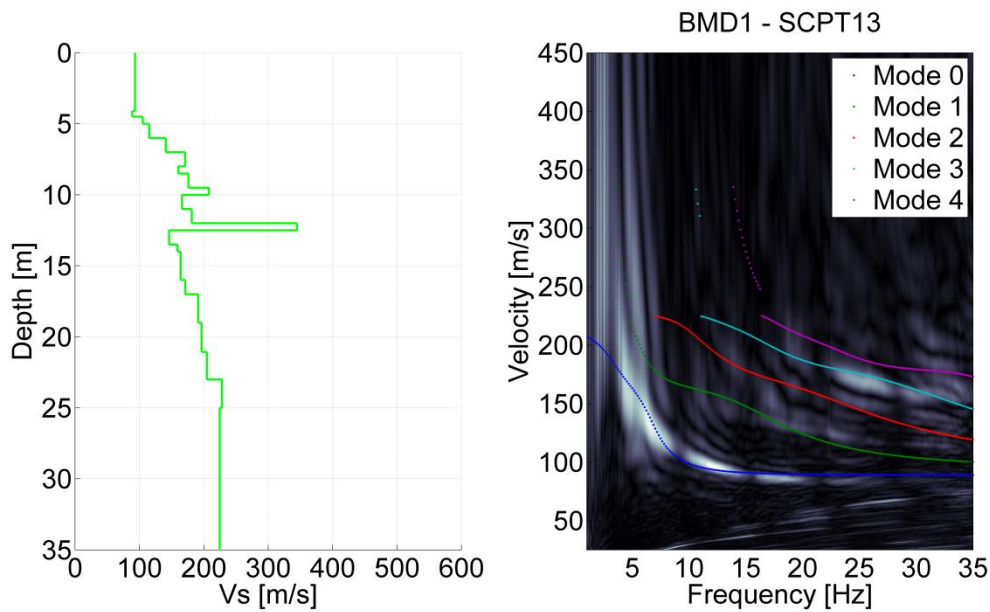


Figure 4.124 Comparison for BMD1 of SCPT13 and MASW result. Left:  $V_s$  profile from SCPT. The  $V_s$  from the top 2 layers of the SCPT is generally unreliable and replaced by the minimum  $V_s$  of the first 3 layers. Right: modelled dispersion curves of different modes based on the SCPT  $V_s$  profile in coloured lines plotted on the energy of MASW dispersion plot in greyscale.

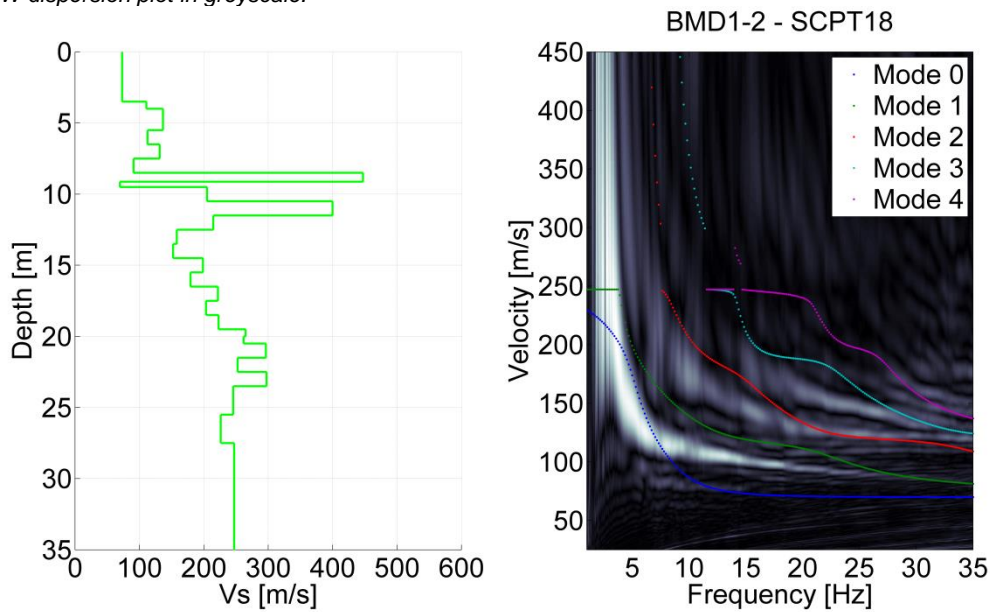


Figure 4.125 Comparison for BMD1 of SCPT18 and MASW result. Left:  $V_s$  profile from SCPT. The  $V_s$  from the top 2 layers of the SCPT is generally unreliable and replaced by the minimum  $V_s$  of the first 3 layers. Right: modelled dispersion curves of different modes based on the SCPT  $V_s$  profile in coloured lines plotted on the energy of MASW dispersion plot in greyscale.

## 4.11.6 Synthesis

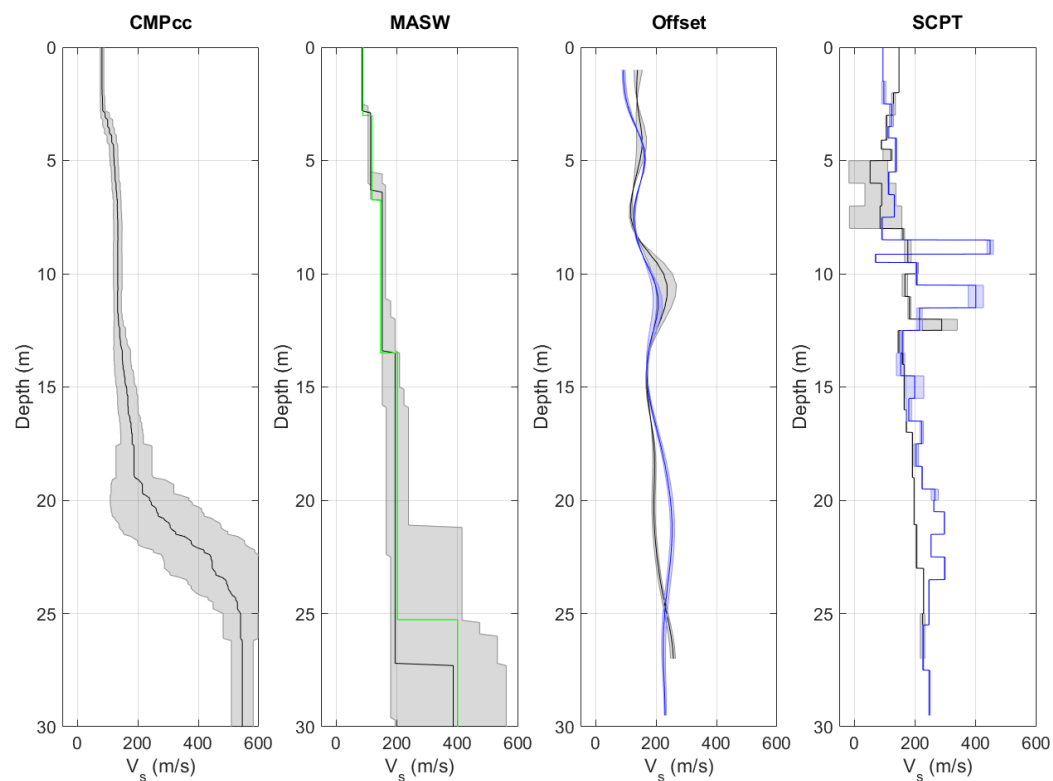


Figure 4.126  $V_s$  profiles from different measurement techniques, including uncertainty bands. From left to right: CMPcc based on active MASW array, shaded band indicates standard deviation; active MASW with manual fit in green and automatic inversion in black with grey shaded band indicating the minimum and the maximum  $V_s$ ; average profile for offset SCPTs between 1 and 5 m offset for 1 or 2 SCPTs with shaded band indicating the minimum and the maximum  $V_s$ ; SCPTs with band indicating variation between left and right blow; cross-hole average profiles for long leg in blue and short leg in grey with shaded band indicating the minimum and the maximum  $V_s$ .

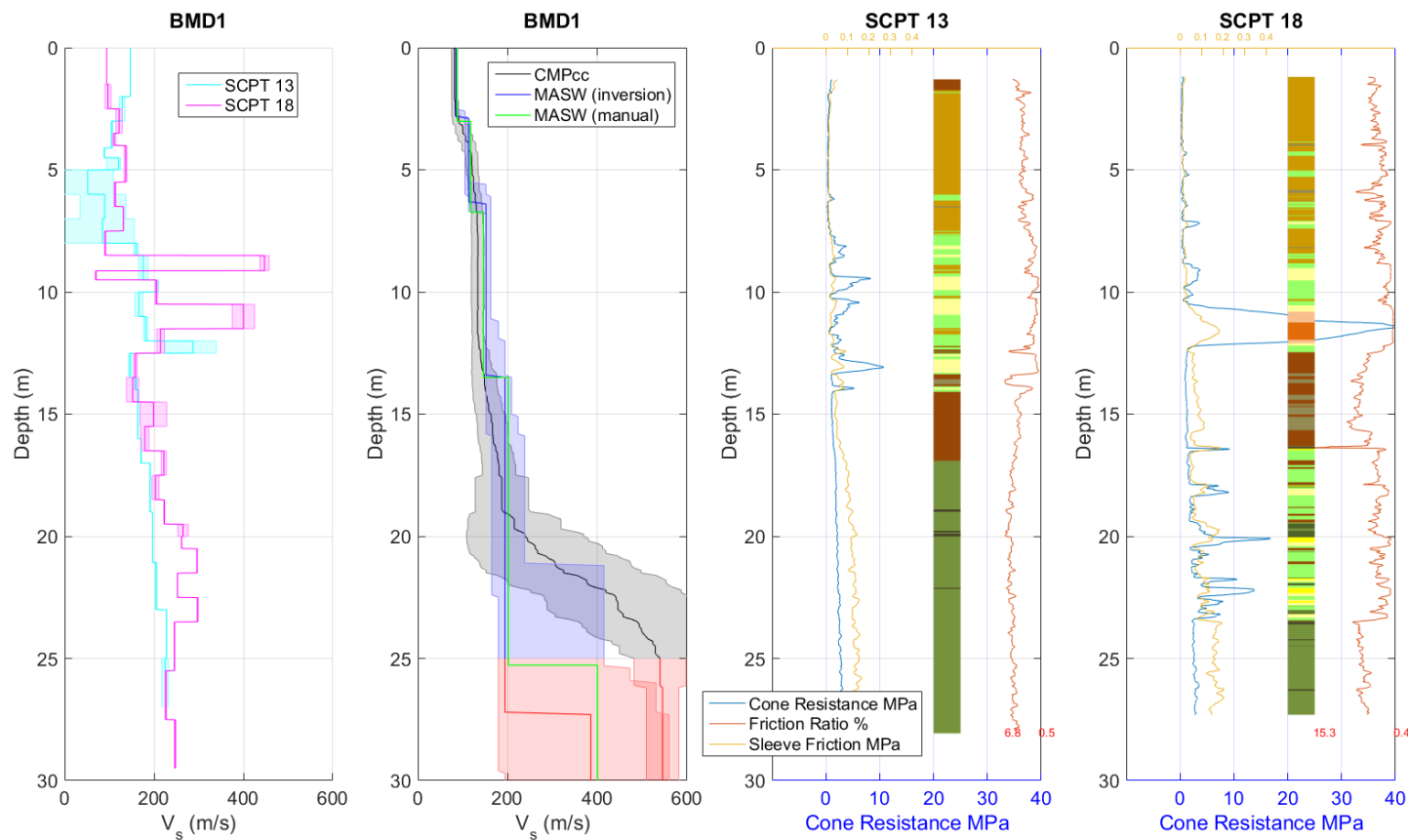


Figure 4.127 Synthesis of  $V_s$  results. Unreliable results are shown in red. From left to right: SCPT with band indicating variation between left and right blow; CMPcc, MASW and average cross-hole results with uncertainty bands; CPT with cone resistance, friction ratio, sleeve friction and automatically generated lithology (indication, for legend see Table 3.1).

## 4.12 Middelstum 2- BMD2

### 4.12.1 Location

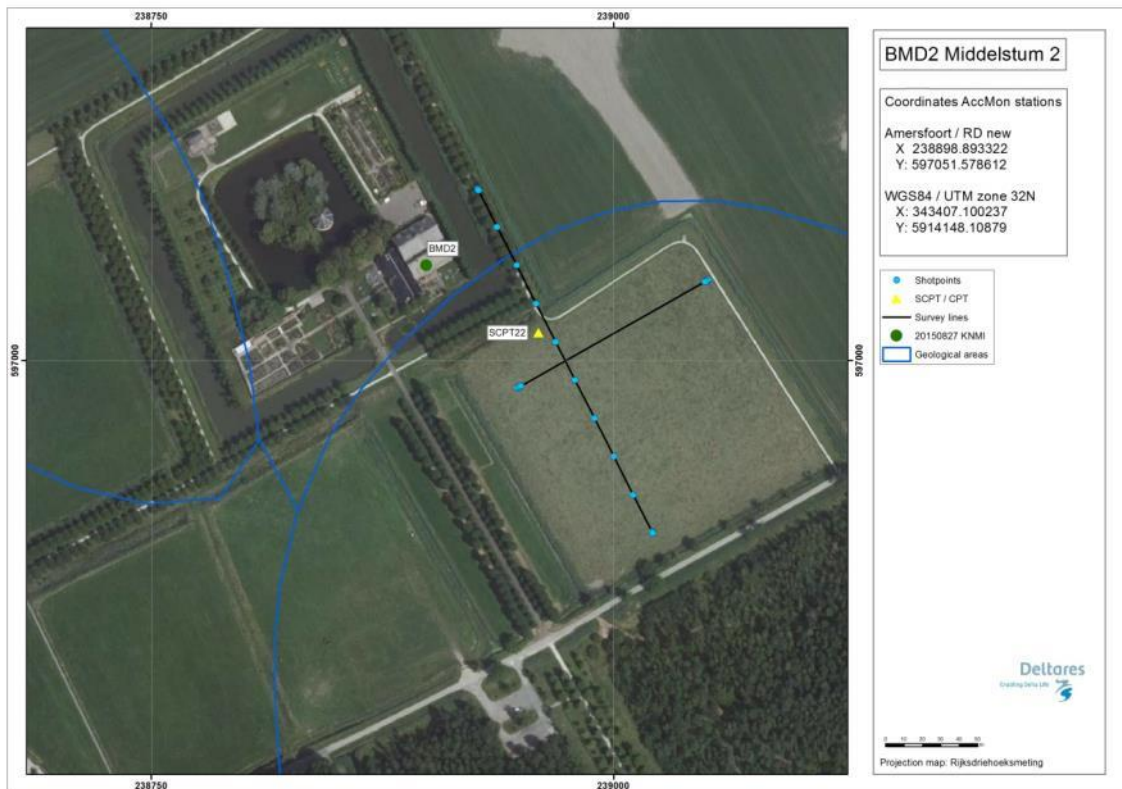


Figure 4.128 Map of location BMD2, showing the KNMI accelerograph station, SCPT location and MASW survey lines and shot locations.

### 4.12.2 Geological setting

The location is situated in a non-erosive area bordering a small erosive valley in the West at a distance of 100 metres with a depth up to 15 metres. Pleistocene is covered by Holocene deposits with a thickness of approximately 10 metres. The deposits can be divided in a coverage layer of clay with a thickness of approximately 3 metres on a sandy layer. The basal peat and older Clay were not eroded and are still present.

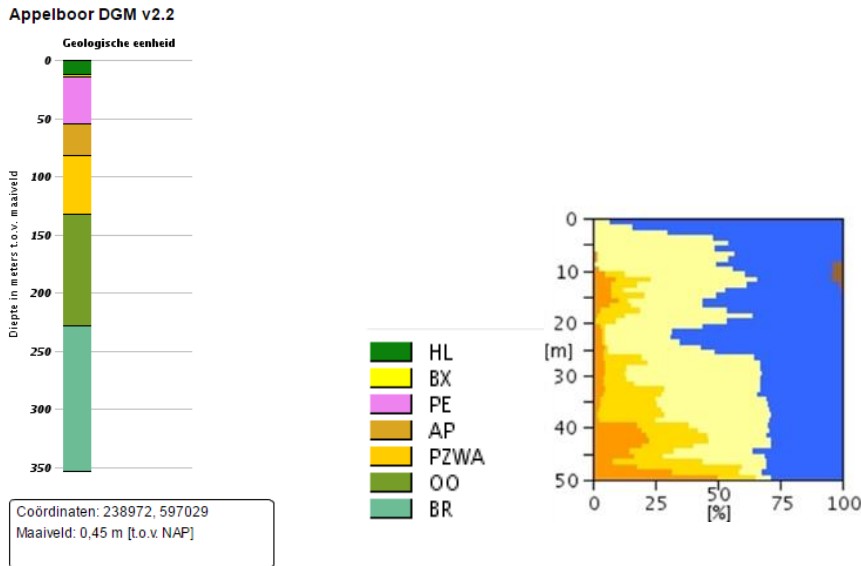


Figure 4.129 Geological information at station BMD2. Left: 1D section from the DGM model. Right: Section from the “delfstoffen online” model (GDN-TNO). Colour coding: brown = peat, blue = clay, yellow to orange = fine sand to coarse sand. The horizontal scale shows the volume percentage of each of the lithologies present at the location, the vertical scale is depth below the surface.

Table 4.12 Descriptions of representative deep boreholes near station BMD2 from the DINO database (www.dinoloket.nl).

Drilling	Distance from drilling	top	bottom	sediment type	Min. grain size	Max. grain size	Formation
B07B0001	750mtr SW	1,86	-1,04	Clay			Formation of Naaldwijk
		-1,04	-9,19	Sand	Very fine		Formation of Naaldwijk
		-9,19	-9,64	Clay			Formation of Naaldwijk
		-9,64	-9,94	Peat			Formation of Nieuwkoop
		-9,94	-10,89	Sand	Fine		Formation of Boxtel
		-10,89	-54,14	Clay			Formation of Peelo
		-54,14	-68,14	Sand	Coarse		Formation of Appelscha
		-68,14	-68,34	Sand	Medium coarse		Formation of Peize

1210624-000-BGS-0007, Version 2, 27 June 2016, final

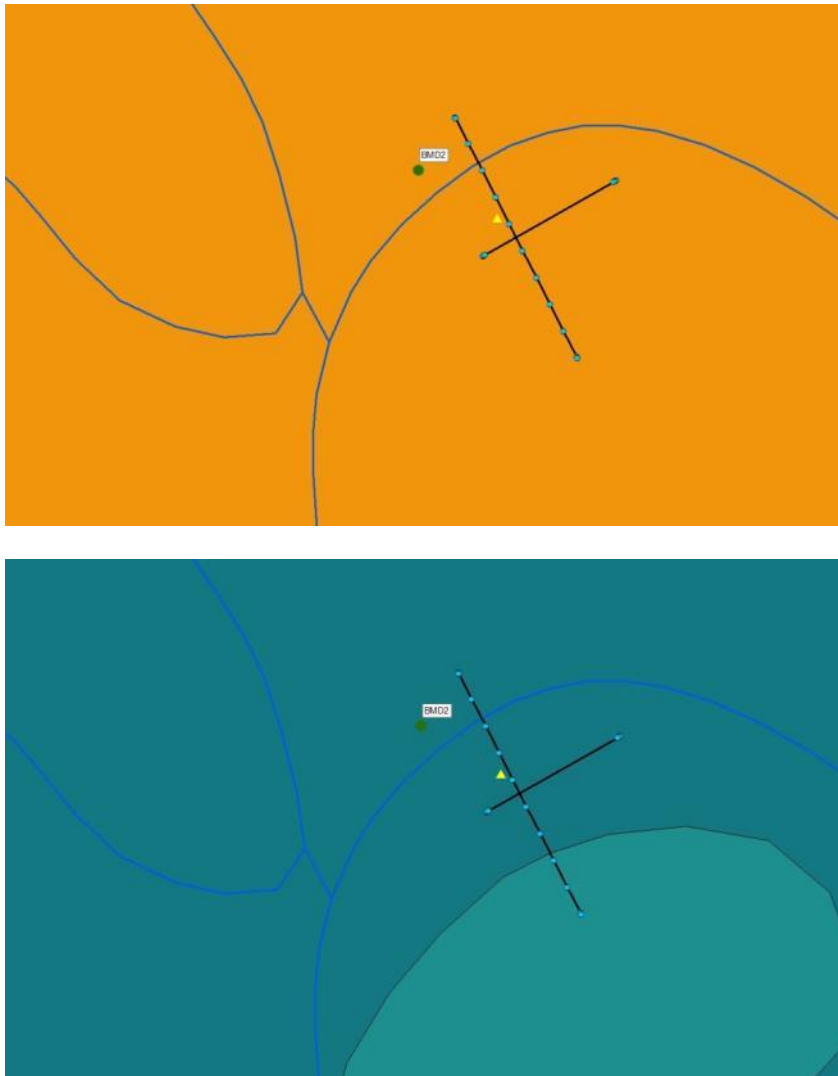


Figure 4.130 Overview map of geological setting based on beta version of GeoTOP model. Top panel: Thickness of the Peelo Formation, blue colour indicates thick Peelo layer, hence in the centre of the channel; red and orange colour indicates thin Peelo layers, hence areas outside the channel; yellow indicates transition zone. Lower panel: Top of Pleistocene surface relative to Dutch Ordnance Datum NAP.

## 4.12.3 SCPT

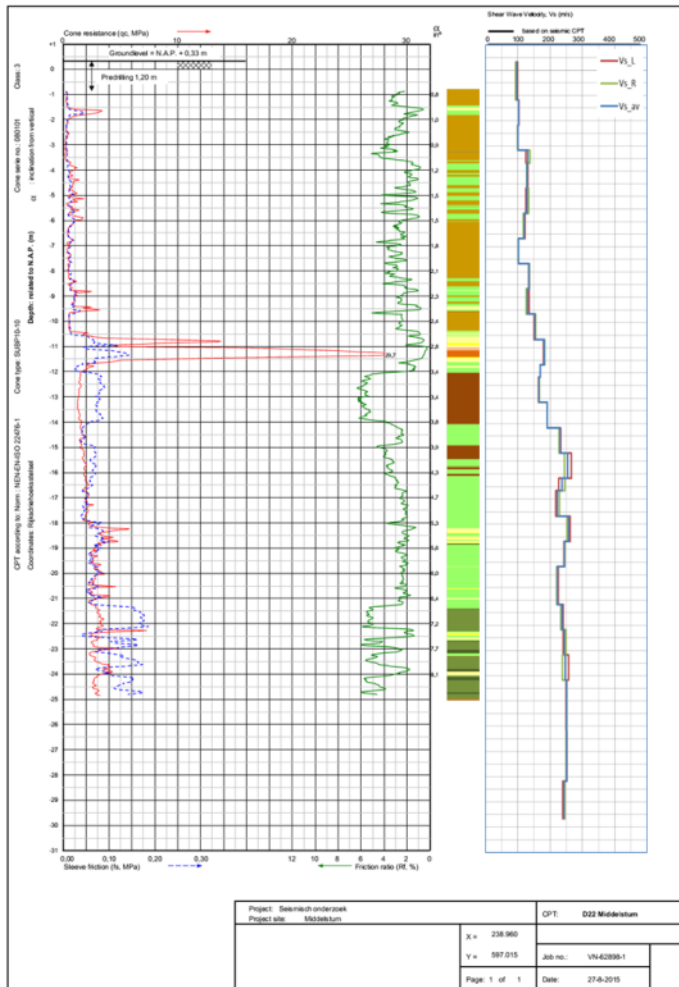


Figure 4.131 SCPT22. From left to right: CPT measurement, showing tip resistance, sleeve friction and friction ratio; automatically generated lithology (indication, for legend see Table 3.1);  $V_s$  profile (red = left blow, green = right blow, blue = average).

## 4.12.4 OSCPT

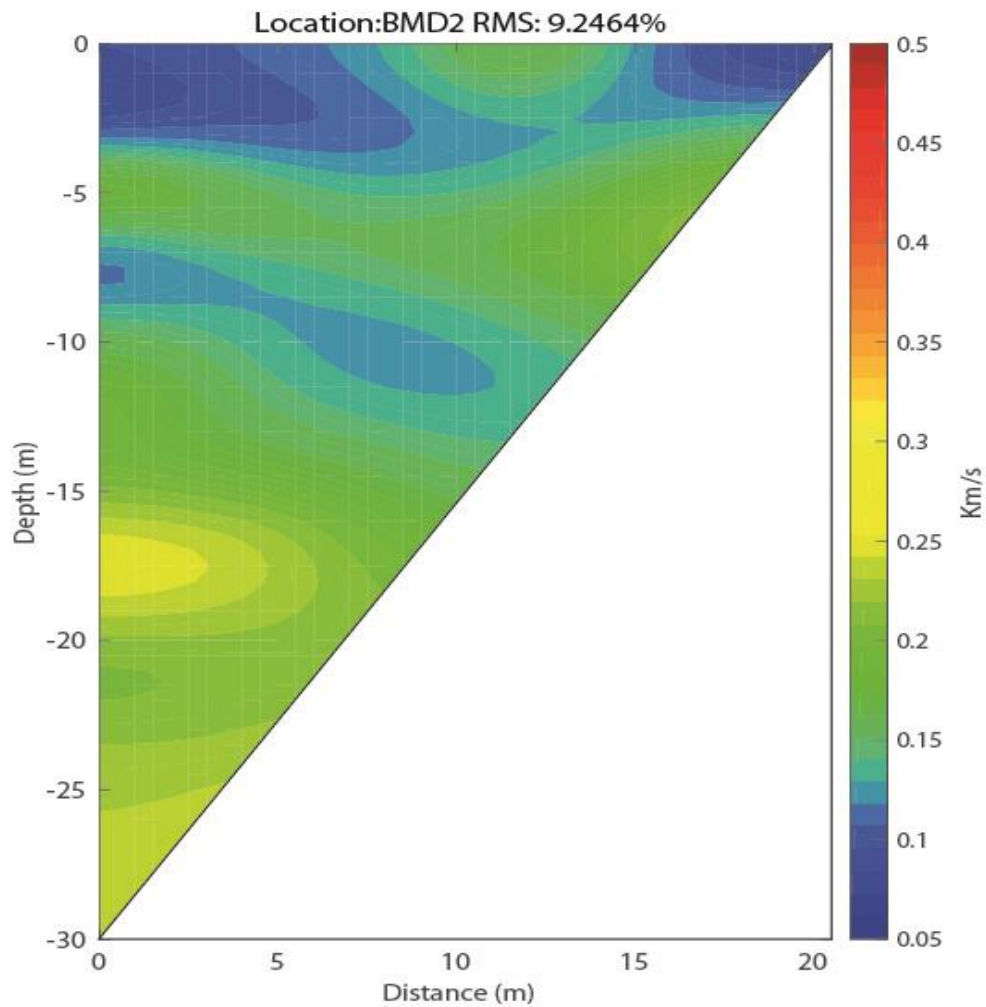


Figure 4.132 Tomographic images based on OSCPT result from SCPT for station BMD2 (SCPT22).

## 4.12.5 MASW

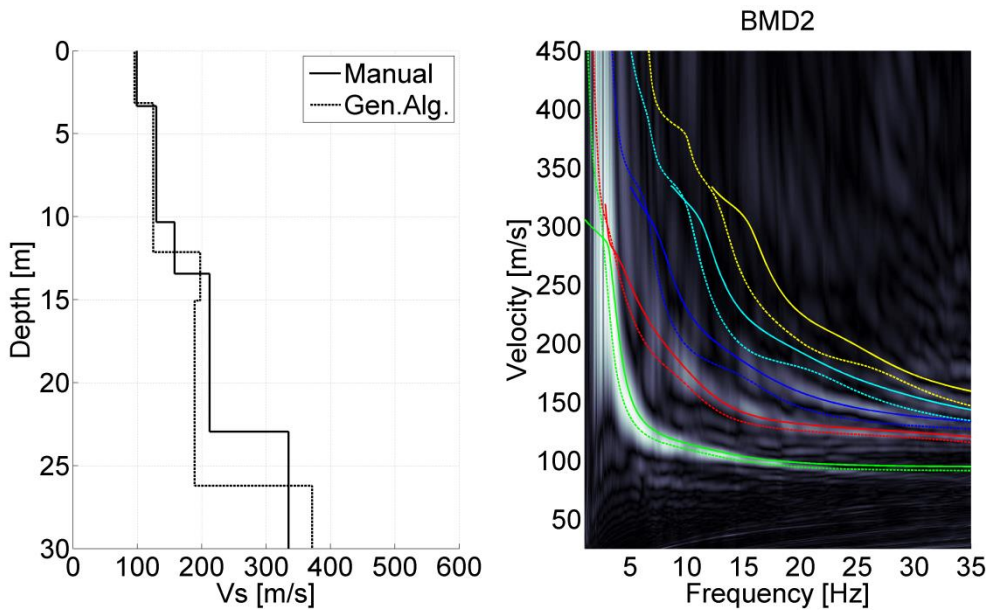


Figure 4.133 MASW result for station BMD2. Left panel:  $V_s$  profiles from active MASW. Solid line from manual fitting of dispersion curves; dashed line for automatic inversion. Right panel: energy in the dispersion plot in greyscale; solid lines are the modelled dispersion curves for different modes of the manually fitted  $V_s$  profile; dashed lines for the different modes of the automatically inverted  $V_s$  profile.

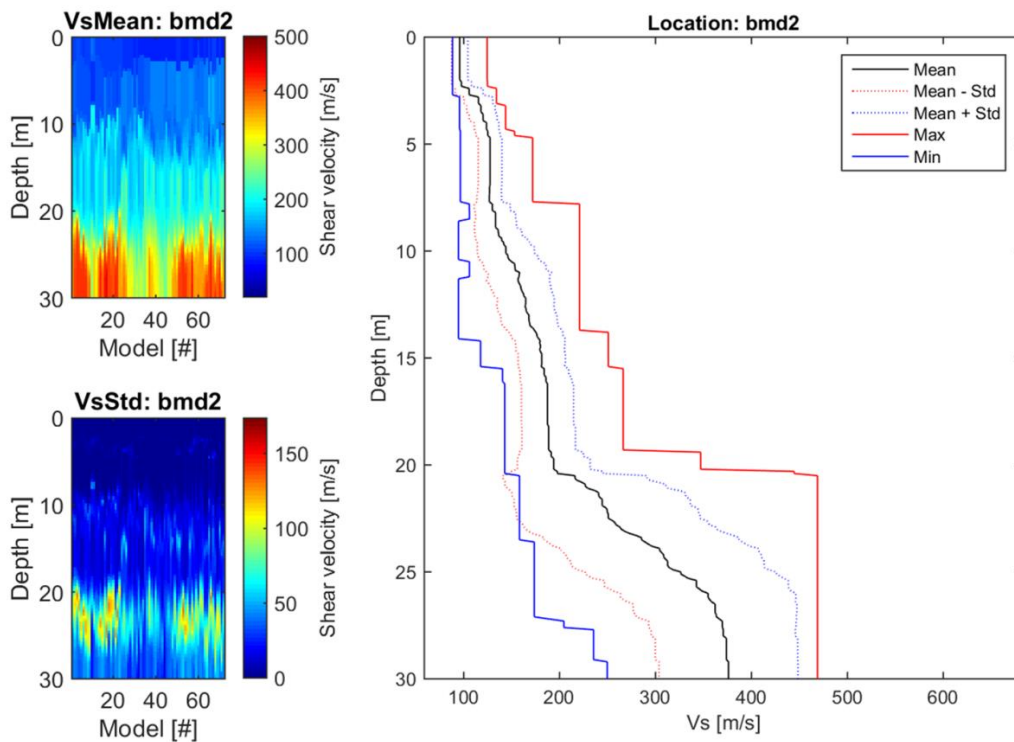


Figure 4.134 CMPcc result for BMD2. Top left: average  $V_s$  along the CMPcc array. Bottom left: standard deviation of  $V_s$  along the CMPcc array. Right: best fit curve of the 72 models with the maximum and minimum value observed in the whole CMPcc and the standard deviation from all models.

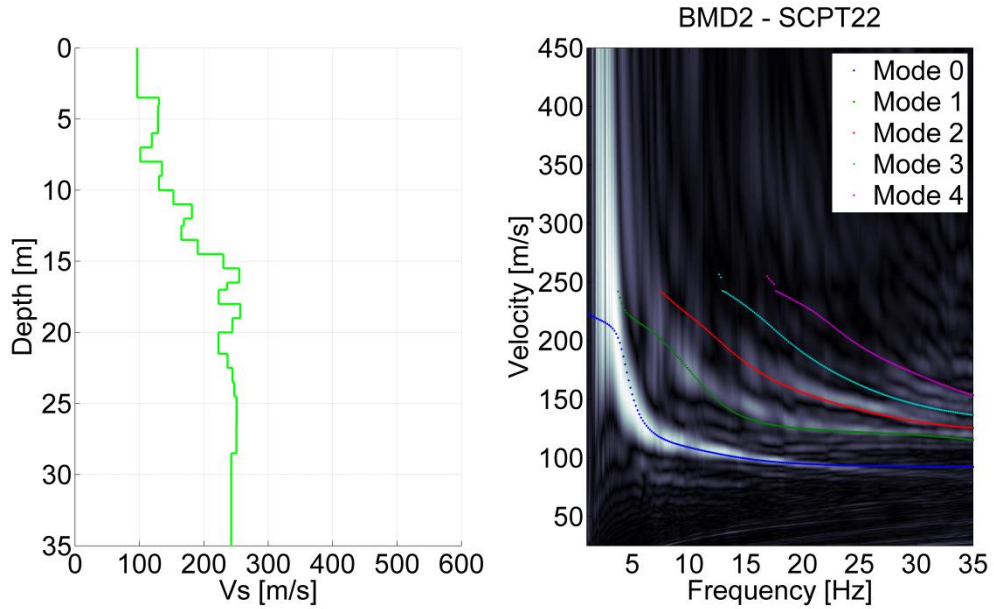


Figure 4.135 Comparison for BMD2 of SCPT22 and MASW result. Left:  $V_s$  profile from SCPT. The  $V_s$  from the top 2 layers of the SCPT is generally unreliable and replaced by the minimum  $V_s$  of the first 3 layers. Right: modelled dispersion curves of different modes based on the SCPT  $V_s$  profile in coloured lines plotted on the energy of MASW dispersion plot in greyscale.



## 4.12.6 Synthesis

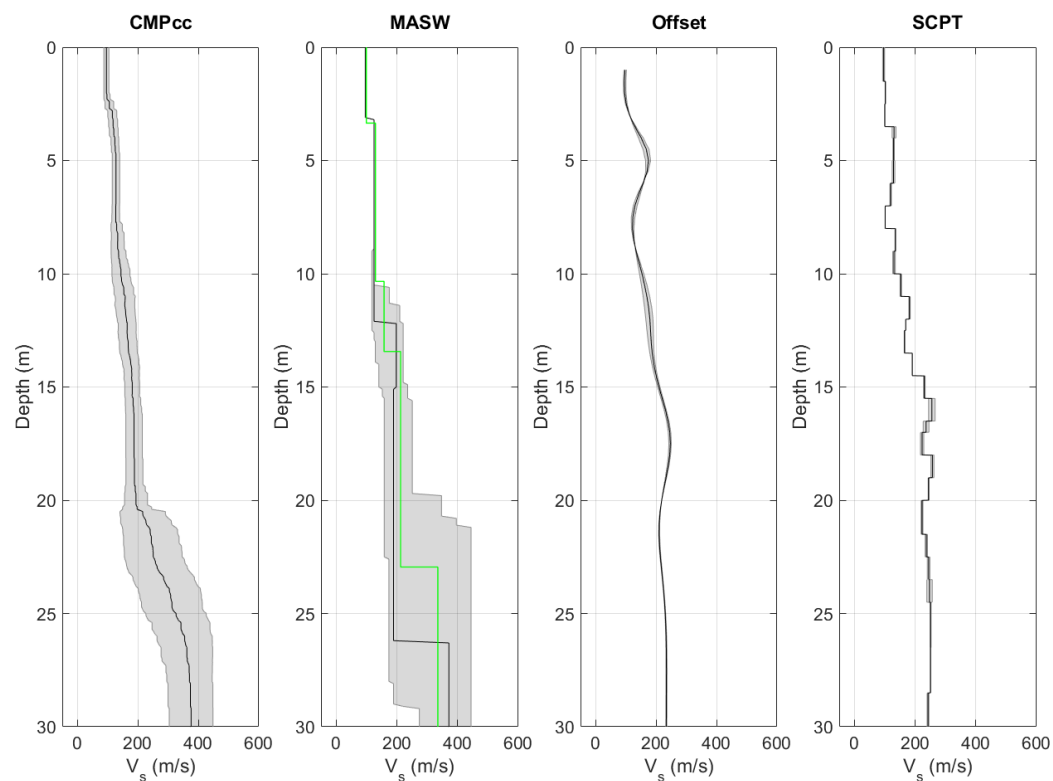


Figure 4.136  $V_s$  profiles from different measurement techniques, including uncertainty bands. From left to right: CMPcc based on active MASW array, shaded band indicates standard deviation; active MASW with manual fit in green and automatic inversion in black with grey shaded band indicating the minimum and the maximum  $V_s$ ; average profile for offset SCPTs between 1 and 5 m offset for 1 or 2 SCPTs with shaded band indicating the minimum and the maximum  $V_s$ ; SCPTs with band indicating variation between left and right blow; cross-hole average profiles for long leg in blue and short leg in grey with shaded band indicating the minimum and the maximum  $V_s$ .

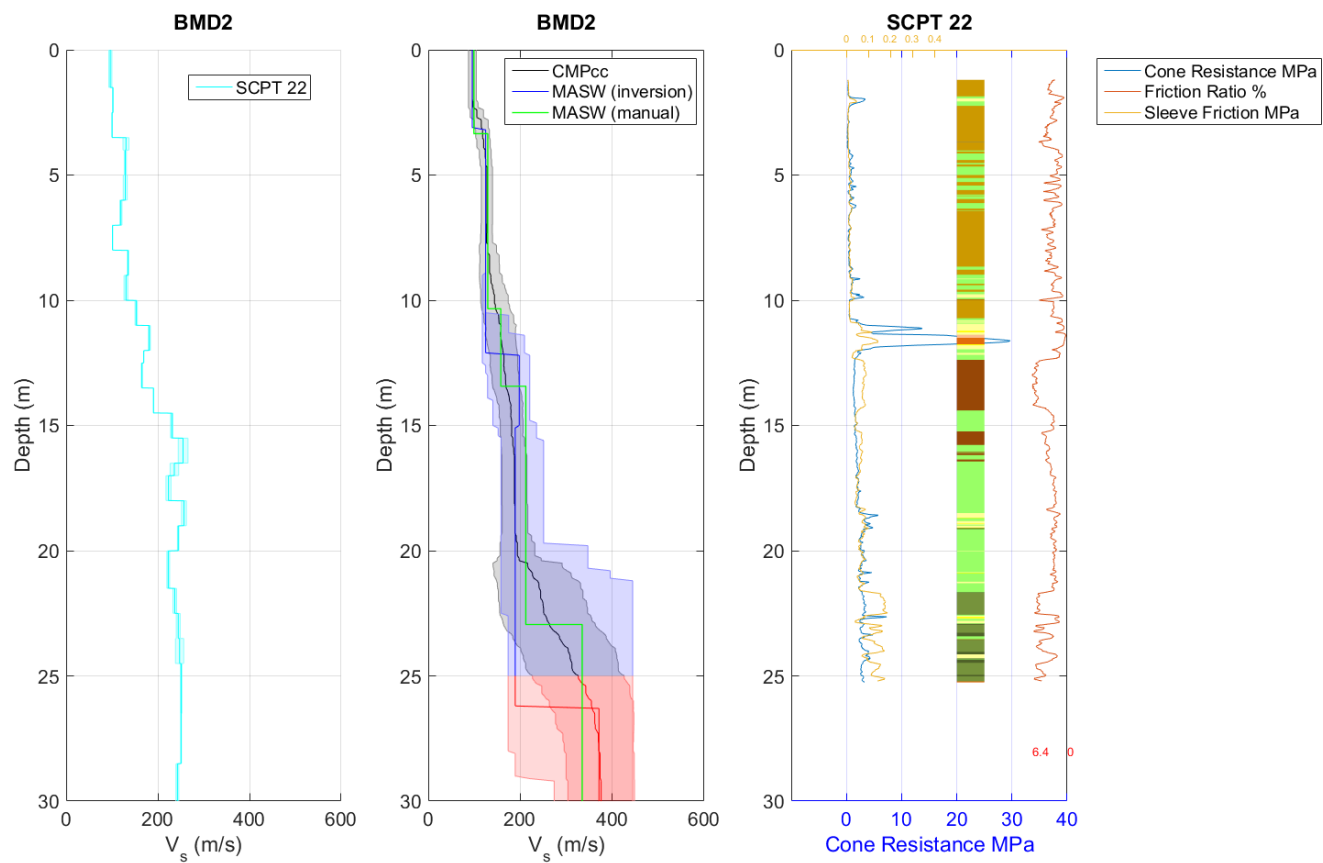


Figure 4.137 Synthesis of  $V_s$  results. Unreliable results are shown in red. From left to right: SCPT with band indicating variation between left and right blow; CMPcc, MASW and average cross-hole results with uncertainty bands; CPT with cone resistance, friction ratio, sleeve friction and automatically generated lithology (indication, for legend see Table 3.1).

## 4.13 Oosternieland- BONL

### 4.13.1 Location

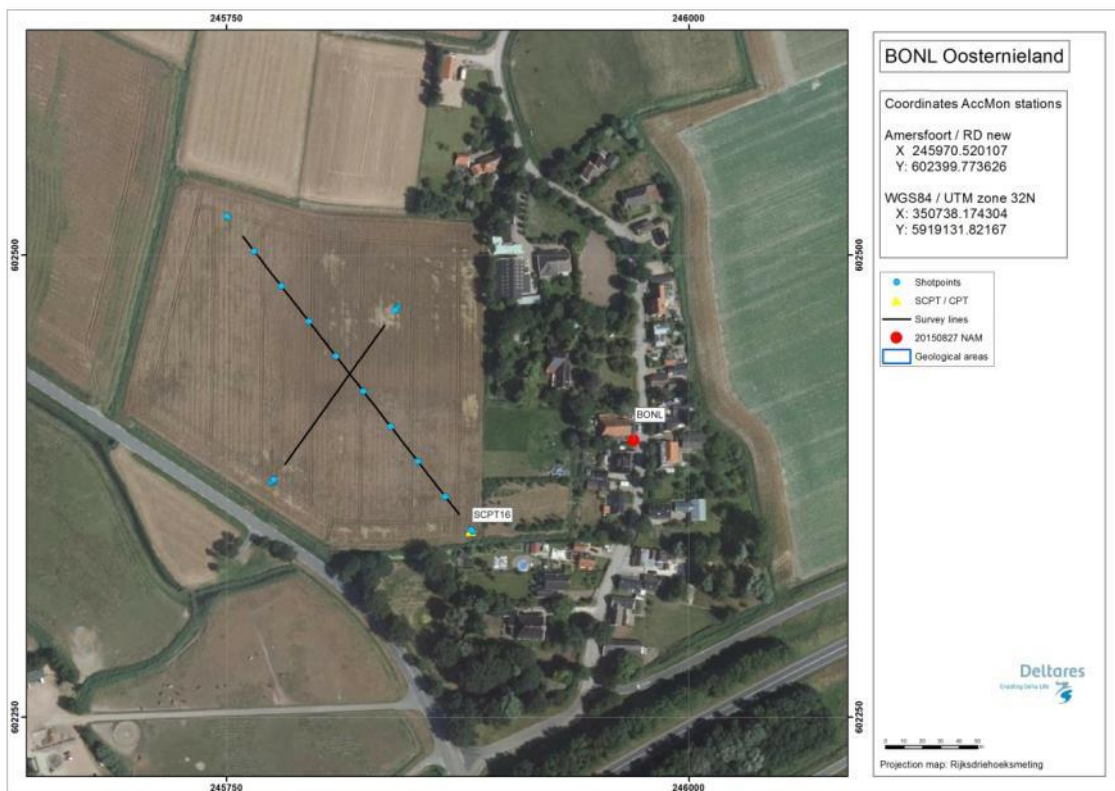


Figure 4.138 Map of location BONL, showing the KNMI accelerograph station, SCPT location and MASW survey lines and shot locations.

### 4.13.2 Geological setting

The location is situated on a NW – SE running ridge with a width of 1500 metres and sided with Holocene erosion valleys with a depth up to approximately 25 metres. The Pleistocene is covered with approximately 14 metre of Holocene deposits mostly consisting of sand with clay layers. The base of the Holocene consists of basal peat or humid clay and therefore the top of the Pleistocene is not eroded.

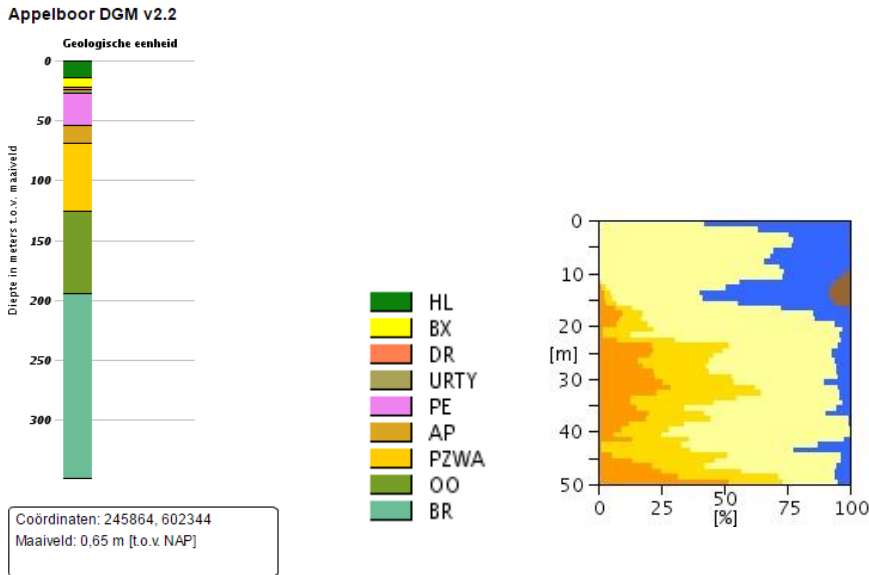


Figure 4.139 Geological information at station BONL. Left: 1D section from the DGM model. Right: Section from the “delfstoffen online” model (GDN-TNO). Colour coding: brown = peat, blue = clay, yellow to orange = fine sand to coarse sand. The horizontal scale shows the volume percentage of each of the lithologies present at the location, the vertical scale is depth below the surface.

Table 4.13 Descriptions of representative deep boreholes near station BONL from the DINO database ([www.dinoloket.nl](http://www.dinoloket.nl)).

Drilling	Distance from drilling	top of layer	bottom of layer	sediment type	Minimum grainsize	Maximum grainsize	Formation
B03G0027	600 mtr NW	1,80	-9,80	Sand	Very fine		Formation of Naaldwijk
		-9,80	-13,60	Clay			Formation of Naaldwijk
		-13,60	-21,80	Sand	Medium fine	Medium coarse	Formation of Boxtel
		-21,80	-23,80	Sand	Extreme coarse		Formation of Drente
		-23,80	-27,80	Sand	Medium coarse	Extreme coarse	Formation of Urk/Tynje
		-27,80	-56,80	Sand	Very coarse	Extreme coarse	Formation of Peelo
		-56,80	-108,80	Sand	Extreme coarse		Formation of Appelscha/Peize

1210624-000-BGS-0007, Version 2, 27 June 2016, final

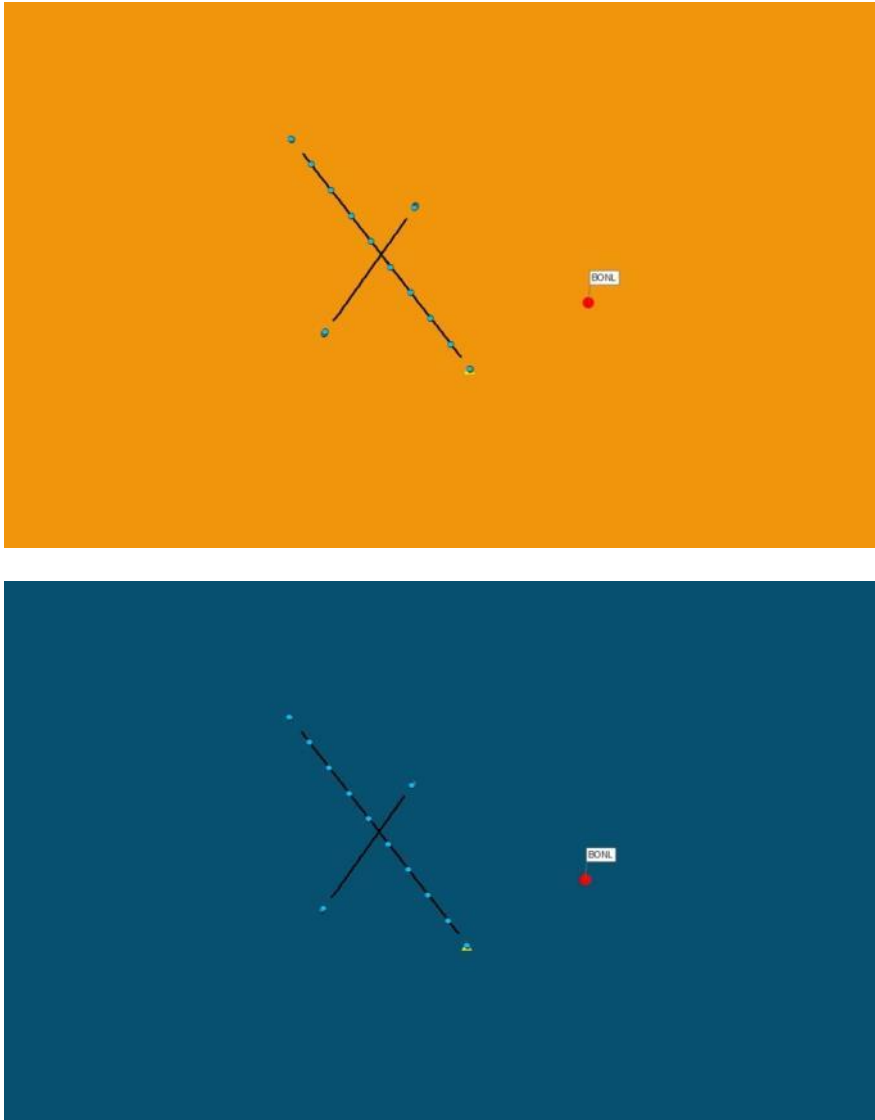


Figure 4.140 Overview map of geological setting based on beta version of GeoTOP model. Top panel: Thickness of the Peelo Formation, blue colour indicates thick Peelo layer, hence in the centre of the channel; red and orange colour indicates thin Peelo layers, hence areas outside the channel; yellow indicates transition zone. Lower panel: Top of Pleistocene surface relative to Dutch Ordnance Datum NAP.

## 4.13.3 SCPT

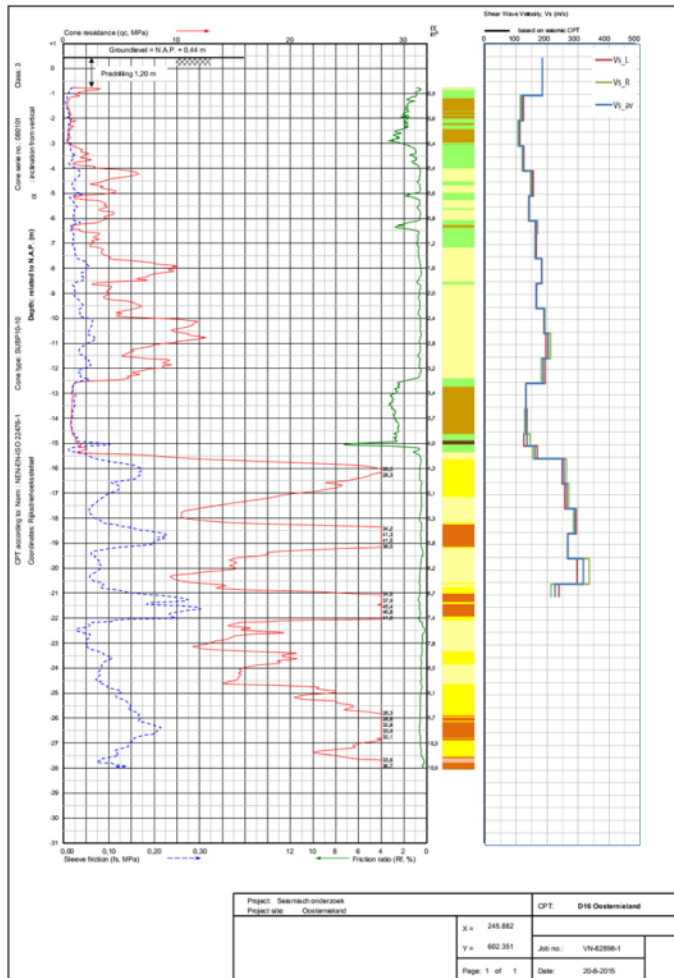


Figure 4.141 SCPT16. From left to right: CPT measurement, showing tip resistance, sleeve friction and friction ratio; automatically generated lithology (indication, for legend see Table 3.1);  $V_s$  profile (red = left blow, green = right blow, blue = average).

## 4.13.4 OSCPT

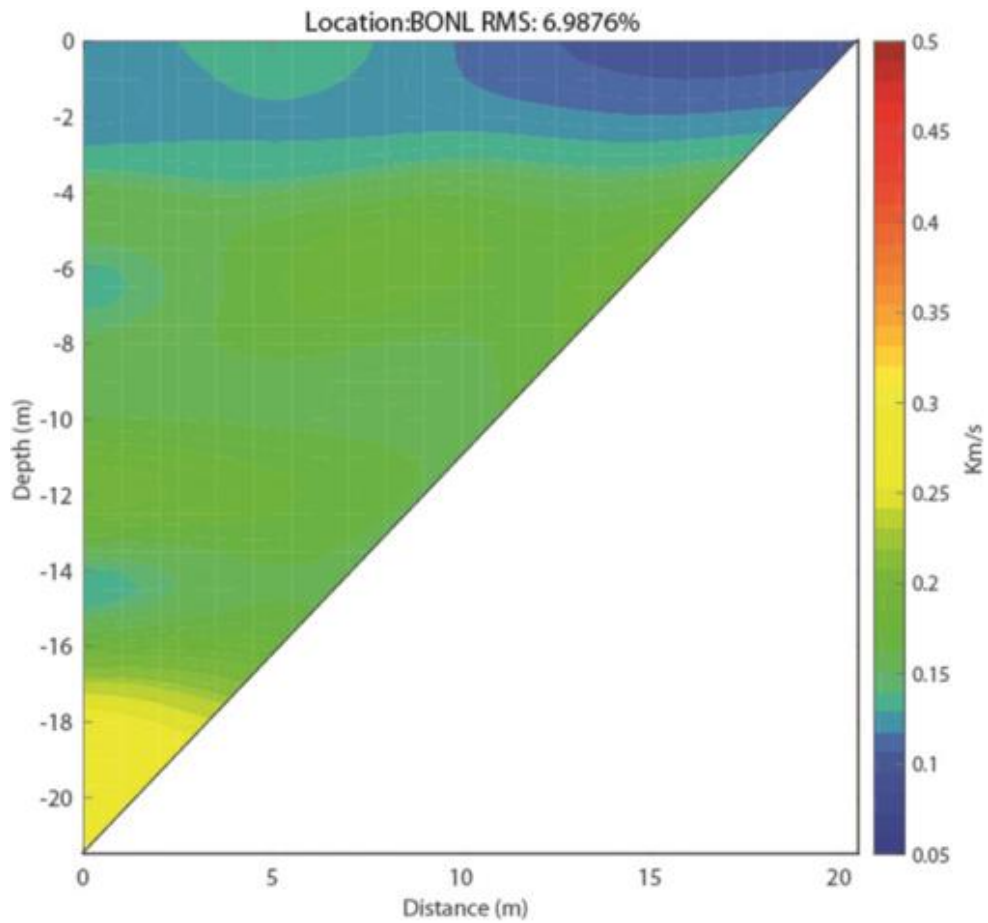


Figure 4.142 Tomographic images based on OSCPT result from SCPT for station BONL (SCPT16).

## 4.13.5 MASW

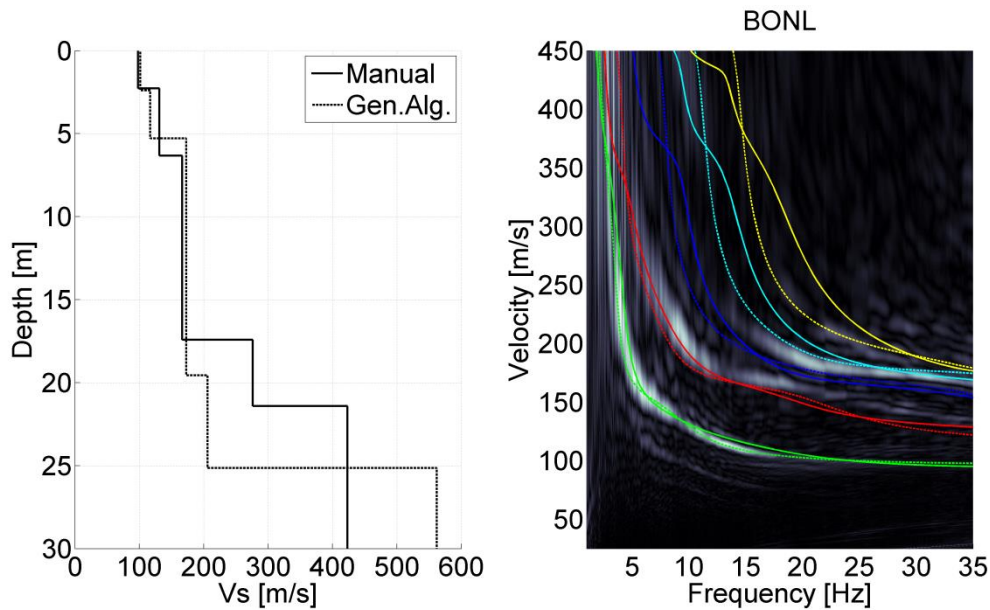


Figure 4.143 MASW result for station BONL. Left panel:  $V_s$  profiles from active MASW. Solid line from manual fitting of dispersion curves; dashed line for automatic inversion. Right panel: energy in the dispersion plot in greyscale; solid lines are the modelled dispersion curves for different modes of the manually fitted  $V_s$  profile; dashed lines for the different modes of the automatically inverted  $V_s$  profile.

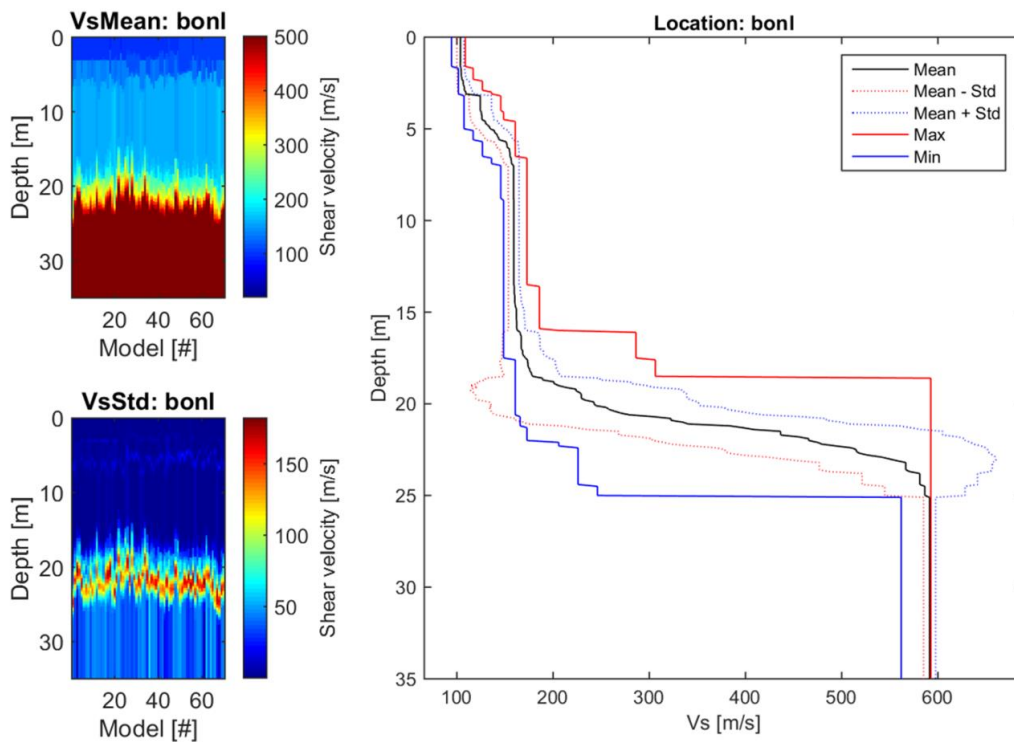


Figure 4.144 CMPcc result for BONL. Top left: average  $V_s$  along the CMPcc array. Bottom left: standard deviation of  $V_s$  along the CMPcc array. Right: best fit curve of the 72 models with the maximum and minimum value observed in the whole CMPcc and the standard deviation from all models.

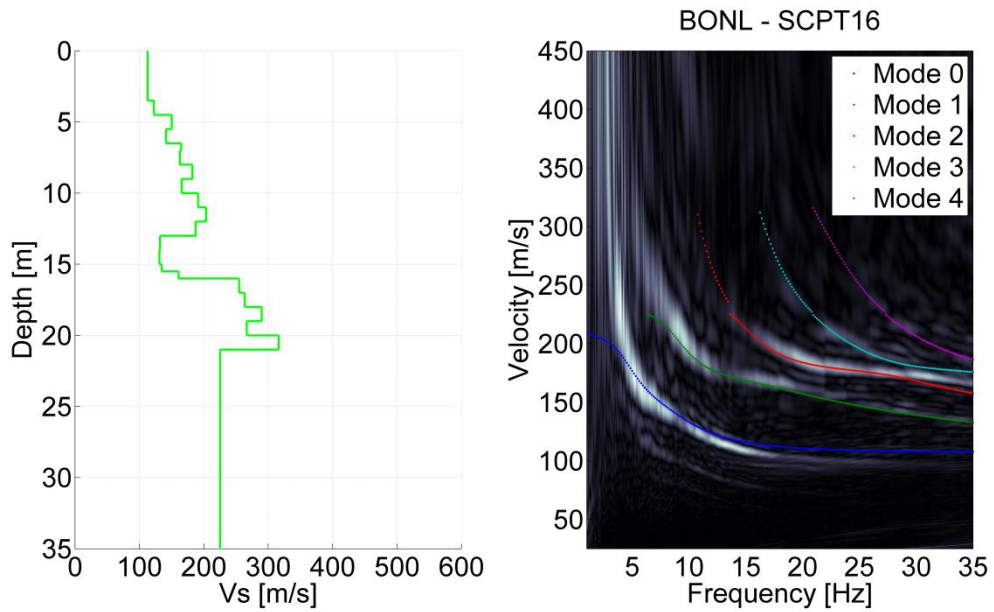


Figure 4.145 Comparison for BONL of SCPT16 and MASW result. Left: VS profile from SCPT. The VS from the top 2 layers of the SCPT is generally unreliable and replaced by the minimum VS of the first 3 layers. Right: modelled dispersion curves of different modes based on the SCPT  $V_s$  profile in coloured lines plotted on the energy of MASW dispersion plot in greyscale.



## 4.13.6 Synthesis

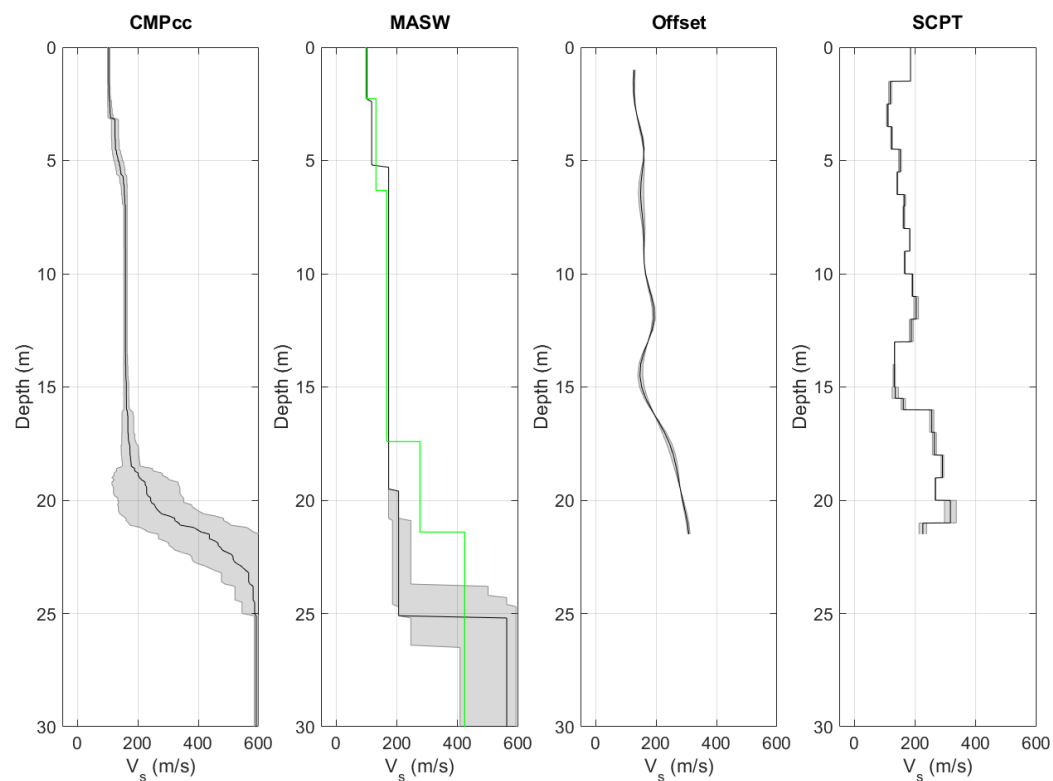


Figure 4.146  $V_s$  profiles from different measurement techniques, including uncertainty bands. From left to right: CMPcc based on active MASW array, shaded band indicates standard deviation; active MASW with manual fit in green and automatic inversion in black with grey shaded band indicating the minimum and the maximum  $V_s$ ; average profile for offset SCPTs between 1 and 5 m offset for 1 or 2 SCPTs with shaded band indicating the minimum and the maximum  $V_s$ ; SCPTs with band indicating variation between left and right blow; cross-hole average profiles for long leg in blue and short leg in grey with shaded band indicating the minimum and the maximum  $V_s$ .

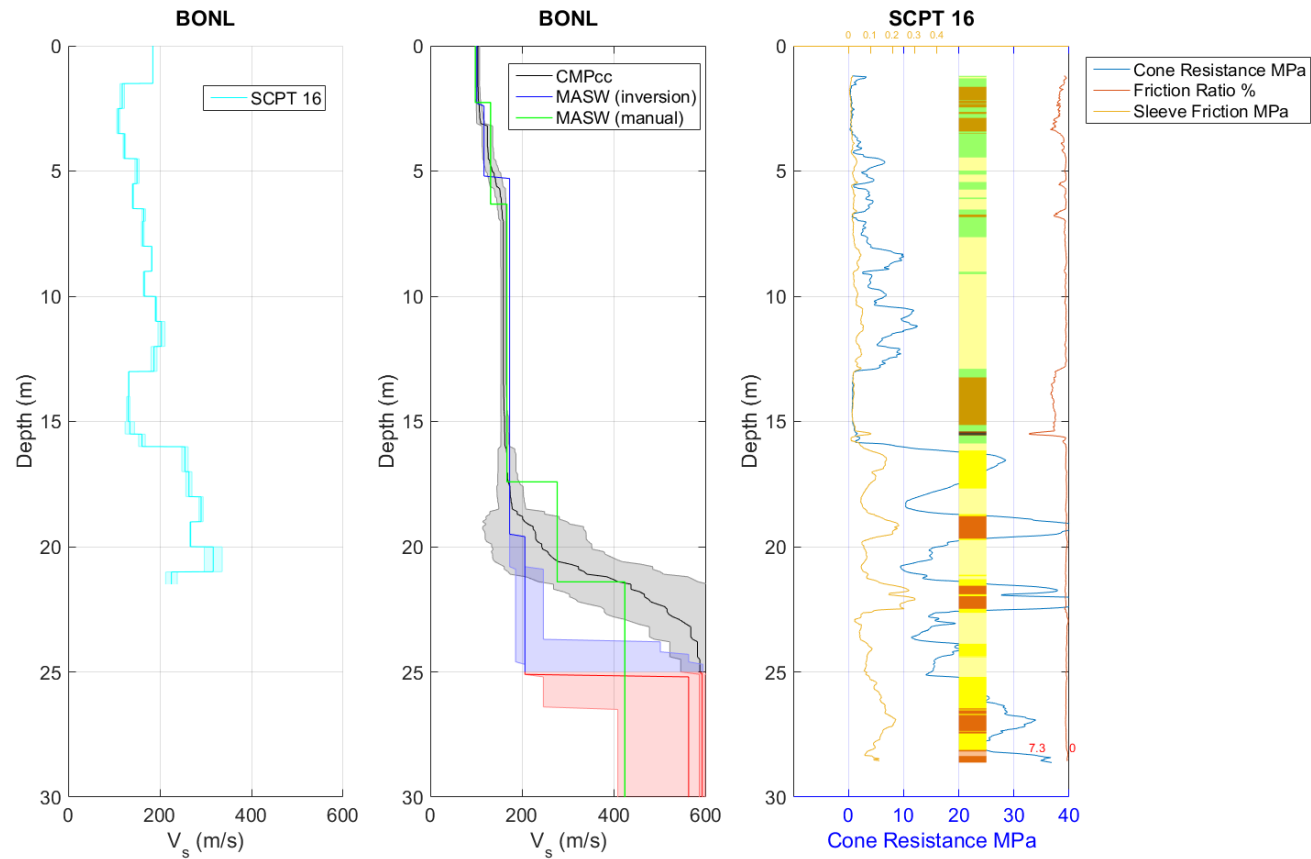


Figure 4.147 Synthesis of  $V_s$  results. Unreliable results are shown in red. From left to right: SCPT with band indicating variation between left and right blow; CMPcc, MASW and average cross-hole results with uncertainty bands; CPT with cone resistance, friction ratio, sleeve friction and automatically generated lithology (indication, for legend see Table 3.1).

## 4.14 Oosterwijtdwerd- BOWW

### 4.14.1 Location

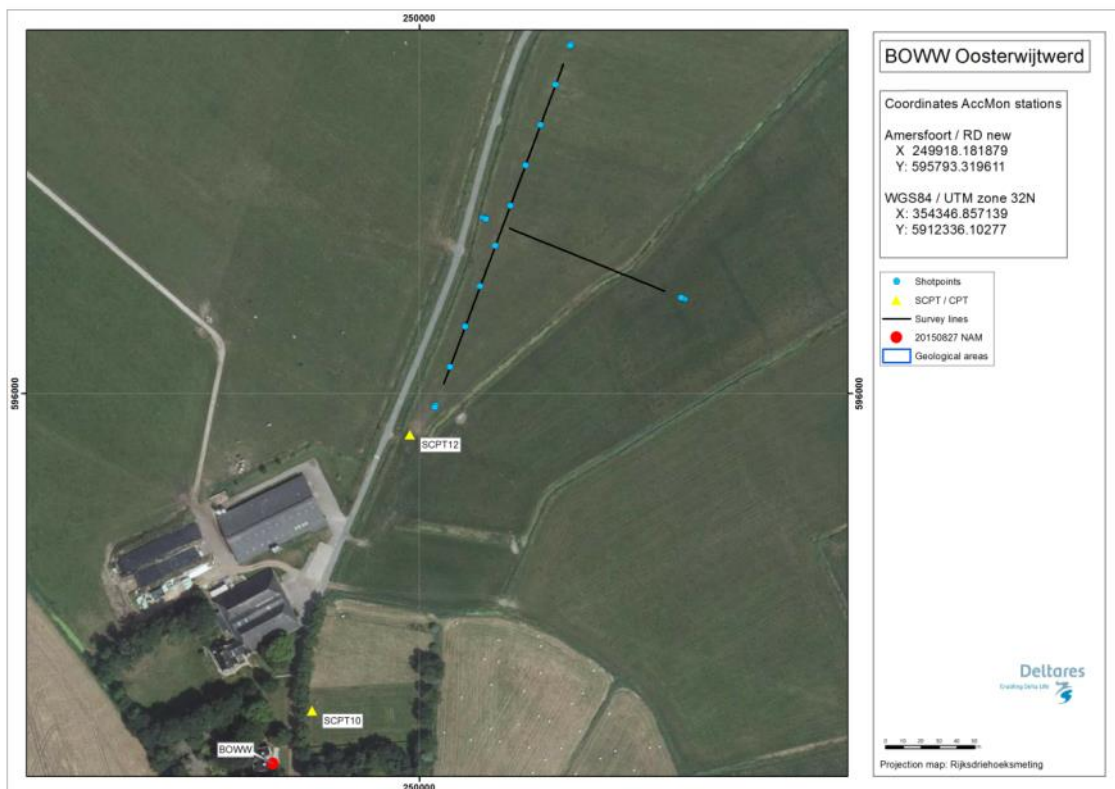


Figure 4.148 Map of location BOWW, showing the KNMI accelerograph station, SCPT location and MASW survey lines and shot locations.

### 4.14.2 Geological setting

The location is situated in a non-erosive area. The top of the Pleistocene is situated at a depth of 8 to 10 metres. The Holocene deposits consist of a clay layer with a peat layer in between at a depth of approximately 2.5 metres. Basal peat is present in this area. To the east at a distance of 500 metres is a small erosive valley with clay on top of boulder clay from the formation of Drente. The top of the boulder clay is found at a depth of 10 metres. The location is situated on the bottom of a Peelo valley with a depth of 100 metres.

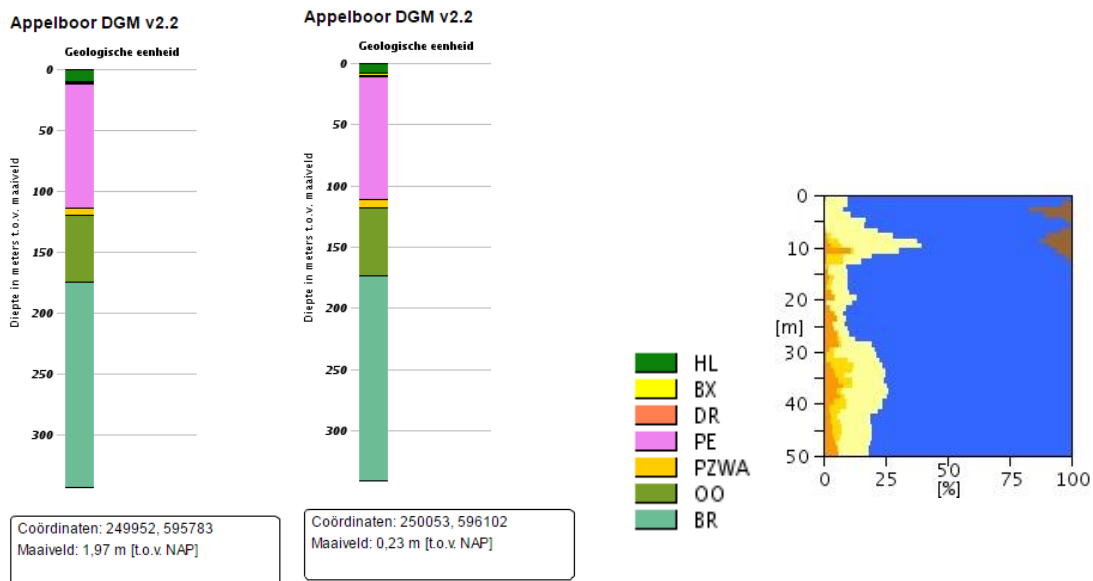


Figure 4.149 Geological information at station BOWW. Left: 1D section from the DGM model. Right: Section from the “delfstoffen online” model (GDN-TNO). Colour coding: brown = peat, blue = clay, yellow to orange = fine sand to coarse sand. The horizontal scale shows the volume percentage of each of the lithologies present at the location, the vertical scale is depth below the surface.

Table 4.14 Descriptions of representative deep boreholes near station BOWW from the DINO database ([www.dinoloket.nl](http://www.dinoloket.nl)).

Drilling	Distance from drilling	top	bottom	sediment type	Min. grain size	Max. grain size	Formation
B07E0031	1200 NE	0,42	-3,80	Clay			Formation of Naaldwijk
		-3,80	-5,58	Sand	Very fine		Formation of Naaldwijk
		-5,58	-7,58	Clay			Formation of Naaldwijk
		-7,58	-10,38	Sand	Fine		Formation of Boxtel
		-10,38	-59,58	Clay			Formation of Peelo
		-59,58	-64,58	Sand	Fine		Formation of Peelo
		-64,58	-75,58	Clay			Formation of Peelo
B07F0005	3200mtr SE	0,38	-2,13	Clay			Formation of Naaldwijk
		-2,13	-3,13	Peat			Formation of Nieuwkoop
		-3,13	-5,88	Clay			Formation of Naaldwijk
		-5,88	-5,98	Peat			Formation of Nieuwkoop
		-5,98	-9,88	Sand	Fine		Formation of Boxtel
		-9,88	-114,38	Clay			Formation of Peelo
		-	-181,38	Sand	Fine		Formation of Peelo
		114,38					

1210624-000-BGS-0007, Version 2, 27 June 2016, final

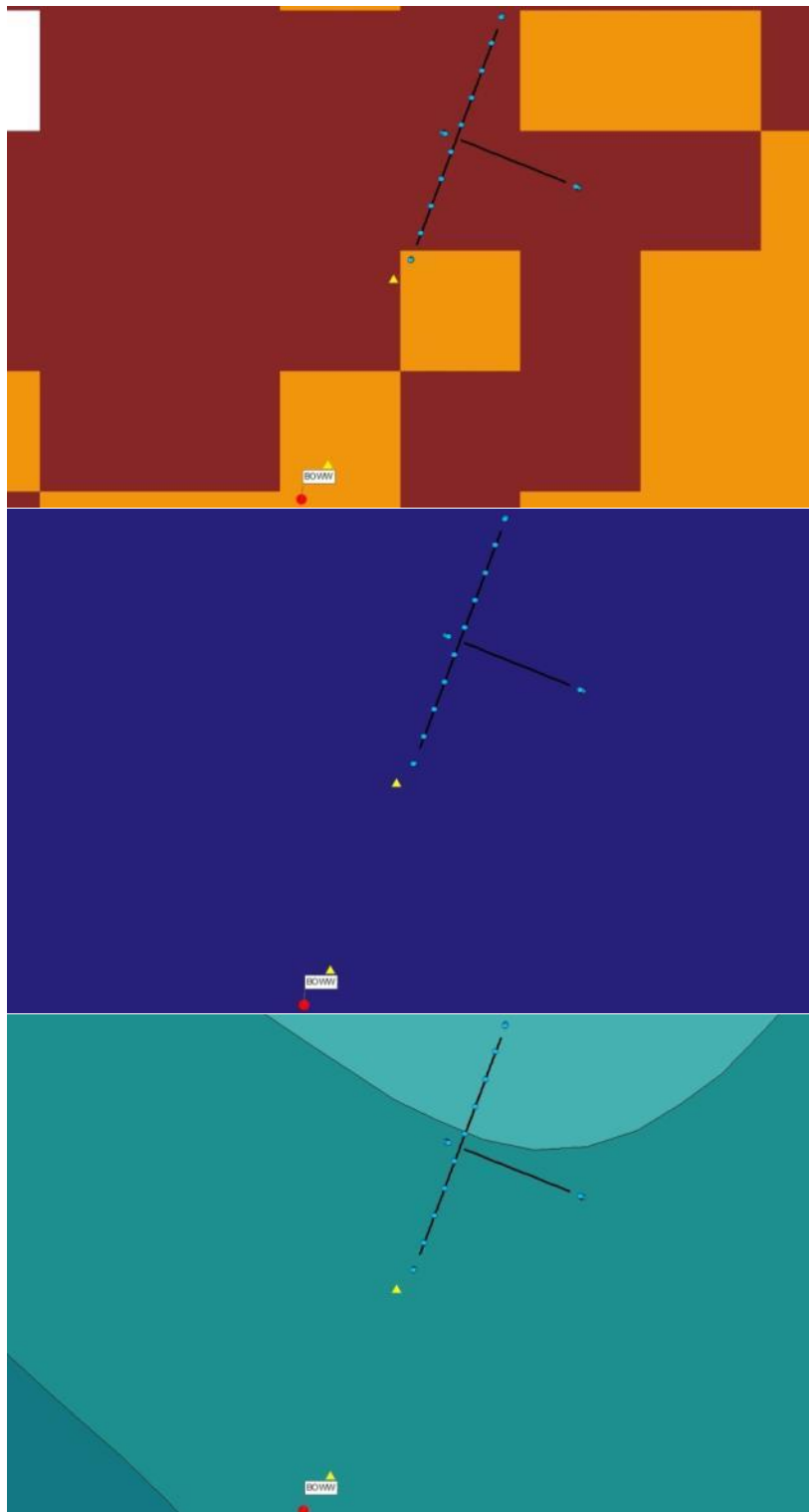


Figure 4.150 Overview map of geological setting based on beta version of GeoTOP model. Top panel: Thickness of the Holocene peat. Middle panel: Thickness of the Peelo Formation, blue colour indicates thick Peelo layer, hence in the centre of the channel; red and orange colour indicates thin Peelo layers, hence areas outside the channel; yellow indicates transition zone. Lower panel: Top of Pleistocene surface relative to Dutch Ordnance Datum NAP.

## 4.14.3 SCPT

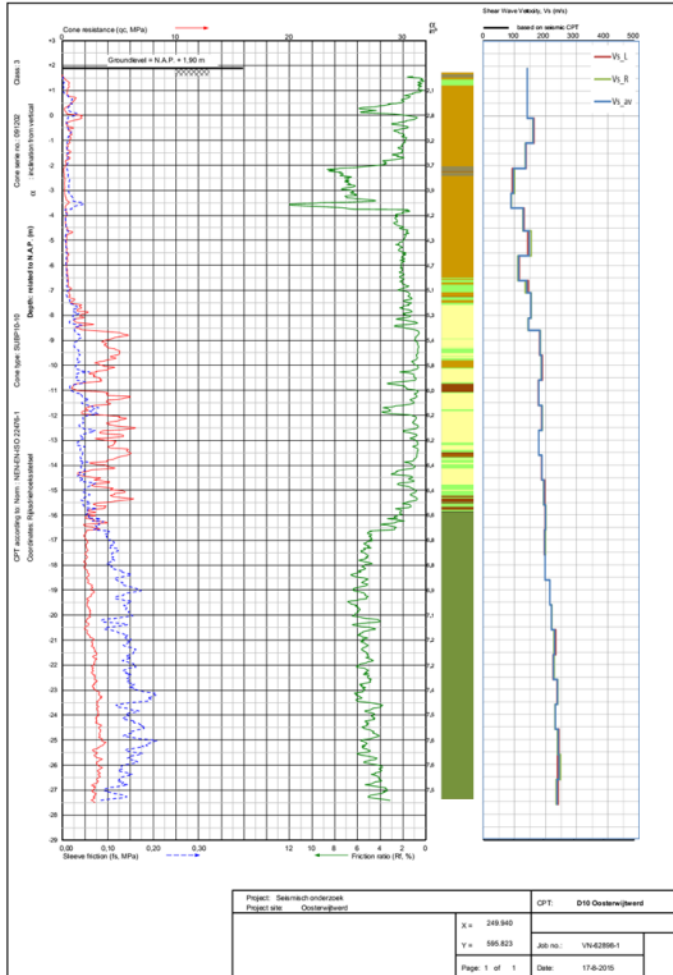


Figure 4.151 SCPT10. From left to right: CPT measurement, showing tip resistance, sleeve friction and friction ratio; automatically generated lithology (indication, for legend see Table 3.1);  $V_s$  profile (red = left blow, green = right blow, blue = average).

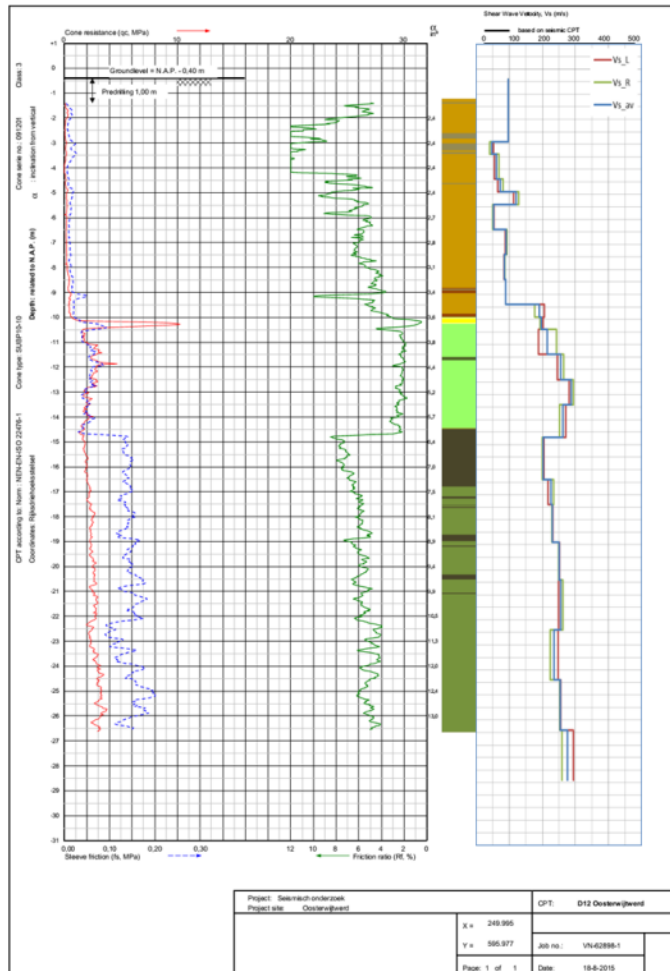


Figure 4.152 SCPT12. From left to right: CPT measurement, showing tip resistance, sleeve friction and friction ratio; automatically generated lithology (indication, for legend see Table 3.1);  $V_s$  profile (red = left blow, green = right blow, blue = average).

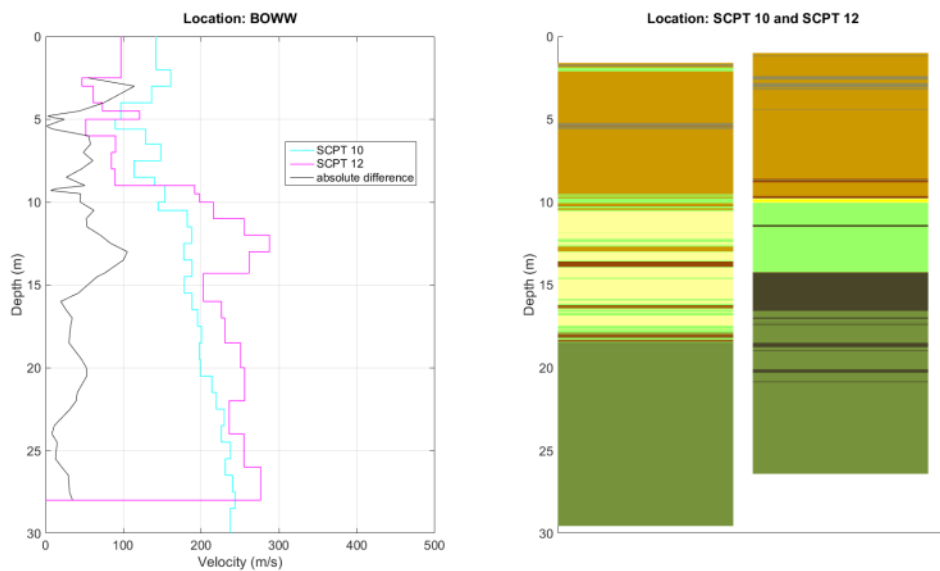


Figure 4.153 Station BOWW. Left: Difference between the two SCPTs measured at the same station location. Right: automatically generated lithology (indication).

## 4.14.4 OSCPT

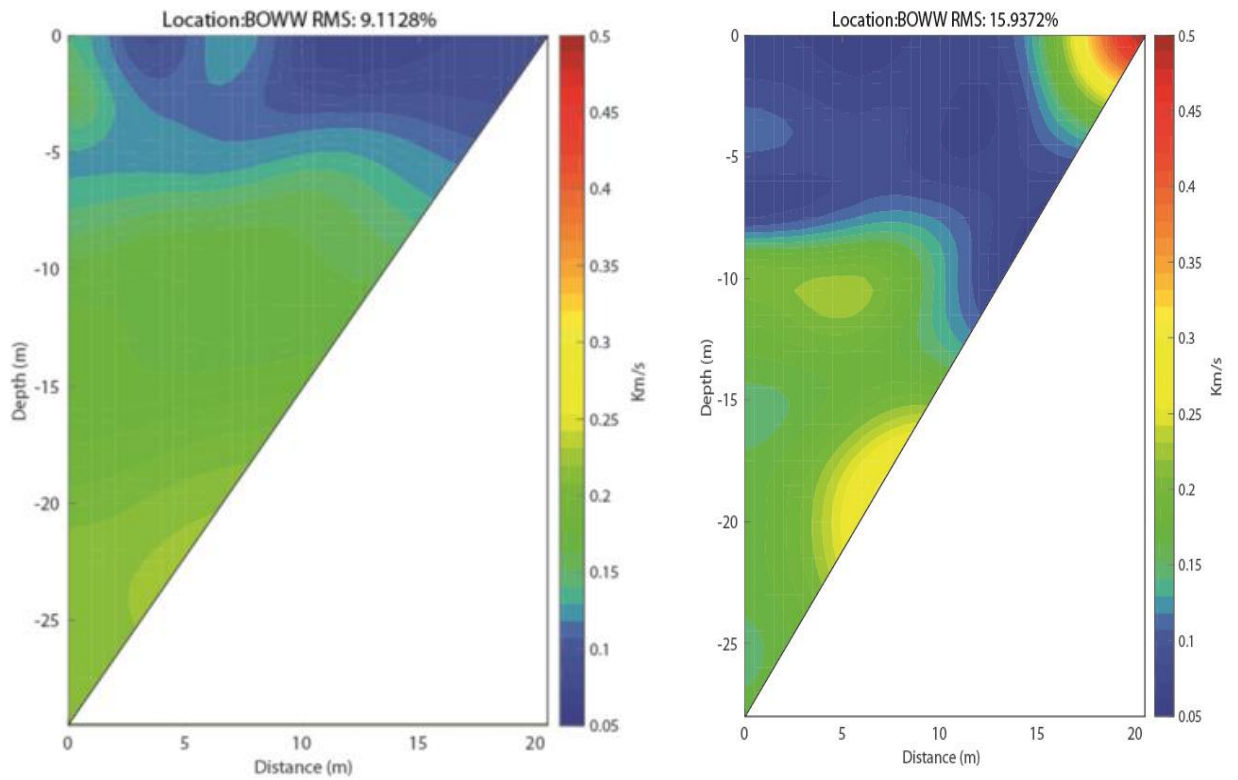


Figure 4.154 Tomographic images based on OSCPT results from two SCPTs for station BOWW (left SCPT10; right SCPT12).

## 4.14.5 MASW

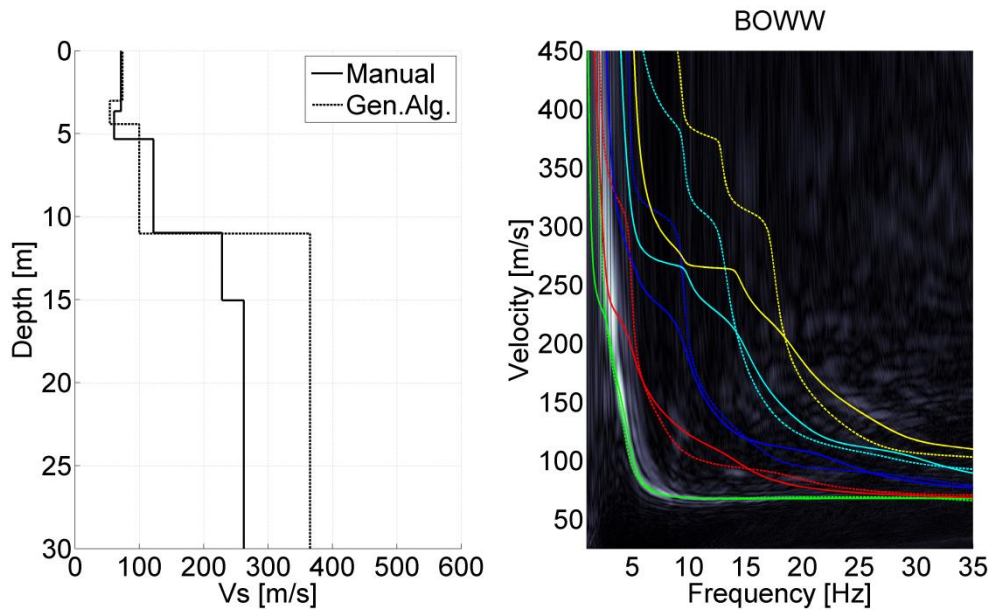


Figure 4.155 MASW result for station BOWW. Left panel:  $V_s$  profiles from active MASW. Solid line from manual fitting of dispersion curves; dashed line for automatic inversion. Right panel: energy in the dispersion plot in greyscale; solid lines are the modelled dispersion curves for different modes of the manually fitted  $V_s$  profile; dashed lines for the different modes of the automatically inverted  $V_s$  profile.

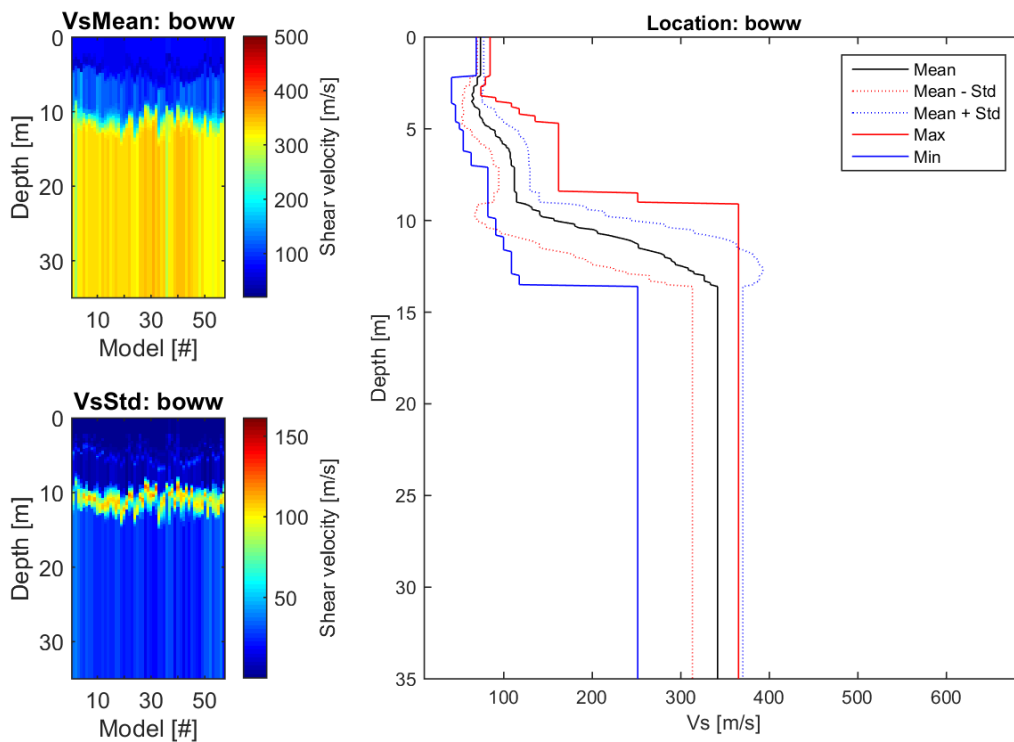


Figure 4.156 CMPcc result for BOWW. Top left: average  $V_s$  along the CMPcc array. Bottom left: standard deviation of  $V_s$  along the CMPcc array. Right: best fit curve of the 72 models with the maximum and minimum value observed in the whole CMPcc and the standard deviation from all models.

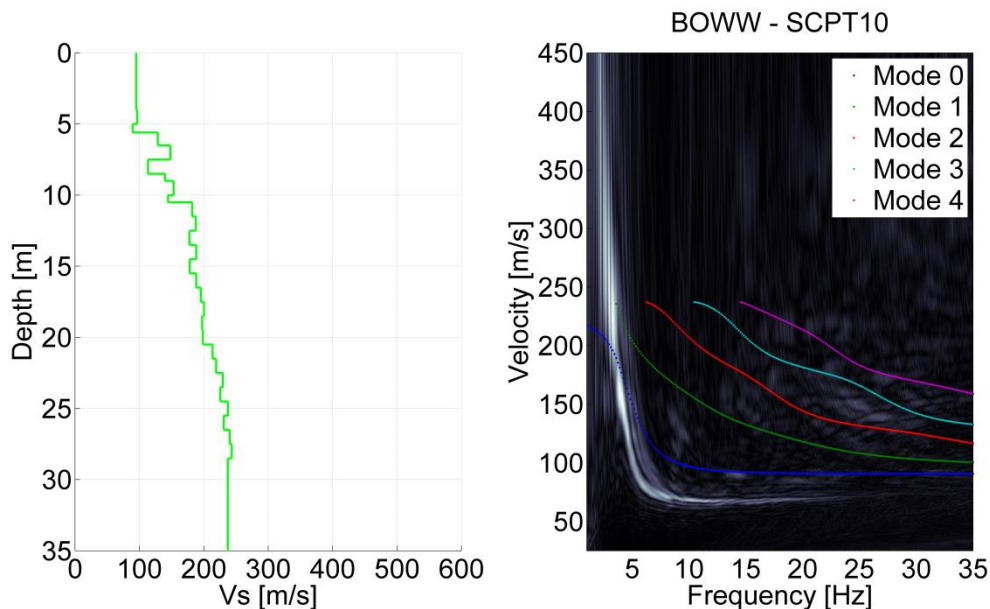


Figure 4.157 Comparison for BOWW of SCPT10 and MASW result. Left:  $V_s$  profile from SCPT. The  $V_s$  from the top 2 layers of the SCPT is generally unreliable and replaced by the minimum  $V_s$  of the first 3 layers. Right: modelled dispersion curves of different modes based on the SCPT  $V_s$  profile in coloured lines plotted on the energy of MASW dispersion plot in greyscale.

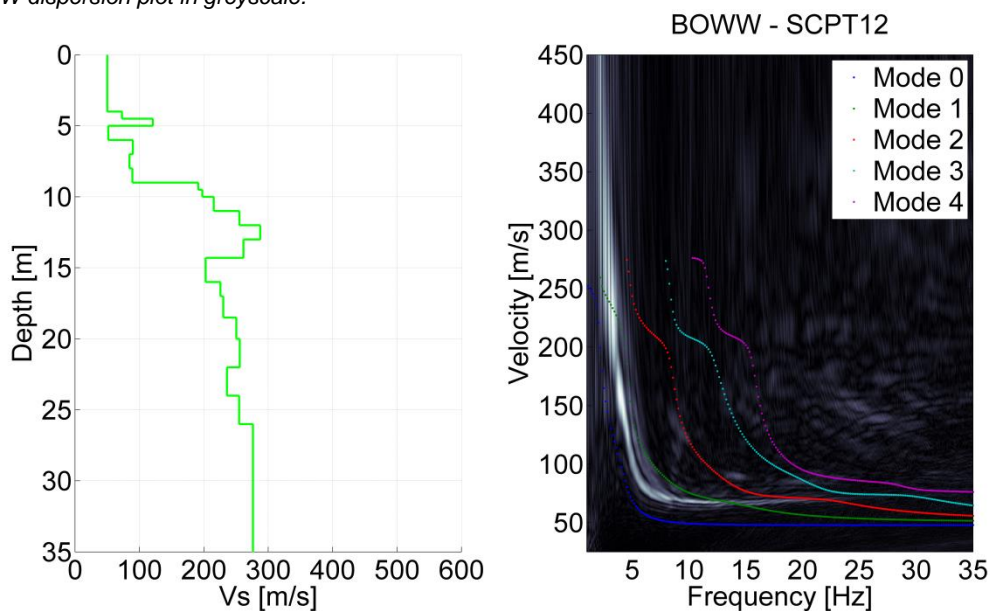


Figure 4.158 Comparison for BOWW of SCPT12 and MASW result. Left:  $V_s$  profile from SCPT. The  $V_s$  from the top 2 layers of the SCPT is generally unreliable and replaced by the minimum  $V_s$  of the first 3 layers. Right: modelled dispersion curves of different modes based on the SCPT  $V_s$  profile in coloured lines plotted on the energy of MASW dispersion plot in greyscale.



## 4.14.6 Synthesis

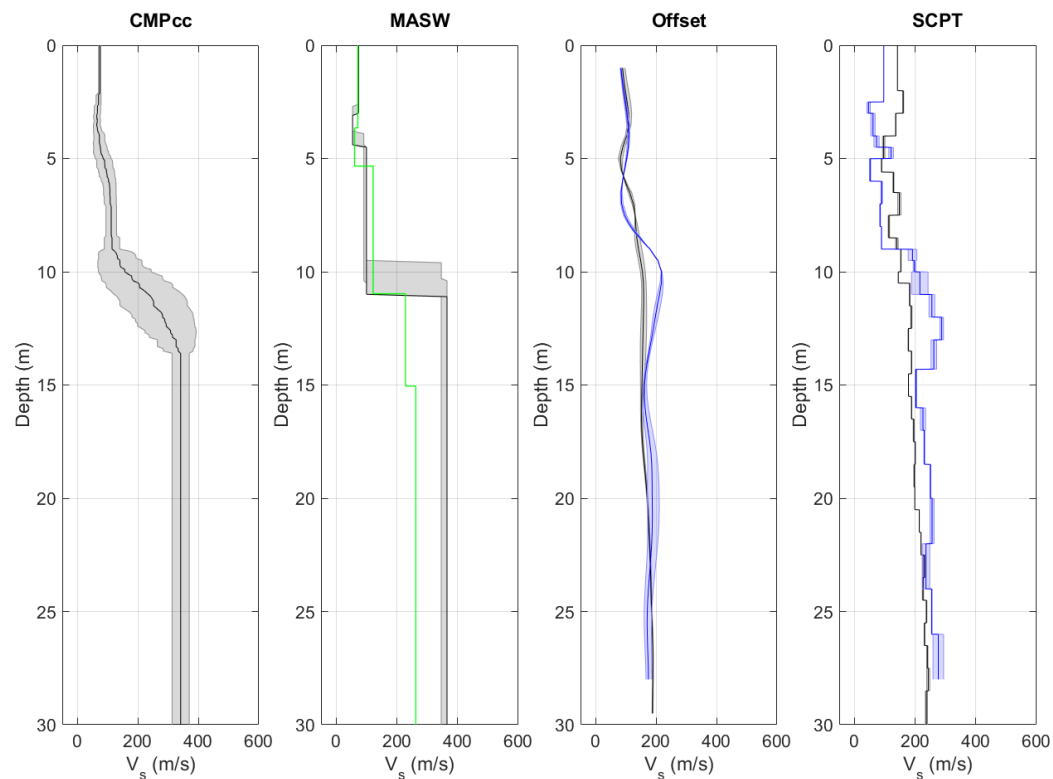


Figure 4.159  $V_s$  profiles from different measurement techniques, including uncertainty bands. From left to right: CMPcc based on active MASW array, shaded band indicates standard deviation; active MASW with manual fit in green and automatic inversion in black with grey shaded band indicating the minimum and the maximum  $V_s$ ; average profile for offset SCPTs between 1 and 5 m offset for 1 or 2 SCPTs with shaded band indicating the minimum and the maximum  $V_s$ ; SCPTs with band indicating variation between left and right blow; cross-hole average profiles for long leg in blue and short leg in grey with shaded band indicating the minimum and the maximum  $V_s$ .

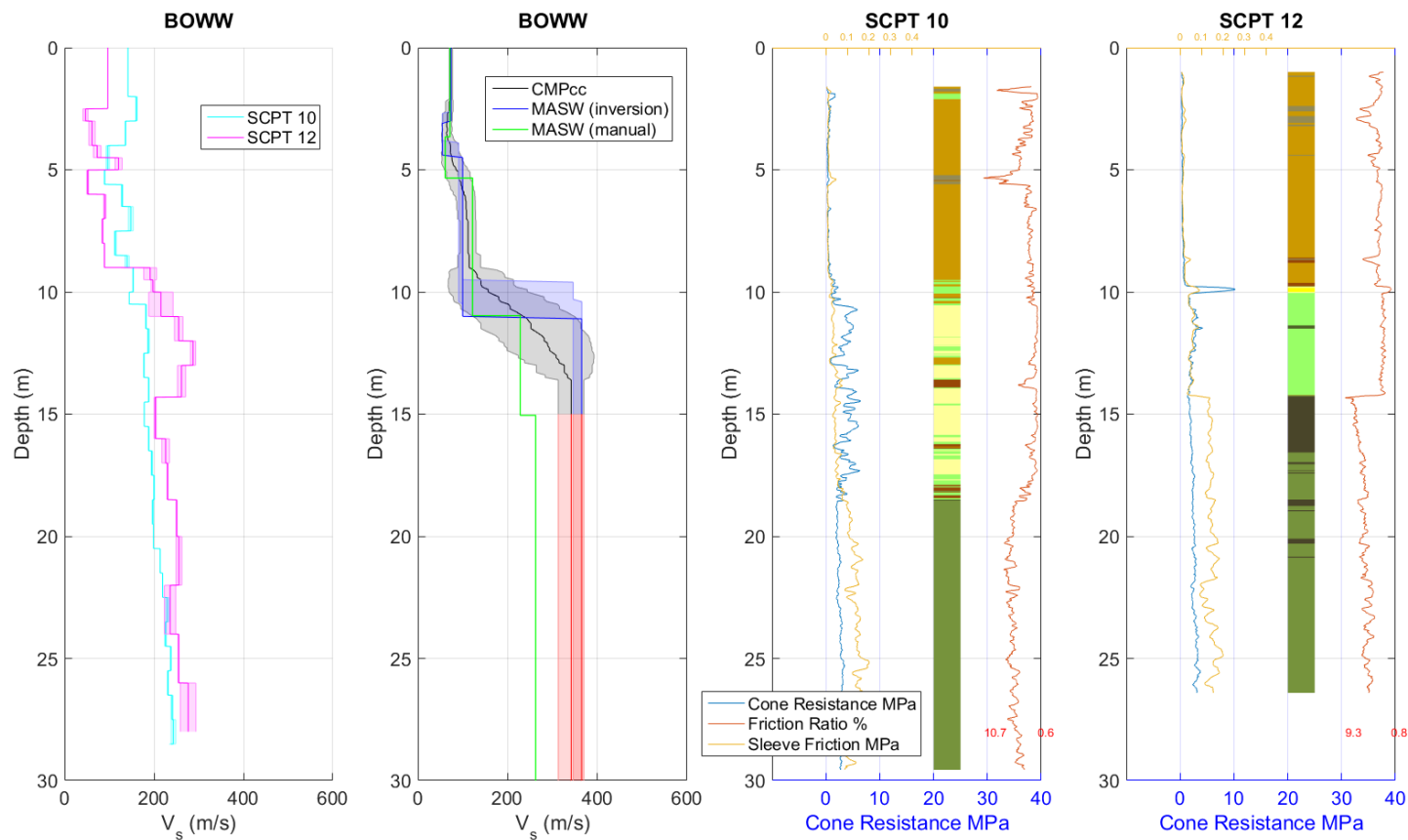


Figure 4.160 Synthesis of  $V_s$  results. Unreliable results are shown in red. From left to right: SCPT with band indicating variation between left and right blow; CMPcc, MASW and average cross-hole results with uncertainty bands; CPT with cone resistance, friction ratio, sleeve friction and automatically generated lithology (indication, for legend see Table 3.1).

## 4.15 Stedum- BSTD

### 4.15.1 Location



Figure 4.161 Map of location BSTD, showing the KNMI accelerograph station, SCPT location and MASW survey lines and shot locations.

### 4.15.2 Geological setting

The location is situated in a non-erosive area. The top of the Pleistocene is situated at a depth of approximately 9 metres. The Holocene deposits are clay layers. The basal peat is present in this area. Possibly part of the survey line is positioned on a small erosive channel. The location is situated on the declining slope of a Peelo valley that reaches from 40 metres at the location up to the maximum depth of 136 metres in the centre over a distance of 2.5 kilometres to the east. At the site of the fieldwork the local geological setting appears to be slightly different: thin layer of Boxtel and Drente sands are present which are probably not present under the accelerograph (according to the DGM model)

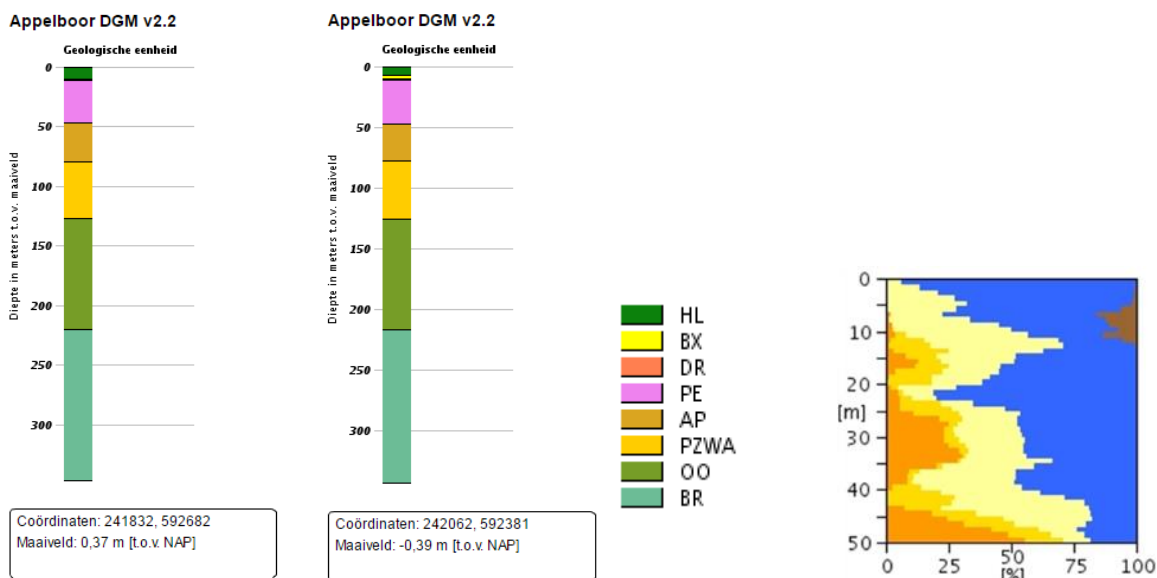


Figure 4.162 Geological information at station BSTD. Left: 1D section from the DGM model. Right: Section from the “delfstoffen online” model (GDN-TNO). Colour coding: brown = peat, blue = clay, yellow to orange = fine sand to coarse sand. The horizontal scale shows the volume percentage of each of the lithologies present at the location, the vertical scale is depth below the surface.

Table 4.15 Descriptions of representative deep boreholes near station BSTD from the DINO database (www.dinoloket.nl).

Drilling	Distance from drilling	top	bottom	sediment type	Min. grain size	Max. grain size	Formation
B07E0042	1200mtr W	0,36	-5,64	Clay			Formation of Naaldwijk
		-5,64	-14,64	Sand	Medium fine	Medium coarse	Formation of Naaldwijk/Boxtel
		-14,64	-23,64	Clay			Eem Formation
		-23,64	-35,64	Sand	Medium fine	Medium coarse	Eem Formation/ Formation of Drente
		-35,64	-41,64	Clay			Formation of Peelo
		-41,64	-44,64	Sand	Fine		Formation of Peelo
		-44,64	-62,64	Sand	Medium coarse		Formation of Appelscha

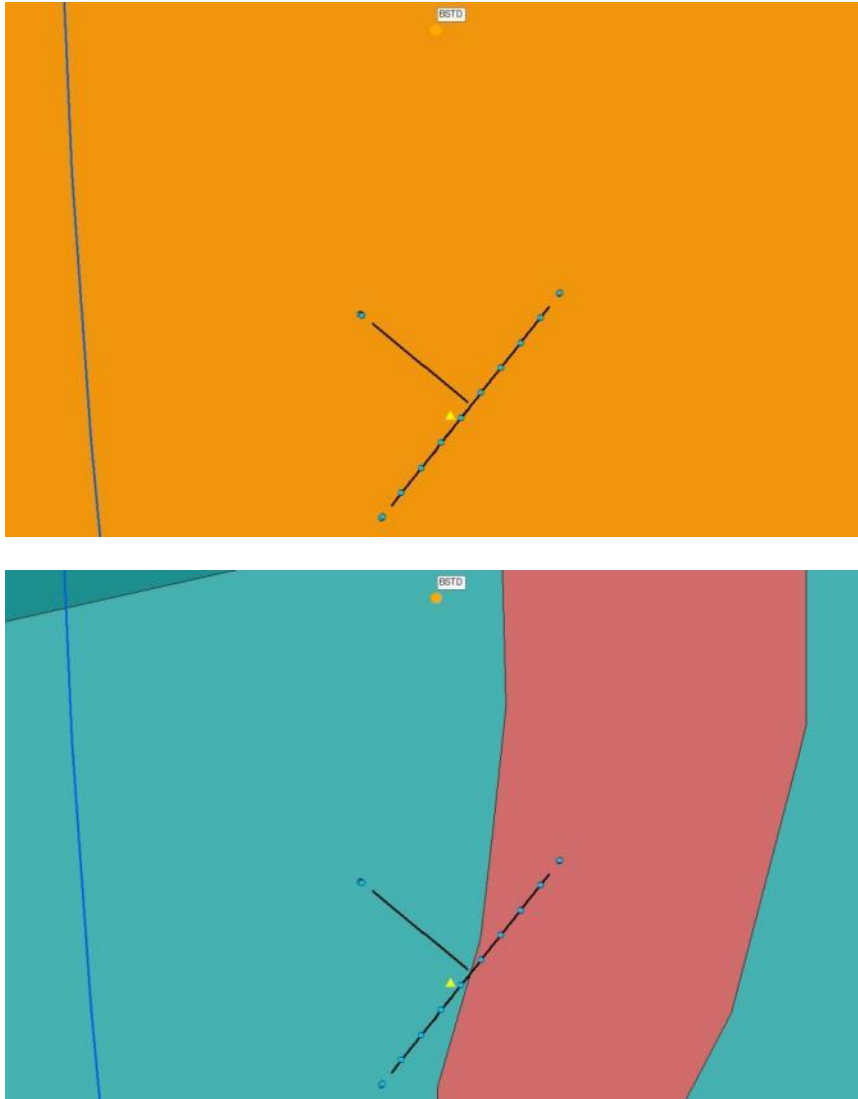


Figure 4.163 Overview map of geological setting based on beta version of GeoTOP model. Top panel: Thickness of the Peelo Formation, blue colour indicates thick Peelo layer, hence in the centre of the channel; red and orange colour indicates thin Peelo layers, hence areas outside the channel; yellow indicates transition zone. Lower panel: Top of Pleistocene surface relative to Dutch Ordnance Datum NAP.

## 4.15.3 SCPT

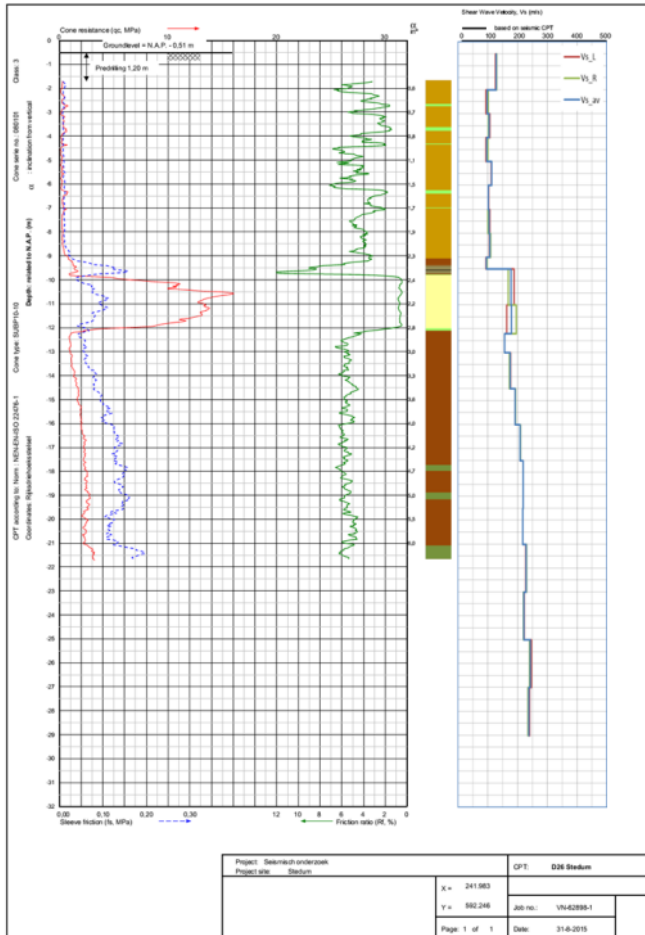


Figure 4.164 SCPT26. From left to right: CPT measurement, showing tip resistance, sleeve friction and friction ratio; automatically generated lithology (indication, for legend see Table 3.1);  $V_s$  profile (red = left blow, green = right blow, blue = average).

## 4.15.4 OSCPT

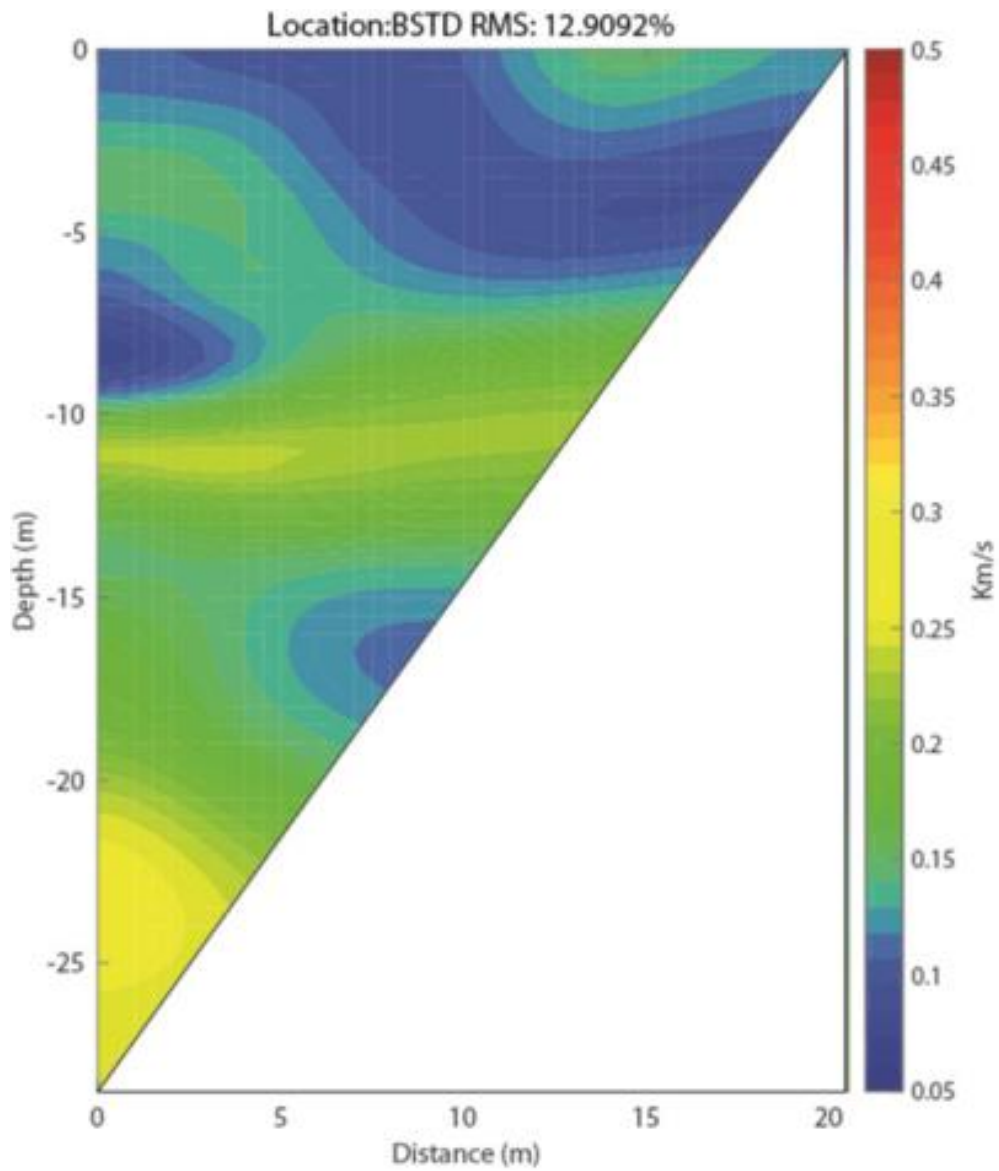


Figure 4.165 Tomographic images based on OSCPT result from SCPT for station BSTD (SCPT26).

## 4.15.5 MASW

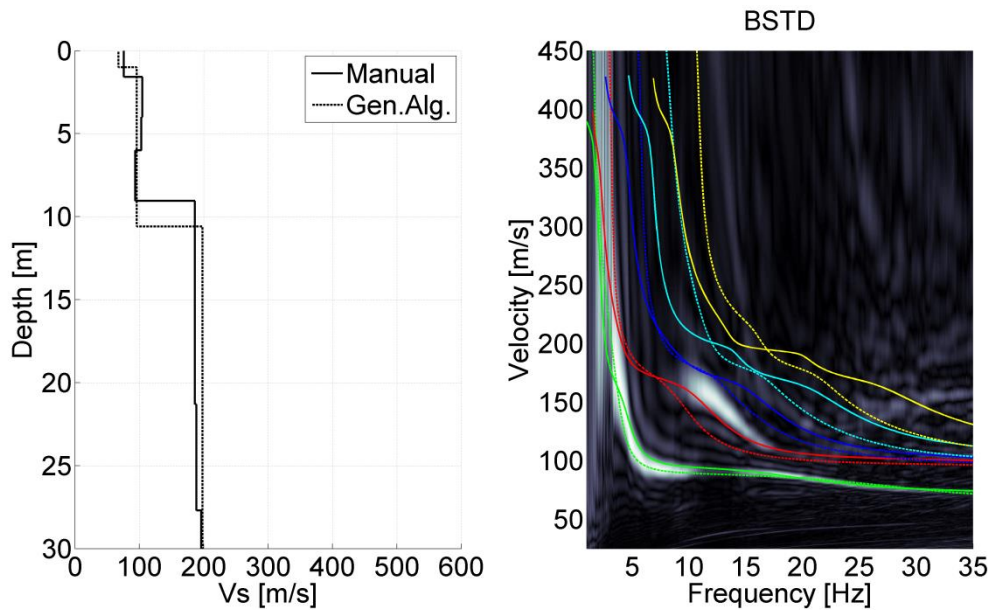


Figure 4.166 MASW result for station BSTD. Left panel:  $V_s$  profiles from active MASW. Solid line from manual fitting of dispersion curves; dashed line for automatic inversion. Right panel: energy in the dispersion plot in greyscale; solid lines are the modelled dispersion curves for different modes of the manually fitted  $V_s$  profile; dashed lines for the different modes of the automatically inverted  $V_s$  profile.

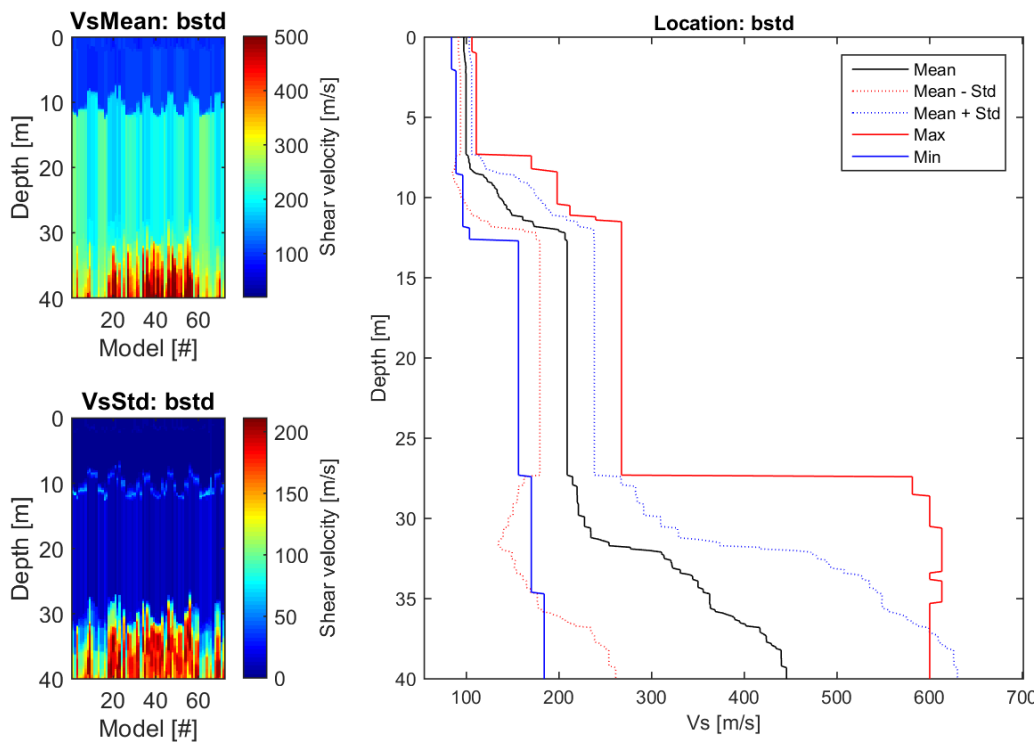


Figure 4.167 CMPcc result for BSTD. Top left: average  $V_s$  along the CMPcc array. Bottom left: standard deviation of  $V_s$  along the CMPcc array. Right: best fit curve of the 72 models with the maximum and minimum value observed in the whole CMPcc and the standard deviation from all models.

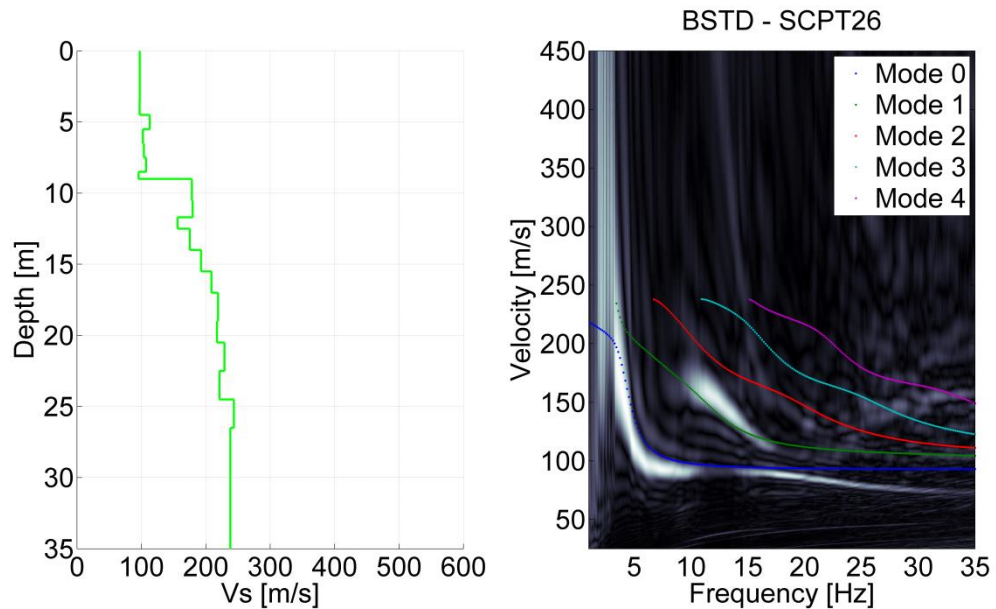


Figure 4.168 Comparison for BSTD of SCPT26 and MASW result. Left:  $V_s$  profile from SCPT. The  $V_s$  from the top 2 layers of the SCPT is generally unreliable and replaced by the minimum  $V_s$  of the first 3 layers. Right: modelled dispersion curves of different modes based on the SCPT  $V_s$  profile in coloured lines plotted on the energy of MASW dispersion plot in greyscale.



## 4.15.6 Synthesis

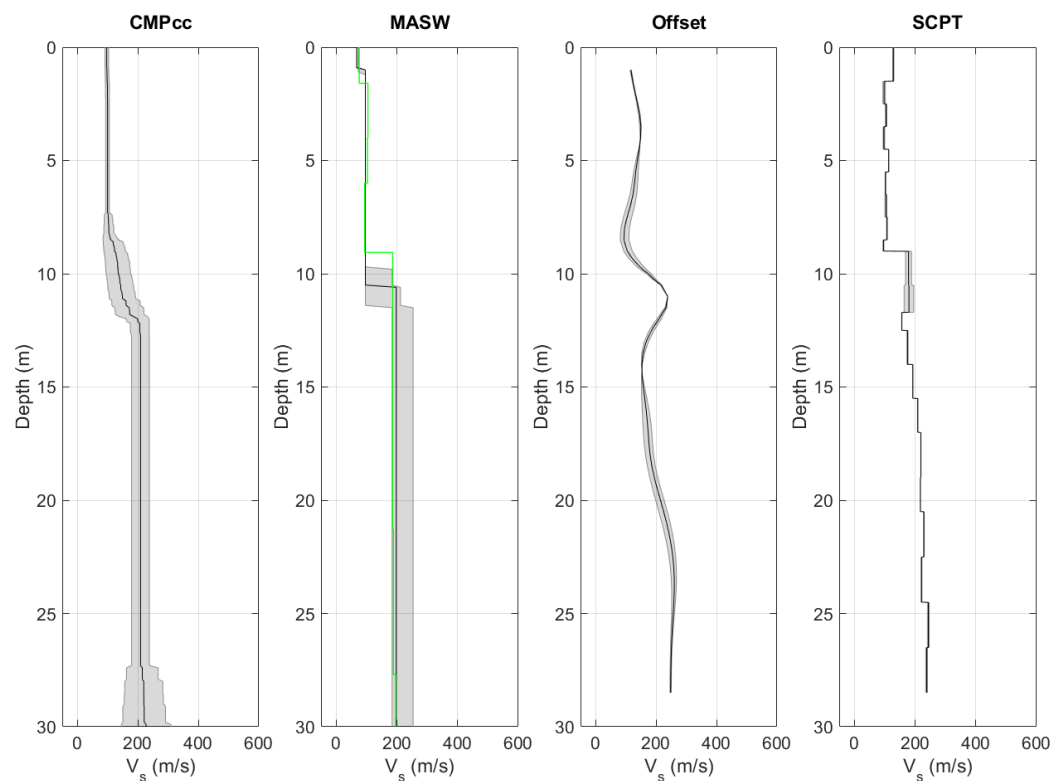


Figure 4.169  $V_s$  profiles from different measurement techniques, including uncertainty bands. From left to right: CMPcc based on active MASW array, shaded band indicates standard deviation; active MASW with manual fit in green and automatic inversion in black with grey shaded band indicating the minimum and the maximum  $V_s$ ; average profile for offset SCPTs between 1 and 5 m offset for 1 or 2 SCPTs with shaded band indicating the minimum and the maximum  $V_s$ ; SCPTs with band indicating variation between left and right blow; cross-hole average profiles for long leg in blue and short leg in grey with shaded band indicating the minimum and the maximum  $V_s$ .

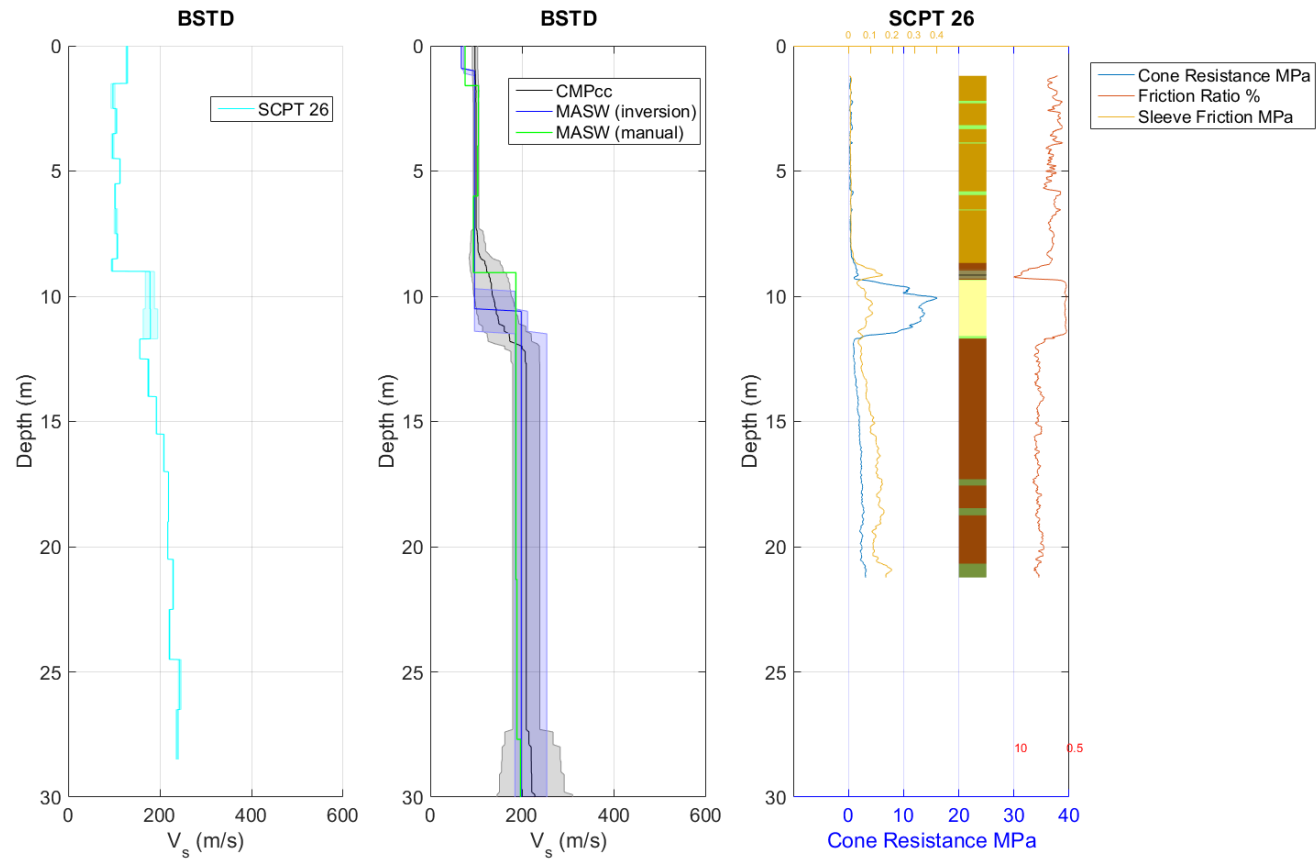


Figure 4.170 Synthesis of  $V_s$  results. Unreliable results are shown in red. From left to right: SCPT with band indicating variation between left and right blow; CMPcc, MASW and average cross-hole results with uncertainty bands; CPT with cone resistance, friction ratio, sleeve friction and automatically generated lithology (indication, for legend see Table 3.1).

## 4.16 Winneveer- BWIN

### 4.16.1 Location



Figure 4.171 Map of location BWIN, showing the KNMI accelerograph station (exact location ambiguous), SCPT location and MASW survey lines and shot locations.

### 4.16.2 Geological setting

The location is situated in a non-erosive area. The top of the Pleistocene is situated at a depth of 6 to 7 metres. The Holocene deposits consist of a clay layer with a peat layer in between, at a depth of approximately 3 metres. The basal peat is present in this area. The location is situated on the bottom of a Peelo valley with a depth of 135 metres.

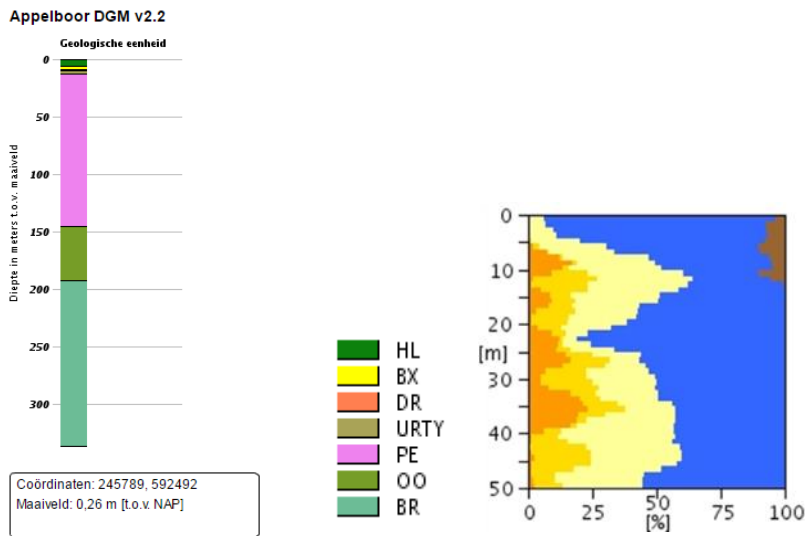
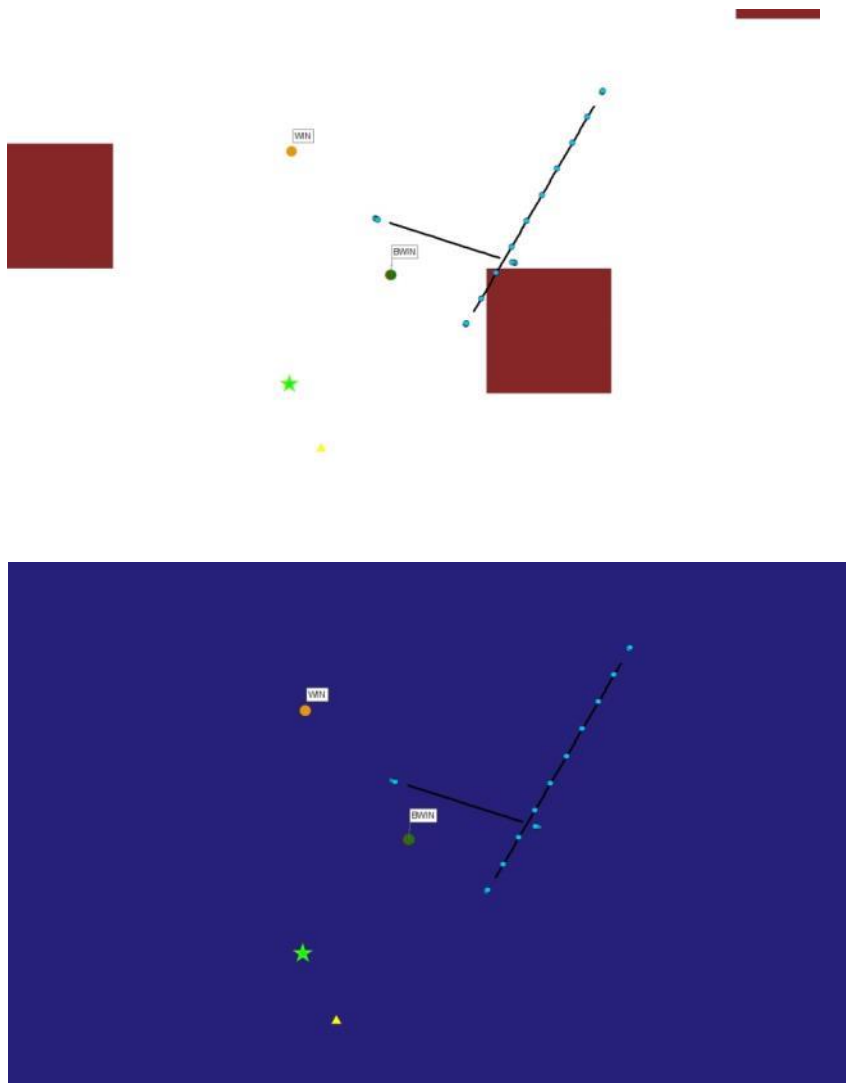


Figure 4.172 Geological information at station BWIN. Left: 1D section from the DGM model. Right: Section from the “delfstoffen online” model (GDN-TNO). Colour coding: brown = peat, blue = clay, yellow to orange = fine sand to coarse sand. The horizontal scale shows the volume percentage of each of the lithologies present at the location, the vertical scale is depth below the surface.

Table 4.16 Descriptions of representative deep boreholes near station BWIN from the DINO database ([www.dinoloket.nl](http://www.dinoloket.nl)).

Drilling	Distance from drilling	top	bottom	sediment type	Min. grain size	Max. grain size	Formation
B07E0004	550mtr S	0,00	-7,80	Clay			Formation of Naaldwijk
		-7,80	-12,30	Sand	Fine		Formation of Boxtel
		-12,30	-77,00	Clay			Formation of Peelo
		-77,00	-99,00	Sand	Fine		Formation of Peelo
		-99,00	-118,30	Sand	Medium coarse		Formation of Peelo
		-118,30	-130,00	Sand	Fine		Formation of Peelo

1210624-000-BGS-0007, Version 2, 27 June 2016, final



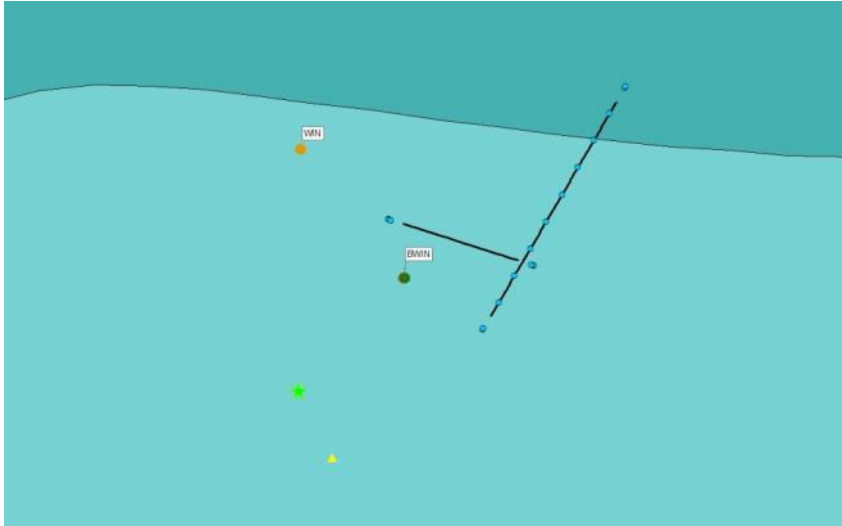


Figure 4.173 Overview map of geological setting based on beta version of GeoTOP model. Top panel: Thickness of the Holocene peat. Middle panel: Thickness of the Peelo Formation, blue colour indicates thick Peelo layer, hence in the centre of the channel; red and orange colour indicates thin Peelo layers, hence areas outside the channel; yellow indicates transition zone. Lower panel: Top of Pleistocene surface relative to Dutch Ordnance Datum NAP.

## 4.16.3 SCPT

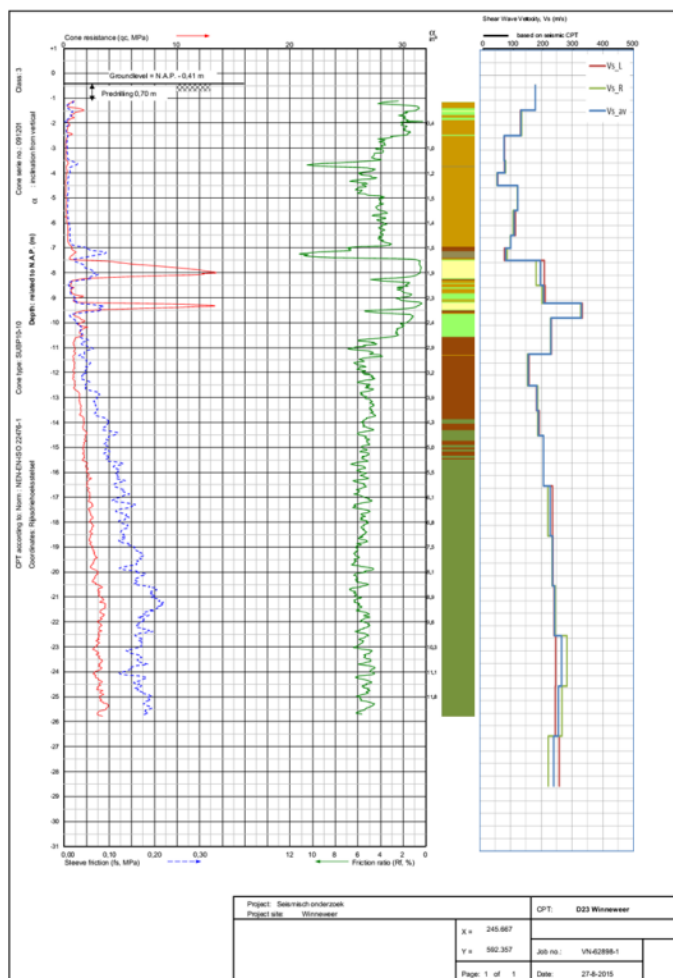


Figure 4.174 SCPT23. From left to right: CPT measurement, showing tip resistance, sleeve friction and friction ratio; automatically generated lithology (indication, for legend see Table 3.1);  $V_s$  profile (red = left blow, green = right blow, blue = average).

## 4.16.4 OSCPT

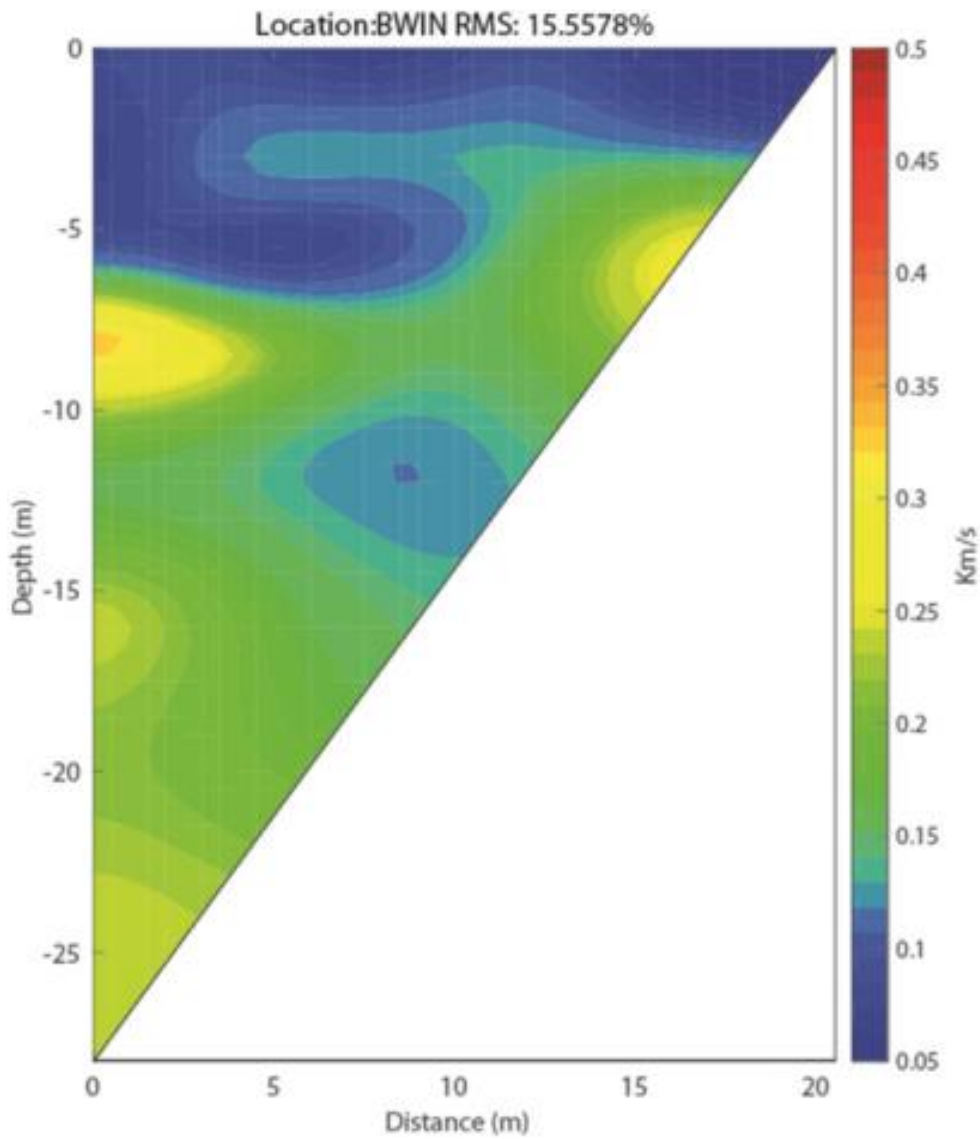


Figure 4.175 Tomographic images based on OSCPT result from SCPT for station BWIN (SCPT23).

## 4.16.5 MASW

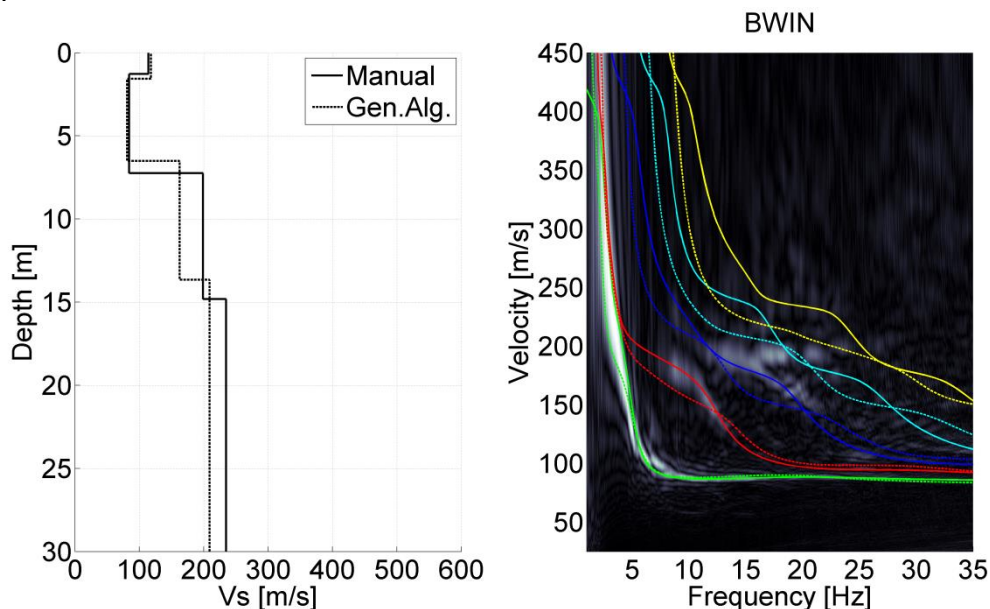


Figure 4.176 MASW result for station BWIN. Left panel:  $V_s$  profiles from active MASW. Solid line from manual fitting of dispersion curves; dashed line for automatic inversion. Right panel: energy in the dispersion plot in greyscale; solid lines are the modelled dispersion curves for different modes of the manually fitted  $V_s$  profile; dashed lines for the different modes of the automatically inverted  $V_s$  profile.

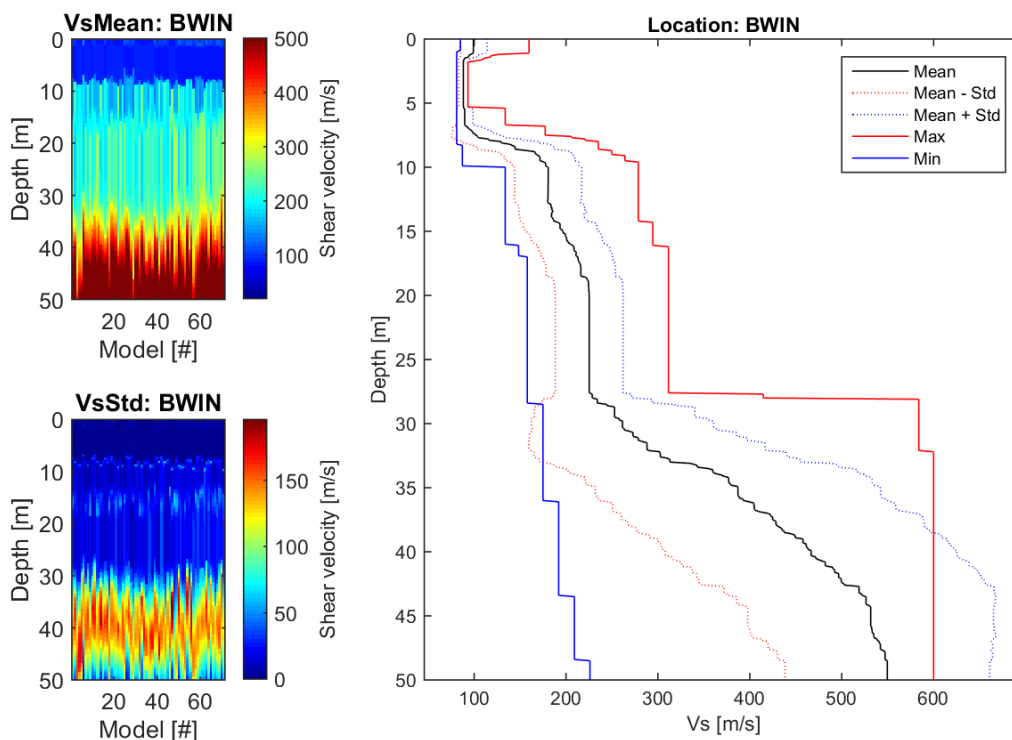


Figure 4.177 CMPcc result for BWIN. Top left: average  $V_s$  along the CMPcc array. Bottom left: standard deviation of  $V_s$  along the CMPcc array. Right: best fit curve of the 72 models with the maximum and minimum value observed in the whole CMPcc and the standard deviation from all models.

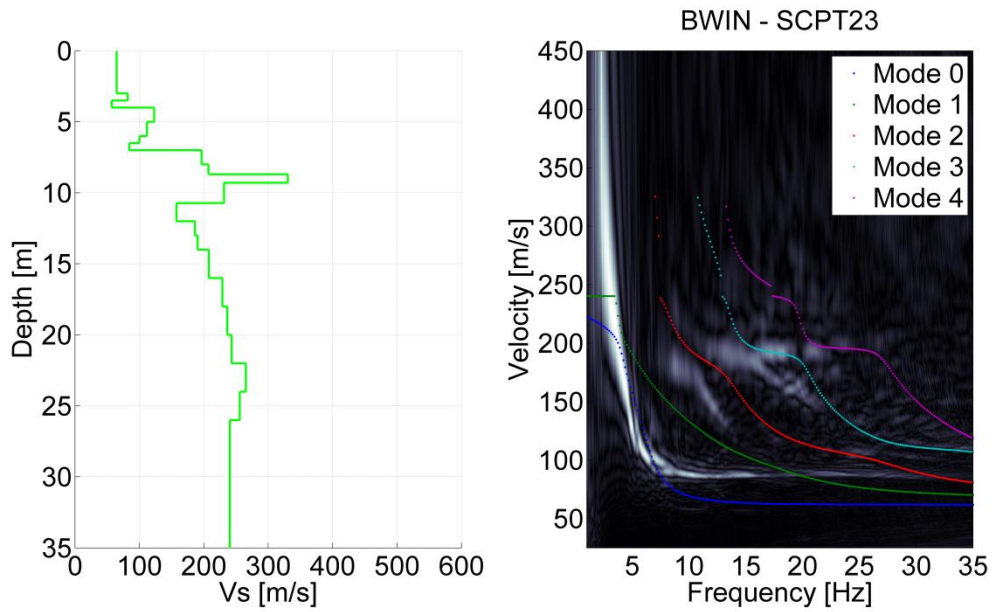


Figure 4.178 Comparison for BWIN of SCPT23 and MASW result. Left:  $V_s$  profile from SCPT. The  $V_s$  from the top 2 layers of the SCPT is generally unreliable and replaced by the minimum  $V_s$  of the first 3 layers. Right: modelled dispersion curves of different modes based on the SCPT  $V_s$  profile in coloured lines plotted on the energy of MASW dispersion plot in greyscale.

## 4.16.6 Synthesis

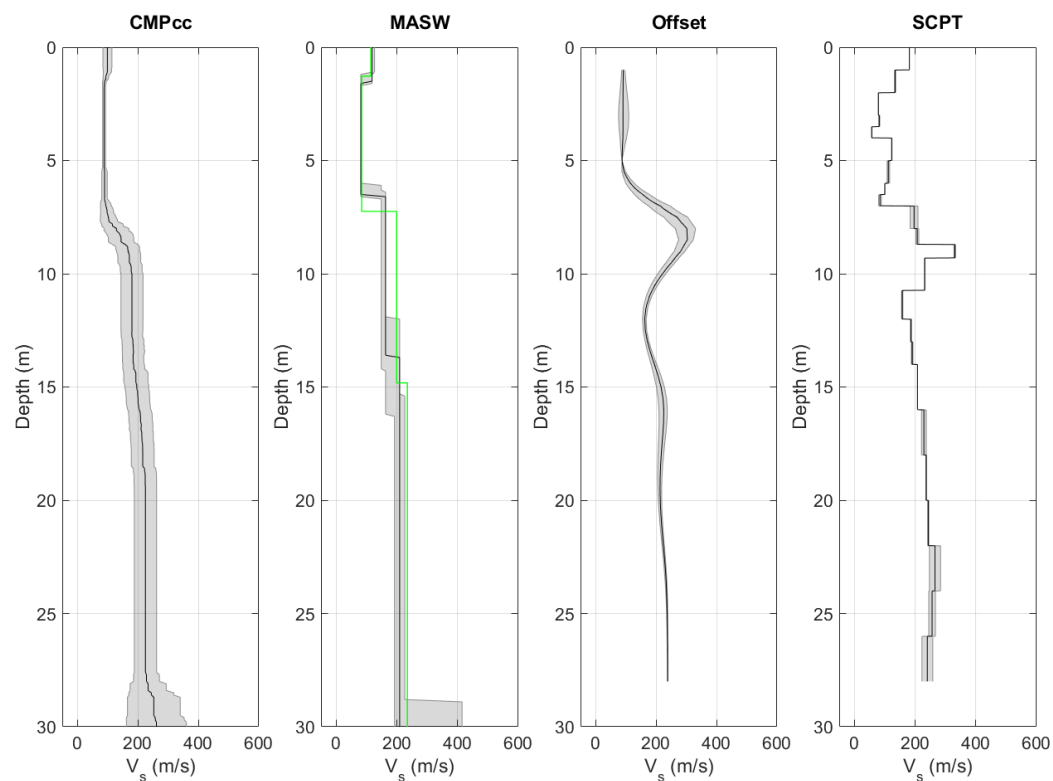


Figure 4.179  $V_s$  profiles from different measurement techniques, including uncertainty bands. From left to right: CMPcc based on active MASW array, shaded band indicates standard deviation; active MASW with manual fit in green and automatic inversion in black with grey shaded band indicating the minimum and the maximum  $V_s$ ; average profile for offset SCPTs between 1 and 5 m offset for 1 or 2 SCPTs with shaded band indicating the minimum and the maximum  $V_s$ ; SCPTs with band indicating variation between left and right blow; cross-hole average profiles for long leg in blue and short leg in grey with shaded band indicating the minimum and the maximum  $V_s$ .

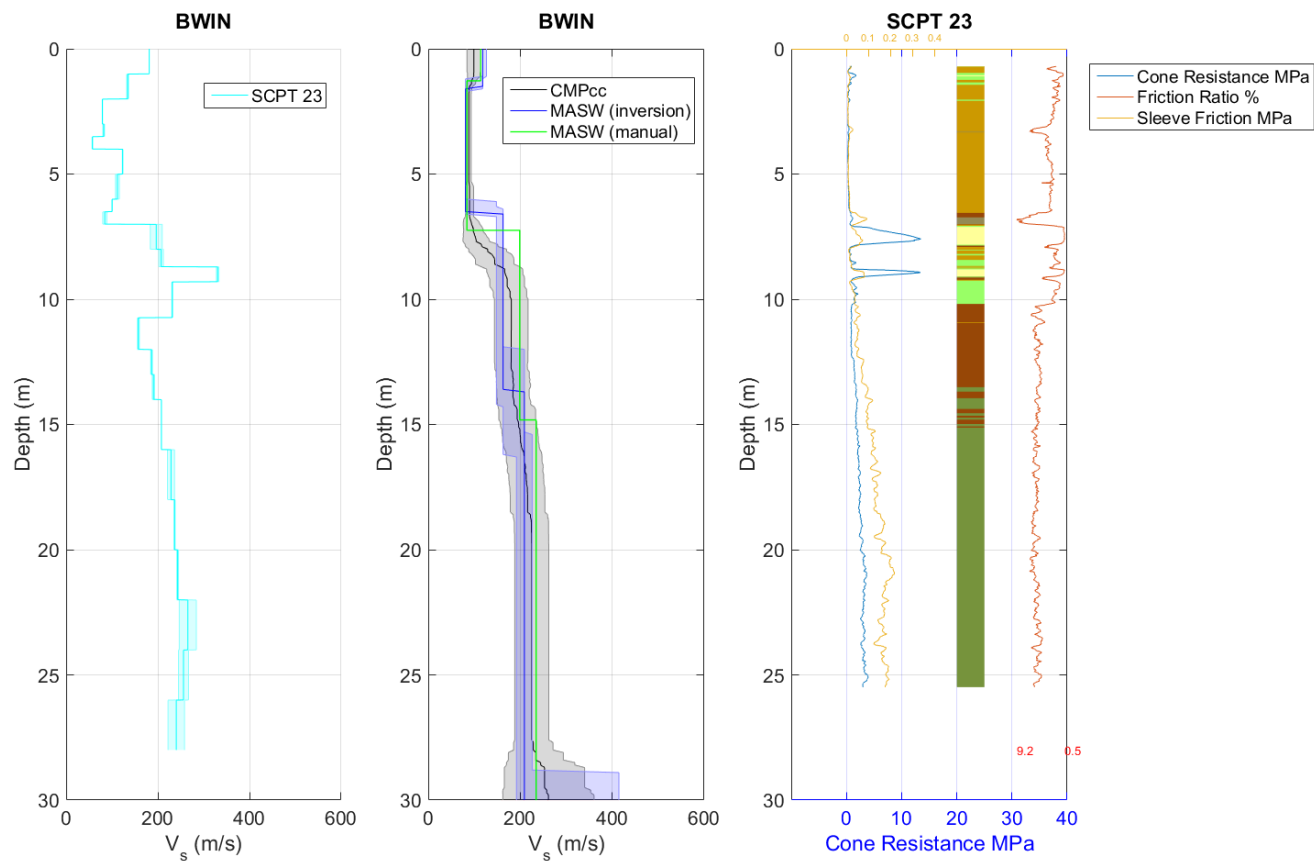


Figure 4.180 Synthesis of  $V_s$  results. Unreliable results are shown in red. From left to right: SCPT with band indicating variation between left and right blow; CMPcc, MASW and average cross-hole results with uncertainty bands; CPT with cone resistance, friction ratio, sleeve friction and automatically generated lithology (indication, for legend see Table 3.1).

## 4.17 Wirdum- BWIR

### 4.17.1 Location



Figure 4.181 Map of location BWIR, showing the KNMI accelerograph station (exact location ambiguous), SCPT location and MASW survey lines and shot locations.

### 4.17.2 Geological setting

The location is situated in a non-erosive area. The top of the Pleistocene is situated at a depth of 6 to 7 metres. The Holocene deposits consist of a clay layer with a peat layer in between at a depth of approximately 3 metres. The basal peat is present in this area. The location is situated on a declining slope of a Peelo valley that reaches from 109 metres at the location up to the maximum depth of 115 metres in the centre over a distance of 0.5 kilometre to the northwest.

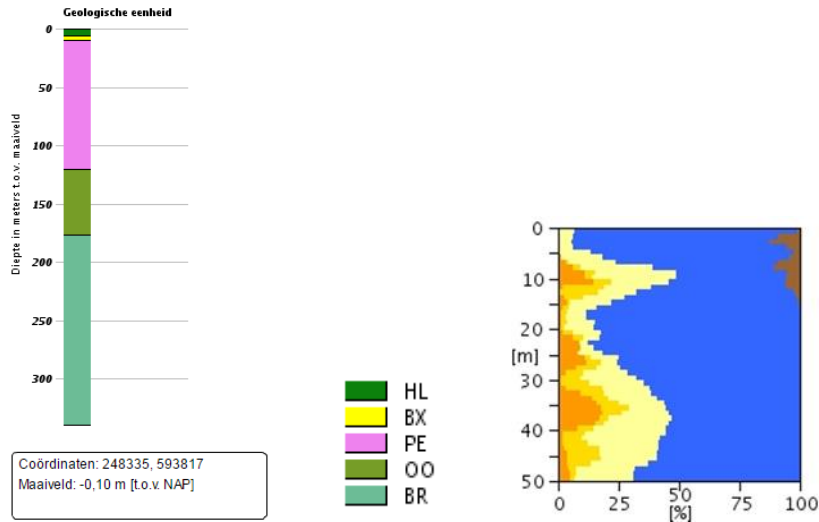
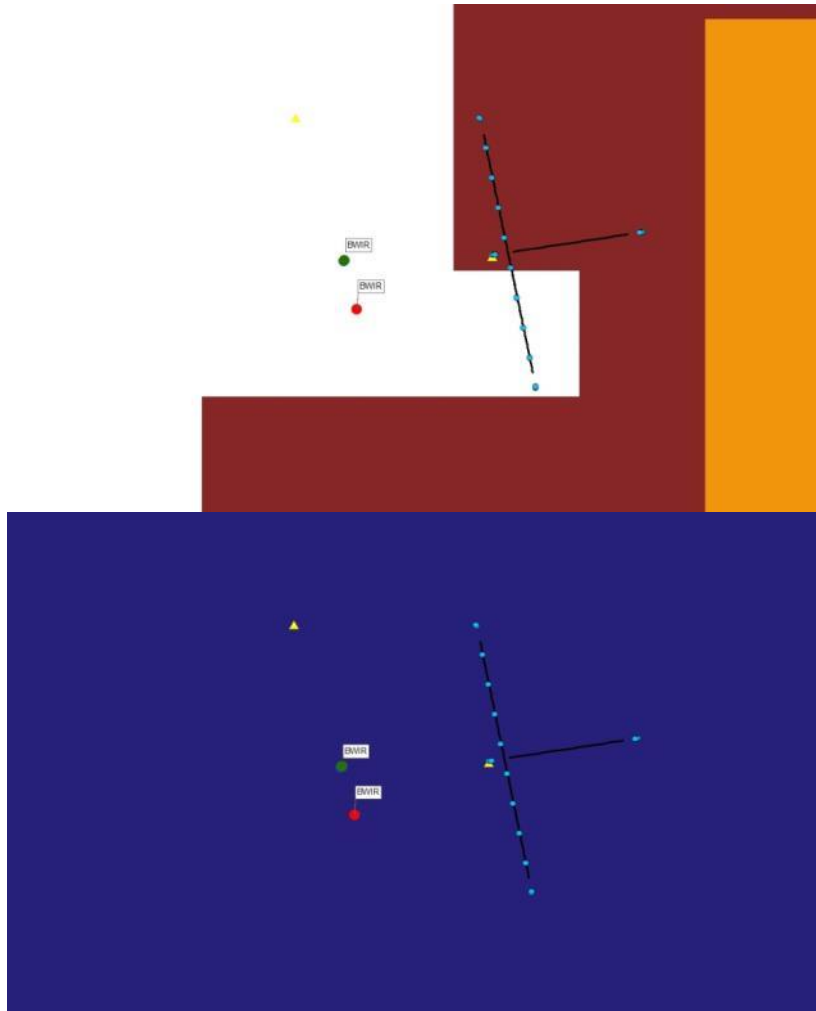


Figure 4.182 Geological information at station BWIR. Left: 1D section from the DGM model. Right: Section from the “delfstoffen online” model (GDN-TNO). Colour coding: brown = peat, blue = clay, yellow to orange = fine sand to coarse sand. The horizontal scale shows the volume percentage of each of the lithologies present at the location, the vertical scale is depth below the surface.

Table 4.17 Descriptions of representative deep boreholes near station BWIR from the DINO database ([www.dinoloket.nl](http://www.dinoloket.nl)).

Drilling	Distance from drilling	top	bottom	sediment type	Min. grain size	Max. grain size	Formation
B07F0005	4000mtr E	0,38	-2,13	Clay			Formation of Naaldwijk
		-2,13	-3,13	Peat			Formation of Nieuwkoop
		-3,13	-5,88	Clay			Formation of Naaldwijk
		-5,88	-5,98	Peat			Formation of Nieuwkoop
		-5,98	-9,88	Sand	Fine		Formation of Boxtel
		-9,88	-114,38	Clay			Formation of Peelo
B07E0004	3300mtr S	-114,38	-181,38	Sand	Fine		Formation of Peelo
		0,00	-7,80	Clay			Formation of Naaldwijk
		-7,80	-12,30	Sand	Fine		Formation of Boxtel
		-12,30	-77,00	Clay			Formation of Peelo
		-77,00	-99,00	Sand	Fine		Formation of Peelo
		-99,00	-118,30	Sand	Medium coarse		Formation of Peelo
-118,30	-130,00	Sand	Fine		Formation of Peelo		

1210624-000-BGS-0007, Version 2, 27 June 2016, final



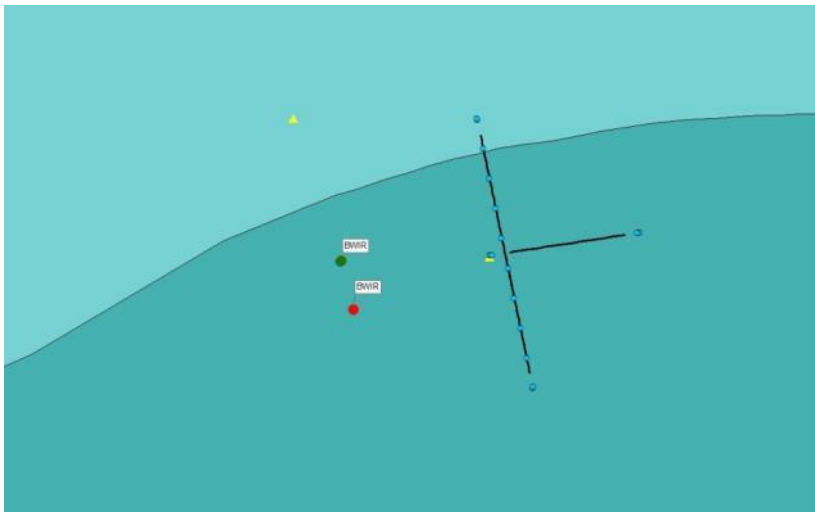


Figure 4.183 Overview map of geological setting based on beta version of GeoTOP model. Top panel: Thickness of the Holocene peat. Middle panel: Thickness of the Peelo Formation, blue colour indicates thick Peelo layer, hence in the centre of the channel; red and orange colour indicates thin Peelo layers, hence areas outside the channel; yellow indicates transition zone. Lower panel: Top of Pleistocene surface relative to Dutch Ordnance Datum NAP.

## 4.17.3 SCPT

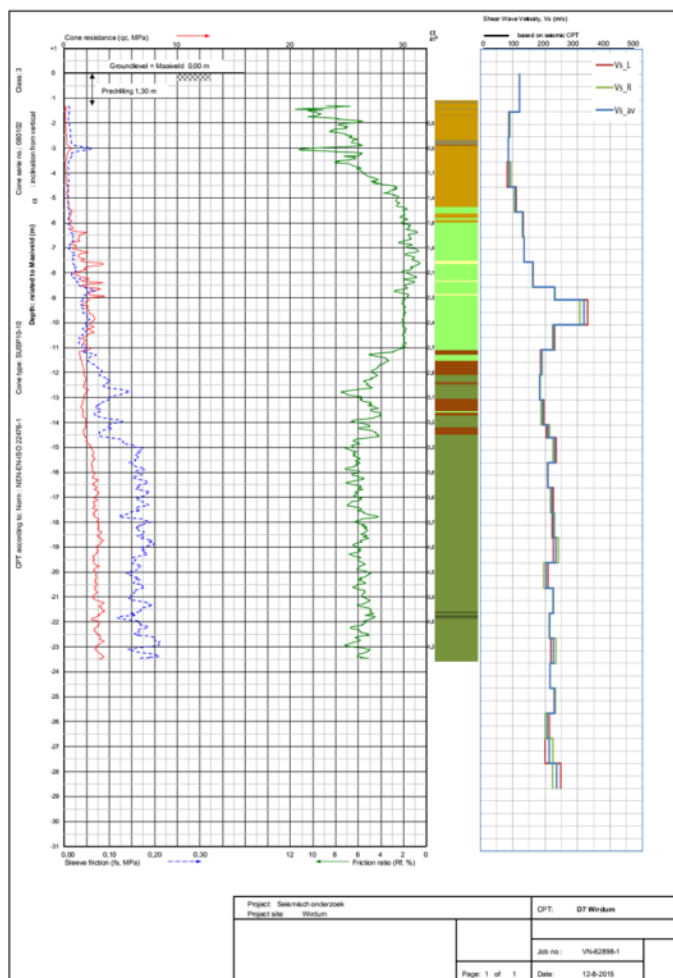


Figure 4.184 SCPT07. From left to right: CPT measurement, showing tip resistance, sleeve friction and friction ratio; automatically generated lithology (indication, for legend see Table 3.1);  $V_s$  profile (red = left blow, green = right blow, blue = average).

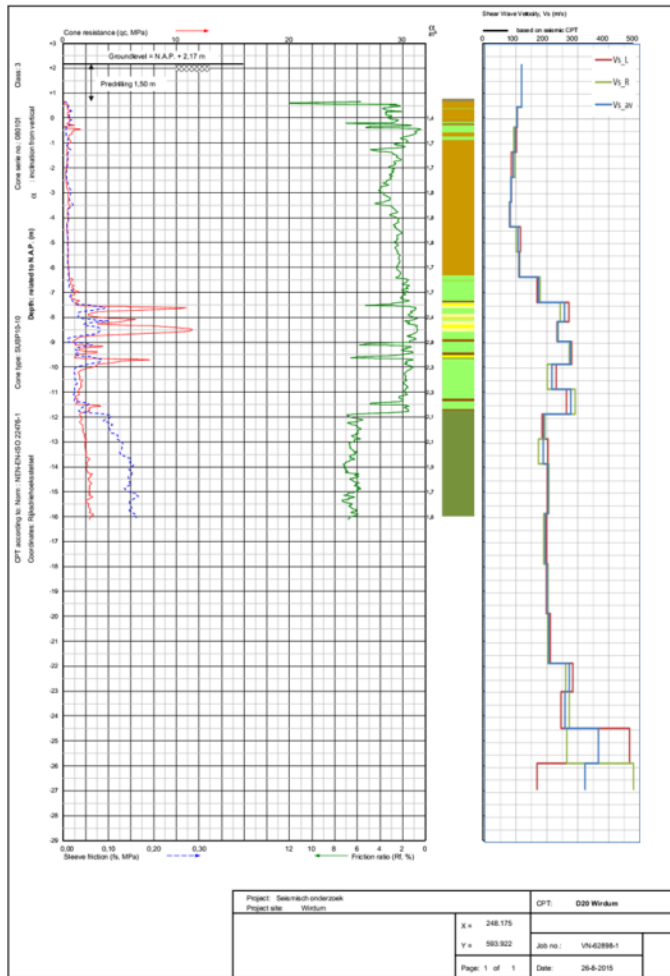


Figure 4.185 SCPT20. From left to right: CPT measurement, showing tip resistance, sleeve friction and friction ratio; automatically generated lithology (indication, for legend see Table 3.1);  $V_s$  profile (red = left blow, green = right blow, blue = average).

1210624-000-BGS-0007, Version 2, 27 June 2016, final

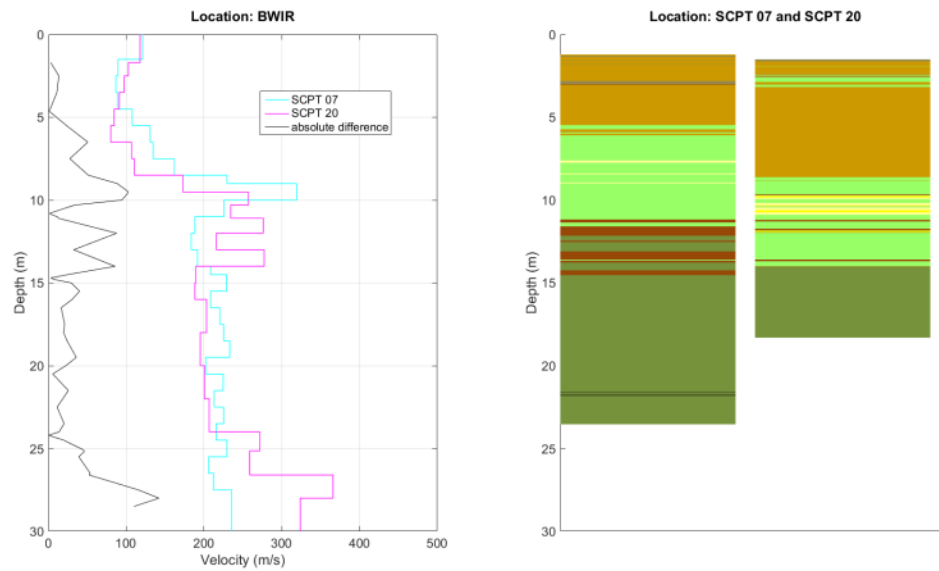


Figure 4.186 Station BWIR. Left: Difference between the two SCPTs measured at the same station location. Right: automatically generated lithology (indication).

## 4.17.4 OSCPT

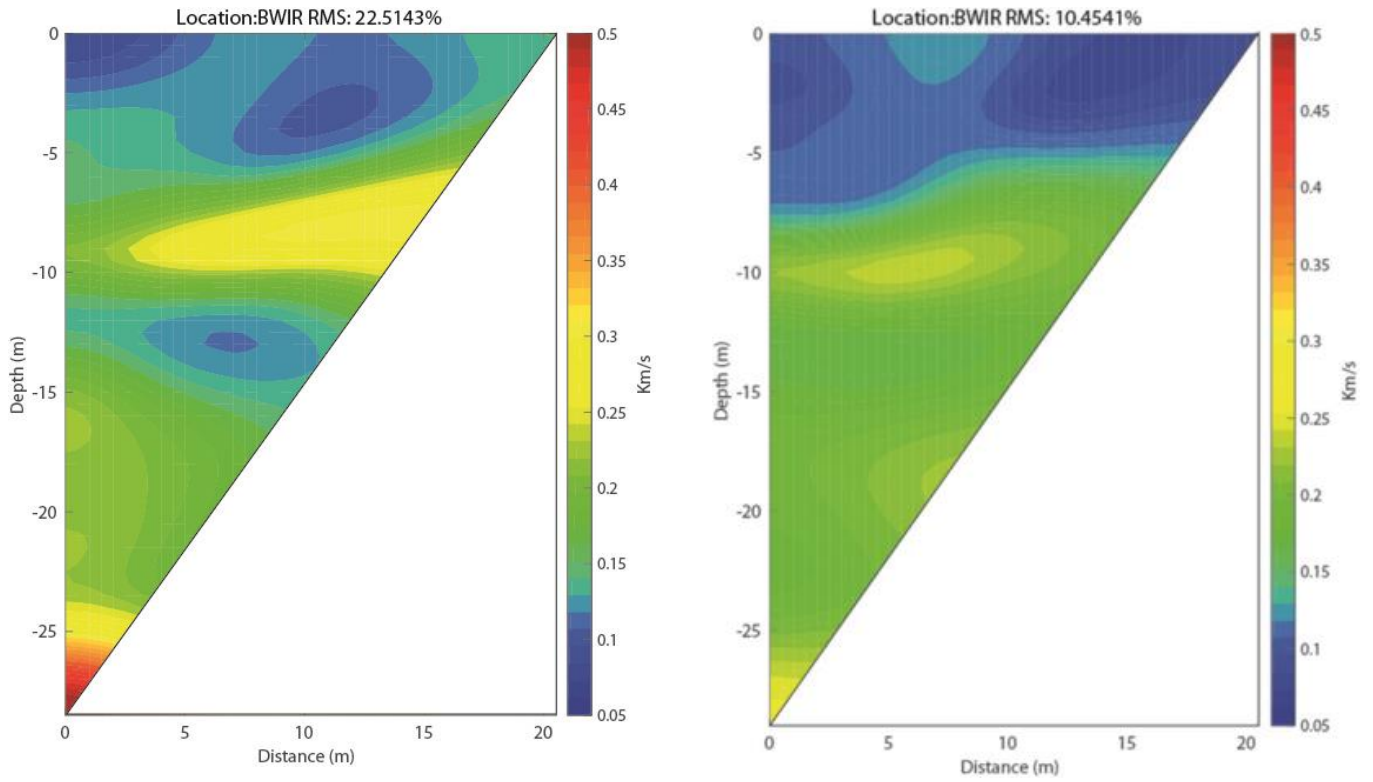


Figure 4.187 Tomographic images based on OSCPT results from two SCPTs for station BWIR (left SCPT07; right SCPT20).

## 4.17.5 MASW

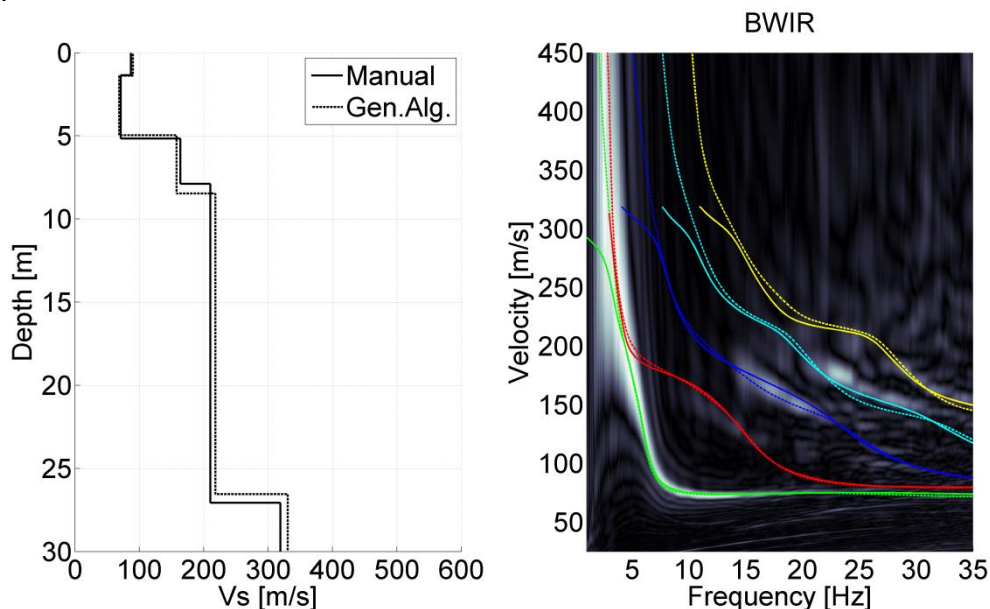


Figure 4.188 MASW result for station BWIR. Left panel:  $V_s$  profiles from active MASW. Solid line from manual fitting of dispersion curves; dashed line for automatic inversion. Right panel: energy in the dispersion plot in greyscale; solid lines are the modelled dispersion curves for different modes of the manually fitted  $V_s$  profile; dashed lines for the different modes of the automatically inverted  $V_s$  profile.

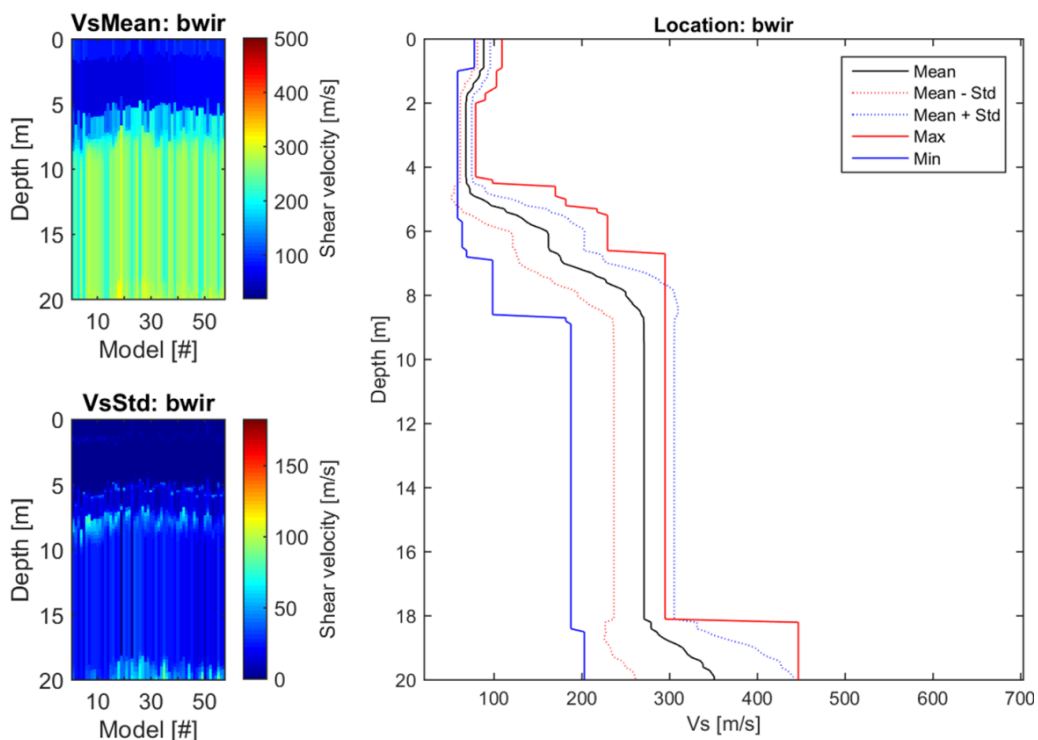


Figure 4.189 CMPcc result for BWIR. Top left: average  $V_s$  along the CMPcc array. Bottom left: standard deviation of  $V_s$  along the CMPcc array. Right: best fit curve of the 72 models with the maximum and minimum value observed in the whole CMPcc and the standard deviation from all models.

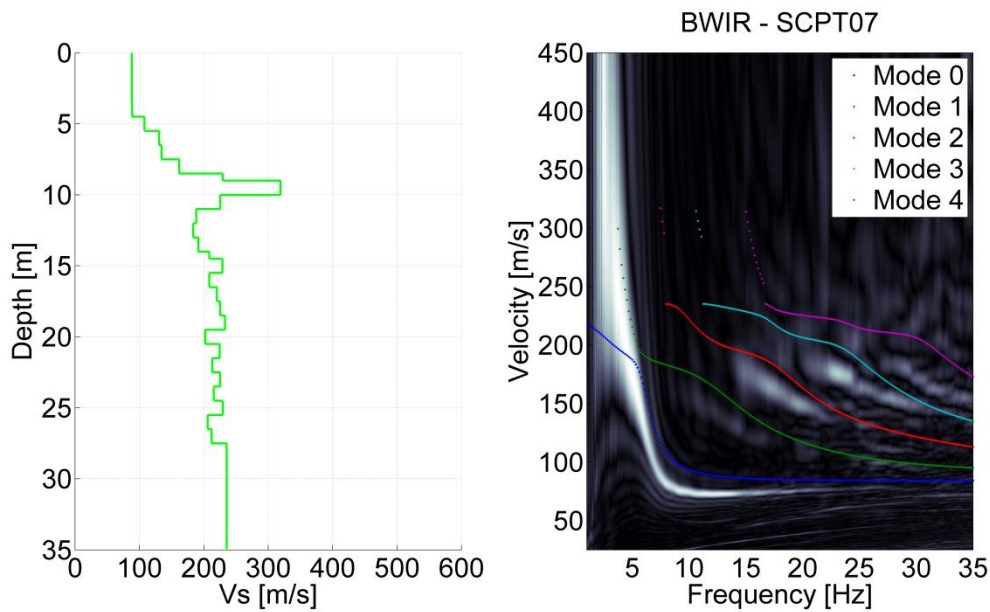


Figure 4.190 Comparison for BWIR of SCPT07 and MASW result. Left:  $V_s$  profile from SCPT. The  $V_s$  from the top 2 layers of the SCPT is generally unreliable and replaced by the minimum  $V_s$  of the first 3 layers. Right: modelled dispersion curves of different modes based on the SCPT  $V_s$  profile in coloured lines plotted on the energy of MASW dispersion plot in greyscale.

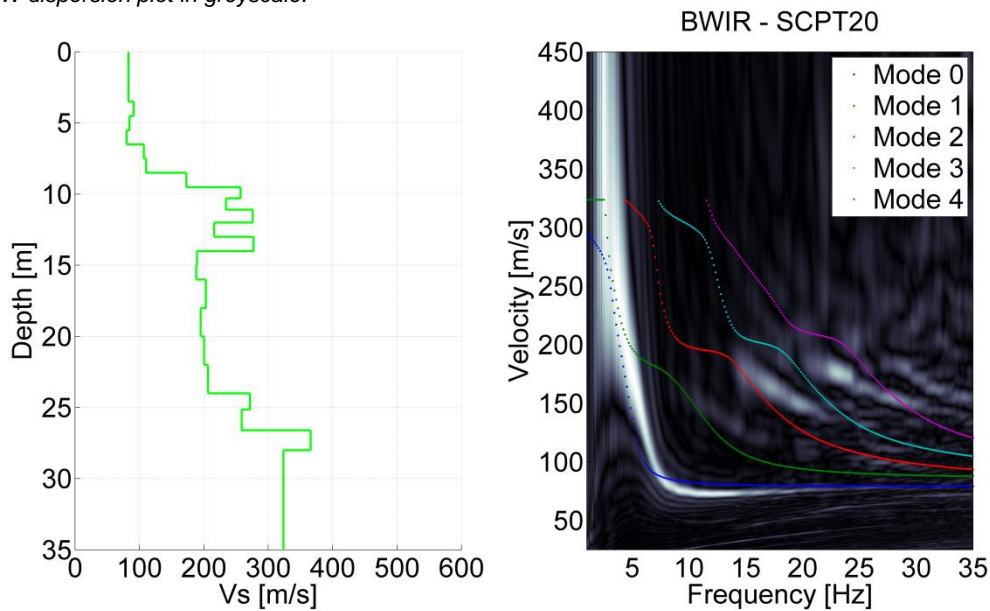


Figure 4.191 Comparison for BWIR of SCPT20 and MASW result. Left:  $V_s$  profile from SCPT. The  $V_s$  from the top 2 layers of the SCPT is generally unreliable and replaced by the minimum  $V_s$  of the first 3 layers. Right: modelled dispersion curves of different modes based on the SCPT  $V_s$  profile in coloured lines plotted on the energy of MASW dispersion plot in greyscale.

## 4.17.6 Synthesis

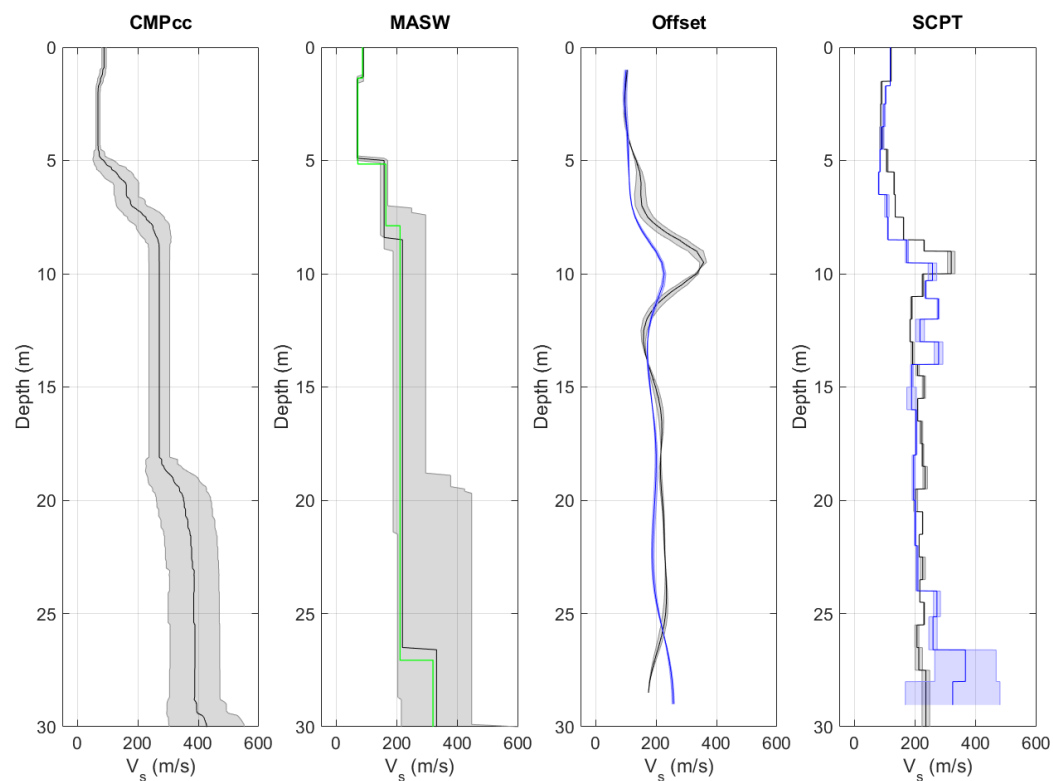


Figure 4.192  $V_s$  profiles from different measurement techniques, including uncertainty bands. From left to right: CMPcc based on active MASW array, shaded band indicates standard deviation; active MASW with manual fit in green and automatic inversion in black with grey shaded band indicating the minimum and the maximum  $V_s$ ; average profile for offset SCPTs between 1 and 5 m offset for 1 or 2 SCPTs with shaded band indicating the minimum and the maximum  $V_s$ ; SCPTs with band indicating variation between left and right blow; cross-hole average profiles for long leg in blue and short leg in grey with shaded band indicating the minimum and the maximum  $V_s$ .

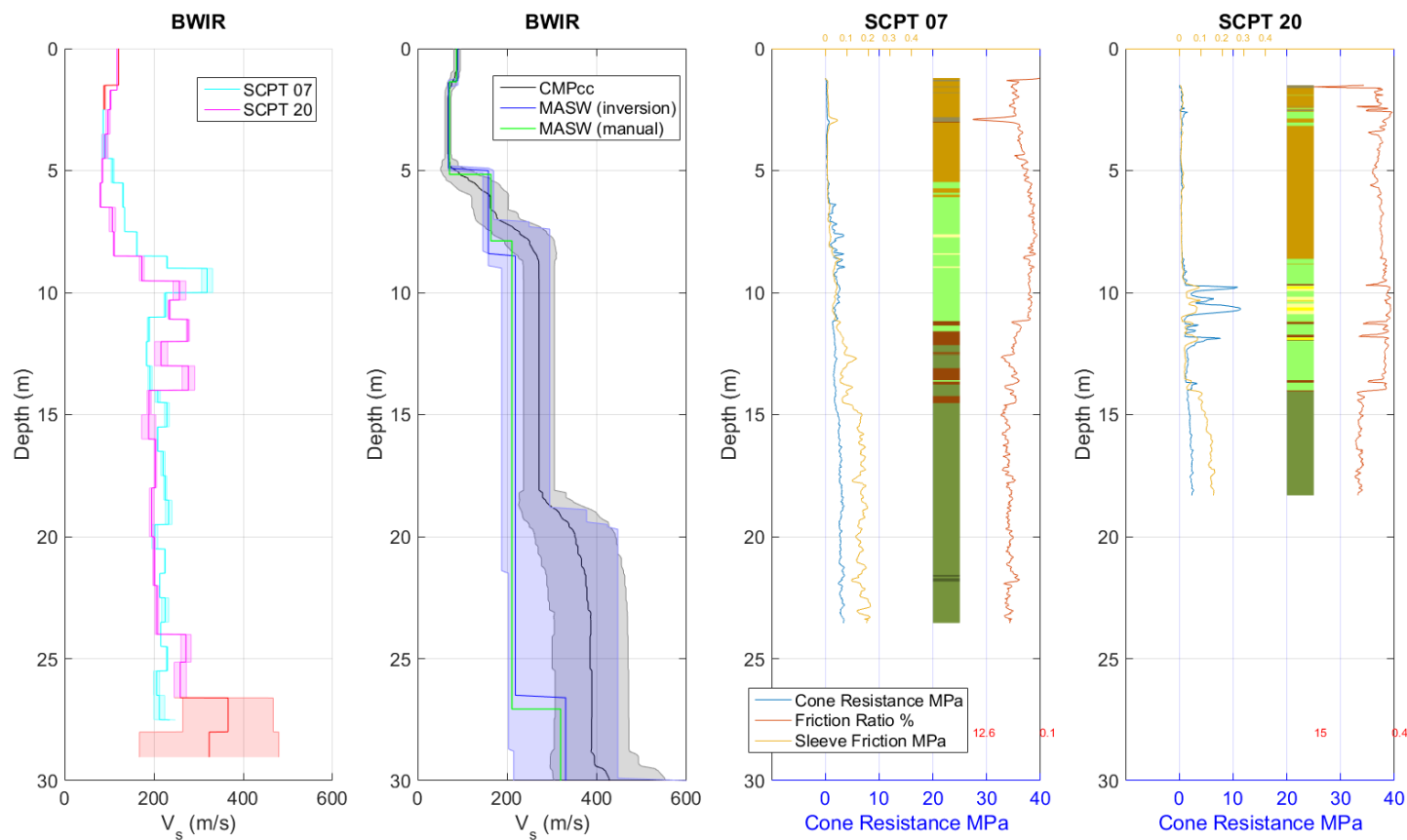


Figure 4.193 Synthesis of  $V_s$  results. Unreliable results are shown in red. From left to right: SCPT with band indicating variation between left and right blow; CMPcc, MASW and average cross-hole results with uncertainty bands; CPT with cone resistance, friction ratio, sleeve friction and automatically generated lithology (indication, for legend see Table 3.1).

## 4.18 't Zandt- BZN1

### 4.18.1 Location



Figure 4.194 Map of location BZN1, showing the KNMI accelerograph station, SCPT location and MASW survey lines and shot locations.

### 4.18.2 Geological setting

The location is situated in a non-erosive area. The Pleistocene is covered with Holocene deposits consisting mostly of sand that is part of an erosive system but at the base older clay and the basal peat has remained untouched. Thickness of the Holocene is up to approximately 12 metres. The location is situated outside the Peelo valleys.

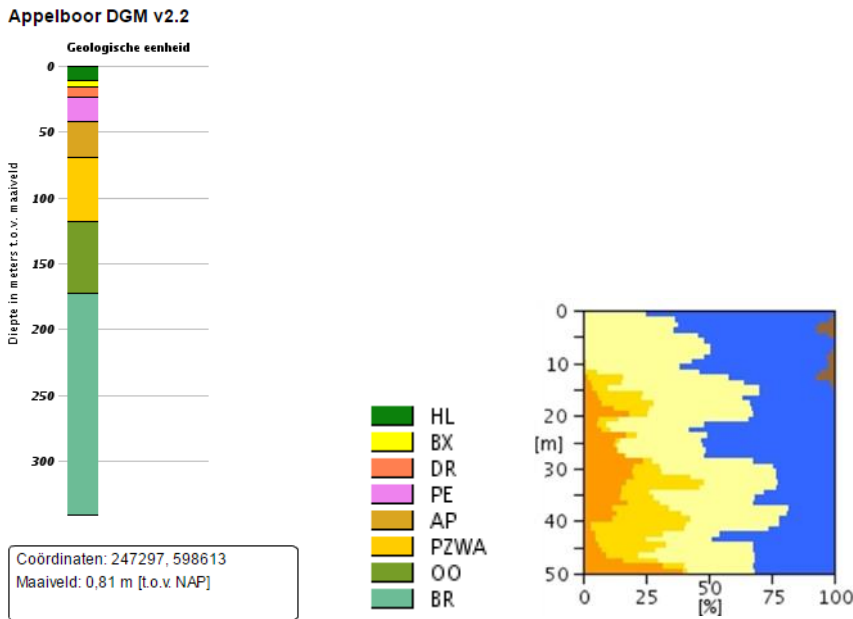


Figure 4.195 Geological information at station BZN1. Left: 1D section from the DGM model. Right: Section from the “delfstoffen online” model (GDN-TNO). Colour coding: brown = peat, blue = clay, yellow to orange = fine sand to coarse sand. The horizontal scale shows the volume percentage of each of the lithologies present at the location, the vertical scale is depth below the surface.

Table 4.18 Descriptions of representative deep boreholes near station BZN1 from the DINO database ([www.dinoloket.nl](http://www.dinoloket.nl)).

<b>Drilling</b>	<b>Distance from drilling</b>	<b>top</b>	<b>bottom</b>	<b>sediment type</b>	<b>Min. grain size</b>	<b>Max. grain size</b>	<b>Formation</b>	
B07E0047	700mtr NE	1,30	-3,30	Clay			Formation of Naaldwijk	
		-3,30	-6,90	Sand	Extreme fine		Formation of Naaldwijk	
		-6,90	-9,50	Clay			Formation of Naaldwijk	
		-9,50	-10,00	Peat			Formation of Nieuwkoop	
		-10,00	-14,90	Sand	Medium fine	Very coarse	Formation of Boxtel	
		-14,90	-16,70	Clay			Formation of Peelo	
		-16,70	-40,70	Sand	Medium fine	Medium coarse	Formation of Peelo	
		-40,70	-55,70	Sand	Very coarse	Extreme coarse	Formation of Appelscha	
		-55,70	-63,70	Sand	Very coarse	Extreme coarse	Formation of Appelscha	
B07E1146	2000mtr NE Just for the lower part	-63,70	-84,70	Sand	Medium fine	Medium coarse	Formation of Peize	
		-84,70	-93,70	Sand	Medium fine	Medium coarse	Formation of Peize	
		-93,70	-100,00	Sand	Medium fine	Medium coarse	Formation of Peize	

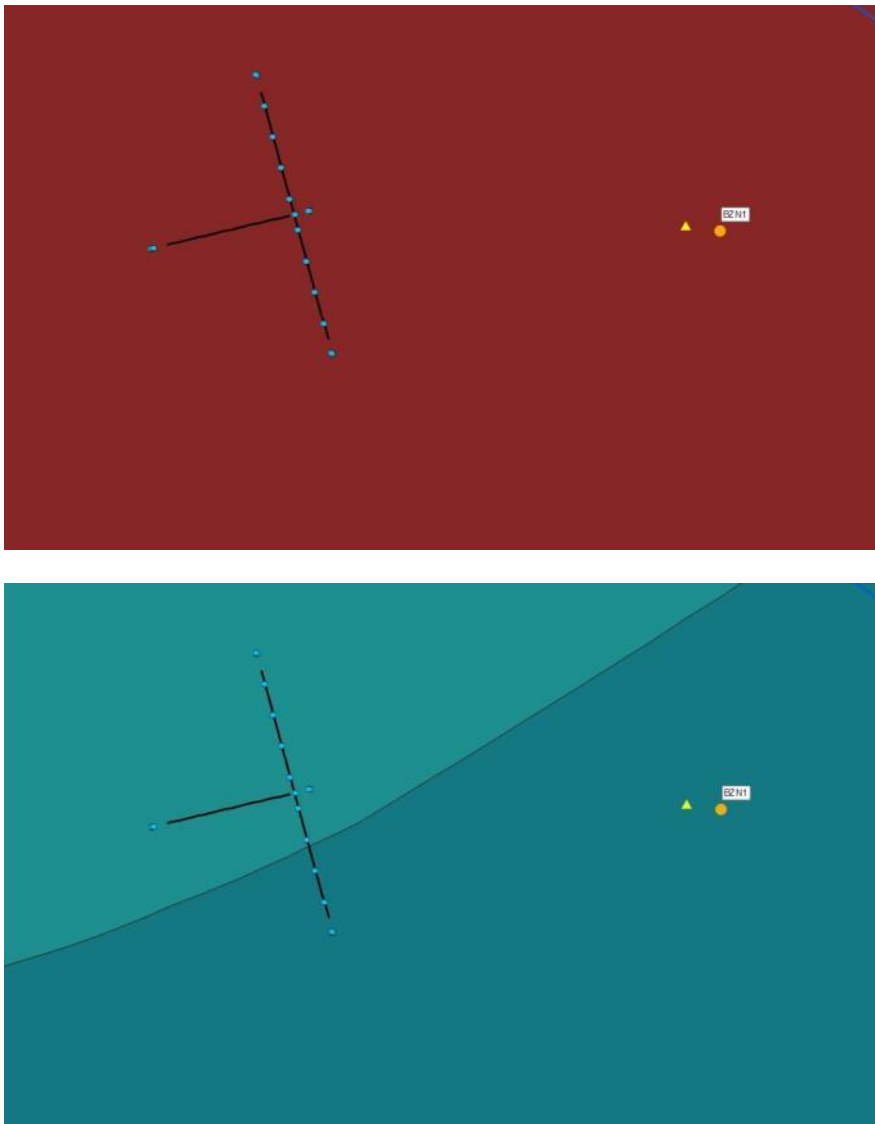


Figure 4.196 Overview map of geological setting based on beta version of GeoTOP model. Top panel: Thickness of the Peelo Formation, blue colour indicates thick Peelo layer, hence in the centre of the channel; red and orange colour indicates thin Peelo layers, hence areas outside the channel; yellow indicates transition zone. Lower panel: Top of Pleistocene surface relative to Dutch Ordnance Datum NAP.

## 4.18.3 SCPT

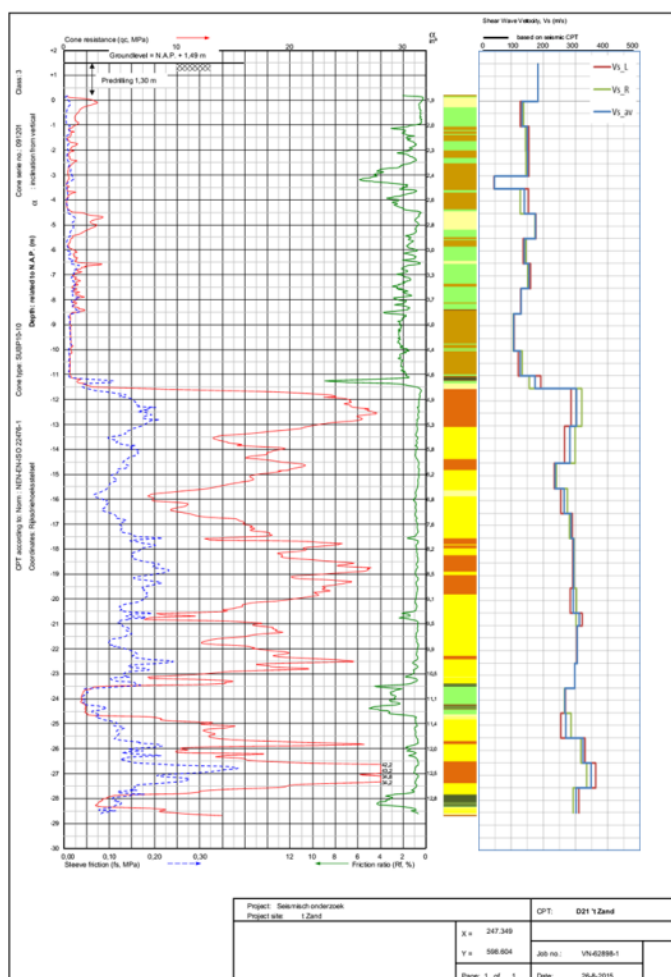


Figure 4.197 SCPT21. From left to right: CPT measurement, showing tip resistance, sleeve friction and friction ratio; automatically generated lithology (indication, for legend see Table 3.1);  $V_s$  profile (red = left blow, green = right blow, blue = average).

## 4.18.4 OSCPT

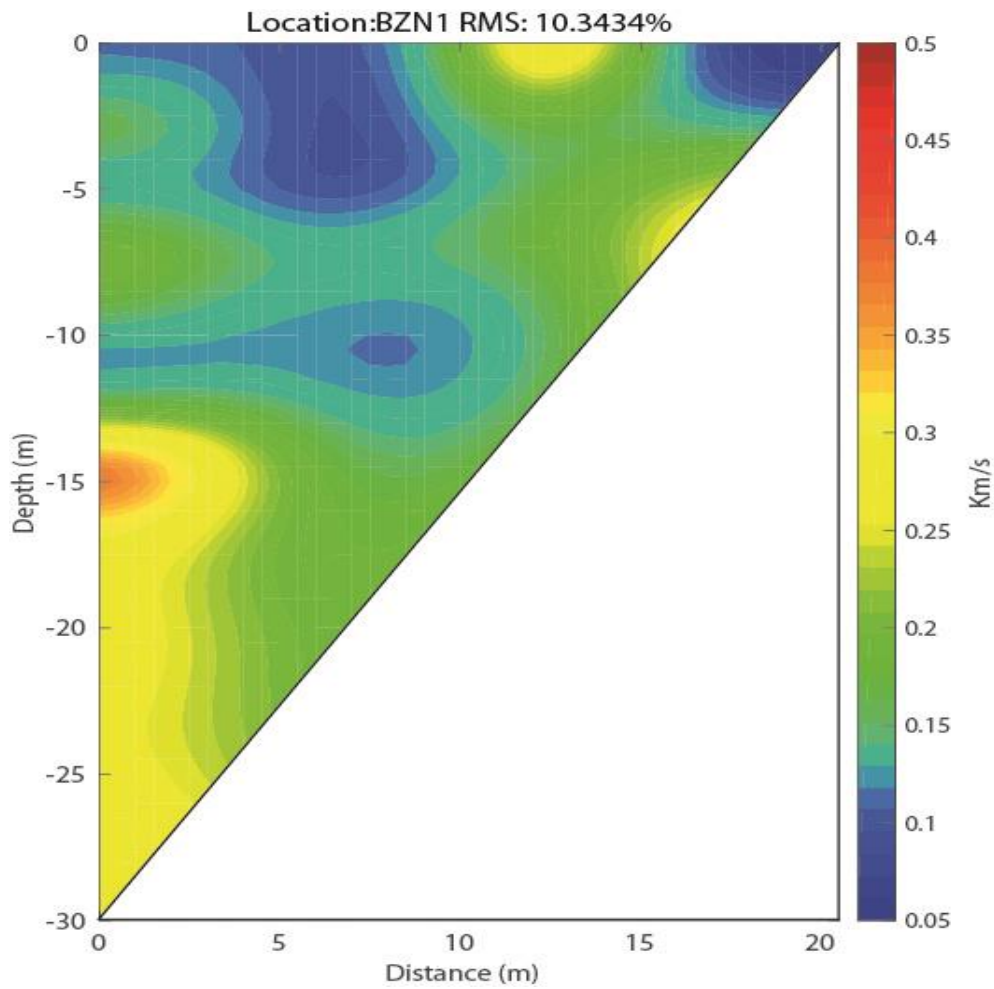


Figure 4.198 Tomographic images based on OSCPT result from SCPT for station BZN1 (SCPT21).

## 4.18.5 MASW

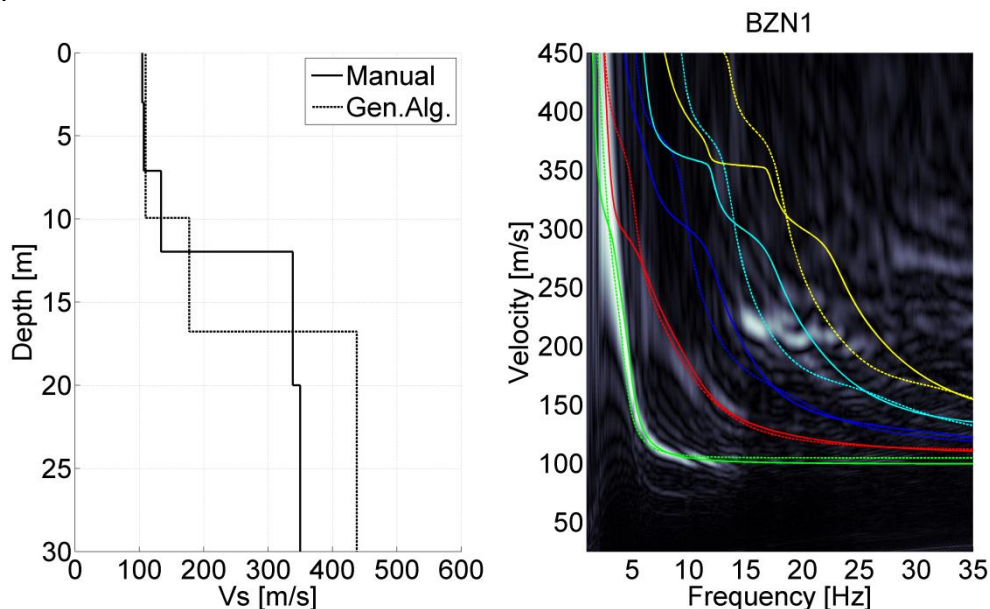


Figure 4.199 MASW result for station BZN1. Left panel:  $V_s$  profiles from active MASW. Solid line from manual fitting of dispersion curves; dashed line for automatic inversion. Right panel: energy in the dispersion plot in greyscale; solid lines are the modelled dispersion curves for different modes of the manually fitted  $V_s$  profile; dashed lines for the different modes of the automatically inverted  $V_s$  profile.

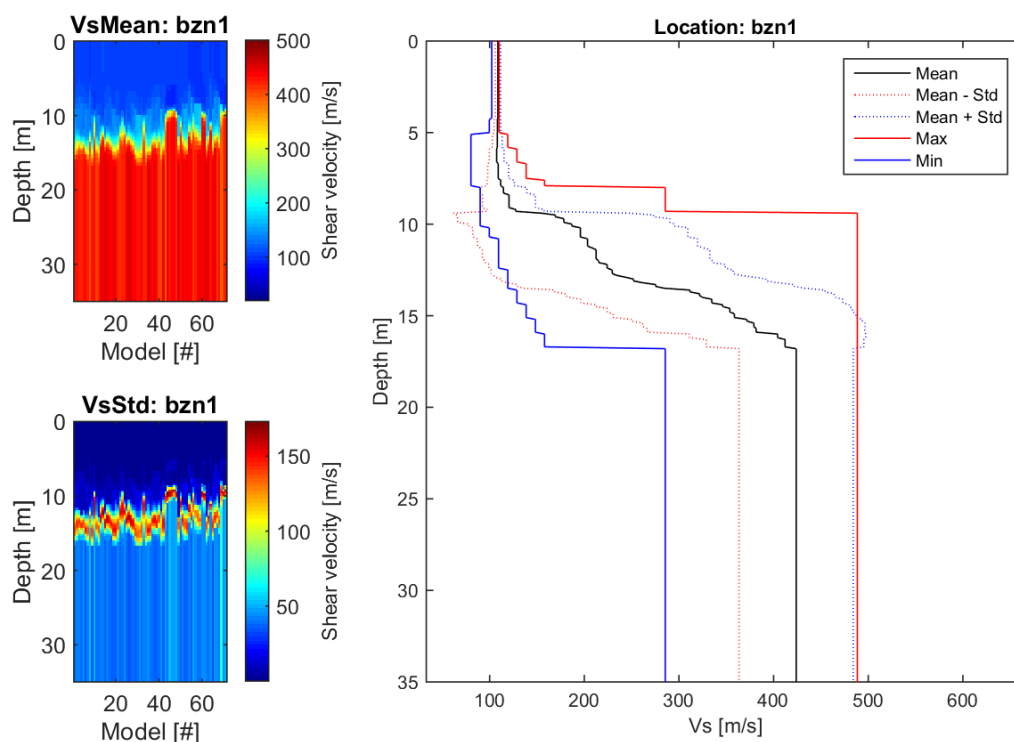


Figure 4.200 CMPcc result for BZN1. Top left: average  $V_s$  along the CMPcc array. Bottom left: standard deviation of  $V_s$  along the CMPcc array. Right: best fit curve of the 72 models with the maximum and minimum value observed in the whole CMPcc and the standard deviation from all models.

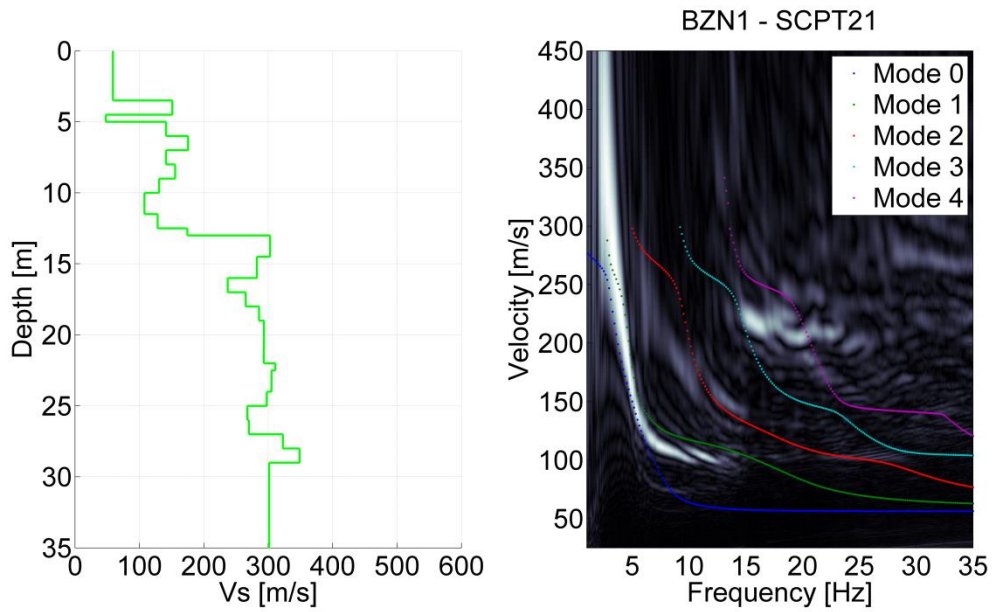


Figure 4.201 Comparison for BZN1 of SCPT21 and MASW result. Left:  $V_s$  profile from SCPT. The  $V_s$  from the top 2 layers of the SCPT is generally unreliable and replaced by the minimum  $V_s$  of the first 3 layers. Right: modelled dispersion curves of different modes based on the SCPT  $V_s$  profile in coloured lines plotted on the energy of MASW dispersion plot in greyscale.

## 4.18.6 Synthesis

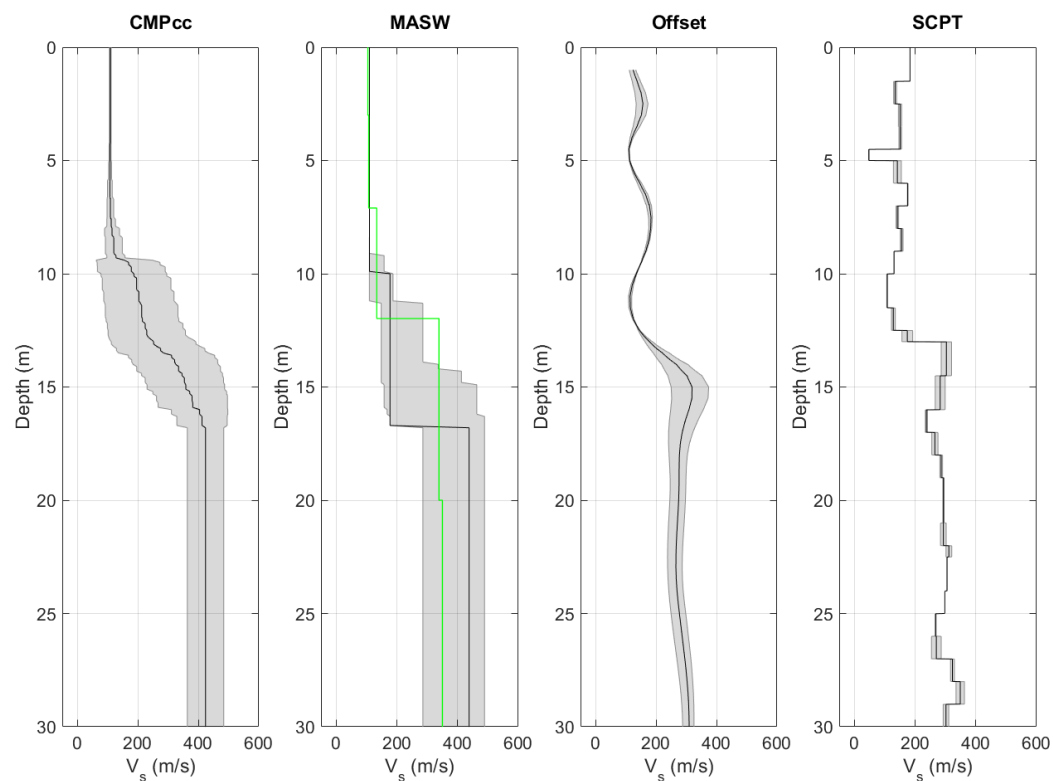


Figure 4.202  $V_s$  profiles from different measurement techniques, including uncertainty bands. From left to right: CMPcc based on active MASW array, shaded band indicates standard deviation; active MASW with manual fit in green and automatic inversion in black with grey shaded band indicating the minimum and the maximum  $V_s$ ; average profile for offset SCPTs between 1 and 5 m offset for 1 or 2 SCPTs with shaded band indicating the minimum and the maximum  $V_s$ ; SCPTs with band indicating variation between left and right blow; cross-hole average profiles for long leg in blue and short leg in grey with shaded band indicating the minimum and the maximum  $V_s$ .

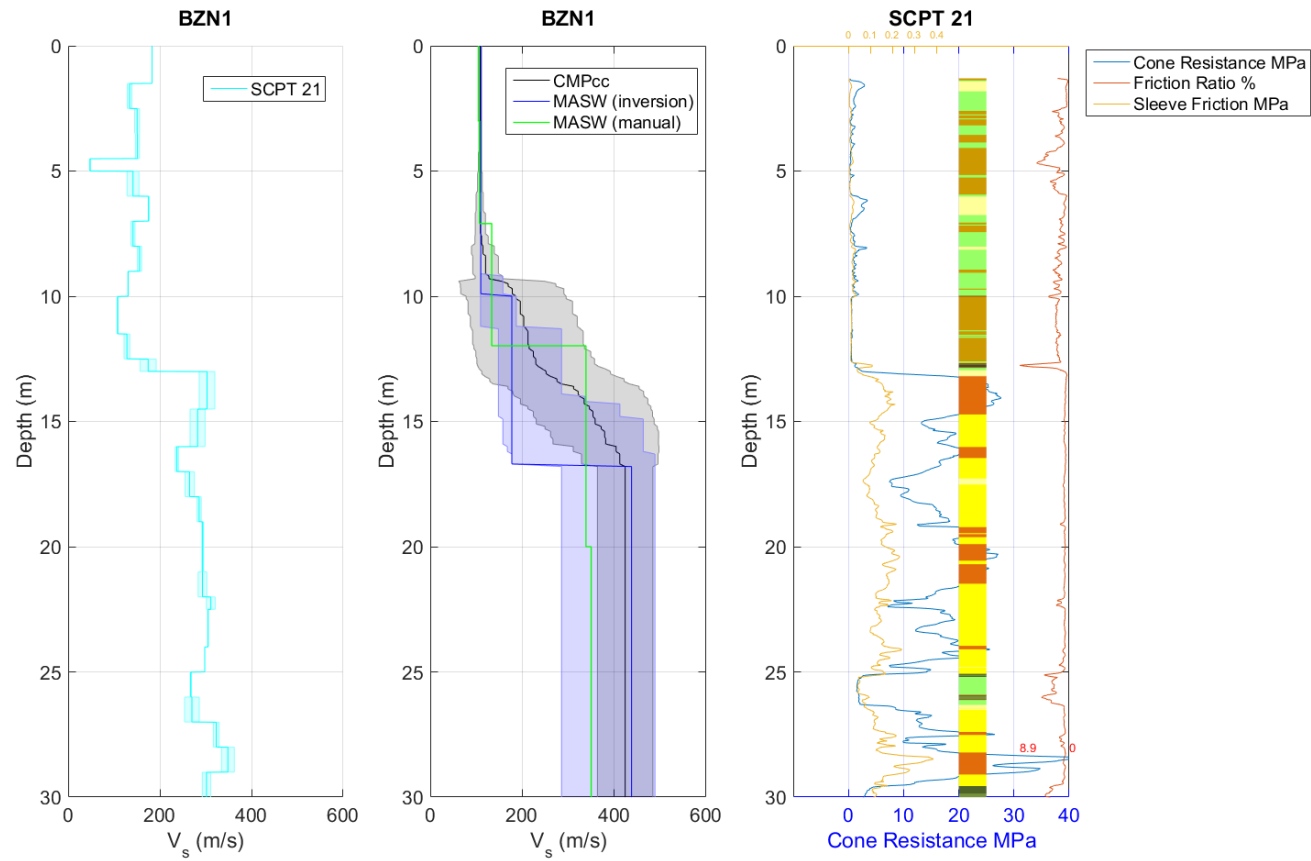


Figure 4.203 Synthesis of  $V_s$  results. Unreliable results are shown in red. From left to right: SCPT with band indicating variation between left and right blow; CMPcc, MASW and average cross-hole results with uncertainty bands; CPT with cone resistance, friction ratio, sleeve friction and automatically generated lithology (indication, for legend see Table 3.1).

## 4.19 Zeerijp- BZN2

### 4.19.1 Location

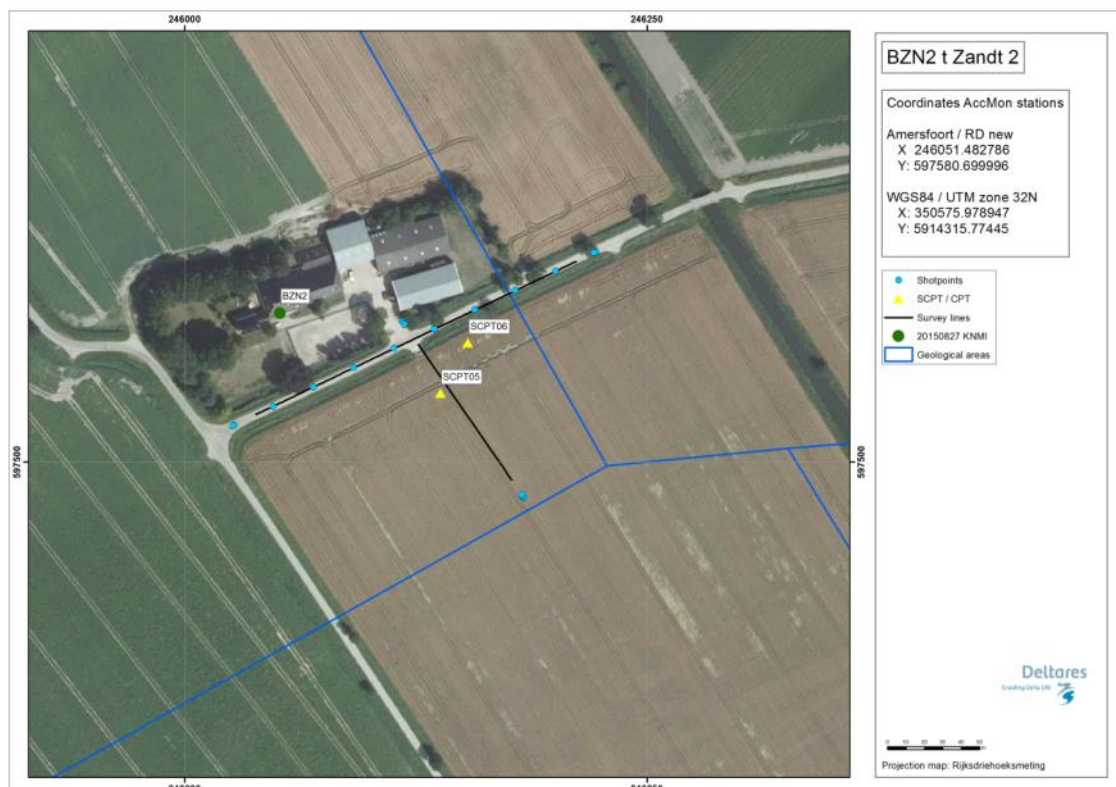


Figure 4.204 Map of location BZN2, showing the KNMI accelerograph station, SCPT location and MASW survey lines and shot locations.

### 4.19.2 Geological setting

The location is situated in a non-erosive area bordering an erosive valley in the West The Pleistocene is covered with Holocene deposits consisting mostly of sand that is part of an erosive system but at the base older clay and basic peat has remained untouched. Thickness of the Holocene is up to approximately 12 metres. The location is situated outside the Peelo valleys.

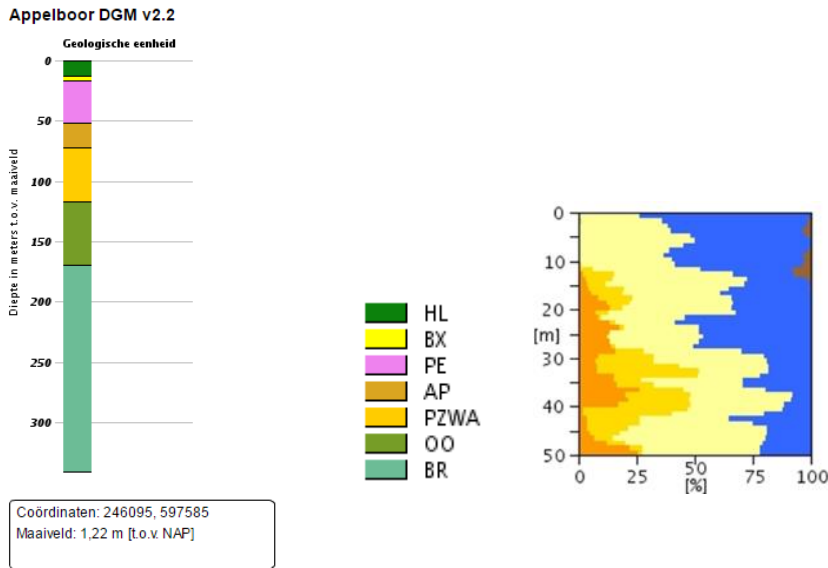


Figure 4.205 Geological information at station BZN2. Left: 1D section from the DGM model. Right: Section from the “delfstoffen online” model (GDN-TNO). Colour coding: brown = peat, blue = clay, yellow to orange = fine sand to coarse sand. The horizontal scale shows the volume percentage of each of the lithologies present at the location, the vertical scale is depth below the surface.

Table 4.19 Descriptions of representative deep boreholes near station BZN2 from the DINO database ([www.dinoloket.nl](http://www.dinoloket.nl)).

Drilling	Distance from drilling	top	bottom	sediment type	Min. grain size	Max. grain size	Formation
B07E0046	1300mtr SE	0,80	-2,00	Clay			Formation of Naaldwijk
		-2,00	-2,40	Peat			Formation of Nieuwkoop
		-2,40	-3,70	Clay			Formation of Naaldwijk
		-3,70	-6,20	Sand	Extreme fine		Formation of Naaldwijk
		-6,20	-11,65	Clay			Formation of Naaldwijk
		-11,65	-15,20	Sand	Medium fine	Medium coarse	Formation of Boxtel
		-15,20	-22,20	Sand	Medium coarse	Extreme coarse	Formation of Drente
		-22,20	-26,90	Clay			Formation of Peelo
		-26,90	-35,20	Sand	Medium fine	Extreme coarse	Formation of Peelo
		-35,20	-53,20	Sand	Medium coarse	Extreme coarse	Formation of Peelo/Appelscha

1210624-000-BGS-0007, Version 2, 27 June 2016, final

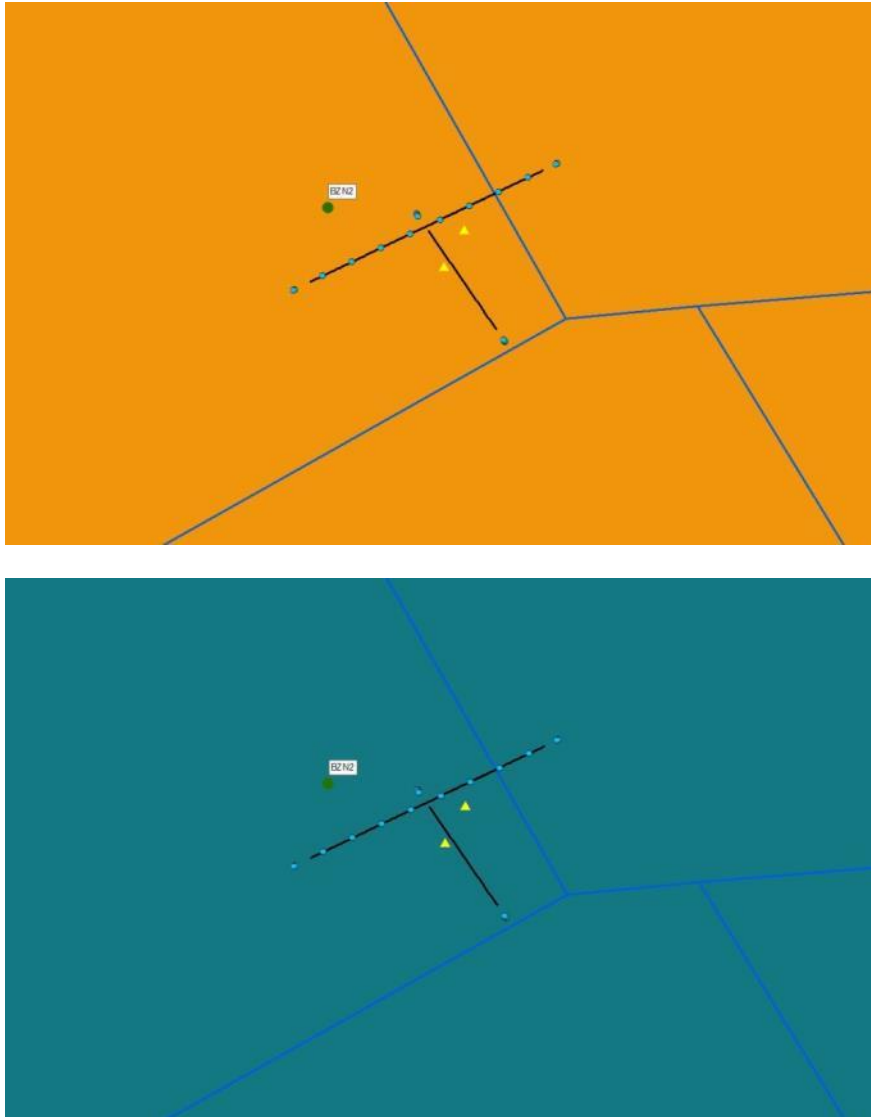


Figure 4.206 Overview map of geological setting based on beta version of GeoTOP model. Top panel: Thickness of the Peelo Formation, blue colour indicates thick Peelo layer, hence in the centre of the channel; red and orange colour indicates thin Peelo layers, hence areas outside the channel; yellow indicates transition zone. Lower panel: Top of Pleistocene surface relative to Dutch Ordnance Datum NAP.

## 4.19.3 SCPT

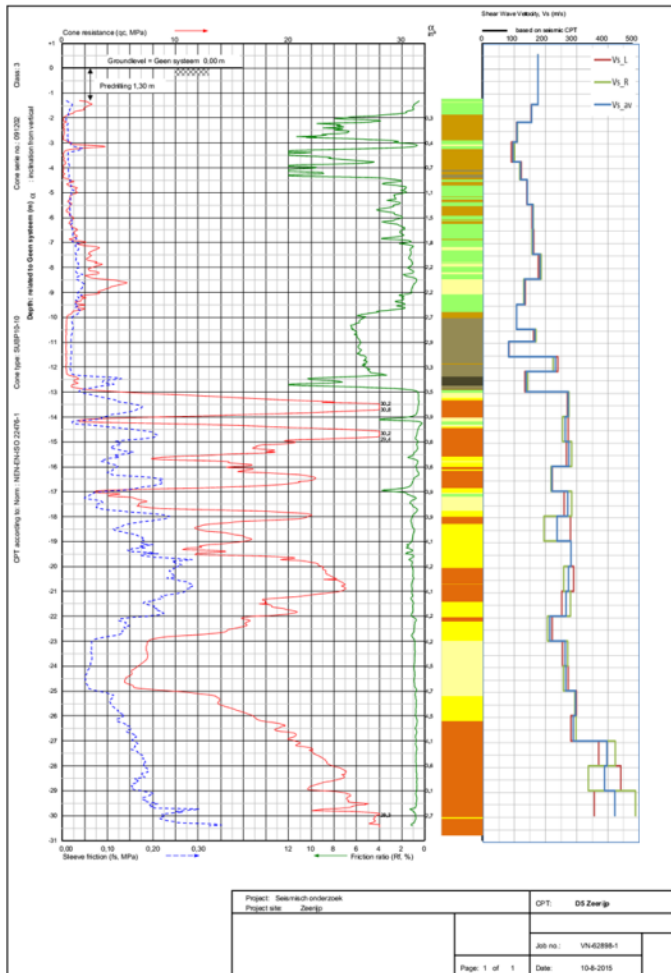


Figure 4.207 SCPT05. From left to right: CPT measurement, showing tip resistance, sleeve friction and friction ratio; automatically generated lithology (indication, for legend see Table 3.1);  $V_s$  profile (red = left blow, green = right blow, blue = average).

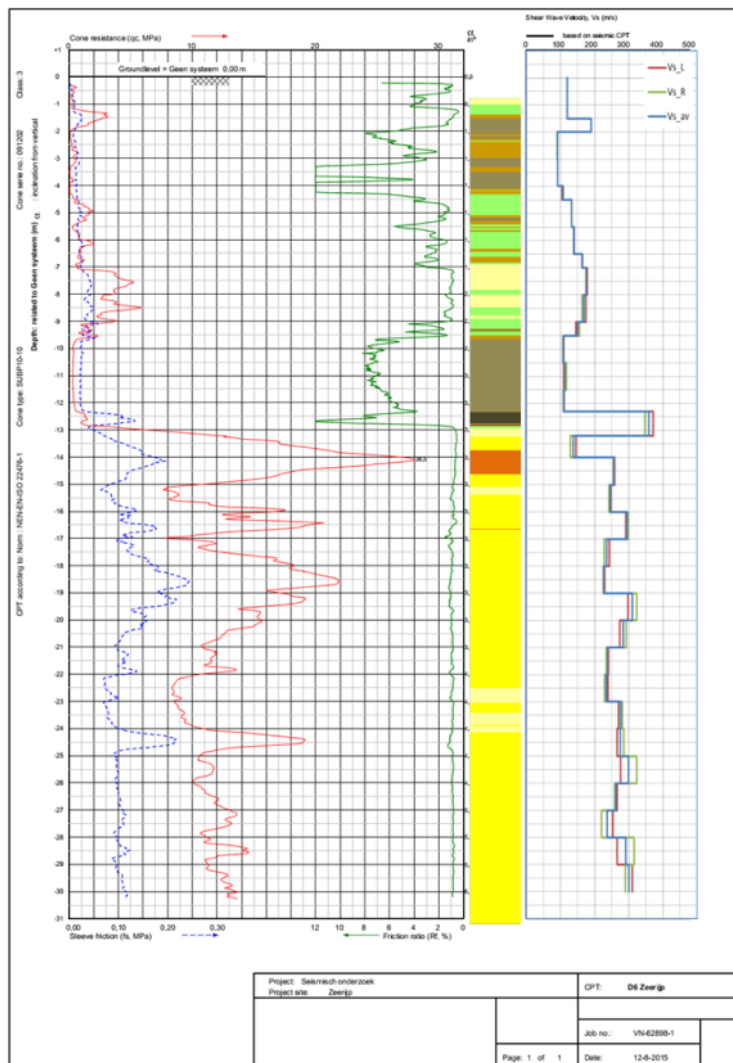


Figure 4.208 SCPT06. From left to right: CPT measurement, showing tip resistance, sleeve friction and friction ratio; automatically generated lithology (indication, for legend see Table 3.1);  $V_s$  profile (red = left blow, green = right blow, blue = average).

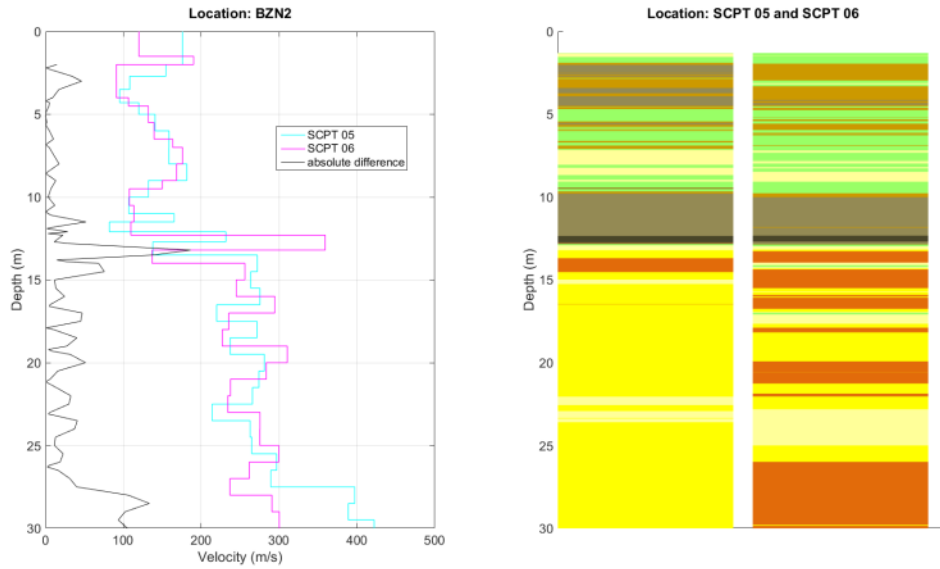


Figure 4.209 Station BZN2. Left: Difference between the two SCPTs measured at the same station location. Right: automatically generated lithology (indication).

## 4.19.4 OSCPT

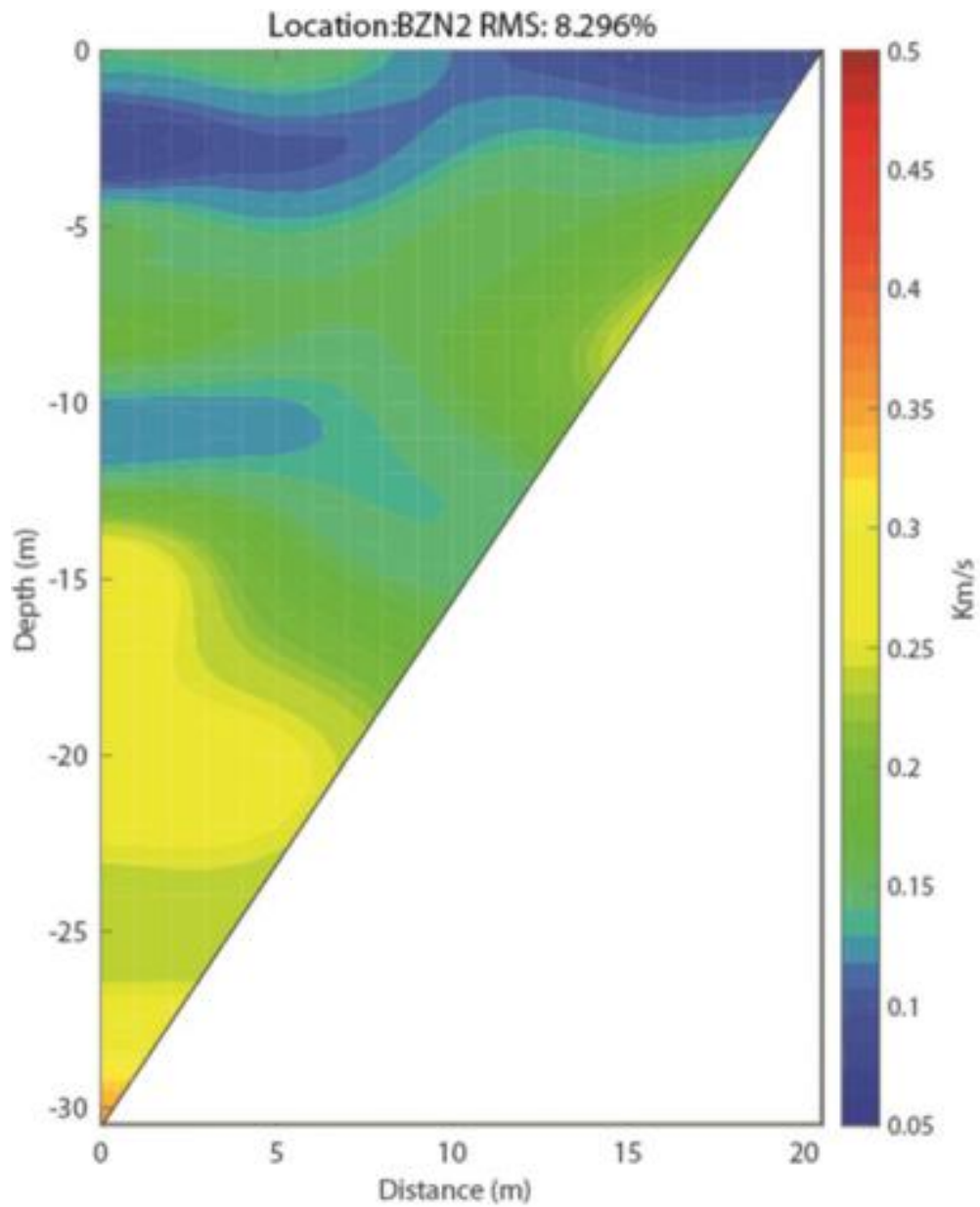


Figure 4.210 Tomographic images based on OSCPT result from SCPT for station BZN2 (SCPT05).

## 4.19.5 MASW

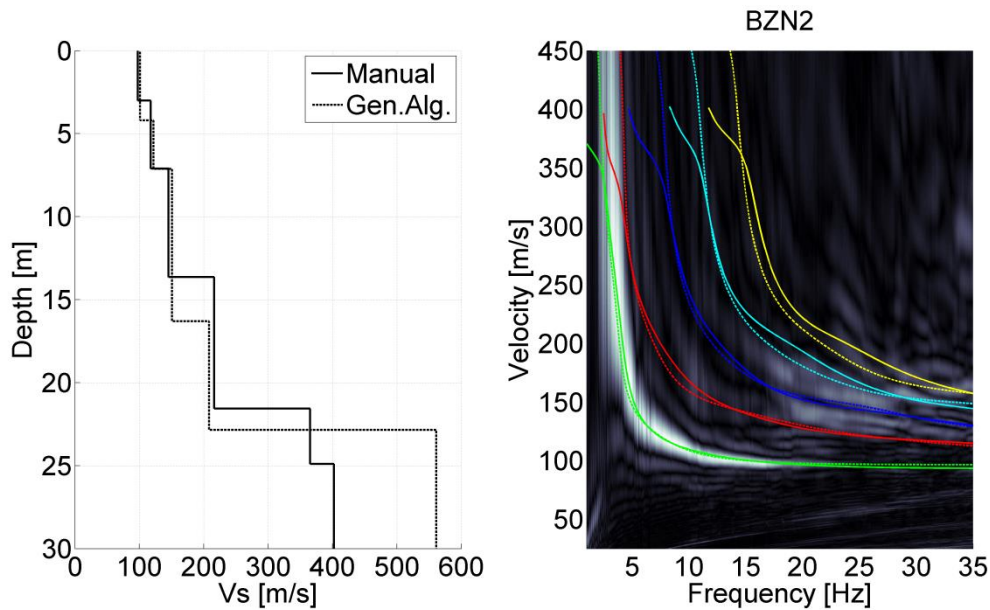


Figure 4.211 MASW result for station BZN2. Left panel:  $V_s$  profiles from active MASW. Solid line from manual fitting of dispersion curves; dashed line for automatic inversion. Right panel: energy in the dispersion plot in greyscale; solid lines are the modelled dispersion curves for different modes of the manually fitted  $V_s$  profile; dashed lines for the different modes of the automatically inverted  $V_s$  profile.

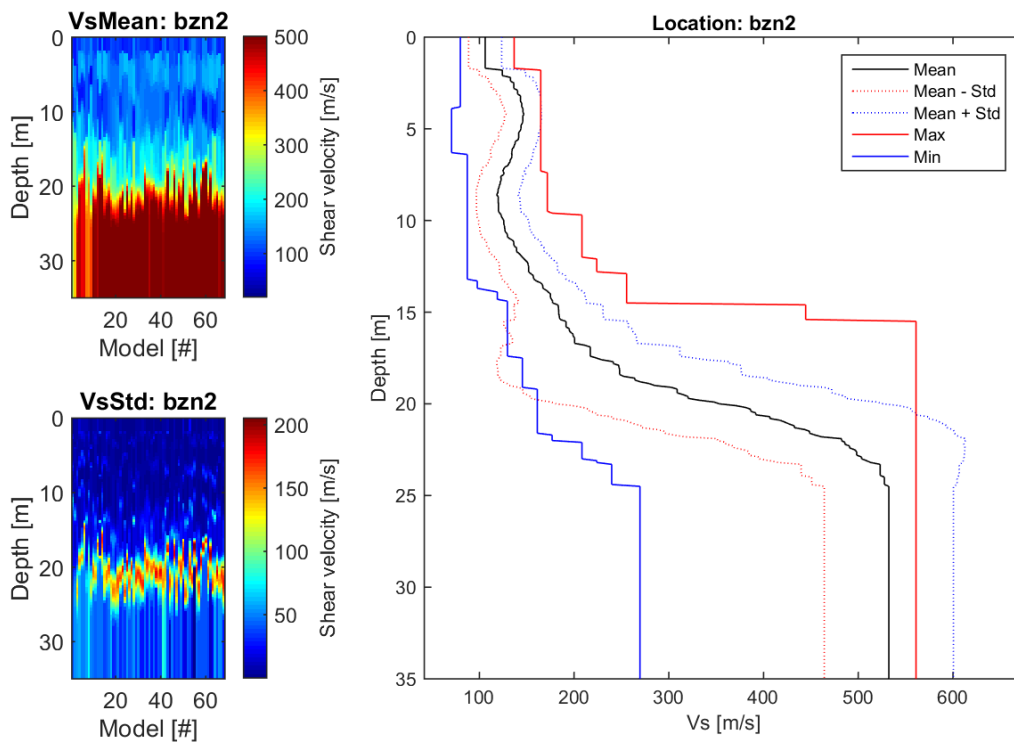


Figure 4.212 CMPcc result for BZN2. Top left: average  $V_s$  along the CMPcc array. Bottom left: standard deviation of  $V_s$  along the CMPcc array. Right: best fit curve of the 72 models with the maximum and minimum value observed in the whole CMPcc and the standard deviation from all models.

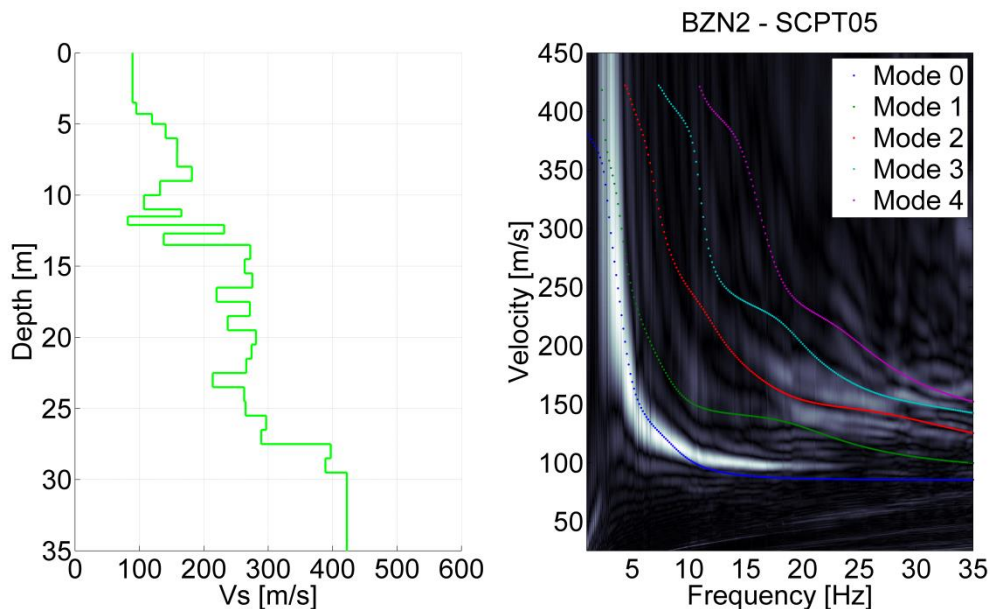


Figure 4.213 Comparison for BZN2 of SCPT05 and MASW result. Left:  $V_s$  profile from SCPT. The  $V_s$  from the top 2 layers of the SCPT is generally unreliable and replaced by the minimum  $V_s$  of the first 3 layers. Right: modelled dispersion curves of different modes based on the SCPT  $V_s$  profile in coloured lines plotted on the energy of MASW dispersion plot in greyscale.

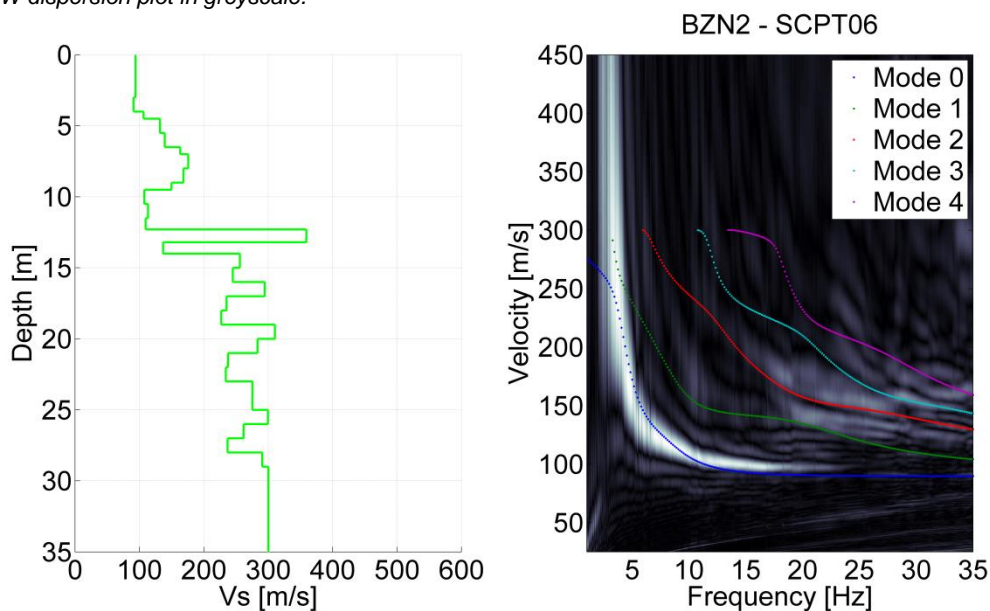


Figure 4.214 Comparison for BZN2 of SCPT06 and MASW result. Left:  $V_s$  profile from SCPT. The  $V_s$  from the top 2 layers of the SCPT is generally unreliable and replaced by the minimum  $V_s$  of the first 3 layers. Right: modelled dispersion curves of different modes based on the SCPT  $V_s$  profile in coloured lines plotted on the energy of MASW dispersion plot in greyscale.



## 4.19.6 Synthesis

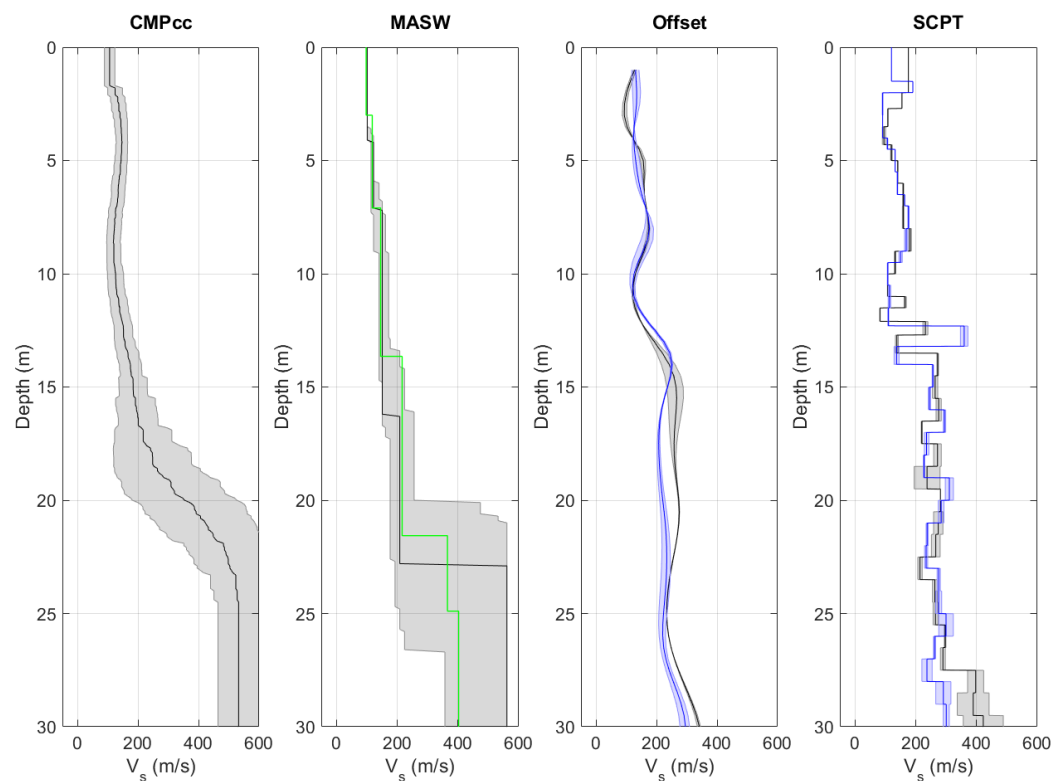


Figure 4.215  $V_s$  profiles from different measurement techniques, including uncertainty bands. From left to right: CMPcc based on active MASW array, shaded band indicates standard deviation; active MASW with manual fit in green and automatic inversion in black with grey shaded band indicating the minimum and the maximum  $V_s$ ; average profile for offset SCPTs between 1 and 5 m offset for 1 or 2 SCPTs with shaded band indicating the minimum and the maximum  $V_s$ ; SCPTs with band indicating variation between left and right blow; cross-hole average profiles for long leg in blue and short leg in grey with shaded band indicating the minimum and the maximum  $V_s$ .

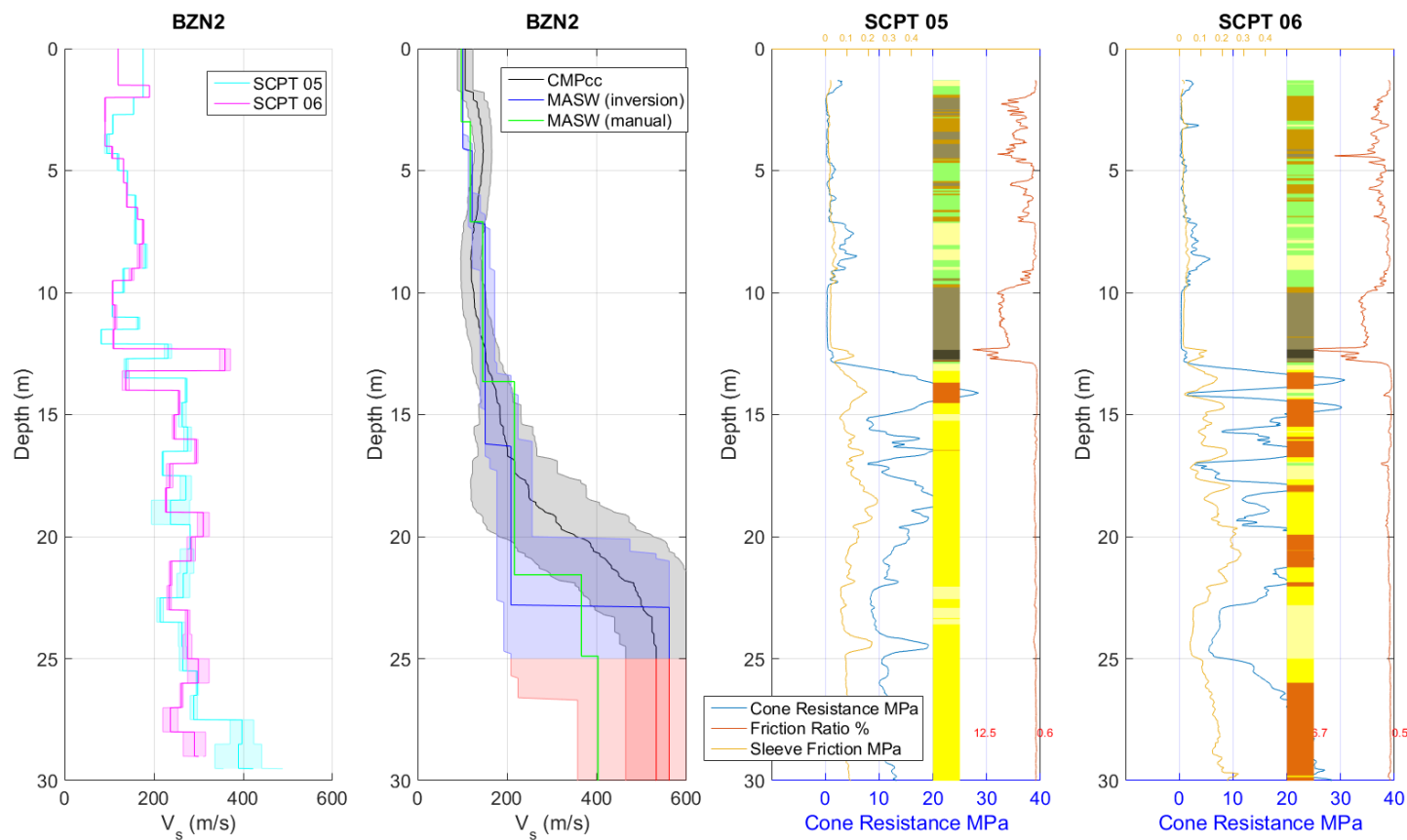


Figure 4.216 Synthesis of  $V_s$  results. Unreliable results are shown in red. From left to right: SCPT with band indicating variation between left and right blow; CMPcc, MASW and average cross-hole results with uncertainty bands; CPT with cone resistance, friction ratio, sleeve friction and automatically generated lithology (indication, for legend see Table 3.1).

## 5 Final $V_S$ profiles from the measurements

### 5.1 General observations

The results of all methods at the station location are presented in chapter 4. In general, the  $V_S$  profiles from all measurement methods show excellent agreement at all locations. As expected, differences between the interpreted profiles of the surface and penetrometer/borehole techniques become apparent with increasing depth. On average, an excellent agreement is found to a depth of 20 m. Below this depth, the uncertainty of the surface techniques increases, resulting in an increase of differences between the  $V_S$  profiles of the various techniques. From the processing and interpretation and the synthesis plots, several general observations are made. These are listed below.

#### **SCPT**

The SCPTs give detailed, but very local profiles of  $V_S$ . At some locations only one SCPT was measured. At other locations, two SCPTs were measured. In the latter case, the  $V_S$  profiles are generally comparable, but there are differences in the details. Certain layers are present in one and absent in the other SCPT. Additionally, layers might be present at both locations, but at different depths and with different thicknesses. These variations are linked to the heterogeneity of the subsurface and can even be visible within short spatial scales, such as in the example of the trajectory of 6 CPTs at location BFB2 (section 4.5.3) and the two SCPTs at location BOWW (section 4.14.3).

The data quality in the top layers of the SCPT measurement also varies. In some cases, the shear wave is difficult to pick, because of interference between direct and refracted waves. This generally results in overestimation of  $V_S$  in the top layers. As a result, the  $V_S$  values in the top meters (max 3.4 m in this data set) are unreliable in 6 of the 27 SCPTs. This is indicated by the red part of the profiles in the synthesis sections.

#### **MASW**

Values of  $V_S$  and layer thickness of the top layer are very well constrained by the active MASW technique. The data resolution and accuracy rapidly decreases with depth. Depending on the local geological setting and the  $V_S$  present, the  $V_S$  profile cannot always be well constrained over the full 30 m depth range. This is indicated by the red part of the profiles in the synthesis sections.

#### **SCPT and MASW combination**

To compare the SCPT and MASW methods, the dispersion curve belonging to the SCPT  $V_S$  profile was determined and plotted on the MASW dispersion map. The SCPT dispersion curve generally did not match the MASW dispersion map well. The top part of the SCPT  $V_S$ , as indicated above, might not be reliable. Therefore, we replaced the top part of the SCPT  $V_S$  profile by a more realistic estimate. This considerably improved the fit between the SCPT dispersion curve and the MASW dispersion map, shown in the last plot of the MASW sections in chapter 4.

The analysis shows that both methods are complementary. Although the resolution of the MASW decreases rapidly with depth, it does constrain the top most layers very well. On the

other hand, the SCPT has poor accuracy for the top part of the profile. In principle, the combined use leads to a more reliable final  $V_S$  profile.

### **Subsurface heterogeneity**

Both the cross-hole tomography and the OSCPT provide information on the level of heterogeneity at the station locations. The OSCPT tomographic images give insight in the amount of heterogeneity near the classic SCPT measurement. In the current data set, there are examples of quite homogeneous  $V_S$  distributions (e.g. for BGAR, SCPT 11, Figure 4.66) and examples of highly heterogeneous  $V_S$  distributions (e.g. BWIN, SCPT23, Figure 4.174 or BAPP, SCPT01 and SCPT02, Figure 4.4 and Figure 4.5). In the heterogeneous case, the SCPT would look very different if the position was chosen e.g. 10 m away. The fact that a classic SCPT is very local representation of  $V_S$  should always be kept in mind.

Although the cross-hole method involves a large logistical effort, it does provide the most detailed information on the lateral variation on a scale equal to the typical size of a building. The cross-hole tomographic images at station locations BAPP, BUHZ and BWSE show various levels of heterogeneity. The tomogram of BUHZ (Figure 4.28) shows relatively homogeneous  $V_S$  layers. The bottom layer, however, is dipping. The tomogram of BWSE (Figure 4.44) shows the clear transition between Holocene (low  $V_S$ ) and Pleistocene (high  $V_S$ ) deposits at 9 to 10 m depth. There are, however, patches of relatively high and low  $V_S$  in the Pleistocene part of the cross section. Additionally, the low  $V_S$  zone in the top is dipping. The tomogram of BAPP (Figure 4.13) shows a large amount of lateral heterogeneity. An SCPT at e.g. 13 m distance between borehole B007 and B009 would look very different from one at 24 m, even though they are only ~ 10 m apart.

The cross-hole tomography did not only result in tomograms for  $V_S$  but also for  $V_P$ . This enables a direct measure of how well these two velocities can be translated to one another. From the three pilot locations we observe that both velocity tomograms have very distinct structures. Therefore, at least for this depth range, converting  $V_P$  profiles to  $V_S$  profiles is not trivial. Part of the  $V_S$  model of GMPE V3 (Bommer et al., 2016) is based on the conversion from  $V_P$  to  $V_S$  using a depth dependent factor. Although this factor has applied to the deeper parts (>70m), the cross-hole observations (0-30 m) suggest that this conversion might need more attention.

### **Smoothing of spatial data**

To compare the OSCPT and the cross-hole tomographic results with the other results in the plots of the synthesis sections, an average  $V_S$  profile was determined. This process resulted in loss of information on the lateral variation and the curves are inevitably smoothed. Generally, the average OSCPT  $V_S$  curve follows the same trends as the SCPT  $V_S$  profile, but with a lot less detail.

A degree of smoothing also occurs in the representation of the CMPcc results. All 72 individual CMPcc curves are averaged into one overall profile with an uncertainty band. This final CMPcc profile shows no discrete steps and varies very smoothly with depth.

## **5.2 Selection of final $V_S$ profile**

The original objective was to construct a representative  $V_S$  profile for each station that was a weighted average of the  $V_S$  results for all methods. The weighting would take into account the DOI, level of resolution and sampling volume of the various techniques. However, during the discussion meeting of experts held at Deltares in January 2016, the objective was revised for

pragmatic reasons. It was decided that the final  $V_S$  profile would consist of the  $V_S$  from the SCPT positioned closest to the station. The discussion on how valuable information of sampling volumes and spatial representativeness of the various techniques should be included is still pending.

For the **original objective**, i.e. a representative  $V_S$  profile from a weighted average of the  $V_S$  results for all methods, the following considerations were made:

- SCPT measurements are included over the entire depth range. The top few meters are less reliable, due to the relative large errors in picking of arrival times in the SCPT record.
- The OSCPT curves are not used in the weighted average  $V_S$ , and were used qualitatively only to obtain an impression of spatial variation in  $V_S$  near the SCPT. This was mainly done, because the OSCPT curves generally follow the SCPT curves but with less resolution.
- The 1D average  $V_S$  profiles constructed from the 2D cross-hole long and short leg (sections on synthesis in chapter 4) are included over the entire depth range for the stations where these measurements were performed.
- The first layer of the  $V_S$  profile obtained with MASW is very well constrained, often superior to the SCPT  $V_S$  result. However, the reliable depth range does not always reach the full 30 m, due to the very low  $V_S$  observed at the locations. MASW  $V_S$  layers are only included in the weighted average in the reliable depth range.
- The CMPcc reliable depth range corresponds to the MASW range, unless the smearing of the profile (section 3.3.2) starts at a shallower depth. In that case, the onset of the smearing is taken as the maximum reliable depth for CMPcc.

The **revised** approach, i.e. use SCPT only to construct  $V_S$  profiles, was based on the following scheme:

1. Review all the measured  $V_S$  profiles at each station and reject those viewed as unreliable or unreliable below some depth. For example, the first arrival of the shear wave could not be determined for the first three measurements of SCPT01 due to bad quality data. Therefore, no reliable  $V_S$  could be determined for the first 3.4 m of the SCPT.
2. Plot the modelled dispersion curves based on the SCPT  $V_S$  profile on top of the MASW dispersion results at locations of closely spaced SCPTs, for quality control.
3. Select the SCPT profile that is closest to the recording station unless
  - a. They are two both at the same distance. In that case, the one better matching the MASW was selected.
  - b. The difference in maximum depth is large. In that case, the deeper profile could be selected even if the SCPT was located further from the station. This, however, was never the case.

There are a few exceptions to the revised approach of constructing  $V_S$  from SCPT only. When the first few SCPT measurements were unreliable, the  $V_S$  values in the top layers were replaced by the  $V_S$  from MASW. This is indicated in Table 5.1.

Generally, the maximum extent corresponds to the maximum depth of penetration of the SCPT. For two SCPTs (SCPT09 and SCPT20) the bottom part was unreliable and the maximum  $V_S$  depth is slightly less than the maximum SCPT penetration depth.

For one station, BOWW, the SCPTs were very different, both in  $V_S$  values and in composition of the subsoil, and, no clear choice could be made for the most representative SCPT. In the GMPE model step, both stations SCPT10 and SCPT12 (see Figure 5.1, red and black line) were considered; SCPT10 was selected as the most useful one by Bommer et al (2016).

The final  $V_S$  profiles to a maximum depth of 30 m below the surface are shown in Figure 5.1. The considerations and choices to arrive at these profiles are summarised in Table 5.1. These  $V_S$  profiles, based on measurements, were combined in a later stage with  $V_S$  models to provide  $V_S$  profiles over the full depth at the stations required for the GMPE (Bommer et al, 2016).

Table 5.1 Considerations for choices in selection of SCPT

Station	Name	Min depth (m)	Max depth (m)	Remark	Choice for SCPT	Reasoning
BAPP	SCPT01	3.4	30	Top unreliable, bad quality data		
BAPP	SCPT02	1.8	29.1	Top 3.6 m has bad quality data (unreliable). Top 1.8 m gives wrong $V_S$ values, between 1.8 and 3.6 good agreement with MASW	SCPT02	Characteristics of MASW better captured and closer to station
BFB2	SCPT14	0	30		SCPT14	Close to station
BFB2	SCPT15	0	25			
BGAR	SCPT11	0	30	Still good although large distance	SCPT11	
BHAR	SCPT17	0	30		SCPT17	
BHKS	SCPT09	1	21.5	SCPT stopped because of very dense sand, continue with high $V_S$	SCPT09	
BKAN	SCPT24	0	27		SCPT24	
BLOP	SCPT19	1.5	30	Top 1.5 m is anthropogenic, replace $V_S$ by just below = 117 m/s to represent natural soil	SCPT19	Closest to station
BLOP	SCPT25	0	24			
BMD1	SCPT13	0	27	Top is anthropogenic material of dwelling mound, same as for station	SCPT13	Closest to station
BMD1	SCPT18	0	29.5	Far from station, in between BMD1 and BMD2		
BMD2	SCPT22	0	30		SCPT22	
BONL	SCPT16	0	21.5		SCPT16	
BOWW	SCPT10	0	29.5	Close to station	SCPT10	Closest to station
BOWW	SCPT12	0	28	Further from station, very different from SCPT10	SCPT12	Consider both SCPTs, no choice made
BSTD	SCPT26	0	28.5	SCPT does not show channel infill. $V_S$ in top possibly lower, 76 m/s based on MASW (not changed)	SCPT26	
BUHZ	SCPT08	2.5	23.05	Top unreliable, replace $V_S$ by extrapolation of third $V_S$ layer	SCPT08	Close to station

BUHZ	SCPT27	0	23	On MASW line, very far from station, different local geological setting than station.		
BWIN	SCPT23	0	28		SCPT23	
BWIR	SCPT07	2.5	28.5	In field next to dwelling mound		
BWIR	SCPT20	0	26.6	On dwelling mound, deepest two SCPT layers unreliable	SCPT20	
BWSE	SCPT03	0	30	Different peaks for sand in two SCPTs	SCPT03	MASW results
BWSE	SCPT04	0	30.1	Different peaks for sand in two SCPTs		
BZN1	SCPT21	0	30		SCPT21	
BZN2	SCPT05	0	30.5			
BZN2	SCPT06	0	30	Better quality data than SCPT05	SCPT06	MASW results and better quality SCPT

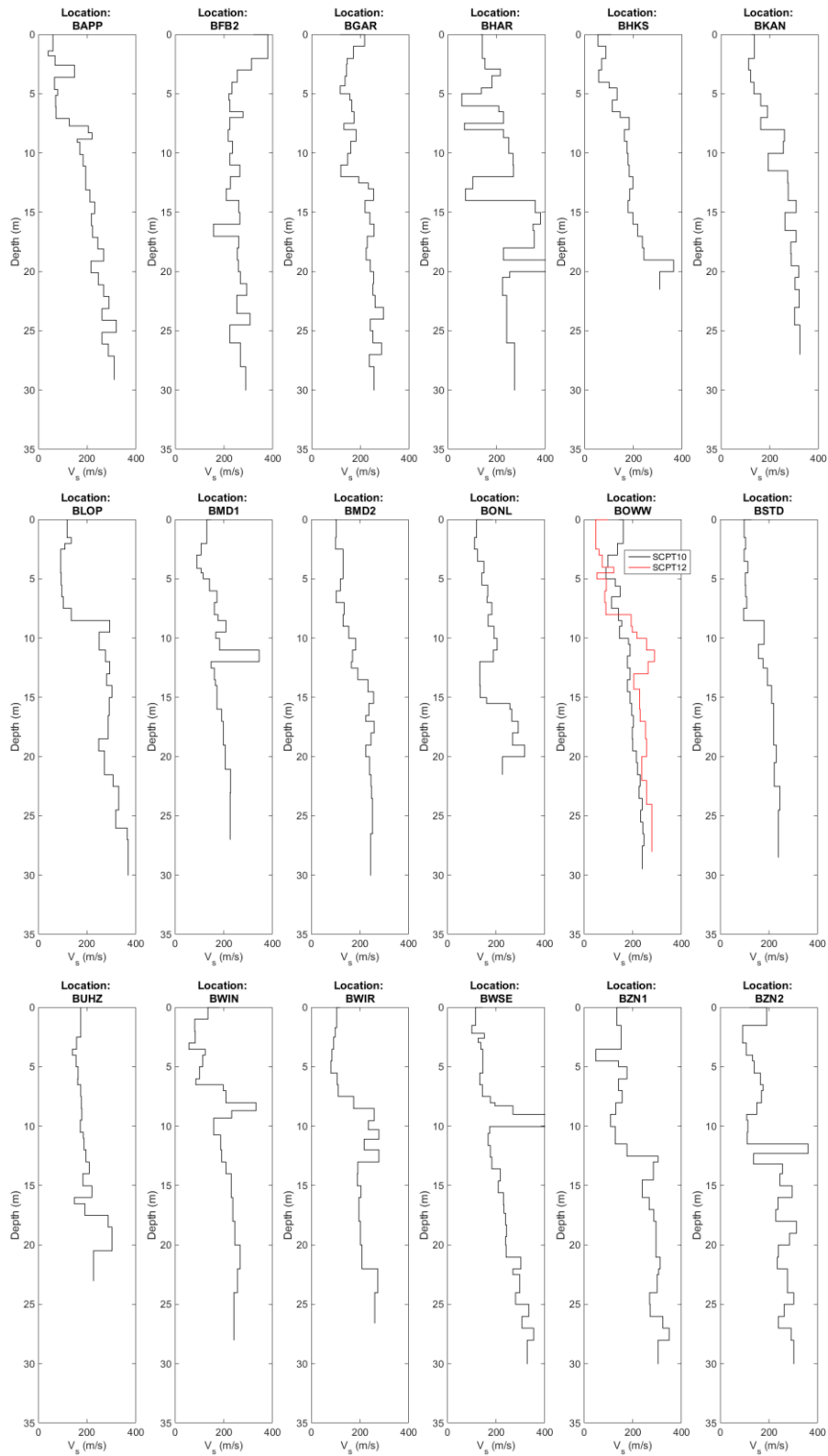


Figure 5.1 Final measured  $V_s$  profiles based on SCPT (except for a limited number of intervals, see Table 5.1) that serve as input for the site response analyses that feed into the GMPE.

### 5.3 Link between $V_S$ and local geological setting

The average  $V_S$  is linked to the age of the deposits (Holocene or Pleistocene) and the lithology (peat, clay, sand). The general ranges of  $V_S$  for the Groningen deposits listed as follows (from the  $V_S$  analysis in Bommer et al., 2016):

- Holocene peat < 100 m/s
- Holocene clay and sand and Pleistocene peat 100-200 m/s
- Pleistocene clay and fine sand 200-250 m/s
- Pleistocene medium and coarse sand > 250 m/s

The  $V_S$  profiles characteristics are given alongside the local geological setting descriptions in Table 5.2. For reference, the  $V_{S30}$  at the station is given as well.  $V_{S30}$  is generally high if no Holocene deposits are present, e.g. for BFB2. The transition between Holocene deposits (relatively low  $V_S$ ) and Pleistocene deposits (relatively high  $V_S$ ) is often easily recognised in the profiles by a jump from low  $V_S$  in the shallow layers to higher  $V_S$  values in the deeper layers.

Table 5.2  $V_S$  characteristics at the stations linked to local geological setting. See Table 4.1 for geological nomenclature.

Location	Measured $V_{S30}$ (m/s)	$V_S$ profile characteristic	Link to local geological setting
BAPP	138	Very low $V_S$ in top 7 m, below 7 m increasing $V_S$ with depth	NIHO and NIBA peat layers and Holocene clay present, transition from Holocene to Pleistocene at 7.1 m depth. Pleistocene dominated by Peelo clay
BFB2	251	Almost constant, high $V_S$	No Holocene deposits present. Dominated by Pleistocene sands, in places cemented.
BGAR	193	Medium $V_S$ in top 12 m, high $V_S$ below 12 m	Only thin layer of NIBA present, sandy Holocene, transition from Holocene to Pleistocene at 12.5 m depth. Pleistocene mostly sandy.
BHAR	184	Relatively high $V_S$ with distinct low $V_S$ layers	No Holocene deposits, upper half contains few intermittent clay and fine sand layers. Peelo clay at 20 m depth
BHKS	159	Very low $V_S$ in top 4 m, low $V_S$ to 7 m, overall increasing $V_S$ with depth	NIHO and NIBA peat layers present, transition from Holocene to Pleistocene at 4.5 m depth, Peelo clay at 8 m depth. SCPT ends in high density Peelo sand at ~ 20 m
BKAN	213	Medium $V_S$ in top 8 m, overall increasing $V_S$ with depth	No peat present, sandy Holocene, transition from Holocene to Pleistocene at 9 m depth, fine sands to 18.5 m, next Peelo clay with relatively high $V_S$
BLOP	187	Low $V_S$ in top 9 m, high $V_S$ below 9 m	Only NIHO and Holocene clay, transition from Holocene to Pleistocene at 9.5 m depth, Pleistocene dominated by Peelo sand
BMD1	172	Low to medium $V_S$ in top 12 m, medium $V_S$ below 12 m	Top anthropogenic, NIHO and Holocene (sandy) clay present, transition from Holocene to Pleistocene at 12.5 m depth, Pleistocene dominated by Peelo clay with relatively low $V_S$
BMD2	168	Low $V_S$ in top 7 m, increase to 14 m, constant $V_S$ below 14 m	No peat present, sandy clay Holocene, transition from Holocene to Pleistocene at 11 m depth, Pleistocene dominated by Peelo clay
BONL	192	Low to medium $V_S$ in top 15 m, high $V_S$ below 15 m	Holocene dominated by fine sands to 13 m, clay to 15.5 m, thin layer of NIBA present, transition from Holocene to Pleistocene at 16 m depth, Pleistocene dominated by sand

BOWW - SCPT10	172	Medium $V_S$ increasing with depth	Top anthropogenic, Holocene clay with thin layer of NIHO, transition from Holocene to Pleistocene at 10.5 m depth, Pleistocene dominated by clay
BOWW - SCPT12	147	Very low $V_S$ in top 8 m, medium to high $V_S$ below 8 m	Holocene dominated by clay and peat (NIHO and NIBA), transition to Pleistocene at 9 m depth, Pleistocene dominated by clay with systematically higher $V_S$ than SCPT10
BSTD	163	Low $V_S$ in top 8 m, increasing $V_S$ with depth below 8 m	Holocene clay and thin NIBA present, transition from Holocene to Pleistocene at 9 m depth, Pleistocene dominated by clay
BUHZ	200	Medium $V_S$ with overall increase with depth	Sandy Holocene with NIBA present, transition from Holocene to Pleistocene at 17.5 m depth, Pleistocene dominated by sand
BWIN	176	Low to very low $V_S$ in top 7 m, high $V_S$ layer at 9 m, slight increase with depth from 10 m on	Holocene clay, with thin NIHO and NIBA present, transition from Holocene to Pleistocene at 7 m depth, Pleistocene dominated by Peelo clay
BWIR	164	Low $V_S$ in top 7.5 m, high $V_S$ to 13 m, medium $V_S$ below 13 m, with high $V_S$ below 26 m	Holocene (sandy) clay, transition from Holocene to Pleistocene at 9.5 m depth, Pleistocene consists of thick sand layer overlying Peelo clay, bottom of Peelo clay with relatively high $V_S$
BWSE	198	Low $V_S$ in top 8 m, high $V_S$ layer at 10 m, increasing from medium to high $V_S$ below 10 m	No peat present, Holocene sandier with depth, transition from Holocene to Pleistocene at 8 m depth, Pleistocene consists of mainly Peelo with transition from dominantly clay to dominantly sand at 21 m
BZN1	192	Medium $V_S$ in top 12 m, with low $V_S$ layers, high $V_S$ below 12 m	Holocene (clayey) sand with thin layer of clay and NIBA, transition from Holocene to Pleistocene at 13 m depth, Pleistocene dominated by sand
BZN2	178	Low to medium $V_S$ in top 12 m, high, irregular $V_S$ below 12 m	Holocene succession of NIHO, (clayey) sand, clay and NIBA, transition from Holocene to Pleistocene at 14 m depth, Pleistocene dominated by sand

## 5.4 Comparison of measured $V_{S30}$ and GMPE V3 $V_{S30}$ map

The final  $V_S$  profiles presented in section 5.2 were used in GMPE V3 to convert earthquake signals as measured by the KNMI monitoring network at the surface to the reference baserock horizon (Bommer et al., 2016). GMPE V3 also contains a modelled  $V_{S30}$  map (section 3.8). In this section, the measured  $V_{S30}$  values are compared to the modelled  $V_{S30}$  map.

The final  $V_S$  profiles from the measurements were converted to  $V_{S30}$  values using Eq. 3.1. Next, the measured  $V_{S30}$  at the stations were compared to the modelled  $V_{S30}$  values for the zones of the GMPE for the station locations (Table 5.3). In general, the modelled  $V_{S30}$  are generally in agreement with the observations, i.e. measured  $V_{S30}$  are mostly within one standard deviation ( $\epsilon < 1$ ) from modelled  $V_{S30}$ . The exceptions are BAPP, BHAR and BKAN, where local characteristics are different from the average characteristics. Therefore, it is important to acquire local information, e.g. to be able to minimise station residuals in GMPE as was done in GMPE V3 (Bommer et al., 2016) or derive location specific ground motions.

Table 5.3 Comparison of measured and modelled  $V_{S30}$  values at the stations.

Location	Measured $V_{S30}$ (m/s)	$\epsilon = (\text{measured-} \\ \text{av}_{\text{zone}})/\text{stdev}_{\text{zone}}$	GMPE V3 $V_{S30}$ map (Bommer et al. 2016, Krüver et al., 2016b)		
			Zone	Average $V_{S30}$ of zone (m/s)	Standard deviation of $V_{S30}$ of zone
BAPP	138	-1.2	2111	171	28
BFB2	251	-0.1	3115	256	40
BGAR	193	0.5	1001	178	28
BHAR	184	-1.4	3118	233	34
BHKS	159	-0.6	2110	177	29
BKAN	213	1.4	604	168	33
BLOP	187	0.4	1032	175	28
BMD1	172	-0.1	1002	175	29
BMD2	168	-0.3	1001	178	28
BONL	192	0.3	1011	184	31
BOWW-SCPT10	172	0.0	2111	171	28
BOWW-SCPT12	147	-0.9	2111	171	28
BSTD	163	-0.7	1037	182	29
BUHZ	200	0.4	801	185	36
BWIN	176	0.0	2110	177	29
BWIR	164	-0.3	2111	171	28
BWSE	198	0.5	602	183	32
BZN1	192	0.8	1004	171	26
BZN2	178	0.1	1032	175	28



## 6 Conclusions and recommendations

As part of the development of Ground Motion Prediction Equations (GMPE) for the Groningen field, a fieldwork campaign was conducted to determine the shear-wave velocity ( $V_S$ ) in situ at 18 recording stations of the KNMI monitoring network. The measured  $V_S$  profiles serve as input for the calibration of the GMPE using records of earthquake motions registered by the network.

The  $V_S$  profiles have been determined using a combination of geophysical techniques. Data has been collected on different scales, from small to large:

- 1 Seismic Cone Penetration Tests (SCPT, 1 metre scale, 1D).
- 2 Offset SCPT (OSCPT, up to 20 metre, 1D).
- 3 Cross-hole tomography (10-25 metre, 2D), only for 3 locations.
- 4 P-S suspension logging (1D), only for 2 locations.
- 5 Multichannel Analysis of Surface Waves-CMPcc (CMPcc, 100 metre scale with internal variation).
- 6 MASW-200m array (200 metre average).

Borehole logging and CPTs provided additional information on the stratigraphy at the sites. All these fieldwork methods and processing techniques were applied at three pilot locations. Generally, the results of the various methods compare well. The SCPT and MASW performed well and are fast acquisition techniques to determine  $V_S$ . These two techniques were selected for the remaining 15 locations, because speed was a critical issue at that stage of the project. The cross-hole tomography technique, yielding detailed 2D images and lateral heterogeneity of  $V_S$  between the boreholes, was not selected for the remainder of the stations, because of the logistics of the boreholes required for these measurements (i.e. inconvenience caused by drilling rigs, time needed for drilling, relatively large distance to accelerograph station). P-S suspension logging was not applied at the remaining locations, since the results were not satisfactory at the pilot locations. This was probably related to the grouting of the borehole, rather than to the principles of the technique. Time pressure did not permit further investigation of the causes of poor performance and possible improvements of the technique in the Groningen setting.

In order to build a representative  $V_S$  profile based on the field measurements, scale and resolution effects should be taken into account. The scales vary from location to location, due to the significant lateral and vertical variations in velocities. Therefore, 'upscaling' from point observations to larger regions should be considered carefully. Originally, the representative  $V_S$  profile at the station was to be determined as a weighted average over the various techniques. This approach, however, was abandoned for pragmatic reasons and time pressure. The final  $V_S$  profiles were solely based on one SCPT per station, with the exception of a limited number of shallow depth intervals where the SCPT results were unreliable. In those cases, the  $V_S$  of MASW was chosen. The final  $V_S$  profiles that serve as input for the GMPE are presented in chapter 5. However, the discussion on sampling of varying volumes of soil by the different methods and scales is still pending.

We provide the following recommendations for future fieldwork campaigns in the Groningen region for the purpose of improving the GMPE:

- Field measurements:
  - Active MASW: in order to obtain an increased depth of investigation, a repeatable source containing low frequencies with an undistorted signal is needed. There are currently good possibilities (i.e., know-how and technical capability) to build such a device. Additionally, the field setup can be improved when passive and active

# Deltares

MASW do not need to be combined because of time pressure. The field setup can be optimised for active MASW to obtain the best quality data.

- Passive MASW: the current setup of the fieldwork did not yield additional frequency information relative to the active MASW. The field setup can be improved by (amongst others) a different layout and longer duration of measurement.
- Representativeness of  $V_S$ :
  - Scales and sampling: the pragmatic choice of using primarily  $V_S$  from SCPT as representative for the  $V_S$  profile at the station location was made under pressure of time. This choice needs to be substantiated by theoretical considerations and discussion by an expert panel.
  - We recommend combining different techniques in all cases, because of their complementary information regarding scale and resolution. Additionally, unreliable results of one technique can be supplemented with the results of another technique.
  - It pays off to acquire local  $V_S$  data rather than using average characteristics, e.g. to reduce GMPE residuals at the station locations.
- Other: the coordinates of several stations are not clear. There are differences in the list of coordinates provided by KNMI and by NAM. It was beyond the scope of the fieldwork to verify the true location of the stations.

Additionally, from the discussions on the improvement of the GMPE and related fieldwork in general, we recommend the following:

- This fieldwork was focused on the in-situ determination of  $V_S$ , while damping is another key parameter in site response calculations. We recommend adjusting future fieldwork design to include determination of damping as well.
- The depth of investigation of this fieldwork was limited to 30 metres below the surface. The amount of actual  $V_S$  data for deeper sediments is very limited, while the site response analysis and GMPE require  $V_S$  information to a depth of ~ 800 m. We recommend increasing the depth of investigation of field measurements to fully cover the range that is relevant for site response and GMPE.
- Processing: investigation of possibilities to derive damping from the SCPT and MASW data is no standard procedure and an approach for that needs to be developed.
- SCPT: improvement of results is possible by using better receivers, including more offsets and the development of an automated and repeatable source.

## A References

Baziw, E. (2002). Derivation of Seismic Cone Interval Velocities Utilizing Forward Modeling and the Downhill Simplex Method, *Can. Geotech. J.*, vol. 39, pp.1-12.

Bommer, J.J., B. Dost, B. Edwards, P.P. Kruiver, P. Meijers, M. Ntinalexis, A. Rodriguez-Marek & P.J. Stafford (2016). Development of Version 3 GMPEs for Response Spectral Accelerations and Significant Durations from Induced Earthquakes in the Groningen Field. Report prepared for NAM.

Douglas, B.J. & R.S. Olsen (1981) Soil classification using electric cone penetrometre. American Society of Civil Engineers, ASCE, Proceedings of Conference on Cone Penetration Testing and Experience, St. Louis, October 26 - 30, pp. 209 – 227

ISO 22476-1:2012(E). Geotechnical investigation and testing — Field testing — Part 1: Electrical cone and piezocone penetration test.

Kruiver, P.P., G. de Lange, A. Wiersma, P. Meijers, M. Korff, J. Peeters, J. Stafleu, R. Harting, R. Dambrink, F. Busschers & J. Gunnink (2015). Geological schematisation of the shallow subsurface of Groningen - For site response to earthquakes for the Groningen gas field. Deltares Report No. 1209862-005-GEO-0004-v5-r, 16 March 2015.

Kruiver, P.P. & A. Wiersma (2016a) Modifications of the Geological model for Site response at the Groningen Field - For GMPE version 3. Deltares report 1209862-005-GEO-0009.

Kruiver, P.P., E. van Dedem, R. Romijn, G.L. de Lange, M. Korff, J. Stafleu, J.L. Gunnink, A. Rodriguez-Marek, J.J. Bommer, J. van Elk, D. Doornhof (2016b) An integrated shear-wave velocity model for the Groningen gas field, The Netherlands. Submitted to *Bulletin of Earthquake Engineering*.

Metzger, L.F. & J.A. Izbicki (2013). Electromagnetic-Induction Logging to Monitor Changing Chloride Concentrations. *Ground water*, 51(1), 108-121.

NAM (2016) Winningsplan Groningen Gasveld 2016. NAM Document EP201604259068, 1 April 2016.

NAM (2016) Technical Addendum to the Winningsplan Groningen 2016. Production, Subsidence, Induced Earthquakes and Seismic Hazard and Risk Assessment in the Groningen Field. PART III Hazard. NAM Document EP201603238413, 1 April 2016.

NAM (2016) Technical Addendum to the Winningsplan Groningen 2016. Production, Subsidence, Induced Earthquakes and Seismic Hazard and Risk Assessment in the Groningen Field. PART IV Risk. NAM Document EP201603238413, 1 April 2016.

Sethian, J.A. (1999). Fast Marching Methods, *SIAM Review*, 41 (2), 199-235.

Watanabe, T., T. Matsuoka & Y. Ashida (1999) Seismic traveltime tomography using Fresnel volume approach. *SEG Technical Program Expanded Abstracts*. Vol. 18.



## B Abbreviations

CPT – Cone Penetration Test

CMPcc – Common Mid Point cross-correlation

DGM – Digital Geological Model

DOI – Depth of investigation

FMDSM – Forward Modelling/Downhill Simplex Method

GDN-TNO – Geological Survey of The Netherlands - TNO

GMPE – Ground Motion Prediction Equation

MASW – Multichannel Analysis of Surface Waves

MBAS – Multi-Station Borehole Acquisition System

P-wave – compressional wave

SCPT – Seismic Cone Penetration Test

SH – horizontally polarised shear wave

S-wave – shear wave

OSCPT – Offset Seismic Cone Penetration Test

QC – Quality Control

$V_P$  – compressional wave velocity

$V_S$  – shear wave velocity

$V_{S30}$  – time averaged shear wave velocity in the first 30 m below the surface

Abbreviations for geological nomenclature are given in Table 4.1.



## C Results of borehole logging

### Uithuizen

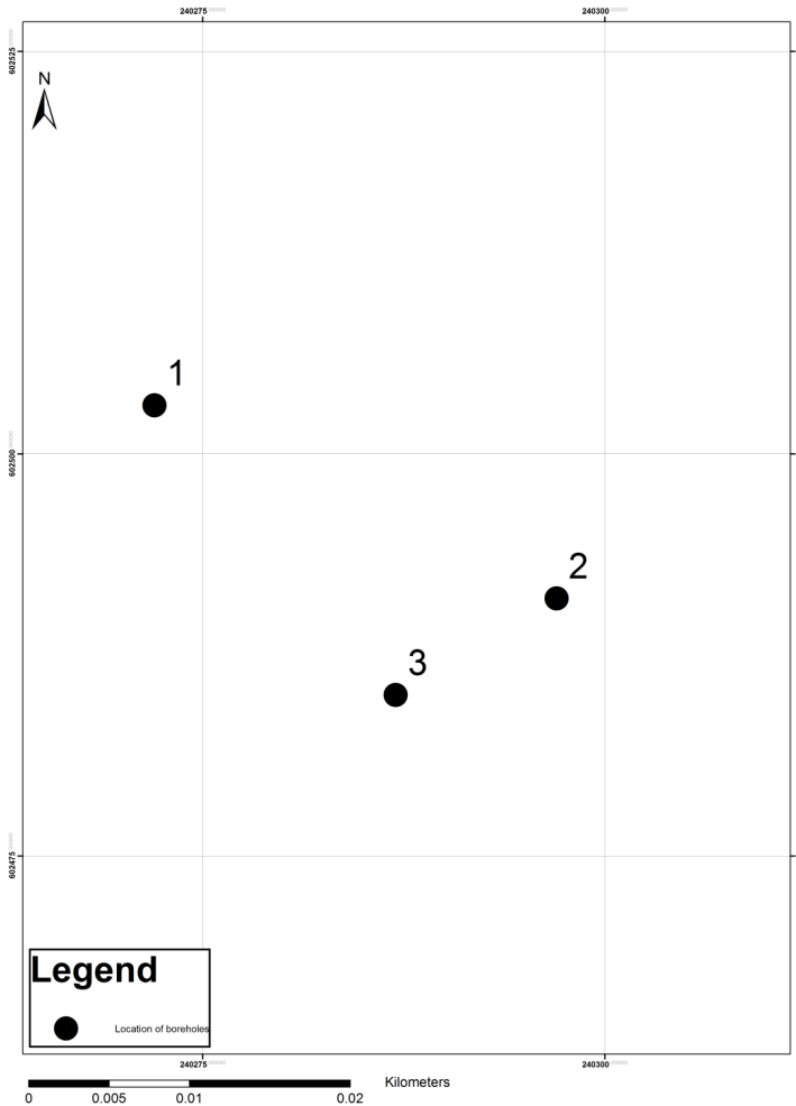


Figure C.1 Locations of the boreholes 1, 2 and 3 in Uithuizen. See Table C.1 for the X,Y coordinates of the boreholes.

# Deltares

## Westeremden

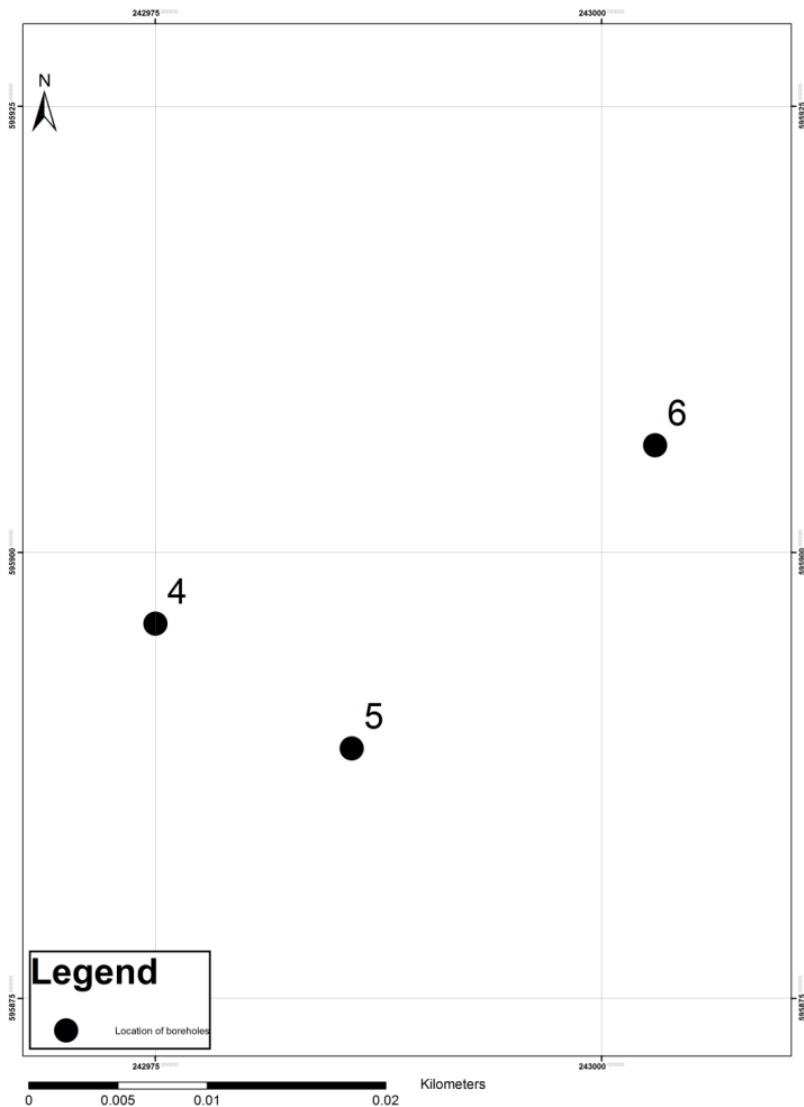


Figure C.2 Locations of the boreholes 4, 5 and 6 in Westeremden. See Table C.1 for the X,Y coordinates of the boreholes.

# Appingedam

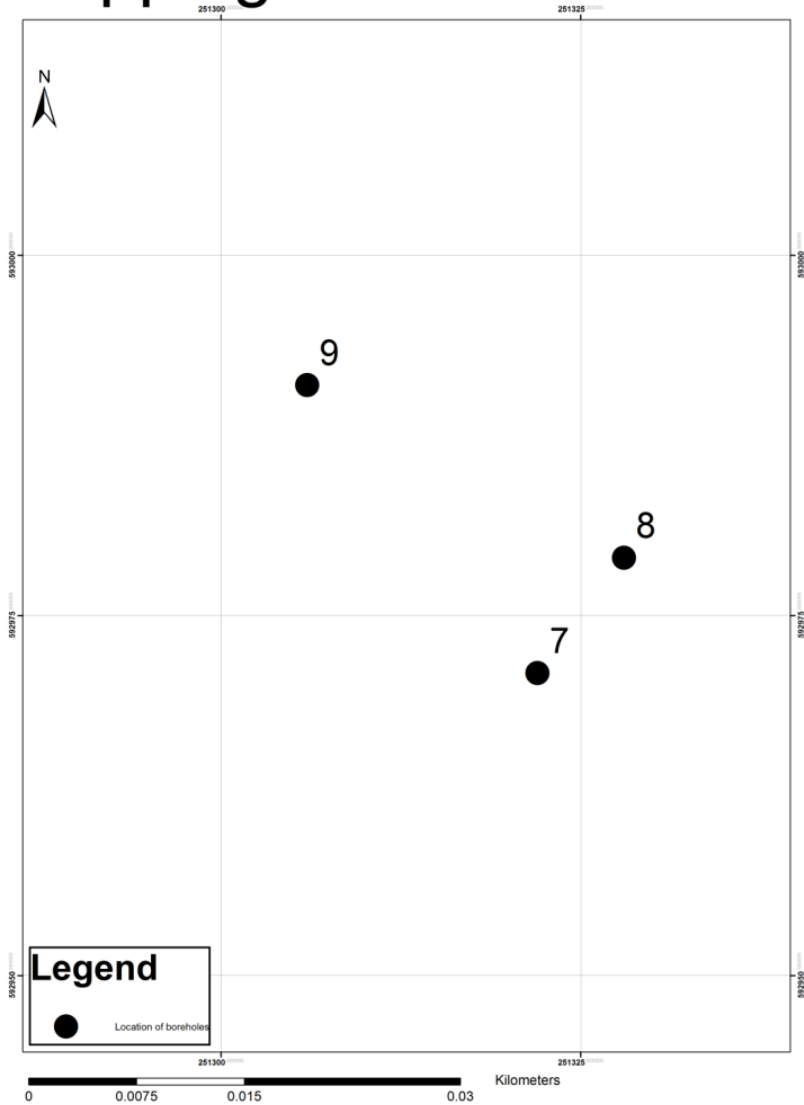


Figure C.3 Locations of the boreholes 7,8 and 9 in Appingedam. See Table C.1 for the X,Y coordinates of the boreholes.

Table C.1 Coordinates of boreholes

Location	Station	Well Id	X (RD)	Y (RD)	Groundlevel (m+NAP)
Uithuizen	BUHZ	1	240272	602503	1.05
Uithuizen	BUHZ	2	240297	602491	1.08
Uithuizen	BUHZ	3	240287	602485	1.1
Westeremden	BWSE	4	242975	595896	0.2
Westeremden	BWSE	5	242986	595889	0.32
Westeremden	BWSE	6	243003	595906	0.36
Appingedam	BAPP	7	251322	592971	-0.82
Appingedam	BAPP	8	251328	592979	-0.85
Appingedam	BAPP	9	251306	592991	-0.7

# Deltares

Information		Location			 Enabling Delta Life
Well id:	1	City:	Uithuizen		
Date:	10-07-2015	Street:	-		
Client:	N.A.M.	X,Y coördinates:	240272, 602503		
Drilling company:	Wiertsema & Partners	Groundlevel height:	1.05m NAP (AHN)		
Drilling method:	Sonic drilling				
Diameter wel:	-				
Depth drilling:	29.6m -BGL				
Depth measurement:	29.6m -BGL				

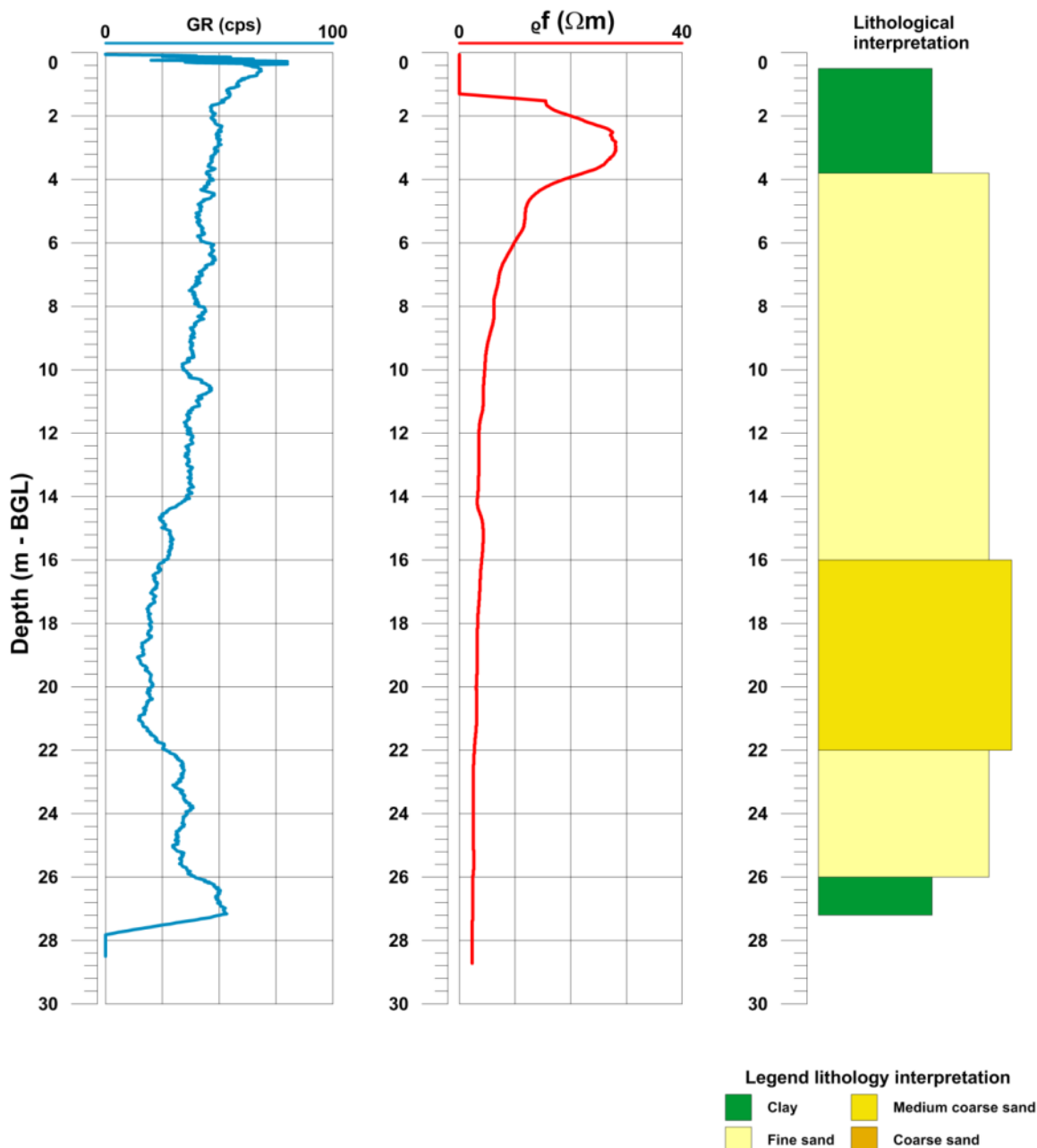


Figure C.4 Borehole logging results, from left to right: GR = gamma ray, pf = induction resistivity and indicative lithological interpretation.

Information		Location	
Well id:	2	City:	Ulthuisen
Date:	10-07-2015	Street:	-
Client:	N.A.M.	X,Y coördinates:	240297, 602491
Drilling company:	Wiertsema & Partners	Groundlevel height:	1.08m NAP (AHN)
Drilling method:	Sonic drilling		
Diameter well:	-		
Depth drilling:	29.82m -BGL		
Depth measurement:	29.82m -BGL		





Enabling Delta Life

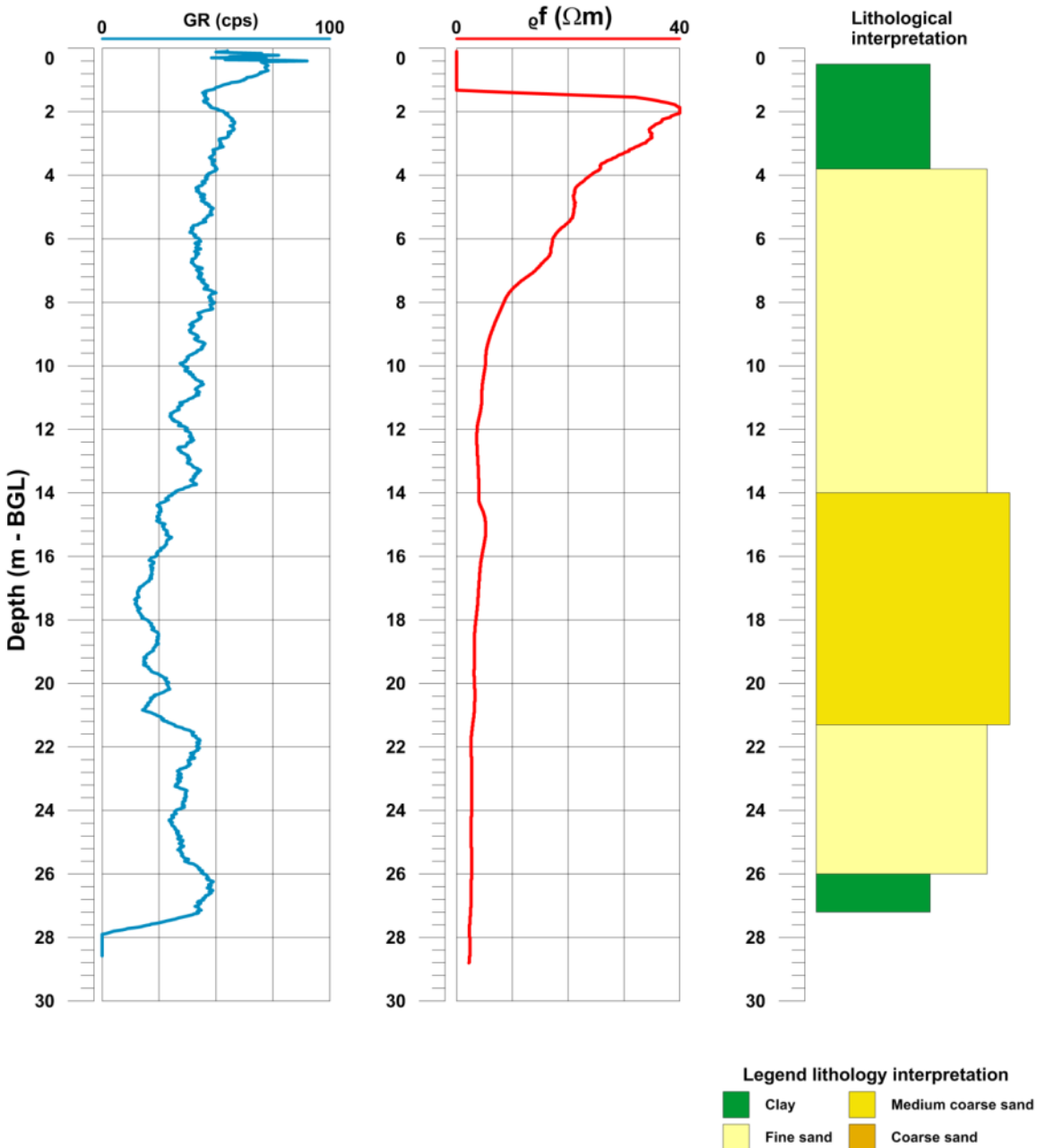


Figure C.5 Borehole logging results, from left to right: GR = gamma ray, pf = induction resistivity and indicative lithological interpretation.

# Deltares

Information		Location	
Well id:	3	City:	Uithuizen
Date:	10-07-2015	Street:	-
Client:	N.A.M.	X,Y coördinates:	240287, 602485
Drilling company:	Wiertsema & Partners	Groundlevel height:	1.10m NAP (AHN)
Drilling method:	Sonic drilling		
Diameter wel:	-		
Depth drilling:	29.83m -BGL		
Depth measurement:	29.83m -BGL		





Enabling Delta Life 

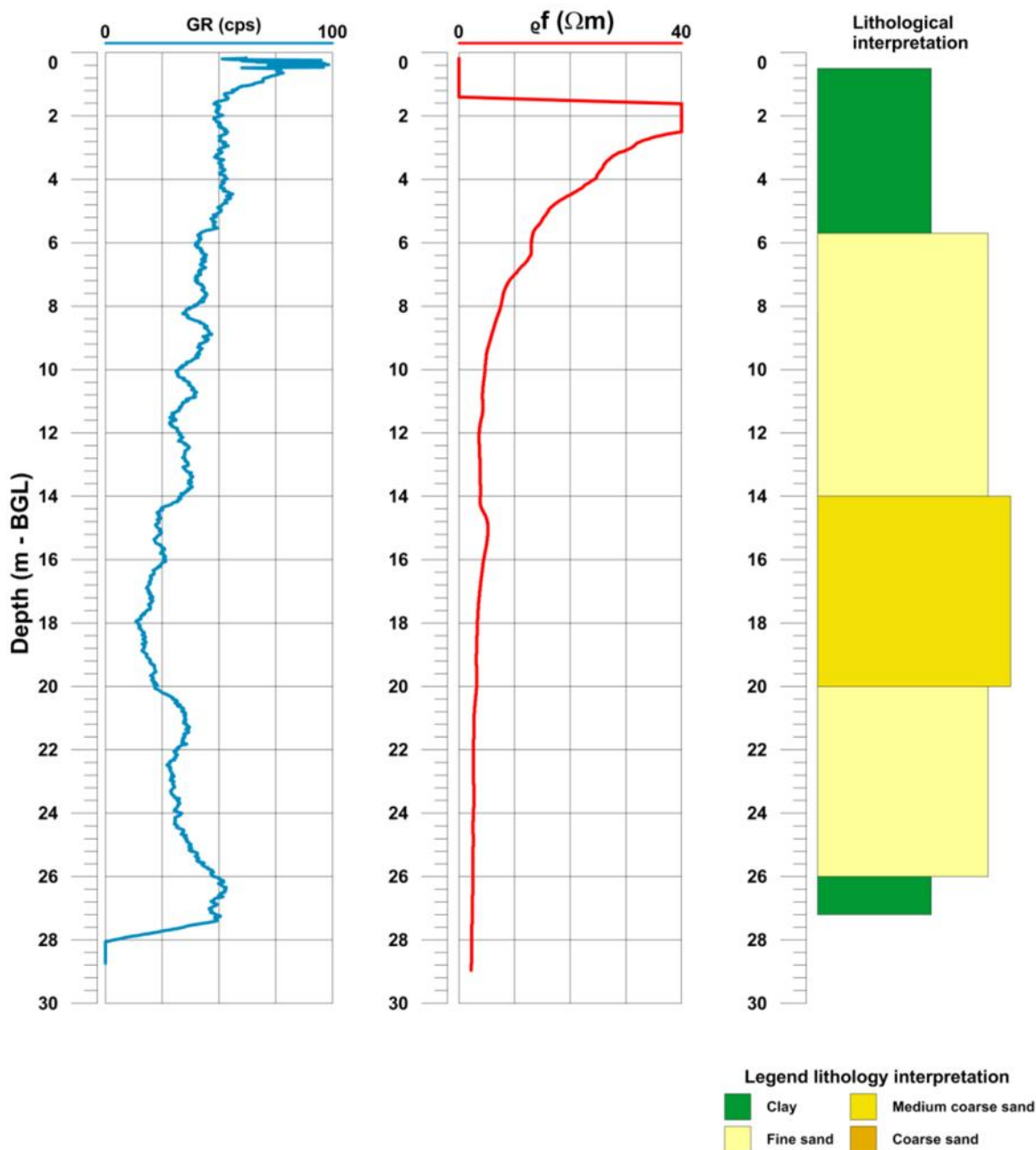


Figure C.6 Borehole logging results, from left to right: GR = gamma ray, pf = induction resistivity and indicative lithological interpretation.

Information		Location	
Well id:	4	City:	Westeremden
Date:	10-07-2015	Street:	-
Client:	N.A.M.	X,Y coördinates:	242975, 595896
Drilling company:	Wiertsema & Partners	Groundlevel height :	0.2m NAP (AHN)
Drilling method:	Sonic drilling		
Diameter well:	-		
Depth drilling:	29.65m -BGL		
Depth measurement:	29.65m -BGL		





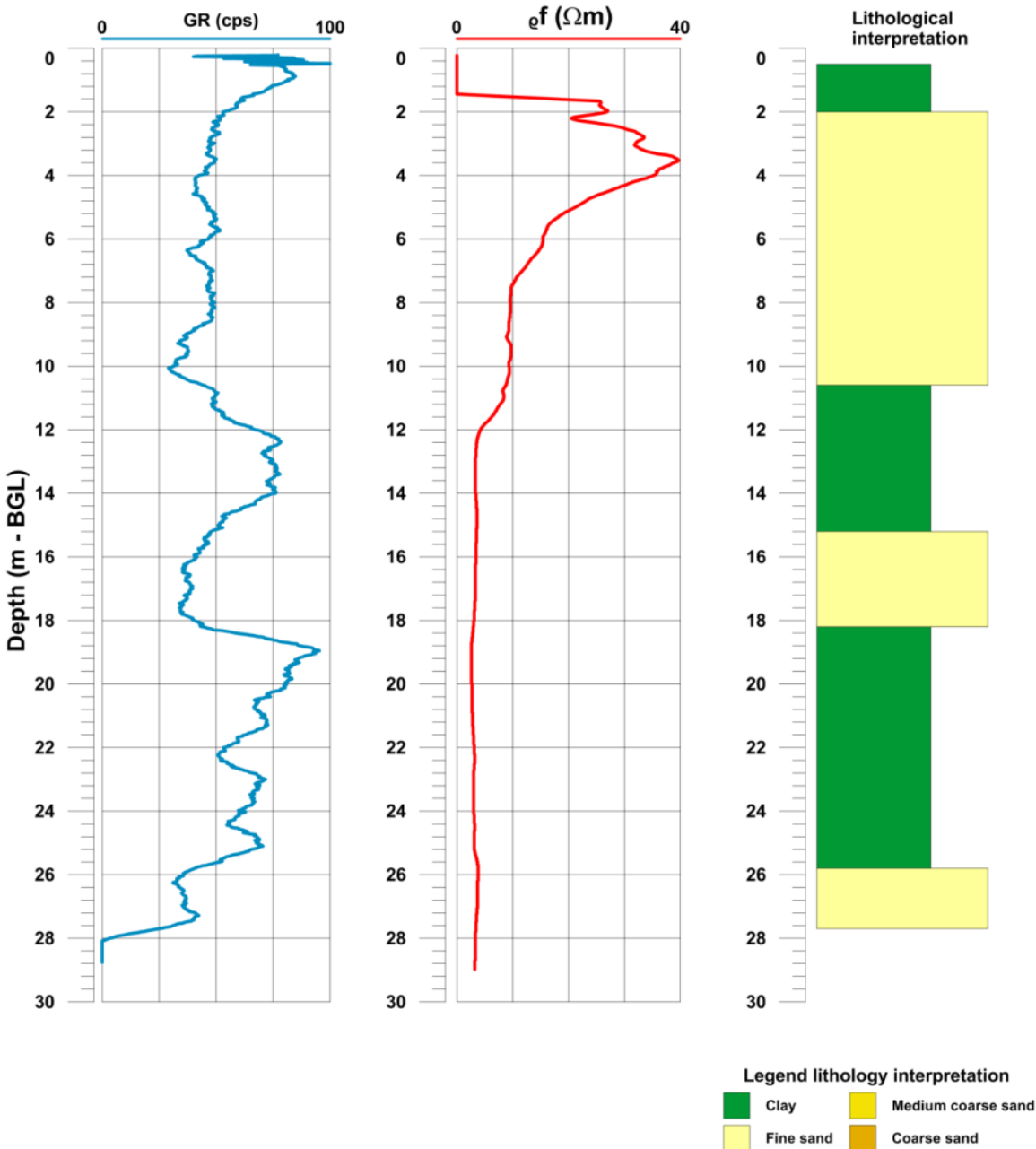


Figure C.7 Borehole logging results, from left to right: GR = gamma ray, pf = induction resistivity and indicative lithological interpretation.

# Deltares

Information		Location	
Well id:	5	City:	Westeremden
Date:	10-07-2015	Street:	-
Client:	N.A.M.	X,Y coördinates:	242986, 595889
Drilling company:	Wiertsema & Partners	Groundlevel height:	0.32m NAP (AHN)
Drilling method:	Sonic drilling		
Diameter wel:	-		
Depth drilling:	29.65m -BGL		
Depth measurement:	29.65m -BGL		





Enabling Delta Life 

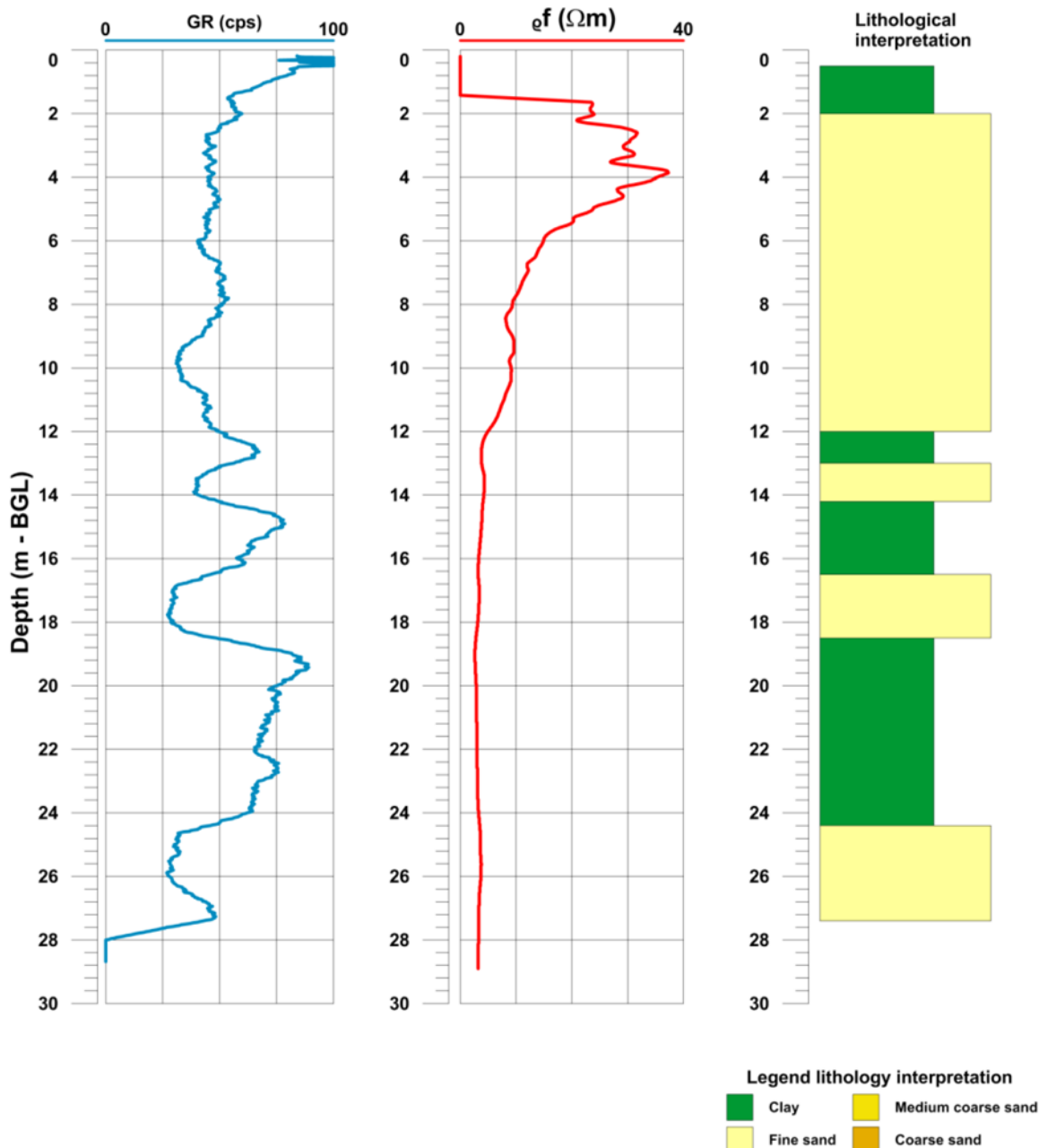


Figure C.8 Borehole logging results, from left to right: GR = gamma ray, pf = induction resistivity and indicative lithological interpretation.

Information		Location	
Well id:	6	City:	Westeremden
Date:	10-07-2015	Street:	-
Client:	N.A.M.	X,Y coördinates:	243003, 595906
Drilling company:	-	Groundlevel height:	0.36m NAP (AHN)
Drilling method:	Sonic drilling		
Diameter well:	-		
Depth drilling:	29.65m -BGL		
Depth measurement:	29.65m -BGL		





Enabling Delta Life

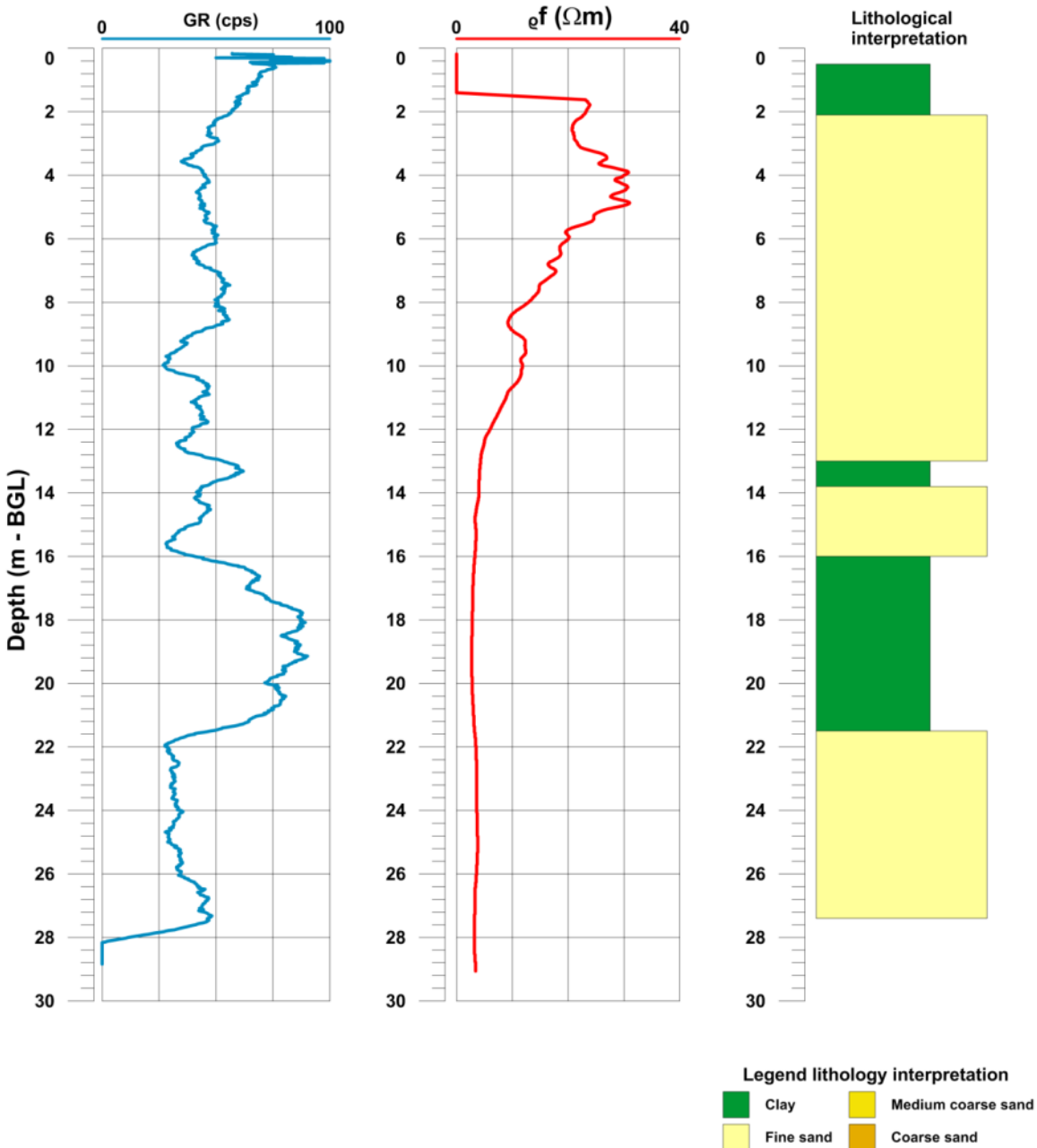


Figure C.9 Borehole logging results, from left to right: GR = gamma ray, pf = induction resistivity and indicative lithological interpretation.

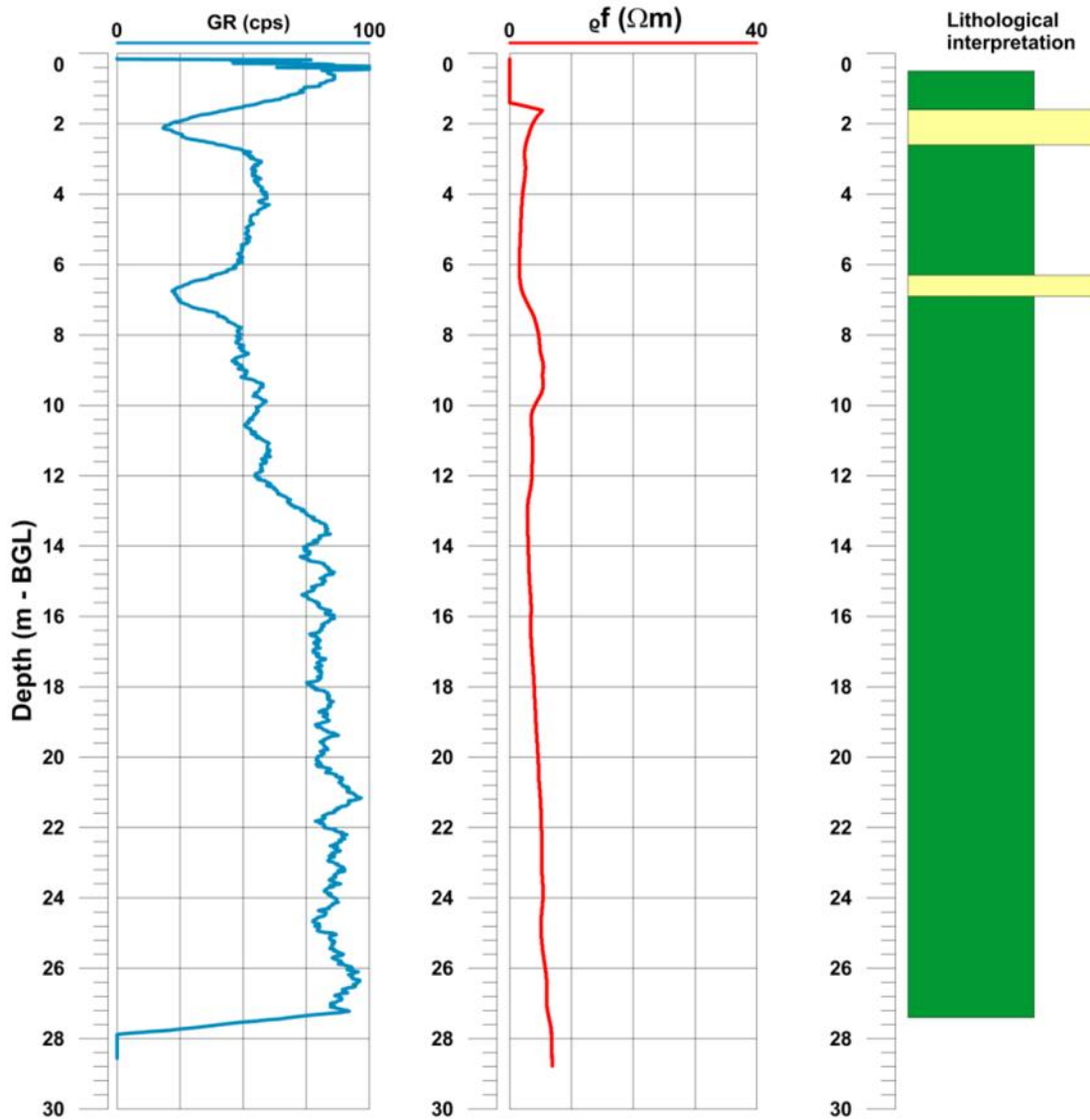
# Deltares

Information		Location	
Well id:	7	City:	Appingedam
Date:	24-07-2015	Street:	-
Client:	N.A.M.	X,Y coördinates:	251322, 592971
Drilling company:	Wiertsema & Partners	Groundlevel height:	-0.82m NAP (AHN)
Drilling method:	Sonic drilling		
Diameter wel:	-		
Depth drilling:	29.65m -BGL		
Depth measurement:	29.65m -BGL		





Enabling Delta Life 



**Legend lithology interpretation**

	Clay		Medium coarse sand
	Fine sand		Coarse sand

Figure C.10 Borehole logging results, from left to right: GR = gamma ray, pf = induction resistivity and indicative lithological interpretation.

Information		Location	
Well id:	8	City:	Appingedam
Date:	24-07-2015	Street:	-
Client:	N.A.M.	X,Y coördinates:	251328, 592979
Drilling company:	Wiertsema & Partners	Groundlevel height:	-0.85m NAP (AHN)
Drilling method:	Sonic drilling		
Diameter well:	-		
Depth drilling:	29.65m -BGL		
Depth measurement:	29.65m -BGL		





Enabling Delta Life



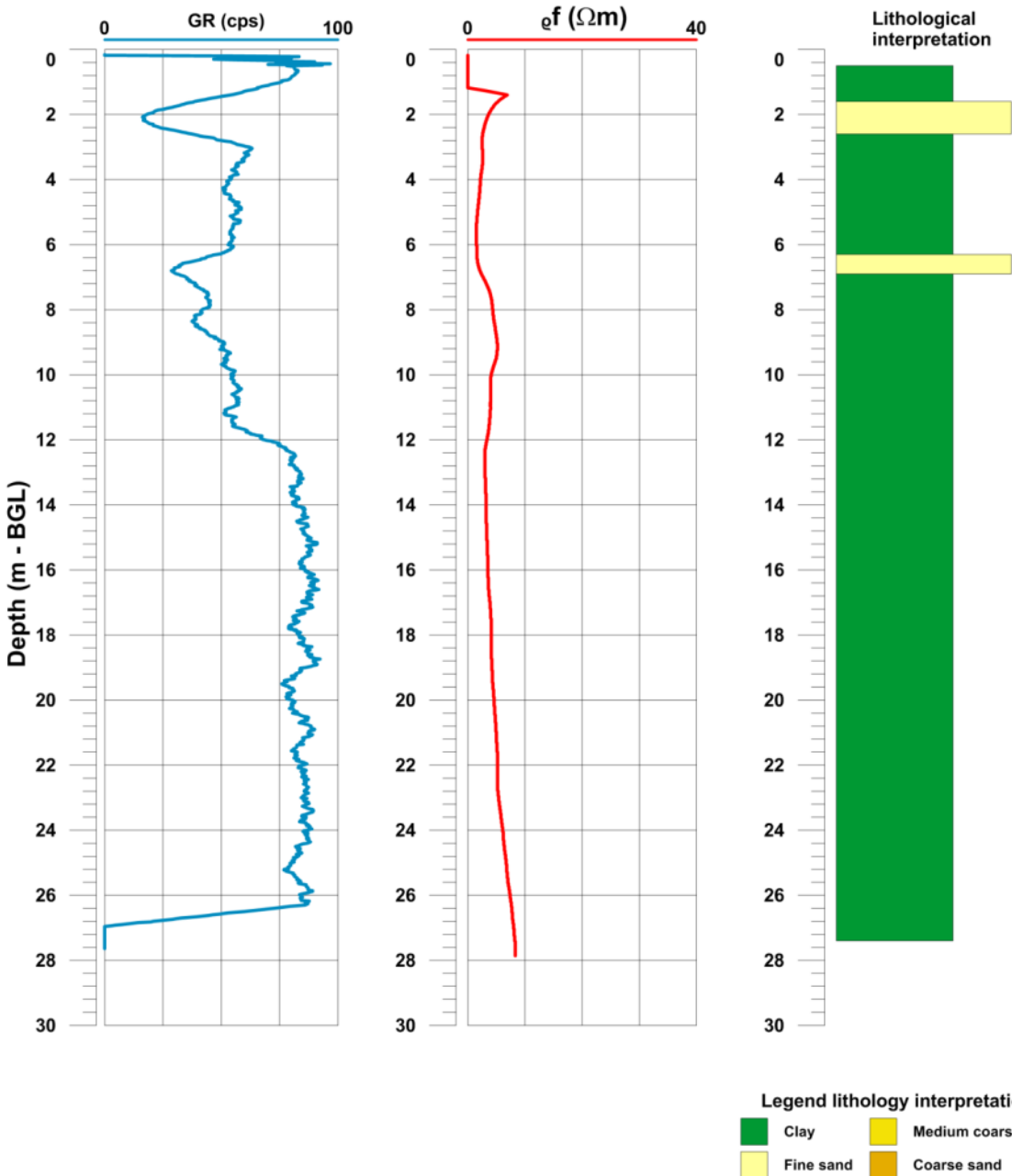


Figure C.11 Borehole logging results, from left to right: GR = gamma ray, pf = induction resistivity and indicative lithological interpretation.

# Deltares

Information		Location	
Well id:	9	City:	Appingedam
Date:	24-07-2015	Street:	-
Client:	N.A.M.	X,Y coördinates:	251306, 592991
Drilling company:	-Wiertsema & Partners	Groundlevel height :	-0.70m NAP (AHN)
Drilling method:	Sonic drilling		
Diameter wel:	-		
Depth drilling:	29.65m -BGL		
Depth measurement:	29.65m -BGL		





Enabling Delta Life 

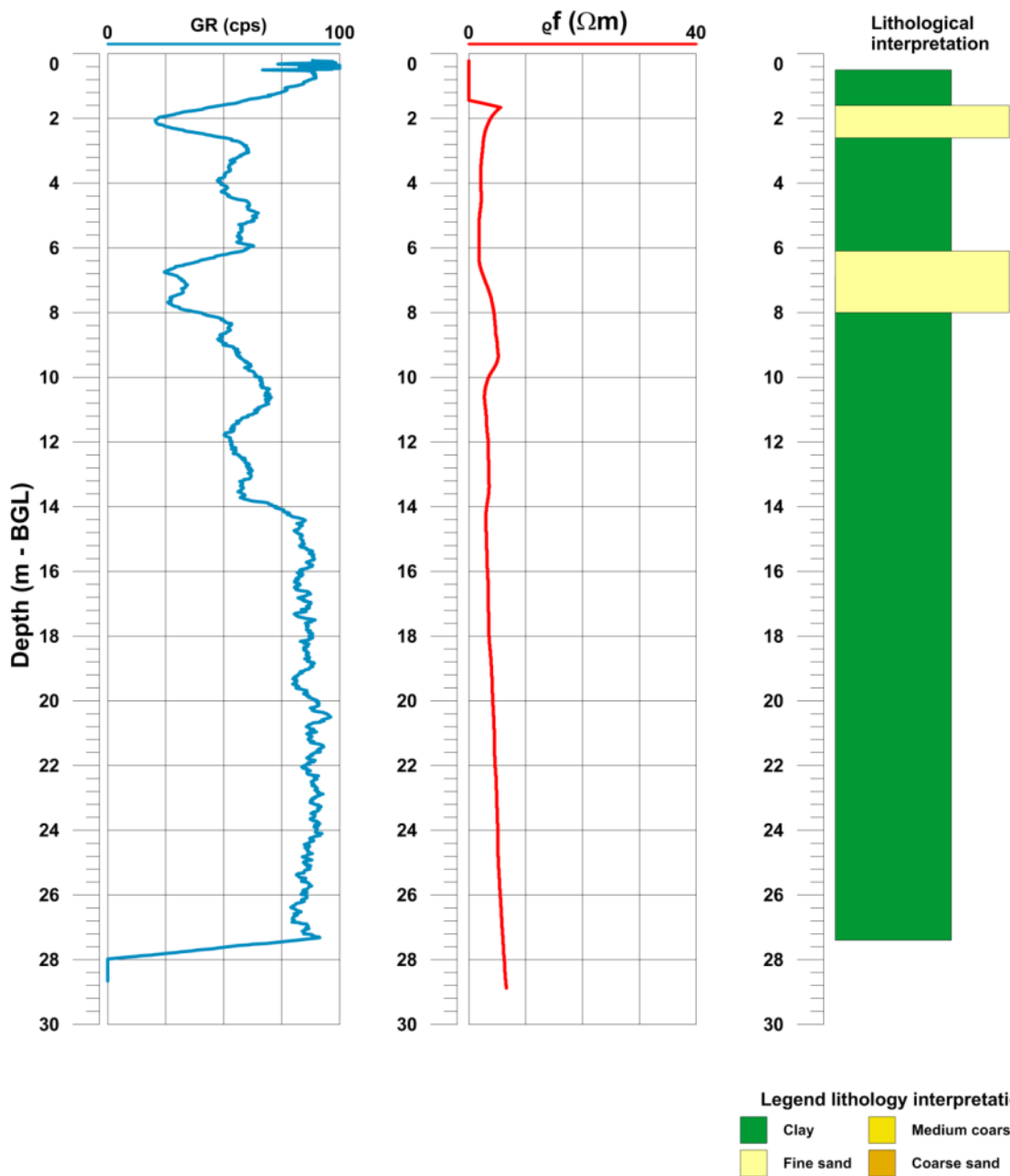


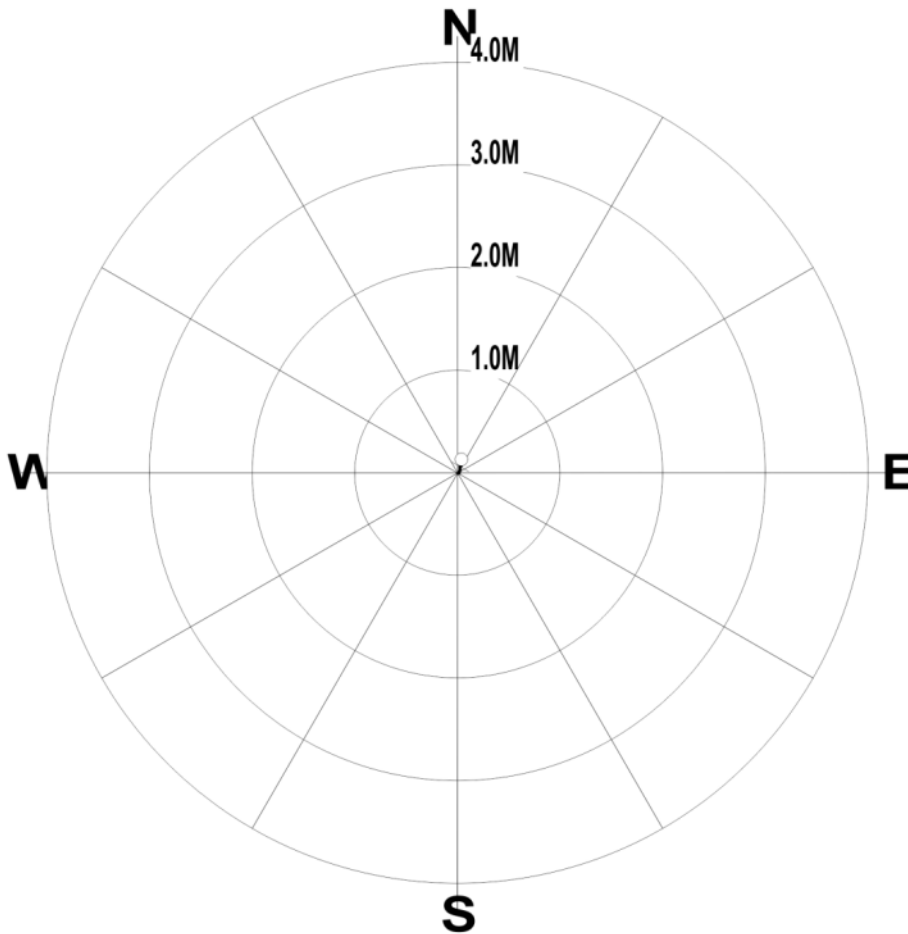
Figure C.12 Borehole logging results, from left to right: GR = gamma ray, pf = induction resistivity and indicative lithological interpretation

## PLAN VIEW COMPU-LOG DEVIATION

CLIENT:  
LOCATION: UITHUIZEN  
HOLE ID: 1  
DATE OF LOG: 07/10/15  
PROBE: 9622C 1056

  
MAG DECL: 3.6

SCALE: 1 M/CM  
TRUE DEPTH: 27.82 M  
AZIMUTH: 19.4  
DISTANCE: 0.1 M  
+ = 20 M INCR  
○ = BOTTOM OF HOLE



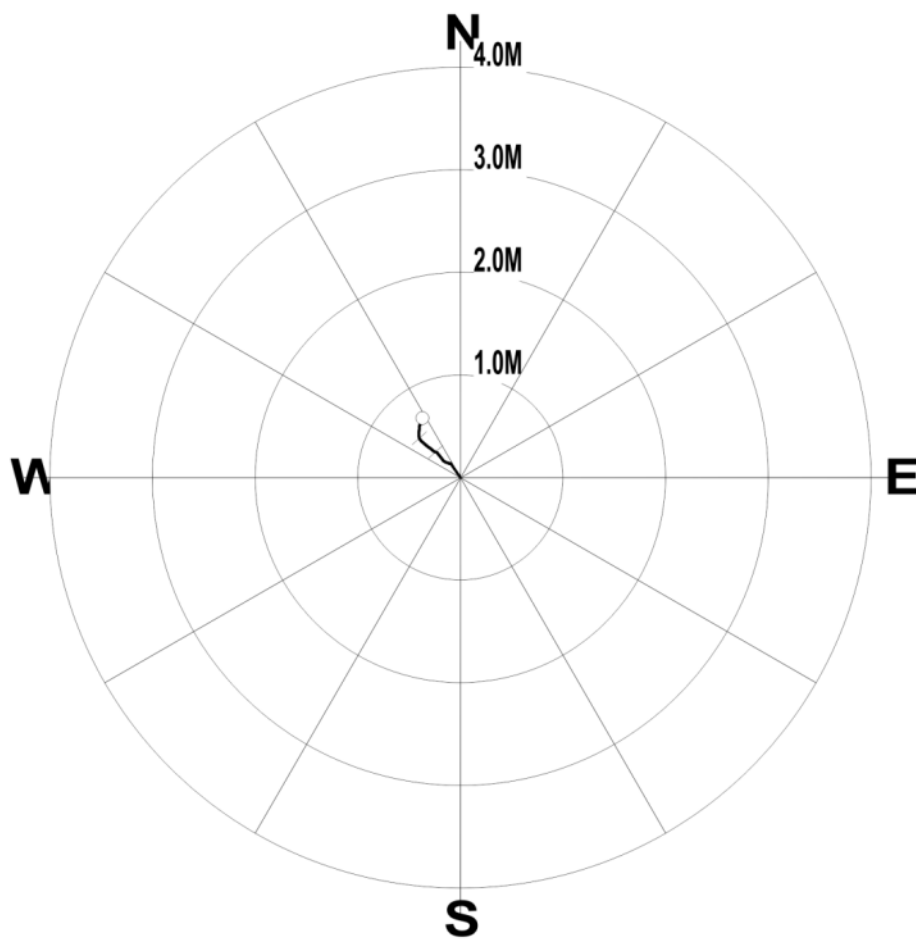
# Deltares

## PLAN VIEW COMPU-LOG DEVIATION

CLIENT:  
LOCATION: WESTEMDEN  
HOLE ID: 4  
DATE OF LOG: 07/10/15  
PROBE: 9622C 1056



SCALE: 1 M/CM  
TRUE DEPTH: 27.77 M  
AZIMUTH: 327.5  
DISTANCE: 0.7 M  
+ = 10 M INCR  
○ = BOTTOM OF HOLE

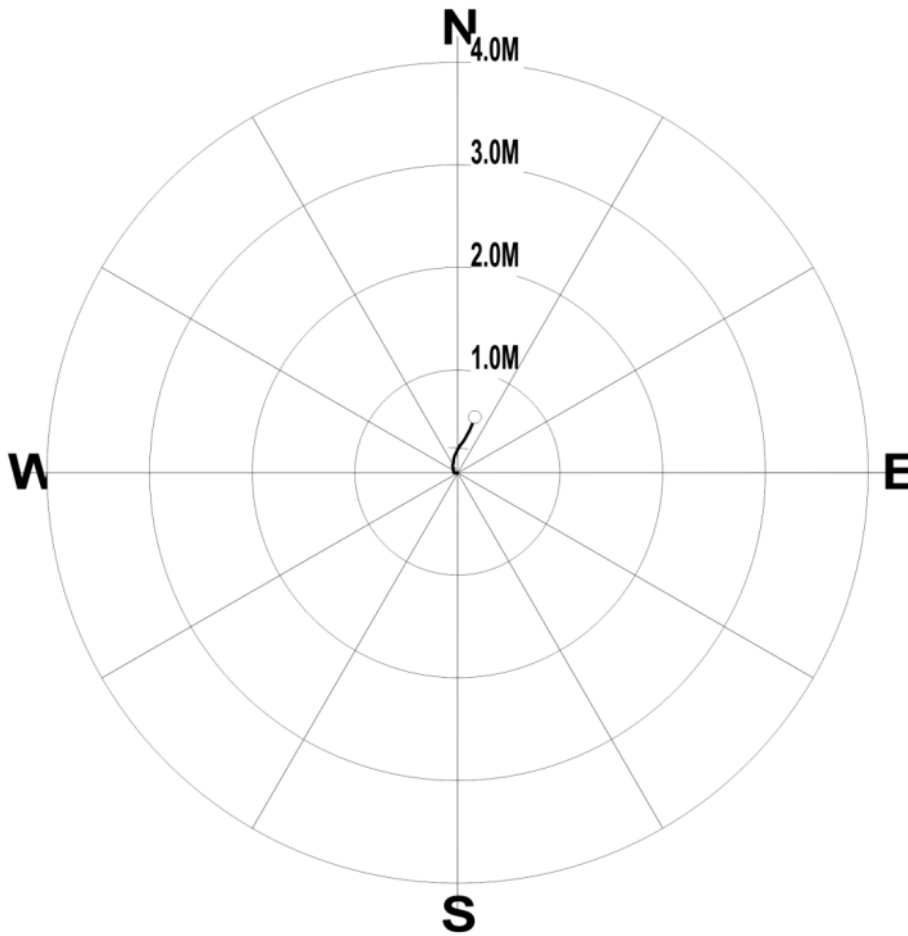


## PLAN VIEW COMPU-LOG DEVIATION

CLIENT:  
LOCATION: WESTEMDEN  
HOLE ID: 5  
DATE OF LOG: 07/10/15  
PROBE: 9622C 1056

  
MAG DECL: 3.6

SCALE: 1 M/CM  
TRUE DEPTH: 28.03 M  
AZIMUTH: 17.4  
DISTANCE: 0.6 M  
+ = 20 M INCR  
○ = BOTTOM OF HOLE



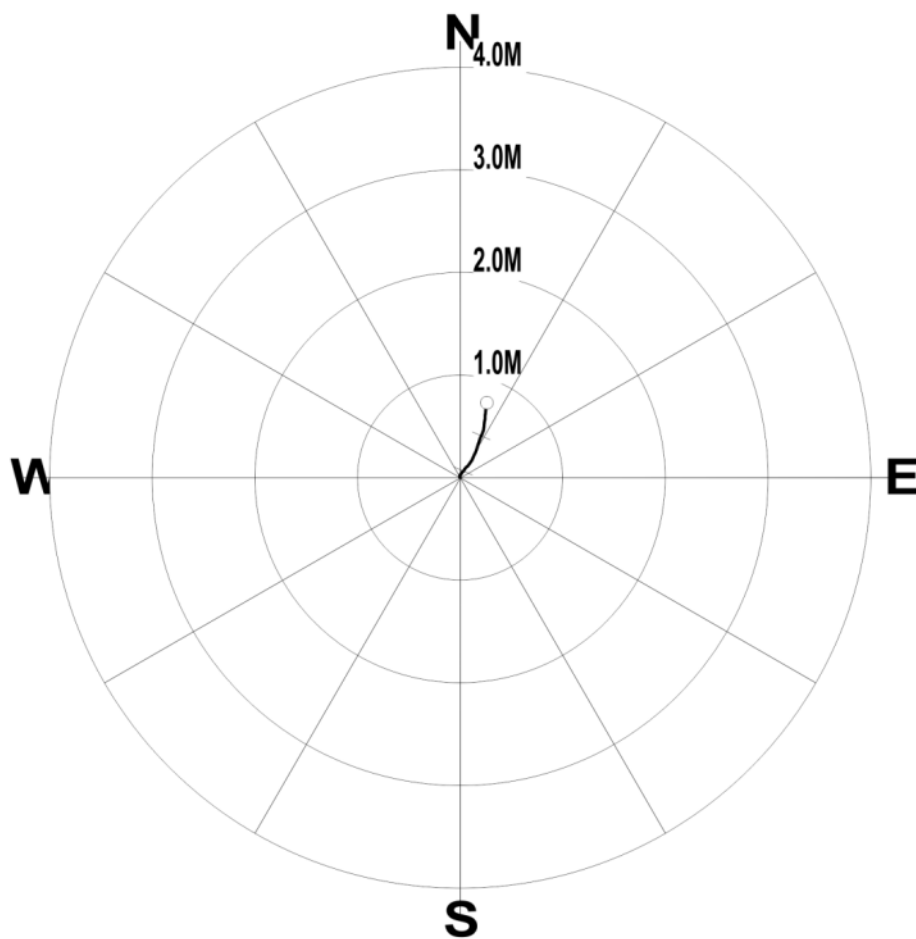
# Deltares

## PLAN VIEW COMPU-LOG DEVIATION

CLIENT:  
LOCATION: WESTEMDEN  
HOLE ID: 6  
DATE OF LOG: 07/10/15  
PROBE: 9622C 1056



SCALE: 1 M/CM  
TRUE DEPTH: 28.06 M  
AZIMUTH: 19.4  
DISTANCE: 0.8 M  
+ = 10 M INCR  
○ = BOTTOM OF HOLE

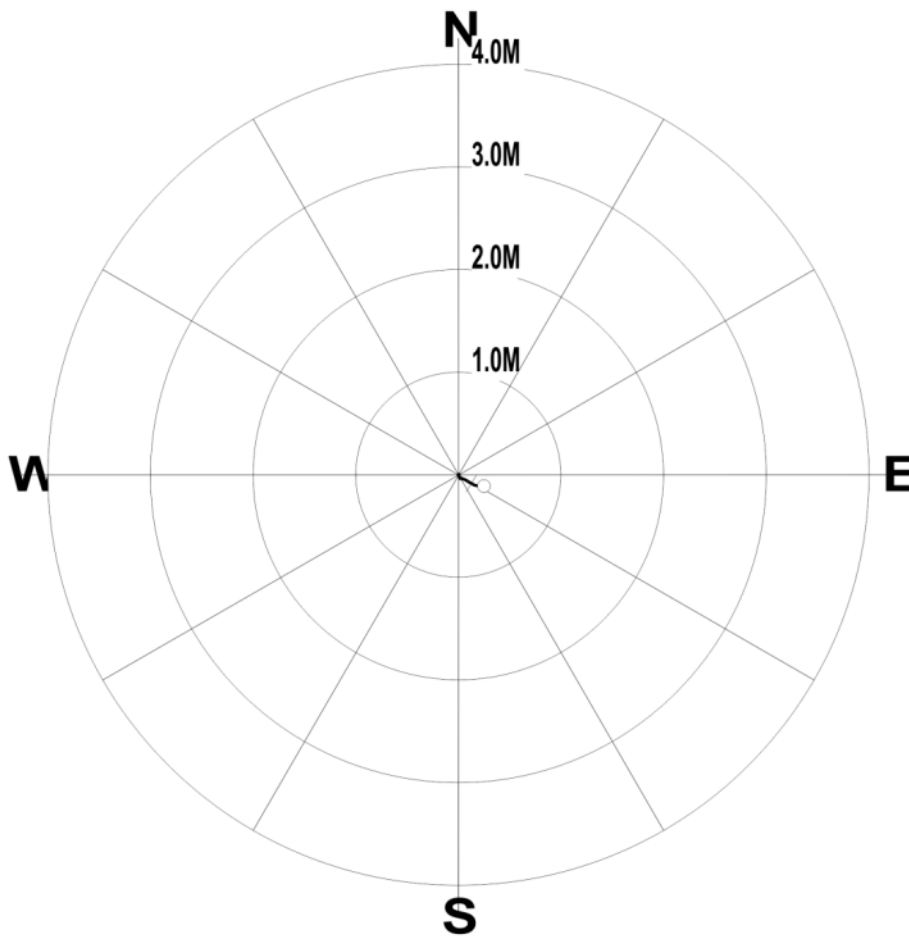


# PLAN VIEW COMPU-LOG DEVIATION

CLIENT:  
LOCATION: APPINGEDAM  
HOLE ID: 7DEV  
DATE OF LOG: 07/24/15  
PROBE: 9622C 1056



SCALE: 1 M/CM  
TRUE DEPTH: 27.90 M  
AZIMUTH: 114.3  
DISTANCE: 0.3 M  
+ = 20 M INCR  
○ = BOTTOM OF HOLE



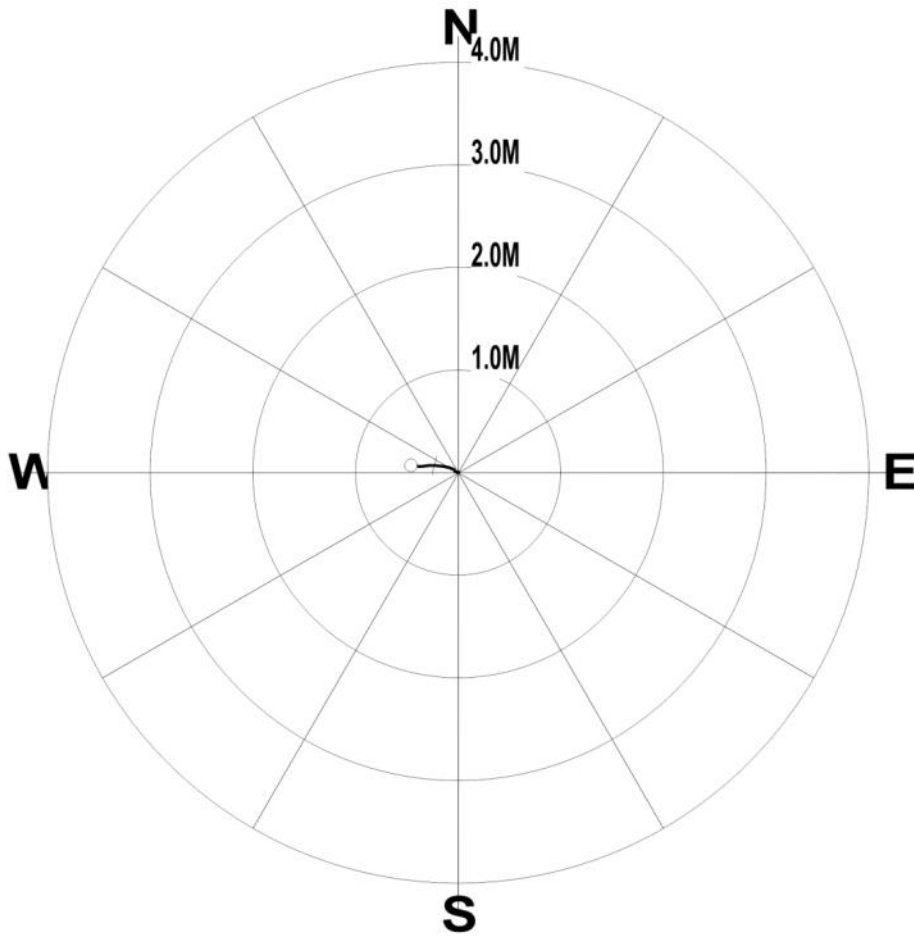
# Deltares

## PLAN VIEW COMPU-LOG DEVIATION

CLIENT:  
LOCATION: APPINGEDAM  
HOLE ID: 8DEV  
DATE OF LOG: 07/24/15  
PROBE: 9622C 1056



SCALE: 1 M/CM  
TRUE DEPTH: 26.99 M  
AZIMUTH: 278.8  
DISTANCE: 0.5 M  
+ = 20 M INCR  
○ = BOTTOM OF HOLE

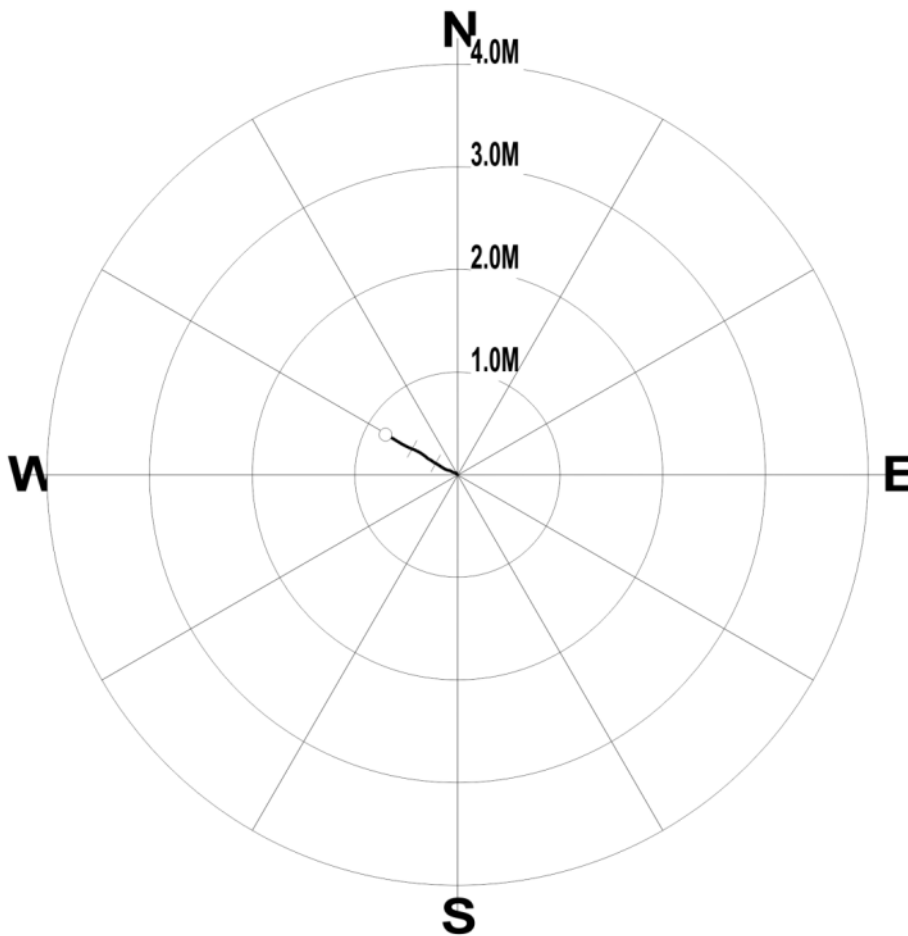


## PLAN VIEW COMPU-LOG DEVIATION

CLIENT:  
LOCATION: APPINGEDAM  
HOLE ID: 9DEV  
DATE OF LOG: 07/24/15  
PROBE: 9622C 1056

  
MAG DECL: 3.6

SCALE: 1 M/CM  
TRUE DEPTH: 27.94 M  
AZIMUTH: 299.4  
DISTANCE: 0.8 M  
+ = 10 M INCR  
○ = BOTTOM OF HOLE



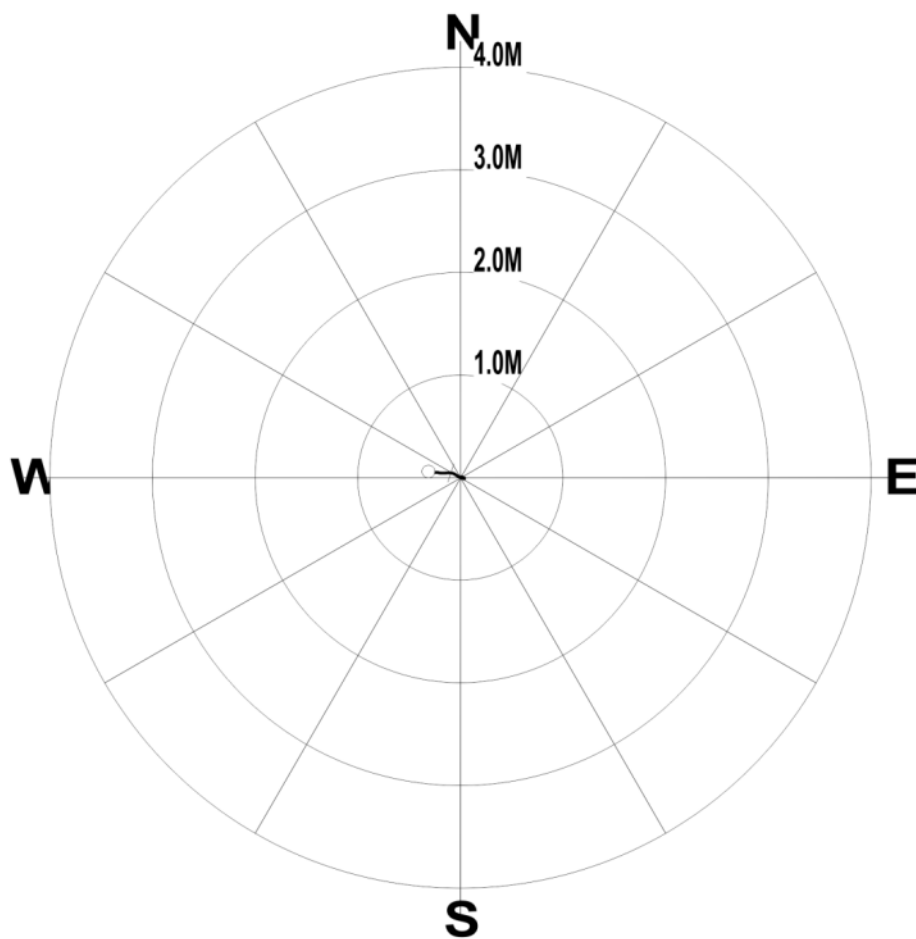
# Deltares

## PLAN VIEW COMPU-LOG DEVIATION

CLIENT:  
LOCATION: UITHUIZEN  
HOLE ID: 2  
DATE OF LOG: 07/10/15  
PROBE: 9622C 1056



SCALE: 1 M/CM  
TRUE DEPTH: 28.04 M  
AZIMUTH: 281.3  
DISTANCE: 0.3 M  
+ = 20 M INCR  
○ = BOTTOM OF HOLE

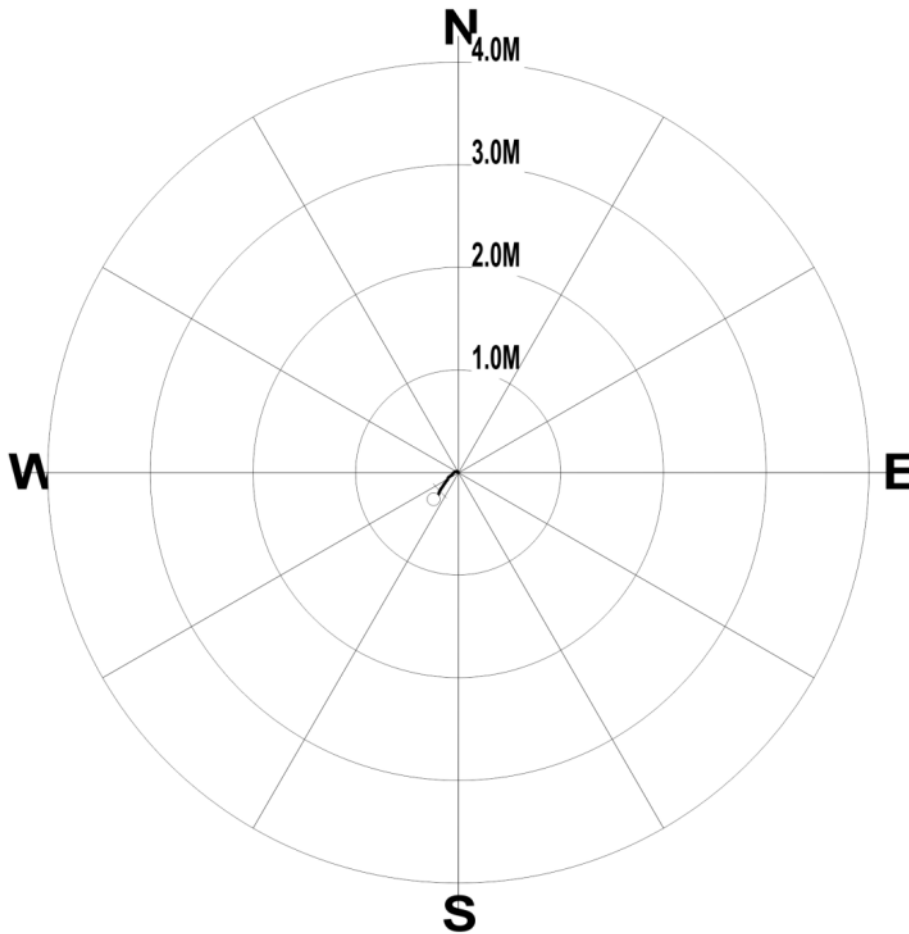


## PLAN VIEW COMPU-LOG DEVIATION

CLIENT:  
LOCATION: UITHUIZEN  
HOLE ID: 3  
DATE OF LOG: 07/10/15  
PROBE: 9622C 1056

  
MAG DECL: 3.6

SCALE: 1 M/CM  
TRUE DEPTH: 28.04 M  
AZIMUTH: 222.1  
DISTANCE: 0.3 M  
+ = 20 M INCR  
○ = BOTTOM OF HOLE





## D SCPT locations and station codes

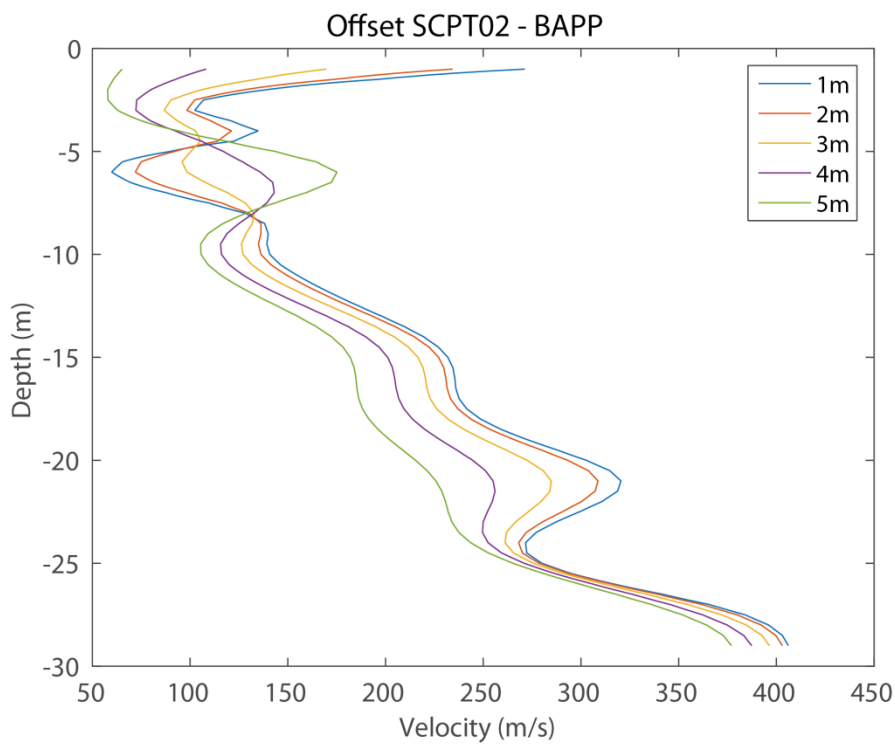
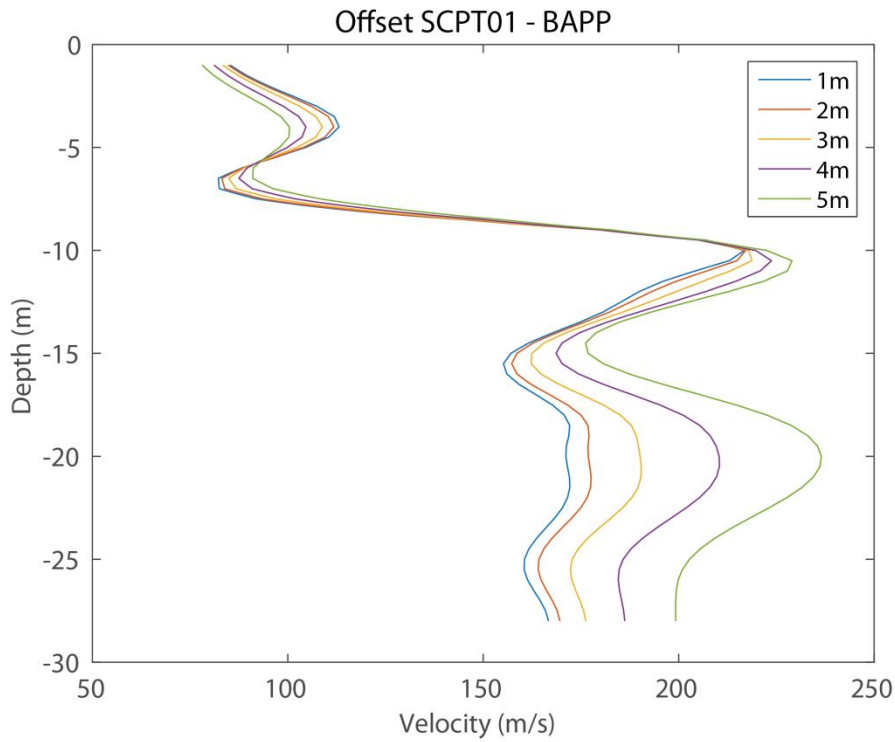
Table D.1 Coordinates of SCPTs and station codes.

(S)CPT code	Station code	Town	(S)CPT code Wiertsema	X (RD)	Y (RD)	Z (m relative to NAP)
CPT201	BFB2	Kolham	201 Kolham	247119.22	578615.36	-0.170
CPT202	BFB2	Kolham	202 Kolham	247119.33	578590.64	-0.030
CPT203	BFB2	Kolham	203 Kolham	247119.58	578565.15	-0.070
CPT204	BFB2	Kolham	204 Kolham	247119.55	578543.22	-0.060
SCPT01	BAPP	Appingedam	DKPS001	251323.25	592977.15	-1.016
SCPT02	BAPP	Appingedam	DKMS002	251393.71	592935.83	-1.102
SCPT03	BWSE	Westeremden	DKPS003	243046.52	595820.66	0.364
SCPT04	BWSE	Westeremden	DKPS004	242978.64	595873.06	0.132
SCPT05	BZN2	Zeerijp	5 Zeerijp	246138.32	597537.37	0.570
SCPT06	BZN2	Zeerijp	6 Zeerijp	246153.25	597564.53	0.500
SCPT07	BWIR	Wirdum	7 Wirdum	248330.93	593811.69	-0.520
SCPT08	BUHZ	Uithuizen	8 Uithuizen	240538.57	603027.21	1.810
SCPT09	BHKS	Garrelsw eer	9 Garrelsw eer	248187.29	590337.60	-1.480
SCPT10	BOWW	Oosterwijdwerd	10 Oosterwijdwerd	249940.09	595822.76	1.900
SCPT11	BGAR	Gartshuizen	11 Garsthuizen	243072.37	598725.17	0.510
SCPT12	BOWW	Oosterwijdwerd	12 Oosterwijdwerd	249994.82	595977.10	-0.400
SCPT13	BMD1	Middelstum	13 Middelstum	238547.74	596407.28	2.340
SCPT14	BFB2	Kolham	14 Kolham	247122.28	578665.08	0.030
SCPT15	BFB2	Kolham	15 Kolham	247120.36	578518.33	-0.080
SCPT16	BONL	Oosternieland	16 Oosternieland	245882.31	602350.75	0.440
SCPT17	BHAR	Harkstede	17 Harkstede	243258.72	583356.34	-1.860
SCPT18	BMD1-2	Middelstum	18 Middelstum	238560.41	596735.55	0.550
SCPT19	BLOP	Loppersum	19 Loppersum	245504.47	595072.65	0.680
SCPT20	BWIR	Wirdum	20 Wirdum	248175.10	593921.60	2.170
SCPT21	BZN1	t Zandt	21 't Zand	247349.32	598603.80	1.490
SCPT22	BMD2	Middelstum	22 Middelstum	238959.63	597015.21	0.330
SCPT23	BWIN	Winneweer	23 Winneweer	245667.41	592356.91	-0.410
SCPT24	BKAN	Kantens	24 Kantens	239877.74	599764.05	0.390
SCPT25	BLOP	Loppersum	25 Loppersum	245523.99	595153.02	0.310
SCPT26	BSTD	Stedum	26 Stedum	241982.98	592245.98	-0.510
SCPT27	BUHZ	Uithuizen	27 Uithuizen	240279.10	602505.38	1.060

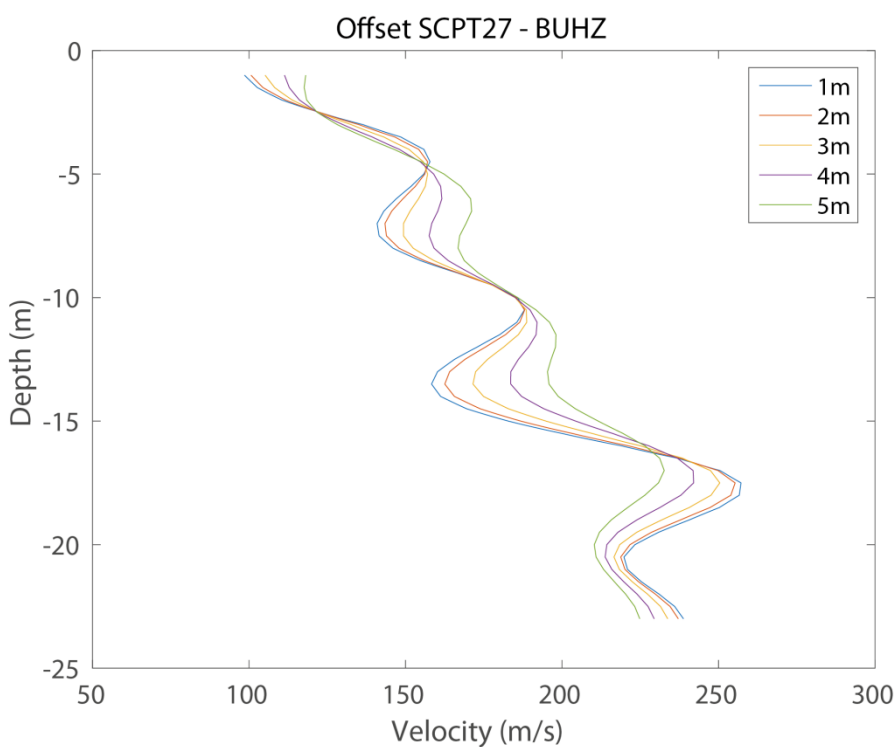
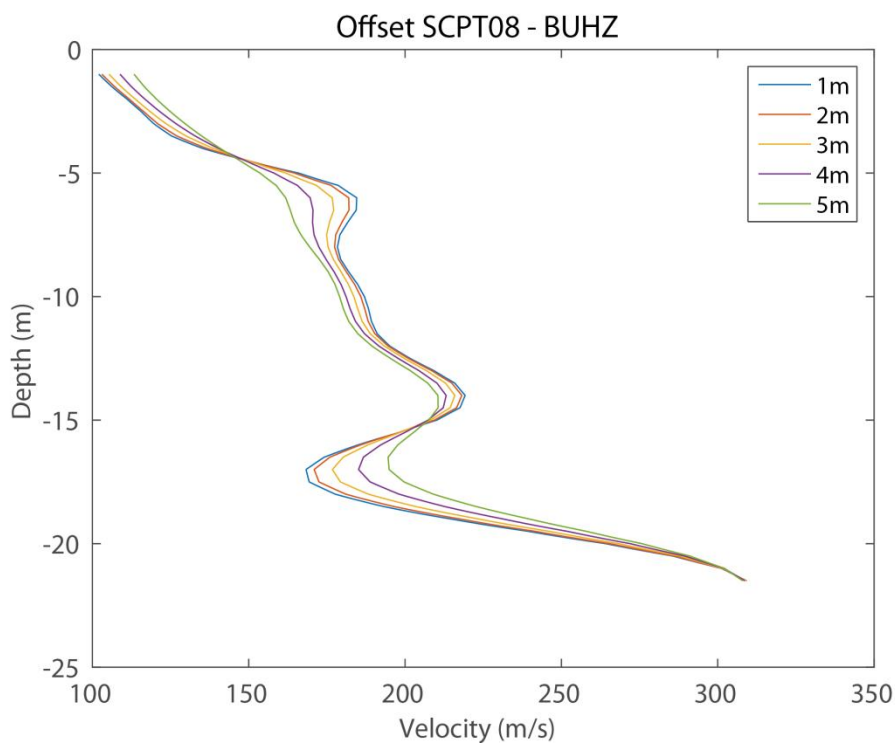


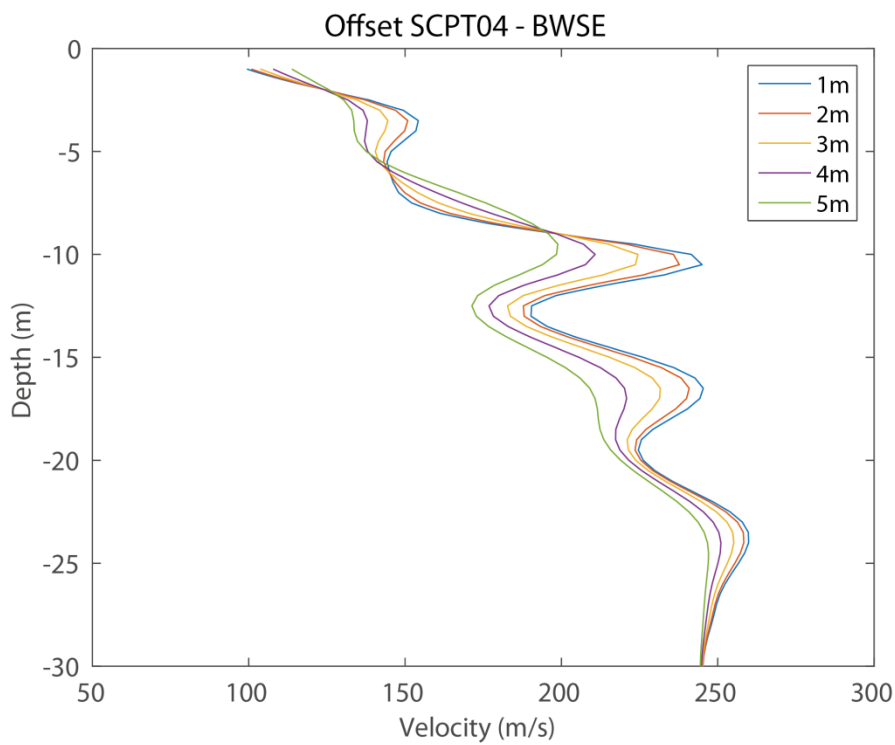
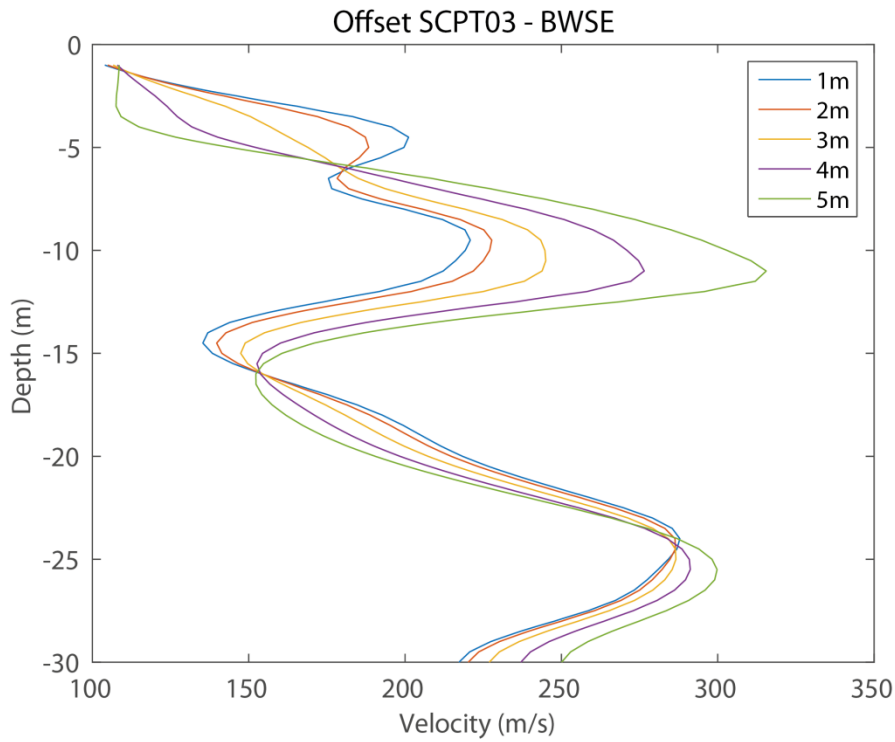
## E OSCPT profiles

This appendix presents the detailed OSCPT profiles of the first 5 m next to the SCPT location, based on the OSCPT tomograms.

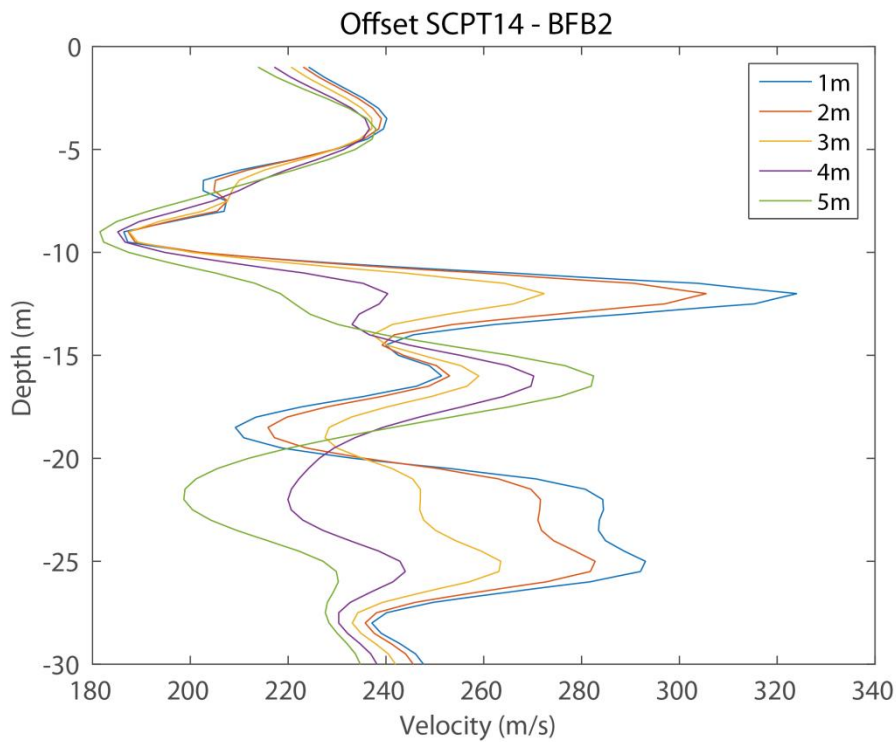


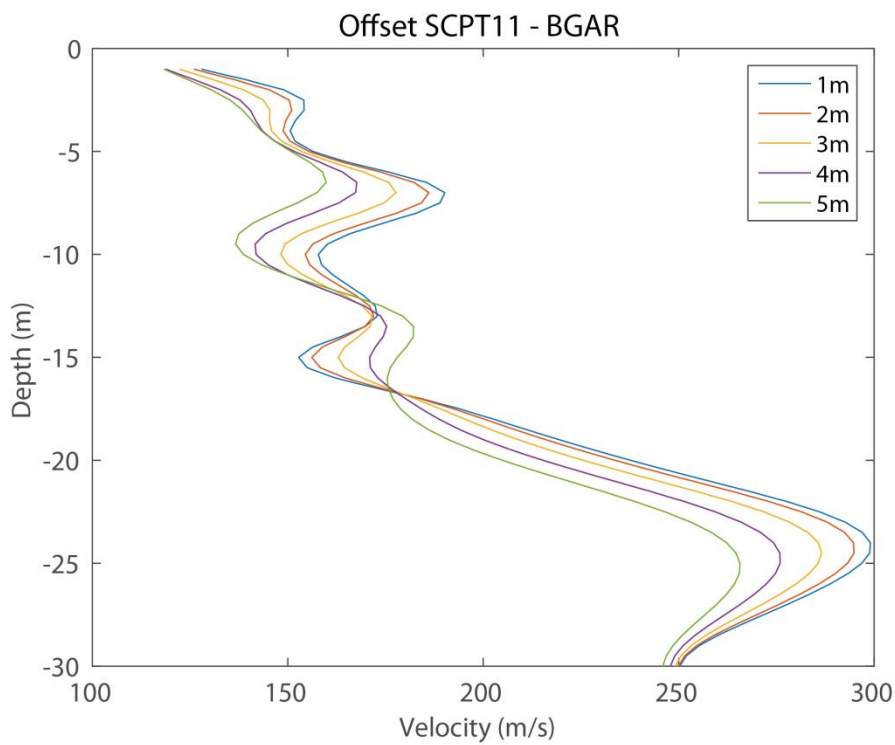
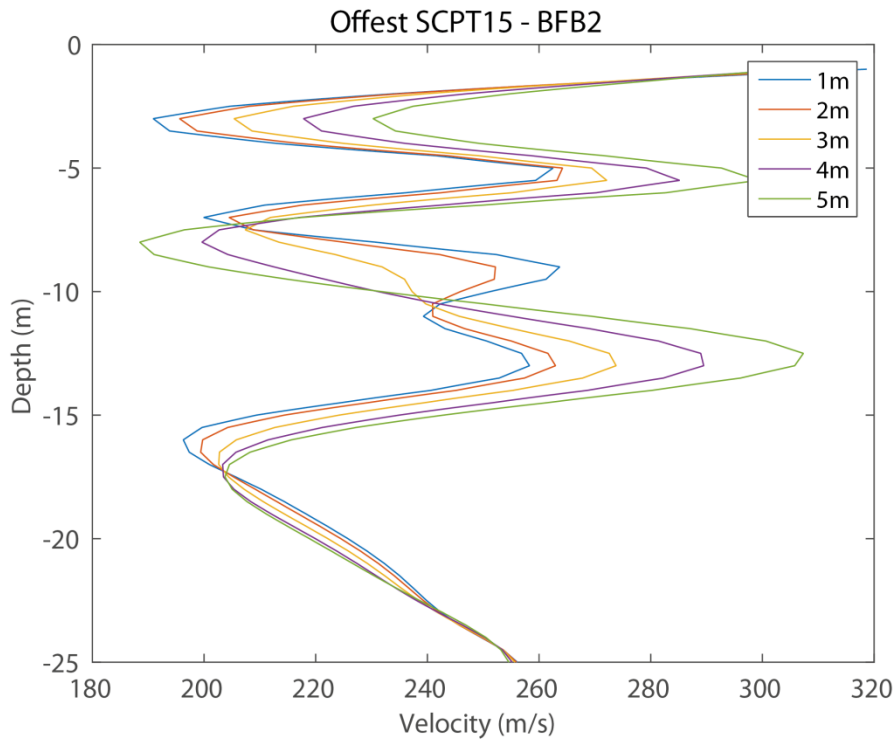
# Deltares



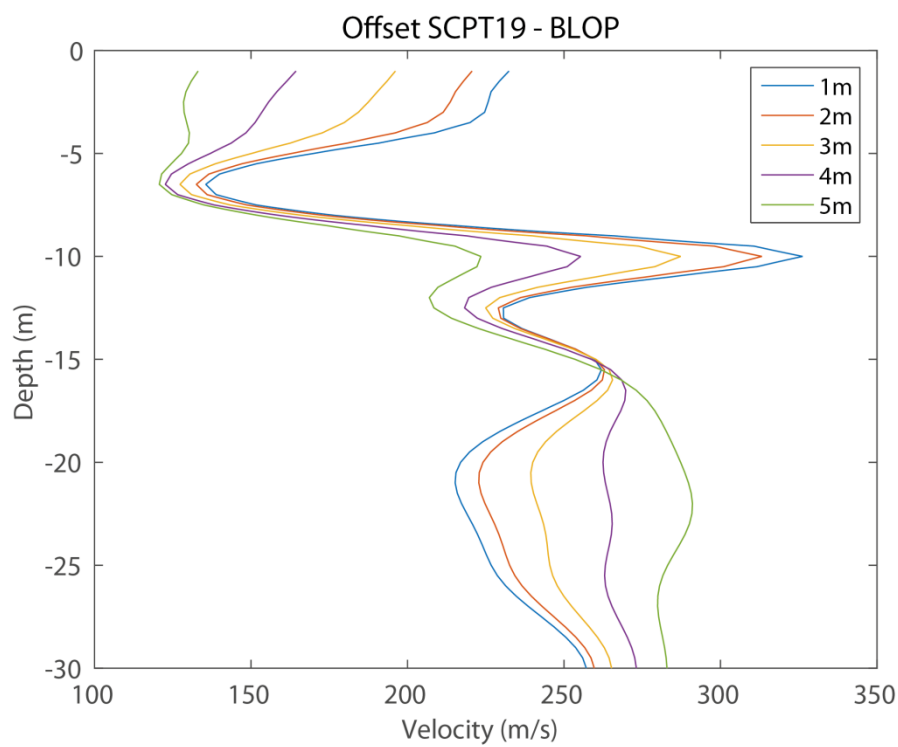
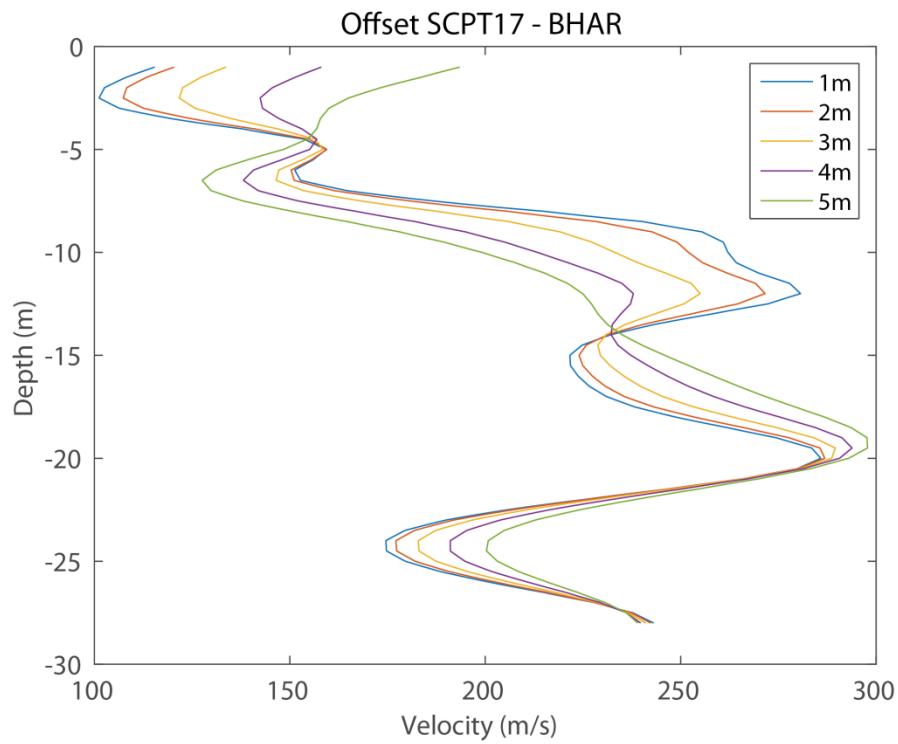


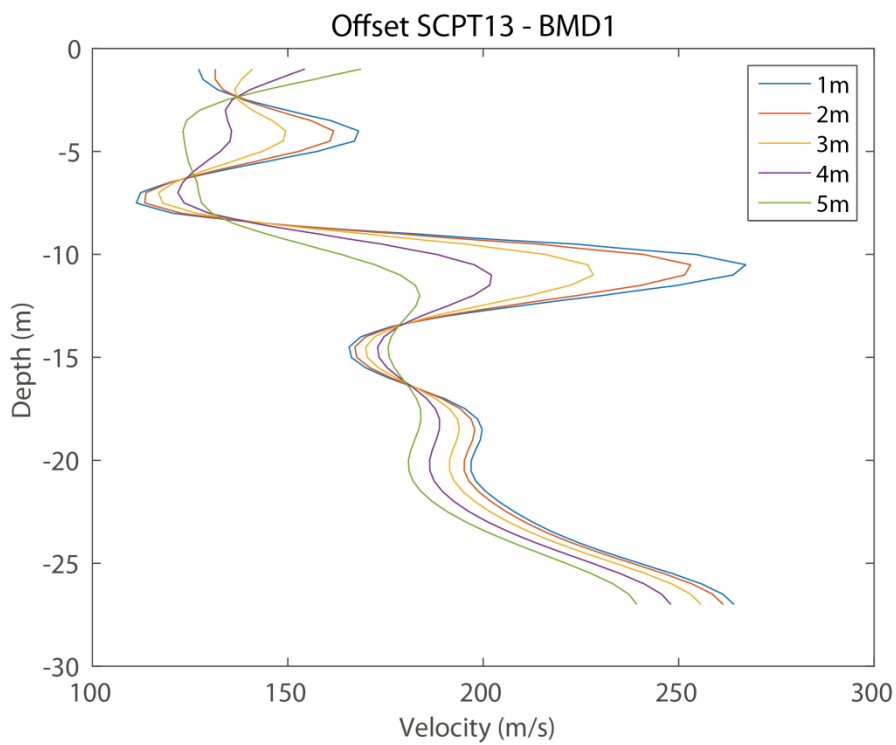
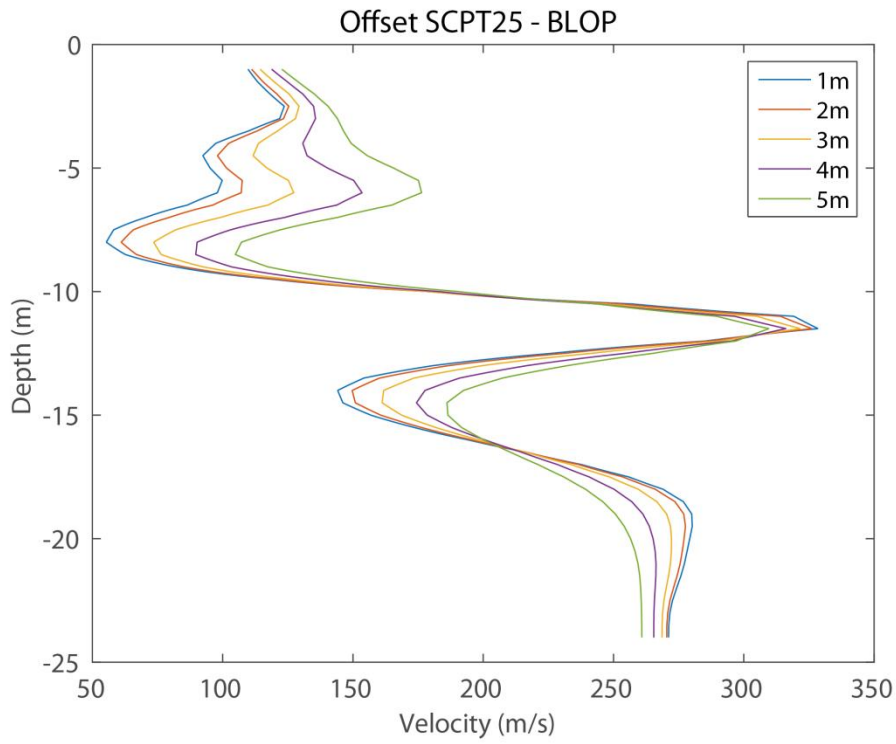
# Deltares



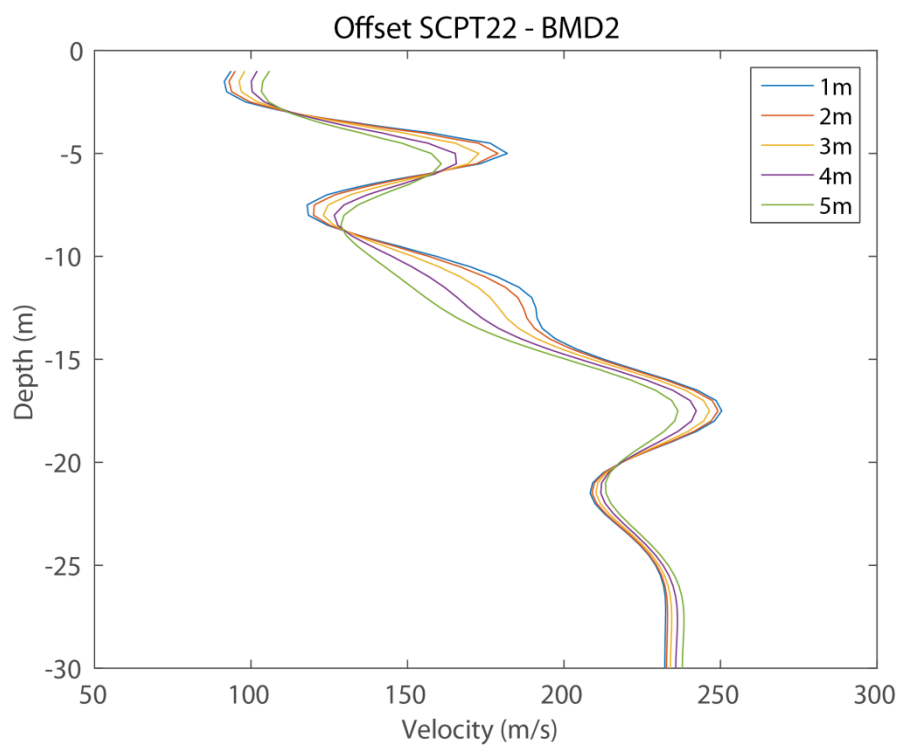
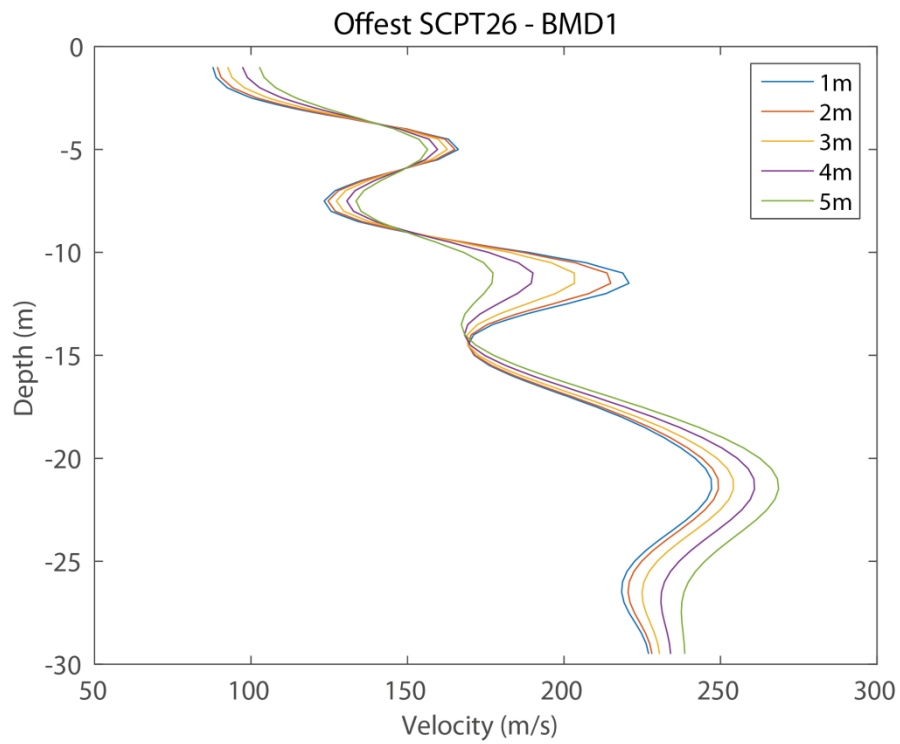


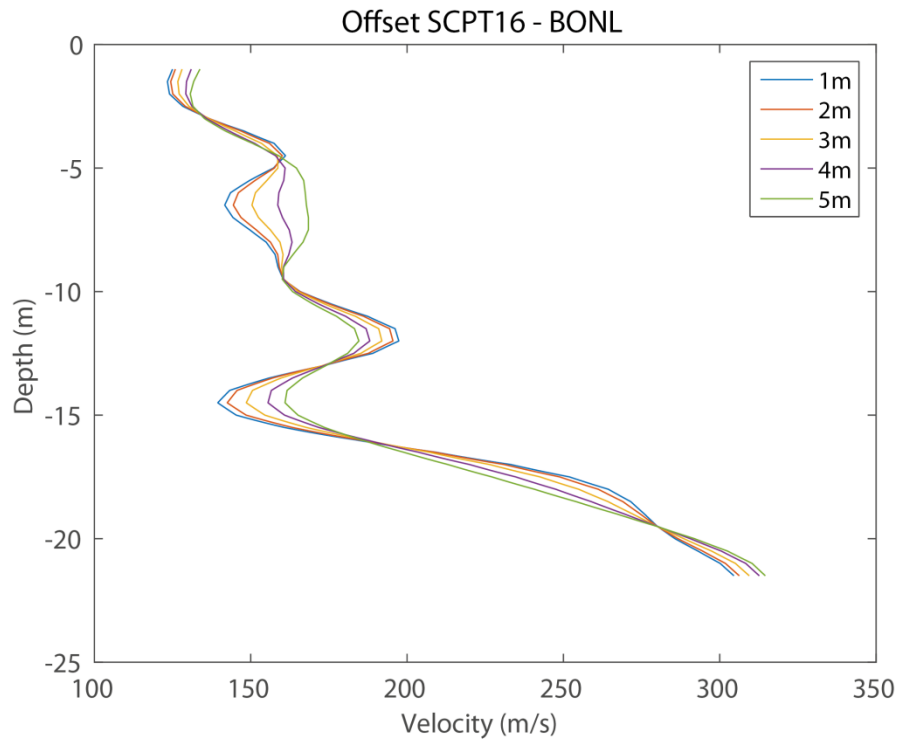
# Deltares



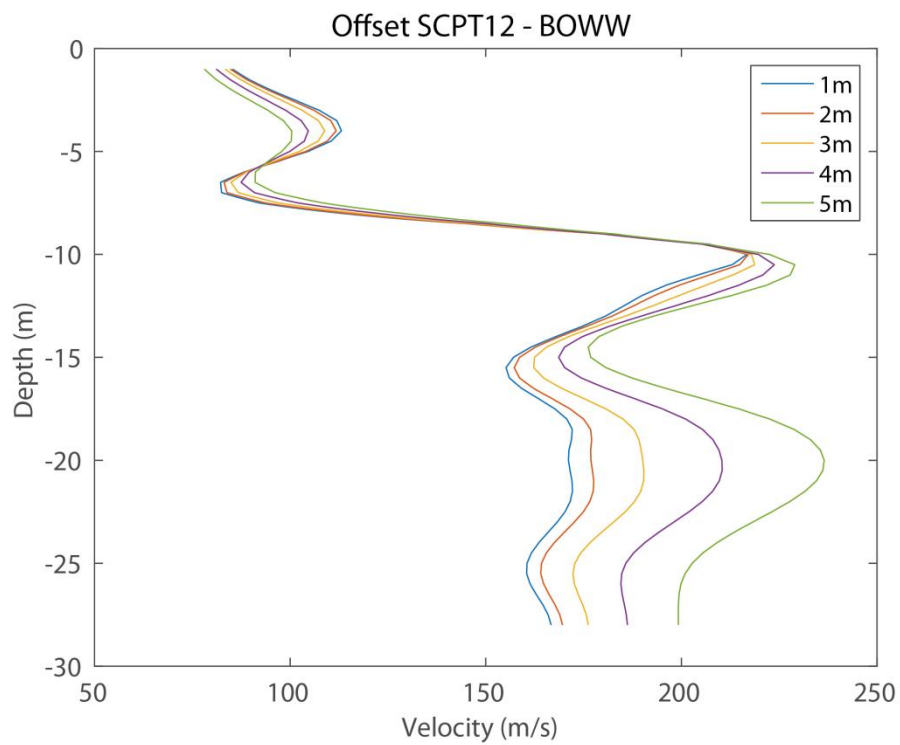
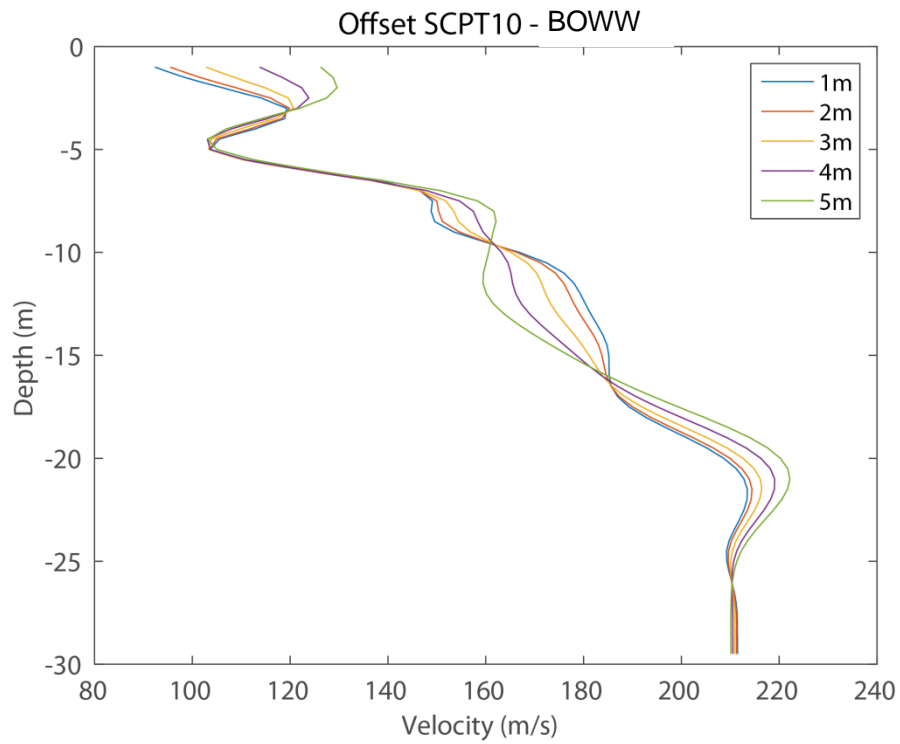


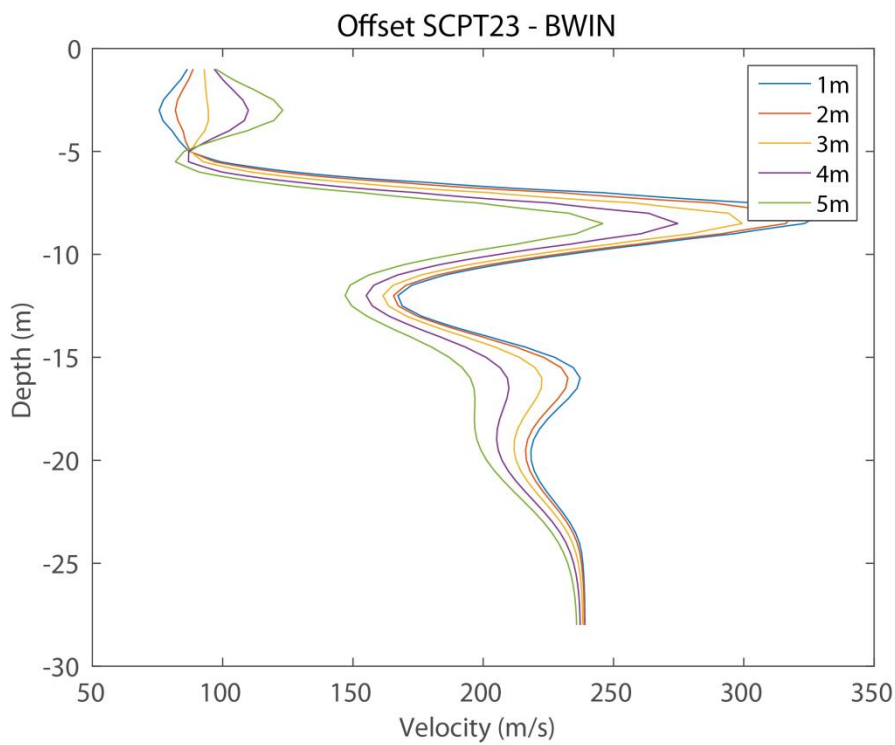
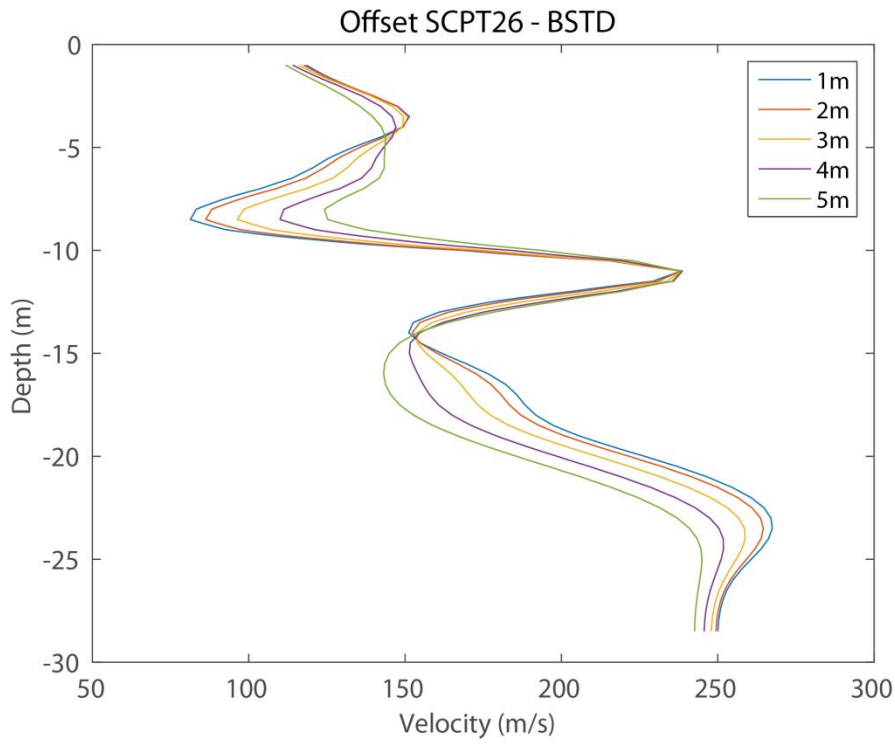
# Deltares



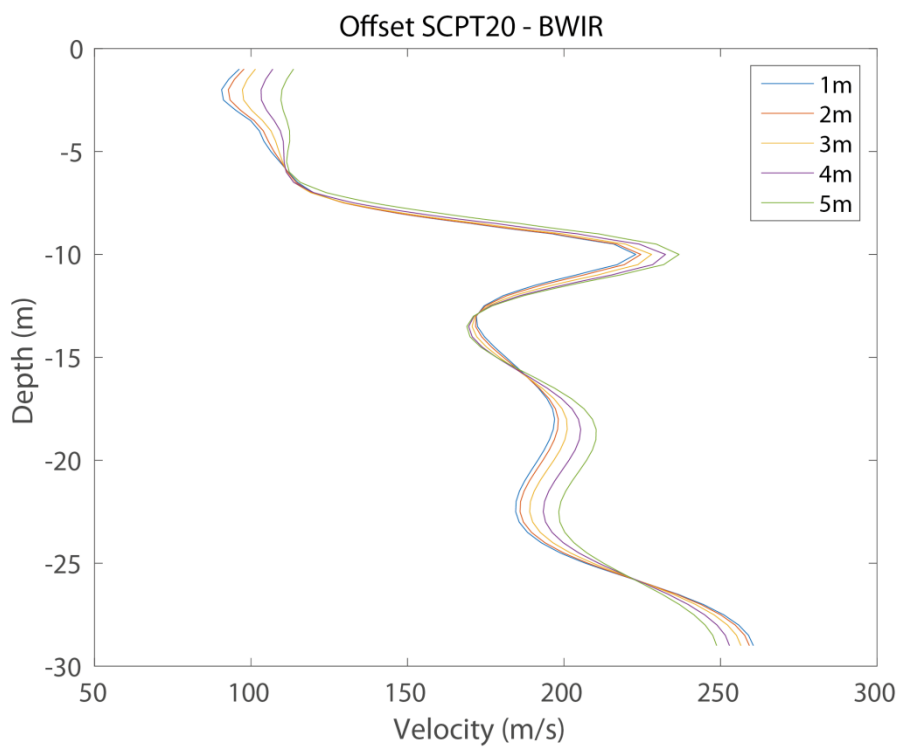
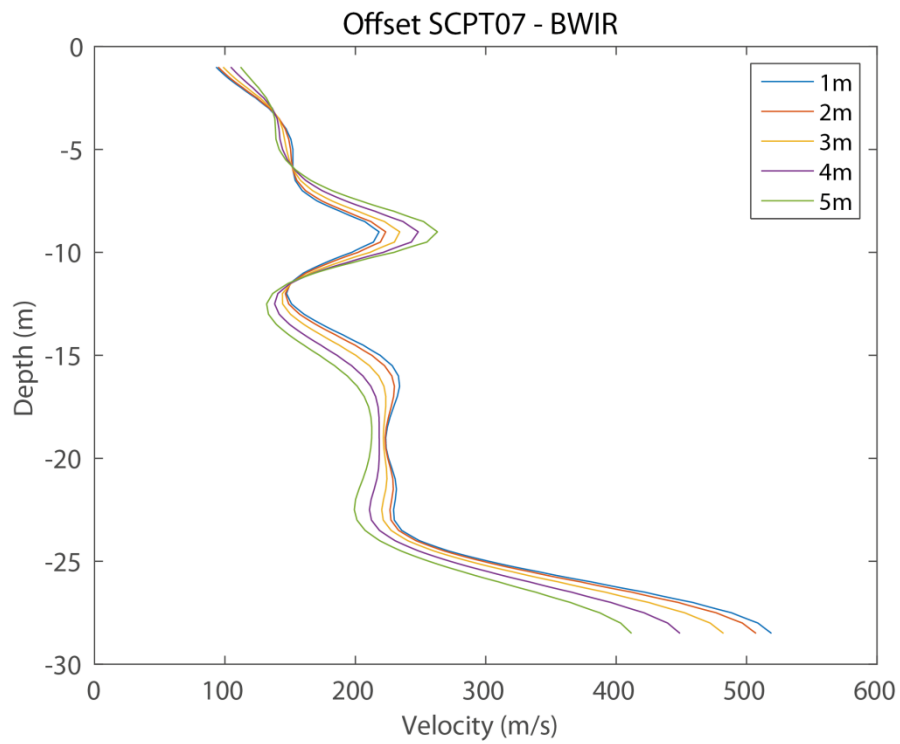


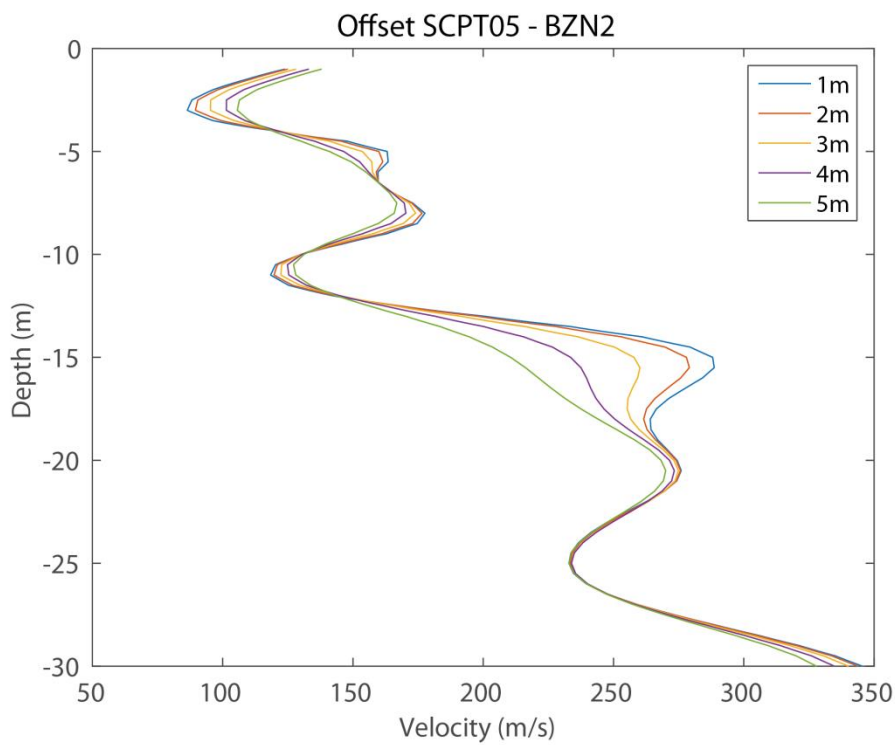
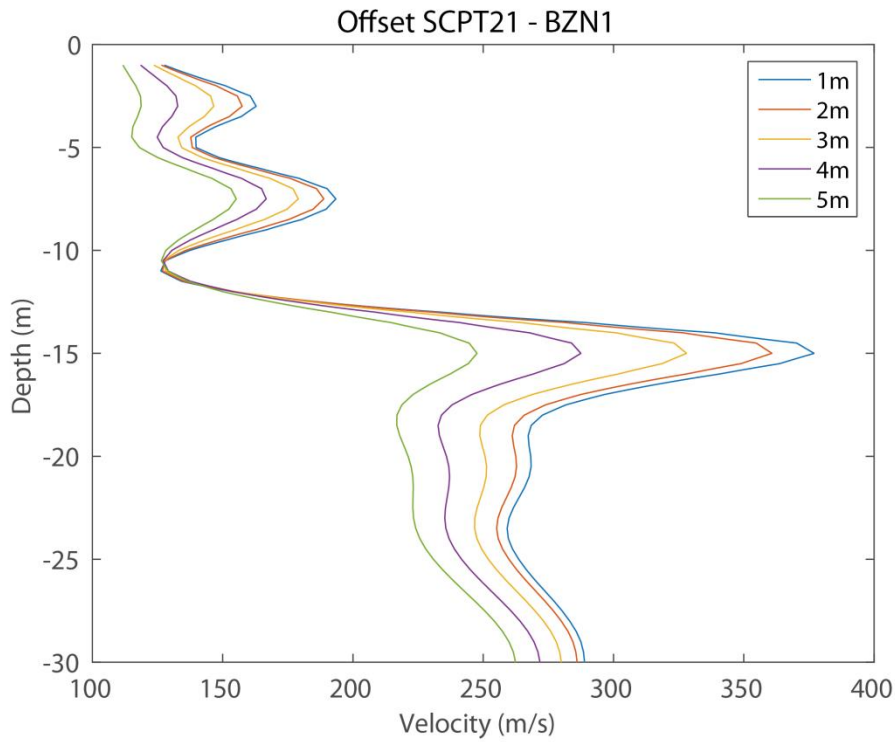
# Deltares





# Deltares



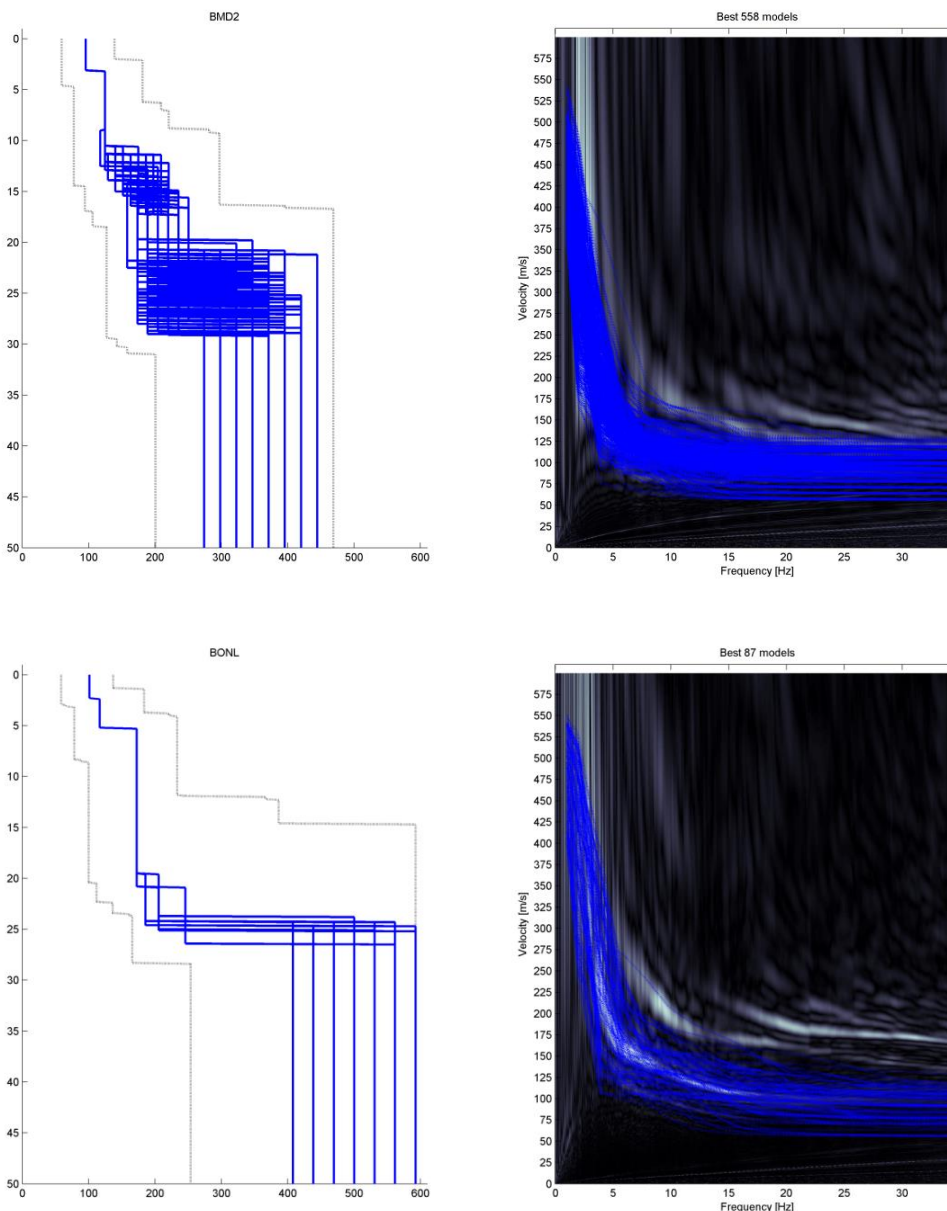




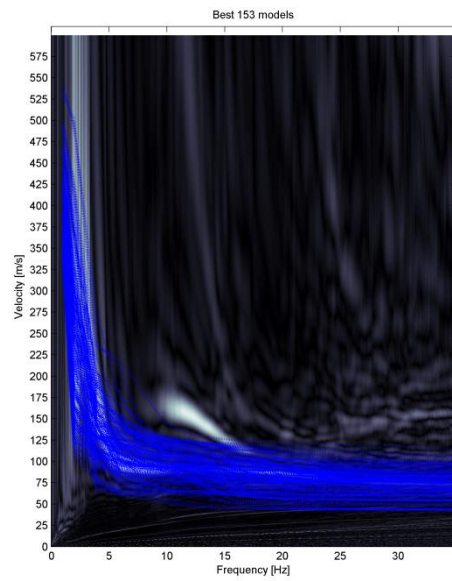
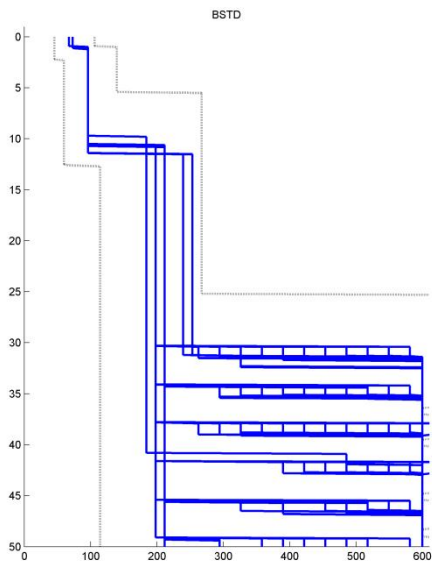
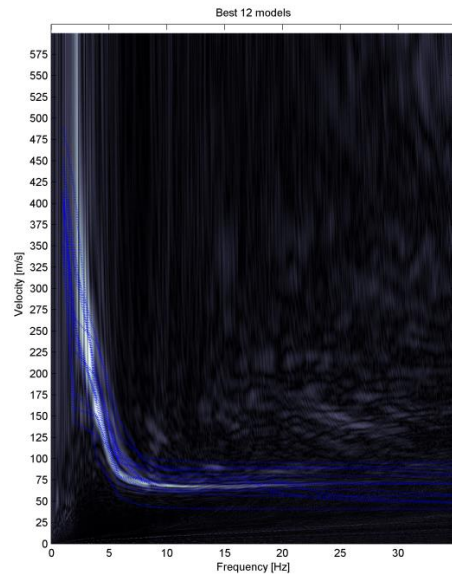
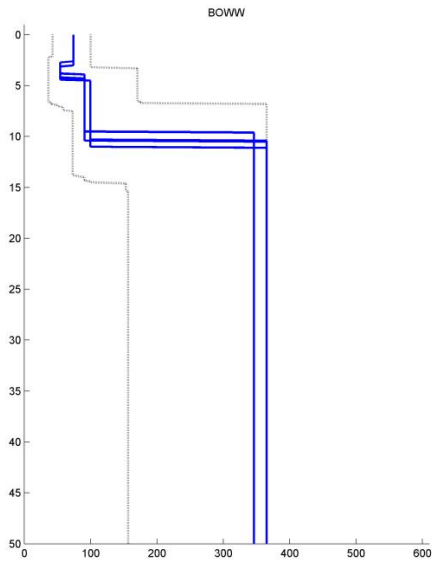
## F Dispersion fitting plots MASW 200m array

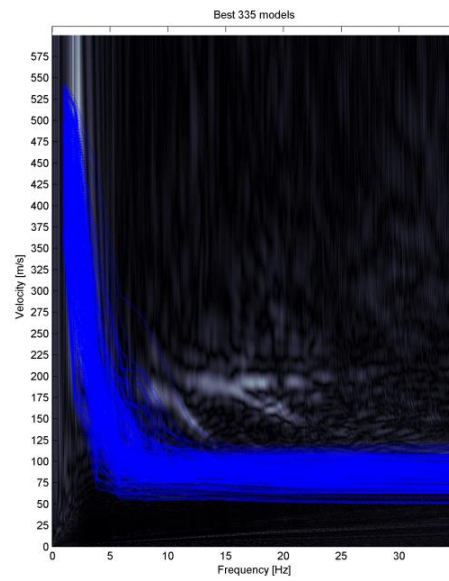
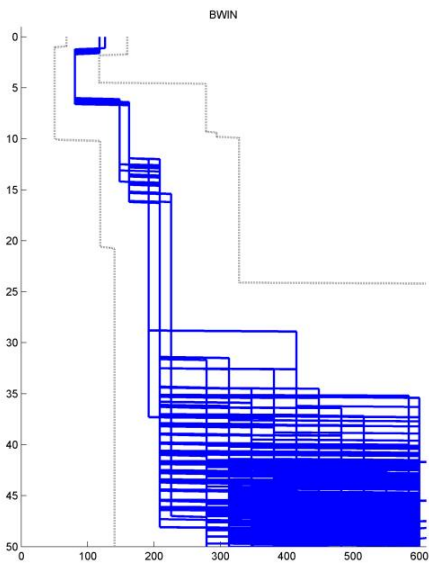
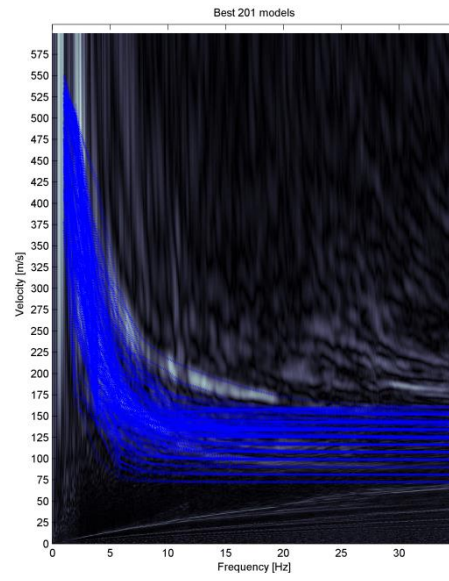
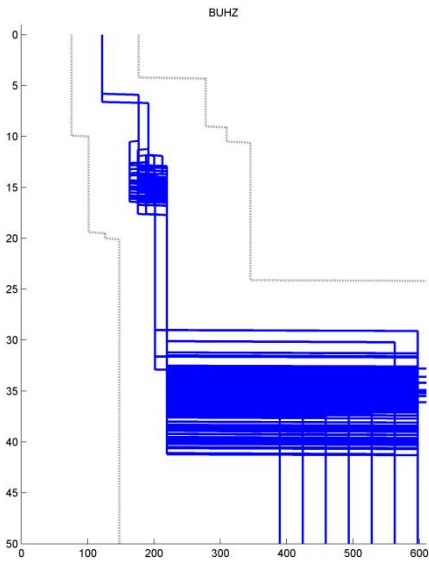
This appendix shows the top 1% (best fit) of the fitted models on top of the dispersion plots (right panels) and the resulting  $V_S$  models (left panels). Each curve represents a model which fits the dispersion plot. For each curve the misfit is calculated and the best 1% models are shown, the number varies greatly from location to location. This method is not optimal for fitting the higher modes. Therefore, we selected a hybrid approach using these models as a starting model and next determine with expert judgement and using a priori information to select the most likely model as presented in chapter 4.

The plots presented in this appendix show average velocity profile/models for the 200 m line.

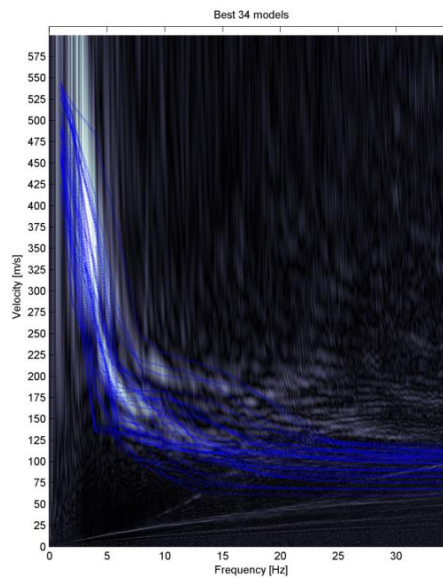
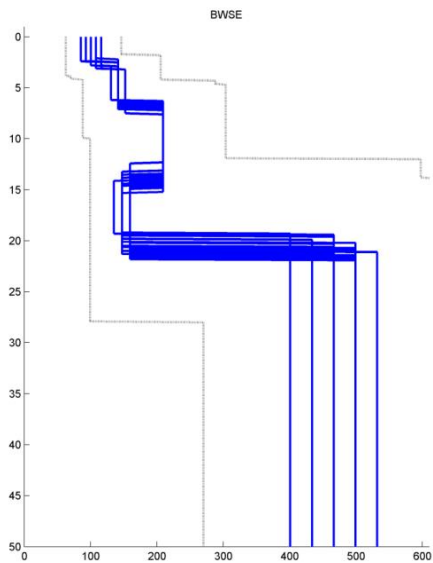
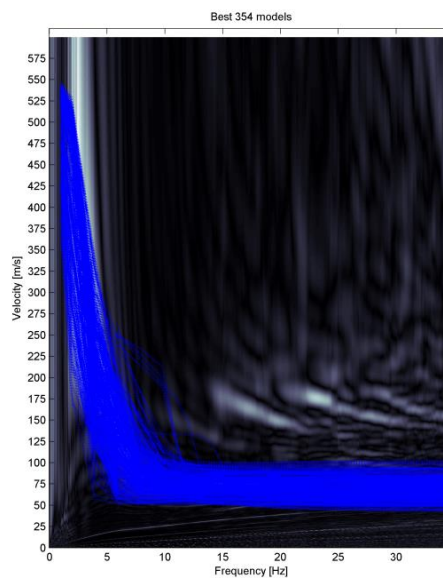
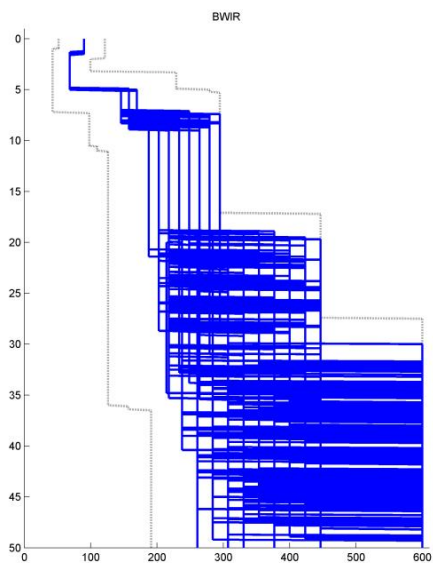


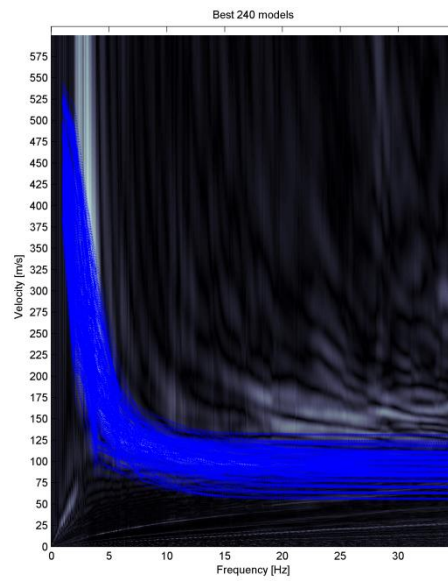
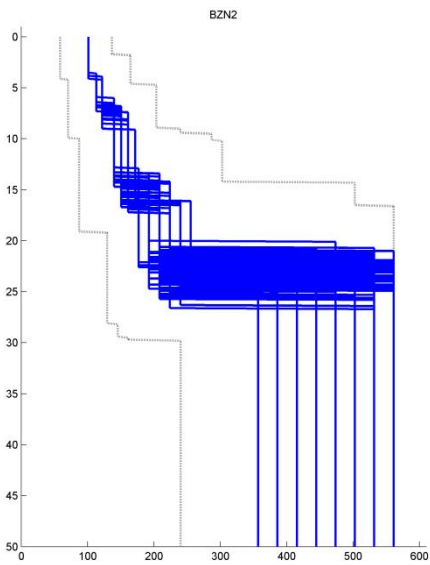
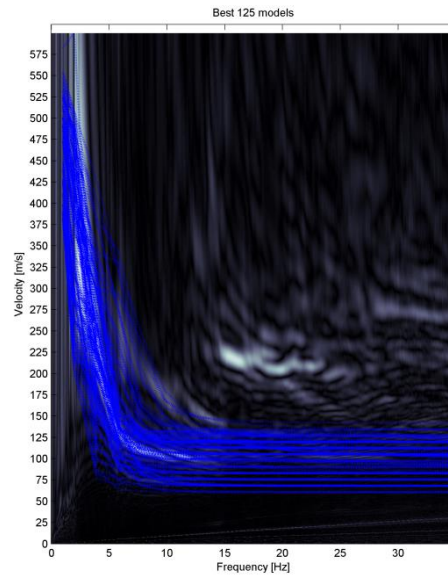
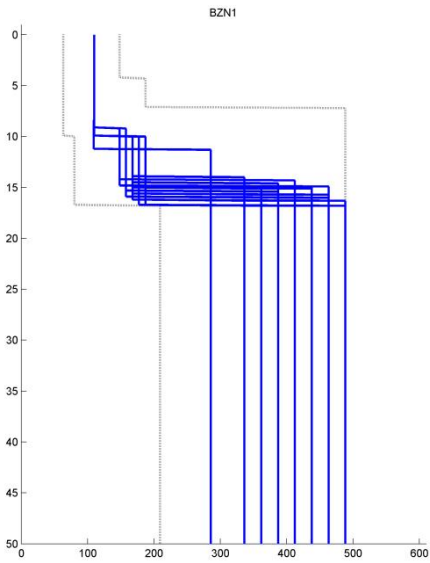
# Deltares



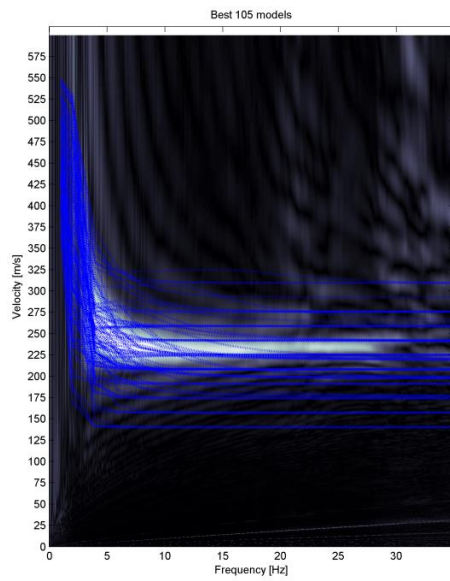
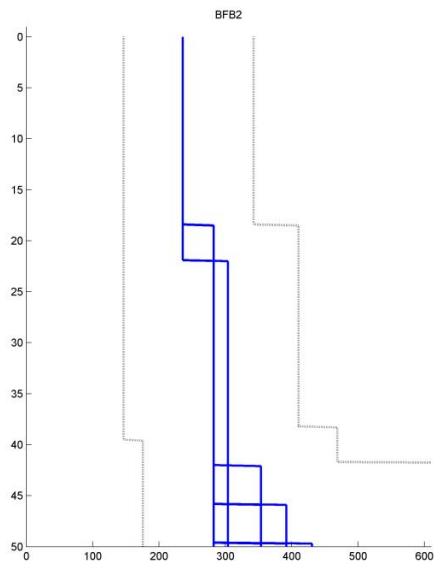
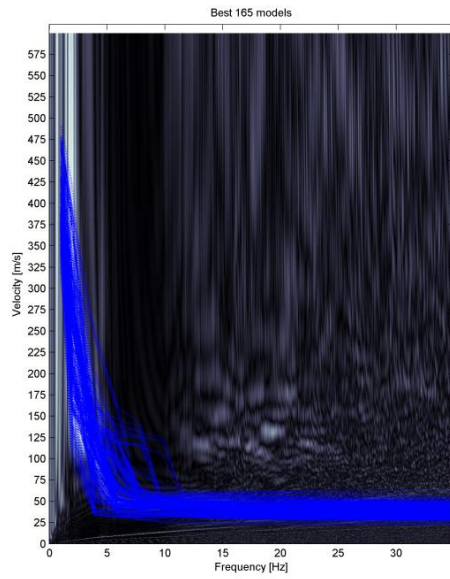
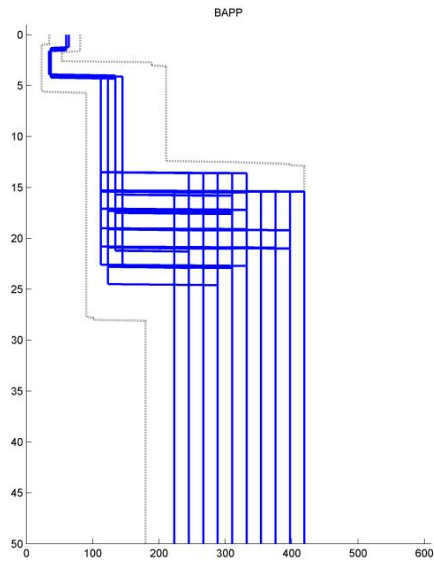


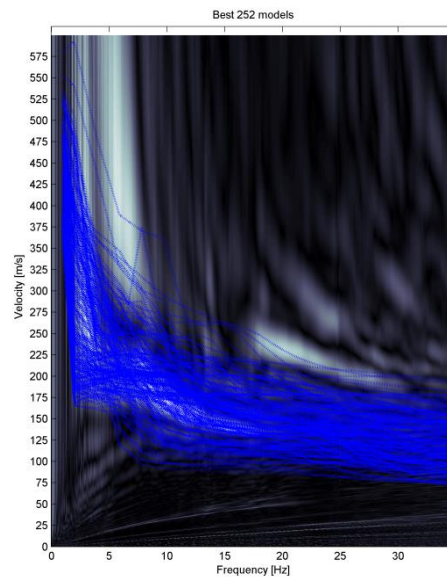
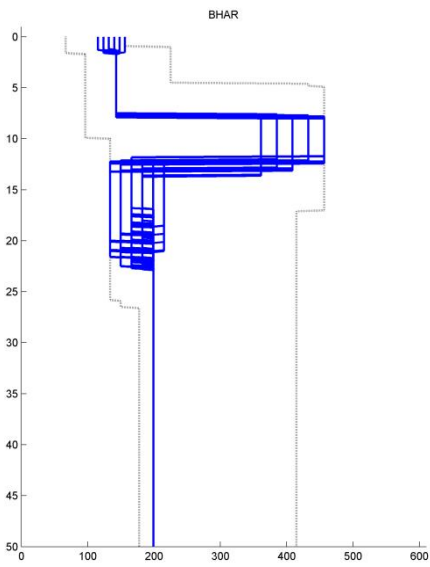
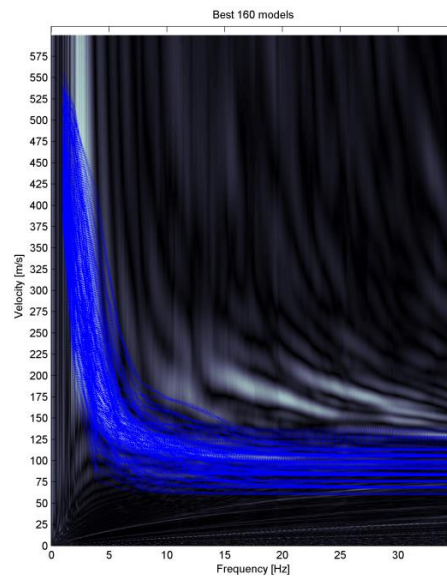
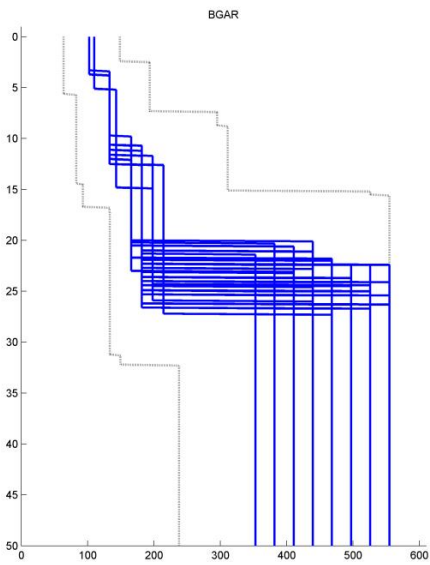
# Deltares



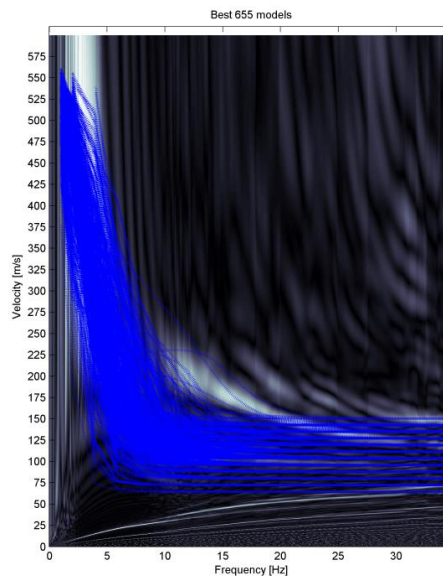
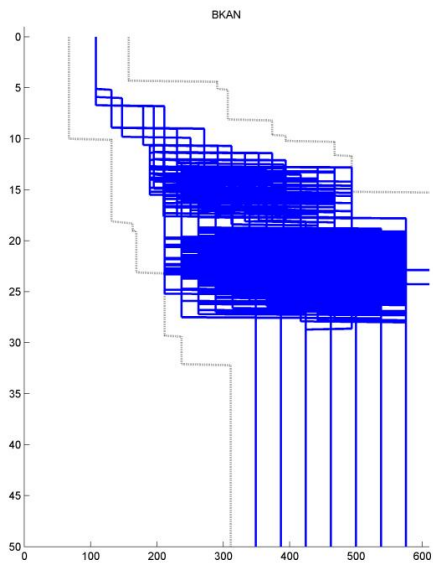
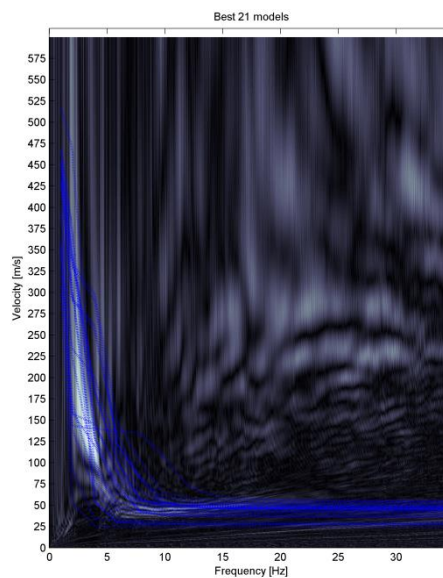
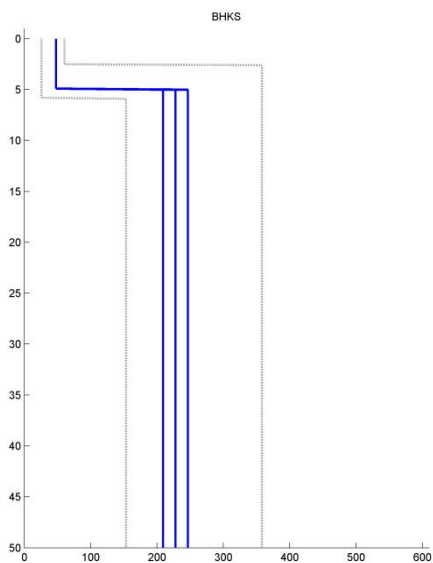


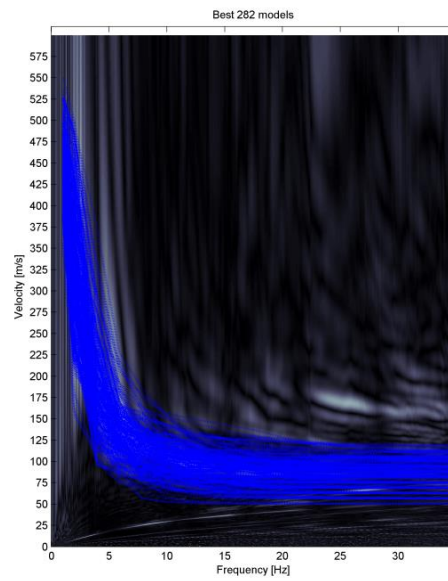
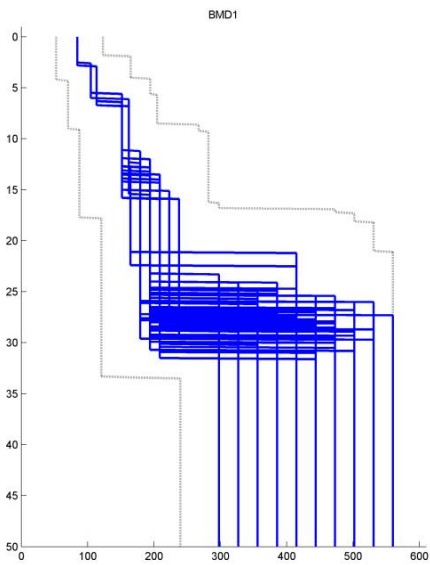
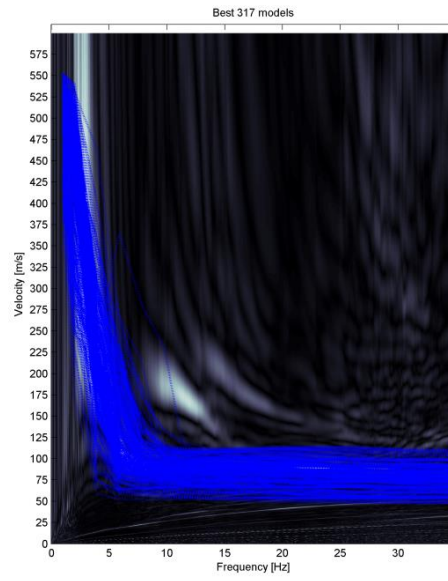
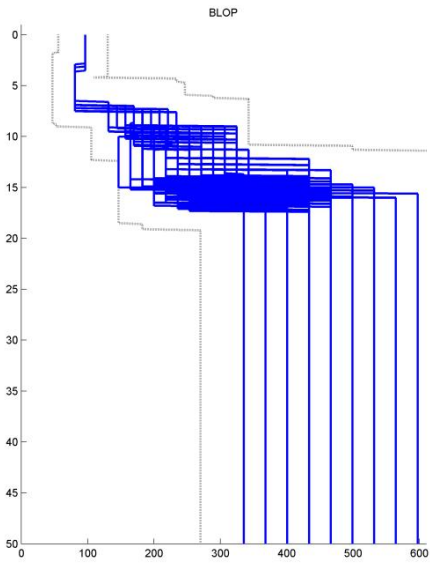
# Deltares





# Deltares







## G Dispersion envelopes CMPcc

In this appendix, the total envelope of energy for the CMPcc method (i.e. all energy from the 72 subsections) are plotted in these graphs. These can be regarded as average energy along the CMPcc array. However, interpretation of these graphs is not straightforward: Red parts indicate dispersions parts that are visible in ALL locations. This means that a completely red dispersion curve represents limited lateral variation along the CMPcc array. On the other hand, a dispersion curve that seems to split or fade out could indicate lateral variation. The colour axis always covers the range of values within the 72 subsections at that particular station.

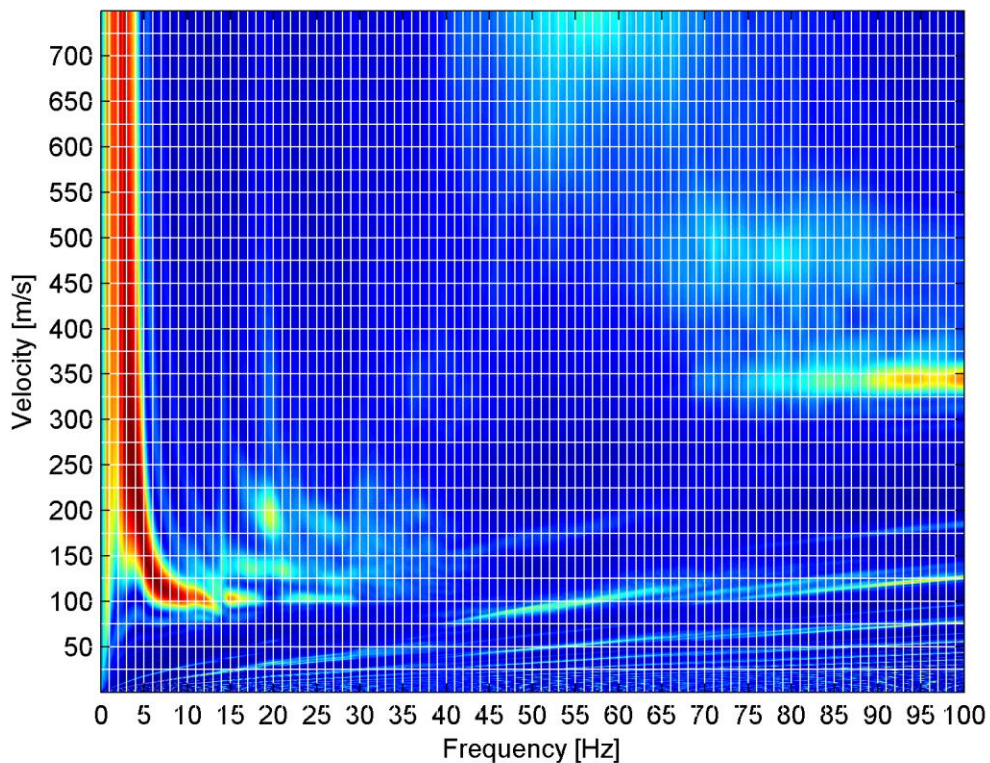


Figure G.1 BZN1

# Deltares

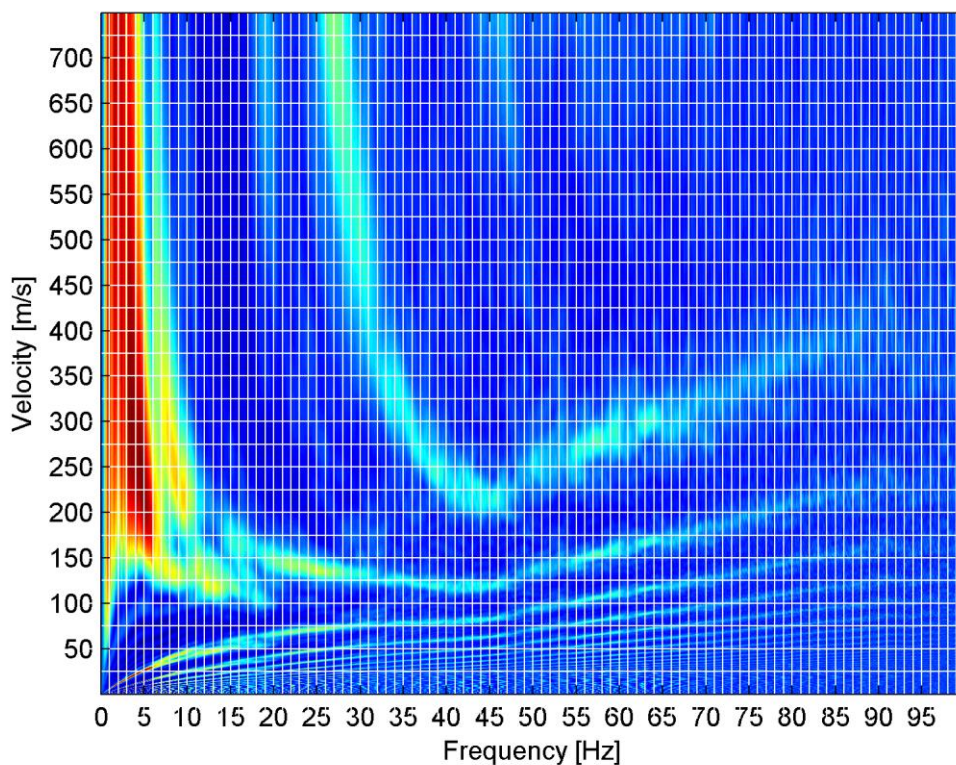


Figure G.2 BSWE

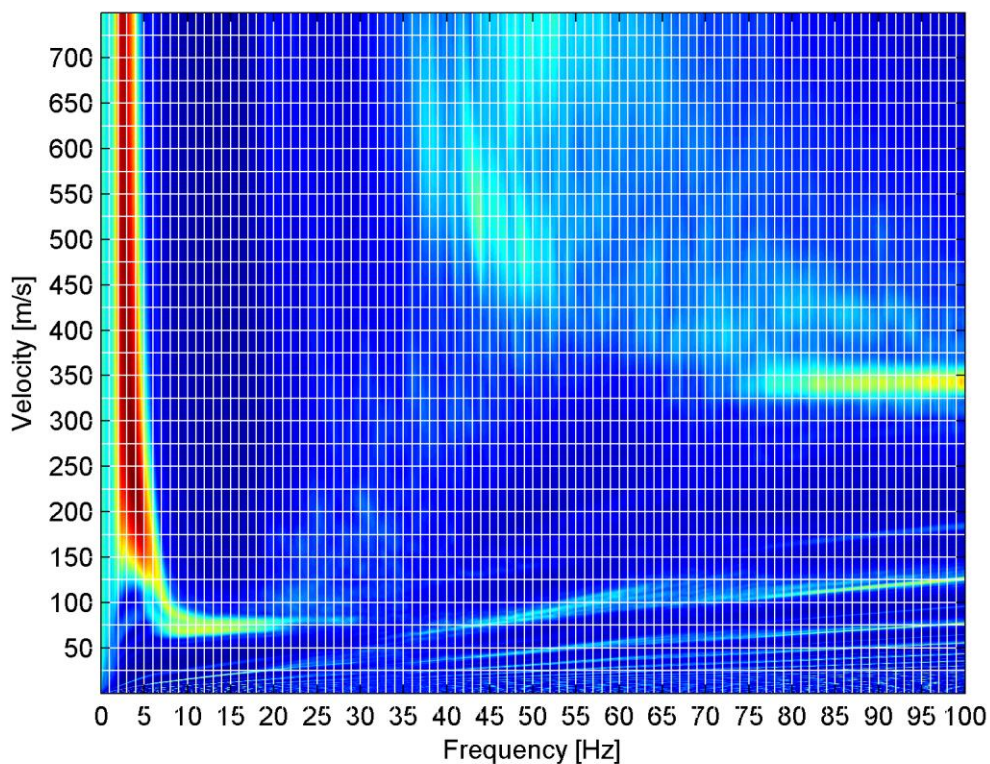


Figure G.3 BWIR

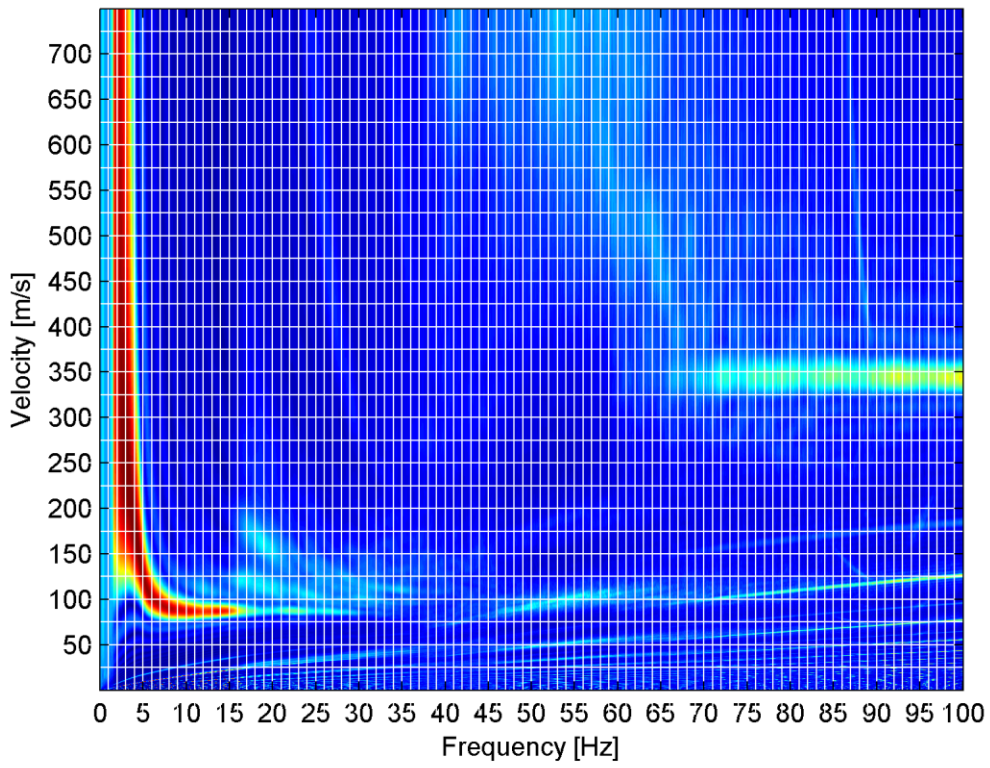


Figure G.4 BWIN

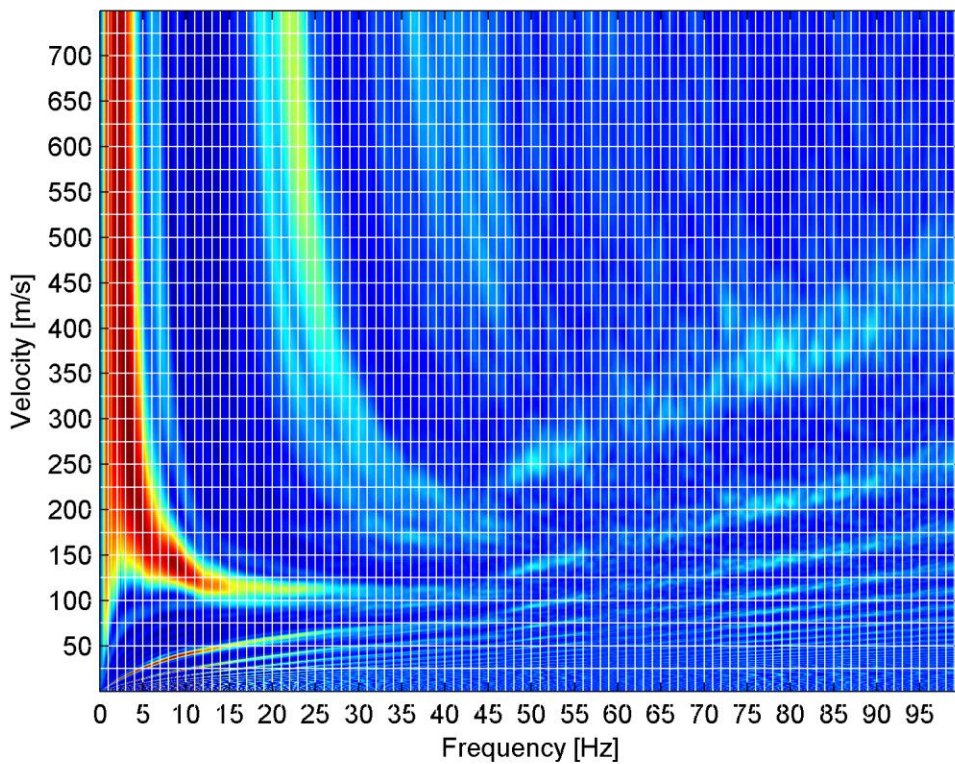


Figure G.5 BUHZ

# Deltares

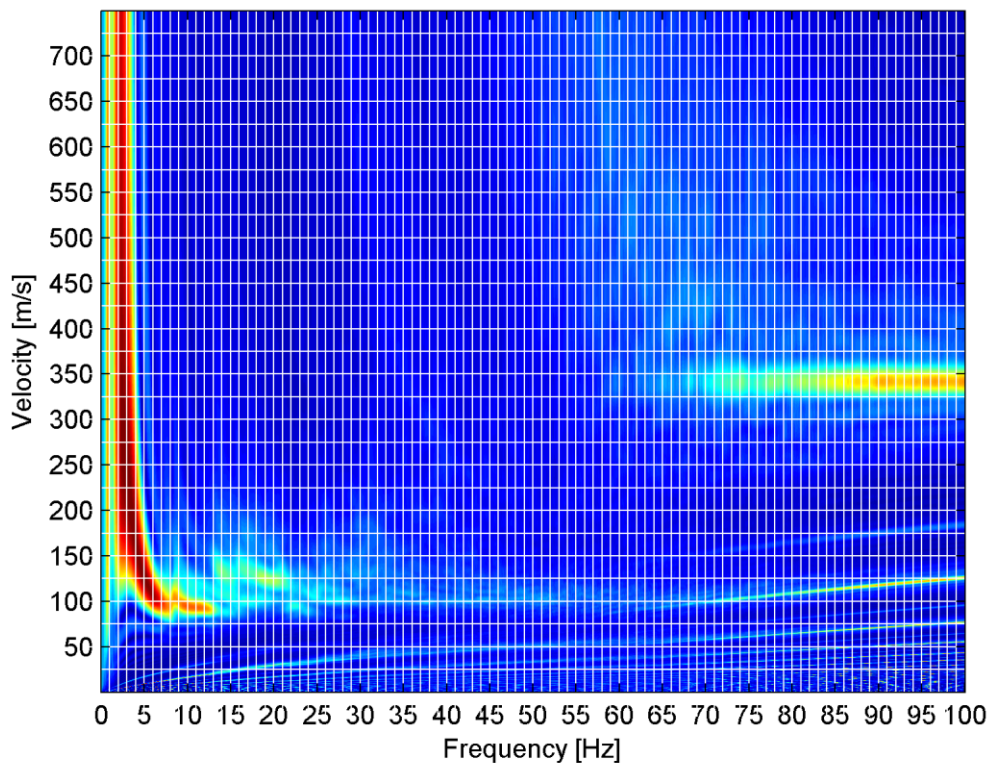


Figure G.6 BSTD

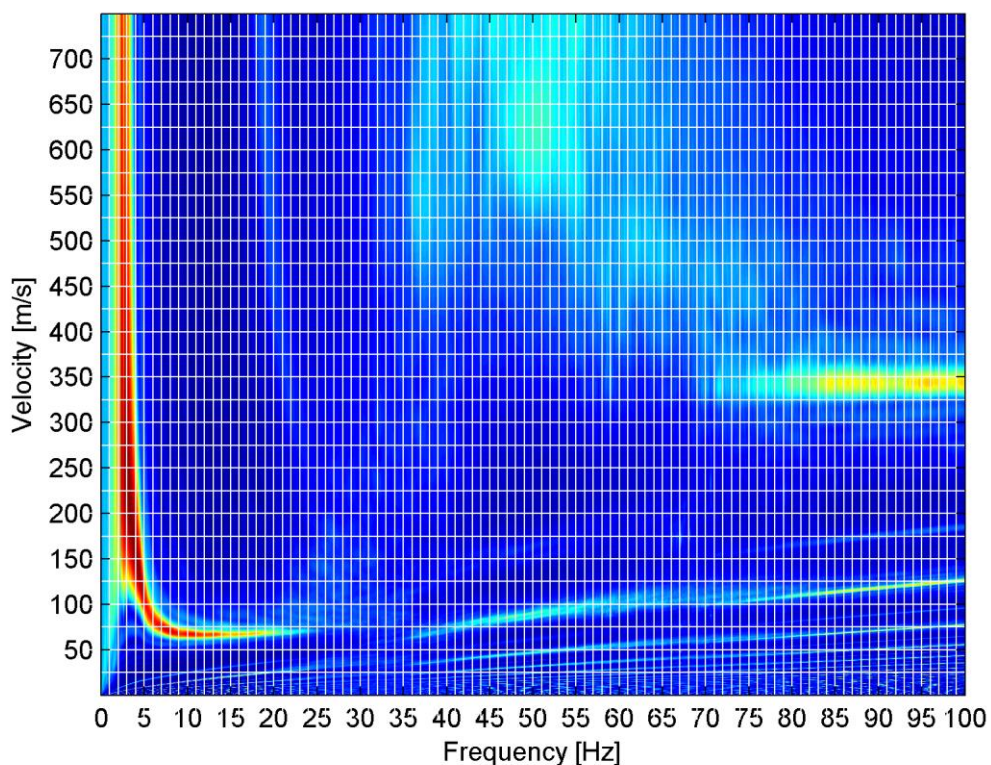


Figure G.7 BOWW

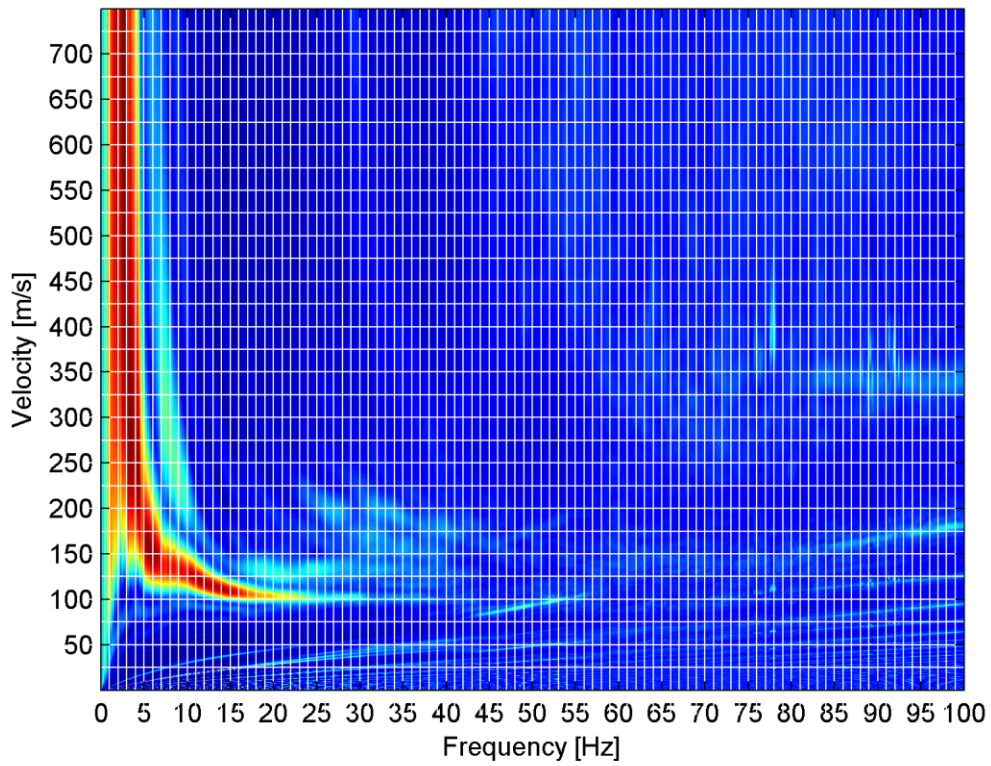


Figure G.8 B0NL

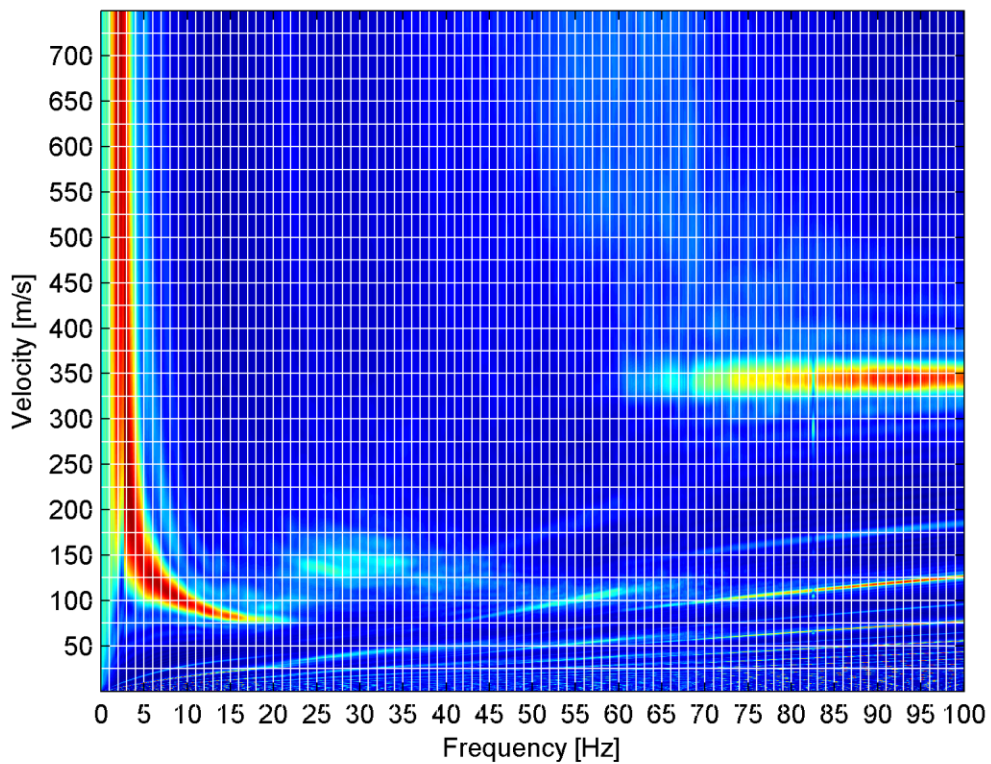


Figure G.9 BMD1

# Deltares

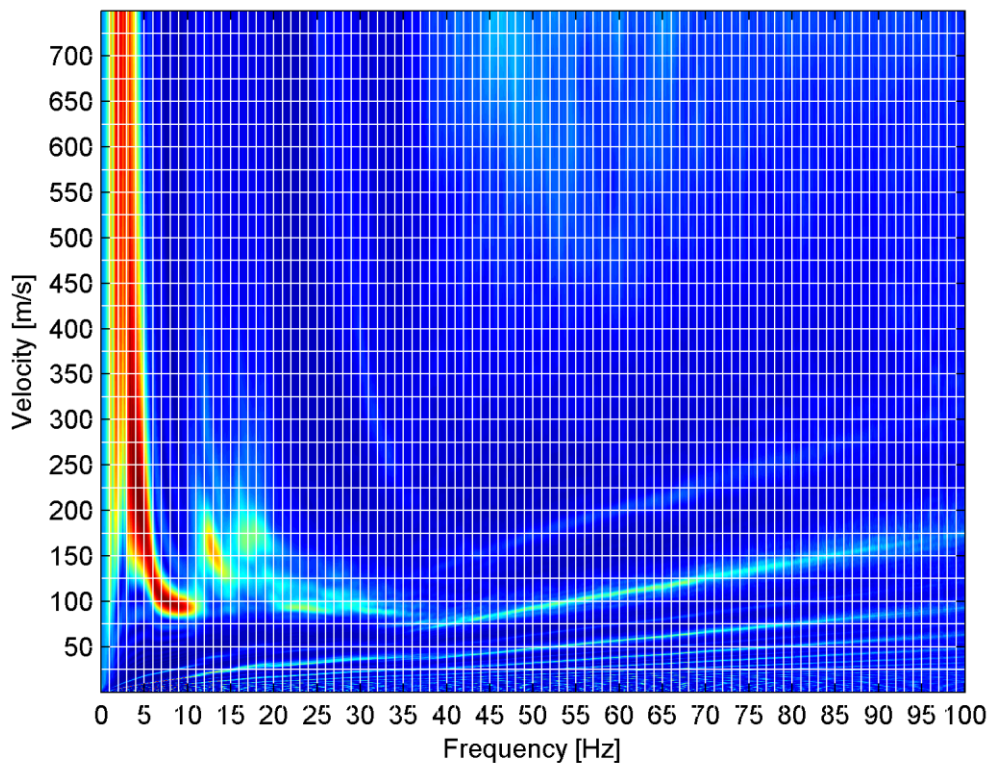


Figure G.10 BLOP

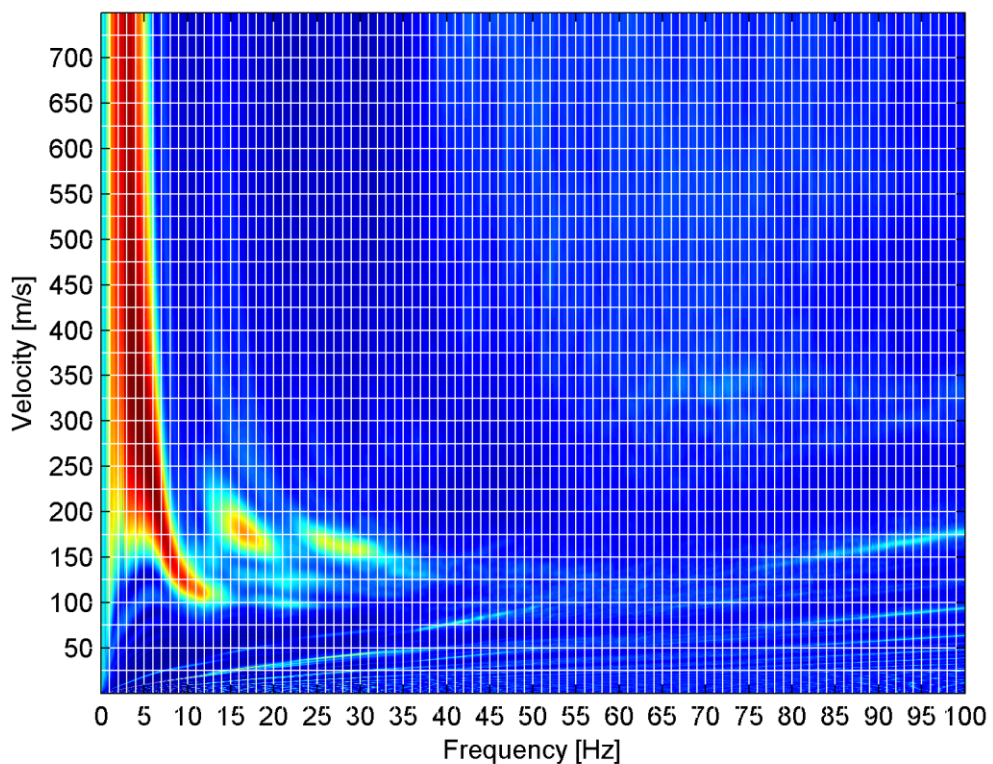


Figure G.11 BKAN

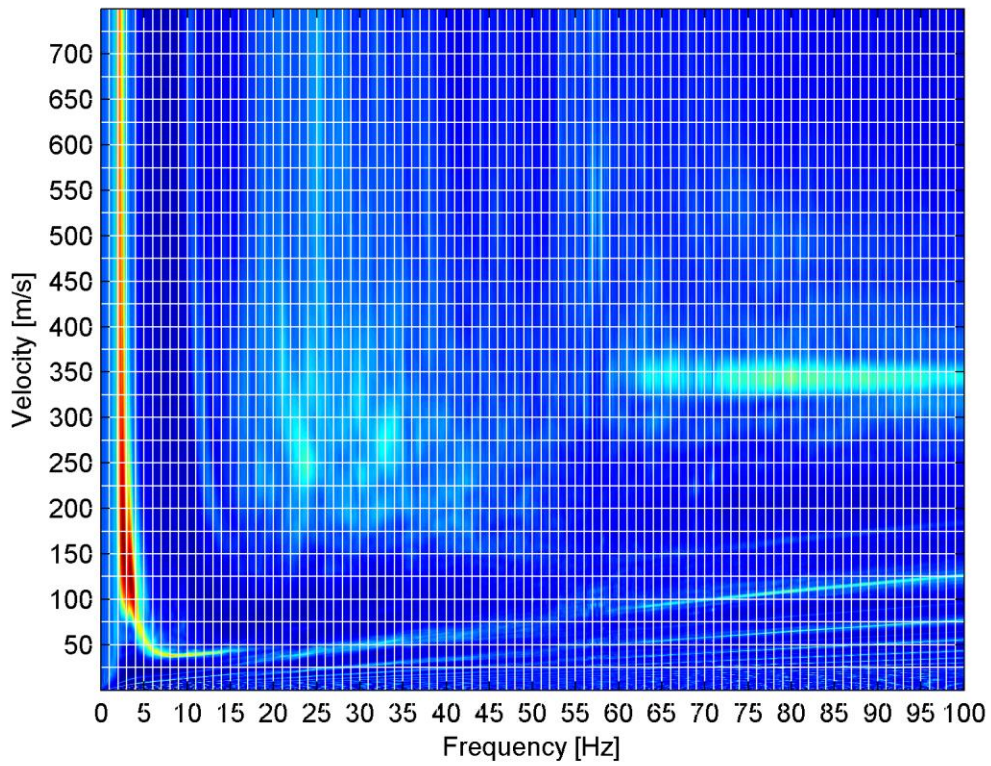


Figure G.12 BHKS

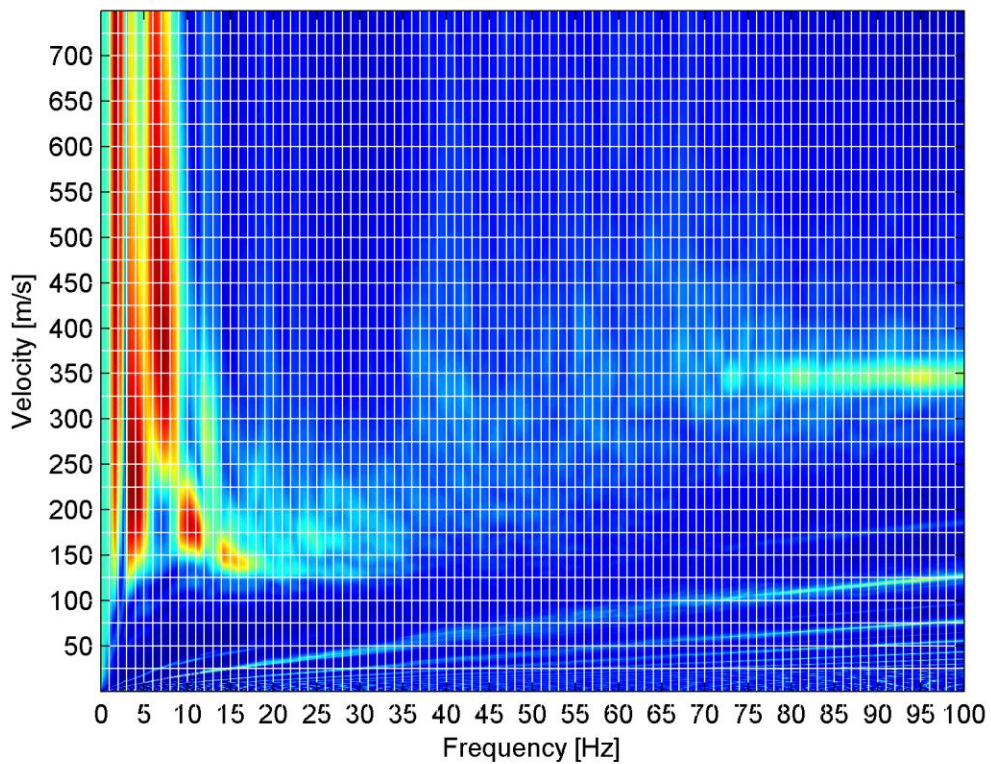


Figure G.13 BHAR

# Deltares

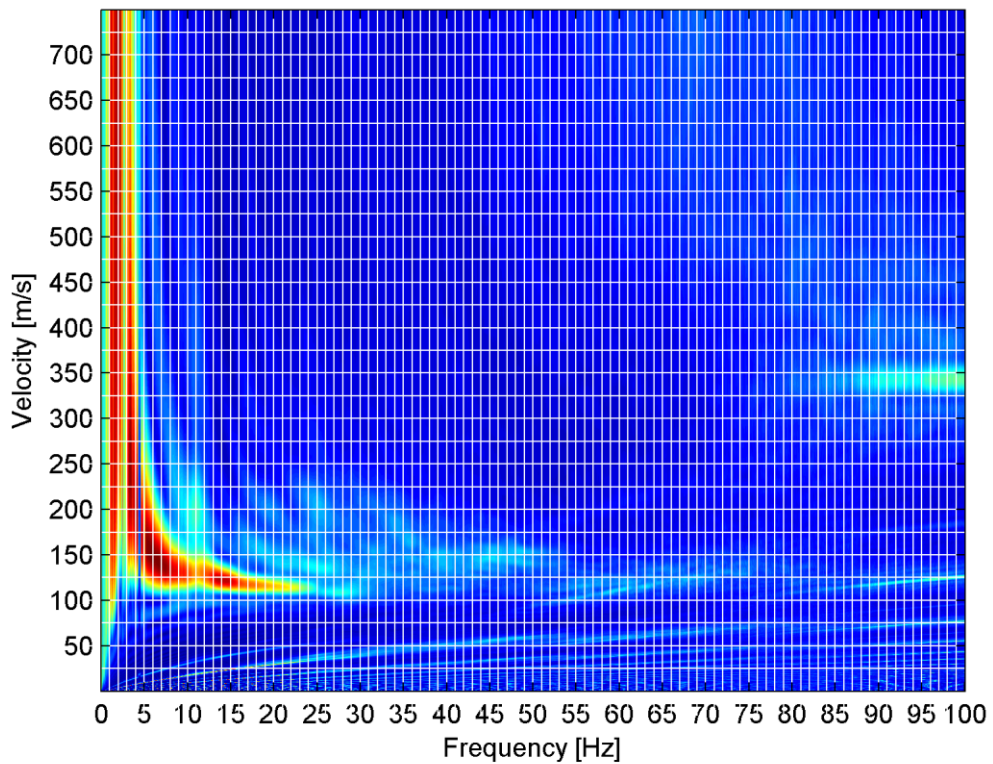


Figure G.14 BGAR

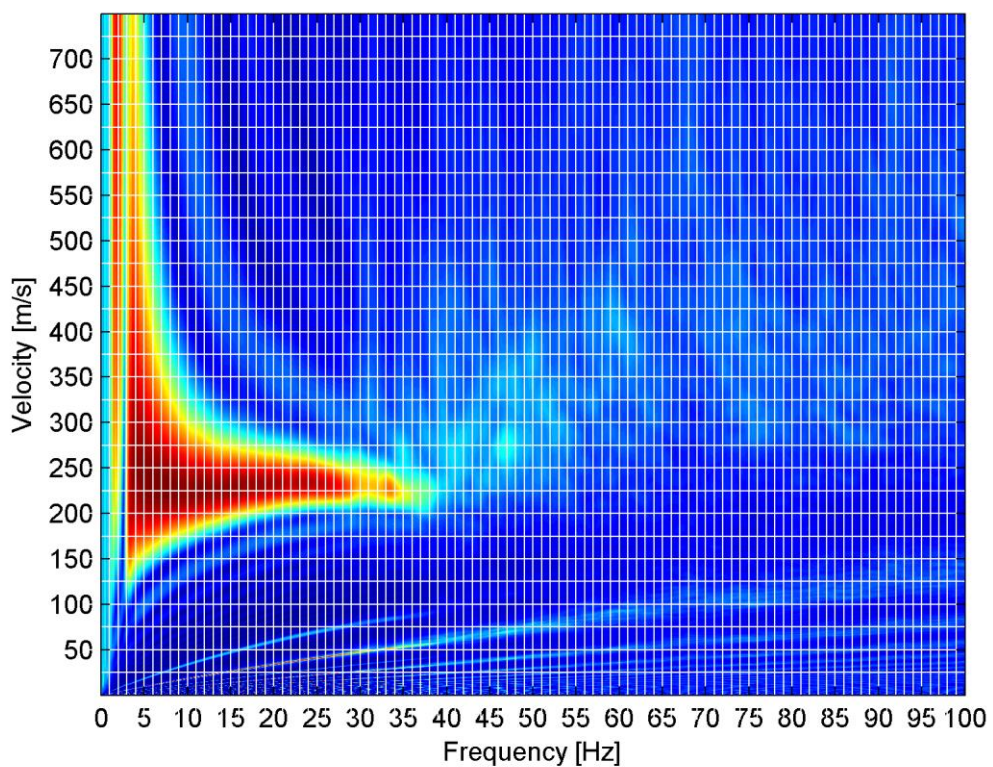


Figure G.15 BFB2

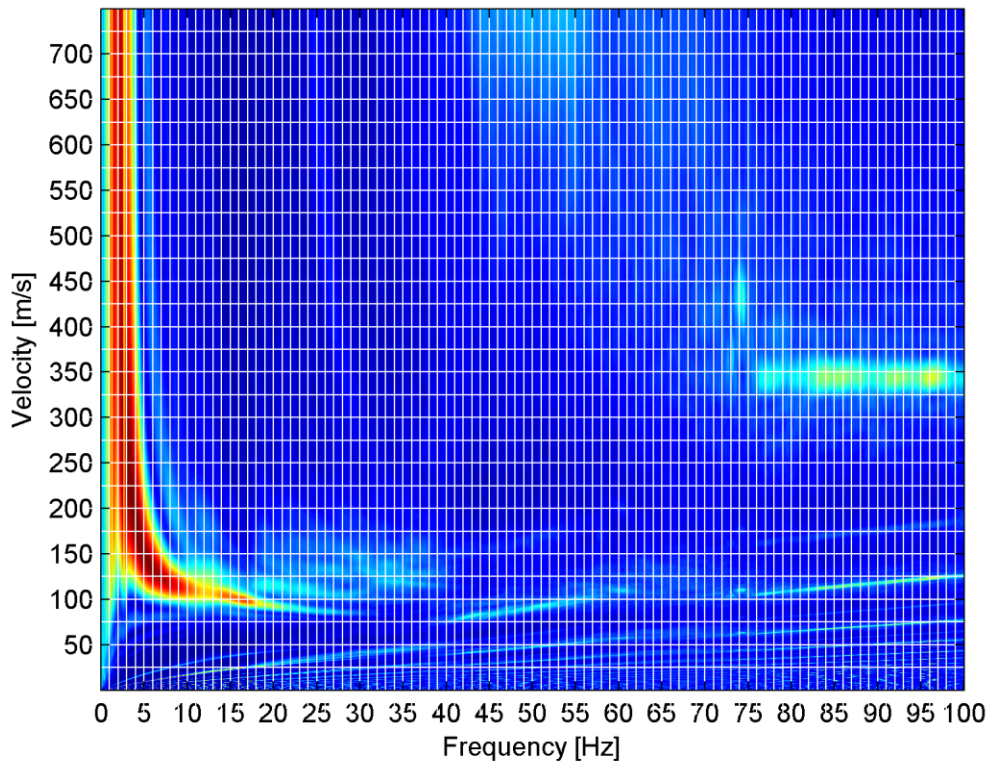


Figure G.16 BMD2

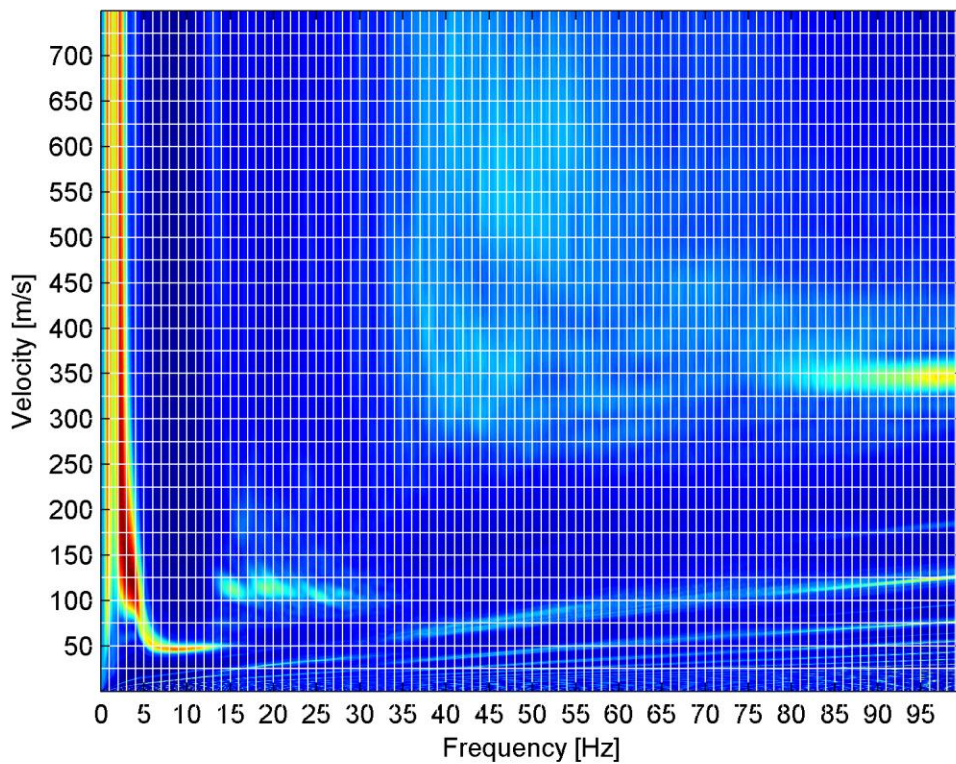


Figure G.17 BAPP

# Deltares

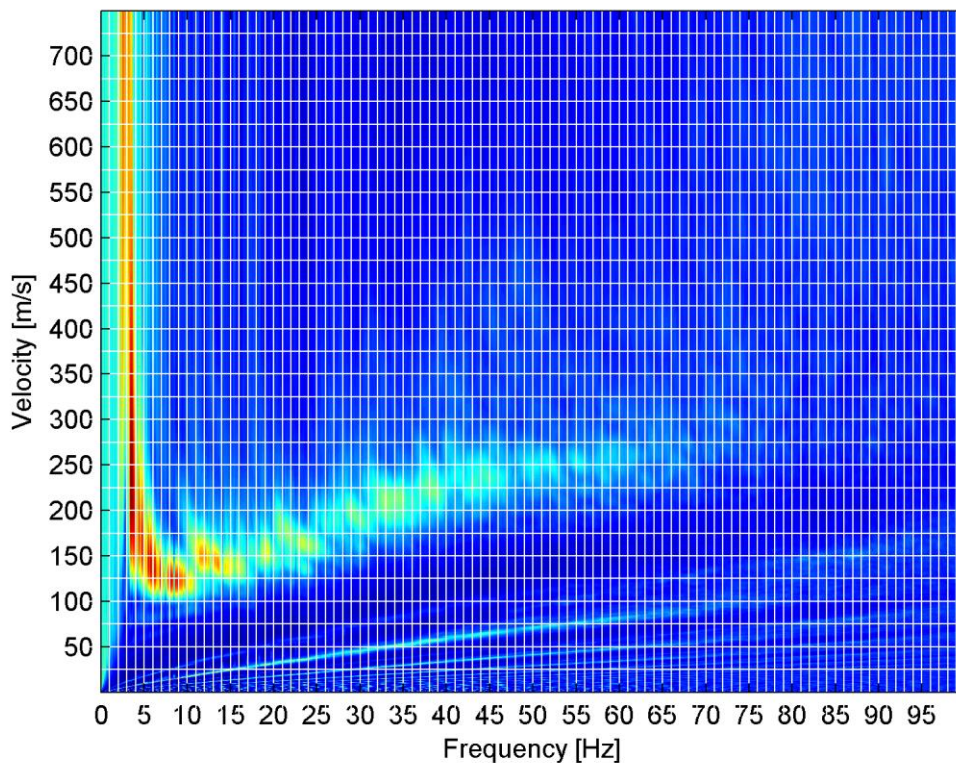


Figure G.18 BZN2

## H Tomography reports from Geotomographie

# *GEOTOMOGRAPHIE GmbH*

Am Tonnenberg 18, 56567 Neuwied, Germany  
Tel.: + 49 2631 778135 / Fax.: + 49 2631 778136

## Report

<b>Project:</b>  Tomographic Surveying at Uithuizen (BUHZ test site)
<b>Client:</b>  Deltares P.O. Box 177 2600 MH Delft  The Netherlands
<b>Print: 1 of 1</b>  <b>Pages: 10</b> <b>Date: 29<sup>th</sup> July 2015</b>
<b>Sign:</b>    Dr. Th. Fechner (Dipl.-Geophysiker)

**C O N T E N T**

	page
<b>1. Executive Summary .....</b>	<b>1</b>
<b>2. Basics and Site Description .....</b>	<b>2</b>
<b>3. P-Wave Seismic Tomography .....</b>	<b>4</b>
3.1 General description .....	4
3.2 Tomography measurements.....	4
3.3 Testing equipment .....	4
3.4 Seismic data processing .....	5
3.5 Results .....	6
<b>4. S-Wave Seismic Tomography .....</b>	<b>6</b>
4.1 General description .....	6
4.2 Tomography measurements.....	6
4.3 Testing equipment .....	7
4.4 Seismic data processing .....	8
4.5 Results .....	9
<b>5. Conclusion and Summary .....</b>	<b>10</b>

## **1. Executive Summary**

Geotomographie GmbH was commissioned to conduct a ground condition survey at the Groningen test site using P- and S-wave seismic tomography.

Three cased boreholes with depths down to about 30 m were available to conduct the tomographic survey. The survey was performed between the 9<sup>th</sup> and 11<sup>th</sup> July 2015.

The seismic data quality obtained ranges from very good to excellent for all source and receiver configurations.

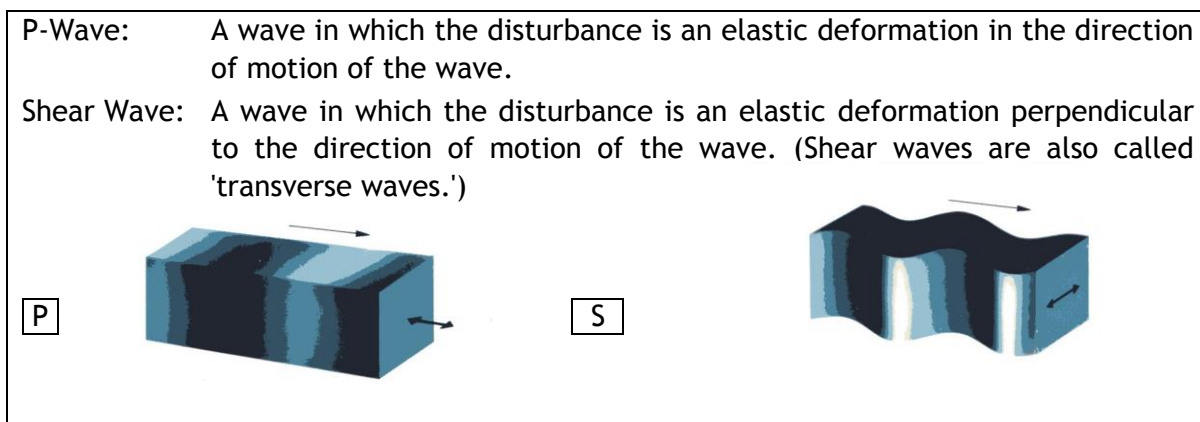
The geology of the test site is comprised of unconsolidated soft sediments.

## 2. Basics and Site Description

Generally, evaluating the subsurface is carried out by drilling boreholes, which possess a high vertical resolution. However, boreholes are limited by sampling only a very small one-dimensional part of the subsurface and are thus unsuitable in predicting the spatial continuity of sediments and their properties. Therefore, the interpretation of the continuity of soil structures will be ambiguous. Remaining uncertainties are often quantified using spatial statistics of the data and the subsurface is then described as a random media with average statistical properties. Geophysical testing along surface or between boreholes can provide such spatial data with excellent quality.

Construction safety demands knowledge on subsurface parameters. In particular, geotechnical shear and stiffness parameters have to be known to avoid subsidence of installations. Among others, shear wave (S-wave) velocity is a crucial rock parameter, which has to be known to calculate soil shear stiffness or other elastic soil parameters. These parameters can be obtained by crosshole and downhole testing.

While compressional seismic waves (P-waves) have a good capability of revealing subsurface structures, shear seismic waves (S-waves) represents a suitable means of recognising lithological features of a deposit and providing additional information, such as different elastic parameters. In recent years, the use of information derived from shear wave exploration has increasingly become routine.



Detecting the S-waves takes a carefully planned survey with specialised survey equipment. Seismic sources and receivers have to be built which can generate and record shear wave arrivals reliably. This is not a simple process because compressional and shear waves often arrive at similar times and mask each other. Much effort, therefore, must be made to circumvent the interaction of both wave types.

This report describes the seismic tests carried out containing three boreholes in an L-shaped arrangement, each about 30 m deep. The coordinates and elevations are shown in Table 1.



### 3. P-Wave Seismic Tomography

#### 3.1 General description

Seismic tomography is used as a geophysical method to delineate structures between boreholes. Seismic waves are generated by an impulsive source in one borehole. The propagation of the seismic waves is influenced by the varying rock properties between the boreholes leading to slow or fast wave arrivals in the second borehole.

To receive the seismic signals, hydrophones connected in a vertical multichannel string with 24 or more sensors are used in the second borehole. Once sufficient signal data quality is achieved, the seismic source is moved to the next position in the borehole and the shooting is repeated. As a result, ray tracing from one borehole to the other builds up very dense and detailed ray coverage.

During seismic data processing, first arrival travel times of the waves related to the p-waves are picked for each source-hydrophone pair. Using an iterative numerical inversion procedure, a seismic velocity distribution between the two boreholes can be calculated based on the travel times and the known source and hydrophone locations.

#### 3.2 Tomography measurements

In total two tomograms have been gathered between B001 - B002 and B003 - B002. The tomograms cover the whole length of the boreholes and provide vertical sections of the p-wave distribution between the boreholes. The vertical spacing between the shot points and the receiver points was 1 m. The individual test configurations for each tomogram are summarised in Table 2.

Table 2: Shooting configuration P-wave tomography (depth below the top of the casing)

Date	Survey	Hydrophone range [m]	Source range [m]
9 <sup>th</sup> July	Slice A B001 → B002	29m to 1m in B002	29,5 to 1m in B001
9 <sup>th</sup> July	Slice B B003 → B002	29m to 1m in B002	29 to 1m in B003

#### 3.3 Testing equipment

In order to generate the high frequency signals which are needed for a good structural resolution, Geotomographie's sparker source system was used. The basic seismic sparker source equipment consists of the electric surge generator, a remote control unit and a downhole probe (see Figure 3). Various source types can be connected (P and S wave generation) to the surge generator. Triggering of the seismic acquisition system is performed by the remote control unit. The remote control unit converts the reference signal of the surge generator into a trigger signal.

Sparker pulses are released by manual or automatic triggering of the generator steered by the remote unit. The downhole p-wave sparker probe consists of the probe housing and a rubber tube system. At the probe housing a plastic protection cover is attached supporting the rubber tube. The closed tube is filled with water and accommodates the sparker electrodes. The electrical discharge occurs within this chamber generating high

frequency pulses. A hydrophone array type BHC2 with 24 channels at 1m spacing, was used to receive the signals (Wester Atlas 2512). A specialised 24 channel compact seismograph was used for data acquisition. Data were stored on laptop and backup was made on memory stick.



Fig. 3: P-wave sparker equipment with 5KV HV unit (upper left), downhole probe SBS42 (upper middle), remote control unit (upper right) and hydrophone (lower middle)

### 3.4 Seismic data processing

Data processing followed several steps in order to convert travel times for tomographic inversion. Seismic data records were depth-sorted and spatial information were assigned to each record. Then, first arrival times of the seismic waves were determined by manual picking using proprietary software. First arrival times are related to the seismic p-wave velocity, which is the most common seismic parameter to describe sediment properties.

The seismic data showed excellent quality throughout all records in the lower parts of the tomograms. Towards the surface the quality decreased slightly but remained on a very high level.

Results are subjected to quality control to ensure a consistency in picked travel times. Travel times of subsequent shots were loaded, compared to adjacent waveforms and if needed, corrected during the travel time picking procedure. In total about 1500 travel times were analysed during the processing of the data.

For the purpose of modelling, the subsurface was numerically divided into 3D-cells. A SIRT algorithm was used for travel time inversion. The algorithm is iterative and minimises the residual of the observed and calculated seismic travel times by a correction of the seismic slowness, i.e. the reciprocal of the seismic velocity in each cell. Seismic waves are assumed to propagate along curved ray paths. The tomograms for each borehole set are processed separately. A vertical and a horizontal cell size of approx. 1m were chosen for all tomograms. No borehole deviation was included.

### **3.5 Results**

The measured P-wave tomograms are shown in Appendix A. The P-wave velocities determined range from about 1000 to 1400m/s within the upper meter above groundwater table and from about 1500m/s to 1800m/s below the ground water table. The lateral velocity changes observed are low. Seismic tomography sections are dominated by a horizontal layering of the sediments.

## **4. S-Wave Seismic Tomography**

### **4.1 General description**

S-wave tomography is a direct way to measure soil stiffness if soil density is known. Another advantage of the S-wave is that it is not influenced by the groundwater table thus resolution of the method is not reduced compared to P-wave tomography under same conditions.

Generation of the S-wave requires a source which is able to generate SH or SV waves in opposite directions. Typically geophones are used to receive the signals. In order to allow a rapid surveying a multi-borehole station tool is required.

Data processing requires different steps compared to P-wave tomography, as typically the number of receivers is limited and identification of the S-wave requires the overlap of the opposite shot directions. Arrival travel times of the S-waves have to be determined. Using an iterative numerical inversion procedure a seismic velocity distribution between the two boreholes can be calculated based on the travel times and known source and hydrophone locations.

### **4.2 Tomography measurements**

In total two tomograms have been gathered between B001 - B002 and B003 - B002. The tomograms cover the whole length of the boreholes and provide vertical sections of the S-wave distribution between the boreholes. The vertical spacing between the shot points and the receiver points was 1 m. The individual test configurations for each tomogram are summarised in Table 3.

Table 3: Shooting configuration S-wave tomography (depth below the top of the casing)

Date	Survey	Receiver range [m] in B002	Source range [m] In B001
10 <sup>th</sup> July	Slice A B001 → B002	Layout 1: 29m to 23m Layout 2: 22m to 16m Layout 3: 15m to 9m Layout 4: 8m to 2m	Layout 1: 29m to 17m Layout 2: 29m to 10m Layout 3: 21m to 3m Layout 4: 14m to 1m
11 <sup>th</sup> July	Slice B B003 → B002	Layout 1: 29m to 23m Layout 2: 22m to 16m Layout 3: 15m to 9m Layout 4: 8m to 2m Layout 5: 7m to 1m	Layout 1: 29m to 17m Layout 2: 28m to 10m Layout 3: 21m to 3m Layout 4: 14m to 1m Layout 5: 7m to 1m

### 4.3 Testing equipment

In order to generate S-waves the Geotomographie SH-wave source type BIS-SH was used. The borehole source BIS-SH generates horizontally polarized shear waves (SH) and compressional waves (P). The seismic signals are highly repeatable.

The source works in dry or water filled boreholes. Energy released by the 5000 V HV unit discharges through a system of electromagnetic coils adjacent to a copper plate. When the plate is rejected a mechanical impact to the borehole wall is generated. The borehole source is coupled to the borehole wall by a pneumatic clamping system (inflatable bladder). The orientation of the source is controlled from surface by a torsionally stiff hose.

The seismic strike direction was aligned perpendicular to the receiver borehole in order to generate SH-waves. To get the opposite strike direction the source was rotated by 180°. In this way one can generate S-waves with opposing polarities. For each shot direction a separate seismic record was acquired and stored.

The seismic signals were received using the Multi-Station Borehole Acquisition System (MBAS) receiver unit. The MBAS is a digital three-component geophone string used to receive P- and S-waves in dry or water filled boreholes. Up to ten individual stations with tri-axial sensors can be connected.

The MBAS stations are aligned to ensure that all horizontal sensors are oriented in the same direction. The system can be oriented from the surface by a torsionally stiff hose. Each station is clamped to the borehole wall by two pneumatic cylinders. An external trigger can be plugged into the USB interface on surface which is connected to a laptop. The operation is entirely controlled by the acquisition software. A separate seismograph is not required.

An MBAS unit with seven 3C units at 1m station interval was used. The MBAS unit was aligned with their X-sensor direction parallel to the source strike direction. Thus, these sensors should give the best seismic signal when evaluating the horizontally polarised shear wave. According to the MBAS layouts given in table 3, the MBAS was pneumatically clamped to the borehole wall. The S-wave source was moved in the other borehole in 1m intervals.



Fig. 4: SH-wave equipment with 5 kV HV unit (upper left), downhole probe BIS-SH (upper middle), remote control unit (upper right) and MBAS receiver (lower middle)

#### 4.4 Seismic data processing

Data processing followed several steps in order to determine travel times for tomographic inversion. Each receiver layout described in table 4 contains 7 stations each with 3C sensors (XYZ). As already described the X-sensor was aligned to be optimal in respect to the strike direction of the source. For example, for layout 1 a total of 13 shot positions were carried out. At every shot position two opposite strike directions

were recorded, i.e. equal to a total of 2 x 13 records (and each record contains 7 x 3 traces). Records were splitted according to their depth and into their X, Y and Z components and then component-wise compiled into one X, Y and Z component record for each strike direction per layout.

Seismic data records were depth-sorted and spatial information were assigned to each record. Then, arrival times of the seismic waves were determined by manually picking of the overlaid records for opposite strike directions.

Travel times are quality controlled to ensure a consistent picking. In total about 1000 travel times were analysed during the processing of the data.

For the purpose of modelling, the subsurface was numerically divided into 3D-cells. A SIRT algorithm was used for travel time inversion. The algorithm is iterative and minimises the residual of the observed and calculated seismic travel times by a correction of the seismic slowness, i.e. the reciprocal of the seismic velocity in each cell. Seismic waves are assumed to propagate along curved ray paths. The tomograms for each borehole set are processed separately. A vertical and a horizontal cell size of approx. 1 m were chosen for all S-wave tomograms.

No borehole deviation was included.

#### 4.5 Results

The measured S-wave tomograms are shown in Appendix B. The determined S-wave velocities range from about 100 to 300 m/s. Seismic tomography sections are dominated by a horizontal layering of the sediments. Three layers can be identified in the S-wave tomograms, similar to the layering observed in the P-wave tomograms. The upper layer ranges from 0 to 5 m below ground and S-wave velocities of around 100 to 150 m/s. This suggests that the upper layer is very weak. The second layer is in a depth from 5 m to about 13 m with S-wave velocities ranging from 150 m/s to 200 m/s. A third layer having seismic velocities above 200 m/s is below a depth of 13 m.

In contrast to the P-wave tomogram the third S-wave layer dips South-East towards B001 and B002. It is unknown why there is a local S-wave decrease or  $V_p/V_s$  increase.

## 5. Conclusion and Summary

This report describes the seismic measurements performed at the Uithuizen test site near Groningen. The survey was carried out between the 9<sup>th</sup> and 11<sup>th</sup> July 2015.

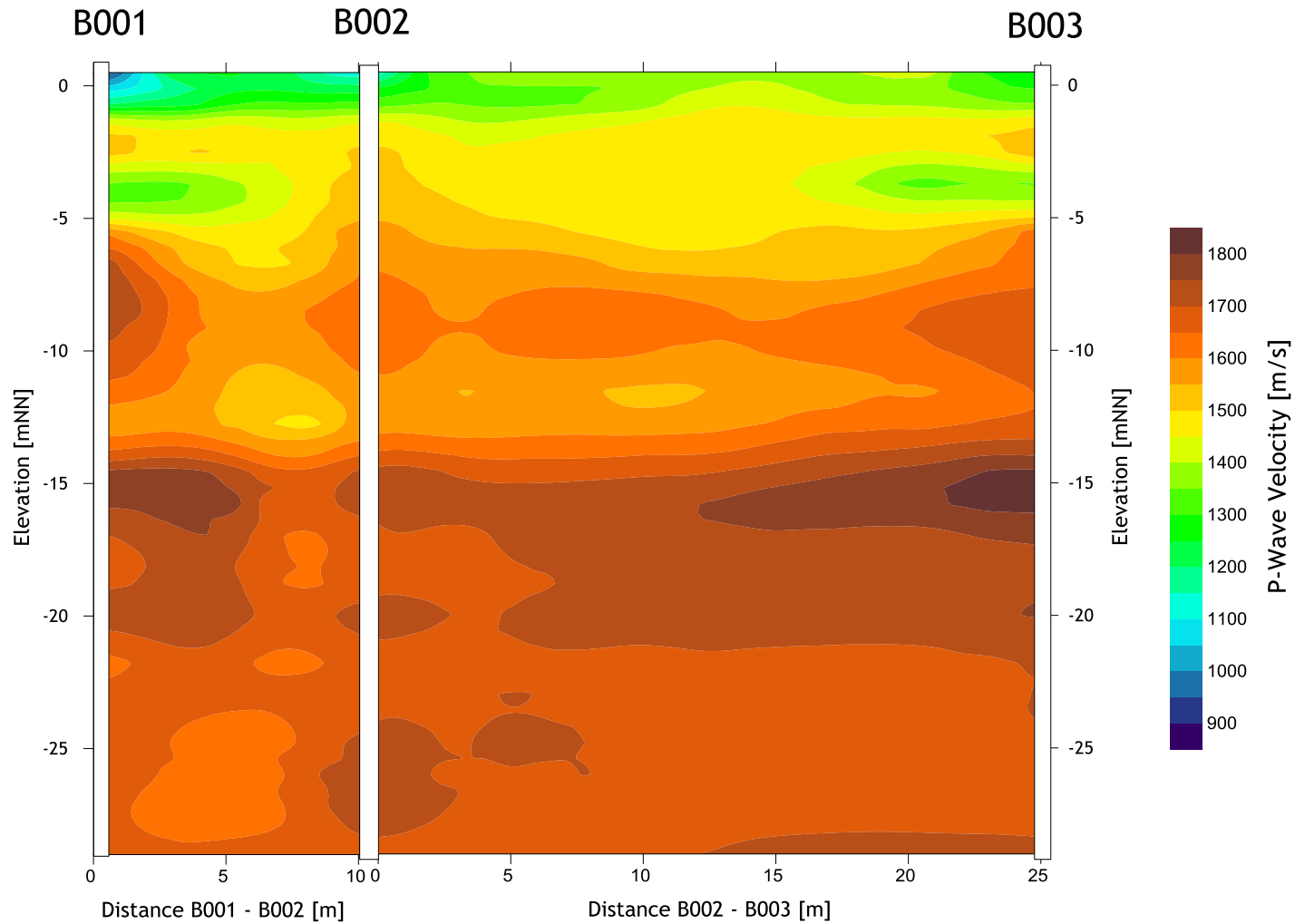
A tomographic P- and S-wave survey was carried out each resulting in two tomograms. The testing interval was 1 m for each test.

The depths of the boreholes were approximately 30 m and distances ranging from 10 m to about 25 m. A borehole source of the type SBS42 generating P-waves was used for the P-wave tomography. The S-wave tomography was carried out using a borehole source type BIS-SH. To receive signals a hydrophone string was used for P-wave tomography. For S-wave tomography the MBAS digital borehole system was used in a 7 station configuration at 1m intervals.

In general, the results show P-wave velocities between 1000 m/s and 1800 m/s and S-wave velocities between 100 and 300 m/s. P-wave velocities below around 1450m/s are due to semi- or unsaturated sediments. Sometimes even saturated sediments might show low velocities if a high content of organic material is present. The high content of organic material causes bacterial degradation which generates gas. Even very small portions of gas can cause a significant drop in velocity.

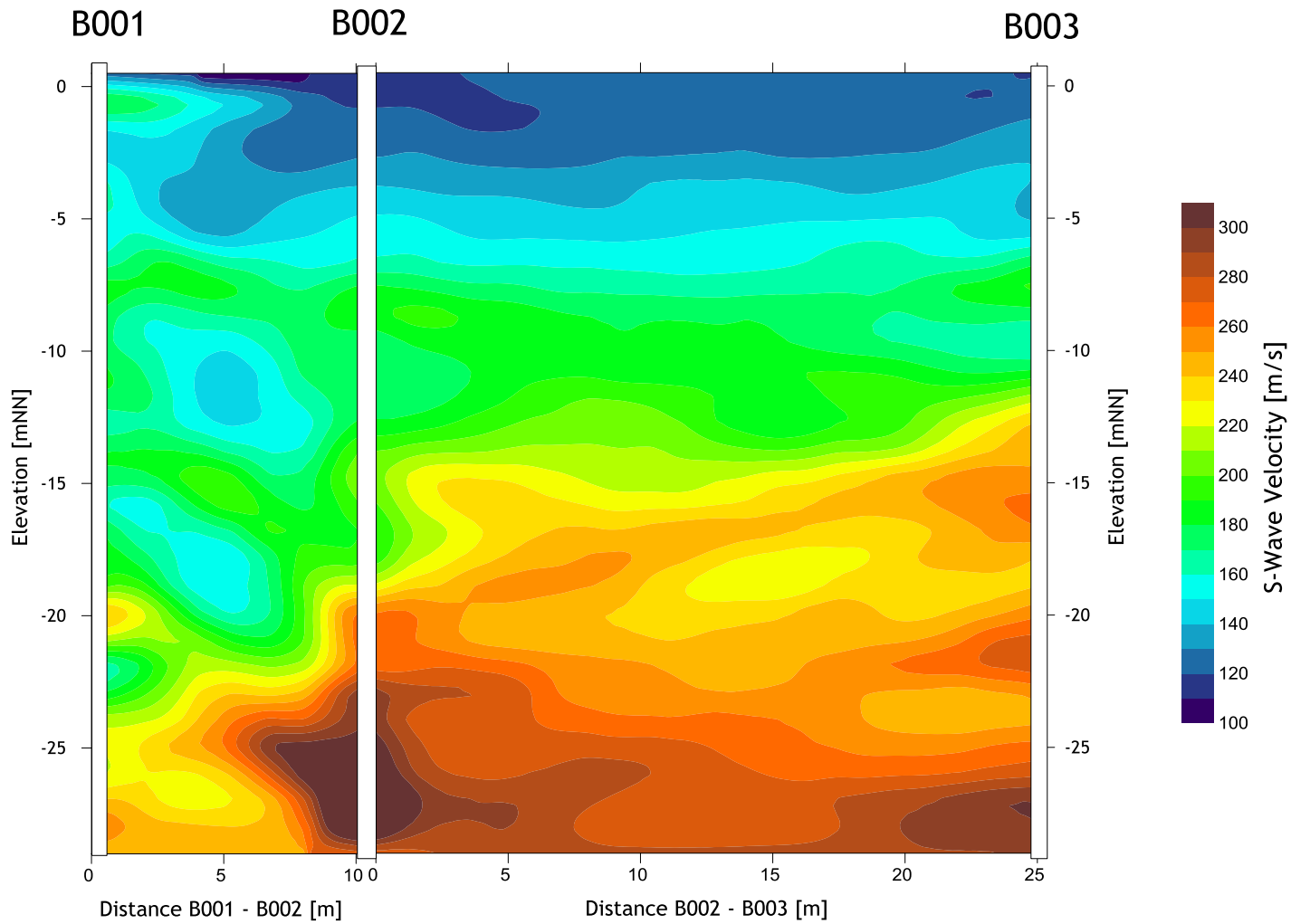
In general three layers can be identified. The upper layer ranges from 0 to 5 m below ground with P-wave velocities from 1000 to 1500 m/s and S-wave velocities from 100 to 150 m/s. The second layer is in a depth from 5 m to about 13 m with P-wave velocities from 1500 to 1700 m/s and S-wave velocities ranging from 150 m/s to 200 m/s. The third layer below 13 m depth shows P-wave velocities above 1700 m/s and S-wave velocities up to 300 m/s. In contrast to the P-wave tomogram the third S-wave layer dips South-East towards B002 and B001. At the time this report was written it is unknown why there is a local S-wave decrease or  $V_p/V_s$  increase.

# P-Wave Tomograms



Geotomographie GmbH – Geophysikalische Spezialmessungen	
56567 Neuwied, Am Tonnenberg 18   Tel.: + 49 2361 778135 Fax.: 778136	
Client: Deltares	
Project: Tomography, Uithuizen	30.07.2015
Content: P-Wave Tomograms	Appendix 1

### S-Wave Tomograms



Geotomographie GmbH – Geophysikalische Spezialmessungen	
56567 Neuwied, Am Tonnenberg 18   Tel.: + 49 2361 778135 Fax.: 778136	
Client: Deltares	
Project: Tomography, Uithuizen	30.07.2015
Content: S-Wave Tomograms	Appendix 2

# *GEOTOMOGRAPHIE GmbH*

Am Tonnenberg 18, 56567 Neuwied, Germany

Tel.: +49 2631 778135 / Fax.: +49 2631 778136

## Report

<b>Project:</b> Tomographic Surveying at the Westeremden (BWSE) test site
<b>Client:</b>  Deltares P.O. Box 177 2600 MH Delft  The Netherlands
<b>Print:</b> 1 of 1 <b>Pages:</b> 10 <b>Date:</b> 7 <sup>th</sup> August 2015
<b>Sign:</b>  Dr. Th. Fechner (Dipl.-Geophysiker)

**C O N T E N T**

	page
<b>1. Executive Summary .....</b>	<b>1</b>
<b>2. Basics and Site Description .....</b>	<b>2</b>
<b>3. P-Wave Seismic Tomography .....</b>	<b>4</b>
3.1 General description .....	4
3.2 Tomography measurements.....	4
3.3 Testing equipment .....	4
3.4 Seismic data processing .....	5
3.5 Results .....	6
<b>4. S-Wave Seismic Tomography .....</b>	<b>6</b>
4.1 General description .....	6
4.2 Tomography measurements.....	7
4.3 Testing equipment .....	7
4.4 Seismic data processing .....	8
4.5 Results .....	9
<b>5. Conclusion and Summary .....</b>	<b>10</b>

## **1. Executive Summary**

Geotomographie GmbH was commissioned to conduct a ground condition survey at the Westeremden test site using P- and S-wave seismic tomography.

Three cased boreholes with depths down to about 30 m were available to conduct the tomographic survey. The survey was performed on the 15<sup>th</sup> and 16<sup>th</sup> July 2015.

The seismic data quality obtained ranges from very good to excellent for all source and receiver configurations.

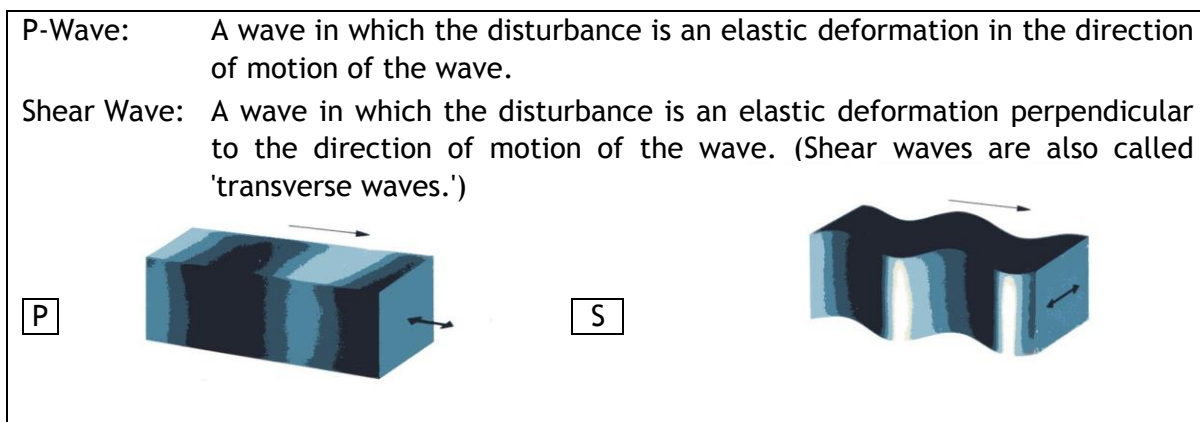
The geology of the test site is comprised of unconsolidated soft sediments.

## 2. Basics and Site Description

Generally, evaluating the subsurface is carried out by drilling boreholes, which possess a high vertical resolution. However, boreholes are limited by sampling only a very small one-dimensional part of the subsurface and are thus unsuitable in predicting the spatial continuity of sediments and their properties. Therefore, the interpretation of the continuity of soil structures will be ambiguous. Remaining uncertainties are often quantified using spatial statistics of the data and the subsurface is then described as a random media with average statistical properties. Geophysical testing along surface or between boreholes can provide such spatial data with excellent quality.

Construction safety demands knowledge on subsurface parameters. In particular, geotechnical shear and stiffness parameters have to be known to avoid subsidence of installations. Among others, shear wave (S-wave) velocity is a crucial rock parameter, which has to be known to calculate soil shear stiffness or other elastic soil parameters. These parameters can be obtained by crosshole and downhole testing.

While compressional seismic waves (P-waves) have a good capability of revealing subsurface structures, shear seismic waves (S-waves) represents a suitable means of recognising lithological features of a deposit and providing additional information, such as different elastic parameters. In recent years, the use of information derived from shear wave exploration has increasingly become routine.



Detecting the S-waves takes a carefully planned survey with specialised survey equipment. Seismic sources and receivers have to be built which can generate and record shear wave arrivals reliably. This is not a simple process because compressional and shear waves often arrive at similar times and mask each other. Much effort, therefore, must be made to circumvent the interaction of both wave types.

This report describes the seismic tests carried out containing three boreholes in an L-shaped arrangement, each about 30 m deep. The coordinates and elevations are shown in Table 1.

Table 1: Surface coordinates of the boreholes

Borehole	Easting [m]	Northing [m]	Elevation [m]
B004	242977.406	595894.962	0.193
B005	242984.716	595888.116	0.298
B006	243000.955	595905.912	0.317



Fig. 1: Location of Site 2 (Westeremden)

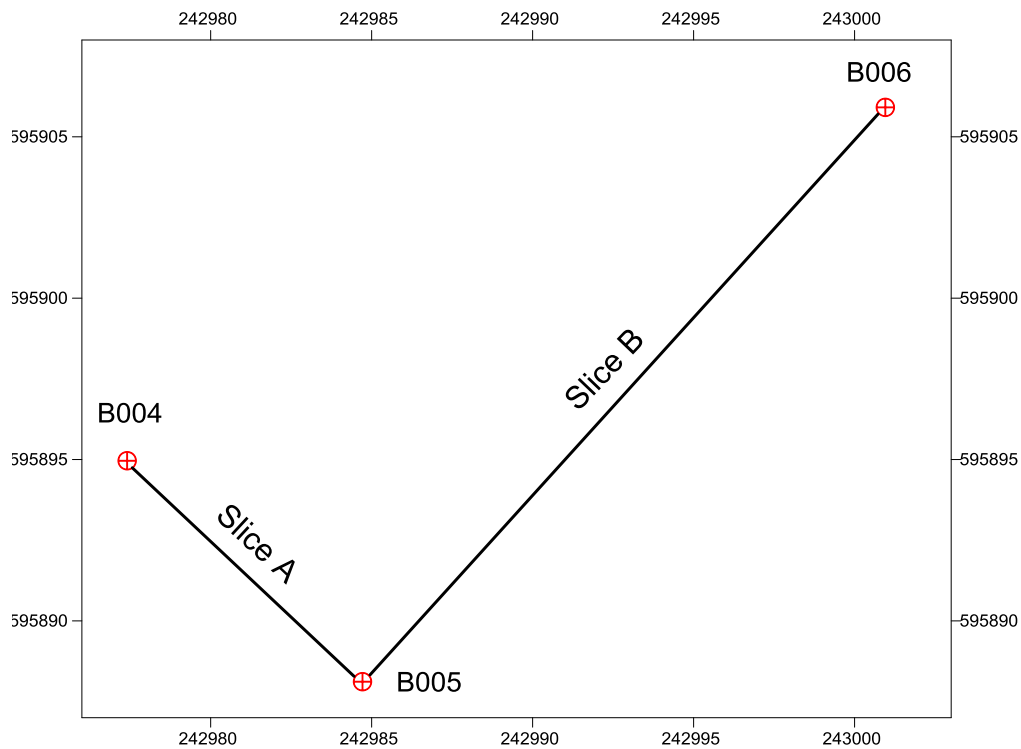


Fig. 2: Plan view of boreholes and tomographic slices

### 3. P-Wave Seismic Tomography

#### 3.1 General description

Seismic tomography is a geophysical method used to delineate structures between boreholes. Seismic waves are generated by an impulsive source in one borehole. The propagation of the seismic waves is influenced by the varying rock properties between the boreholes leading to slow or fast wave arrivals in the second borehole.

To receive the seismic signals, hydrophones connected in a vertical multichannel string with 24 or more sensors are used in the second borehole. Once sufficient signal data quality is achieved, the seismic source is moved to the next position in the borehole and the shooting is repeated. As a result, ray tracing from one borehole to the other builds up very dense and detailed ray coverage.

During seismic data processing, first arrival travel times of the waves related to the p-waves are picked for each source-hydrophone pair. Using an iterative numerical inversion procedure, a seismic velocity distribution between the two boreholes can be calculated based on the travel times and the known source and hydrophone locations.

#### 3.2 Tomography measurements

In total two tomograms have been gathered between boreholes B004 - B005 and B006 - B005. The tomograms provide vertical sections of the p-wave distribution between the boreholes. The vertical spacing between the shot points and the receiver points was 1 m. The individual test configurations for each tomogram are summarised in Table 2. The receiver range was limited to a depth of 27 m, as the hydrophone string was unable to advance further during the field measurements.

Table 2: Shooting configuration P-wave tomography (depth below top of casing)

Date	Survey	Hydrophone range [m]	Source range [m]
15 <sup>th</sup> July	Slice A B004 → B005	27 to 1 m in B005	29 to 1m in B004
15 <sup>th</sup> July	Slice B B005 → B006	27 to 1 m in B005	29 to 1m in B006

#### 3.3 Testing equipment

The equipment used to measure the P-wave arrival times consists of an electric surge generator, a remote control unit and a downhole probe (see Figure 3). Various source types can be connected (P and S wave generation) to the surge generator. Triggering of the seismic acquisition system is performed by the remote control unit. The remote control unit converts the reference signal of the surge generator into a trigger signal.

Due to the good transmission properties of the soil, it was decided to use the same source for both the P- and S-wave tomographic measurements. Therefore, the Geotomographie SH-wave source type BIS-SH source was used for both P- and S-wave measurements, as the BIS-SH generates both horizontally polarized shear waves (SH) and compressional waves (P) with a high repeatability.

Energy released by the 5000 V HV unit discharges through a system of electromagnetic coils adjacent to a copper plate. When the plate is rejected, a mechanical impact to the borehole wall is generated. The borehole source is coupled to the borehole wall by a pneumatic clamping system (inflatable bladder). The orientation of the source is controlled from surface by a torsionally stiff hose.

The seismic strike direction was aligned towards the receiver borehole in order to generate P-waves with the highest amplitude. For the P-wave tomography measurements, one record was recorded for each depth interval.

A hydrophone array type BHC2 with 24 channels at 1m spacing, was used to receive the signals (Western Atlas 2512). A specialised 24 channel compact seismograph was used for data acquisition. Data were stored on laptop and backup was made on memory stick.



Fig. 3: P-wave tomography equipment with 5 kV HV unit (upper left), downhole probe BIS-SH (upper middle), remote control unit (upper right) and hydrophone (lower middle)

### 3.4 Seismic data processing

Data processing followed several steps in order to convert travel times for tomographic inversion. Seismic data records were depth-sorted and spatial information were assigned to each record. Then, first arrival times of the seismic waves were determined by manual picking using proprietary software. First arrival times are related to the seismic p-wave velocity, which is the most common seismic parameter to describe sediment properties.

The seismic data showed excellent quality throughout all records in the lower parts of the tomograms. Towards the surface the quality decreased slightly but remained on a very high level for Slice A and on an acceptable level for Slice B.

Results are subjected to quality control to ensure a consistency in picked travel times. Travel times of subsequent shots were loaded, compared to adjacent waveforms and if needed, corrected during the travel time picking procedure. In total about 1800 travel times were analysed during the processing of the data.

For the purpose of modelling, the subsurface was numerically divided into 3D-cells. A SIRT algorithm was used for travel time inversion. The algorithm is iterative and minimises the residual of the observed and calculated seismic travel times by a correction of the seismic slowness, i.e. the reciprocal of the seismic velocity in each cell. Seismic waves are assumed to propagate along curved ray paths. The tomograms for each borehole set are processed separately. A vertical and a horizontal cell size of approx. 1 m were chosen for all tomograms. No borehole deviation was included.

### **3.5 Results**

The measured P-wave tomograms are shown in Appendix A. The seismic velocity measurements are dominated by horizontal layering, with four distinguishable layers. Within the upper most two meters above groundwater table, the P-wave velocities range from about 1000 to 1400 m/s. Subsequently, the P-wave velocities increase up to 1500 m/s for depths of 2 m to 6 m. Thereafter, a lower velocity layer follows with P-wave velocities of about 1300 m/s. Below, the P-wave velocities range from 1600 to 1800 m/s.

## **4. S-Wave Seismic Tomography**

### **4.1 General description**

S-wave tomography is a direct way to measure soil stiffness if soil density is known. Another advantage of the S-wave is that it is not influenced by the groundwater table thus resolution of the method is not reduced compared to P-wave tomography under the same conditions.

Generation of an S-wave requires a source which is able to generate SH or SV waves in opposite directions. Typically geophones are used to receive the signals. In order to allow a rapid surveying a multi-borehole station tool is required.

Data processing requires different steps compared to P-wave tomography, as typically the number of receivers is limited and identification of the S-wave requires the overlap of the opposite shot directions. Arrival travel times of the S-waves have to be determined. Using an iterative numerical inversion procedure a seismic velocity distribution between the two boreholes can be calculated based on the travel times and known source and hydrophone locations.

## 4.2 Tomography measurements

In total two tomograms have been gathered between boreholes B004 - B005 and B006 - B005. The tomograms cover the whole length of the boreholes and provide vertical sections of the S-wave distribution between the boreholes. The vertical spacing between the shot points and the receiver points was 1 m. The individual test configurations for each tomogram are summarised in Table 3.

Table 3: Shooting configuration S-wave tomography (depth below top of casing)

Date	Survey	Receiver range [m] in B002	Source range [m] In B001
15 <sup>th</sup> July	Slice A B004 → B005	Layout 1: 29 to 23 Layout 2: 22 to 16 Layout 3: 15 to 9 Layout 4: 8 to 2 Layout 5: 7 to 1	Layout 1: 29 to 17 Layout 2: 29 to 9 Layout 3: 22 to 2 Layout 4: 15 to 1 Layout 5: 8 to 1
16 <sup>th</sup> July	Slice B B006 → B005	Layout 1: 29 to 23 Layout 2: 22 to 16 Layout 3: 15 to 9 Layout 4: 8 to 2 Layout 5: 7 to 1	Layout 1: 29 to 16 Layout 2: 29 to 9 Layout 3: 22 to 2 Layout 4: 15 to 1 Layout 5: 8 to 1

## 4.3 Testing equipment

In order to generate S-waves the Geotomographie SH-wave source type BIS-SH was used. The borehole source BIS-SH generates horizontally polarized shear waves (SH) and compressional waves (P). The seismic signals are highly repeatable.

The source works in dry or water filled boreholes. Energy released by the 5000 V HV unit discharges through a system of electromagnetic coils adjacent to a copper plate. When the plate is rejected, a mechanical impact to the borehole wall is generated. The borehole source is coupled to the borehole wall by a pneumatic clamping system (inflatable bladder). The orientation of the source is controlled from surface by a torsionally stiff hose.

The seismic strike direction was aligned perpendicular to the receiver borehole in order to generate SH-waves. To get the opposite strike direction the source was rotated by 180° and thus generating S-waves with opposing polarities. For each shot direction a separate seismic record was acquired and stored.

The seismic signals were received using the Multi-Station Borehole Acquisition System (MBAS) receiver unit. The MBAS is a digital three-component geophone string used to receive P- and S-waves in dry or water filled boreholes. Up to ten individual stations with tri-axial sensors can be connected.

The MBAS stations are aligned to ensure that all horizontal sensors are oriented in the same direction. The system can be oriented from the surface by a torsionally stiff hose. Each station is clamped to the borehole wall by two pneumatic cylinders. An external

trigger can be plugged into the USB interface on surface which is connected to a laptop. The operation is entirely controlled by the acquisition software. A separate seismograph is not required.

An MBAS unit with seven 3C units at 1m station interval was used. The MBAS unit was aligned with their X-sensor direction parallel to the source strike direction. Thus, these sensors should give the best seismic signal when evaluating the horizontally polarised shear wave. According to the MBAS layouts given in table 3, the MBAS was pneumatically clamped to the borehole wall. The S-wave source was moved in the other borehole in 1m intervals.



Fig. 4: SH-wave equipment with 5 kV HV unit (upper left), downhole probe BIS-SH (upper middle), remote control unit (upper right) and MBAS receiver (lower middle)

#### 4.4 Seismic data processing

Data processing followed several steps in order to determine travel times for tomographic inversion. Each receiver layout described in table 3 contains 7 stations each with 3C sensors (XYZ). As already described the X-sensor was aligned to be optimal in respect to the strike direction of the source. For example, for layout 1 a total of 13 shot positions were carried out. At every shot position two opposite strike directions were recorded, i.e. equal to a total of  $2 \times 13$  records (and each record contains  $7 \times 3$

traces). Records were split according to their depth and into their X, Y and Z components and then component-wise compiled into one X, Y and Z component record for each strike direction per layout.

Subsequently, the traces were resorted and grouped according to the different receiver positions. At the beginning of this resorting, one record corresponded to one shot at a certain depth (polarized either in the plus or minus direction) and displayed seven traces of a single component (either X, Y or Z). After this resorting, one record corresponded to one receiver position and displayed the traces of the shots at different depths. This proved beneficial when picking the data, as more traces could be viewed at the same time and trends in S-wave arrival were easier to identify.

Spatial information was assigned to each record and arrival times of the seismic waves were determined by manually picking of the overlaid records for opposite strike directions. These travel times were quality controlled to ensure consistent picking and borehole deviation data was incorporated. In total about 950 travel times were analysed during the processing of the data.

For the purpose of modelling, the subsurface was numerically divided into 3D-cells. A SIRT algorithm was used for travel time inversion. The algorithm is iterative and minimises the residual of the observed and calculated seismic travel times by a correction of the seismic slowness, i.e. the reciprocal of the seismic velocity in each cell. Seismic waves are assumed to propagate along curved ray paths. The tomograms for each borehole set are processed separately. A vertical and a horizontal cell size of approx. 1 m were chosen for all S-wave tomograms.

#### **4.5 Results**

The measured S-wave tomograms are shown in Appendix B. The determined S-wave velocities range from about 100 to 300 m/s. Seismic tomography sections are dominated by a horizontal layering of the sediments. Two layers can be identified in the S-wave tomograms, which correspond to the layering observed in the P-wave tomograms. The upper layer ranges from 0 to about 9 m and is characterised by S-wave velocities of around 100 to 150 m/s. This suggests that the upper layer is very weak. The second layer with S-wave velocities above 200 m/s is below a depth of 9 m. Due to the proportionally higher S-wave velocity contrasts, the S-wave tomograms show a distinctly higher resolution compared to the P-wave tomograms, especially for the lower layer below a depth of 9 m.

## 5. Conclusion and Summary

This report describes the seismic measurements performed at the Westeremden (BWSE) test site near Groningen. The survey was carried out on the 15<sup>th</sup> and 16<sup>th</sup> July 2015.

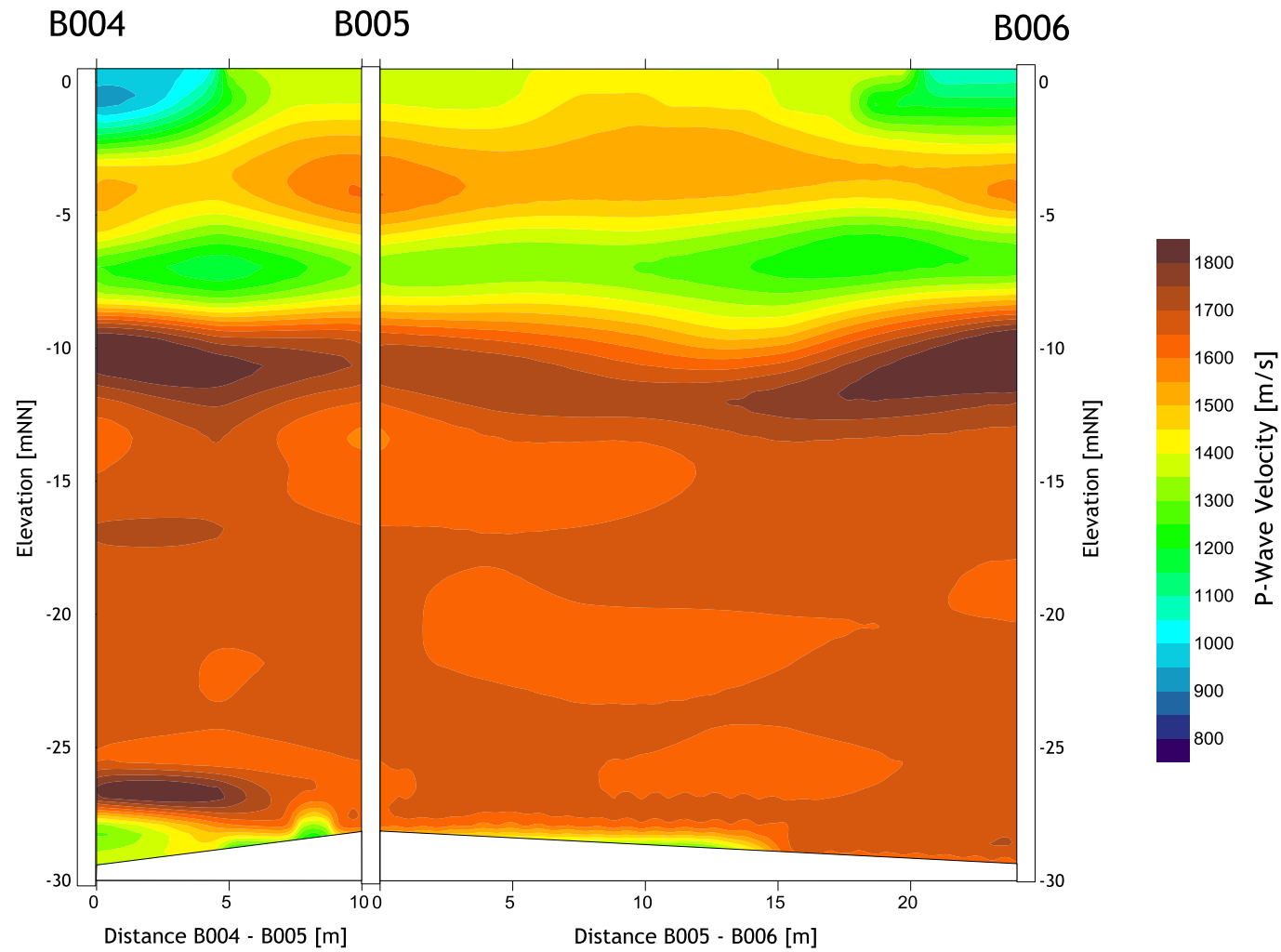
A tomographic P- and S-wave survey was carried out each resulting in two tomograms. The testing interval was 1 m for each test.

The depths of the boreholes were approximately 30 m and inter-borehole distances ranging from about 10 m to 24 m. Both P-wave and S-wave tomographic surveys were carried out with the borehole source type BIS-SH. To receive signals a hydrophone string was used for P-wave tomography. For S-wave tomography the MBAS digital borehole system was used in a 7 station configuration at 1m intervals.

In general, the results show P-wave velocities between 1000 m/s and 1800 m/s and S-wave velocities between 100 and 300 m/s. P-wave velocities below around 1450m/s are due to semi- or unsaturated sediments. Sometimes even saturated sediments might show low velocities if a high content of organic material is present. The high content of organic material causes bacterial degradation which generates gas. Even very small portions of gas can cause a significant drop in velocity.

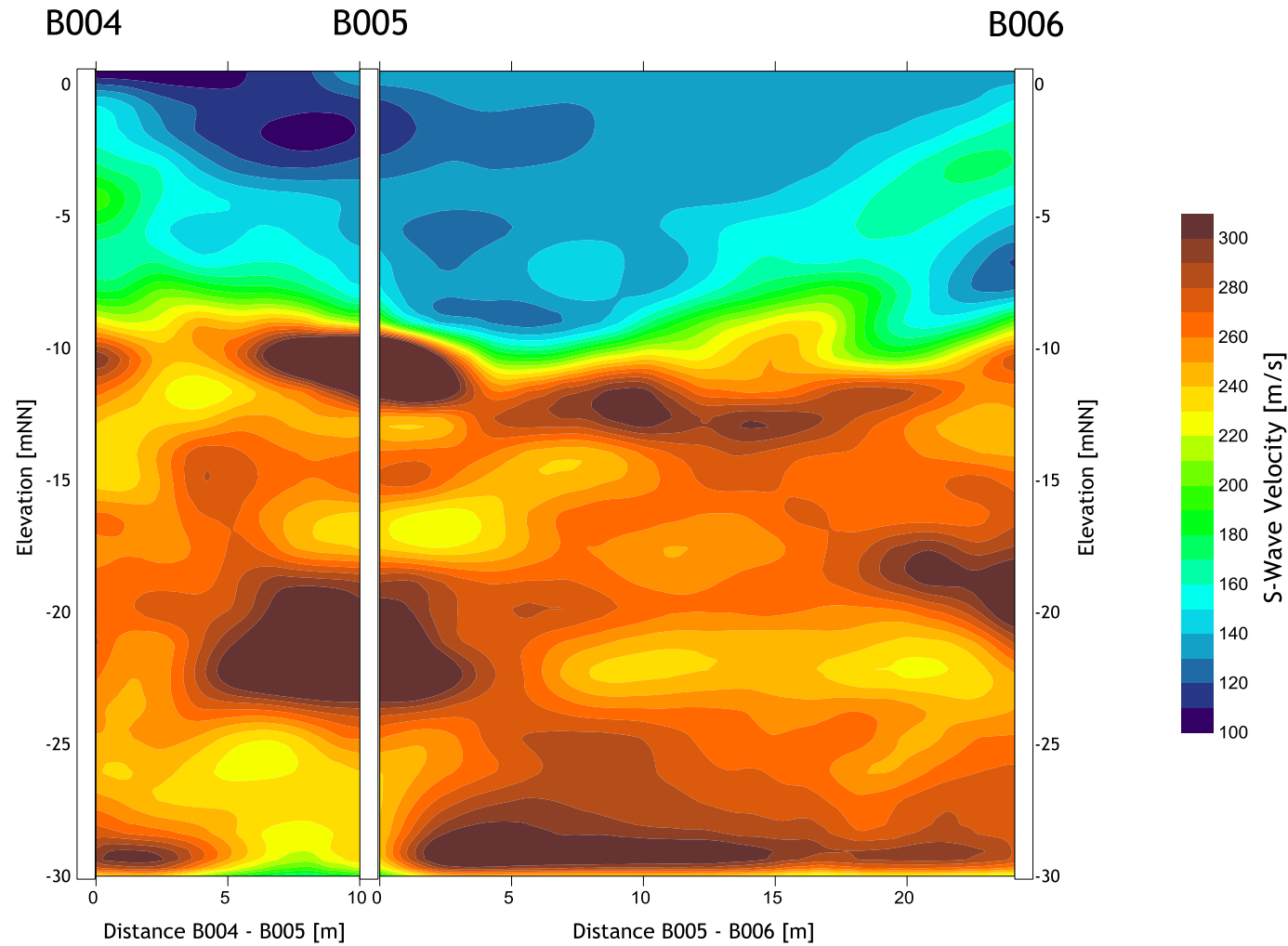
In general two layers can be identified. The upper layer ranges from 0 to 9 m below ground with P-wave velocities from 1000 to 1500 m/s and S-wave velocities from 100 to 150 m/s. The second layer below a depth of about 9 m shows P-wave velocities above 1600 m/s and S-wave velocities between 200 and 300 m/s.

# P-Wave Tomograms



Geotomographie GmbH – Geophysikalische Spezialmessungen	
56567 Neuwied, Am Tonnenberg 18   Tel.: +49 2361 778135 Fax.: 778136	
Client: Deltares	
Project: Tomography, Westerlanden	07.08.2015
Content: P-Wave Tomograms	Appendix 1

# S-Wave Tomograms



Geotomographie GmbH – Geophysikalische Spezialmessungen	
56567 Neuwied, Am Tonnenberg 18   Tel.: +49 2361 778135 Fax.: 778136	
Client: Deltares	
Project: Tomography, Westerlanden	07.08.2015
Content: S-Wave Tomograms	Appendix 2

# *GEOTOMOGRAPHIE GmbH*

Am Tonnenberg 18, 56567 Neuwied, Germany

Tel.: +49 2631 778135 / Fax.: +49 2631 778136

## Report

<b>Project:</b> Tomographic Surveying at the Appingedam (BAPP) test site
<b>Client:</b>  Deltares P.O. Box 177 2600 MH Delft  The Netherlands
<b>Print:</b> 1 of 1 <b>Pages:</b> 10 <b>Date:</b> 11 <sup>th</sup> August 2015
<b>Sign:</b>    Dr. Th. Fechner (Dipl.-Geophysiker)

**C O N T E N T**

	page
<b>1. Executive Summary .....</b>	<b>1</b>
<b>2. Basics and Site Description .....</b>	<b>2</b>
<b>3. P-Wave Seismic Tomography .....</b>	<b>4</b>
3.1 General description .....	4
3.2 Tomography measurements.....	4
3.3 Testing equipment .....	4
3.4 Seismic data processing .....	5
3.5 Results .....	6
<b>4. S-Wave Seismic Tomography .....</b>	<b>6</b>
4.1 General description .....	6
4.2 Tomography measurements.....	7
4.3 Testing equipment .....	7
4.4 Seismic data processing .....	9
4.5 Results .....	9
<b>5. Conclusion and Summary .....</b>	<b>10</b>

## **1. Executive Summary**

Geotomographie GmbH was commissioned to conduct a ground condition survey at the Appingedam (BAPP) test site using P- and S-wave seismic tomography.

Three cased boreholes with depths down to about 30 m were available to conduct the tomographic survey. The survey was performed on the 21<sup>st</sup> and 22<sup>nd</sup> July 2015.

The obtained seismic data varies in its quality. Below a depth of 8 m the quality is excellent for all source receiver configurations. Above 8 m the data quality is moderate to poor, due to the poor transmission properties of the soft soil.

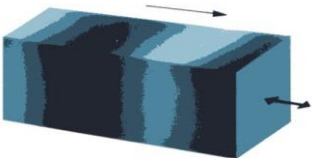
The geology of the test site is comprised of unconsolidated soft sediments.

## 2. Basics and Site Description

Generally, evaluating the subsurface is carried out by drilling boreholes, which possess a high vertical resolution. However, boreholes are limited by sampling only a very small one-dimensional part of the subsurface and are thus unsuitable in predicting the spatial continuity of sediments and their properties. Therefore, the interpretation of the continuity of soil structures will be ambiguous. Remaining uncertainties are often quantified using spatial statistics of the data and the subsurface is then described as a random media with average statistical properties. Geophysical testing along surface or between boreholes can provide such spatial data with excellent quality.

Construction safety demands knowledge on subsurface parameters. In particular, geotechnical shear and stiffness parameters have to be known to avoid subsidence of installations. Among others, shear wave (S-wave) velocity is a crucial rock parameter, which has to be known to calculate soil shear stiffness or other elastic soil parameters. These parameters can be obtained by crosshole and downhole testing.

While compressional seismic waves (P-waves) have a good capability of revealing subsurface structures, shear seismic waves (S-waves) represents a suitable means of recognising lithological features of a deposit and providing additional information, such as different elastic parameters. In recent years, the use of information derived from shear wave exploration has increasingly become routine.

P-Wave:	A wave in which the disturbance is an elastic deformation in the direction of motion of the wave.		
Shear Wave:	A wave in which the disturbance is an elastic deformation perpendicular to the direction of motion of the wave. (Shear waves are also called 'transverse waves'.)		
P		S	

Detecting the S-waves takes a carefully planned survey with specialised survey equipment. Seismic sources and receivers have to be built which can generate and record shear wave arrivals reliably. This is not a simple process because compressional and shear waves often arrive at similar times and mask each other. Much effort, therefore, must be made to circumvent the interaction of both wave types.

This report describes the seismic tests carried out containing three boreholes in an L-shaped arrangement, each about 30 m deep. The coordinates and elevations are shown in Table 1.

Table 1: Surface coordinates of the boreholes

Borehole	Easting [m]	Northing [m]	Elevation [m]
B007	251319.717	592970.822	-0.957
B008	251325.703	592978.547	-1.022
B009	251303.459	592990.938	-0.841

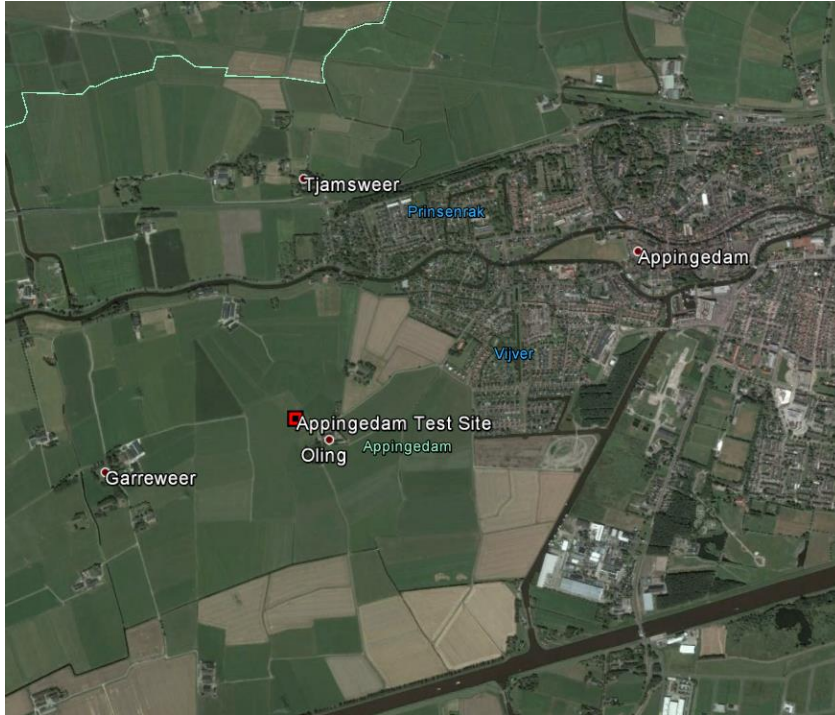


Fig. 1: Location of Site 3 (Appingedam)

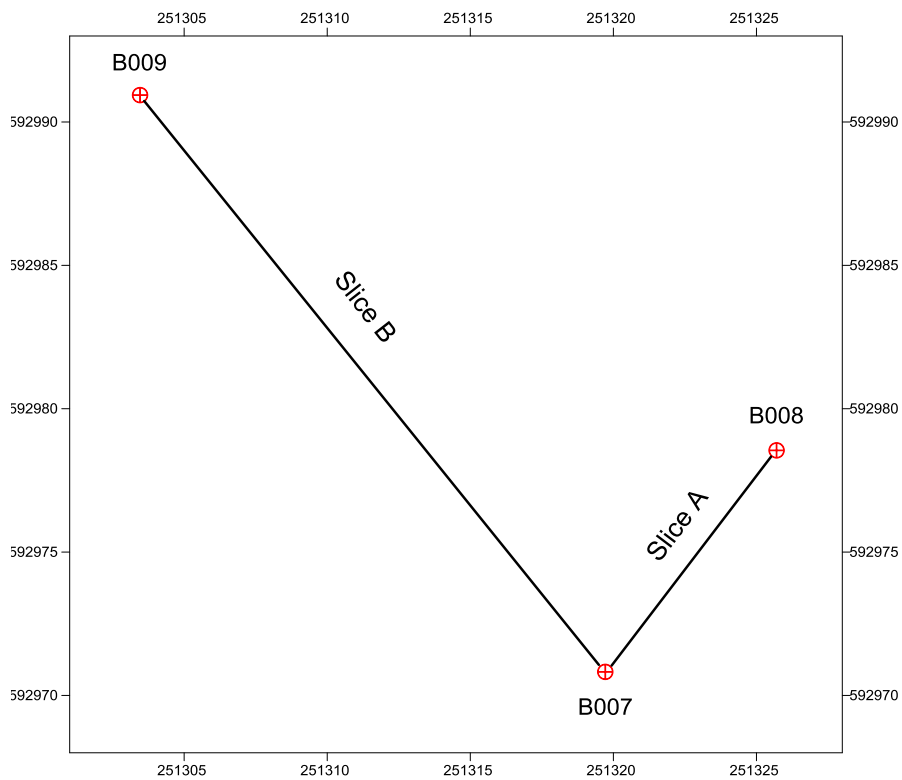


Fig. 2: Plan view of boreholes and tomographic slices

### 3. P-Wave Seismic Tomography

#### 3.1 General description

Seismic tomography is a geophysical method used to delineate structures between boreholes. Seismic waves are generated by an impulsive source in one borehole. The propagation of the seismic waves is influenced by the varying rock properties between the boreholes leading to slow or fast wave arrivals in the second borehole.

To receive the seismic signals, hydrophones connected in a vertical multichannel string with 24 or more sensors are used in the second borehole. Once sufficient signal data quality is achieved, the seismic source is moved to the next position in the borehole and the shooting is repeated. As a result, ray tracing from one borehole to the other builds up very dense and detailed ray coverage.

During seismic data processing, first arrival travel times of the p-waves are picked for each source-hydrophone pair. Using an iterative numerical inversion procedure, a seismic velocity distribution between the two boreholes can be calculated based on the travel times and the known source and hydrophone locations.

#### 3.2 Tomography measurements

In total two tomograms have been gathered between boreholes B007 - B008 and B007 - B009. The tomograms provide vertical sections of the p-wave distribution between the boreholes. The vertical spacing between the shot points and the receiver points was 1 m. The individual test configurations for each tomogram are summarised in Table 2. For Slice A the source was limited to the borehole B008 depth of 28 m.

Table 2: Shooting configuration P-wave tomography (depth below top of casing)

Date	Survey	Hydrophone range [m]	Source range [m]
21 <sup>st</sup> July	Slice A B008 → B007	29 to 1 m in B007	28 to 1m in B008
21 <sup>st</sup> July	Slice B B009 → B007	29 to 1 m in B007	29 to 1m in B009

#### 3.3 Testing equipment

The equipment used to measure the P-wave arrival times consists of an electric surge generator, a remote control unit and a downhole probe (see Figure 3). Various source types can be connected (P and S wave generation) to the surge generator. Triggering of the seismic acquisition system is performed by the remote control unit. The remote control unit converts the reference signal of the surge generator into a trigger signal.

Due to the good transmission properties of the soil, it was decided to use the same source for both the P- and S-wave tomographic measurements. Therefore, the Geotomographie SH-wave source type BIS-SH source was used for both P- and S-wave measurements, as the BIS-SH generates both horizontally polarized shear waves (SH) and compressional waves (P) with a high repeatability.

Energy released by the 5000 V HV unit discharges through a system of electromagnetic coils adjacent to a copper plate. When the plate is rejected, a mechanical impact to the borehole wall is generated. The borehole source is coupled to the borehole wall by a pneumatic clamping system (inflatable bladder). The orientation of the source is controlled from surface by a torsionally stiff hose.

The seismic strike direction was aligned towards the receiver borehole in order to generate P-waves with the highest amplitude. For the P-wave tomography measurements, one record was recorded for each depth interval.

A hydrophone array type BHC2 with 24 channels at 1m spacing, was used to receive the signals (Western Atlas 2512). A specialised 24 channel compact seismograph was used for data acquisition. Data were stored on laptop and backup was made on memory stick.



Fig. 3: P-wave tomography equipment with 5 kV HV unit (upper left), downhole probe BIS-SH (upper middle), remote control unit (upper right) and hydrophone (lower middle)

### 3.4 Seismic data processing

Data processing followed several steps in order to convert travel times for tomographic inversion. Seismic data records were depth-sorted and spatial information were assigned to each record. Then, first arrival times of the seismic waves were determined by manual picking using proprietary software. First arrival times are related to the seismic p-wave velocity, which is the most common seismic parameter to describe sediment properties.

The seismic data showed excellent quality throughout all records in the lower parts of the tomograms. Towards the surface the quality decreased due to the very soft soil and the poor transmission of seismic waves in such an environment. However, the quality remained on a moderate level for Slice A and on an acceptable level for Slice B. The ground water level is inferred at a depth of approximately 5 m, which causes a high level of refraction for waves in the upper 5 m. Thus, traveltimes for the upper 5 m were omitted from the inversion, as the inclusion would have caused artefacts in the tomograms.

Results are subjected to quality control to ensure a consistency in picked travel times. Travel times of subsequent shots were loaded, compared to adjacent waveforms and if needed, corrected during the travel time picking procedure. In total about 1300 travel times were analysed during the processing of the data.

For the purpose of modelling, the subsurface was numerically divided into 3D-cells. A SIRT algorithm was used for travel time inversion. The algorithm is iterative and minimises the residual of the observed and calculated seismic travel times by a correction of the seismic slowness, i.e. the reciprocal of the seismic velocity in each cell. Seismic waves are assumed to propagate along curved ray paths. The tomograms for each borehole set are processed separately. A vertical and a horizontal cell size of approx. 1 m were chosen for all tomograms. The borehole deviation was incorporated in the inversion process.

### **3.5 Results**

The measured P-wave tomograms are shown in Appendix A. The seismic velocity measurements are dominated by horizontal layering, with three distinguishable layers. No traveltimes for the upper five meters above ground water table were included in the inversion process and thus no information is available. Velocities for depths of 5 to 8 m ranged from approximately 1000 to 1600 m/s. This layer is followed by a thin high velocity zone, extending from depths of 8 to 11 m with p-wave velocities of 1700 to 2000 m/s. Below, the P-wave velocity is around 1600 m/s.

## **4. S-Wave Seismic Tomography**

### **4.1 General description**

S-wave tomography is a direct way to measure soil stiffness if soil density is known. Another advantage of the S-wave is that it is not influenced by the groundwater table thus resolution of the method is not reduced compared to P-wave tomography under the same conditions.

Generation of an S-wave requires a source which is able to generate horizontally (SH) or vertically (SV) polarized S-waves in two opposing directions. Typically, geophones are used to receive the signals. In order to allow a rapid surveying a multi-borehole station tool is required.

Data processing requires different steps compared to P-wave tomography, as typically the number of receivers is limited and identification of the S-wave requires the overlapping of the opposite shot directions. Arrival travel times of the S-waves have to

be determined. Using an iterative numerical inversion procedure a seismic velocity distribution between the two boreholes can be calculated based on the travel times and known source and hydrophone locations.

#### 4.2 Tomography measurements

In total two tomograms have been gathered between boreholes B007 - B008 and B007 - B009. The measurements cover the whole length of the boreholes for Slice A. For Slice B the measurements cover depths of 29 to 2 m. The upper station at a depth of 1 m was omitted due to poor wave transmission in the upper meter. The vertical spacing between the shot points and the receiver points was set to 1 m. The individual test configurations for each tomogram are summarised in Table 3.

Table 3: Shooting configuration S-wave tomography (depth below top of casing)

Date	Survey	Receiver range [m] in B002	Source range [m] In B001
22 <sup>nd</sup> July	Slice A B008 → B007	Layout 1: 29 to 23 Layout 2: 22 to 16 Layout 3: 15 to 9 Layout 4: 8 to 2 Layout 5: 7 to 1	Layout 1: 28 to 17 Layout 2: 28 to 9 Layout 3: 22 to 2 Layout 4: 15 to 1 Layout 5: 8 to 1
22 <sup>nd</sup> July	Slice B B009 → B007	Layout 1: 29 to 23 Layout 2: 22 to 16 Layout 3: 15 to 9 Layout 4: 8 to 2	Layout 1: 29 to 16 Layout 2: 29 to 9 Layout 3: 22 to 2 Layout 4: 15 to 1

#### 4.3 Testing equipment

In order to generate S-waves the Geotomographie SH-wave source type BIS-SH was used. The borehole source BIS-SH generates horizontally polarized shear waves (SH) and compressional waves (P). The seismic signals are highly repeatable.

The source works in dry or water filled boreholes. Energy released by the 5000 V HV unit discharges through a system of electromagnetic coils adjacent to a copper plate. When the plate is rejected, a mechanical impact to the borehole wall is generated. The borehole source is coupled to the borehole wall by a pneumatic clamping system (inflatable bladder). The orientation of the source is controlled from surface by a torsionally stiff hose.

The seismic strike direction was aligned perpendicular to the receiver borehole in order to generate SH-waves. To get the opposite strike direction the source was rotated by 180° and thus generating S-waves with opposing polarities. For each shot direction a separate seismic record was acquired and stored.

The seismic signals were received using the Multi-Station Borehole Acquisition System (MBAS) receiver unit. The MBAS is a digital three-component geophone string used to receive P- and S-waves in dry or water filled boreholes. Up to ten individual stations with tri-axial sensors can be connected.

The MBAS stations are aligned to ensure that all horizontal sensors are oriented in the same direction. The system can be oriented from the surface by a torsionally stiff hose. Each station is clamped to the borehole wall by two pneumatic cylinders. An external trigger can be plugged into the USB interface on surface which is connected to a laptop. The operation is entirely controlled by the acquisition software. A separate seismograph is not required.

An MBAS unit with seven 3C units at 1m station interval was used. The MBAS unit was aligned with their X-sensor direction parallel to the source strike direction. Thus, these sensors should give the best seismic signal when evaluating the horizontally polarised shear wave. According to the MBAS layouts given in Table 3, the MBAS was pneumatically clamped to the borehole wall. The S-wave source was moved in the other borehole in 1m intervals.



Fig. 4: SH-wave equipment with 5 kV HV unit (upper left), downhole probe BIS-SH (upper middle), remote control unit (upper right) and MBAS receiver (lower middle)

#### 4.4 Seismic data processing

Data processing followed several steps in order to determine travel times for tomographic inversion. Each receiver layout described in Table 3 contains 7 stations each with 3C sensors (XYZ). As already described the X-sensor was aligned to be optimal in respect to the strike direction of the source. For example, for layout 1 a total of 13 shot positions were carried out. At every shot position two opposite strike directions were recorded, i.e. equal to a total of 2 x 13 records (and each record contains 7 x 3 traces). Records were split according to their depth and into their X, Y and Z components and then component-wise compiled into one X, Y and Z component record for each strike direction per layout.

Subsequently, the traces were resorted and grouped according to the different receiver positions. At the beginning of this resorting, one record corresponded to one shot at a certain depth (polarized either in the plus or minus direction) and displayed seven traces of a single component (either X, Y or Z). After this resorting, one record corresponded to one receiver position and displayed the traces of the shots at different depths. This proved beneficial when picking the data, as more traces could be viewed at the same time and trends in S-wave arrival were easier to identify.

Spatial information was assigned to each record and arrival times of the seismic waves were determined by manually picking of the overlaid records for opposite strike directions. These travel times were quality controlled to ensure consistent picking and borehole deviation data was incorporated. In total about 800 travel times were analysed during the processing of the data.

For the purpose of modelling, the subsurface was numerically divided into 3D-cells. A SIRT algorithm was used for travel time inversion. The algorithm is iterative and minimises the residual of the observed and calculated seismic travel times by a correction of the seismic slowness, i.e. the reciprocal of the seismic velocity in each cell. Seismic waves are assumed to propagate along curved ray paths. The tomograms for each borehole set are processed separately. A vertical and a horizontal cell size of approximately 1 m were chosen for all S-wave tomograms. The borehole deviation was incorporated in the inversion process.

#### 4.5 Results

The measured S-wave tomograms are shown in Appendix B. The determined S-wave velocities range from about 30 to 350 m/s. Seismic tomography sections are dominated by a horizontal layering of the sediments. Three layers can be identified in the S-wave tomograms. The upper layer ranges from 0 to about 8 m and is characterised by S-wave velocities of around 30 to 100 m/s. This suggests that the upper layer is very weak. The velocity increase at 8 m corresponds to the boundary observed in the P-wave tomograms. The second layer with S-wave velocities of around 150 to 250 m/s is observed between depths of 8 and 20 m. Below 20 m, the third layer possesses S-wave velocities of around 300 m/s. Due to the proportionally higher S-wave velocity contrasts, the S-wave tomograms show a distinctly higher resolution compared to the P-wave tomograms.

## 5. Conclusion and Summary

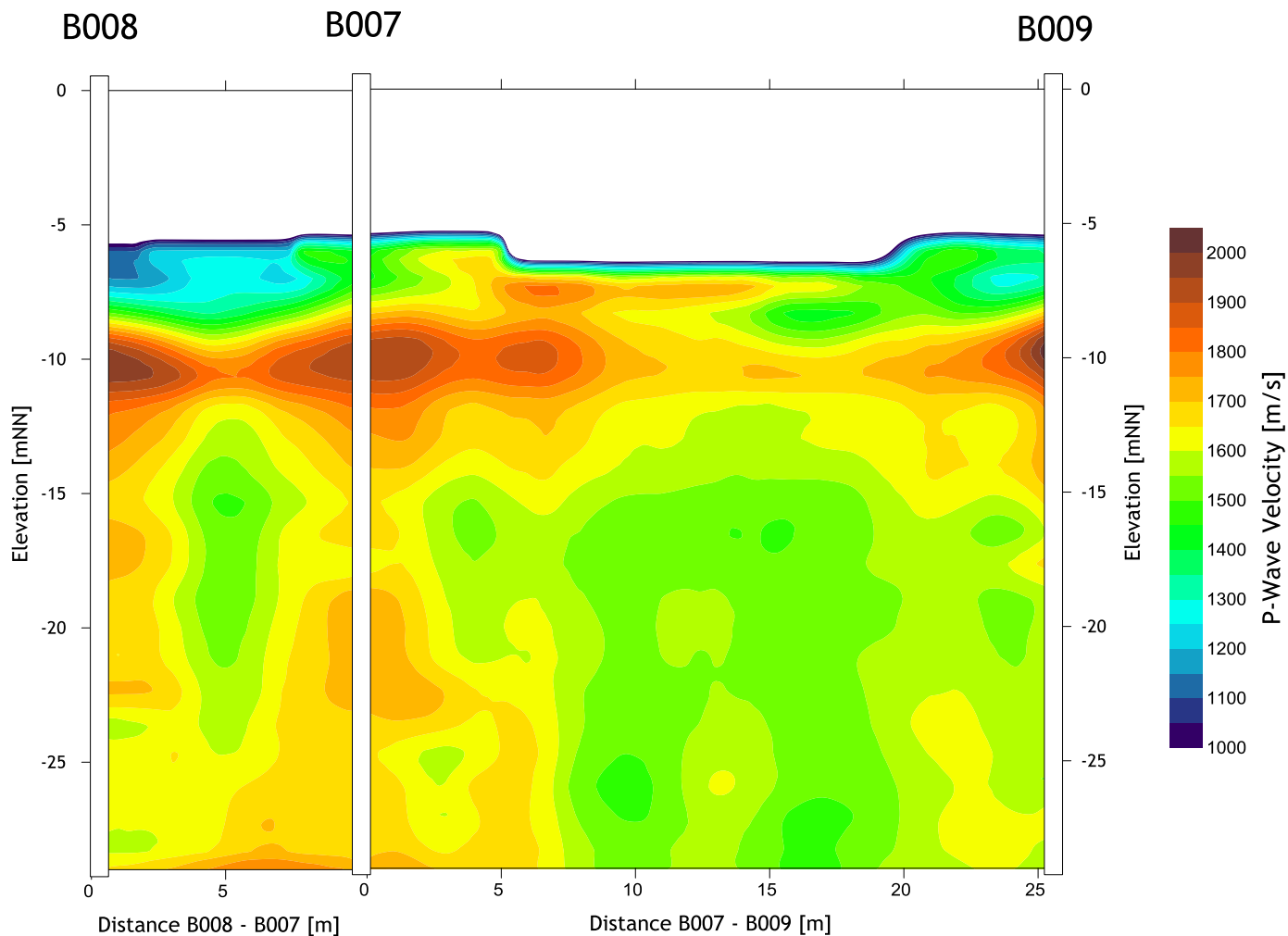
This report describes the seismic measurements performed at the Appingedam (BAPP) test site near Delfzijl. The survey was carried out on the 21<sup>st</sup> and 22<sup>nd</sup> July 2015. A tomographic P- and S-wave survey was carried out each resulting in two tomograms. The sampling interval was set to 1 m for both tomography measurements.

The depths of the boreholes were approximately 30 m and inter-borehole distances ranging from about 10 m to 26 m. Both P-wave and S-wave tomographic surveys were carried out with the borehole source type BIS-SH. To receive signals a hydrophone string was used for P-wave tomography. For S-wave tomography the MBAS digital borehole system was used in a 7 station configuration at 1m intervals.

In general, the results show P-wave velocities between 1000 m/s and 2000 m/s and S-wave velocities between 30 and 350 m/s. P-wave velocities below around 1450m/s are due to semi- or unsaturated sediments. Sometimes even saturated sediments might show low velocities if a high content of organic material is present. The high content of organic material causes bacterial degradation which generates gas. Even very small portions of gas can cause a significant drop in velocity.

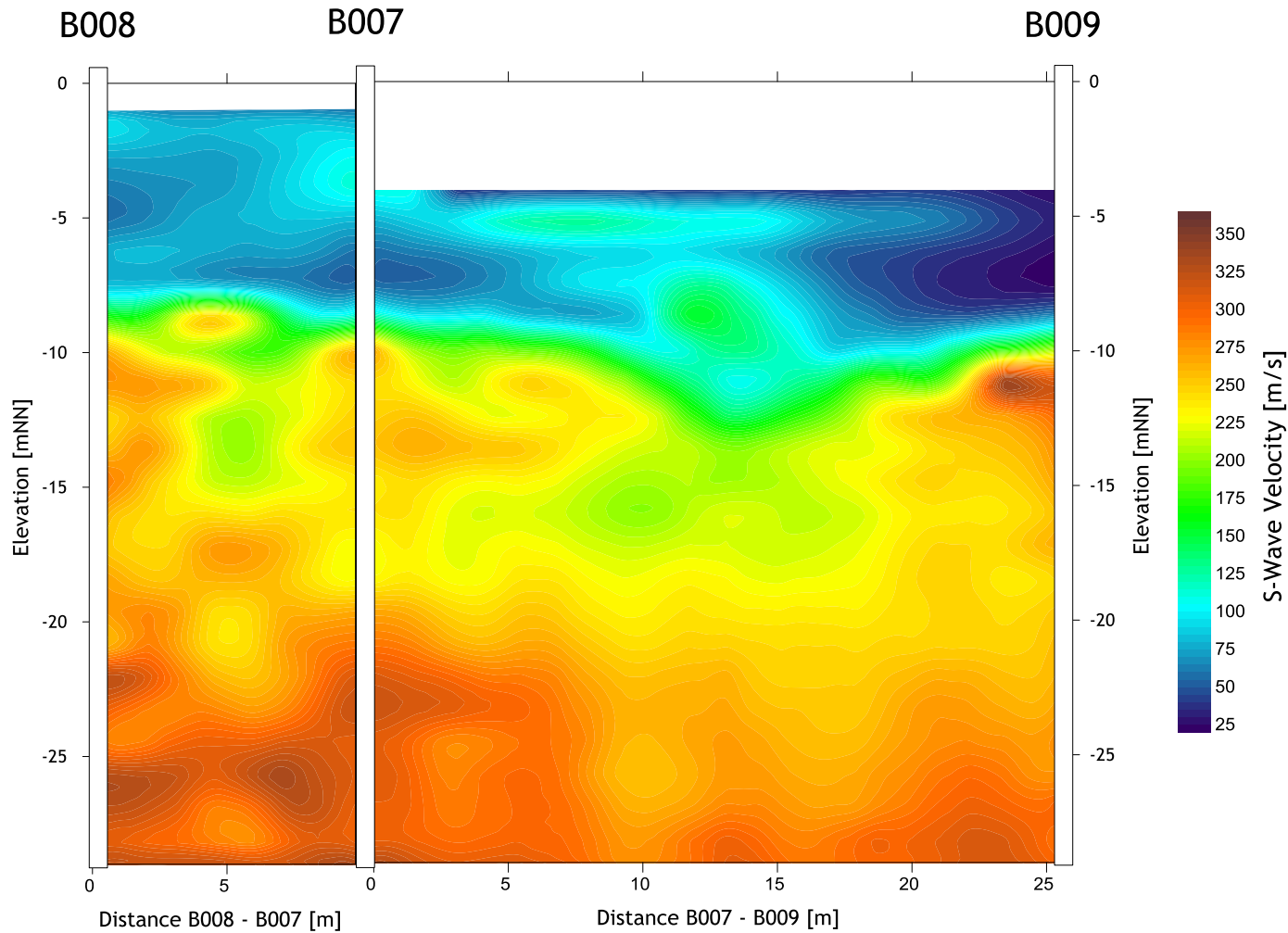
In general three layers can be identified in the two tomograms. The upper layer ranges from 0 to 8 m below ground with P-wave velocities from 1000 to 1600 m/s and S-wave velocities from 30 to 100 m/s, which indicates a very weak layer. The second layer at depths of 8 to 11 m shows higher P-wave velocities of around 1700 to 2000 m/s. This layer shows up as a transition zone in the S-wave tomograms, where S-wave velocities increase from 100 to around 250 m/s sharply. A third layer is consistent in both tomograms below a depth of 11 m with P-wave velocities of around 1600 m/s and S-wave velocities between 200 and 350 m/s. A fourth layer might be present below a depth of 20 m. At this boundary the S-wave velocities increase from 250 to over 300 m/s. This boundary is not visible in the P-wave tomograms which could be due to the lower resolution of the P-wave tomograms.

# P-Wave Tomograms



Geotomographie GmbH – Geophysikalische Spezialmessungen	
56567 Neuwied, Am Tonnenberg 18   Tel.: +49 2361 778135 Fax.: 778136	
Client: Deltares	
Project: Tomography, Appingedam	11.08.2015
Content: P-Wave Tomograms	Appendix 1

# S-Wave Tomograms



Geotomographie GmbH – Geophysikalische Spezialmessungen	
56567 Neuwied, Am Tonnenberg 18   Tel.: +49 2361 778135 Fax.: 778136	
Client: Deltares	
Project: Tomography, Appingedam	11.08.2015
Content: S-Wave Tomograms	Appendix 2